

SHOCK WAVE AND
HIGH PRESSURE PHENOMENA

G. Ben-Dor

Shock Wave Reflection Phenomena

Second Edition



Springer

Shock Wave and High Pressure Phenomena

Series Editor-in-Chief

L. Davison, USA

Y. Horie, USA

Founding Editor

R. A. Graham, USA

Advisory Board

V. E. Fortov, Russia

Y. M. Gupta, USA

R. R. Asay, USA

G. Ben-Dor, Israel

K. Takayama, Japan

F. Lu, USA

Shock Wave and High Pressure Phenomena

- L.L. Altgilbers, M.D.J. Brown, I. Grishnaev, B.M. Novac, I.R. Smith, I. Tkach, and Y. Tkach:* Magnetocumulative Generators
- T. Antoun, D.R. Curran, G.I. Kanel, S.V. Razorenov, and A.V. Utkin:* Spall Fracture
- J. Asay and M. Shahinpoor (Eds.):* High-Pressure Shock Compression of Solids
- S.S. Batsanov:* Effects of Explosion on Materials: Modification and Synthesis Under High-Pressure Shock Compression
- R. Cherét:* Detonation of Condensed Explosives
- L. Davison, D. Grady, and M. Shahinpoor (Eds.):* High-Pressure Shock Compression of Solids II
- L. Davison and M. Shahinpoor (Eds.):* High-Pressure Shock Compression of Solids III
- L. Davison, Y. Horie, and M. Shahinpoor (Eds.):* High-Pressure Shock Compression of Solids IV
- L. Davison, Y. Horie, and T. Sekine (Eds.):* High-Pressure Shock Compression of Solids V
- A.N. Dremin:* Toward Detonation Theory
- Y. Horie, L. Davison, and N.N. Thadhani (Eds.):* High-Pressure Shock Compression of Solids VI
- R. Graham:* Solids Under High-Pressure Shock Compression
- J.N. Johnson and R. Cherét (Eds.):* Classic Papers in Shock Compression Science
- V.F. Nesterenko:* Dynamics of Heterogeneous Materials
- M. Sučeska:* Test Methods of Explosives
- J.A. Zukas and W.P. Walters (Eds.):* Explosive Effects and Applications
- G.I. Kanel, S.V. Razorenov, and V.E. Fortov:* Shock-Wave Phenomena and the Properties of Condensed Matter
- V.E. Fortov, L.V. Altshuler, R.F. Trunin, and A.I. Funtikov:* High-Pressure Shock Compression of Solids VII
- L.C. Chhabildas, L. Davison, and Y. Horie (Eds.):* High-Pressure Shock Compression of Solids VIII
- R.P. Drake:* High-Energy-Density Physics
- D. Grady:* Fragmentation of Rings and Shells
- M. V. Zhernokletov and B. L. Glushak (Eds.):* Material Properties under Intensive Dynamic Loading
- G. Ben-Dor:* Shock Wave Reflection Phenomena

G. Ben-Dor

Shock Wave Reflection Phenomena

Second Edition

With 194 Figures



Springer

Gabi Ben-Dor
Ben-Gurion University of Negev
Institute for Applied Research
Beer-Sheva, Israel
E-mail: bendorg@bgu.ac.il

Series Editors-in-Chief:

Lee Davison
39 Cañoncito Vista Road
Tijeras, NM 87059, USA
E-mail: leedavison@aol.com

Yasuyuki Horie
AFRL/MNME Munitions Directorate
2306 Perimeter Road
Eglin AFB, FL 32542, USA
E-mail: yasuyuki.horie@eglin.af.mil

Library of Congress Control Number: 2007928738

ISSN 8063-7200
ISBN 978-3-540-71381-4 2nd ed. Springer Berlin Heidelberg New York
ISBN 978-3-540-97707-2 1st ed. Springer Berlin Heidelberg New York

This work is subject to copyright. All rights are reserved, whether the whole or part of the material is concerned, specifically the rights of translation, reprinting, reuse of illustrations, recitation, broadcasting, reproduction on microfilm or in any other way, and storage in data banks. Duplication of this publication or parts thereof is permitted only under the provisions of the German Copyright Law of September 9, 1965, in its current version, and permission for use must always be obtained from Springer. Violations are liable for prosecution under the German Copyright Law.

Springer is a part of Springer Science+Business Media
springer.com
© Springer-Verlag Berlin Heidelberg 1991, 2007

The use of general descriptive names, registered names, trademarks, etc. in this publication does not imply, even in the absence of a specific statement, that such names are exempt from the relevant protective laws and regulations and therefore free for general use.

Typesetting by the author and SPi using a Springer L^AT_EX macro package
Cover design: WMX design GmbH, Heidelberg

Printed on acid-free paper SPIN: 11519492 54/SPi 5 4 3 2 1 0

To **Professor Ozer Igra** who introduced me to the world of shock tubes
and waves,

to **Professor Irvine Israel Glass** who led me into the world of shock wave
reflection phenomena,

to **my colleagues** all over the world with whom I have been investigating
the fascinating phenomena of shock wave reflection for over 30 years,
and finally,

to **Ms. Edna Magen**, and our three children, **Shai, Lavi and Tsachit**,
who provided me with an excellent atmosphere and support to accomplish
all my goals.

Acknowledgment

I would like to thank Dr. Li Huaidong, currently at the Jet Propulsion Laboratory, California Institute of Technology, in Pasadena, who was my Ph.D. student and Post Doctoral Fellow during the years 1992–1997, for his invaluable contribution to many of the findings of my researches in the area of shock wave reflection, which are the reason for putting together this second edition of my monograph.

Preface

Nothing is more exciting to a scientist than realizing that his/her areas of expertise are developing and that the state-of-the-knowledge yesterday is outdated today.

The distinguished philosopher Ernst Mach first reported the phenomenon of shock wave reflection over 125 years ago in 1878. The study of this fascinating phenomenon was then abandoned for a period of about 60 years until Professors John von Neumann and Bleakney initiated its investigation in the early 1940s. Under their supervision, 15 years of intensive research related to various aspects of the reflection of shock waves in pseudosteady flows were carried out. It was during this period that the four basic shock wave reflection configurations, regular, single-Mach, transitional-Mach and double-Mach reflections, were discovered. Then, for a period of about 10 years from the mid-1950s until the mid-1960s, the investigation of the reflection phenomenon of shock waves was kept on a low flame all over the world (e.g. Australia, Japan, Canada, USA, USSR, etc.) until Professor Tatyana Bazhenova from the USSR, Professor Irvine Israel Glass from Canada, and Professor Roy Henderson from Australia re-initiated the study of this and related phenomena. Under their scientific leadership, numerous findings related to this phenomenon were reported. Probably the most productive research group in the mid-1970s was that led by Professor Irvine Israel Glass in the Institute of Aerospace Studies of the University of Toronto. In 1978, exactly 100 years after Ernst Mach first reported his discoveries on the reflection phenomenon; I published my Ph.D. thesis in which, for the first time, analytical transition criteria between the various shock wave reflection configurations were established.

For reasons which for me are yet unknown, the publication of my Ph.D. findings triggered intensive experimental and analytical studies of the shock wave reflection phenomenon over a variety of geometries and properties of the reflecting surface and in a variety of gases. The center of the experimental investigation was shifted from Canada to Japan, in general, and to the Shock Wave Research Center that was led by Professor Kazuyoshi Takayama, in particular. Under his supervision flow visualization techniques reached such

VIII Preface

a stage that the phrase “*cannot be resolved experimentally*” almost ceased to exist in the scientific dictionary, especially after Dr. Harald Kleine joined his research group for a couple of years.

In the same year that I published my Ph.D. thesis, I published my first journal paper related to the shock wave reflection phenomenon. This paper, entitled “Nonstationary Oblique Shock Wave Reflections: Actual Isopycnics and Numerical Experiments” was co-authored with my Ph.D. supervisor, Professor Irvine Israel Glass. In the conclusion to the paper we wrote *Undoubtedly, numerical codes will evolve in the future which will reliably predict not only RR and SMR but also CMR and DMR in real gases*. I wish my lottery predictions were as successful as this prediction, since probably the most remarkable progress in the study of the shock wave reflection phenomenon in the following decade (i.e., in the 1980s) was made by American computational fluid dynamicists, who demonstrated that almost nothing is beyond their simulation capability. At one time, it was feared that the computational fluid dynamicists would put the experimentalists out of business. Fortunately, this did not occur. Instead, experimentalists, computational fluid dynamicists, and theoreticians worked together in harmony under the orchestration of Professor John Dewey, who realized, in 1981, that scientists interested in the reflection phenomenon of shock waves will benefit the most if they meet once every one/two years and exchange views and ideas. In 1981, he initiated the International Mach Reflection Symposium, which became the framework for excellent cooperation between scientists from all over the world who are interested in better understanding the shock wave reflection phenomenon.

Ten years later, in 1991, I completed writing my monograph entitled *Shock Wave Reflection Phenomena*, which summarized the state-of-the-knowledge at that time.

Three major developments, which shattered this state-of-the-knowledge, took place in the 15 years that has passed since then.

- The first (in the early 1990s), was the discovery of the hysteresis phenomenon in the reflection of shock waves in steady flows.
- The second (in the mid-1990s), was a re-initiation of a abandoned approach considering an overall shock wave diffraction process that results from the interaction of two sub-processes, namely, the shock-wave reflection process and the shock-induced flow deflection process. This approach led to the development of new analytical models for describing the transitional- and the double-Mach reflections; and
- The third (in the late 1990s and the mid-2000s), was the resolution of the well-known von Neumann paradox.

As a result, only one out of the four main chapters of the monograph could be still considered as relevant and providing updated information. Unlike this chapter, the other four are simply outdated. Consequently, the monograph has been re-written, to again describe the state-of-the-knowledge of the fascinating

phenomena of shock wave reflection, which I have been investigating for over three decades.

As a final remark I would like to point out that this book comes as close as possible to summarizing almost all that I know about shock wave reflection phenomena from a phenomenological point of view. Thirty-one years ago, when I first met Professor Irvine Israel Glass, I almost knew nothing about the reflection of shock waves. When he assigned me the investigation of this phenomenon, I thought that it would take a lifetime to understand and explain it. Now I can state wholeheartedly that I was lucky to have been assigned to investigate this fascinating phenomenon and to have met and worked under the supervision of Professor Irvine Israel Glass. I have been even luckier to become a part of a wonderful group of scientists from all over the world with whom I have been collaborating throughout the past thirty years, and with whom I hope to continue collaborating in the future.

Contents

1	General Introduction	1
1.1	Introduction and Historical Background	3
1.2	Reasons for the Reflection	9
1.2.1	Reason for the Reflection in Steady Flows	11
1.2.2	Reasons for the Reflection in Pseudosteady and Unsteady Flows	12
1.3	Analytical Approaches for Describing Regular and Mach Reflections	13
1.3.1	Two-Shock Theory (2ST) for an Inviscid Flow	14
1.3.2	Three-Shock Theory (3ST) for an Inviscid Flow	16
1.4	Shock Polars	18
1.4.1	Shock-Polar Presentation of the Flow Field Near the Reflection Point of a Regular Reflection	21
1.4.2	Shock-Polar Presentation of the Flow Field Near the Triple Point of a Mach Reflection	22
1.5	Suggested RR \rightleftharpoons IR Transition Criteria	25
1.5.1	Detachment Criterion	25
1.5.2	Mechanical-Equilibrium Criterion	29
1.5.3	Sonic Criterion	30
1.5.4	Length-Scale Criterion	32
1.5.5	Summary, Critique, and Discussion	33
	References	36
2	Shock Wave Reflections in Steady Flows	39
2.1	Categories of Steady Reflection Phenomena	42
2.1.1	Curved Incident Shock Wave Reflections over Straight Reflecting Surfaces	42
2.1.2	Straight Incident Shock Wave Reflections over Curved Reflecting Surfaces	43
2.1.3	Curved Incident Shock Wave Reflections over Curved Reflecting Surfaces	44

2.1.4	Straight Incident Shock Wave Reflections over Straight Reflecting Surfaces	44
2.2	Modifications of the Perfect Inviscid Two- and Three-Shock Theories	48
2.2.1	Nonstraight Discontinuities	49
2.2.2	Viscous Effects	49
2.2.3	Thermal Conduction Effects	51
2.2.4	Real Gas Effects	52
2.3	Prediction of the Mach Reflection Shape and the Mach Stem Height	53
2.3.1	Assumptions and Concepts of the Models	54
2.3.2	Governing Equations	58
2.3.3	Derivation of a General Expression for a Curved Line as a Function of Some Boundary Conditions at Its Ends	64
2.3.4	Estimation of the Strength of the Expansion Waves that are Reflected at the Slipstream	66
2.3.5	Geometric Relations of the Wave Configuration Shown in Figs. 2.12 and 2.15	67
2.3.6	Results	70
2.4	Hysteresis Processes in the RR \rightleftharpoons MR Transition	76
2.4.1	Introduction	76
2.4.2	Hysteresis Processes in the Reflection of Symmetric Shock Waves	79
2.4.3	Hysteresis Process in the Reflection of Asymmetric Shock Waves	90
2.4.4	Hysteresis Process in the Reflection of Axisymmetric (Conical) Shock Waves	101
	References	131
3	Shock Wave Reflections in Pseudosteady Flows	135
3.1	“Old” State-of-the-Knowledge	139
3.1.1	Reflection Configurations	140
3.1.2	The Transition Criteria	143
3.1.3	Second Triple Point Trajectory and Some Critical Remarks Regarding the Old State-of-the-Knowledge	151
3.2	“New” (Present) State-of-the-Knowledge	156
3.2.1	Introductory Remarks	156
3.2.2	Shock-Diffraction Process	157
3.2.3	Transition Criteria	159
3.2.4	Single-Mach Reflection (SMR)	161
3.2.5	Formation of Transitional-Mach Reflection (TMR) or Double-Mach Reflection (DMR)	161
3.2.6	Transitional-Mach Reflection (TMR)	162
3.2.7	Double-Mach Reflection – DMR	167

3.2.8	SMR \rightleftharpoons PTMR/TMR/DMR and the TMR \rightleftharpoons DMR Transition Criteria and Domains of Different Types of Reflection	175
3.2.9	Triple-Mach Reflection	176
3.2.10	Summary of the New State-of-the-Knowledge	177
3.2.11	Domains and Transition Boundaries	179
3.2.12	Weak Shock Wave Reflection Domain	180
3.3	Summary, Critique, and Discussion	190
3.4	Modifications of the Perfect Inviscid Two- and Three-Shock Theories	194
3.4.1	Nonsteady Effects	194
3.4.2	Nonstraight Discontinuities	195
3.4.3	Real Gas Effects	196
3.4.4	Viscous Effects	201
3.4.5	Thermal Conduction Effects	222
3.4.6	Noninfinitely Thin Contact Discontinuity	224
3.4.7	Non-Self-Similar Effects	227
3.5	Additional Considerations	230
3.5.1	Flow Deflection Domains	230
3.5.2	Shock Wave Diffraction Domains	232
3.5.3	Comparison Between Steady and Pseudosteady Reflection Domains	233
	References	235
4	Shock Wave Reflections in Unsteady Flows	247
4.1	Constant Velocity Shock Wave Reflections Over Nonstraight Surfaces	250
4.1.1	Shock Wave Reflections Over Cylindrical Concave Surfaces	250
4.1.2	Shock Wave Reflections Over Cylindrical Convex Surfaces	282
4.1.3	Shock Wave Reflections Over Double Wedges	291
4.2	Nonconstant Velocity Shock Wave Reflections Over Straight Surfaces	297
4.3	Spherical Shock Wave Reflections Over Straight and Nonstraight Surfaces	297
	References	304
5	Source List	307
5.1	Scientific Journals	308
	References	308
5.2	Reports	332
	References	332
	Index	339

1

General Introduction

List of symbols

Latin Letters

C_P	Specific heat capacity at constant pressure
C_V	Specific heat capacity at constant volume
h_i	Enthalpy in state (i)
ℓ_w	Length scale required for the formation of an MR
M_i	Flow Mach number in state (i)
M_S	Incident shock wave Mach number
p_i	Static pressure in state (i)
T_i	Static temperature in state (i)
u_i	Flow velocity in state (i) with respect to the reflection point, R , in RR or the triple point, T , in MR
V_i	Flow velocity in state (i) in a laboratory frame of reference.
V_S	Incident shock wave velocity in a laboratory frame of reference.

Greek Letters

χ	First triple point trajectory angle
χ'	Second triple point trajectory angle
$\delta_{\max}(M_i)$	Maximum flow deflection angle for a flow having a Mach number M_i through an oblique shock wave
ϕ_i	Angle of incidence between the flow and the oblique shock wave across which the flow enters into state (i)
γ	Specific heat capacities ratio ($= C_P/C_V$)
μ	Mach angle
θ_i	Angle of deflection of the flow while passing across an oblique shock wave and entering into state (i)
θ_W	Reflecting wedge angle
θ_W^C	Complementary wedge angle ($= 90^\circ - \phi_1$)
ρ_i	Flow density in state (i)

ω_i Angle between the incident shock wave and the reflecting surface

ω_r Angle between the reflected shock wave and the reflecting surface

Abbreviations (not in alphabetic order)

R Reflection point

T Triple point

i Incident shock wave

r Reflected shock wave

m Mach stem

s Slipstream

T Triple point

RR Regular reflection

IR Irregular reflection

MR Mach reflection

WMR Weak Mach reflection

vMR von Neumann reflection

VR Vasilev reflection

GR Guderley reflection

DiMR Direct-Mach reflection

StMR Stationary-Mach reflection

InMR Inverse-Mach reflection

TRR Transitioned regular reflection

SMR Single-Mach reflection

PTMR Pseudo-transitional-Mach reflection

TMR Transitional-Mach reflection

DMR Double-Mach reflection

DMR⁺ Positive double-Mach reflection

DMR⁻ Negative double-Mach reflection

TerDMR Terminal double-Mach reflection

Subscripts

0 Flow state ahead of the incident shock wave, i, or the Mach stem, m

1 Flow state behind the incident shock wave, i

2 Flow state behind the reflected shock wave, r

3 Flow state behind the Mach stem, m

m Maximum deflection point (also known as the detachment point) on the shock polar

s Sonic point on the shock polar

Superscripts

R With respect to the reflection point R

T with respect to the triple point T

s Strong solution

w Weak solution

When a shock wave propagating in a medium with given acoustic impedance obliquely encounters another medium, having a different acoustic impedance, it experiences a reflection that is known in the literature as oblique shock wave reflection.

1.1 Introduction and Historical Background

Ernst Mach, who reported his discovery as early as 1878, was probably the first scientist to notice and record the reflection phenomenon of shock waves. In his ingenious experimental study, which was surveyed by Reichenbach (1983) and re-conducted by Krehl & van der Geest (1991), he recorded two different shock wave reflection configurations. The first, a two shock wave configuration is known nowadays as regular reflection, RR, and the second, a three shock wave configuration, was named after him, and is known nowadays as Mach reflection, MR.

Intensive research of the reflection phenomena of shock waves was re-initiated in the early 1940s by von Neumann. Since then it has been realized that the Mach reflection wave configuration can be further divided into more specific wave structures. In addition, three new types of reflection were recognized:

- The first, a von Neumann reflection, vNR, was forwarded in the early 1990s.
- The second, a reflection that has been named Guderley reflection, GR, after Guderley (1947) who was the first one to hypothesize it.
- The third, an intermediate wave configuration that appears for conditions between those appropriate for the establishment and existence of vNR and GR. Since it was first mentioned by Vasilev [see e.g., Vasilev & Kraiko (1999)] it will be referred to in this monograph as Vasilev reflection, VR.

In general, the reflection of shock waves can be divided into:

- Regular reflection, RR, or
- Irregular reflections, IR.

The RR wave configuration consists of two shock waves, the incident shock wave, i , and the reflected shock wave, r , that meet at the reflection point, R , which is located on the reflecting surface. A schematic illustration of the wave configuration of an RR is shown in Fig. 1.1. All the other wave configurations are termed irregular reflections, IR.

The IR-domain is divided, in general, into four subdomains:

- A subdomain inside which the three-shock theory of von Neumann (see Sect. 1.3.2) has a “standard” solution that corresponds to an MR
- A subdomain inside which the three-shock theory has a “nonstandard” solution that corresponds to a vNR

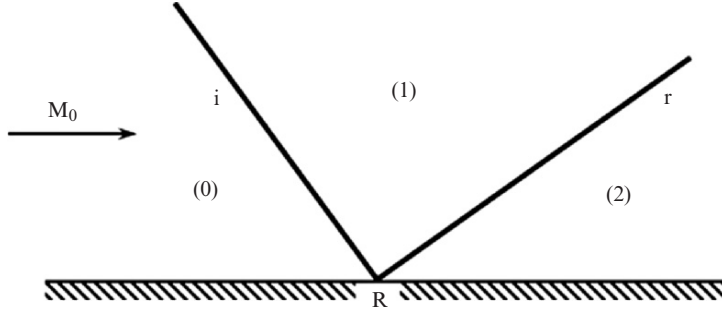


Fig. 1.1. Schematic illustration of a regular reflection wave configuration – RR

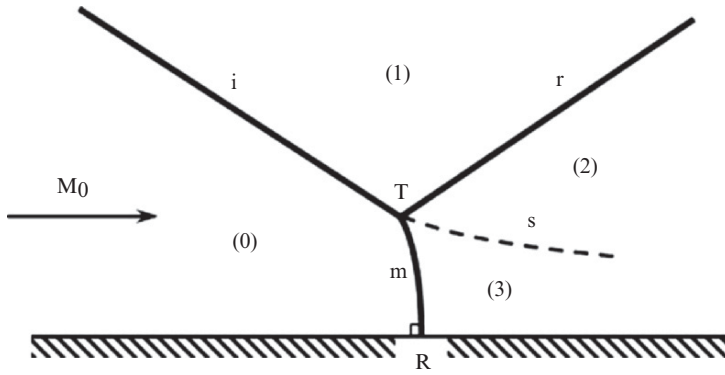


Fig. 1.2. Schematic illustration of a Mach reflection wave configuration – MR

- A subdomain inside which the three-shock theory does not have any solution, but experimental evidences reveal inside it wave configurations that resemble MR wave configuration.¹ The wave configuration in this case is a GR
- A subdomain, which extends between the just-mentioned vNR- and the GR-domains inside which the reflection is a VR

The subdomains of vNR, VR and GR, which are typified by weak shock waves and small reflecting wedge angles, have been referred to by many investigators as the weak-shock wave reflection domain.

The MR wave configuration consists of three shock waves, namely; the incident shock wave, i, the reflected shock wave, r, the Mach stem, m, and one slipstream, s. These four discontinuities meet at a single point that is known as the triple point, T, which is located above the reflecting surface. A clear discontinuity in the slope between the incident shock wave and the Mach stem exists at the triple point. A schematic illustration of the wave configuration of an MR is shown in Fig. 1.2. The reflection point, R is at the foot of the Mach stem where it is perpendicular to the reflecting surface.

¹ This phenomenon is known as the von Neumann paradox.

While trying to resolve the above-mentioned von Neumann paradox, Colella & Henderson (1990), investigated, numerically, the weak-shock wave reflection domain and found that there were cases in which there was no apparent discontinuity in the slope between the incident shock wave and the Mach stem, the slipstream was ill defined and the reflected shock wave degenerated near the triple point to a band of compression wave. In such cases they claimed that the reflection was not an MR, but another reflection that they termed as von Neumann reflection, vNR. Note that some researchers (see e.g., Olim & Dewey 1992) termed this reflection as weak-Mach reflection, WMR.

Vasilev & Kraiko (1999), who also investigated the weak-shock wave reflection domain, found by means of a high-resolution numerical study that an additional wave configuration exists in the WMR-domain. The reflection that they observed, in the subdomain in which the three-shock theory has no solution, was a four-wave pattern that was originally suggested by Guderely (1947) about 60 years ago. Based on their numerical study, an expansion wave exists immediately behind the reflected shock wave. The four-wave configuration that was revealed in the course of their study consisted of three shock waves and a centered extremely narrow expansion fan. Owing to this fact, it should not be surprising that the three-shock theory failed to predict a four-wave configuration. This means, in turn, that there is no paradox in the three-shock theory of von Neumann. Skews & Ashworth (2005) who investigated recently the weak-shock wave reflection domain claimed that a solution of the inviscid transonic equations indicated the possible existence of a very small, multi-wave structure immediately behind the three-shock confluence. In their experimental study they obtained schlieren photographs that showed a structure consisting of an expansion wave followed by a small shock situated behind the confluence point, with some indication of smaller scale structures in some experiments. Skews & Ashworth (2005) suggested naming this four-wave reflection pattern, which was hypothesized first by Guderley (1947), as Guderley reflection, GR. In their conclusion, they mentioned that since their experiments only covered a very small part of the parameter space identified in the literature as falling within the weak-shock wave domain further research is needed to better understand the reflection phenomenon of weak shock waves.

Vasilev & Kraiko (1999) who numerically investigated recently the weak-shock wave reflection domain revealed that there is an intermediate domain, between the vNR- and the GR-domains inside which a yet not fully understood reflection takes place. This reflection will be referred to in the followings as Vasilev reflection, VR.

Since the picture regarding the weak-shock wave reflection domain is not fully understood at this stage, the IR-reflection will be considered as divided into two types: an MR or a WMR, which could be a vNR, a VR or a GR.

Following the re-initiation of the investigation of the shock wave reflection phenomena in the early 1940s, Courant & Freidrichs (1948) indicated that, theoretically, three different types of MR wave configurations are possible,

depending on the direction of propagation of the triple point with respect to the reflecting surface:

- The MR is direct, DiMR, if the triple point moves away from the reflecting surface.
- The MR is stationary, StMR, if the triple point moves parallel to the reflecting surface.
- The MR is inverse, InMR, if the triple point moves towards the reflecting surface.²

The existence of these three types of MR wave configurations was later validated experimentally by Ben-Dor & Takayama (1986/7). Schematic illustrations of a DiMR, an StMR, and an InMR are shown in Fig. 1.3a–c, respectively. While the DiMR is possible both in pseudosteady and unsteady flows, the StMR and the InMR are possible only in unsteady flows.

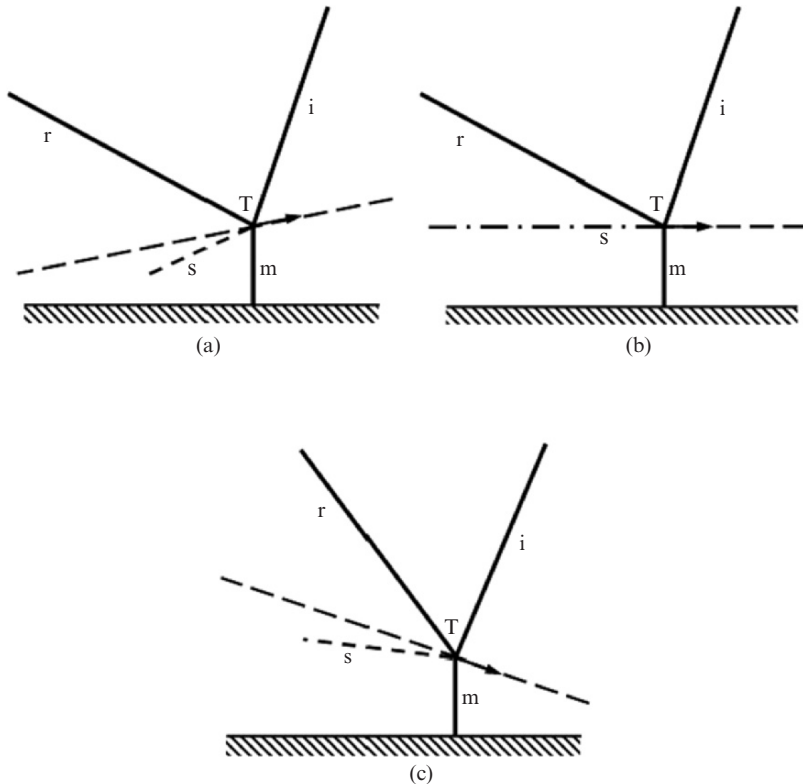


Fig. 1.3. Schematic illustrations of the wave configurations of (a) a direct-Mach reflection – DiMR; (b) a stationary-Mach reflection – StMR; (c) an inverse-Mach reflection – InMR

² Courant & Friedrichs termed this wave configuration as inverted-Mach reflection.

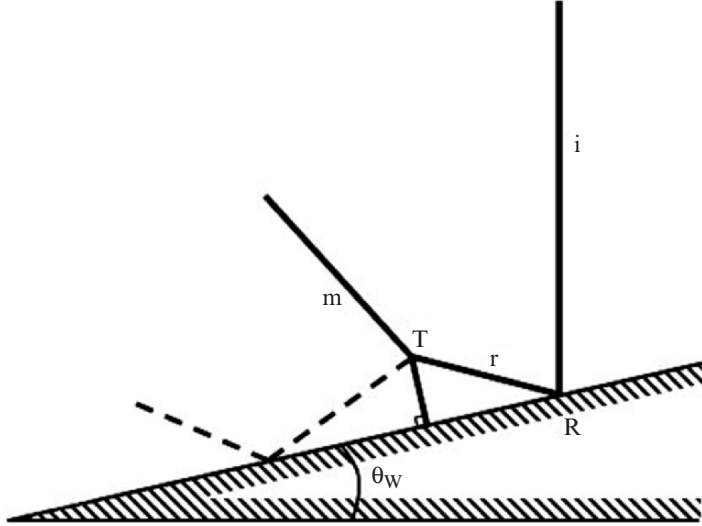


Fig. 1.4. Schematic illustration of a transitioned regular reflection wave configuration – TRR

Since the InMR is an MR in which the triple point moves towards the reflecting surface, it terminates as soon as its triple point collides with the reflecting surface. The termination of the InMR leads to the formation of a new wave configuration that was mentioned first by Ben-Dor & Takayama (1986/7). The wave configuration of this reflection consists of an RR followed by an MR. A schematic illustration of this wave configuration is shown in Fig. 1.4. Since this wave configuration is formed following a transition from an InMR, and since its main structure is an RR, it is called transitioned regular reflection, TRR.

As will be shown subsequently, in pseudosteady flows the shock wave reflection process over the reflecting surface interacts with a flow deflection process around the leading edge of the reflecting wedge. This interaction results in three different MR wave configurations, which were all discovered during the Manhattan project. Until the early 1940s the only two wave configurations that were known to exist in pseudosteady flows were the regular reflection, RR, and the Mach reflection, MR, that as mentioned earlier were first observed by Mach (1878). Smith (1945) investigated the shock wave reflection phenomenon and noted that in some cases the reflected shock wave of the MR had a kink or a reversal of curvature. However, only after White (1951) discovered a completely different type of reflection, which he called double-Mach reflection, DMR, was the wave configuration observed by Smith (1945), i.e., an MR with a kink or a reversal of curvature in the reflected shock wave, recognized as a unique type of reflection. Following White's (1951) finding the reflection that was first observed by Mach (1878) was named simple-Mach reflection, SMR, the reflection that was discovered by Smith (1945) was

named complex-Mach reflection, CMR, and the reflection that was discovered by White (1951) was termed double-Mach reflection, DMR, because its structure (see Fig. 3.9) consisted of two triple points. In the 1970s when it was realized that the so-called simple-Mach reflection is not simple at all, it was renamed and is known nowadays as single-Mach reflection, SMR. Similarly, since the so-called complex-Mach reflection is less complex than some of the other reflection configurations, DMR for example, and since, as will be shown subsequently, it can be viewed as an intermediate wave configuration between the SMR and the DMR, it was re-named and is called nowadays transitional-Mach reflection,³ TMR. Li & Ben-Dor (1995) showed that there is an additional wave configuration, a pseudo-transitional-Mach reflection, PTMR. A PTMR is, in fact, a TMR in which the reflected shock wave does not have a reversal of curvature, and as a result, its appearance is identical to a SMR. An SMR, a TMR and a DMR are shown in Figs. 3.7–3.9, respectively.

In summary, the MR wave configuration consists, in pseudo steady flows, of four types:

- A single-Mach reflection, SMR
- A pseudo-transitional-Mach reflection, PTMR
- A transitional-Mach reflection, TMR
- A double-Mach reflection, DMR

Ben-Dor (1981) showed that, depending on the initial conditions, the trajectory angle of the second triple point, χ' , could be either larger ($\chi' > \chi$) or smaller ($\chi' < \chi$) than the trajectory angle of the first triple point, χ . Lee & Glass (1984) termed the DMR for which $\chi' > \chi$ as DMR^+ and the DMR for which $\chi' < \chi$ as DMR^- . Photographs of a DMR^+ and a DMR^- are shown in Fig. 3.11a, b, respectively. An intermediate DMR for which $\chi' = \chi$ is shown in Fig. 3.11c. Lee & Glass (1984) argued that there could be conditions for which the second triple point, T' , would be located on the reflecting surface, i.e., $\chi' = 0$. They termed this wave configuration as a terminal double-Mach reflection, TerDMR. A TerDMR is shown in Fig. 3.12.

In summary, there are 13 different possible wave configurations, which are associated with the reflection of a shock wave over an oblique surface, namely: RR, WMR (i.e., vNR, VR, and GR), StMR, InMR, TRR, SMR, PTMR, TMR, DMR^+ , DMR^- , and TerDMR. In steady flows only RR and SMR (usually referred to only as MR) are possible. Pseudosteady flows, where, as will be shown subsequently, there is an interaction between two processes, the shock wave reflection over the reflecting wedge and the shock-induced flow deflection around the leading edge of the reflecting wedge, give rise, in addition to RR and SMR, to WMR (i.e., vNR, VR, and GR), PTMR, TMR, DMR^+ , DMR^- , and TerDMR. In unsteady flows three additional wave configurations are possible: StMR, InMR, and TRR. The just mentioned 13 different wave configurations are shown in an evolution tree type presentation in Fig. 1.5.

³ This name was originally suggested by Professor I.I. Glass.

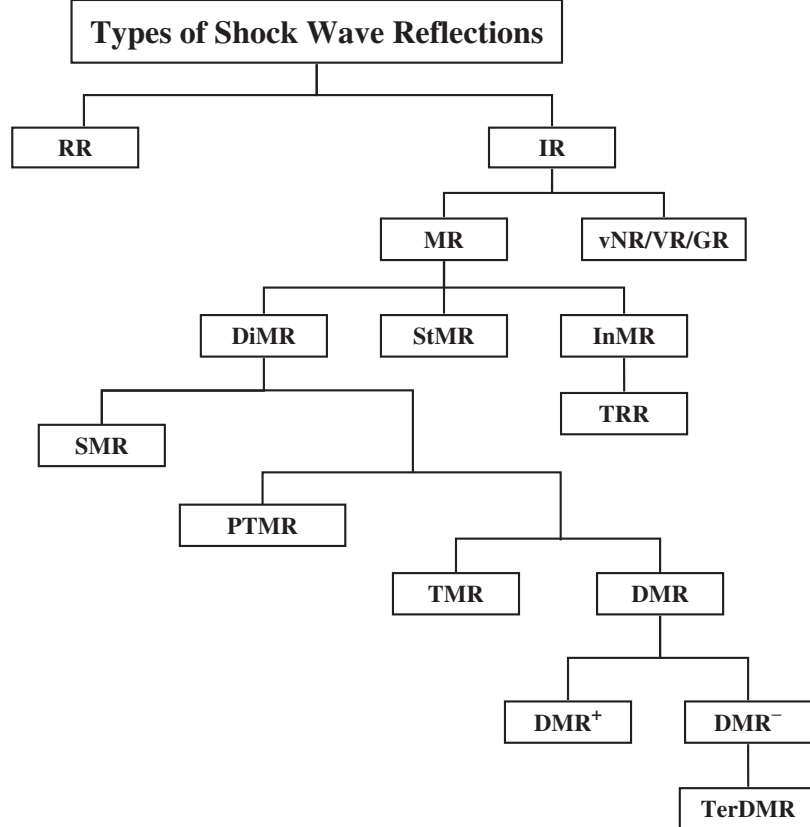


Fig. 1.5. The 13 possible shock wave reflection configurations

Because of the fact that different types of flow give rise to different types of reflections, the presentation of the shock wave reflection phenomenon will be divided, in this book, into three parts:

- Reflection in steady flows in Chap. 2
- Reflection in pseudosteady flows in Chap. 3
- Reflection in unsteady flows in Chap. 4.

1.2 Reasons for the Reflection

Now that the shock wave reflection phenomenon has been introduced briefly, it is appropriate to explain the physical reasons for its occurrence.

The major reason for the occurrence of the reflection phenomenon arises from a very basic gas dynamic phenomenon. Consider Fig. 1.6 where three different cases in which a flow with Mach number M_0 moves towards a wedge

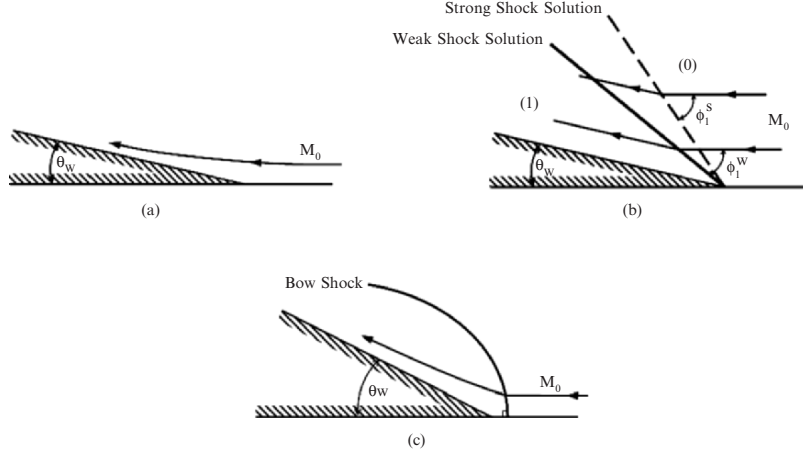


Fig. 1.6. Flow over a wedge in a steady flow: (a) $M_0 < 1$, smooth subsonic turning; (b) $M_0 > 1$ and $\theta_W < \delta_{\max}(M_0)$, straight and attached oblique shock wave; (c) $M_0 > 1$ and $\theta_W > \delta_{\max}(M_0)$, detached curved (bow) shock wave

having an angle θ_W are illustrated. In the first case, Fig. 1.6a, the flow is subsonic, $M_0 < 1$. Therefore, the flow “knows” well in advance that an obstacle is awaiting it, and hence it “adjusts” itself, well before it reaches the wedge, to negotiate the obstacle through a continuous smooth subsonic turning. However, if the flow is supersonic, $M_0 > 1$, it is “unaware” of the obstacle ahead of it, and the only way by which it can negotiate the obstacle which suddenly blocks its propagation path, is by means of a shock wave (as shown in Fig. 1.6b, c). There are two general cases for this situation: a straight and attached shock wave, which deflects the flow instantaneously to become parallel to the reflecting wedge surface, as is shown in Fig. 1.6b, and a curved and detached shock wave, which changes the supersonic flow along the surface to subsonic, as is shown in Fig. 1.6c. It is well known (Liepmann & Roshko, 1957) that for a given combination of M and θ_W there are two possible straight and attached shock waves by which the required flow deflection could be achieved, provided $\theta_W < \delta_{\max}(M_0)$, where $\delta_{\max}(M_0)$ is the maximum possible deflection of a flow having a Mach number M_0 by any oblique shock wave. The two shock waves are illustrated in Fig. 1.6b. The solid line shows the first shock, known as the weak shock since it corresponds to the so-called weak-shock solution. The angle of incidence between it and the oncoming flow is ϕ_1^W . A dashed line shows the second shock, known as the strong shock since it corresponds to the so-called strong-shock solution. The angle of incidence between it and the oncoming flow, ϕ_1^S , is always greater than ϕ_1^W . The flow behind the shock wave is supersonic if the shock wave corresponds to the weak-shock solution and it is subsonic if the shock wave corresponds to the strong-shock solution. It is an experimental fact, that unless special measures are taken, the

shock wave corresponding to the weak-shock solution is the one that usually occurs. Figure 1.6c illustrates the case when $\theta_W > \delta_{\max}(M_0)$. For this case, an attached oblique shock wave is impossible. Instead, a curved detached shock wave⁴ is obtained. Upon passing through the foot of the curved detached shock wave, the flow becomes subsonic and, as such, it negotiates the obstacle that is imposed by the wedge through a continuous smooth subsonic turning.

1.2.1 Reason for the Reflection in Steady Flows

Figure 1.7 illustrates a wedge with an angle of $\theta_W < \delta_{\max}(M_0)$ mounted in a steady supersonic flow, $M_0 > 1$. This situation is analogous to the case shown in Fig. 1.6b, and hence, upon encountering the wedge, a straight and attached oblique shock wave is generated at the leading edge of the wedge. The flow passing through this shock wave is deflected by an angle of $\theta_1 = \theta_W$ to become parallel to the reflecting wedge surface. Since, as mentioned earlier, this oblique shock wave arises from the weak-shock solution, the flow behind it, in state (1), is supersonic, $M_1 > 1$. Thus, one obtains in state (1) a situation in which a supersonic flow is directed obliquely towards the bottom wall. This situation is again analogous to either one of the two cases shown in Fig. 1.6b, c, i.e., a supersonic flow having a Mach number M_1 that must negotiate an “imaginary wedge” with an angle θ_W (see Fig. 1.7). If $\theta_W < \delta_{\max}(M_1)$, where $\delta_{\max}(M_1)$ is the maximum possible deflection of a flow having a Mach number M_1 by any oblique shock wave, the flow negotiates the bottom wall and becomes parallel to it by means of an “attached” shock wave. This shock wave, which should emanate from the reflection point, point R, results in an RR wave configuration. However, if $\theta_W > \delta_{\max}(M_1)$, the flow negotiates

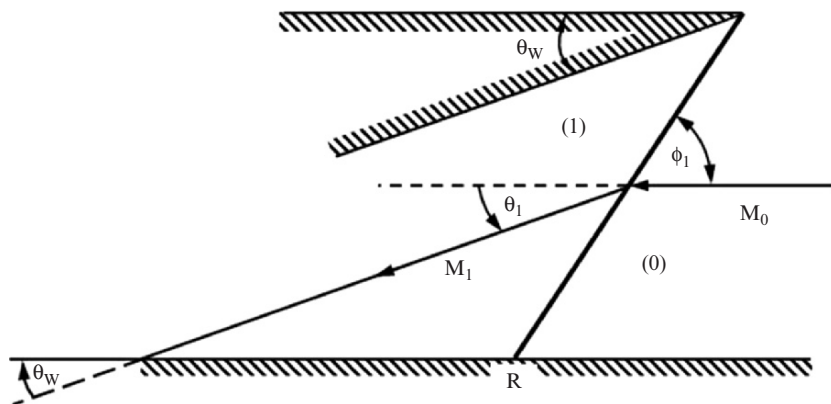


Fig. 1.7. Schematic illustration of the reason for the reflection of shock waves in steady flows

⁴ Also known as bow shock wave.

the bottom wall by a “detached” shock wave which, in turn, results in an MR wave configuration.

1.2.2 Reasons for the Reflection in Pseudosteady and Unsteady Flows

Consider a planar incident shock wave, i, having a Mach number M_S , colliding with a sharp compressive wedge having an angle θ_W , as shown in Fig. 1.8a. The flow states ahead and behind it are (0) and (1), respectively. Let us consider the flow field from a frame of reference attached to the reflection point, R, where the foot of the incident shock wave touches the reflecting wedge surface. In this coordinate system the flow in state (0) moves parallel to the reflecting wedge surface and approaches the incident shock wave with a supersonic velocity $u_0 = V_s / \sin \phi_1$, or a flow Mach number $M_0 = M_S / \sin \phi_1$, where $\phi_1 = \frac{\pi}{2} - \theta_W$ is the angle of incidence. While passing through the incident shock wave the flow is deflected towards the reflecting wedge surface by an angle of θ_1 from its original direction and its dynamic and thermodynamic properties are changed. The deflection results in a situation in which the flow in state (1) approaches the reflecting wedge surface obliquely at an angle θ_1 . Unlike the previous case of a steady flow, where ϕ_1 is always appropriate to the weak-shock solution, and hence the flow in state (1) is always supersonic, $M_1 > 1$, here the value of ϕ_1 is controlled by θ_W since $\phi_1 = \frac{\pi}{2} - \theta_W$. Thus, if θ_W is small enough, ϕ_1 can be large enough to fall into the strong-shock solution domain. Hence, the flow Mach number in state (1) in a frame of reference attached to the reflection point R, i.e., M_1^R , can be either supersonic or subsonic, depending upon the value of θ_W .

Let us first consider the situation when $M_1^R > 1$ that is analogous to either one of the two steady cases shown in Fig. 1.6b or c. If $\theta_1 < \delta_{\max}(M_1^R)$, then

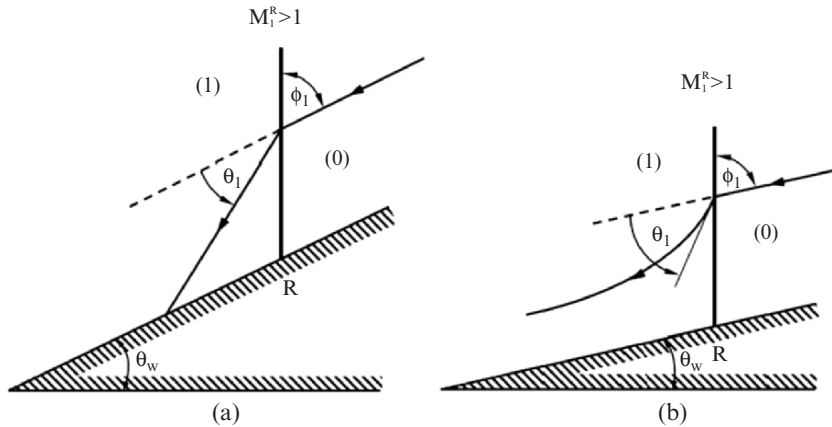


Fig. 1.8. Schematic illustrations of the reason for shock wave reflection in pseudosteady flows: (a) $M_1^R > 1$; (b) $M_1^R < 1$

an attached oblique shock wave emanating from the reflection point R will deflect the flow away from the reflecting wedge surface, while forming an RR wave configuration, and if $\theta_1 > \delta_{\max}(M_1^R)$, the flow deflection will be achieved by a detached shock wave, which will evolve into an MR wave configuration.

If, however, $M_1^R < 1$, the analogy to Fig. 1.6a suggests that the subsonic flow should negotiate the wedge surface continuously and smoothly, as shown schematically in Fig. 1.8b, without any need for a shock wave. In reality, however, this is not the case. For all the combinations of M_0 and θ_W for which $M_1^R < 1$ an MR or a WMR (i.e., vNR, VR, or GR) wave configuration is obtained. The exact reason for this lies probably in the following explanation.

Consider Fig. 1.8b, where the subsonic flow obtained behind the incident shock wave is seen to negotiate the wedge by a continuous turn. Although it was noted earlier that this situation is analogous to the one shown in Fig. 1.6a, there is one important difference. While in Fig. 1.6a the flow “knows” about the obstacle awaiting it when it is far away from the wedge, and hence it starts adjusting its streamline to negotiate the obstacle long before actually encountering it, in the situation shown in Fig. 1.8b the flow streamline adjacent to the reflecting wedge surface does not “know” about the obstacle until it passes through the foot of the incident shock, i.e. Hence, upon passing through the foot of the incident shock wave it “finds” itself in a situation in which it must negotiate a new boundary condition that is suddenly imposed on it. This sudden change in the boundary condition is, most probably, the reason for generating an additional shock wave, which in turn results in a reflection for a situation where the flow Mach number behind the incident shock wave is subsonic with respect to the reflection point R.

1.3 Analytical Approaches for Describing Regular and Mach Reflections

The analytical approaches for describing the RR and the MR wave configurations were initiated both by von Neumann (1943a and 1943b). The one describing the RR is known as the *two-shock theory* – 2ST while the one describing the MR is known as the *three-shock theory* – 3ST. Both theories make use of the inviscid conservation equations across an oblique shock wave, together with appropriate boundary conditions.

Consider Fig. 1.9 where an oblique shock wave and the associated flow fields are illustrated. The flow states ahead and behind the oblique shock wave are (i) and (j), respectively. The angle of incidence between the oncoming flow and the oblique shock wave is ϕ_j . While passing through the oblique shock wave, from state (i) to state (j), the flow is deflected by an angle θ_j . The conservation equations across an oblique shock wave, relating states (i) and (j) for a steady inviscid flow are:

- The conservation of mass:

$$\rho_i u_i \sin \phi_j = \rho_j u_j \sin (\phi_j - \theta_j) \quad (1.1)$$

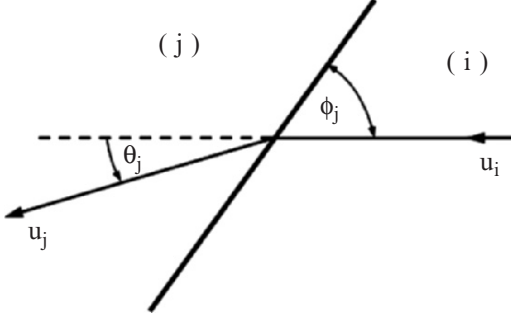


Fig. 1.9. Definition of parameters across an oblique shock wave

– The conservation of normal momentum:

$$p_i + \rho_i u_i^2 \sin^2 \phi_j = p_j + \rho_j u_j^2 \sin^2 (\phi_j - \theta_j). \quad (1.2)$$

– The conservation of tangential momentum

$$\rho_i \tan \phi_j = \rho_j \tan (\phi_j - \theta_j). \quad (1.3)$$

– The conservation of energy

$$h_i + \frac{1}{2} u_i^2 \sin^2 \phi_j = h_j + \frac{1}{2} u_j^2 \sin^2 (\phi_j - \theta_j) \quad (1.4)$$

Here u is the flow velocity in a frame of reference attached to the oblique shock wave, and ρ , p , and h are the flow density, flow static pressure and flow enthalpy, respectively.

If thermodynamic equilibrium is assumed to exist on both sides of the oblique shock wave, then two thermodynamic properties are sufficient to fully define a thermodynamic state, e.g., $\rho = \rho(p, T)$ and $h = h(p, T)$, where T is the flow temperature. Consequently, under this assumption the above set of four conservation equations contains eight parameters, namely, p_i , p_j , T_i , T_j , u_i , u_j , ϕ_j and θ_j . Thus, if four of these parameters are known, the above set of the conservation equations is solvable in principle.

1.3.1 Two-Shock Theory (2ST) for an Inviscid Flow

The two-shock theory (2ST) is the analytical model for describing the flow field near the reflection point, R, of an RR. The wave configuration of an RR and some associated parameters are shown schematically in Fig. 1.10. The RR consists of two discontinuities: the incident shock wave, i, and the reflected shock wave, r. These two shock waves intersect at the reflection point, R, which is located on the reflecting surface. Since the reflection of shock waves is not a linear phenomenon, the RR wave configuration is not linear either, i.e., $\omega_i \neq \omega_r$.

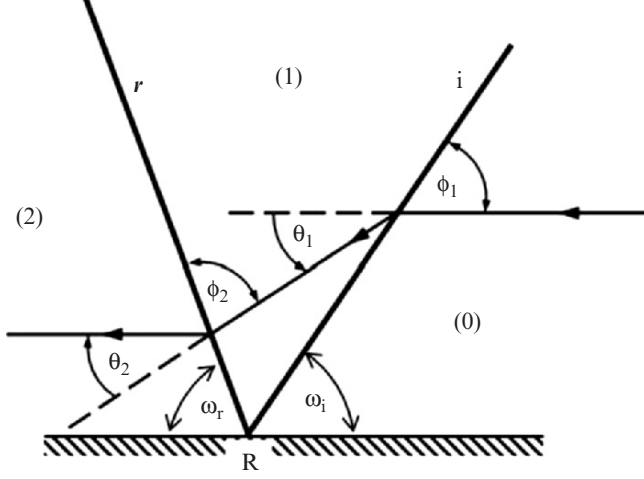


Fig. 1.10. Schematic illustration of the wave configuration of a regular reflection – RR

Applying the oblique shock wave equations, given in Sect. 1.3, on the two oblique shock waves, i and r, that are associated with the wave configuration of an RR, results in the following set of governing equations for an RR in an inviscid flow.

Across the incident shock wave, i:

$$\rho_0 u_0 \sin \phi_1 = \rho_1 u_1 \sin (\phi_1 - \theta_1) \quad (1.5)$$

$$p_0 + \rho_0 u_0^2 \sin^2 \phi_1 = p_1 + \rho_1 u_1^2 \sin^2 (\phi_1 - \theta_1) \quad (1.6)$$

$$\rho_0 \tan \phi_1 = \rho_1 \tan (\phi_1 - \theta_1) \quad (1.7)$$

$$h_0 + \frac{1}{2} u_0^2 \sin^2 \phi_1 = h_1 + \frac{1}{2} u_1^2 \sin^2 (\phi_1 - \theta_1) \quad (1.8)$$

Across the reflected shock wave, r:

$$\rho_1 u_1 \sin \phi_2 = \rho_2 u_2 \sin (\phi_2 - \theta_2) \quad (1.9)$$

$$p_1 + \rho_1 u_1^2 \sin^2 \phi_2 = p_2 + \rho_2 u_2^2 \sin^2 (\phi_2 - \theta_2) \quad (1.10)$$

$$\rho_1 \tan \phi_2 = \rho_2 \tan (\phi_2 - \theta_2) \quad (1.11)$$

$$h_1 + \frac{1}{2} u_1^2 \sin^2 \phi_2 = h_2 + \frac{1}{2} u_2^2 \sin^2 (\phi_2 - \theta_2) \quad (1.12)$$

In addition to these eight conservation equations, there is also the condition that the flow behind the reflected shock wave, in state (2), must be parallel to the reflecting wedge surface. Hence, under the assumption of an inviscid flow:

$$\theta_1 - \theta_2 = 0. \quad (1.13)$$

In summary, the two-shock theory (2ST), which describes the flow field of an RR near the reflection point, R, consists of a set of nine governing equations.

If thermodynamic equilibrium is assumed in states (0), (1), and (2) then both the density, ρ , and the enthalpy, h , could be expressed in terms of the pressure, p , and the temperature, T , [i.e., $\rho = \rho(p, T)$ and $h = h(p, T)$] and the above set of nine governing equations consists of only 13 parameters, namely: $p_0, p_1, p_2, T_0, T_1, T_2, u_0, u_1, u_2, \phi_1, \phi_2, \theta_1$ and θ_2 . Consequently, four of these 13 parameters must be known in order to have a closed set, which, in principle, could be solved.

Henderson (1982) showed, that if the gas is assumed to obey the equation of state of a perfect gas, $p = \rho RT$, and to be thermally perfect, $h = C_P T$, then (1.5)–(1.13) could be combined to a single polynomial of the order six. Although a polynomial of order six yields six roots, Henderson (1982) showed that using simple physical considerations four of the six roots could be discarded. This finding implies that equations (1.5) to (1.13) do not result in a unique solution for a given set of initial conditions. This will be further illustrated and discussed in Sect. 1.4.1.

1.3.2 Three-Shock Theory (3ST) for an Inviscid Flow

The three-shock theory is the analytical model for describing the flow field near the triple point of an MR. The wave configuration and some associated parameters of an MR are shown schematically in Fig. 1.11. The MR consists of four discontinuities: three shock waves (the incident shock wave, i , the reflected shock wave, r , and the Mach stem, m) and one slipstream, s . These four discontinuities meet at a single point, known as the triple point, T , which is located above the reflecting surface. The Mach stem is usually curved along its entire length although its curvature could be very small. Depending upon the initial conditions it can be either concave or convex. At its foot, i.e., at the reflection point, R , it is perpendicular to the reflecting surface.

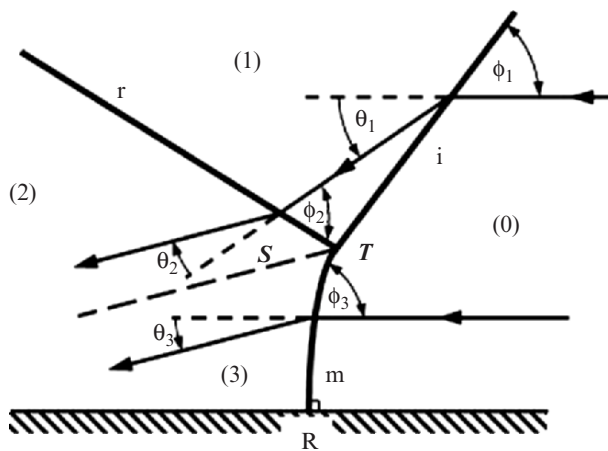


Fig. 1.11. Schematic illustration of the wave configuration of a Mach reflection – MR

Applying the oblique shock wave equations, given in Sect. 1.3, on the three oblique shock waves, i, r and m, that are associated with the wave configuration of an MR, results in the following set of governing equations for an MR in an inviscid flow.

Across the incident shock wave, i:

$$\rho_0 u_0 \sin \phi_1 = \rho_1 u_1 \sin (\phi_1 - \theta_1) \quad (1.14)$$

$$p_0 + \rho_0 u_0^2 \sin^2 \phi_1 = p_1 + \rho_1 u_1^2 \sin^2 (\phi_1 - \theta_1) \quad (1.15)$$

$$\rho_0 \tan \phi_1 = \rho_1 \tan (\phi_1 - \theta_1) \quad (1.16)$$

$$h_0 + \frac{1}{2} u_0^2 \sin^2 \phi_1 = h_1 + \frac{1}{2} u_1^2 \sin^2 (\phi_1 - \theta_1) \quad (1.17)$$

Across the reflected shock wave, r:

$$\rho_1 u_1 \sin \phi_2 = \rho_2 u_2 \sin (\phi_2 - \theta_2) \quad (1.18)$$

$$p_1 + \rho_1 u_1^2 \sin^2 \phi_2 = p_2 + \rho_2 u_2^2 \sin^2 (\phi_2 - \theta_2) \quad (1.19)$$

$$\rho_1 \tan \phi_2 = \rho_2 \tan (\phi_2 - \theta_2) \quad (1.20)$$

$$h_1 + \frac{1}{2} u_1^2 \sin^2 \phi_2 = h_2 + \frac{1}{2} u_2^2 \sin^2 (\phi_2 - \theta_2) \quad (1.21)$$

Across the Mach stem, m:

$$\rho_0 u_0 \sin \phi_3 = \rho_3 u_3 \sin (\phi_3 - \theta_3) \quad (1.22)$$

$$p_0 + \rho_0 u_0^2 \sin^2 \phi_3 = p_3 + \rho_3 u_3^2 \sin^2 (\phi_3 - \theta_3) \quad (1.23)$$

$$\rho_0 \tan \phi_3 = \rho_3 \tan (\phi_3 - \theta_3) \quad (1.24)$$

$$h_0 + \frac{1}{2} u_0^2 \sin^2 \phi_3 = h_3 + \frac{1}{2} u_3^2 \sin^2 (\phi_3 - \theta_3). \quad (1.25)$$

In addition to these 12 conservation equations, there are also two boundary conditions, which arise from the fact that the flow states (2) and (3) are separated by a contact surface across which the pressure remains constant, i.e.,

$$p_2 = p_3 \quad (1.26)$$

Furthermore, under the assumptions of an inviscid flow and an infinitely thin contact surface the streamlines on both sides of the contact surface are parallel. This implies that:

$$\theta_1 \mp \theta_2 = \theta_3 \quad (1.27)$$

Equation (1.27) gives rise to two possible three-shock theories:

$$\theta_1 - \theta_2 = \theta_3 \quad (1.28a)$$

A three-shock theory fulfilling the requirement given by (1.28a) will be referred to in the followings as the “standard” three-shock theory, as opposed to a “nonstandard” three-shock theory, which fulfills the condition:

$$\theta_1 + \theta_2 = \theta_3. \quad (1.28b)$$

As will be shown subsequently, the solution of the standard three-shock theory yields an MR, while the solution of the nonstandard three-shock theory yields a vNR.

Thus, the three-shock theory (either the standard or the nonstandard), which describes the flow field near the triple point, T, consists of 14 governing equations. Again, if thermodynamic equilibrium is assumed in states (0), (1), (2) and (3) then the set of 14 governing equations contains 18 parameters, namely: $p_0, p_1, p_2, p_3, T_0, T_1, T_2, T_3, u_0, u_1, u_2, u_3, \phi_1, \phi_2, \phi_3, \theta_1, \theta_2$ and θ_3 . Consequently, four of these 18 parameters must be known in order to have a closed set of equations, which, in principle, could be solved.

Henderson (1982) showed that if the gas is assumed to obey the equation of state of a perfect gas, $p = \rho RT$, and to be thermally perfect, $h = C_P T$, then (1.14) to (1.27) could be reduced to a single polynomial of order ten, with the pressure ratio p_3/p_0 as the polynomial variable. The polynomial coefficients were taken to be a function of the specific heat capacities ratio, $\gamma = C_P/C_V$, the flow Mach number in state (0), M_0 , and the incident shock wave strength in terms of the pressure ratio across it, p_1/p_0 . Although a polynomial of degree ten yields ten roots, Henderson (1982) showed that seven out of the ten roots could be discarded by using simple physical considerations and the possibility of double roots. This implies that (1.14)–(1.27) do not yield a unique solution for a given set of initial conditions. This is further illustrated and discussed in Sect. 1.4.2.

1.4 Shock Polars

Kawamura & Saito (1956) were the first to suggest that owing to the fact that the boundary conditions of an RR (1.13) and an MR (1.26 and 1.27) are expressed in terms of the flow deflection angles, θ and the flow static pressures, p , the use of (p, θ) -polars could be of great advantage in better understanding the shock wave reflection phenomenon.

The graphical presentation of the relationship between the pressure, p_j , obtained behind an oblique shock wave (see Fig. 1.9) and the angle, θ_j , by which the flow is deflected while passing through an oblique shock wave, for a fixed flow Mach number, M_i , and different angles of incidence, ϕ_j , is known as the a pressure-deflection shock polar. A typical pressure-deflection shock polar is shown in Fig. 1.12. Four special points are indicated on the shown shock polar:

- Point “a” illustrates a situation in which the flow state behind the oblique shock wave is identical to the flow state ahead of it. This situation is obtained when the angle of incidence between the oblique shock wave and the oncoming flow, ϕ_j , is equal to the Mach angle $\mu_i = \sin^{-1}(1/M_i)$. In this case the pressure does not change across the oblique shock wave, $p_j/p_i = 1$, and the flow deflection is zero, $\theta_j = 0$.

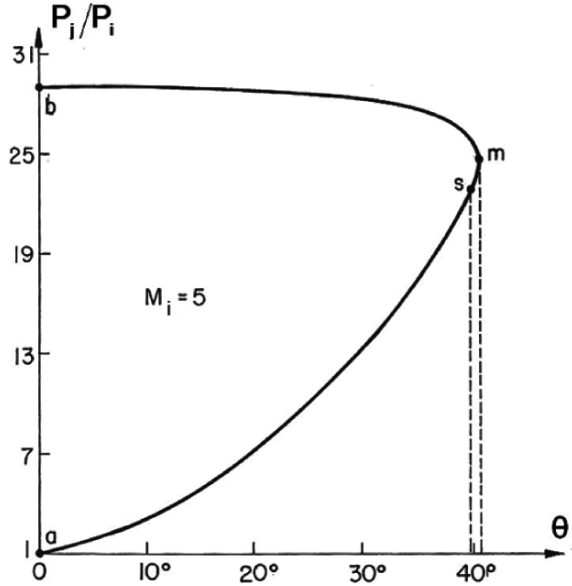


Fig. 1.12. A typical, accurately drawn to scale, $(p_j/p_i, \theta_j)$ -polar for $M_i = 5$ and $\gamma = 1.4$

- Point, “b” indicates the flow state, which is obtained from state (i) by passing through the strongest possible oblique shock wave, namely; a normal shock wave for which $\phi_j = 90^\circ$. In this case, the pressure jump across the normal shock wave, p_j/p_i , is maximal and the flow deflection is again zero, $\theta_j = 0$.
- Point “s” divides the shock polar into two portions. Along the portion between points “a” and “s” the flow Mach number that is obtained behind the oblique shock wave is supersonic, i.e., $M_j > 1$, and along the portion between points “s” and “b” the flow Mach number that is obtained behind the oblique shock wave is subsonic, $M_j < 1$. Thus, point “s” indicates the situation when the flow that is obtained behind the oblique shock wave is exactly sonic, $M_j = 1$. The “a–s” and “s–b” portions of the shock polar are known as the weak and strong portions of the shock polar, respectively. In fact, the earlier-mentioned weak- and strong-shock solutions (see Sect. 1.2) refer to solutions on these two portions.
- Point “m,” which is sometimes denoted as “d” is known as the point of maximum deflection or the detachment point. It indicates the maximum deflection by which a given supersonic flow can be deflected by an oblique shock wave. As can be seen from Fig. 1.12 the difference between θ_s and θ_m is very small. It is equal to zero for $M_i = 1$ and it approaches zero as $M_i \rightarrow \infty$. Depending on the specific heat capacities ratio, γ , it assumes maximal values of a few degrees at moderate values of M_i . For this reason

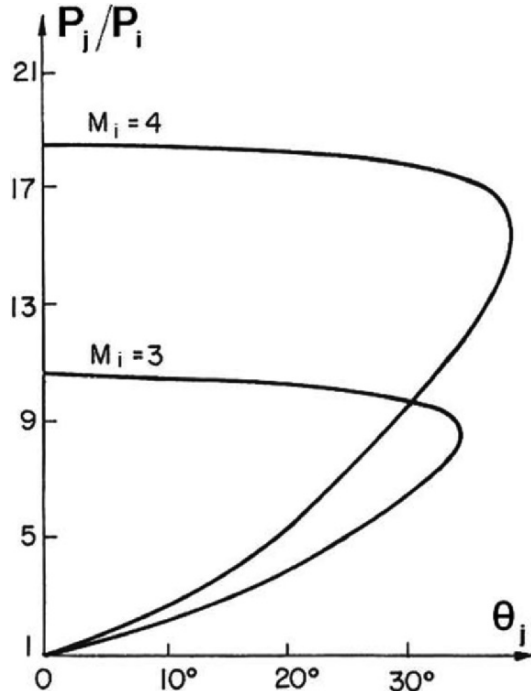


Fig. 1.13. The dependence of the $(p_j/p_i, \theta_j)$ -polar on the incident flow Mach number, M_i , for $\gamma = 1.4$

it is a common practice to treat points “s” and “m,” especially from an engineering point of view, as practically a single point.

It is well known that the larger the flow Mach number, M_i , is the larger is the corresponding shock polar. This is illustrated in Fig. 1.13 where the shock polars for a perfect diatomic gas ($\gamma = 1.4$) and for $M_i = 3$ and $M_i = 4$ are accurately drawn to scale.

Real gas effects also change the size of the $(p_j/p_i, \theta_j)$ -polar as can be seen in Fig. 1.14. Both the maximum deflection angle and the pressure jump across the oblique shock wave increase because of the relaxation of the internal degrees of freedom of the gas. For the particular case that is shown in Fig. 1.14 for $M_i = 10$, $p_i = 15$ Torr and $T_i = 300$ K, $\theta_{j_m} = 42.7^\circ$ for a perfect nitrogen and $\theta_{j_m} = 49^\circ$ for a nitrogen in dissociational equilibrium.

As mentioned in Sects. 1.3.1 and 1.3.2, in many phenomena involving shock wave interactions there is a possibility of more than one theoretical solution. In such cases shock polars can be useful in discarding unrealistic solutions and indicating the actual solution or solutions.

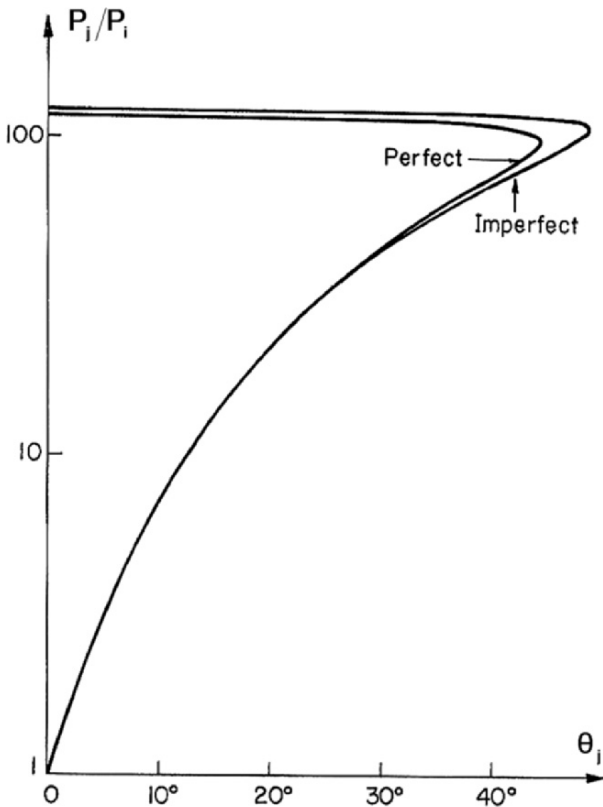


Fig. 1.14. The dependence of the $(p_j/p_i, \theta_j)$ -polar on real gas effects for nitrogen at $M_i = 10, p_i = 15$ Torr and $T_i = 300$ K

1.4.1 Shock-Polar Presentation of the Flow Field Near the Reflection Point of a Regular Reflection

Figure 1.15 presents the $(p_i/p_0, \theta_i^R)$ -polar solution of the flow field near the reflection point, R, of an RR. The flow deflection angles, θ_i^R , are measured with respect to the direction of the oncoming flow when the frame of reference is attached to the reflection point, R. State (0) at which $p_i = p_0$, i.e., $p_i/p_0 = 1$, and $\theta_i^R = \theta_0^R = 0$, is at the origin. The locus of all the flow states that could be obtained from state (0) by passing through any oblique shock wave is represented by the I-polar. Consequently, state (1), which is obtained from state (0) by passing through the incident shock wave, i, is on the I-polar at the point p_1/p_0 and θ_1^R . The locus of all the flow states that could be obtained from state (1) by passing through any oblique shock wave is represented by the R-polar. Note that since reflected shock wave deflects the flow in a direction opposite to that of the incident shock wave, the R-polar is drawn in an orientation that is opposite to that of the I-polar. Consequently, state

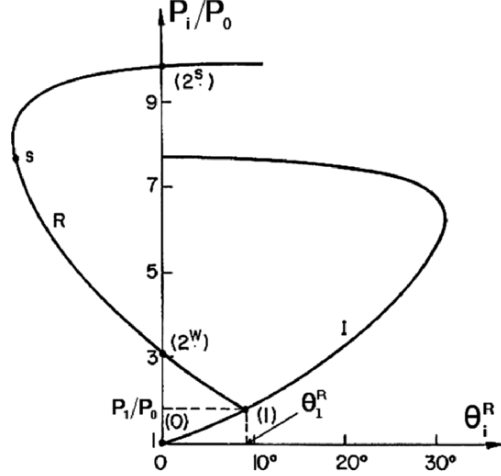


Fig. 1.15. $(p_i/p_0, \theta_i^R)$ -polar solution of a regular reflection

(2), which is obtained from state (1) by passing through the reflected shock wave, is on the R-polar. The boundary condition for an RR (1.13) implies that $\theta_2^R = 0$, therefore, state (2) is obtained at the point where the R-polar intersects the p-axis, i.e., the line along which $\theta^R = 0$.

Figure 1.15 implies that two different points, (2^w) and (2^s) , fulfill the just-mentioned requirement. Each one of these two points indicates a possible solution of the governing equations of an RR [(1.5)–(1.13)]. Point (2^w) is known as the “weak-shock solution” and point (2^s) is known as the “strong-shock solution.” Note that none of these two solutions could be discarded on theoretical grounds. However, it is an experimental fact that, unless special measures are taken, the weak-shock solution is the one that usually occurs. Consequently, the flow state behind the reflected shock wave is represented by point (2^w) of Fig. 1.15. In the following this state will be labeled as (2) only. Note that the just-described situation in which the graphical solution of the governing equations of an RR, using $(p_i/p_0, \theta_i^R)$ -polar, implies that there are two possible solutions of an RR for a given set of initial conditions was already mentioned in Sect. 1.3.1.

1.4.2 Shock-Polar Presentation of the Flow Field Near the Triple Point of a Mach Reflection

Figure 1.16 presents the $(p_i/p_0, \theta_i^T)$ -polar solution of the flow field in the vicinity of the triple point, T, of an MR. The flow deflection angles, θ_i^T , are measured with respect to the direction of the oncoming flow when the frame of reference is attached to the triple point, T. State (0) at which $p_i = p_0$, i.e., $p_i/p_0 = 1$, and $\theta_i^T = \theta_0^T = 0$, is at the origin. The locus of all the flow states that could be obtained from state (0) by passing through any oblique

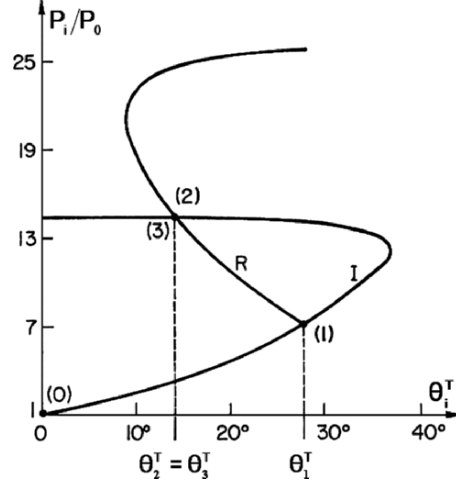


Fig. 1.16. $(p_i/p_0, \theta_i^T)$ -polar solution of a Mach reflection

shock wave is represented by the I-polar. Consequently, state (1), which is obtained from state (0) by passing through the incident shock wave is on the I-polar at the point p_1/p_0 and θ_1^T . The locus of all the flow states that could be obtained from state (1) by passing through any oblique shock wave is represented by the R-polar. Hence, state (1) is the origin of the R-polar, which for the above explained reason that was given in Sect. 1.4.1, is drawn in a direction opposite to the I-polar. State (2), behind the reflected shock wave, lies on the R-polar, and state (3), behind the Mach stem, lies on the I-polar since it is also obtained from state (0) by passing through the Mach stem. Since the pressures in states (2) and (3) are equal, i.e., $p_2 = p_3$ (1.26), and since the flows in states (2) and (3) are parallel, i.e., $\theta_2^T = \theta_3^T$ (1.27 in a frame of reference moving along the triple point trajectory), states (2) and (3) are obtained at the point where the I- and R-polars intersect. Note that since $\theta_1^T > \theta_3^T$ the shock polar solution shown in Fig. 1.16 represents a typical “standard” solution of the three-shock theory, i.e., an MR.

Figure 1.17 presents three cases of different possible solutions of the flow field in the vicinity of the triple point of an MR. Unlike Fig. 1.16, where only the right branch of the I-polar is drawn, here the left branch is also shown. Points “a”, “b” and “c” indicate three different possible MR-solutions (i.e., intersections of the I- and R-polars). In the MR-solution at point “a” the net deflection of the flows in states (2) and (3) is positive, (i.e., $\theta_2^T = \theta_3^T = +7^\circ > 0$) with respect to their original direction in state (0). In the MR-solution at point “b” the net deflection of the flows in states (2) and (3) is zero (i.e., $\theta_2^T = \theta_3^T = 0$), and in the MR-solution at point “c” the net deflection of the flows in states (2) and (3) is negative (i.e., $\theta_2^T = \theta_3^T = -8^\circ < 0$). Courant & Freidrichs (1948) termed the corresponding three different types of possible MR wave

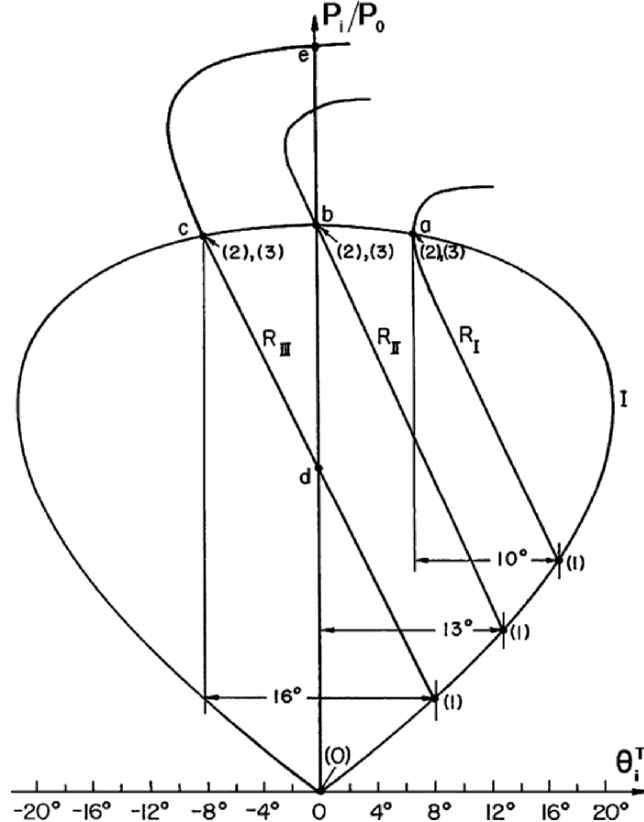


Fig. 1.17. Three different possible MR-solutions resulting in a DiMR at point “a”, an StMR at point “b” and an InMR at point “c”

configurations as: Direct-Mach reflection (DiMR) at point “a”, Stationary-Mach reflection (StMR) at point “b” and Inverse-Mach reflection (InMR) at point “c.”

Note that the (I-R_{II})-polar combination (in Fig. 1.17) indicates, in addition to the StMR at point “b”, also a possible RR-solution at this point since the R_{II}-polar intersects the p -axis at this point. Similarly, the I-R_{III} polar combination indicates, in addition to the InMR at point “c”, a possible RR-solution at point “d” where the R_{III}-polar intersects the p -axis. Thus, it is again evident that based on the graphical solution of the governing equations of an MR, using $(p_i/p_0, \theta_i^T)$ -polar, different reflection configurations can be theoretically obtained for the same initial conditions.

1.5 Suggested RR \rightleftharpoons IR Transition Criteria

The search for the RR \rightleftharpoons IR transition criterion has been the objective of numerous analytical, numerical and experimental studies since von Neumann re-initiated the investigation of the oblique shock wave reflection phenomena in the early 1940s. The reason for the continuous search for the correct RR \rightleftharpoons IR transition criterion arose from the fact that the agreement between the various proposed criteria and the experimental results was never satisfactory enough in the entire range of incident shock wave Mach numbers and reflecting wedge angles.

In the following, the various proposed RR \rightleftharpoons IR transition criteria are discussed in detail using shock polars for explanatory purposes. It should be noted here that von Neumann initiated most of these criteria already in the early 1940s.

1.5.1 Detachment Criterion

Consider Figs. 1.15 and 1.16 and note that while in the case of an RR the R-polar intersects the p -axis at two points, in the case of an MR the R-polar does not intersect the p -axis at all. The limiting case is the case in which the R-polar is tangent to the p -axis and hence intersects it at a single point. This situation is known as the detachment criterion. Two (I-R)-polars combinations illustrating this situation are shown in Fig. 1.18a, b. A slight shift of the R-polar to the right will result in a situation in which the R-polar will not intersect the p -axis at all, and an RR-solution will be impossible.

Since at the detachment criterion, the flow deflection by the reflected shock wave is maximal, i.e., $\theta_2 = \theta_{2m}$, the transition line arising from the detachment criterion can be calculated using the two-shock theory [(1.5)–(1.13)] while replacing θ_2 by θ_{2m} .

Depending on the initial conditions, the point of tangency between the R-polar and the p -axis could be either outside or inside the I-polar as shown in Fig. 1.18a, b, respectively. The limiting situation between these two cases is shown in Fig. 1.18c where the R-polar is tangent to the p -axis exactly at the normal shock wave point of the I-polar.

Following Henderson (1982) incident shock waves, which result in, at detachment, a situation in which the point of tangency of the R-polar to the p -axis is outside the I-polar (such as shown in Fig. 1.18a) are termed “strong” shock waves, while those resulting in a situation in which the point of tangency of the R-polar to the p -axis is inside the I-polar (such as shown in Fig. 1.18b) are termed “weak” shock waves.⁵

Three interesting (I-R)-polars combinations, corresponding to detachment, are possible in the just-presented “weak” shock wave domain. They

⁵ Note that this definition has nothing to do with the earlier mentioned division of the shock polar to strong- and weak-shock solutions.

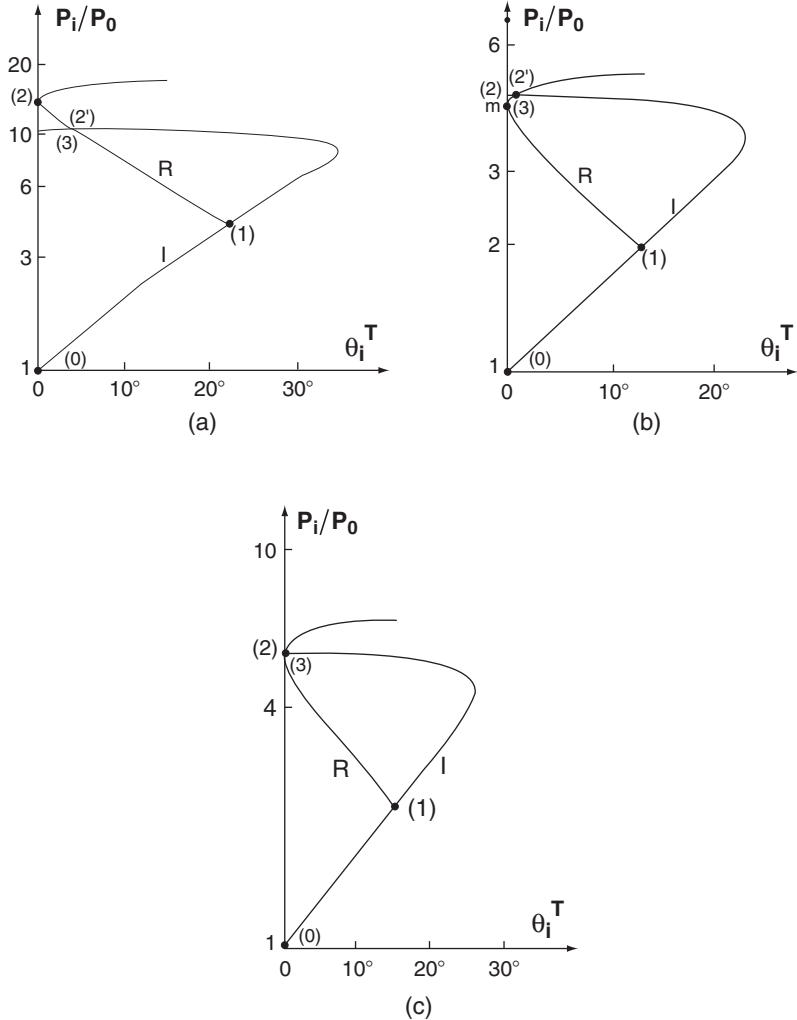


Fig. 1.18. Three different (I–R)-polars combinations at detachment for nitrogen in dissociational equilibrium with $p_0 = 15$ Torr and $T_0 = 300$ K: (a) the R-polar is tangent to the p -axis outside the I-polar ($M_0 = 3, \theta_W = 50.01^\circ$ and $M_S = 1.93$); (b) the R-polar is tangent to the p -axis inside the I-polar ($M_0 = 2, \theta_W = 47.32^\circ$ and $M_S = 1.36$); (c) the R-polar is tangent to the p -axis at the normal shock point of the I-polar ($M_0 = 2.185, \theta_W = 48.46^\circ$ and $M_S = 1.449$)

are shown in Fig. 1.19a–c. Figure 1.19a presents an (I–R)-polars combination for which the net deflection of the flows in state (2), with respect to the triple point, is smaller than that in state (1). Hence the flow originating from state (0) at a point above the triple point trajectory is first deflected towards the wedge surface by the incident shock wave, and then it is deflected away from the wedge surface by the reflected shock wave to result in a situation

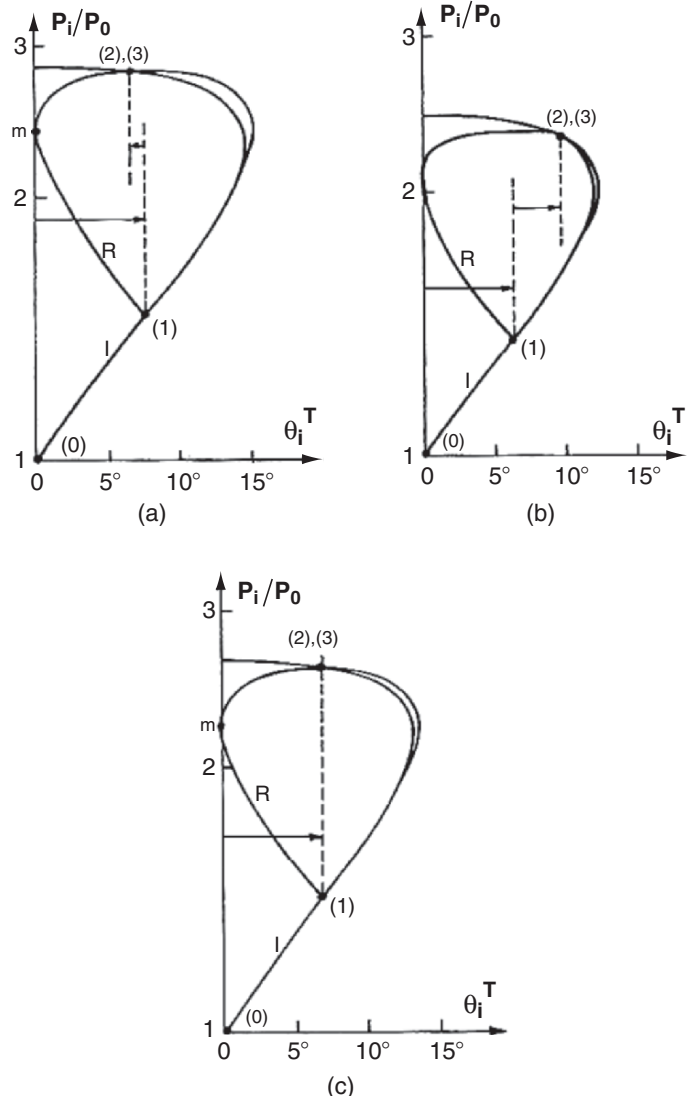


Fig. 1.19. (I-R)-polars presentation of possible solution of the three-shock theory for perfect nitrogen ($\gamma = 1.4$): (a) $\theta_2^T = \theta_3^T < \theta_1^T$ ($M_0 = 1.6, \phi_1 = 47.88^\circ$); (b) $\theta_2^T = \theta_3^T > \theta_1^T$ ($M_0 = 1.5, \phi_1 = 49.67^\circ$); and (c) $\theta_2^T = \theta_3^T = \theta_1^T$ ($M_0 = 1.55, \phi_1 = 41.50^\circ$)

in which $\theta_2^T = \theta_3^T < \theta_1^T$. This situation, which implies that $\theta_1 - \theta_2 = \theta_3$ (1.28a), i.e., a “standard” solution of the three-shock theory (see Sect. 1.3.2), results in an MR. The (I-R)-polar combination shown in Fig. 1.19b illustrates a different solution. It is seen that the flow that is deflected towards the wedge surface while passing through the incident shock wave is not deflected

away from the wedge when it passes through the reflected shock wave but it is further deflected towards the wedge to result in a situation in which $\theta_2^T = \theta_3^T > \theta_1^T$. This situation, which implies that $\theta_1 + \theta_2 = \theta_3$ (1.28b), i.e., a “nonstandard” solution of the three-shock theory (see Sect. 1.3.2), results in a vNR. The limiting (I–R)-polars combination between these two solutions is shown in Fig. 1.19c that indicates that the flow passing through the reflected shock wave is not deflected at all, i.e., $\theta_2 = 0$ and hence $\theta_2^T = \theta_3^T = \theta_1^T$. The boundary condition of the three-shock theory for this case is simply $\theta_1 = \theta_3$.

Schematic drawings of the three possible shock wave configurations that correspond to the three (I–R)-polars combinations that are shown in Fig. 1.19a–c is given in Fig. 1.20a–c, respectively. It should be noted here that

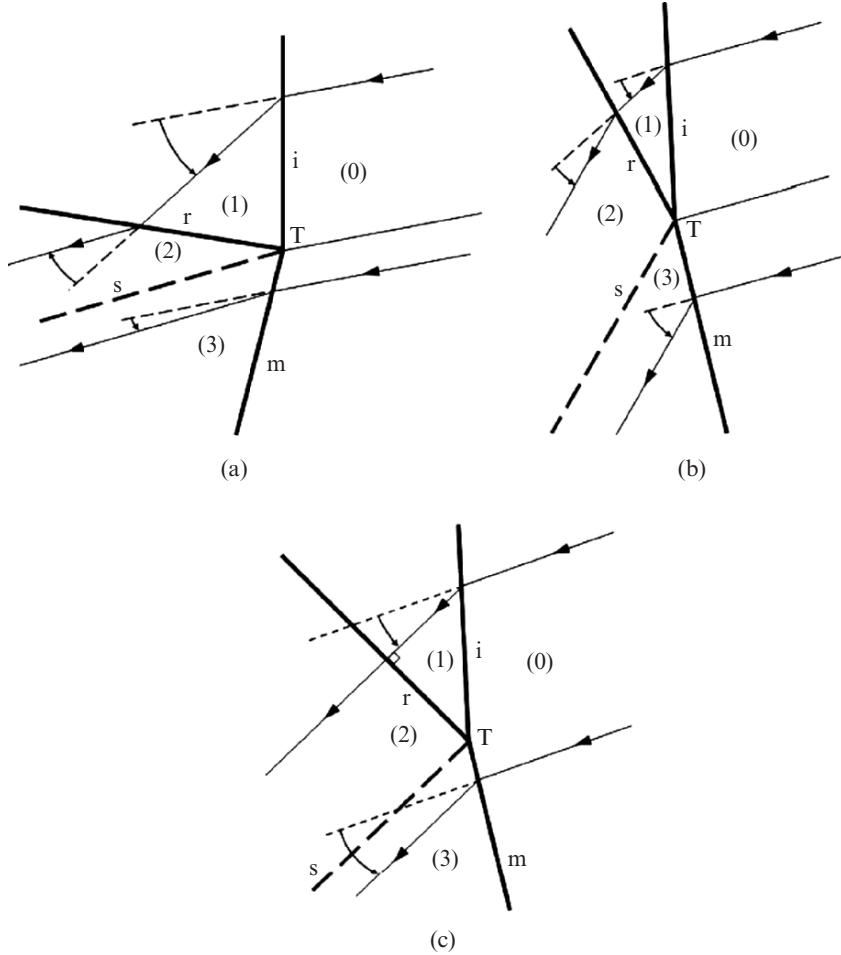


Fig. 1.20. The wave configurations of the three possible solutions of the three-shock theory whose graphical solutions are shown in Fig. 1.19a–c, respectively

the situation shown in Figs. 1.19c, 1.20c implies that the reflected shock wave is normal to the flow in state (1) ahead of it. As will be shown subsequently (see Sect. 3.2.3) this situation represents the MR \rightleftarrows vNR transition criterion. In summary, (I–R)-polars combination that result in situations in which $\theta_2^T = \theta_3^T < \theta_1^T$ correspond to MRs, while (I–R)-polars combination that result in situations in which $\theta_2^T = \theta_3^T > \theta_1^T$ correspond to vNRs. In addition, there are situations for which the R-polar is completely embedded inside the I-polar and does not intersect it at all. In these cases the condition required by (1.27) cannot be satisfied and neither a standard nor a nonstandard three-shock solution exists. As will be shown subsequently this is the case for which the resulted reflection is the earlier mentioned Guderley reflection, GR.

It should be pointed out here that if one wishes to use the three-shock theory in order to calculate the flow properties in the vicinity of the triple point of the three different wave configurations that are shown in Fig. 1.20a–c, then the following boundary conditions for the flow deflection angles should be used. Equation (1.28a) should be used for calculating the MR shown in Fig. 1.20a and (1.28b) should be used for calculating the wave configuration shown in Fig. 1.20b. For the limiting wave configuration that is shown in Fig. 1.20c, either (1.28a) or (1.28b) could be used since for this case, the reflected shock wave is normal to the oncoming flow, and hence $\theta_2 = 0$. Thus, (1.28a) and (1.28b) degenerate to

$$\theta_1 = \theta_3 \quad (1.29)$$

In addition, since two of the dependent variables of the three-shock theory, namely, the angle of incidence between the flow in state (1) and the reflected shock wave, ϕ_2 , and the flow deflection angle of the flow passing through the reflected shock wave, θ_2 , are known, i.e., $\phi_2 = 90^\circ$ and $\theta_2 = 0$, the set of the governing equations of the three-shock theory is significantly simplified for this case as it reduces from 18 to 16 unknowns.

1.5.2 Mechanical-Equilibrium Criterion

This criterion, which was also suggested originally by von Neumann (1943), was re-initiated under this name by Henderson & Lozzi (1975) for the following reason. Consider the (I–R)-polars combinations shown in Fig. 1.18a, b, both of which correspond to the detachment criterion. These (I–R)-polars combinations suggest that if the RR \rightleftharpoons IR transition occurs at detachment, then the termination of the RR and the formation of the IR must be associated with a sudden pressure change, from p_2 to $p_{2'}$ (2 is the point where the R-polar is tangent to the p -axis and $2'$ is the point where the R-polar intersects the I-polar). Henderson & Lozzi (1975) argued that such a sudden pressure change must be supported by either a compression wave (or a shock wave) or an expansion wave, depending upon whether p_2 is greater than (as shown in Fig. 1.18a) or smaller than (as shown in Fig. 1.18b) $p_{2'}$. Since neither of

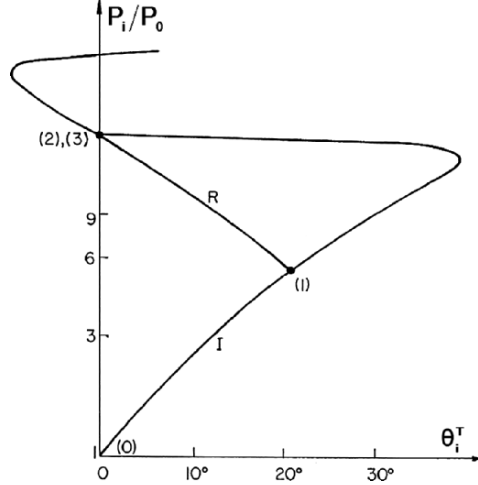


Fig. 1.21. (I–R)-polars combination illustrating the mechanical-equilibrium criterion

these additional waves has ever been observed experimentally, Henderson & Lozzi (1975) concluded that the detachment criterion is not physical. Alternatively, they suggested a transition, which corresponds to the polars combination shown in Fig. 1.21.

In this (I–R)-polars combination the R-polar intersects the p -axis exactly at the normal shock point of the I-polar. Consequently, both an RR and an MR are theoretically possible at the intersection point. Hence, if this point is indeed the $\text{RR} \rightleftharpoons \text{IR}$ transition point, then from the pressures point of view, the transition would be continuous and mechanical equilibrium would be maintained during the transition. The mechanical equilibrium transition line can be obtained by solving equations (1.14)–(1.28a) and requiring that $\theta_1 - \theta_2 = \theta_3 = 0$.

1.5.3 Sonic Criterion

This transition criterion, which was also first introduced, as a possible transition criterion, by von Neumann (1943), is based on the argument that the $\text{RR} \rightleftharpoons \text{IR}$ transition depends on whether the corner-generated signals can catch-up with the reflection point, R, of the RR. Hence, as long as the flow Mach number behind the reflected shock wave is supersonic, the reflection point is isolated from the corner-generated signals, and they cannot reach it.

Consider Fig. 1.22a, b where two different (I–R)-polars combinations are shown. While in Fig. 1.22a, the R-polar intersects the p -axis along its “weak” portion in Fig. 1.22b the R-polar intersects the p -axis along its “strong” portion. Thus, while the flow behind the reflected shock wave is supersonic for the former case, it is subsonic for the latter. The limit between these two cases is

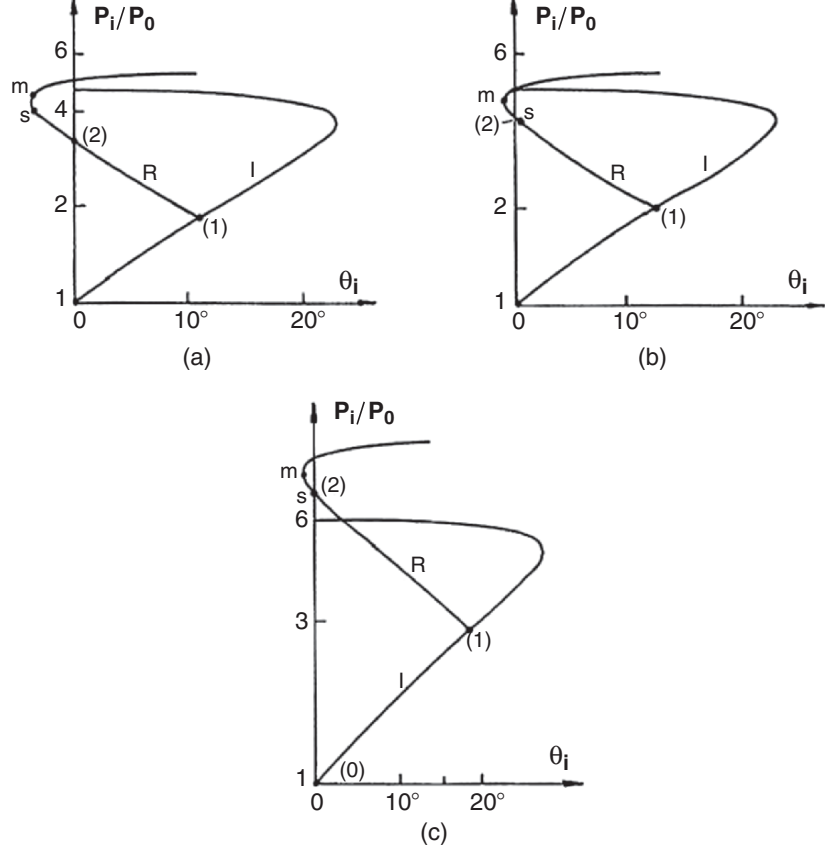


Fig. 1.22. $(p_i/p_0, \theta_i^T)$ -polar solutions of three different RRs for perfect nitrogen: (a) supersonic flow behind the reflected shock wave ($M_0 = 2$, $\phi_1 = 40.41^\circ$, $\theta_W = 49.59^\circ$ and $M_s = 1.3$); (b) subsonic flow behind the reflected shock wave ($M_0 = 2$, $\phi_1 = 42.54^\circ$, $\theta_W = 47.46^\circ$ and $M_s = 1.35$); (c) sonic flow behind the reflected shock wave

shown in Fig. 1.22c where the R-polar intersects the p -axis exactly at its sonic point, s . This (I-R)-polars combination is appropriate to the sonic criterion, or the catch-up condition, since this is the limit for which the corner-generated signals can catch-up with the reflection point, R , of the regular reflection. The transition line arising from the sonic criterion can be calculated by solving the governing equations of the two-shock theory, i.e., (1.5)–(1.13), and replacing θ_2 by θ_{2s} .

It is worthwhile noting that since the sonic and the detachment points are very close to each other, the sonic criterion results in transition conditions that are very close to those of the detachment criterion. In many cases the difference between them in terms of the value of the reflecting wedge angle is only a

fraction of a degree. For this reason, it is almost impossible to distinguish experimentally between the sonic and detachment criteria.

Lock & Dewey (1989) developed an ingenious experimental set-up by which they were able to experimentally distinguish between the “sonic” and the “detachment” criteria. Their experimental investigation led to the conclusion that, in pseudosteady flows, the $RR \rightleftharpoons IR$ transition occurs when the corner-generated signals manage to catch-up with the reflection point, R, i.e., at the sonic condition rather than the detachment one.

1.5.4 Length-Scale Criterion

The length-scale criterion was introduced by Hornung et al. (1979). The physical reasoning of this criterion is based on their argument that, unlike the wave configuration of an RR that is not associated with any length scale, since both the incident and reflected shock waves extend to infinity (see Fig. 1.1), the wave configuration of an MR inherently includes a length scale, namely the finite length of the Mach stem that extends from the reflection point, R, on the reflecting surface to the triple point, T (see Fig. 1.2). Thus they argued that in order for an MR to be formed, i.e., in order for a shock wave with a finite length to exist, a physical length scale must be available at the reflection point, namely, pressure signals must be communicated to the reflection point of the RR. This argument eventually led them to conclude that there are two different conditions for the termination of the RR depending on whether the flow under consideration is steady or pseudosteady.

Consider the pseudosteady RR in Fig. 1.23a and note that the length of the reflecting surface, ℓ_w , can be communicated to the reflection point, R, only if a subsonic flow is established between points Q and R (in a frame of reference attached to R). This requirement corresponds to the polars combination shown in Fig. 1.22c, which, as discussed earlier, corresponds also to the sonic criterion. In a steady flow (Fig. 1.23b) the length, ℓ_w , of the wedge that is used to generate the incident shock wave can be communicated to the reflection point, R, only if a propagation path exists between points Q and R via the expansion wave at point Q' . This is possible only if the flow between points R and Q' is subsonic. According to Hornung et al. (1979) this could happen if an MR existed, since the flow behind the Mach stem of an MR is always subsonic. Consequently, they argued that the $RR \rightarrow MR$ transition takes place the very first time the MR becomes theoretically possible. This requirement corresponds to the (I-R)-polars combination shown in Fig. 1.21, which, as discussed earlier, corresponds also to the mechanical-equilibrium criterion.

Thus, the length-scale concept of Hornung et al. (1979) led to two different transition lines. In steady flows it predicts transition at the point predicted by the mechanical-equilibrium criterion, $\theta_1 - \theta_2 = \theta_3 = 0$, and in pseudosteady flows it predicts transition at the point predicted by the sonic

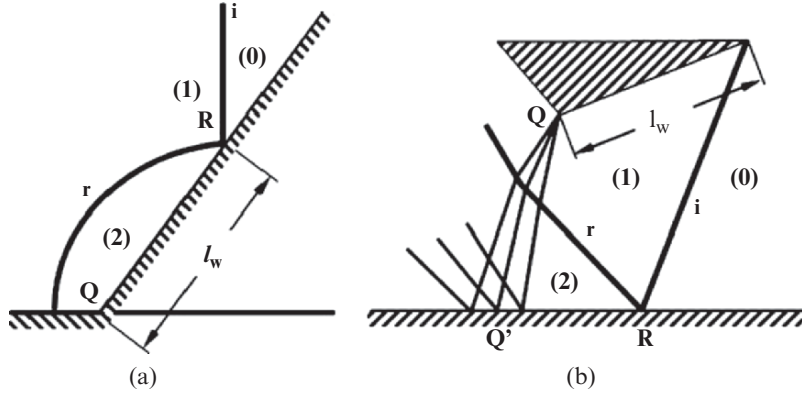


Fig. 1.23. Definition of the physical length, ℓ_w , which should be communicated to the reflection point, R, in order to enable the RR \rightarrow MR transition: (a) pseudosteady flows; and (b) steady flows

criterion, $\theta_1 - \theta_{2_s} = 0$, which is practically identical to the detachment criterion, $\theta_1 - \theta_{2_m} = 0$.

1.5.5 Summary, Critique, and Discussion

The four foregoing suggested transition criteria yield three different RR \rightleftharpoons IR transition lines, which can be calculated in the following manner:

- The transition line arising from the detachment criterion is calculated using the two-shock theory while requiring that

$$\theta_2 = \theta_{2_m}. \quad (1.30)$$

- The transition line arising from the sonic criterion is calculated using the two-shock theory while requiring that

$$\theta_2 = \theta_{2_s} \quad (1.31)$$

- The transition line arising from the mechanical-equilibrium criterion is calculated using the three-shock theory while requiring that

$$\theta_1 - \theta_2 = \theta_3 = 0. \quad (1.32)$$

Recall that the transition lines arising from the length-scale concept are given by (1.31) for pseudosteady flows and by (1.32) for steady flows. It should also be mentioned that the transition lines as calculated by (1.30) and (1.31) are practically identical.

Figure 1.24 illustrates three different (I-R)-polars combinations. The (I-R_i)-polars combination corresponds to the mechanical-equilibrium condition; the (I-R_{iii})-polars combination corresponds to the detachment/sonic condition; and the (I-R_{ii})-polars combination corresponds to an intermediate

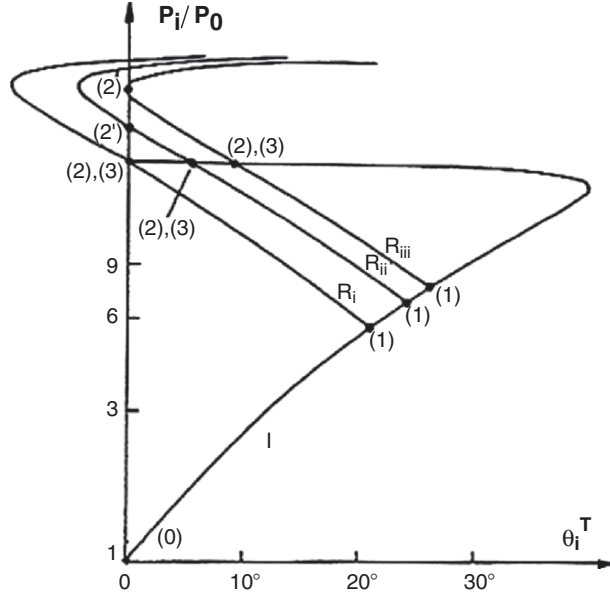


Fig. 1.24. Various (I-R)-polars combinations: the (I-R_i)-polars combination corresponds to the mechanical-equilibrium criterion; the (I-R_{iii})-polars combination corresponds to the detachment/sonic criterion; the (I-R_{ii})-polars combination corresponds to an intermediate situation

situation. For the latter polars combination the mechanical-equilibrium criterion predicts an MR at the point where the R_{ii}-polar intersects the I-polar [points (2) and (3)] while the detachment criterion predicts an RR at the point where the R_{ii}-polar intersects the p -axis [point (2')]. For all the R-polars between the R_i- and the R_{iii}-polars, two solutions, RR or MR, are theoretically possible.

Figure 1.25 illustrates the size of the dual-solution region in the (M_S, θ_w^C) -plane, where θ_w^C is the complementary angle of ϕ_1 , i.e., $\theta_w^C = 90^\circ - \phi_1$. It is seen clearly that the area of disagreement between the mechanical-equilibrium and the detachment criteria is very large. Note that if the transition line arising from the sonic criterion had been added to Fig. 1.25 it would have laid slightly above the detachment transition line.

Although Henderson & Lozzi (1975) reported that excellent agreement was obtained between the mechanical-equilibrium criterion and their experiments in steady flows, i.e., wind tunnel experiments, there are unfortunately some difficulties associated with the physical concept upon which this criterion is based.

First, as can be seen in Fig. 1.25, the mechanical-equilibrium criterion does not apply over the entire range of incident shock wave Mach numbers, M_S . It exists only for values of M_S larger than the value where the mechanical equilibrium transition line emanates from the detachment transition line. This

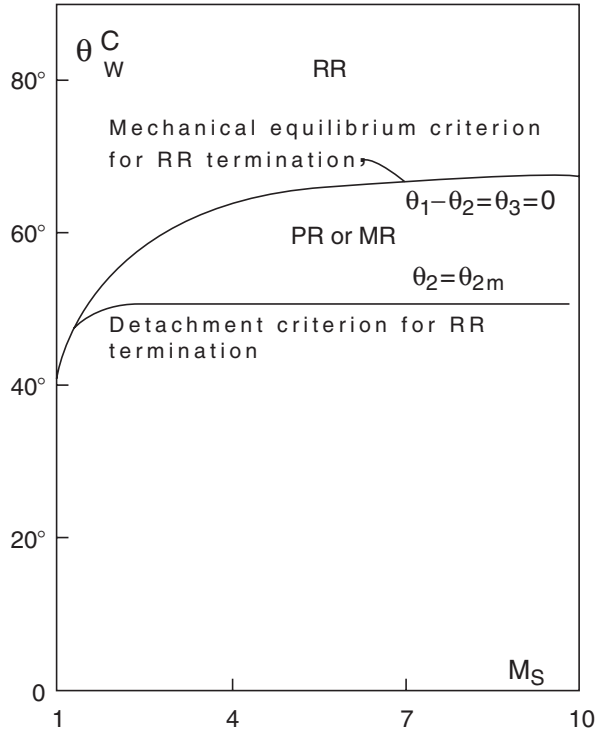


Fig. 1.25. Domains of RR and MR in the (M_S, θ_W^C) -plane as defined by the mechanical-equilibrium and the detachment criteria. $\theta_W^C = 90^\circ - \phi_1$

in turn implies that since $M_S = M_0 \sin \phi_1$ there are combinations of M_0 and ϕ_1 for which the condition given by (1.32) cannot be met.

Second, in their experiments in pseudosteady flows, e.g., shock tube experiments, they observed that RR wave configurations persisted not only inside the dual-solution region shown in Fig. 1.25 but also slightly below the detachment transition line, where RR is theoretically impossible. In the weak-shock wave domain the persistence was up to 5° while in the strong-shock wave domain RR prevailed to about 2° below its theoretical limit. Other investigators who also studied experimental, the RR \rightleftharpoons IR transition obtained similar results. Henderson & Lozzi (1975) attempted to resolve this anomaly by advancing a hypothesis that the RR wave configurations that were observed beyond the limit predicted by the mechanical-equilibrium criterion were, in fact, undeveloped MR wave configurations in which the Mach stem, the slipstream and the triple point were too close together and too small to be resolved as is the case in a well developed MR wave configuration. However, in pseudosteady flows, the shock wave configuration grows with time. Thus the triple point should eventually show up if a long enough reflecting

wedge is used. This, unfortunately, did not occur even in experiments where the reflecting surface was very long.

Finally, Henderson and Lozzi's requirement of mechanical equilibrium is not justified when the flow under consideration is either steady or pseudo-steady, since for these cases, depending upon the initial conditions, either an RR or an IR wave configuration is established, and the requirement of a continuous pressure change during transition is unnecessary since transition does not take place at all. If, however, the flow under consideration is unsteady, and the reflection actually goes through a transition from RR to IR or from IR to RR, then their argument could apply. However, as will be shown in Chap. 4, in the case of unsteady flows, the additional waves required by Henderson & Lozzi (1975) to be associated with a transition at detachment that arises from the sudden pressure drop do indeed appear in the flow field (see e.g., Fig. 1.4 in which a normal shock wave follows the RR that was obtained when the InMR was terminated and transitioned to a TRR).

In summary, experimental results in both steady and unsteady (including pseudosteady) flows have suggested that in steady flows the $\text{RR} \rightleftharpoons \text{IR}$ transition generally agrees with the condition given by (1.32), while in pseudosteady and unsteady flows the $\text{RR} \rightleftharpoons \text{IR}$ transition seems to agree with the conditions given by either (1.30) or (1.31). Thus it can be concluded that the length-scale concept of Hornung et al. (1979) most likely leads to the adequate criterion for the $\text{RR} \rightleftharpoons \text{IR}$ transition because it results in the correct transition lines in steady, pseudosteady, and unsteady flows.

As will be shown subsequently, the agreement between this transition criterion and careful experimental investigation was never satisfactory enough in the close vicinity of the transition lines. This fact has been motivating investigators to continue searching for the "correct" $\text{RR} \rightleftharpoons \text{IR}$ transition criterion. However, one must recall that the transition criteria are based on the two- and three-shock theories which were developed under the assumption that all the discontinuities are straight in the vicinity of their intersection points and hence that the various flow states bounded by them are uniform. In addition to this assumption, which introduces inherent errors into the transition lines that are calculated based on the two- and three-shock theories, it will be shown subsequently that the inclusion of viscous effects and real gas effects does improve the agreement between the experimental results and predictions based on these two fundamental theories.

References

- Ben-Dor, G., "Relations between first and second triple point trajectory angles in double Mach reflection", AIAA J., 19, 531–533, 1981.
 Ben-Dor, G. & Takayama, K., "The dynamics of the transition from Mach to regular reflection over concave cylinders", Israel J. Tech., 23, 71–74, 1986/7.

- Colella, P. & Henderson, L.F., "The von Neumann paradox for the diffraction of weak shock waves", *J. Fluid Mech.*, 213, 71–94, 1990.
- Courant, R. & Freidrichs, K.O., *Hypersonic Flow and Shock Waves*, Wiley Interscience, New York, N.Y., USA, 1948.
- Guderley, K.G., "Considerations on the structure of mixed subsonic-supersonic flow patterns", Tech. Rep. F-TR-2168-ND, Wright Field, USA, 1947.
- Henderson, L.F., "Exact Expressions for Shock Reflection Transition Criteria in a Perfect Gas", *ZAMM*, 62, 258–261, 1982.
- Henderson, L.F. & Lozzi, A., "Experiments on transition of Mach reflection", *J. Fluid Mech.*, 68, 139–155, 1975.
- Hornung, H.G., Oertel, H. Jr. & Sandeman, R.J., "Transition to Mach reflection of shock waves in steady and pseudo-steady flows with and without relaxation", *J. Fluid Mech.*, 90, 541–560, 1979.
- Kawamura, R. & Saito, H., "Reflection of shock waves-1. Pseudo-stationary case", *J. Phys. Soc. Japan*, 11, 584–592, 1956.
- Krehl, P. & van der Geest, "The discovery of the Mach reflection effect and its demonstration in an auditorium", *Shock Waves*, 1, 3–15, 1991.
- Lee, J.-H. & Glass, I.I., "Pseudo-stationary oblique-shock wave reflections in frozen and equilibrium air", *Prog. Aerospace Sci.*, 21, 33–80, 1984.
- Li, H. & Ben-Dor, G., "Reconsideration of pseudo-steady shock wave reflections and the transition criteria between them", *Shock Waves*, 5(1/2), 59–73, 1995.
- Liepmann, H.W. & Roshko, A., *Elements of Gasdynamics*, John Wiley & Sons, New York, N.Y., USA., 1957.
- Lock, G. & Dewey, J.M., "An experimental investigation of the sonic criterion for transition from regular to Mach reflection of weak shock waves", *Exp. Fluids*, 7, 289–292, 1989.
- Mach, E., "Über den verlauf von funkenwellen in der ebene und im raume", *Sitzungsbr. Akad. Wiss. Wien*, 78, 819–838, 1878.
- Neumann, J. von, "Oblique reflection of shocks", Explos. Res. Rep. 12, Navy Dept., Bureau of Ordnance, Washington, DC, USA., 1943a.
- Neumann, J. von, "Refraction, intersection and reflection of shock waves", NAVORD Rep. 203-45, Navy Dept., Bureau of Ordnance, Washington, DC, U.S.A., 1943b.
- Olim, M. & Dewey, J.M., "A revised three-shock solution for the Mach reflection of weak shock waves", *Shock Waves*, 2, 167–176, 1992.
- Reichenbach, H., "Contribution of Ernst Mach to fluid dynamics", *Ann. Rev. Fluid Mech.*, 15, 1–28, 1983.
- Skews, B. & Ashworth J.T., "The physical nature of weak shock wave reflection", *J. Fluid Mech.*, 542, 105–114, 2005.
- Smith, L.G., "Photographic investigation of the reflection of plane shocks in air", OSRD Rep. 6271, Off. Sci. Res. Dev., Washington, DC., USA., or NDRC Rep. A-350, 1945.

- Vasilev, E. & Kraiko, A., “Numerical simulation of weak shock diffraction over a wedge under the von Neumann paradox conditions”, Comp. Math. & Math. Phys., 39, 1335–1345, 1999.
- White, D.R., “An experimental survey of the Mach reflection of shock waves”, Princeton Univ., Dept. Phys., Tech. Rep. II-10, Princeton, N.J., USA., 1951.

2

Shock Wave Reflections in Steady Flows

List of symbols

Latin Letters

a_i	Speed of sound in state (i)
\bar{a}	Average speed of sound behind a curved Mach stem
d	Maximum horizontal shift of the foot of the Mach stem with respect to the triple point
H	Distances from the leading edge to the line of symmetry/bottom surface
H_m	Distances from the triple point to the line of symmetry/bottom (=length of the Mach stem for a straight Mach stem)
\bar{H}_m	Nondimensional Mach stem height
H_s	The height of the throat (see Fig. 2.12)
H_t	Distance from the trailing edge of the reflecting wedge to the line of symmetry/bottom surface (see Fig. 2.12)
$H_{t,\max}$ (MR)	Maximum distance from the trailing edge of the reflecting wedge to the line of symmetry/bottom surface for obtaining an MR (see Fig. 2.14)
$H_{t,\max}$ (RR)	Maximum distance from the trailing edge of the reflecting wedge to the line of symmetry/bottom surface for obtaining an RR (see Fig. 2.14)
$H_{t,\min}$ (MR)	Minimum distance from the trailing edge of the reflecting wedge to the line of symmetry/bottom surface for obtaining an MR (see Fig. 2.14)
$H_{t,\min}$ (RR)	Minimum distance from the trailing edge of the reflecting wedge to the line of symmetry/bottom surface for obtaining an RR (see Fig. 2.14)
J_{TG} (x, y)	Shape of the Mach stem from the triple point, T, to its foot, G
k	Thermal conductivity
L_w	Length of the slope of the reflecting wedge

L	Length of the reflecting wedge
L	Width (see Fig. 2.41)
\bar{M}	Average flow Mach number behind a curved Mach stem
M_{0C}	Critical flow Mach number below which the mechanical equilibrium does not exist
M_i	Flow Mach number in state (i)
M_f	Flight Mach number
M_{tr}	Flight Mach number at which a transition takes place
p_i	Static pressure in state (i)
p_w	Wake pressure behind the tail of the reflecting wedge
R	Specific gas constant
R	Reflection coefficient (see (2.42))
R_I	Intensity reflection coefficient (see (2.43))
S	Distance (see Fig. 2.41)
t	Time
T_i	Temperature in state (i)
u_i	Flow velocity in state (i)
\bar{u}	Average flow velocity behind a curved Mach stem
w	Length of the reflecting wedge
x	Coordinate
X	Nondimensional horizontal distance ($= S/L$)
y	Coordinate
Z_i	Acoustic impedance at state (i)

Greek Letters

α	Flow direction relative to a horizontal direction
β_i	Incident shock wave angle
β_r	Reflected shock wave angle
β_i^D	Incident shock wave angle at the detachment condition
β_i^N	Incident shock wave angle at the von Neumann condition
β_i^S	Limiting incident shock wave angle for a stable RR
$\delta_{\max}(M_i)$	Maximum deflection angle for a flow having Mach number M_i through an oblique shock wave
ϕ	Angle of incidence
ϕ_i	Angle of incidence between the flow and the oblique shock wave across which the flow enters state (i)
ϕ^*	Limiting angle of incidence (see (2.1))
γ	Specific heat capacities ratio
μ	Dynamic viscosity
μ_i	Mach angle of the flow having a Mach number M_i
$\nu(M)$	Prandtl–Meyer function
θ_i	Angle of deflection of the flow while passing across an oblique shock wave and entering into state (i)
θ_w	Reflecting wedge angle
θ_w^C	Complementary wedge angle

θ_w^D	Reflecting wedge angle at the detachment condition
θ_w^E	Reflecting wedge angle at the condition analogous to detachment condition in the reflection of asymmetric shock waves
θ_w^N	Reflecting wedge angle at the von Neumann condition
θ_w^T	Reflecting wedge angle at the condition analogous to von Neumann condition in the reflection of asymmetric shock waves
ρ_i	Flow density in state (<i>i</i>)
$\bar{\rho}$	Average flow density behind a curved Mach stem
τ	Nondimensional time
<i>Subscripts</i>	
G	Foot of the Mach stem
T	Triple point
0	Flow state ahead of the incident shock wave, i
1	Flow state behind the incident shock wave, i
2	Flow state behind the reflected shock wave, r
3	Flow state behind the Mach stem, m
<i>Superscripts</i>	
D	At detachment criterion
N	At von Neumann criterion
<i>Abbreviations</i>	
Waves and Points	
i	Incident shock wave
m	Mach stem
r	Reflected shock wave
s	Slipstream
T	Triple point
R	Reflection point
Wave Configuration	
IR	Irregular reflection
RR	Regular reflection
sRR	Strong regular reflection (an RR with a strong reflected shock wave)
wRR	Weak regular reflection (an RR with a weak reflected shock wave)
MR	Mach reflection
NR	No reflection
Overall Wave Configuration	
oMR	Overall Mach reflection
oMR[DiMR + DiMR]	An oMR that consists of two DiMRs
oMR[DiMR + StMR]	An oMR that consists of one DiMR and one StMR
oMR[DiMR + InMR]	An oMR that consists of one DiMR and one InMR

oRR	Overall regular reflection
oRR[wRR + sRR]	An oRR that consists of one wRR and one sRR
oRR[wRR + wRR]	An oRR that consists of two wRRs
Types of Mach Reflection	
DiMR	Direct-Mach reflection
InMR	Inverse-Mach reflection
StMR	Stationary-Mach reflection

As mentioned in Chap. 1 only regular reflection (RR) and Mach reflections (MR) are possible in steady flows. Hence, the reflection phenomenon in steady flows is less complicated than in pseudosteady or unsteady flows, and its analytical investigation is much simpler.

Unfortunately, in spite of this obvious advantage, not too many experimental studies on the reflection of shock waves in steady flows have been reported thus far. Furthermore, most of the available basic experimental data (excluding the new data regarding the recently discovered hysteresis phenomena) were obtained more than three decades ago, with experimental equipment and diagnostic technique less accurate than those existing nowadays.

2.1 Categories of Steady Reflection Phenomena

The shock wave reflection phenomenon in steady flows could be divided, in general, into four different categories:

- Reflection of a curved incident shock wave from a straight surface
- Reflection of a straight incident shock wave from a curved surface
- Reflection of a curved incident shock wave from a curved surface
- Reflection of a straight incident shock wave from a straight surface

2.1.1 Curved Incident Shock Wave Reflections over Straight Reflecting Surfaces

If a supersonic flow, $M_0 > 1$, encounters a concave or a convex reflecting wedge, then the shock wave which results in, to enable the flow to negotiate the wedge, is also concave or convex. The regular reflections of the incident shock wave for these two possibilities are shown schematically in Fig. 2.1a, b, respectively. The intermediate case of a straight reflecting wedge, of course, results in a straight attached oblique shock wave provided that the reflecting wedge angle is smaller than the maximum flow deflection appropriate to M_0 , as shown in Fig. 1.6b [i.e., $\theta_w < \delta_{\max}(M_0)$]. If, however, the reflecting wedge angle is greater than the maximum flow deflection, as shown in Fig. 1.6c, then the straight reflecting wedge results in a detached bow shock wave which results in a situation similar to that shown in Fig. 2.1b.

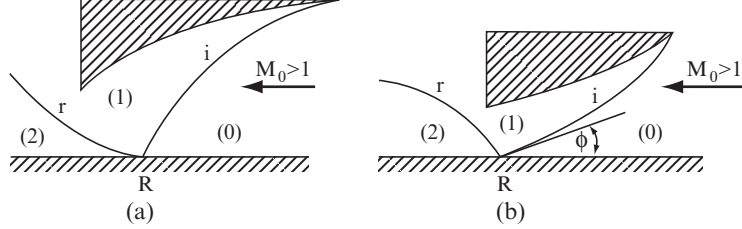


Fig. 2.1. Schematic illustrations of the RR wave configurations of a curved incident shock wave reflection over a straight surface: (a) concave incident shock wave; (b) convex incident shock wave

Pant (1971), who analytically studied the reflection of steady curved shock waves, showed that for weak incident shock waves there is a wave angle, ϕ , (see Fig. 2.1b) for which the reflected shock wave is straight. This specific wave angle, ϕ^* , which was found to be independent of the incident flow Mach number, M_0 , could be obtained from:

$$\phi^* = \cos^{-1} \left(\frac{1}{2} \sqrt{\gamma + 1} \right) \quad (2.1)$$

Thus, in the regular reflection of weak shock waves of all strengths for $\phi < \phi^*$ the incident and the reflected shock waves have curvatures of opposite sign. As the wave angle in the vicinity of the reflection point approaches ϕ^* the reflected shock wave straightens out until it becomes straight at $\phi = \phi^*$. For $\phi > \phi^*$ the curvatures of the incident and the reflected shock waves have the same sign.

Molder (1971) numerically investigated this type of steady flow reflection. In the case of an RR a zero downstream curvature on the streamline behind the reflected shock wave near the reflection point, R, was imposed, and in the case of an MR the pressure gradients and curvatures of the streamlines along the slipstream, in the vicinity of the triple point, T, were matched. Molder's (1971) results showed many possible combinations of reflected-shock curvatures, streamline-curvatures and pressure gradients.

In addition Molder (1971) presented both theoretical arguments and experimental evidence that the RR \rightleftharpoons MR transition occurs when the Mach stem is normal to the incident flow, i.e., at the point predicted by the length scale criterion $\theta_1 - \theta_2 = \theta_3 = \tilde{\theta} = 0$.

Although only RR wave configurations are shown in Fig. 2.1a, b, MR wave configurations are also possible in this steady flow reflection category.

2.1.2 Straight Incident Shock Wave Reflections over Curved Reflecting Surfaces

Two general cases, which belong to this category of RRs in steady flows, are shown schematically in Fig. 2.2a, b. The incident shock waves are straight

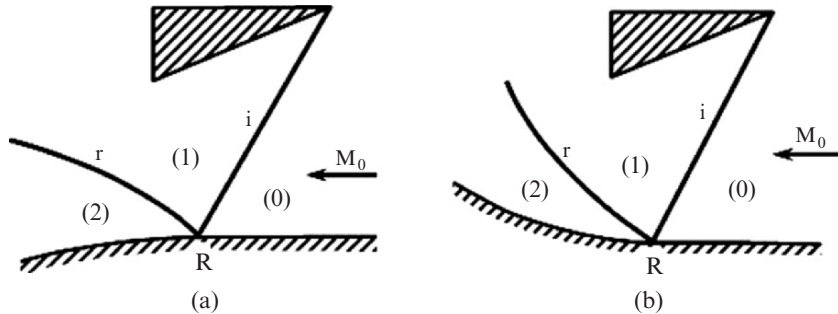


Fig. 2.2. Schematic illustrations of the RR wave configurations of a straight incident shock wave reflecting over a curved surface: (a) convex surface; (b) concave surface

and the reflecting surfaces are straight up to the reflection point, R, after which they are either concave or convex. Depending upon the curvature of the reflecting surface downstream of the reflection point, R, a concave or a convex reflected shock wave is obtained. The curvature of the reflected shock has the same sign as the curvature of the reflecting surface as shown schematically in Fig. 2.2a, b.

Although only RR wave configurations are shown in Fig. 2.2a, b, MR wave configurations are also possible in this steady flow reflection category.

2.1.3 Curved Incident Shock Wave Reflections over Curved Reflecting Surfaces

Four general cases, which belong to this category of shock wave reflections in steady flows, are shown schematically in Fig. 2.3a–d. The incident shock wave in each of these cases is curved and the reflecting surface is straight up to the reflection point, R, beyond which it is either concave or convex. The reflected shock waves assume a curvature with the same sign as the curvature of the reflecting surface, as is shown schematically in Fig. 2.3a–d.

It is obvious that there should be conditions in this steady-flow reflection category, for which MR wave configurations are obtained rather than the RR wave configurations that are shown in Fig. 2.3a–d.

2.1.4 Straight Incident Shock Wave Reflections over Straight Reflecting Surfaces

This category of shock wave reflections in steady flows is undoubtedly the easiest one to treat analytically as the incident shock wave, the reflected shock wave and the reflecting surface are all straight. Most of the reported analytical and experimental studies on the reflection of shock waves in steady flows fall into this steady flow reflection category.

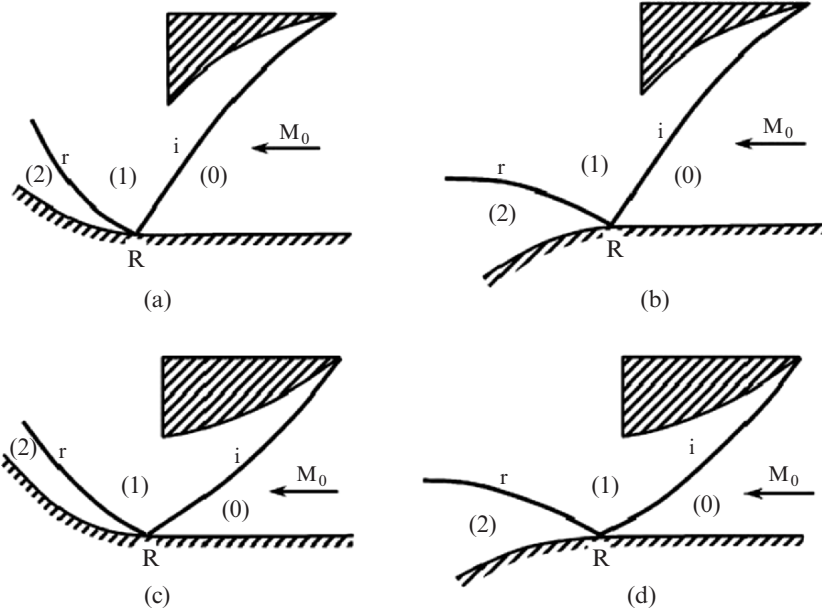


Fig. 2.3. Schematic illustrations of the RR wave configurations of a curved incident shock wave reflecting over a curved surface: (a) concave incident shock wave over a convex surface; (b) concave incident shock wave over a concave surface; (c) convex incident shock wave over a convex surface; (d) convex incident shock wave over a concave surface

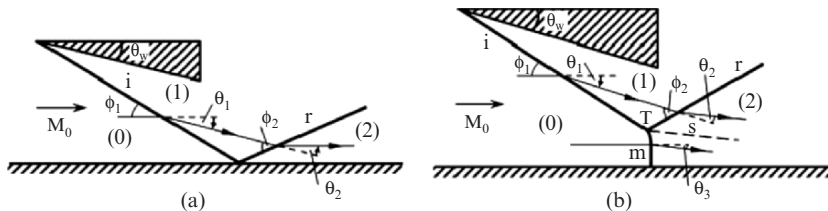


Fig. 2.4. Definition of various flow parameters in: (a) RR; (b) MR

Types of Reflections

Experimental evidence indicates that in this case of steady flows only two reflection configurations are possible, namely, a regular reflection, RR, and a Mach reflection, MR, which in fact is always a single-Mach reflection, SMR.

Schematic illustrations of the wave configurations of an RR and an MR in steady flows are shown in Fig. 2.4a, b, respectively. The interaction between the supersonic flow, M_0 , and the reflecting wedge, θ_w , generates a straight oblique attached shock wave, the incident shock wave, i , through which the flow is deflected by an angle of θ_1 to become parallel to the reflecting wedge

surface, i.e., $\theta_1 = \theta_w$. Since the just-mentioned oblique shock wave arises from the weak solution (see Sect. 1.2), the flow behind the incident shock wave, i , is supersonic. The deflected flow obliquely approaches the bottom surface with an angle θ_w (see Fig. 2.4a). If θ_w is smaller than the maximum deflection angle appropriate to the flow Mach number, M_1 , in state (1), i.e., if $\theta_w < \delta_{\max}(M_1)$, then an RR as shown in Fig. 2.4a could be obtained. If, however, θ_w is greater than the maximum deflection angle of the flow Mach number, M_1 , in state (1), i.e., if $\theta_w > \delta_{\max}(M_1)$, then an RR is impossible, and the resulted reflection is an MR as shown in Fig. 2.4b.

RR \rightleftharpoons MR Transition Criterion

Hornung & Robinson (1982) showed that the RR \rightleftharpoons MR transition is the one arising from the length scale criterion (see Sect. 1.5.4). In the case of steady flows, the length scale criterion results in two different transition formulae depending upon whether the incident flow Mach number, M_0 , is smaller or greater than a certain critical value, M_{0C} . This critical value is the smallest value of M_0 for which the condition imposed by the mechanical equilibrium (see (1.32)) could be satisfied. In fact this is the value of M_0 at which the transition line appropriate to the mechanical equilibrium criterion emanates from the transition line appropriate to the detachment (see Fig. 1.25). The I–R shock polar combination at this critical value of M_{0C} is shown in Fig. 1.18c.

For values of $M_0 > M_{0C}$ the length scale criterion yields a transition at

$$\theta_1 - \theta_2 = \theta_3 = 0. \quad (2.2)$$

This, incidentally, is identical to that predicted by the mechanical equilibrium criterion (see Sect. 1.5.2). For values of $M_0 < M_{0C}$, for which (2.2) cannot be satisfied, the length scale criterion predicts transition at the point where the flow behind the reflected shock wave is sonic, i.e.,

$$M_2 = 1 \quad (2.3)$$

Equation (2.3) which, is also known as the sonic criterion (see Sect. 1.5.3), could be rewritten as:

$$\theta_1 = \theta_{2s} \quad (2.4)$$

The transition lines which result from (2.2) and (2.3) or (2.4) join at the point $M_0 = M_{0C}$. Note that the transition line arising from (2.2) is calculated by means of the three-shock theory while the transition line arising from (2.3) or (2.4) is calculated by means of the two-shock theory. The exact values of M_{0C} for diatomic ($\gamma = 7/5$) and monatomic ($\gamma = 5/3$) perfect gases were calculated by Molder (1979); they are $M_{0C} = 2.202$ and $M_{0C} = 2.470$, respectively.

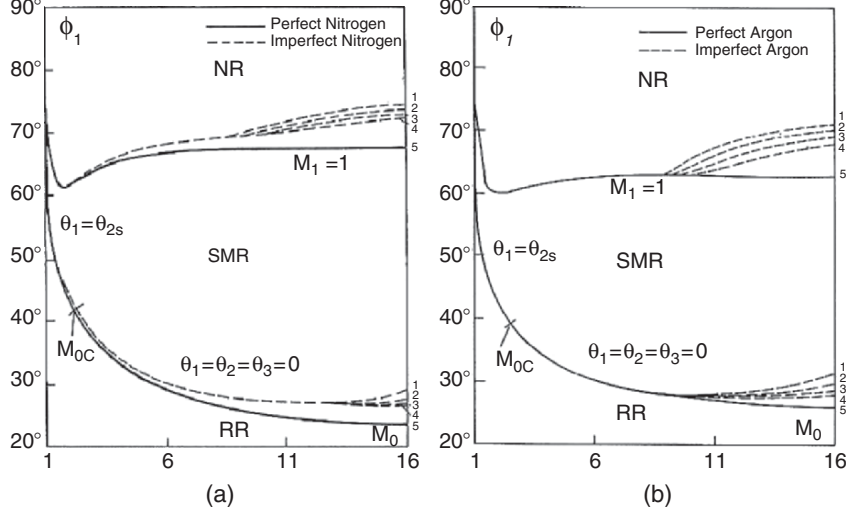


Fig. 2.5. Domains and transition boundaries of various types of shock wave reflection configurations in the (M_0, ϕ_1) -plane. The *solid lines* are for a perfect gas behavior and the *dashed lines* are for an imperfect gas behavior with $T_0 = 300\text{ K}$ and $p_0 = 1, 10, 100, \text{ and } 1,000\text{ Torr}$ for lines 1–4, respectively. (a) Nitrogen: $\gamma = 7/5$ for perfect and in dissociational equilibrium for imperfect behaviors; (b) Argon: $\gamma = 5/3$, for perfect and in ionizational equilibrium for imperfect behaviors

Domains of Different Types of Reflections in the (M_0, ϕ_1) -Plane

The domains of different types of shock wave reflection wave configurations in steady flows in the (M_0, ϕ_1) -plane are shown in Fig. 2.5a, b for nitrogen (N_2) and argon (Ar), respectively. The solid lines are for a perfect gas behavior ($\gamma = 7/5$ for nitrogen and $\gamma = 5/3$ for argon) and the dashed lines are for an imperfect gas behavior (dissociational equilibrium for N_2 and ionizational equilibrium for Ar). Lines (1)–(4) correspond to $p_0 = 1, 10, 100, \text{ and } 1,000\text{ Torr}$, respectively. The NR (no reflection) domains correspond to the unobtainable strong shock solution, for which the flow behind the incident shock wave would have been subsonic, i.e., $M_1 < 1$. Note that for the reason discussed in Sect. 2.1.4 the RR \rightleftharpoons MR transition line is calculated differently depending upon whether M_0 is smaller or greater than M_{0C} . Figure 2.5a, b clearly indicates that real gas effects significantly influence both the RR \rightleftharpoons MR and the RR \rightleftharpoons NR transition lines.

Comparison of Analysis with Experiments

The RR \rightleftharpoons MR transition lines as given by (2.2) and (2.4) were verified experimentally by Henderson & Lozzi (1975, 1979), Hornung et al. (1979) and Hornung & Robinson (1982).

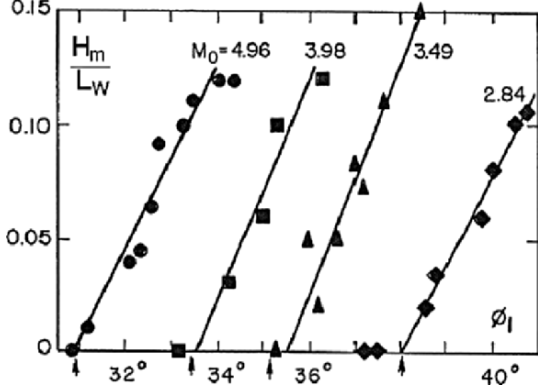


Fig. 2.6. Experimental measurements of the height of the Mach stem as a function of the angle of incidence for different flow Mach numbers and the determination of the transition angle

The results of the experimental investigation of Hornung & Robinson (1982) are shown in Fig. 2.6, where the nondimensional height of the Mach stem, H_m/L_w , as a function of the angle of incidence, ϕ_1 , for different flow Mach numbers, M_0 , is shown (L_w , a characteristic dimension of the reflecting wedge, is defined in Fig. 1.23b). By extrapolating their experimental results to $H_m/L_w = 0$, they showed that the actual $RR \rightleftharpoons MR$ transition occurs at a value of ϕ_1 appropriate to that obtained from (2.2). The analytical values for the given incident flow Mach numbers are shown in Fig. 2.6 by arrowheads.

In spite of the excellent agreement between the experiments and the theory regarding the $RR \rightleftharpoons MR$ transition, one must recall that the two-shock theory as applied to obtain the transition lines shown in Fig. 2.5a, b assumes that the fluid is an ideal one, i.e., inviscid ($\mu = 0$) and thermally nonconductive ($k = 0$), here μ is the dynamic viscosity and k is the thermal conductivity. These, of course, are only simplifying assumptions as a real fluid always has a finite viscosity and thermal conductivity. Discussions on these effects are given in the following sections.

2.2 Modifications of the Perfect Inviscid Two- and Three-Shock Theories

The two- and three-shock theories that were presented in Sects. 1.3.1 and 1.3.2 were developed using simplifying assumptions that are not fully justified, since the reflection phenomenon in steady flows might be affected by nonideal effects. The major assumptions, upon which the two- and three-shock theories were based, are:

- (1) The flow is steady.
- (2) The discontinuities at the reflection point of the RR and the triple point of the MR are straight. This in turns implies that the flow fields bounded by these discontinuities are uniform.
- (3) The flow obeys the equation of state of a perfect gas ($p = \rho RT$).
- (4) The flow is inviscid ($\mu = 0$).
- (5) The flow is thermally nonconductive ($k = 0$).
- (6) The contact discontinuity at the triple point of the MR is infinitely thin, i.e., it is a slipstream.

Beside the first assumption, which for the case of steady shock wave reflections, is fulfilled by definition, the other assumptions could have a meaningful effect. Hence, in the following, the validity of these assumptions is discussed separately.

2.2.1 Nonstraight Discontinuities

Based on experimental observations it is clear that not all the discontinuities of an MR are straight. In fact both the Mach stem and the slipstream are curved. Whether their curvature is meaningful as they approach the triple point is an open question. If yes, then one could assume that the use of the three-shock theory to calculate the flow field near the triple point introduces an inherent error into the predicted results. Note that while in the case of a pseudosteady SMR (see Fig. 3.7), where only the incident shock wave is straight, in the case of a steady MR both the incident and the reflected shock waves are straight. This could imply that predictions based on the three-shock theory should better agree with steady MR-configurations than with pseudosteady SMR-configurations.

2.2.2 Viscous Effects

The flow in state (0) develops a boundary layer along the reflecting surface, and hence the incident shock wave, i , which emanates from the leading edge of the reflecting wedge (see Fig. 2.4a), interacts with this boundary layer to result in a relatively complex structure near the reflection point on the reflecting surface. The interaction with the boundary layer depends on whether the boundary layer is laminar or turbulent as shown in Fig. 2.7, where the interaction of the incident shock wave with the boundary layer near the reflection point, R , of an RR is shown schematically. Figure 2.7 reveals that if one is to solve accurately the flow field near the reflection point, R , of an RR then a very complex flow field must be dealt with.

Henderson (1967) analytically investigated the reflection of a shock wave from a rigid wall in the presence of a boundary layer by treating the problem not as a reflection but as a refraction process. He found that a Mach stem was always present and that the bottom of this wave was bifurcated

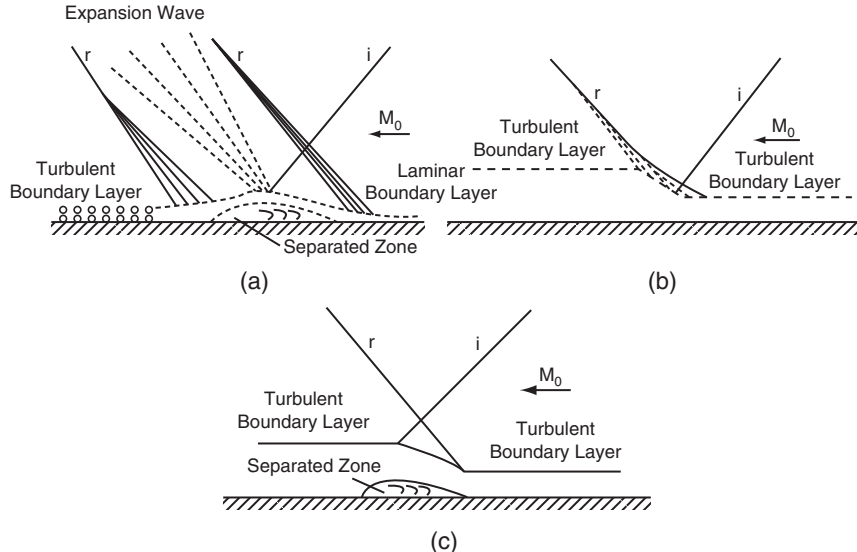


Fig. 2.7. Schematic illustration of the way by which the boundary layer over the reflecting surface could affect the wave structure of an RR near the reflection point

(a lambda foot). The reflection was said to be regular (RR) if the Mach stem and the lambda foot were confined to the boundary layer and irregular (IR) if either the Mach stem or the lambda foot extended into the main stream. Two types of regular reflection were found, one that had a reflected compression wave and the other that had both reflected compression waves and expansion waves. Henderson (1967) presented initial conditions that enable one to decide which type of reflection would appear. Henderson (1967) reported furthermore, that there were two types of IR, one that had a Mach stem present in the main stream and the other that was characterized by a four-wave configuration. There were also two processes by which the RR became IR. One was due to the formation of a downstream shock wave that subsequently swept upstream to establish the irregular system and the other was due to boundary layer separation, which forced the lambda foot into the main stream.

There is, however, a possibility by which the above-mentioned viscous effects could be eliminated in steady flow reflections. By using a relatively simple experimental set-up the above-illustrated interaction with the boundary layer developing over the reflecting surface could be avoided. This is shown in Fig. 2.8 where two identical reflecting wedges are placed in such a way that they produce two symmetrical regular (Fig. 2.8a) and Mach (Fig. 2.8b) reflections. In this case, the line of symmetry replaces the reflecting wedge, thus completely eliminating the development of a boundary layer along it. Hence, it is possible to generate inviscid RR wave configurations in steady flows.

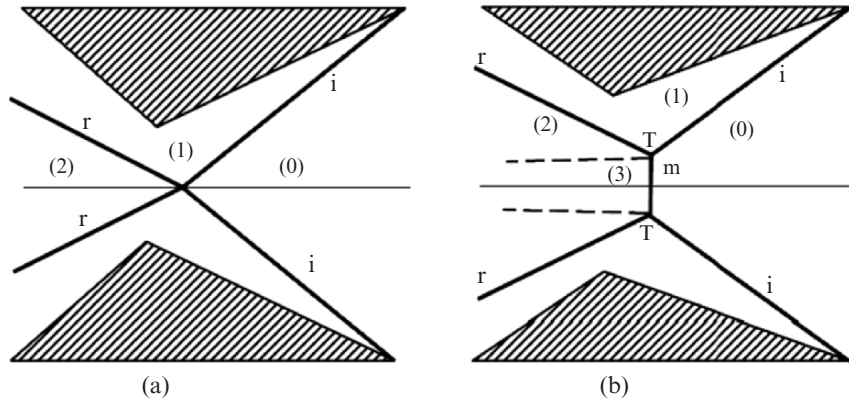


Fig. 2.8. Schematic illustration of an experimental set-up for eliminating the boundary layer effect shown in Fig. 2.7: (a) RR; (b) MR

Things are different in the case of an MR, in which viscous effects along the slipstream of an MR always exist. These effects would have, in the case of a steady MR, similar influence as in the pseudosteady MR (see Sect. 3.4.4). Thus, the modification of the three-shock theory that is presented briefly in Sect. 3.4.4 is probably applicable also to a steady MR if one is to accurately predict the angles between the various discontinuities near the triple point. Using an experimental set-up similar to that mentioned above, the boundary layer with which the foot of the Mach stem interacts could also be eliminated. This is shown in Fig. 2.8b.

Some excellent photographs showing the interactions of both the incident shock wave of an RR and the Mach stem of an MR with the boundary layer could be found in Sect. 28.3 of the book *The Dynamics and Thermodynamics of Compressible Fluid Flow* by Shapiro (1953).

2.2.3 Thermal Conduction Effects

The fact that a real gas has a finite thermal conductivity, introduces an additional mechanism, heat transfer, which might affect the flow fields near the reflection point of an RR and the triple point of an SMR. (For more details of see Sect. 3.4.5 where the effect of thermal conduction for the case of pseudosteady reflections is presented). Unfortunately, neither experimental nor analytical studies of this effect are available.

The foregoing remark on the elimination of viscous effects along the reflecting surface by using a double wedge experimental set-up is also valid for the elimination of heat transfer effects. However, along the slipstream of an MR heat transfer effects might still play an important role.

2.2.4 Real Gas Effects

The question whether real gas effects are important and therefore must be accounted for depends on the ratio between the relaxation length of a certain degree of freedom and the physical characteristic size of the reflection phenomenon.

When the flow fields near the reflection point, R , of an RR or the triple point, T , of an MR are concerned, it is quite appropriate to assume that the flow is frozen with its pre-shock thermodynamic state. However, as the flow moves downstream away from the incident shock front, its internal degrees of freedom are excited (provided the temperatures are sufficiently high) and the flow fields ahead of and behind the reflected shock wave are no longer uniform.

Consider Fig. 2.9 where two reflecting wedges with identical wedge angles, θ_w , that overlap each other are used to produce two RR-configurations, which differ in their size since the surface that is used to reflect the same incident shock wave, i , is located at different distances from the reflecting wedge. The corresponding two reflection points are labeled R_1 and R_2 , respectively. Although the flow fields associated with these two RR-configurations seem to be identical, (one is a linear enlargement of the other) this is not the

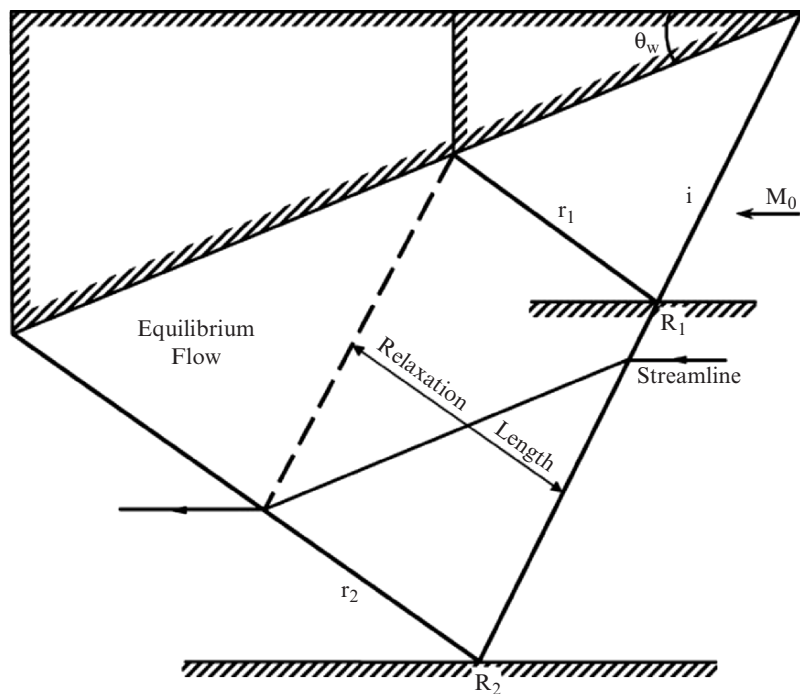


Fig. 2.9. Schematic illustration of the way by which the reflection in steady flows can be affected by the excitation of the internal degrees of freedom

case, because the relaxation length behind the incident shock wave is not scaled, i.e., it remains the same in its size regardless of the size of the reflecting wedge. Note that for illustrative purposes the length of the relaxation zone was chosen such that it extends exactly until the end of the reflected shock wave, r_1 , of the upper RR-configuration. In addition, for simplicity purposes, the reflection of the reflected shock waves (r_1 and r_2) from the surface of the reflecting wedge is not drawn. Thus, while the reflected shock wave of the upper RR-configuration, r_1 , faces a nonequilibrium flow along its entire length, the reflected shock wave of the lower RR-configuration, r_2 , is seen to face an equilibrium flow along its portion that extends beyond the streamline that is added to the figure. This, of course, suggests that the flow fields, which develop behind the shock waves r_1 and r_2 , are different although they were generated using identical initial conditions. Thus, when the shock reflection phenomenon is investigated in steady flows, the influence of real gas effects should be carefully considered prior to their neglect or inclusion.

2.3 Prediction of the Mach Reflection Shape and the Mach Stem Height

As was presented in the foregoing sections the shock wave reflection in steady flows can be regular reflection, RR (Fig. 2.4a) or Mach reflection, MR (Fig. 2.4b). About five decades ago Courant & Friedrichs (1959) and Liepmann & Roshko (1957) and later Emanuel (1986) and Ben-Dor & Takayama (1992) pointed out that one of the unsolved problems associated with the reflection of shock waves in steady flows was the mechanism by which the size of the entire wave configuration of the MR was determined. They pointed out that the height of the Mach stem of a Mach reflection wave configuration was not uniquely determined by von Neumann three-shock theory. Consider Fig. 2.10 where the three solid and one dashed lines describe the four discontinuities of a steady MR wave configuration, namely: the incident shock wave, i , the reflected shock wave, r , the Mach stem, m , and the slipstream, s . These four discontinuities meet at a single point, the triple point, T . If one selects a new point along the incident shock wave, i , and draws there three lines, r' , m' and s' parallel to r , m and s then one would have a new triple point, T' , with its four discontinuities. The two triple points, T and T' , as well as all the other points along the incident shock wave, i , that could have been chosen to be the location of the triple points, completely satisfy the governing equations of the three-shock theory, which is the basis for the analytical description of an MR. However, when experiments with identical initial conditions are repeated in a given facility, only one of the above-mentioned infinite theoretically possible MR wave configurations is obtained. Thus, the three-shock theory is incapable of predicting the actual size of the MR wave configuration (i.e., the Mach stem height) since it is inherently independent of any physical length scale.

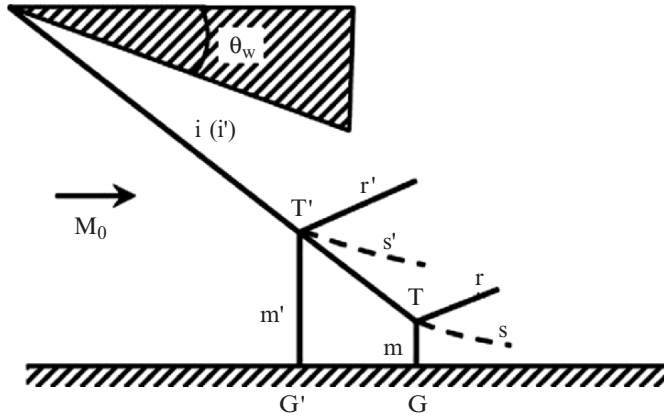


Fig. 2.10. Schematic illustration of two theoretically possible MR wave configurations for identical initial conditions

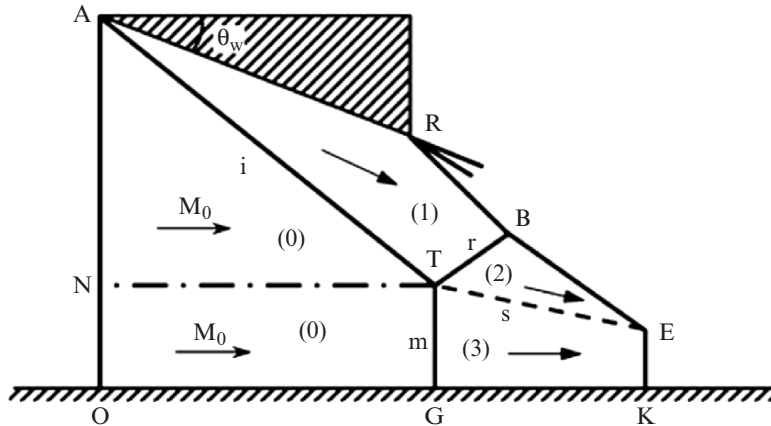


Fig. 2.11. Schematic illustration of an MR wave configuration and definition of parameters relevant to Azevedo & Liu's (1993) model

2.3.1 Assumptions and Concepts of the Models

Soon after the above-mentioned remark by Ben-Dor & Takayama (1992), Azevedo & Liu (1993) suggested a physical model for predicting the height of the Mach stem. Consider Fig. 2.11 where a schematic drawing of a reflecting wedge, which generates an MR, is shown. They assumed in their model that:

- (1) The gas obeys the equation of state of a perfect gas.
- (2) The Mach stem is straight.
- (3) The fluid is ideal, i.e., inviscid and nonconductive.
- (4) The Mach stem, the slipstream and the bottom surface form an effective one-dimensional converging nozzle.

- (5) The throat of this converging nozzle is located at the point where the leading characteristic of the expansion wave (lines RB and BE in Fig. 2.11), that is generated at the trailing edge of the reflecting wedge, intersects the slipstream (point E in Fig. 2.11).
- (6) The flow in region (3) is isentropic and reaches sonic conditions at the throat.

They developed the continuity and momentum equations and some geometric relations for the control volume ARBEKO shown in Fig. 2.11. In order to complete the set of the equations, they applied the three-shock theory for the triple point T. Using their analytical model they obtained relatively good predictions of the Mach stem height for $M_0 = 2.84, 3.49, 3.98$ and 4.96 . (For more details of their model see Sect. 3.3 in the first edition of this monograph, Ben-Dor 1991).

Li & Ben-Dor (1997) raised some doubts about Azevedo & Liu's (1993) model. They argued that:

- The same continuity and momentum conservation equations were used twice in the model, once in the three-shock theory and once in the control volume ARBETN (see Fig. 2.11).
- They applied the quasi-one-dimensional isentropic relation for the control volume TEKG. However, this equation actually originates from the mass and momentum conservation equations.

Therefore, Li & Ben-Dor (1997) presented a modified model (presented subsequently), which provided a better agreement with the experimental results. A half-plane symmetrical MR wave configuration, usually used in the experiments in order to avoid the viscous boundary wall effects, is shown in Fig. 2.12 together with the definition of the relevant parameters. The MR shown in

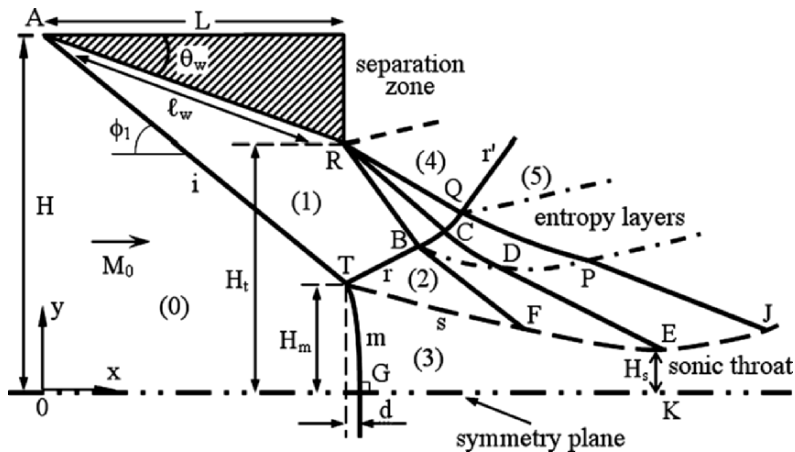


Fig. 2.12. Schematic illustration of an MR wave configuration and definition of parameters relevant to the model of Li & Ben-Dor (1997)

Fig. 2.12 consists of the incident shock, i , the reflected shock, r , the slightly curved Mach stem, m , and the slipstream, s . The flow immediately behind the Mach stem is subsonic. Note that owing to gasdynamic considerations the Mach stem is perpendicular to the plane of symmetry at its foot, point G . The maximum horizontal shift of the foot of the Mach stem is d . Interaction of the reflected shock wave, r , with the centered expansion fan that emanates from the trailing edge of the shock-generating wedge results in a transmitted-reflected shock wave, r' , transmitted expansion waves and an entropy-layers region. Details of shock wave/expansion fan interaction analysis can be found in Li & Ben-Dor (1996). The transmitted expansion waves interact with the slipstream, s , and cause the pressure to drop in the stream wise direction in region (3) behind the Mach stem, thus accelerating the flow to supersonic conditions. As a result, the cross-sectional area of the stream tube between the slipstream and the plane of symmetry decreases to a minimum at a sonic throat (EK in Fig. 2.12) before it increases again in the region of accelerating supersonic flow. A subsonic pocket (TEKG) is formed in an otherwise supersonic flow. The flow downstream of the line RCDEK is supersonic, and hence is isolated from the subsonic pocket. The size and shape of this pocket (eventually the Mach stem height) are solely controlled by the geometry of the upper boundary of region (1) and the distance between the trailing edge of the wedge and the symmetry plane, H_t .

Hornung & Robinson (1982) correctly pointed out that the nondimensional Mach stem height, H_m/ℓ_w , could be expressed in the general form as

$$H_m/\ell_w = f(\gamma, M_0, \theta_w, H_t/\ell_w), \quad (2.5)$$

where γ , M_0 , θ_w , H_t and ℓ_w are the specific heat capacities ratio, the incoming flow Mach number, the reflecting wedge angle, the exit cross-sectional area at the trailing edge and the wedge length, respectively. Unfortunately, Hornung & Robinson (1982) did provide the expression of the function, f .

It is apparent from Fig. 2.12 that in order to get the analytical expression for determining the size of Mach stem, one has to solve:

- The interaction between the expansion fan and the reflected shock wave
- The interaction between the expansion fan and the slipstream
- The flow field in the subsonic pocket (i.e., the converging nozzle)

These solutions, which were presented originally by Li & Ben-Dor (1997), are provided subsequently.

The discussion so far is based on the assumption that a stable MR wave configuration is established for the geometry presented in Fig. 2.12. However, one may ask if there are cases for a combination of M_0 and θ_w for which an MR is theoretically possible but could not be materialized. As shown by Li & Ben-Dor (1997) this indeed happens if H_t is smaller than a certain value, $H_{t,\min}(\text{MR})$, for which the reflected shock wave, r , reaches the reflecting wedge surface as is shown in Fig. 2.13. When the reflected shock wave, r , hits the reflecting wedge before interacting with the expansion fan emanating from the

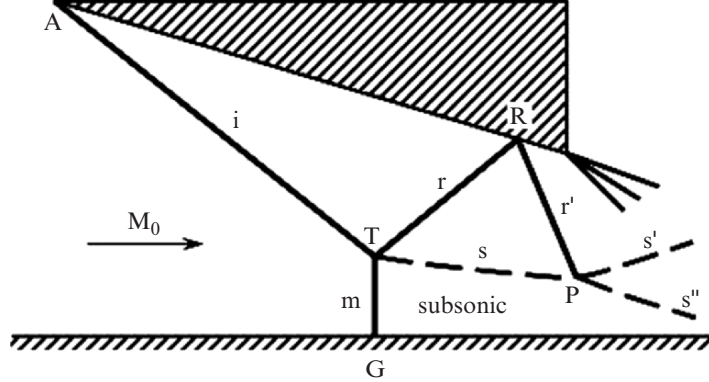


Fig. 2.13. Schematic illustration of a possible transient MR in which its reflected shock wave reflects from the reflecting wedge surface

trailing edge, it reflects as a reflected-reflected shock wave, r' . This shock wave hits the slipstream, s , at point P . Depending upon the impedance matching either a shock wave or an expansion fan reflects from the slipstream, s . Thus a kink should develop in the slipstream at the intersection point, P , and the slipstream should be deflected either upwards as shown by s' or downwards as shown by s'' . Since the flow behind the Mach stem, m , is subsonic, this kink becomes unstable (see Landau & Lifshitz, 1987) and the Mach stem is pushed upstream, until it reaches the leading edge of the reflecting wedge and the flow through the converging nozzle, formed by the reflecting wedge surface and the line of symmetry, becomes unstalled. This process was experimentally observed by Chpoun et al. (1995) and numerically simulated by Vuillon et al. (1995). Therefore, for an MR wave configuration, there exists a minimum value of H_t , i.e., $H_{t,\min}(\text{MR})$, at which the reflected shock wave grazes the trailing edge (see Fig. 2.14). If $H_t < H_{t,\min}(\text{MR})$ the flow is unstalled.

If the combination of M_0 and ϕ_1 is inside the dual solution domain (see Sect. 1.5.5 and Fig. 1.25) where both RR and MR wave configurations are theoretically stable, then as shown schematically in Fig. 2.14 there are in fact four limiting values of H_t , two for RR and two for MR. In similar to $H_{t,\min}(\text{MR})$ there is a value appropriate to the situation in which the reflected shock wave of the RR grazes the trailing edge of the reflecting wedge, $H_{t,\min}(\text{RR})$. Note that $H_{t,\min}(\text{RR}) < H_{t,\min}(\text{MR})$. The fact that the incident shock wave, i , intersects with the leading characteristic of the expansion fan that emanates from the trailing edge of the reflecting wedge, provides two maximal cases for RR and MR, i.e., $H_{t,\max}(\text{RR})$ and $H_{t,\max}(\text{MR})$, since beyond this distances both the orientation and the strength of the incident shock wave are changed. Here again $H_{t,\max}(\text{RR}) < H_{t,\max}(\text{MR})$. Based on the foregoing discussion, for a combination of M_0, θ_w and ℓ_w an MR will take place if $H_{t,\min}(\text{MR}) < H_t < H_{t,\max}(\text{MR})$. Analytical expressions for $H_{t,\min}(\text{MR})$ and $H_{t,\max}(\text{MR})$ are given in Sect. 2.3.6.

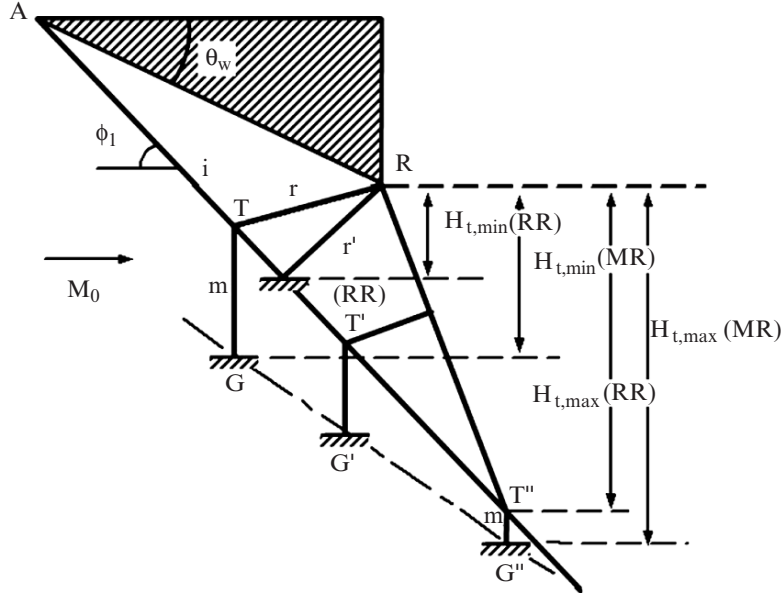


Fig. 2.14. Schematic illustration of the limiting cases of the exit cross-sectional area $H_{t,\min}$ and $H_{t,\max}$ for both RR- and MR-wave configurations

2.3.2 Governing Equations

The derivation of the governing equations is based on the following assumptions:

- (1) The gas is perfect and its heat capacities ratio is constant ($\gamma = 1.4$).
- (2) The fluid is ideal, i.e., its dynamic viscosity and thermal conductivity are equal to zero.
- (3) The flow in region (2) is supersonic (see Fig. 2.12).
- (4) The slipstream and the line of symmetry form a two-dimensional converging/diverging nozzle. Sonic conditions are reached at the throat (EK in Fig. 2.12) of this nozzle provided the flow is free of far-field downstream influences.

The governing equations [(1.14)–(1.27)] of the well-known three-shock-theory (see Sect. 1.3.2) that are used to solve the flow field associated with the triple point T of the MR could be rewritten to read:

$$M_j = F(M_i, \phi_j), \quad (2.6.1)$$

$$\theta_j = G(M_i, \phi_j), \quad (2.6.2)$$

$$p_j = p_i H(M_i, \phi_j), \quad (2.6.3)$$

$$\rho_j = \rho_i E(M_i, \phi_j), \quad (2.6.4)$$

and

$$a_j = a_i A(M_i, \phi_j), \quad (2.6.5)$$

where

$$F(M, \phi) = \left\{ \frac{1 + (\gamma - 1)M^2 \sin^2 \phi + \left[\frac{(\gamma+1)^2}{4} - \gamma \sin^2 \phi \right] M^4 \sin^2 \phi}{[\gamma M^2 \sin^2 \phi - \frac{\gamma-1}{2}] [\frac{\gamma-1}{2} M^2 \sin^2 \phi + 1]} \right\}^{1/2} \quad (2.7.1)$$

$$G(M, \phi) = \arctan \left[2 \cot \phi \frac{M^2 \sin^2 \phi - 1}{M^2(\gamma + \cos 2\phi) + 2} \right], \quad (2.7.2)$$

$$H(M, \phi) = \frac{2}{\gamma + 1} \left(\gamma M^2 \sin^2 \phi - \frac{\gamma - 1}{2} \right), \quad (2.7.3)$$

$$E(M, \phi) = \frac{(\gamma + 1)M^2 \sin^2 \phi}{(\gamma - 1)M^2 \sin^2 \phi + 2}, \quad (2.7.4)$$

and

$$A(M, \phi) = \frac{[(\gamma - 1) M^2 \sin^2 \phi + 2]^{1/2} [2\gamma M^2 \sin^2 \phi - (\gamma - 1)]^{1/2}}{(\gamma + 1)M \sin \phi}. \quad (2.7.5)$$

Based on the forgoing presentation and the flow parameters, which were defined in the schematic illustration of the MR wave configuration shown in Fig. 1.11, the following equations are self-explanatory:

Across the incident shock wave, i:

$$M_1 = F(M_0, \phi_1), \quad (2.8.1)$$

$$\theta_1 = G(M_0, \phi_1), \quad (2.8.2)$$

$$p_1 = p_0 H(M_0, \phi_1), \quad (2.8.3)$$

$$\rho_1 = \rho_0 E(M_0, \phi_1), \quad (2.8.4)$$

$$a_1 = a_0 A(M_0, \phi_1). \quad (2.8.5)$$

Across the reflected shock wave, r:

$$M_2 = F(M_1, \phi_2), \quad (2.9.1)$$

$$\theta_2 = G(M_1, \phi_2) \quad (2.9.2)$$

$$p_2 = p_1 H(M_1, \phi_2), \quad (2.9.3)$$

$$\rho_2 = \rho_1 E(M_1, \phi_2), \quad (2.9.4)$$

$$a_2 = a_1 A(M_1, \phi_2), \quad (2.9.5)$$

Across the Mach stem shock, m, and near the triple point:

$$M_3 = F(M_0, \phi_3), \quad (2.10.1)$$

$$\theta_3 = G(M_0, \phi_3), \quad (2.10.2)$$

$$p_3 = p_0 H(M_0, \phi_3), \quad (2.10.3)$$

$$\rho_3 = \rho_0 E(M_0, \phi_3) \quad (2.10.4)$$

$$a_3 = a_0 A(M_0, \phi_3), \quad (2.10.5)$$

It is obvious that

$$\theta_1 = \theta_w, \quad (2.11)$$

And across the slipstream, s , one has

$$\theta_1 - \theta_2 = \theta_3, \quad (2.12)$$

$$p_2 = p_3. \quad (2.13)$$

The above set of equations consists of 18 equations with 18 unknowns, namely, $M_1, M_2, M_3, \theta_1, \theta_2, \theta_3, p_1, p_2, p_3, \phi_1, \phi_2, \phi_3, \rho_1, \rho_2$ and ρ_3 provided the parameters M_0, p_0, ρ_0 and θ_w are known. Thus, the set of equations is complete and could be solved, in principle.

Generally, the Mach stem is curved (see Fig. 2.12). At its foot (point G) on the line of symmetry, the Mach stem is normal to the upstream flow, M_0 . Therefore, the relations of the normal shock segment for which $\phi_G = \pi/2$ can be written as:

$$M_G = F(M_0, \pi/2) \quad (2.14.1)$$

$$p_G = p_0 H(M_0, \pi/2) \quad (2.14.2)$$

$$\rho_G = \rho_0 E(M_0, \pi/2), \quad (2.14.3)$$

and

$$a_G = a_0 A(M_0, \pi/2). \quad (2.14.4)$$

The shape of the curved Mach stem is determined by the subsonic flow region behind it. Theoretically, it is impossible to get an exact analytical expression of the shape of the Mach stem. However, based on the experimental fact that the Mach stem is only slightly curved and under the first order approximation together with the following boundary conditions at points T and G [see definition of parameters in Fig. 2.12 as well as the chosen (x, y) -coordinate system]:

$$x_T = (H - H_m) \cos \phi_1, \quad (2.15)$$

$$y_T = H_m, \quad (2.16)$$

$$\left. \frac{dx}{dy} \right|_T = -\cot \phi_3, \quad (2.17)$$

$$y_G = 0, \quad (2.18)$$

and

$$\left. \frac{dx}{dy} \right|_G = 0. \quad (2.19)$$

The shape of the Mach stem can be expressed as follows (for further details see Sect. 2.3.3),

$$J_{TG}(x, y) = y^2 \cot \phi_3 + 2H_m x - H_m^2 \cot \phi_3 - 2(H - H_m) H_m \cos \phi_1 = 0, \quad (2.20)$$

where x_T, y_T, x_G and y_G are the coordinates of the triple point, T, and the foot of the Mach stem, G, H and H_m , as shown in Fig. 2.12, are the respective distances from the leading edge, A, and from the triple point, T, to the line of symmetry.

The horizontal shift of the foot of the Mach stem with respect to the triple point is

$$d = x_G - x_T = \frac{H_m \cot \phi_3}{2}. \quad (2.21)$$

The only one unknown parameter in (2.15)–(2.21) is the Mach stem height, H_m .

Interaction of the Expansion Fan with the Reflected Shock Wave and Slipstream

A detailed schematic illustration of the interactions of the centered expansion fan with the reflected shock wave, r, and the slipstream, s, that was mentioned earlier and the definition of the relevant parameters is shown in Fig. 2.15. Based on the foregoing discussion the MR-wave configuration does not depend on the flow parameters in the regions downstream of line RCDE (see Fig. 2.12) provided it is free of downstream influences. Consequently, only the governing equations for solving the relevant flow regions shown in Fig. 2.15 are needed.

The region RBC is a Prandtl–Meyer fan, therefore

$$\nu(M_C) - \nu(M_1) = \theta_w - \alpha \quad (2.22)$$

$$p_C = p_1 \left[\frac{2 + (\gamma - 1)M_1^2}{2 + (\gamma - 1)M_C^2} \right]^{\gamma/\gamma-1}, \quad (2.23)$$

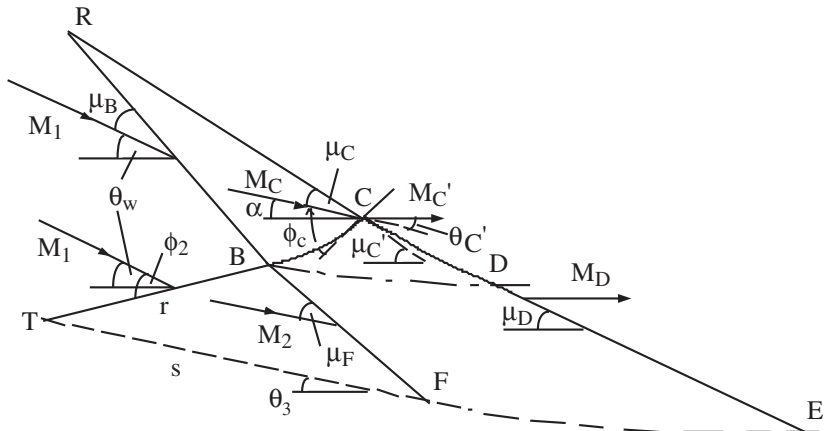


Fig. 2.15. A detailed schematic illustration of the interactions of the centered expansion fan emanating from the trailing edge of the reflecting wedge (see Fig. 2.12) with the reflected shock wave and the slipstream of the MR and definition of parameters

where M_C and p_C are the flow Mach number and the pressure along the characteristic RC , α is the flow direction relative to the horizontal direction, and $\nu(M)$ is the Prandtl–Meyer function, i.e.,

$$\nu(M) = \left(\frac{\gamma + 1}{\gamma - 1} \right)^{1/2} \arctan \left[\frac{(\gamma - 1)(M^2 - 1)}{\gamma + 1} \right]^{1/2} - \arctan(M^2 - 1)^{1/2}. \quad (2.24)$$

Across the curved reflected shock wave at point C, one gets:

$$M_{C'} = F(M_C, \phi_C) \quad (2.25.1)$$

$$\theta_{C'} = G(M_C, \phi_C) \quad (2.25.2)$$

$$p_{C'} = p_C H(M_C, \phi_C) \quad (2.25.3)$$

where $M_{C'}$, $\theta_{C'}$ and $p_{C'}$ are the flow Mach number, the flow deflection angle, and the pressure immediately behind the curved reflected shock at point C, respectively, and the functions F , G and H are given by (2.7.1)–(2.7.3), respectively.

The interaction of the centered expansion fan with the reflected shock wave results in an entropy-layers region (see Fig. 2.12 and 2.15). The dashed-dotted line BD in Fig. 2.15 (BDP in Fig. 2.12) is the weak tangent discontinuity. The region BCD in Fig. 2.15 (or BQP in Fig. 2.12) is filled with infinite such entropy layers. The pressure and the flow direction remain the same across each layer while the entropy, the density and other thermodynamic properties change in infinitesimal increments. Therefore, the overall changes of the flow properties across the entire entropy layers region result in a situation in which the flow directions at points C and D along curve CD are parallel and the pressures are the same, i.e.,

$$\alpha = \theta_{C'} \quad (2.26)$$

$$p_{C'} = p_D, \quad (2.27)$$

where p_D is the pressure at point D.

When the transmitted expansive waves reach the slipstream, s, they partially reflect from it and partially transmit through it. Under the first-order approximation (see Sect. 2.3.3), the reflected expansive waves are very weak and hence could be neglected. Thus, region BFED could be assumed to be a simple wave region. Consequently, the flow parameters along the lines BF and DE remain constant. At point E where the sonic throat is located (see Fig. 2.12), the flow direction should be parallel to the x -axis. Again, by using the Prandtl–Meyer function one gets:

$$\nu(M_D) - \nu(M_2) = \theta_3 \quad (2.28)$$

$$p_D = p_2 \left[\frac{2 + (\gamma - 1)M_2^2}{2 + (\gamma - 1)M_D^2} \right]^{\gamma/\gamma-1} \quad (2.29)$$

The above set of equations (2.22)–(2.29) consists of nine equations with nine unknowns, i.e., $M_C, M_{C'}, M_D, p_C, p_{C'}, p_D, \phi_C, \theta_{C'}$ and α . Therefore, it is complete provided all the other parameters are known, as indeed is the case.

Flow Through the Subsonic Pocket (Region TEKG in Fig. 2.12)

The flow behind the nearly normal Mach stem, in the duct formed by the slipstream and the line of symmetry (TE and GK, respectively, in Fig. 2.12) is subsonic. Theoretically, it is impossible to get an exact analytical solution in this subsonic flow region. However, for the case under consideration the Mach stem is slightly curved and hence $\theta_3 \ll 1$. Consequently, it is reasonable to assume that the flow in the duct TEKG is quasi-one-dimensional. As assumed earlier, the isentropic flow becomes sonic at the throat (EK in Fig. 2.12). The well-known quasi-one-dimensional area-Mach number relation results in

$$\frac{H_m}{H_s} = \frac{1}{\bar{M}} \left[\frac{2}{\gamma + 1} \left(1 + \frac{\gamma - 1}{2} \bar{M}^2 \right) \right]^{\gamma+1/2(\gamma-1)}. \quad (2.30)$$

Here H_s is the height of the throat, and \bar{M} could be regarded as the average flow Mach number behind the curved Mach stem and. It is defined as

$$\bar{M} = \bar{u}/\bar{a}, \quad (2.31)$$

where under a first order approximation

$$\bar{u} = \frac{1}{H_m \bar{\rho}} \int_0^{H_m} \rho \vec{u} \cdot \vec{e}_x dy = \frac{1}{2\bar{\rho}} (\rho_3 u_3 \cos \theta_3 + \rho_G u_G), \quad (2.32.1)$$

$$\bar{a} = \frac{a_3 + a_G}{2}, \quad (2.32.2)$$

and

$$\bar{\rho} = \frac{\rho_3 + \rho_G}{2}. \quad (2.32.3)$$

Substituting (2.32.1)–(2.32.3) into (2.31) results in

$$\bar{M} = \frac{2(\rho_3 u_3 \cos \theta_3 + \rho_G u_G)}{(\rho_3 + \rho_G)(a_3 + a_G)}, \quad (2.33)$$

where $u_3 = M_3 a_3$ and $u_G = M_G a_G$, u_3, M_3, ρ_3 and θ_3 are obtained from the solution of the three-shock theory, i.e., equations (2.8.1) to (2.13), and M_G, ρ_G and a_G are given by (2.14.1), (2.14.3), and (2.14.4).

Recall that the Mach stem height, H_m , is still unknown in the above set of equations, the geometric relations of the wave configuration, given by (2.57) in Sect. 2.3.5, provide the required extra equation to close this set of equations.

It should be pointed out here that the actual flow in the pocket TEKG is two-dimensional, and hence the flow parameters are not uniform in the

cross-sections of the pocket, i.e., along the y -axis (see Fig. 2.12). This could be seen clearly in the numerical simulations of Chpoun et al. (1994) and Ivanov et al. (1995). Under the quasi-one-dimensional flow assumption, the average flow parameters in the cross-sections are used in the related equations. Inspecting the matching conditions across the slipstream indicates that the pressures in region (2), where the flow is supersonic and uniform (TF is a straight line), and in the region downstream of the expansion wave region, are not necessarily equal to the average pressures in the pocket. But the flow directions on the two sides of the slipstream at the sonic throat (EK) where the minimum cross-section area is reached are the same and parallel to the x -axis. The three-shock-theory solution [(2.8.1)–(2.13)] is valid only in the regions near the triple point T. The matching condition across the slipstream at point E is the flow directions (2.28) rather than the pressures.

2.3.3 Derivation of a General Expression for a Curved Line as a Function of Some Boundary Conditions at Its Ends

A monotonous curve Q_1-Q_2 is shown in Fig. 2.16. The coordinates of Q_1 and Q_2 in the (x, y) -coordinates system are (x_1, y_1) and (x_2, y_2) , respectively. The slopes at Q_1 and Q_2 are $\tan \delta_1$ and $\tan \delta_2$, respectively. If the curve $Q_1 - Q_2$ satisfies the condition that $\delta_2 - \delta_1 = \delta \ll 1$, its analytical expression can be obtained under the first-order approximation provided the proper parameters are known. The derivation is given in the following.

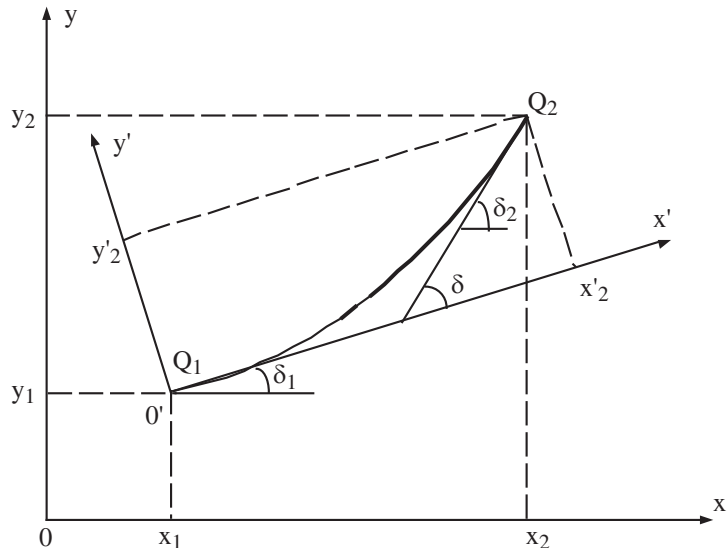


Fig. 2.16. Schematic illustration of a monotonous curve and definition of parameters in both (x, y) - and (x', y') -coordinates

The transformation from the (x, y) - to the (x', y') -coordinates system is (see Fig. 2.16):

$$x' = (x - x_1) \cos \delta_1 + (y - y_1) \sin \delta_1, \quad (2.34a)$$

$$y' = -(x - x_1) \sin \delta_1 + (y - y_1) \cos \delta_1. \quad (2.34b)$$

The coordinates of Q_1 and Q_2 in the (x', y') -coordinates system are $(0, 0)$ and (x'_2, y'_2) , respectively. The slopes at Q_1 and Q_2 are 0 and $\tan(\delta_2 - \delta_1)$, respectively. By assuming that $\tan(\delta_2 - \delta_1) = \epsilon$, where $\epsilon \ll 1$, one could get the following equation for the curve $Q_1 - Q_2$:

$$y' = f(x') < \epsilon x' \leq \epsilon x'_2. \quad (2.35)$$

For the present case, the curve $Q_1 - Q_2$ represents the curves BC, CD, BD or EF (see Fig. 2.12). If the maximum characteristic length is taken as the normalization factor then $x'_2 < 1$. By using Taylor's expansion (2.35) becomes:

$$y' = f(x') = f(0) + f'_{x'}(0)x' + \frac{1}{2}f''_{x'x'}(0)(x')^2 + o(\epsilon) \quad (2.36)$$

Since at Q_1 , $y' = 0$ and $dy'/dx' = 0$, and at Q_2 , $dy'/dx' = \epsilon$, one gets:

$$y' = f(x') = \frac{(x')^2}{2x'_2}\epsilon, \quad (2.37)$$

which at point Q_2 yields:

$$y'_2 = \frac{x'_2}{2}\epsilon. \quad (2.38)$$

Returning to the (x, y) -coordinates system, the following expressions for the curve $Q_1 - Q_2$ could be obtained by substituting (2.34a) and (2.34b) into (2.37) and (2.38)

$$\begin{aligned} J(x, y, x_1, y_1, x_2, y_2, \delta_1, \delta_2) &= [(y - y_1) \tan \delta_1 + (x - x_1)]^2 \tan(\delta_2 - \delta_1) \\ &+ 2[(x_2 - x_1) + (y_2 - y_1) \tan \delta_1][(x - x_1) \tan \delta_1 - (y - y_1)] = 0 \end{aligned} \quad (2.39)$$

and

$$y_2 - y_1 = \tan \Lambda(\delta_1, \delta_2)(x_2 - x_1), \quad (2.40)$$

where

$$\Lambda(\delta_1, \delta_2) = \arctan \left[\frac{2 \tan \delta_1 + \tan(\delta_2 - \delta_1)}{2 - \tan \delta_1 \tan(\delta_2 - \delta_1)} \right] \quad (2.41)$$

Equation (2.39) is a general expression for a curved line as a function of some boundary conditions at its ends.

2.3.4 Estimation of the Strength of the Expansion Waves that are Reflected at the Slipstream

When an incident wave (compression or expansion) collides head-on with a gas interface, it can partially reflect from it and partially transmit through it (see Fig. 2.17). The reflection coefficient, R , can be defined as

$$R = \left| \frac{1 - Z_i/Z_t}{1 + Z_i/Z_t} \right|, \quad (2.42)$$

where Z_i and Z_t are the wave impedances of states (i) and (t) at the acoustic limit, respectively, i.e., $Z_i = \rho_i a_i$ and $Z_t = \rho_t a_t$ (for more details, see Henderson, 1989). The intensity reflection coefficient, R_I , is

$$R_I = R^2 \left| \frac{Z_i}{Z_r} \right|, \quad (2.43)$$

where Z_r is the wave impedance of state (r) at the acoustic limit, i.e., $Z_r = \rho_r a_r$. When the incident wave is an expansion wave as is the present case, Z_r approximately equals to Z_i . Therefore, (2.43) can be simplified to read:

$$R_I = R^2 = \left| \frac{\rho_t a_t - \rho_i a_i}{\rho_t a_t + \rho_i a_i} \right|^2. \quad (2.44)$$

If the incident expansion wave impacts the gas interface obliquely (see Fig. 2.18), the intensity reflection coefficient becomes:

$$R_I = R^2 \cos^2 \beta = \left| \frac{\rho_t a_t - \rho_i a_i}{\rho_t a_t + \rho_i a_i} \right|^2 \cos^2 \beta \quad (2.45)$$

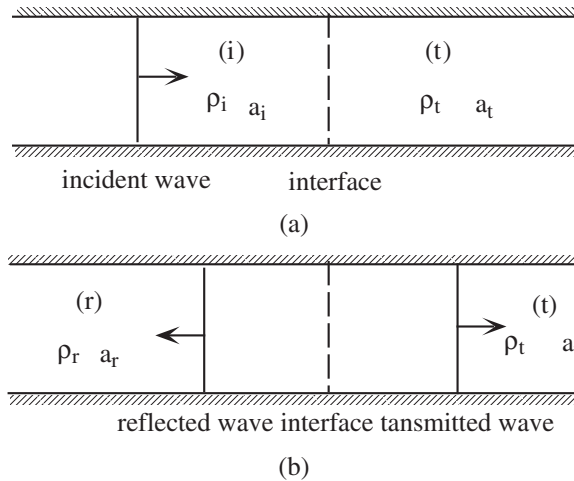


Fig. 2.17. Schematic illustration of head-on interaction of a wave with a gas interface. (a) Before the interaction; (b) After the interaction

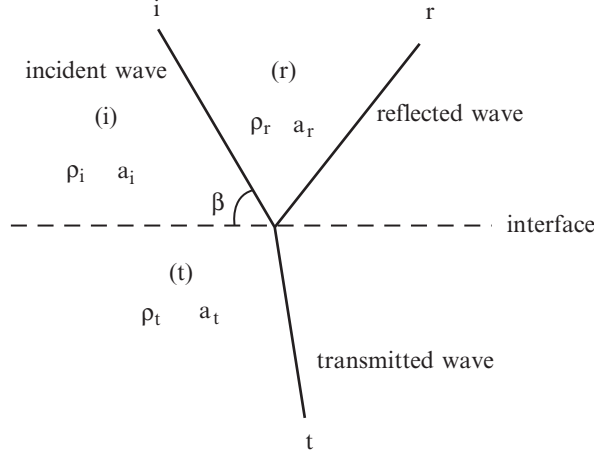


Fig. 2.18. Schematic illustration of oblique interaction of an expansion wave with a gas interface

In the present case, i.e., the gas interface is the slipstream separating regions (2) and (3), i.e., $\rho_i a_i = \rho_2 a_2$ and $\rho_t a_t = \rho_3 a_3$. For combinations of M_0 and θ_w that result in an MR the following inequality is always valid:

$$\left| \frac{\rho_3 a_3 - \rho_2 a_2}{\rho_3 a_3 + \rho_2 a_2} \right| < 0.2. \quad (2.46)$$

By combining (2.45) and (2.46), one obtains the intensity of the reflection coefficient of the expansion wave from region (2) shown in Fig. 2.12 as

$$R_I = \left| \frac{\rho_3 a_3 - \rho_2 a_2}{\rho_3 a_3 + \rho_2 a_2} \right|^2 \cos^2 \beta \leq \left| \frac{\rho_3 a_3 - \rho_2 a_2}{\rho_3 a_3 + \rho_2 a_2} \right|^2 < 0.04. \quad (2.47)$$

Therefore, under the first-order approximation the reflected wave from the slipstream (see Fig. 2.12) is negligibly weak and hence can be neglected.

2.3.5 Geometric Relations of the Wave Configuration Shown in Figs. 2.12 and 2.15

The coordinates of the relevant intersection points shown in Fig. 2.12 are $R(x_R, y_R)$, $B(x_B, y_B)$, $C(x_C, y_C)$, $D(x_D, y_D)$, $E(x_E, y_E)$ and $F(x_F, y_F)$. The straight lines RB can be expressed as

$$y_B - y_R = -\tan(\mu_B + \theta_w)(x_B - x_R), \quad (2.47a)$$

where

$$\mu_B = \arcsin(1/M_1) \quad (2.47b)$$

$$x_R = L = w \sin \theta_w \quad (2.47c)$$

and

$$y_R = w \cos \theta_w. \quad (2.47d)$$

For the straight line RC

$$y_C - y_R = -\tan(\mu_C + \alpha)(x_C - x_R), \quad (2.48a)$$

where

$$\mu_C = \arcsin(1/M_C). \quad (2.48b)$$

For the straight line BF

$$y_F - y_B = -\tan(\mu_2 + \theta_3)(x_F - x_B), \quad (2.49a)$$

where

$$y_F = H_s, \quad (2.49b)$$

and

$$\mu_2 = \arcsin(1/M_2). \quad (2.49c)$$

For the straight line DE

$$y_E - y_D = -\tan \mu_D (x_E - x_D), \quad (2.50a)$$

where

$$\mu_D = \arcsin(1/M_D). \quad (2.50b)$$

For the straight line TB

$$y_B - y_T = \tan(\phi_2 - \theta_w)(x_B - x_T), \quad (2.51a)$$

where

$$y_T = H_m, \quad (2.51b)$$

and

$$x_T = (H - H_m) \cos \phi_1. \quad (2.51c)$$

For the straight line TF

$$y_F - y_T = -\tan \theta_3 (x_F - x_T). \quad (2.52)$$

The exact analytical expressions for the curved lines BC, CD, BD and FE are hard to obtain. However, an inspection of the formation of these lines, which result from the interaction of the expansion waves (weak discontinuities) with the shock wave, slipstream and tangent weak discontinuities, indicates that their slopes change slowly and their total variations are small. Under the first order approximation, their analytical expression could be obtained using the procedure that was presented in Sect. 2.3.3.

The expression of the curved line BC is

$$J[x, y, x_B, y_B, x_C, y_C, \delta_B(BC), \delta_C(BC)] = 0 \quad (2.53a)$$

and

$$y_B - y_C = \tan \Lambda [\delta_B(BC), \delta_C(BC)] (x_B - x_C), \quad (2.53b)$$

where $\delta_B(BC)$ and $\delta_C(BC)$, the angles of inclination of the curve BC at points B and C, respectively, are given by

$$\delta_B(BC) = \phi_2 - \theta_w \quad (2.53c)$$

and

$$\delta_C(BC) = \phi_C - \alpha \quad (2.53d)$$

and the functions J and Λ are given by (2.38) and (2.40) in Sect. 2.3.3, respectively.

For the curved line CD one gets

$$J [x, y, x_C, y_C, x_D, y_D, \delta_C(CD), \delta_D(CD)] = 0 \quad (2.54a)$$

and

$$y_C - y_D = \tan \Lambda [\delta_C(CD), \delta_D(CD)] (x_C - x_D), \quad (2.54b)$$

where $\delta_C(CD)$ and $\delta_D(CD)$, the angles of inclination of the curve CD at points C and D, respectively, are given by

$$\delta_C(CD) = -\mu_{C'} = -\arcsin (1/M_{C'}) \quad (2.54c)$$

and

$$\delta_D(CD) = -\mu_D = -\arcsin (1/M_D). \quad (2.54d)$$

For the curved line BD one gets

$$J [x, y, x_B, y_B, x_D, y_D, \delta_B(BD), \delta_D(BD)] = 0 \quad (2.55a)$$

and

$$y_B - y_D = \tan \Lambda [\delta_B(BD), \delta_D(BD)] (x_B - x_D), \quad (2.55b)$$

where $\delta_B(BD)$ and $\delta_D(BD)$, the angles of inclination of the curve BD at points B and D, respectively, are given by

$$\delta_B(BD) = \theta_3 \quad (2.55c)$$

and

$$\delta_D(BD) = 0. \quad (2.55d)$$

For the curved line FE one gets

$$J [x, y, x_F, y_F, x_E, y_E, \delta_F(FE), \delta_E(FE)] = 0 \quad (2.56a)$$

and

$$y_F - y_E = \tan \Lambda [\delta_F(FE), \delta_E(FE)] (x_F - x_E), \quad (2.56b)$$

where $\delta_F(FE)$ and $\delta_E(FE)$, the angles of inclination of the curve FE at points F and E, respectively, are given by

$$\delta_F(FE) = -\theta_3 \quad (2.56c)$$

and

$$\delta_E(FE) = 0. \quad (2.56d)$$

By combining (2.47a) to (2.56d) one finally gets the following relation between H_m and H_s

$$H_m = R(H_s, H, w, \theta_w, \phi_2, \theta_3, \alpha, M_1, M_2, M_C, M_{C'}, M_D). \quad (2.57)$$

2.3.6 Results

A comparison between the normalized Mach stem heights, H_m/L as predicted by the above-presented model (solid line), and as measured by Hornung & Robinson (1982) (solid squares) is shown in Fig. 2.19a, b for $M_0 = 2.84$ and 3.98 , respectively. The geometry condition is $H_t/L = 0.37$. Azevedo & Liu's (1993) calculated results (dashed line) and Vuillon et al.'s (1995) numerical results (open circles) are added to these figures. The predictions of the above-presented model are better than those predicted by Azevedo & Liu's (1993) model, which were presented in detail in Sect. 3.3 of the 1st edition of this monograph (Ben-Dor, 1991). Furthermore, it is evident that the Mach stem heights based on the present model approach zero exactly at the von Neumann transition point, ϕ_1^N . This indicated that the MR \rightleftharpoons RR transition takes place at von Neumann criterion.

The predicted values of the Mach stem heights, which agree very well with the experimental data for $M_0 = 2.84$ (Fig. 2.19a), are slightly lower than the experimental data and the numerical simulations for the larger value of $M_0 = 3.98$ (Fig. 2.19b). The reason for this is not clear (It could be that the experimental results of Hornung & Robinson, 1982, were either contaminated by three-dimensional effects or influenced by downstream conditions).

As analyzed in Sect. 2.3.1, an MR wave configuration is well established only when the geometrical set-up to which the MR is attached satisfies the condition that $H_{t,\min}(MR) < H_t < H_{t,\max}(MR)$, where $H_{t,\max}(MR)$ and $H_{t,\min}(MR)$ are, respectively, the upper and lower limits of H_t for which an MR is obtainable. These limits could be calculated easily with the parameters defined in Figs. 2.12, 2.14, and 2.15 to read

$$H_{t,\max}(MR) = H_m + \frac{w \sin(\mu_B + \theta_w) \sin(\phi_1 - \theta_w)}{\sin(\mu_B + \theta_w - \phi_1)} \quad (2.34.1)$$

and

$$H_{t,\min}(MR) = H_m + \frac{w \sin(\phi_2 - \theta_w) \sin(\phi_1 - \theta_w)}{\sin(\phi_1 + \phi_2 - \theta_w)}. \quad (2.34.2)$$

If the (M_0, ϕ_1) -combination is inside the dual-solution domain, i.e., $\phi_1^N < \phi_1 < \phi_1^D$ (Fig. 1.25), a stable RR wave configuration is also possible. The upper and

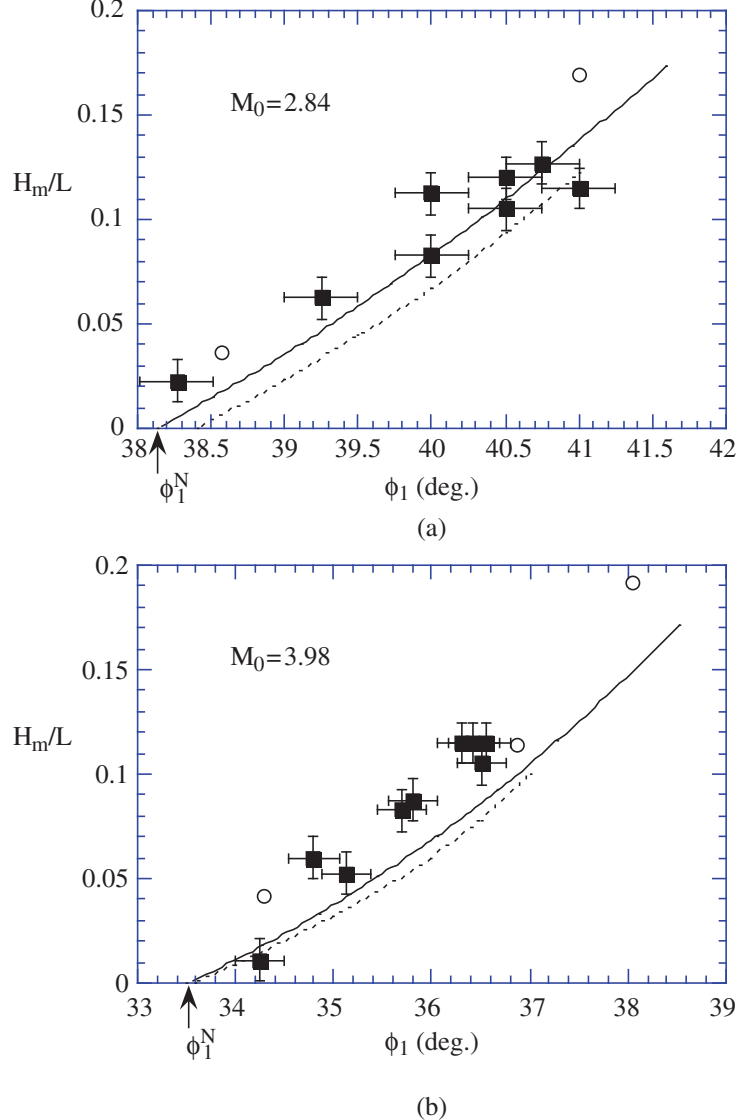


Fig. 2.19. Comparisons of the analytically predicted normalized Mach stem height, with the experiments Hornung & Robinson's (1982) and the numerical simulations of Vuillon et al. (1995) for $H_t/L = 0.37$. (a) $M_0 = 2.84$, and (b) $M_0 = 3.98$

lower limits of H_t for the existence of an RR wave configuration could be calculated also to read

$$H_{t,\max}(\text{RR}) = \frac{w \sin(\mu_B + \theta_w) \sin(\phi_1 - \theta_w)}{\sin(\mu_B + \theta_w - \phi_1)} \quad (2.35.1)$$

and

$$H_{t,\min}(\text{RR}) = \frac{w \sin(\phi_2 - \theta_w) \sin(\phi_1 - \theta_w)}{\sin(\phi_1 + \phi_2 - \theta_w)}, \quad (2.35.2)$$

It should be noted here that while ϕ_2 in (2.34.2) is calculated from an MR solution, ϕ_2 in (2.35.2) is calculated from an RR solution. As it turns out, ϕ_2 of an RR is larger than ϕ_2 of an MR for the same values of M_0 and θ_w . Figure 2.14 also indicated that $H_{t,\max}(\text{RR}) < H_{t,\max}(\text{MR})$ and $H_{t,\min}(\text{RR}) < H_{t,\min}(\text{MR})$.

It is very important to note that an RR wave configuration is still stable when its reflected shock wave hits the reflecting wedge surface, i.e., $H_t(\text{RR}) < H_{t,\min}(\text{RR})$, since the mechanism which causes the MR wave configuration to become unstable when $H_t(\text{MR}) < H_{t,\min}(\text{MR})$ (recall the analysis in Sect. 2.3.1) does not exist in the RR-case.

The dependence of $H_{t,\max}(\text{MR})/\ell_w$ and $H_{t,\min}(\text{MR})/\ell_w$ on ϕ_1 for $M_0 = 5$ (ℓ_w is the length of the slope of the reflecting wedge) is shown in Fig. 2.20. The two vertical dashed lines indicate the RR \rightleftharpoons MR transition values, $\phi_1^N = 30.3^\circ$ and $\phi_1^D = 39.9^\circ$ as obtained from the detachment and the von Neumann transition criteria, respectively. The two horizontal dashed-dotted lines are the upper and the lower limits of RR, i.e., $H_{t,\max}(\text{RR})$ and $H_{t,\min}(\text{RR})$. An MR-configuration can exist only in the domain bounded by the two solid lines. The flow becomes unstarted if the parameters H_t and ϕ_1 lie below $H_{t,\min}(\text{MR})/\ell_w$.

The calculated heights and locations of the Mach stem for $M_0 = 4.96$ and $\theta_w = 25^\circ$ (which correspond to a point inside dual-solution domain) for $w = 1$ is shown in Fig. 2.21. The Mach stem height decreases

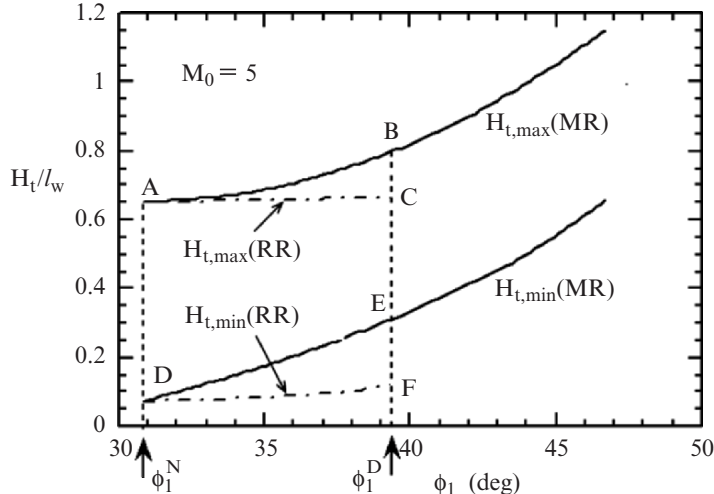


Fig. 2.20. Dependence of the normalized upper and lower limit values of H_t for both RR and MR, on the incident shock wave angle, ϕ_1 , and domains where RR and MR wave configurations are either stable or unstable for $M_0 = 5$

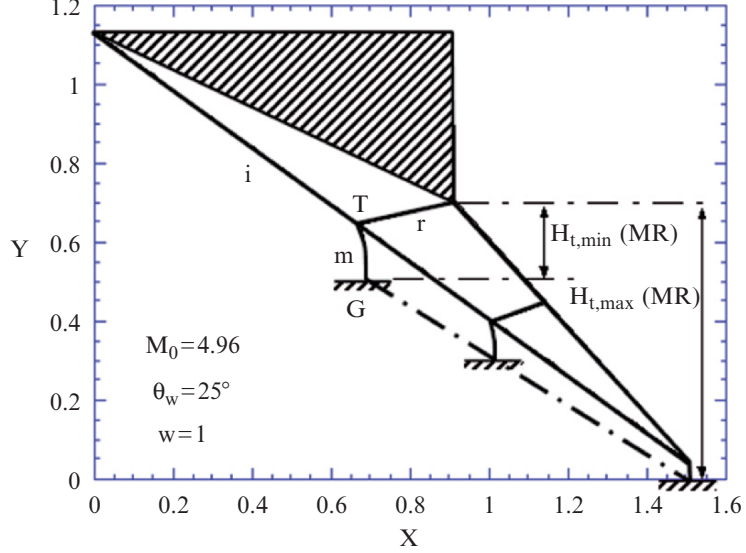


Fig. 2.21. Analytical predictions of the shape and location of Mach reflection wave configuration in the domain $H_{t,\min}(\text{MR}) < H_t < H_{t,\max}(\text{MR})$ for $w = 1$, $M_0 = 4.96$ and $\theta_w = 25^\circ$

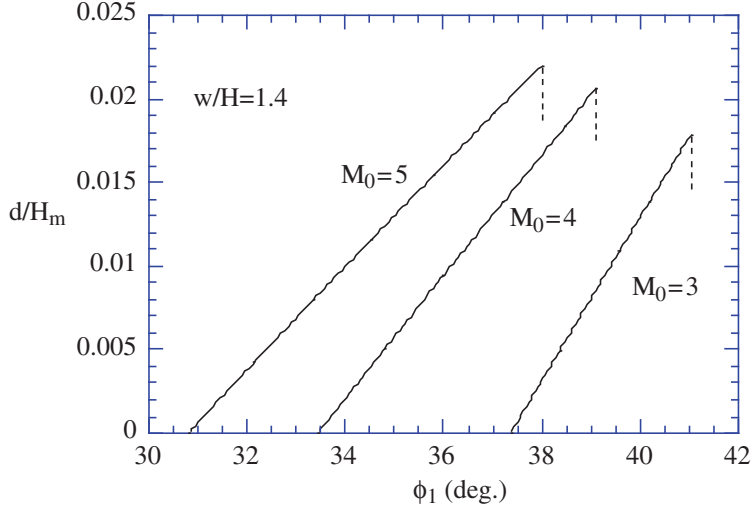


Fig. 2.22. Dependence of the normalized horizontal shift of Mach stem, d/H_m , on the incident shock wave angle, ϕ_1 , for $w/H = 1.4$ and different values of M_0

monotonously as H_t increases, and reaches the maximum and minimum values at $H_t = H_{t,\min}(\text{MR})$ and $H_t = H_{t,\max}(\text{MR})$, respectively.

Figure 2.22 reveals that the dependence of the ratio of the horizontal maximum shift of the foot of the Mach stem to the Mach stem height, d/H_m ,

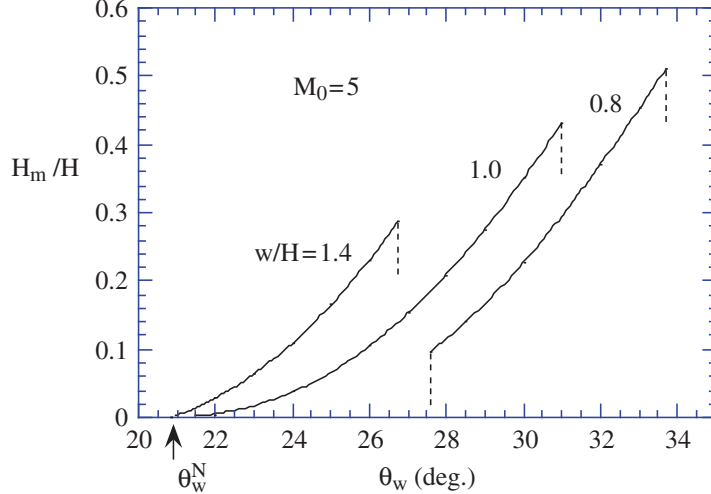


Fig. 2.23. Dependence of the normalized Mach stem height, H_m / H , on the reflecting wedge angle, θ_w , for different values of w/H with the upper and the lower limits (vertical dashed lines) for $M_0 = 5$

on ϕ_1 is almost linear. The maximum value of d/H_m is about 0.02, which implies that the curvatures of Mach stem are indeed very small. These results are consistent with experimental observations. This fact could explain why many investigators who assumed a straight Mach stem did not introduce a pronounced error, although the Mach stem cannot be straight. (A straight Mach stem can be theoretically obtained only at $\phi_1 = \phi_1^N$, but according to the present model under this condition $H_m = 0$).

Figure 2.23 presents the dependence of H_m / H on θ_w for $M_0 = 5$ and different geometrical ratios of w/H . For $w/H = 1.4$ and 1.0, the Mach stem heights smoothly approach zero at the von Neumann point with different slopes. However, for $w/H = 0.8$, the Mach stem height does not approach zero, and instead, it reaches its minimum value $H_m / H = 0.1$, beyond which H_t becomes greater than $H_{t,\max}(\text{MR})$. The vertical dashed lines indicate the maximum values of the Mach stem heights.

Figure 2.24 shows the dependence of $H_{t,\min}(\text{MR})$ on θ_w for $M_0 = 5$. The two vertical dashed lines correspond to the detachment point, $\theta_w^D = 20.9^\circ$, and the von Neumann transition point, $\theta_w^N = 37.8^\circ$, respectively. Based on the previously mentioned analysis, an MR wave configuration could not exist in domains I and II although, based on the three-shock theory, which does not account for the influence of the geometrical condition, an MR wave configuration is theoretically possible there. An MR wave configuration could be established only in domain III. Note that an RR wave configuration can exist in domain I since an RR wave configuration is theoretically possible and stable there.

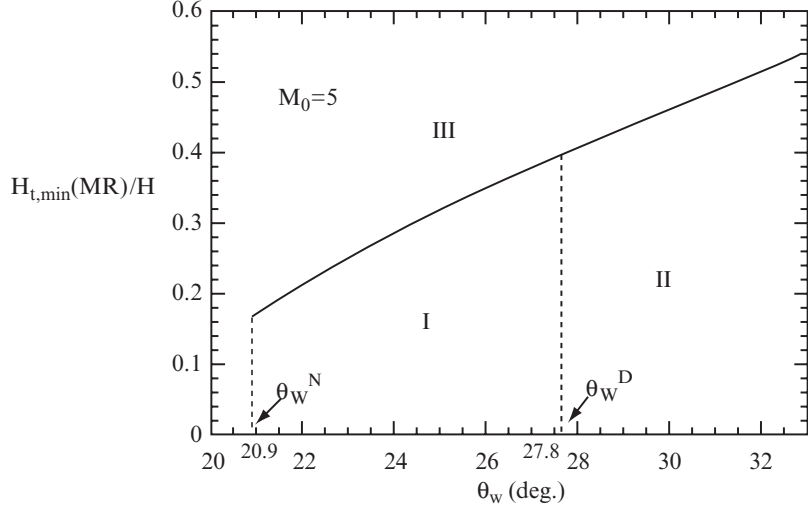


Fig. 2.24. Dependence of $H_{t,\min}$ on the reflecting wedge angle, θ_w , for $M_0 = 5$

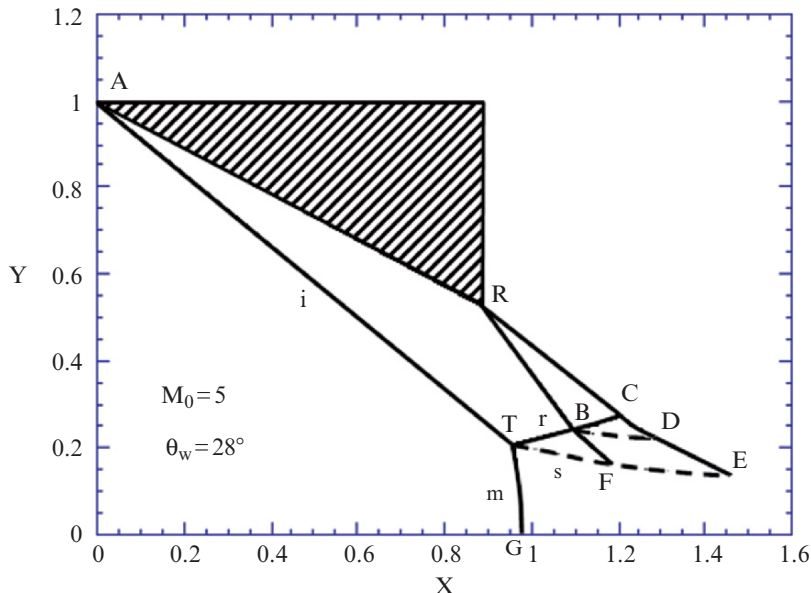


Fig. 2.25. Analytical prediction of a Mach reflection wave configurations for $M_0 = 5$ and $\theta_w = 28^\circ$

The Mach reflection wave configuration for $M_0 = 5$ and $\theta_w = 28^\circ$ is shown in Fig. 2.25. The interaction of the expansion fan that originated at the trailing edge with the reflected shock wave, r , and the slipstream, s , curves the shock wave (BC), the characteristic (CD) and the slipstream (FE).

The sonic throat (point E) is located downstream of point F where the head of the expansion fan intersects the slipstream. (Recall that the basic assumption in Azevedo & Liu's (1993) model was that the sonic throat is located at point F). A mechanism, by which the expansion fan creates the sonic throat and carries information of the upper geometrical conditions through the subsonic pocket to the Mach stem, and hence determines its size and location, is self-explanatory (for details see Sternberg 1959, and Hornung et al. (1979)).

It should be mentioned here that all the foregoing results and discussion were based on the assumption that the MR wave configuration is isolated from downstream influences. Downstream influences could either increase or decrease the Mach stem height. Henderson & Lozzi (1975 and 1979) and Hornung & Robinson (1982) experimentally observed that the Mach stem heights became greater by introducing higher downstream pressures. A study on the influence of downstream pressure on the shock wave reflection is provided subsequently in Sect. 2.4.4.

2.4 Hysteresis Processes in the Regular Reflection \rightleftarrows Mach Reflection Transition

2.4.1 Introduction

As presented in Sect. 1.5.5 there are two extreme conditions for the RR \rightleftarrows MR transition, namely, the detachment condition beyond which an RR wave configuration is theoretically impossible and the von Neumann condition beyond which an MR wave configuration is theoretically impossible. For more details regarding these and other proposed RR \rightleftarrows MR transition criteria see Sect. 1.5. Unlike the detachment condition, which exists for all values of M_0 , the von Neumann condition exists for values of $M_0 \geq M_{0C}$. Molder (1979) calculated the exact value of M_{0C} and found that $M_{0C} = 2.202$ for a perfect diatomic gas ($\gamma = 7/5$) and $M_{0C} = 2.470$ for a perfect monatomic gas ($\gamma = 5/3$). Consequently, while only the transition line arising from the detachment condition exists in the range $1 < M_0 \leq M_{0C}$, two transition lines, arising from the detachment and the von Neumann conditions, exist in the range $M_0 \geq M_{0C}$. The von Neumann transition line emerges from the detachment transition line at $M_0 = M_{0C}$.

By defining the angles of incidence of the incident shock wave that are appropriate to the von Neumann and the detachment conditions as β_i^N and β_i^D , respectively, one obtains that only RR wave configurations are theoretically possible in the range $\beta_i < \beta_i^N$ and only MR wave configurations are theoretically possible in the range $\beta_i > \beta_i^D$. In the intermediate range $\beta_i^N \leq \beta_i \leq \beta_i^D$ both RR and MR wave configurations are theoretically possible. For this reason the intermediate domain, which is bounded by the von Neumann condition, β_i^N , and the detachment condition, β_i^D , is known as the *dual-solution domain*. Note that since $\beta_1 = \beta_1(M_0, \theta_w)$ where M_0 and θ_w are the flow Mach

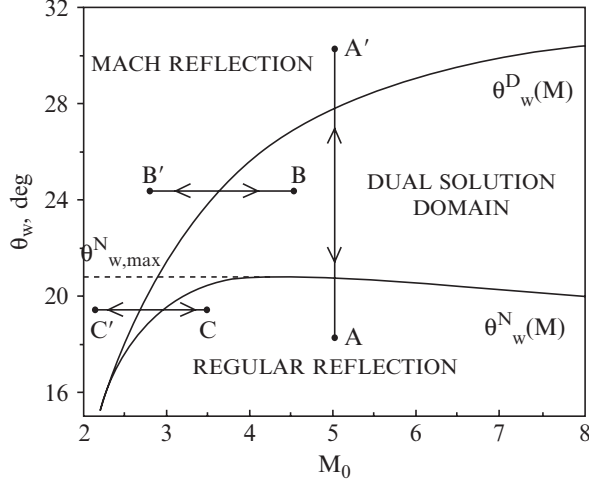


Fig. 2.26. Domains of possible shock wave reflection wave configurations in the (M_0, θ_w) -plane

number and the reflecting wedge angle, respectively, the dual-solution domain can be presented either in the (M_0, β_1) – or the (M_0, θ_w) -planes.

The dual-solution domain in the (M_0, θ_w) -plane is shown in Fig. 2.26. As just mentioned the entire (M_0, θ_w) -plane can be divided into three domains:

- A domain inside which only RR wave configurations are theoretically possible.
- A domain inside which only MR wave configurations are theoretically possible.
- A domain inside which both RR and MR wave configurations are theoretically possible.

The existence of conditions beyond which only RR or only MR wave configurations are theoretically possible and the existence of an intermediate domain inside which both RR and MR wave configurations are theoretically possible led Hornung et al. (1979) to hypothesize that a hysteresis could exist in the $RR \rightleftarrows MR$ transition process.

An inspection Fig. 2.26 indicates that two general hysteresis processes are theoretically possible:

- A *wedge-angle-variation-induced hysteresis*. In this hysteresis process, the flow Mach number is kept constant while the reflecting wedge angle is changed.
- A *flow-Mach-number-variation-induced hysteresis*. In this hysteresis process, the reflecting wedge angle is kept constant while the flow-Mach number is changed.

It is noted that since $\beta_1 = \beta_1(M_0, \theta_w)$ these two hysteresis processes are, in fact, *angle-of-incidence-variation-induced hysteresis processes*.

Henderson & Lozzi (1975, 1979) and Hornung & Robinson (1982) failed in their experimental attempts to record the wedge-angle-variation-induced hysteresis process and concluded that the RR wave configuration is unstable inside the dual-solution domain, and that as a consequence the RR \rightleftharpoons MR transition (i.e., both the RR \rightarrow MR and the MR \rightarrow RR transitions) occurs at the von Neumann condition. Hornung & Robinson (1982) summarized that the RR \rightleftharpoons MR transition occurs at the von Neumann criterion for $M_0 \geq M_{0C}$, and at the sonic condition, which is very close to the detachment criterion for $M_0 \leq M_{0C}$.

Teshukov (1989) analytically proved, by using a linear stability technique, that the RR wave configuration is stable inside the dual-solution domain. Li & Ben-Dor (1996) analytically proved, by applying the principle of minimum entropy production, that the RR wave configuration is stable in most of the dual-solution domain. The results of Li & Ben-Dor (1996) are shown in Fig. 2.27 where the dual-solution domain is drawn in the (M_0, β_1) -plane. The line β_1^S separates the dual-solution domain into two subdomains inside which the RR wave configuration is stable or not.

- RR is stable in the domain $\beta_1^N < \beta_1 < \beta_1^S$ and
- RR is unstable in the domain $\beta_1^S < \beta_1 < \beta_1^D$, which is extremely narrow.

Hence, practically the RR could be considered as stable in the entire dual-solution domain.

Chpoun et al. (1995) were the first to record experimentally both stable RR wave configurations inside the dual-solution domain and a wedge-angle-

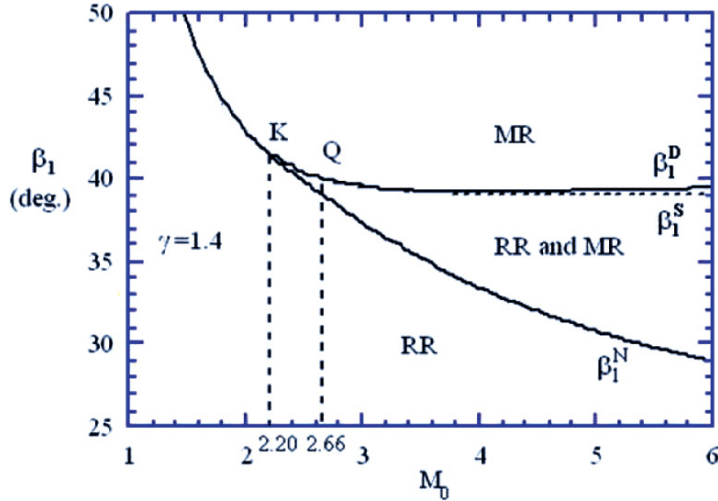


Fig. 2.27. The dual-solution domain in the (M_0, β_1) -plane with the line, β_1^S , separating the domains of stable and unstable RR wave configuration

variation-induced hysteresis in the RR \rightleftharpoons MR transition. As will be discussed subsequently, it was shown later, by some investigators, that the experimental results of Chpoun et al. (1995) were not purely two-dimensional. These investigators claimed and showed that the hysteresis process that was recorded by Chpoun et al. (1995) was influenced and promoted by three-dimensional effects.

Vuillon et al. (1995) were the first to obtain numerically stable RR and MR wave configurations for the same flow-Mach numbers and reflecting wedge angles but different aspect ratios of the geometrical set-up inside the dual-solution domain.

The above-mentioned experimental and numerical findings that the RR wave configuration is stable inside the dual-solution domain and the experimental finding that a hysteresis in the RR \rightleftharpoons MR transition indeed exists, re-initiated the interest of the scientific community in the reflection process in steady flows, in general, and the hysteresis process in the RR \rightleftharpoons MR transition, in particular.

It is important to note here that in spite of the fact that the early reason for studying the hysteresis process in the RR \rightleftharpoons MR transition was purely academic, it turned out that the existence of the hysteresis process has an important impact on flight performance at high supersonic and hypersonic velocities. Consequently, there is a clear aeronautical and aerospace engineering interest in better understanding this complex phenomenon. Some of the geometries that were investigated resemble geometries of supersonic/hypersonic intakes. The findings regarding the existence of hysteresis loops could be relevant to flight performances of vehicles flying at supersonic and hypersonic speeds. The possible dependence of the flow pattern that is established inside an intake, in general, and the accompanied pressure distribution, in particular, on the preceding variations in the speed of flight of a supersonic/hypersonic aircraft should be accounted for in designing intakes and flight conditions for supersonic and hypersonic vehicles. Especially because different flow fields would result in different flow conditions that could significantly affect the combustion process and the entire performance of the vehicle.

2.4.2 Hysteresis Processes in the Reflection of Symmetric Shock Waves

Wedge-Angle-Variation-Induced Hysteresis

As mentioned earlier, Chpoun et al. (1995) were the first to experimentally record the wedge-angle-variation-induced hysteresis in the RR \rightleftharpoons MR transition and thereby verify Hornung et al.'s (1979) hypothesis. An example from the experimental results of Chpoun et al. (1995) is shown in Fig. 2.28 in the (β_i, β_r) -plane, where β_i and β_r are the wave angles of the incident and reflected shock waves, respectively. Note that based on the notation defined in Fig. 1.9 $\beta_i \equiv \phi_1$ and $\beta_r \equiv \phi_2$. Experimentally recorded MR and RR

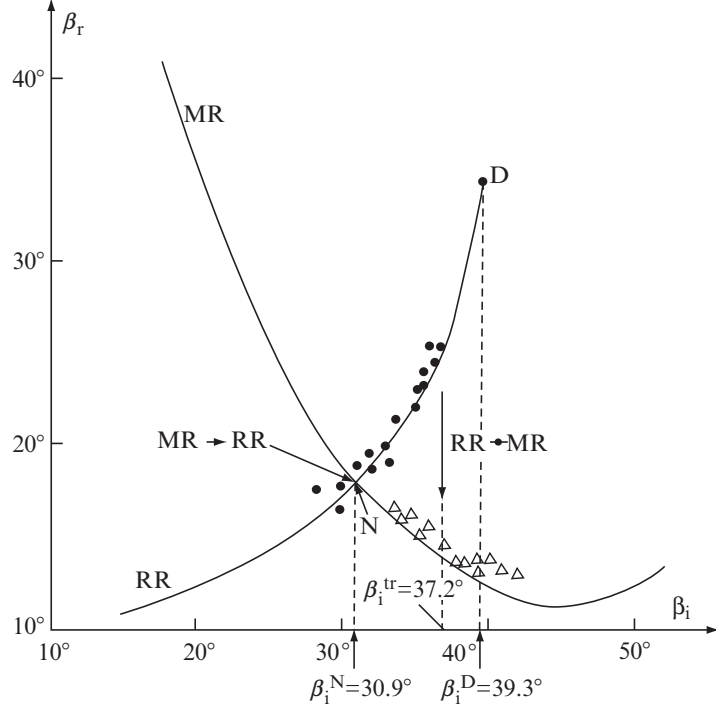


Fig. 2.28. The wedge-angle-variation-induced hysteresis process in the $RR \rightleftharpoons MR$ transition in the (β_i, β_r) -plane as recorded experimentally by Chpoun et al. (1995)

wave configurations are marked with open triangles and closed circles, respectively. The theoretical von Neumann and the detachment transition angles for the flow-Mach number of the experiment, $M_0 = 4.96$, are $\beta_i^N = 30.9^\circ$ and $\beta_i^D = 39.3^\circ$, respectively. The experimental results reveal that the $MR \rightarrow RR$ transition occurred very close to the appropriate theoretical von Neumann angle, i.e., $\beta_i^{tr}(MR \rightarrow RR) \cong \beta_i^N = 30.9^\circ$, while the reversed $RR \rightarrow MR$ transition, took place at about $\beta_i^{tr}(RR \rightarrow MR) = 37.2^\circ$, which is 2.1° smaller than the appropriate theoretical detachment angle. Consequently, a hysteresis phenomenon in the $RR \rightleftharpoons MR$ transition is clearly evident. The very good agreement between the experimental results and the von Neumann criteria and the poor agreement with the detachment criterion might suggest that perhaps the above-mentioned three-dimensional effects (to be discussed in more details subsequently) have a larger influence on the $RR \rightarrow MR$ transition than on the $MR \rightarrow RR$ transition and that the RR wave configuration is perhaps less stable than the MR wave configuration inside the dual-solution domain.

Schlieren photographs of RR and MR wave configurations that illustrate the just-mentioned wedge-angle-variation-induced hysteresis process are shown in Fig. 2.29. Figure 2.29a shows an MR wave configuration at

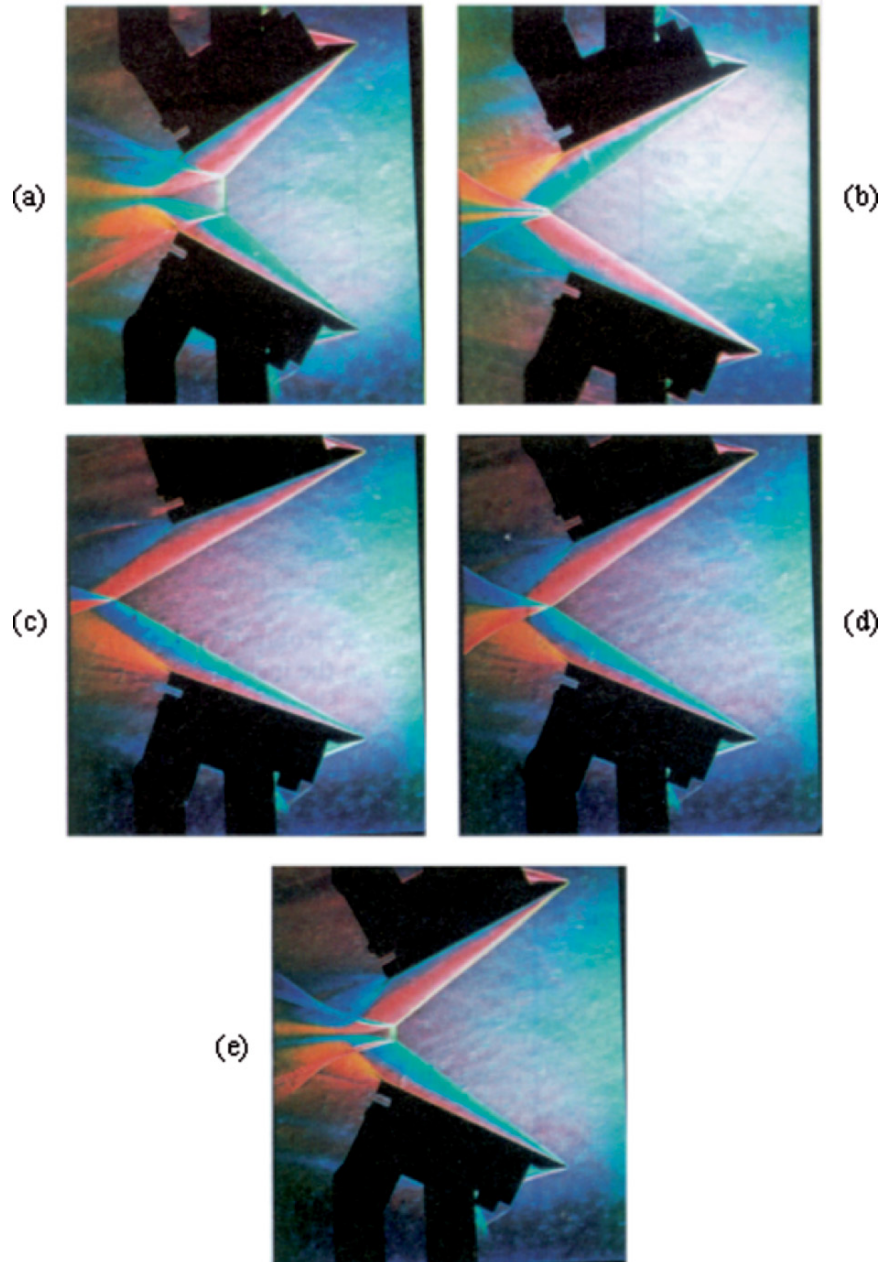


Fig. 2.29. Schlieren photographs from Chpoun et al.'s (1995) experimental investigation illustrating the hysteresis phenomenon in the $\text{RR} \rightleftharpoons \text{MR}$ transition process. (a) An MR at $\beta_i \cong 42^\circ > \beta_i^D$, (b) an MR at $\beta_i^N < \beta_i \cong 34.5^\circ < \beta_i^D$, (c) an RR at $\beta_i \cong 29.5^\circ < \beta_i^N$, (d) an RR at $\beta_i^N < \beta_i \cong 34.5^\circ < \beta_i^D$, (e) an MR at $\beta_i \cong 37.5^\circ < \beta_i^D$. Note that the MR shown in (b) and the RR shown in (d) have the same initial conditions ($M_0 = 4.96$ and $\beta_i \cong 34.5^\circ$)

$\beta_i \cong 42^\circ > \beta_i^D$. When β_i was decreased the MR wave configuration was maintained as shown in Fig. 2.29b where $\beta_i^N < \beta_i \cong 34.5^\circ < \beta_i^D$. When β_i was decreased below β_i^N to $\beta_i \cong 29.5^\circ < \beta_i^N$ the MR wave configuration was terminated and an RR wave configuration was obtained (Fig. 2.29c). When the process was reversed and β_i was increased beyond β_i^N back to $\beta_i^N < \beta_i \cong 34.5^\circ < \beta_i^D$, the wave configuration remained an RR (Fig. 2.29d). Note that the MR wave configuration, shown in Fig. 2.29b, and the RR wave configuration, shown in Fig. 2.29d, had practically the same initial conditions, i.e., $M_0 = 4.96$ and $\beta_i \cong 34.5^\circ$. The fact that both the RR and the MR wave configurations were stable, clearly verifies the fact that a hysteresis exists in the $RR \rightleftarrows MR$ transition process. When β_i was further increased to $\beta_i \cong 37.5^\circ < \beta_i^D$ the RR wave configuration was suddenly terminated and an MR wave configuration was formed (Fig. 2.29e). It is noted here that Ivanov et al. (1998b and 1998c) experimentally recorded a similar hysteresis process a few years later.

Chpoun et al. (1994), using a Navier–Stokes solver, were the first to numerically simulate and thereby verify the existence of a wedge-angle-variation-induced hysteresis in the $RR \rightleftarrows MR$ transition. Unfortunately, however, since their study was published in a French journal it did not catch the attention of the relevant scientific community. Ivanov et al. (1995) conducted, independently, a direct simulation Monte Carlo (DSMC) based study of the phenomenon and confirmed the existence of the hysteresis process. Following their numerical study many investigators using a variety of numerical codes simulated the hysteresis process. Additional direct simulation Monte Carlo (DSMC) calculations were published by Ivanov et al. (1996a), Ben-Dor et al. (1997) and Ivanov et al. (1998c); Ivanov et al. (1996a) also presented high resolution FCT scheme calculations; calculations based on the TVD scheme were presented by Shirozu & Nishida (1995); calculations based on Godunov and van Leer were conducted by Chpoun & Ben-Dor (1995); calculations based on the HLLE MUSCL TVD scheme were conducted by Ivanov et al. (1998c); and calculations based on Steger and Warming flux splitting scheme were presented by Ben-Dor et al. (1999). It is noted here that unlike the experiments, which were partially affected by three-dimensional effects, the numerical simulations were all purely two-dimensional.

A numerical illustration of the wedge-angle-variation-induced hysteresis, for $M_0 = 5$, is shown in Fig. 2.30. This Euler simulation was carried out using a high-order finite volume MUSCL TVD scheme with HLLE approximate Riemann solver. Details of the numerical code could be found in Ivanov et al. (1998c). The simulation starts with a wedge angle $\theta_w = 20^\circ$ that corresponds to an incident shock angle $\beta_i = 29.8^\circ$ for which, as can be seen in frame (1), an RR wave configuration is obtained. Upon increasing the wedge angle (or the angle of incidence) the RR wave configuration is maintained (frames 2–4) until it is suddenly changed to an MR wave configuration between $\theta_w = 27.9^\circ$ (frame 5) and $\theta_w = 28^\circ$ (frame 6). If at this point the direction of changing the wedge angle is reversed the MR wave configuration is seen to persist

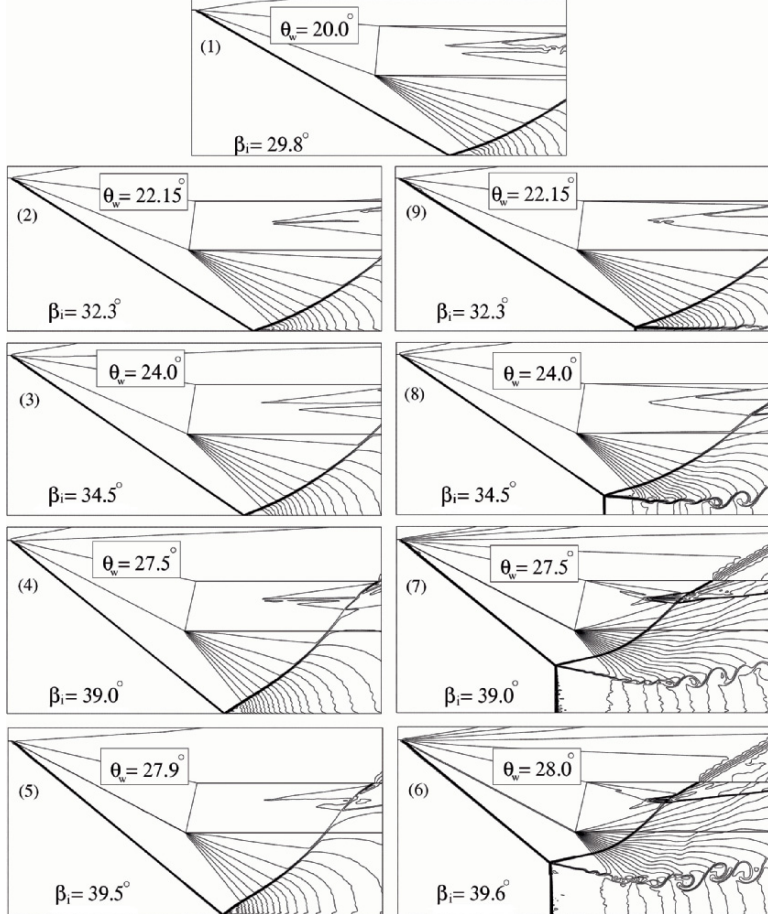


Fig. 2.30. Wedge-angle-variation-induced hysteresis for $M_0 = 5$

(frames 7–9) until it is changed back to an RR wave configuration between $\theta_w = 22.15^\circ$ (frame 9) and $\theta_w = 22.1^\circ$ (not shown in the figure). Finally, when the wedge angle is decreased to its initial value, $\theta_w = 20^\circ$, a steady RR wave configuration, identical to that shown in frame (1), is again obtained. The numerically obtained transition angles do not agree exactly with the appropriate theoretical von Neumann ($\theta_w^N = 20.9^\circ$) and detachment ($\theta_w^D = 27.8^\circ$) wedge angles. The numerical MR \rightarrow RR transition angle is one degree larger than the theoretical von Neumann angle. This is probably because the very small Mach stem, near the von Neumann transition angle, is not resolved well enough in the computations. Grid refinement studies confirmed that the numerically obtained MR \rightarrow RR transition angle approached the theoretical value of $\theta_w^N = 20.9^\circ$ when the grid was refined (see Fig. 2.31 where the normalized Mach stem height versus the wedge angle is given). The minimum

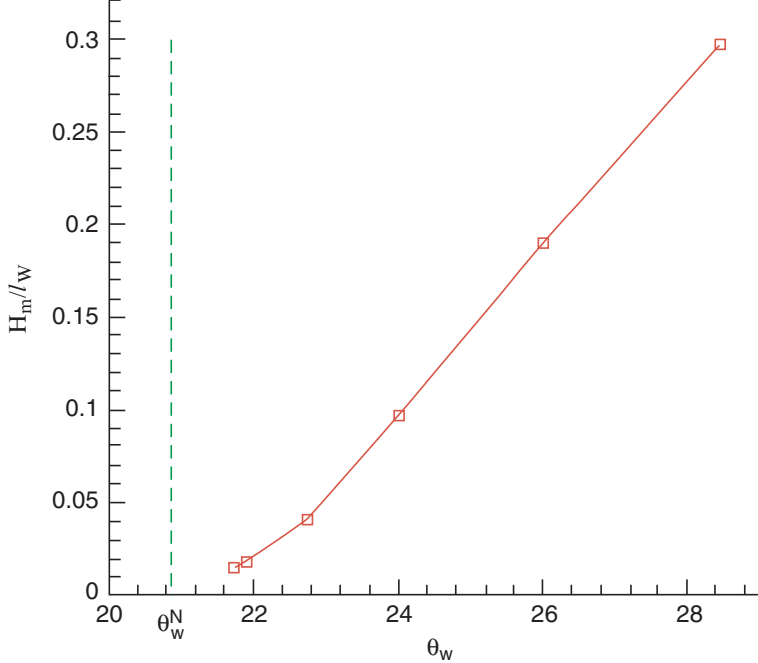


Fig. 2.31. The calculated normalized Mach stem height versus the reflecting wedge angle

normalized Mach stem height $H_m/w \approx 1\%$ was obtained on a very fine grid (the grid cell size in the vertical direction was $\Delta y/\ell_w = 0.001$).

Unlike the MR \rightarrow RR transition angle, the RR \rightarrow MR transition angle does not depend on the grid resolution for fine enough grids but strongly depends on the numerical dissipation inherent in any shock-capturing solver. Large numerical dissipation or low order reconstruction could result in significant differences between the numerical and the theoretical values of the transition angles. For example, the RR \rightarrow MR transition angle, for $M_0 = 4.96$, in the computations of Chpoun & Ben-Dor (1995) who used an INCA code, was 33° , i.e., more than 5° larger than $\theta_w^D = 27.7^\circ$. Applying a high-order shock-capturing scheme resulted in a transition wedge angle of 27.95° , which was only 0.25° larger than the theoretical value.

Three-Dimensional Effects

Researchers who wondered why the hysteresis phenomenon was recorded in the course of some experimental investigations and not in others have forwarded two possible reasons:

- The extent of the experimental hysteresis depends on the type of the wind tunnel in which the experiments were conducted. Fomin et al. (1996),

Ivanov et al. (1998a and 1998b) showed, experimentally, that while in a closed test section wind tunnel the hysteresis was hardly detected, a clear hysteresis was obtained in an open test section wind tunnel. Not surprisingly Henderson & Lozzi (1975, 1979), Hornung et al. (1979) and Hornung & Robinson (1982) who did not detect the hysteresis used closed section wind tunnels, while Chpoun et al. (1995) and Fomin et al. (1996) who did detect it used open jet type wind tunnels.

- Three-dimensional edge effects affect the experiment and promote the hysteresis. Skews et al. (1996), Skews (1997 and 1998) and Ivanov et al. (1998a, 1998b and 1998c), claimed and showed that the experimental investigations, in which hysteresis processes were recorded in the RR \rightleftharpoons MR transition, were all contaminated by three-dimensional edge effects and hence could not be considered as purely two-dimensional. Skews (2000) showed that three-dimensional edge effects are evident in actual wave configurations associated with the reflection of plane shock waves over plane wedges.

It should be noted here that using the same reflecting wedge (i.e., same aspect ratios) a hysteresis was observed in an open test section wind tunnel by Chpoun et al. (1995) and was not observed in a closed test section wind tunnel by Ivanov et al. (1998a and 1998b), in spite of the fact that very similar if not identical three-dimensional effects, that mainly depend on the aspect ratios of the reflecting wedge, were present in both cases. These results clearly indicate that three-dimensional effects by themselves are not enough to promote the hysteresis and that the type of the wind tunnel, i.e., open or closed test section, has a significant, and unfortunately not yet understood, role in the occurrence of hysteresis in the RR \rightleftharpoons MR transition in steady flows.

Figure 2.32 shows numerically generated schlieren-like photographs of RR (a and b) and MR (c and d) wave configurations in a purely two-dimensional flow, on the left side, and a supposedly two-dimensional flow, which is affected by three-dimensionally edge effects, on the right side, for $M_0 = 4$. Beside the clear differences between the two-dimensional and the three-dimensionally affected wave configurations, the dramatic shortening of the Mach stem height, owing to the three-dimensional edge effects, should be noted (compare parts c and d). Consequently, the numerically calculated height of a purely two-dimensional MR wave configuration, for a given geometry and flow conditions, could be used as a measure of the two-dimensionality of the actual MR wave configuration that is recorded experimentally.

Kudryavtsev et al. (1999) demonstrated numerically and experimentally that increasing the aspect ratio could reduce the influence of the three-dimensional edge effects. Figure 2.33 indicates that by increasing the aspect ratio, the actual Mach stem height approaches the numerically calculated height, which is appropriate to a purely two-dimensional MR wave configuration. Hence, an actual MR wave configuration cannot be considered as free of three-dimensional edge effects as long as the height of its Mach stem

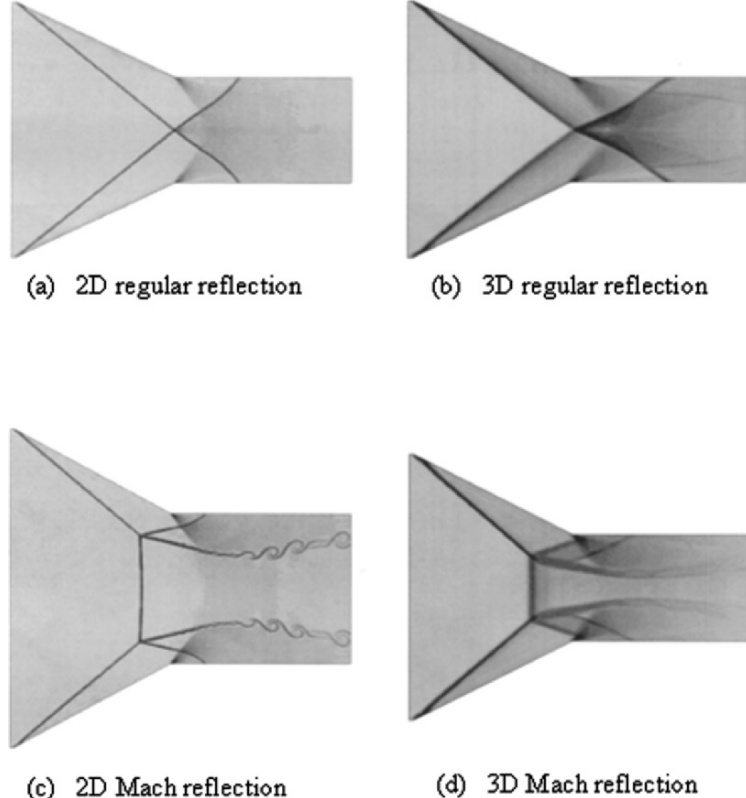


Fig. 2.32. Numerically generated schlieren-like photographs of RR (on the *top*) and MR (on the *bottom*) wave configurations in a purely two-dimensional flow (on the *left*) and a supposedly two-dimensional flow, which is affected by three-dimensionally edge effect (on the *right*) for $M_0 = 4$. Parts a and b: $\beta_i = 39^\circ$; Parts c and d: $\beta_i = 40^\circ$

is smaller than that appropriate to a calculated purely two-dimensional MR wave configuration. This condition is a necessary but not a sufficient one for ensuring a purely two-dimensional MR wave configuration.

Flow-Mach-Number-Variation-Induced Hysteresis

As mentioned earlier keeping the wedge angle constant and changing the oncoming flow-Mach number could also lead to a hysteresis process in the $RR \rightleftharpoons MR$ transition. Figure 2.26 reveals that two possible hysteresis processes exist for this case:

- If $\theta_w > \theta_{w,\max}^N$ the Mach number could be changed along the path B–B'–B from a value inside the dual-solution domain where both RR and

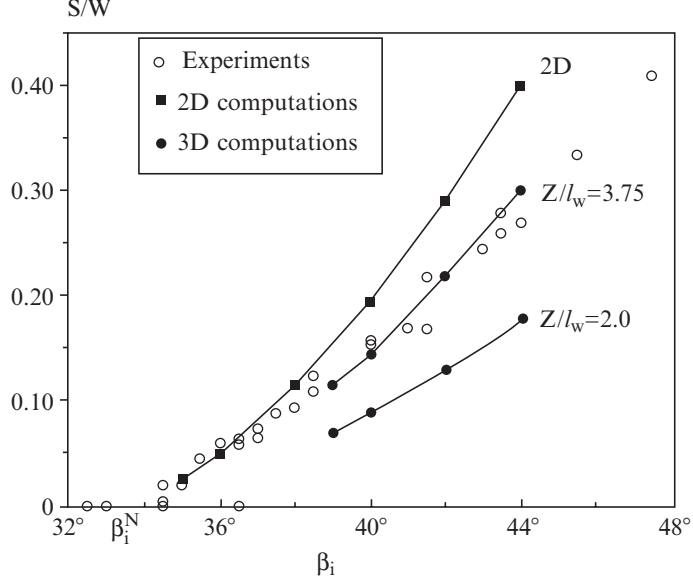


Fig. 2.33. Dependence of the Mach stem height on the aspect ratio. Equality between the Mach stem height of an actual Mach reflection and the one numerically calculated, using a 2D code, is a necessary but not sufficient condition for the actual Mach reflection to be two-dimensional, i.e., free of three-dimensional effects

MR wave configurations are theoretically possible, to a value outside the dual-solution domain for which only an MR wave configuration is theoretically possible and then back to the initial value. If one starts inside the dual-solution domain with an RR wave configuration¹ then after transition to an MR wave configuration, the wave configuration never returns to be an RR wave configuration because the MR \rightarrow RR transition is not compulsory on the return path. Note that the above-described loop does not represent a full hysteresis loop, though both RR and MR wave configurations could be observed for the same values of the reflecting wedge angle and the flow-Mach number.

- If $\theta_w < \theta_{w,\max}^N$ the Mach number could be changed from a value for which only an RR wave configuration is theoretically possible to a value for which only an MR wave configuration is theoretically possible and then back to the initial value crossing both $\theta_w^N(M)$ and $\theta_w^D(M)$ curves (see the

¹ Depending on the way by which the flow is initiated numerically, either an RR or an MR wave configuration can be established inside the dual-solution domain. If the computation is initiated with an oncoming supersonic flow having a Mach number, M_0 , a stable RR will be established. However, if the computation is initiated with an oncoming normal shock wave behind which the induced flow has a Mach number equal to M_0 , a stable MR will be established.

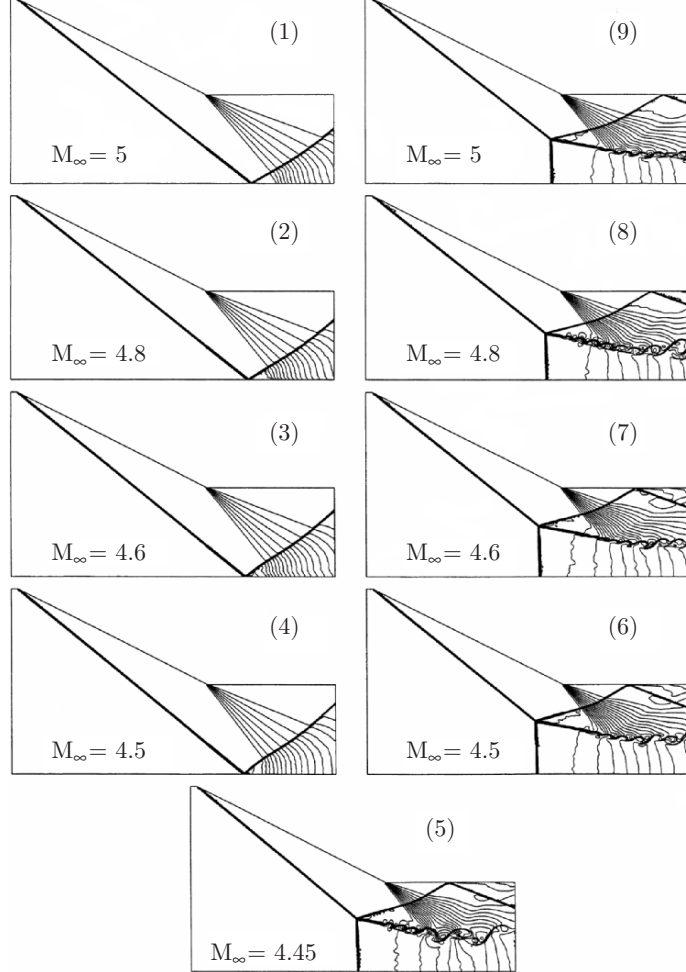


Fig. 2.34a.

path C–C'–C in Fig. 2.26). Consequently, in similar to the wedge-angle-variation-induced hysteresis, a full hysteresis loop is obtained for this case, with a return to the initial wave configuration.

The above two cases were numerically investigated by Ivanov et al. (2001). Typical results for the former case ($\theta_w > \theta_{w,\max}^N = 20.92^\circ$) are shown in Fig. 2.34b. The reflecting wedge angle was kept constant at $\theta_w = 27^\circ$ while the oncoming flow-Mach number, M_0 , was first decreased from 5 to 4.45 and then increased back to its initial value. The first frame, with $M_0 = 5$, shows an RR wave configuration inside the dual-solution domain. When M_0 was decreased, the detachment transition line, $\theta_w^D(M)$, beyond which an RR wave

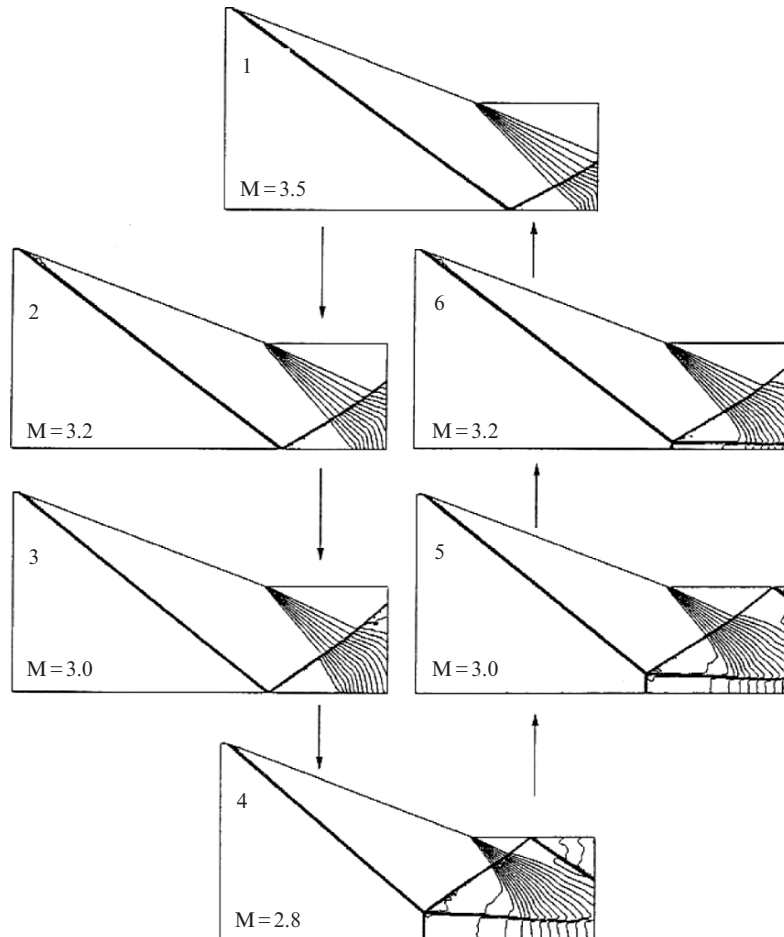


Fig. 2.34b. Flow-Mach-number-variation-induced hysteresis for: (a) $\theta_w = 27^\circ$ and (b) $\theta_w = 20.5^\circ$

configuration is theoretically impossible, was reached at $M_0 = 4.57$. The RR \rightarrow MR transition took place between frames (4) and (5) when M_0 was changed from 4.5 to 4.45, i.e., at $M_0 = 4.475 \pm 0.025$. This numerical value is in reasonable agreement with the theoretical value of 4.57. The existence of RR wave configuration slightly beyond the theoretical limit was observed also in other numerical simulations of the wedge-angle-variation-induced hysteresis and could be attributed to the influence of numerical viscosity that is inherent in shock-capturing codes. Once an MR wave configuration was established, M_0 was increased back to its initial value of $M_0 = 5$. Since theoretically an MR wave configuration can exist for values of M_0 , which are inside the dual-solution domain, the reversed transition, MR \rightarrow RR, did not

take place at the detachment transition line. As a result, two different wave configurations, an RR and an MR, were obtained for identical flow conditions (same values of M_0 and θ_w). See e.g., the pairs of the frames (1) and (9), (2) and (8) and (3) and (7) and (4) and (6) in which the first frame shows an RR wave configuration and the second one shows an MR wave configuration.

Typical results for the latter case ($\theta_w < \theta_{w,\max}^N = 20.92^\circ$) are shown in Fig. 2.34b. The reflecting wedge angle was kept constant at $\theta_w = 20.5^\circ$. For this value of θ_w , the flow Mach number values that correspond to the von Neumann criterion are 3.47 and 6.31 while that corresponding to the detachment criterion is 2.84. The oncoming flow Mach number was decreased from $M_0 = 3.5$ to $M_0 = 2.8$ and then increased back to the initial value. Some frames showing the sequence of events that were encountered are shown in Fig. 2.34b. The RR \rightarrow MR transition occurred between the frames appropriate to $M_0 = 2.9$ (not shown in the figure) and $M_0 = 2.8$ in close agreement with the theoretical value, while the reversed MR \rightarrow RR transition was observed between the frames appropriate to $M_0 = 3.2$ and $M_0 = 3.3$ (not shown in the figure), which is slightly earlier than the theoretical value. This disagreement could be attributed to the very small height of the Mach stem near the von Neumann criterion, which made its numerical resolution very difficult.

It should be noted here that Onofri & Nasuti (1999) conducted an independent investigation of the flow-Mach-number-variation-induced hysteresis. The results obtained by them were in close agreement with those obtained by Ivanov et al. (2001).

2.4.3 Hysteresis Process in the Reflection of Asymmetric Shock Waves

The reflection process of asymmetric shock waves was investigated experimentally by Chpoun & Lengrand (1997), both analytically and experimentally by Li et al. (1999) and numerically by Ivanov et al. (2002).

Overall Wave Configuration

Li et al. (1999) conducted a detailed analysis of the two-dimensional reflection of asymmetric shock waves in steady flows. In similar to the interaction of symmetric shock waves in steady flows, the interaction of asymmetric shock waves leads to two types of overall wave configurations, namely; an overall regular reflection (oRR) and an overall Mach reflection (oMR). These two overall wave configurations are shown schematically in Fig. 2.35a, b, respectively.

An oRR wave configuration (Fig. 2.35a) consists of two incident shock waves (i_1 and i_2), two reflected shock waves (r_1 and r_2), and one slipstream (s). These five discontinuities meet at a single point (R). The slipstream results

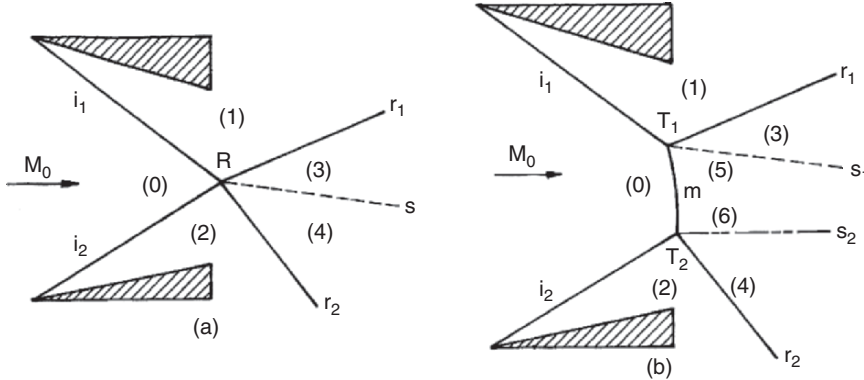


Fig. 2.35. Schematic illustration of the two general overall wave configurations which could be obtained from the reflection of asymmetric shock waves in steady flows: (a) An overall regular reflection (oRR); and (b) an overall Mach reflection (oMR)

from the fact that the streamlines of the oncoming flow pass through two unequal shock wave sequences, i.e., the (i_1, r_1) - and (i_2, r_2) -sequences. If the flow deflection angles are $\theta_1, \theta_2, \theta_3$ and θ_4 through the i_1, i_2, r_1 and r_2 shock waves, respectively, then the boundary condition for an oRR is $\theta_1 - \theta_3 = \theta_2 - \theta_4 = \delta$. (Recall that in the reflection of symmetric shock waves $\theta_1 = \theta_3$ and $\theta_2 = \theta_4$ and hence $\delta = 0$).

Li et al. (1999) showed that two different oRR wave configurations are theoretically possible:

- An oRR wave configuration that consists of RRs that are both weak, wRR, and hence it is labelled as oRR[wRR + wRR]
- An oRR wave configuration that also consists of two RRs of which one is weak, wRR, and the other is strong, sRR, and hence it is labelled as oRR[wRR + sRR].

Figure 2.35b indicates that in addition to the incident and reflected shock waves (i_1, i_2, r_1 and r_2) a common Mach stem (m) appears in an oMR wave configuration. The common Mach stem bridges two triple points (T_1 and T_2) from which two slipstreams (s_1 and s_2) emanate. If the flow deflection angles are again $\theta_1, \theta_2, \theta_3$ and θ_4 through the i_1, i_2, r_1 and r_2 shock waves, respectively, then the boundary conditions for an oMR wave configuration are $\theta_1 - \theta_3 = \delta_1$ and $\theta_2 - \theta_4 = \delta_2$. (Recall that in the reflection of symmetric shock waves $\theta_1 = \theta_2$ and $\theta_3 = \theta_4$ and hence, $\delta_1 = \delta_2$).

The theoretically possible wave configurations, which can result from the reflection of asymmetric shock waves, could be determined with the aid of shock polars (for details see Li et al. (1999)). Figure 2.36 illustrate seven shock polar combinations. For all the combinations, the flow Mach number

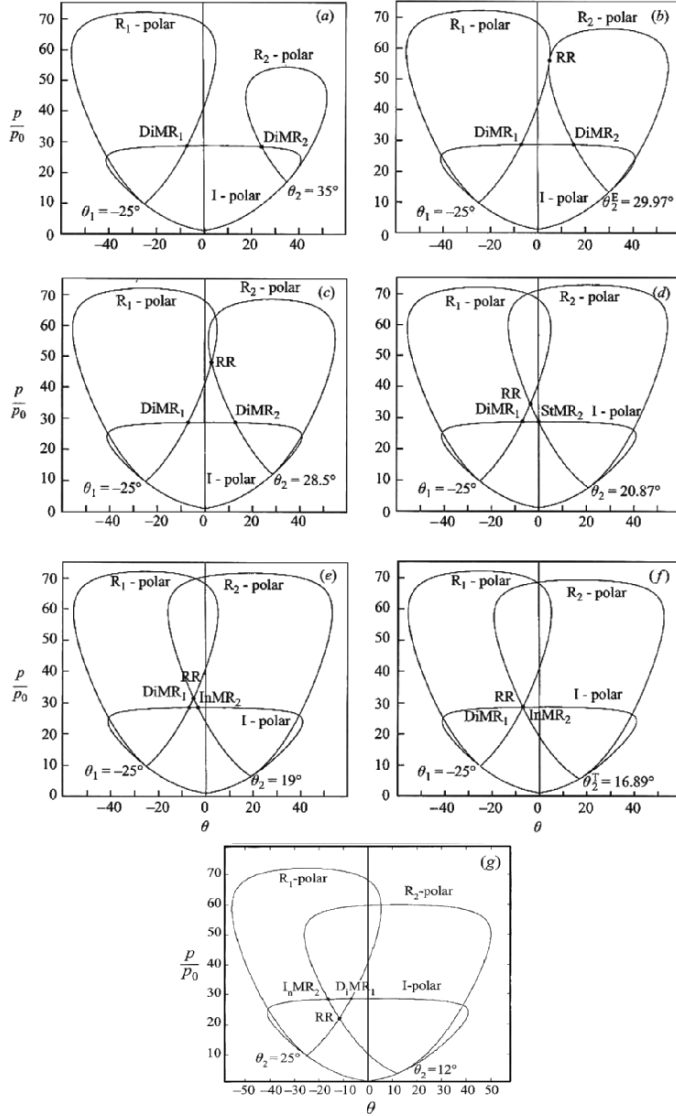


Fig. 2.36. Pressure-deflection polar combinations illustrating various theoretically possible solutions in the reflection of asymmetric shock waves for a fixed flow Mach number, $M_0 = 4.96$, and one fixed wedge angle $\Theta_{w1} = 25^\circ$

is $M_0 = 4.96$ and hence the I-polar is identical. Furthermore, since the angle of one reflecting wedge is kept constant at $\theta_{w1} = 25^\circ$, all the R₁-polars are also identical. Note that the intersection of the I- and the fixed R₁-polars in Fig. 2.36a–g predicts a direct-Mach reflection (DiMR). The shock polar combination of Fig. 2.36a is for $M_0 = 4.96$, $\theta_{w1} = 25^\circ$ and $\theta_{w2} = 35^\circ$.

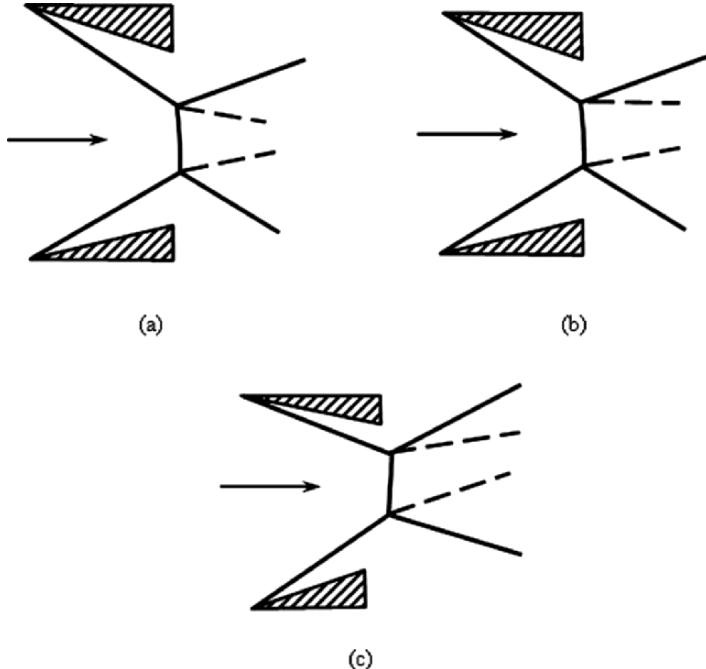


Fig. 2.37. Schematic illustrations of the wave configurations of various overall Mach reflections: (a) an oMR[DiMR + DiMR], i.e., an oMR that consists of two DiMRs, (b) An oMR[DiMR+StMR], i.e., an oMR that consists of one DiMR and one StMR, and (c) An oMR[DiMR + InMR], i.e., an oMR that consists of one DiMR and one InMR

As can be seen the intersection of the R₂- and the I-polars results in a DiMR. Consequently, the shock polar combination shown in Fig. 2.36a represents the solution of an oMR wave configuration that consists of two DiMRs. A schematic illustration of this oMR wave configuration is shown in Fig. 2.37a. Note that since the oMR wave configurations consists of two DiMRs their slip-streams form a converging stream tube. Hence, the subsonic flow behind the Mach stem accelerates, in similar to the situation obtained in the reflection of symmetric shock waves. When θ_{w2} is decreased to 29.97° the shock polars combination shown in Fig. 2.36b is obtained. Here the R₁- and R₂-polars are tangent to each other. As a result, in addition to an oMR wave configuration, similar to that shown in Fig. 2.37a, which consists of two DiMRs (DiMR₁ and DiMR₂) here an oRR wave configuration, at the point where the R₁- and R₂-polars are tangent to each other is also theoretically possible. The shock polar combination shown in Fig. 2.36b is analogous to the detachment condition in the reflection over a single wedge or the reflection of symmetric shock waves (see Sect. 1.5.1). When θ_{w2} is further decreased to 28.5° the shock polar combination shown in Fig. 2.36c is reached. Here again

both an oMR wave configuration which consists of two DiMRs (DiMR_1 and DiMR_2) and an oRR wave configuration are theoretically possible. Upon a further decrease in θ_{w2} , to 20.87° the situation shown in Fig. 2.36d is obtained. In similar to the cases shown in Fig. 2.36b, c, the overall reflection here again can be either an oMR or an oRR. However, unlike the previous cases, where the oMR wave configurations consisted of two DiMRs (DiMR_1 and DiMR_2), here the oMR wave configuration consists of a DiMR_1 and an StMR₂. A schematic illustration of the overall wave configuration corresponding to this case is shown in Fig. 2.37b. Note that the slipstream of the stationary-Mach reflection wave configuration is parallel to the oncoming flow. In similar to the wave configuration shown in Fig. 2.37a the two slipstreams in Fig. 2.37b also form a converging stream tube. A further decrease in θ_{w2} , to 19° results in the situation shown in Fig. 2.36e. Again two solutions are theoretically possible: an oRR or an oMR. However, unlike the previously described case, here the oMR wave configuration consists of a DiMR_1 and an InMR₂. A schematic drawing of the overall wave configuration corresponding to this case is shown in Fig. 2.37c. Note the orientation of the slipstream of the InMR, which is shown in the upper part of Fig. 2.37c. It should be noted here again that the stream tube formed by the two slipstreams is converging. An interesting shock polar combination is obtained when θ_{w2} is further decreased and reaches the value 16.89° . At this condition the three polars, namely the I-, R₁- and R₂-polars meet at a single point as shown in Fig. 2.36f. This combination is, in fact, analogous to the von Neumann condition in the reflection over a single wedge or the reflection of symmetric shock waves (see Sect. 1.5.2). Based on the foregoing discussion the shock polar combinations shown in Fig. 2.36b, f are the two extreme situations between which both an oRR and an oMR wave configurations are theoretically possible. Hence, they are, in fact, the upper ($\theta_{w2} = 29.97^\circ$, see Fig. 2.36b) and the lower ($\theta_{w2} = 16.89^\circ$, see Fig. 2.36f) bounds of the dual-solution domain for $M_0 = 4.96$ and $\theta_{w1} = 25^\circ$. When θ_{w2} is further reduced, e.g., to 12° , the resulting shock polar combination, which is shown in Fig. 2.36g, suggests an oRR wave configuration at the point where the R₁- and R₂-polars intersect. The other theoretical solution suggested by this shock polars combination, i.e., an oMR wave configuration, which consists of a DiMR_1 and an InMR₂, is not physical since it implies a wave configuration, in which the slipstreams of the two MR wave configurations form a diverging stream tube. Such a stream tube cannot be negotiated by the subsonic flow behind the Mach stem.

In summary three different oMR wave configurations are theoretically possible. They are:

- An oMR wave configuration that consists of two direct-Mach reflections, DiMR, and hence it is labeled as oMR[DiMR + DiMR]
- An oMR wave configuration that consists of one direct-Mach reflection, DiMR, and one stationary-Mach reflection, StMR, and hence it is labeled as oMR[DiMR + StMR]

- An oMR wave configuration that consists of one direct-Mach reflection, DiMR, and one inverse-Mach reflection, InMR, and hence it is labeled as oMR[DiMR + InMR]

Schematic illustrations of these three oMR wave configurations are shown in Fig. 2.37a–c, respectively.

Details regarding the direct-, stationary- and inverse-Mach reflections can be found in Courant & Friedrichs (1959), Takayama & Ben-Dor (1985) and Ben-Dor (1991).

Dual-Solution Domain

As just shown there are two extreme transition criteria that are analogous to the two extreme transition criteria in the case of the reflection of symmetric shock waves, namely the detachment and the von Neumann criteria. In similar to the case of the reflection of symmetric shock waves, the two extreme transition criteria also result in a dual-solution domain.

The dual-solution domain, in the $(\theta_{w1}, \theta_{w2})$ -plane for $M_0 = 4.96$ is shown in Fig. 2.38. (Note that the wedge angles θ_{w1} and θ_{w2} are symmetric.) The transition lines analogous to the “detachment”, θ_{w2}^E , and the “von Neumann”, θ_{w2}^T , criteria are drawn as solid lines. The dual-solution domain, inside which the overall wave configuration can be either an oRR or an oMR, extends between these two transition lines. The two dashed lines, marked θ_{w1}^N and θ_{w2}^N , indicate the von Neumann condition for the shock wave reflection over a single wedge (i.e., a symmetric reflection). On one of its sides the MR wave configuration is direct, DiMR, and on its other side the MR wave configuration is inverse, InMR, on the line itself the MR wave configuration is stationary, StMR.

Based on Fig. 2.38 the dual-solution domain can be divided into two parts:

- In one part, labeled “3 + 2” the overall wave configuration could be either an oRR or an oMR[DiMR + DiMR].
- In the other part, labeled “3 + 1” the overall wave configuration could be either an oRR or an oMR [DiMR + InMR]

Wedge-Angle-Variation-Induced Hysteresis

Figure 2.38 suggests that one can start with an oRR wave configuration having a value of $\theta_{w2} < \theta_{w2}^T$ and then increase θ_{w2} until the “detachment” transition line, θ_{w2}^E , above which an oRR wave configuration is theoretically impossible, is crossed. At the “detachment” transition line the oRR wave configuration must change to an oMR wave configuration. If, after the transition, the direction of changing θ_{w2} is reversed and it is decreased, the oMR wave configuration can continue to exist until the “von Neumann” transition line, θ_{w2}^T , below which an oMR wave configuration is theoretically impossible, will be reached.

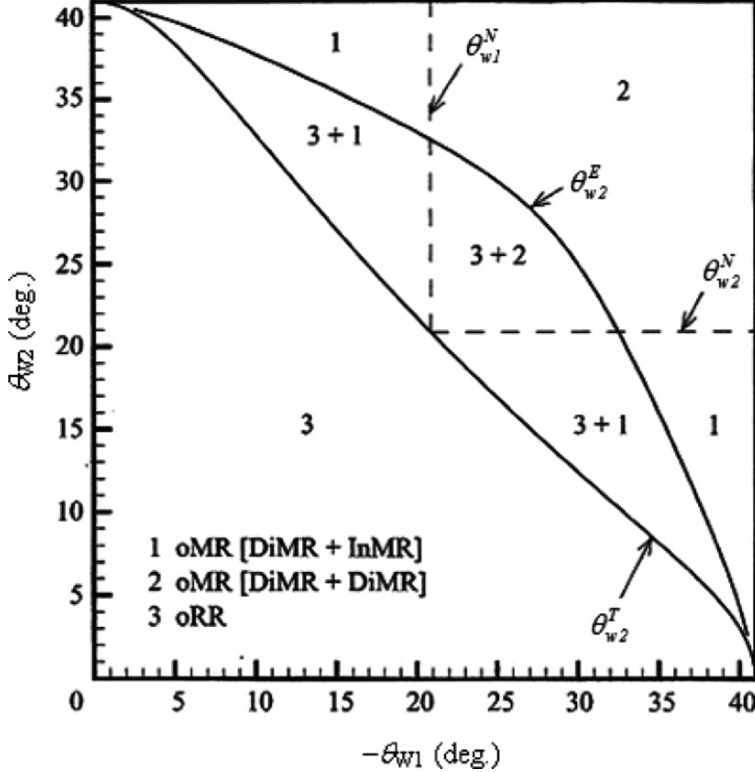


Fig. 2.38. The dual-solution domain in the reflection of asymmetric shock waves

At the “von Neumann” transition line the oMR wave configuration must change back to an oRR wave configuration.

Based on Fig. 2.38, which corresponds to $M_0 = 4.96$, it is evident that depending on whether θ_{w1} is smaller or larger than θ_{w1}^N , two different sequences of transition of the overall reflection wave configuration are theoretically possible during the above-described process of first increasing θ_{w2} and then decreasing it back to its initial value:

- For $\theta_{w1} < \theta_{w1}^N$ the process starts with an oRR wave configuration that is maintained until the “detachment” transition line, θ_{w2}^E , is reached. At this point the oRR \rightarrow oMR[DiMR + InMR] transition takes place. On the reverse path the oMR[DiMR + InMR] wave configuration is maintained until the “von Neumann” transition line, θ_{w2}^T , is reached. At this point the reversed oMR[DiMR + InMR] \rightarrow oRR transition takes place.
- For $\theta_{w1} > \theta_{w1}^N$ the process again starts with an oRR wave configuration that is maintained until the “detachment” transition line, θ_{w2}^E , is reached. At this point the oRR \rightarrow oMR[DiMR + DiMR] transition takes place. On the reverse path the oMR[DiMR + DiMR] wave configuration is main-

tained until the line θ_{w2}^N is reached. Exactly on this line the reflection wave configuration becomes an oMR[DiMR + StMR]. Then it changes to an oMR[DiMR + InMR] wave configuration. The oMR[DiMR + InMR] is maintained until the “von Neumann” transition line, θ_{w2}^T , is reached. At this point the reversed oMR[DiMR + InMR] \rightarrow oRR transition takes place.

Chpoun & Lengrand (1997) and Li et al. (1999) experimentally verified both the existence of an oMR[DiMR + InMR] wave configuration and the existence of a wedge-angle-variation-induced hysteresis in the oRR \rightleftharpoons oMR transition. Owing to resolution limitations of their experimental facility, the above-described two theoretically possible sequences of events in the oRR \rightleftharpoons oMR transition were not recorded. The experimental results of Li et al. (1999) agreed very well with the analytical transition lines.

It is important to note here that the experimental and geometrical set-ups of the reflection experiments over asymmetric wedges were very similar to those over symmetric wedges, which were described in the previous chapter. Hence, the three-dimensional edge effects in both cases were probably also similar. The fact that very good agreement between the analytical predictions and the experimental results were obtained regarding both the transition and the wave angles might suggest that the influence of the three-dimensional effects was not too significant.

Typical color schlieren photographs showing an oMR wave configuration, and an oRR wave configuration, for identical values of $M_0 = 4.96$, $\theta_{w1} = 28^\circ$ and $\theta_{w2} = 24^\circ$ are shown in Fig. 2.39a, b, respectively. These two schlieren photographs are clear evidence that different overall wave configurations can be obtained for identical flow conditions when two asymmetric shock waves interact.

Ivanov et al. (2002) numerically investigated the wedge-angle-variation-induced hysteresis. Numerical simulations of the above-mentioned two different sequences of events are shown in Fig. 2.40a, b for $M_0 = 4.96$ and $\theta_{w1} = 18^\circ$ and for $M_0 = 4.96$ and $\theta_{w1} = 28^\circ$, respectively. Constant density contours are shown in each of these figures. Each sequence starts at the top frame and then continuous in a counter clockwise direction. The flow conditions for each horizontal pair of the frames are the same. Hence, the wedge-angle-variation-induced hysteresis is clearly evident.

The sequence in Fig. 2.40b starts with an oRR wave configuration at $\theta_{w2} = 22^\circ$. When θ_{w2} is increased the oRR wave configuration still exists at $\theta_{w2} = 28^\circ$. At $\theta_{w2} = 36^\circ$, which is above the corresponding value of θ_{w2}^E , an oRR wave configuration can no longer exist and the overall reflection wave

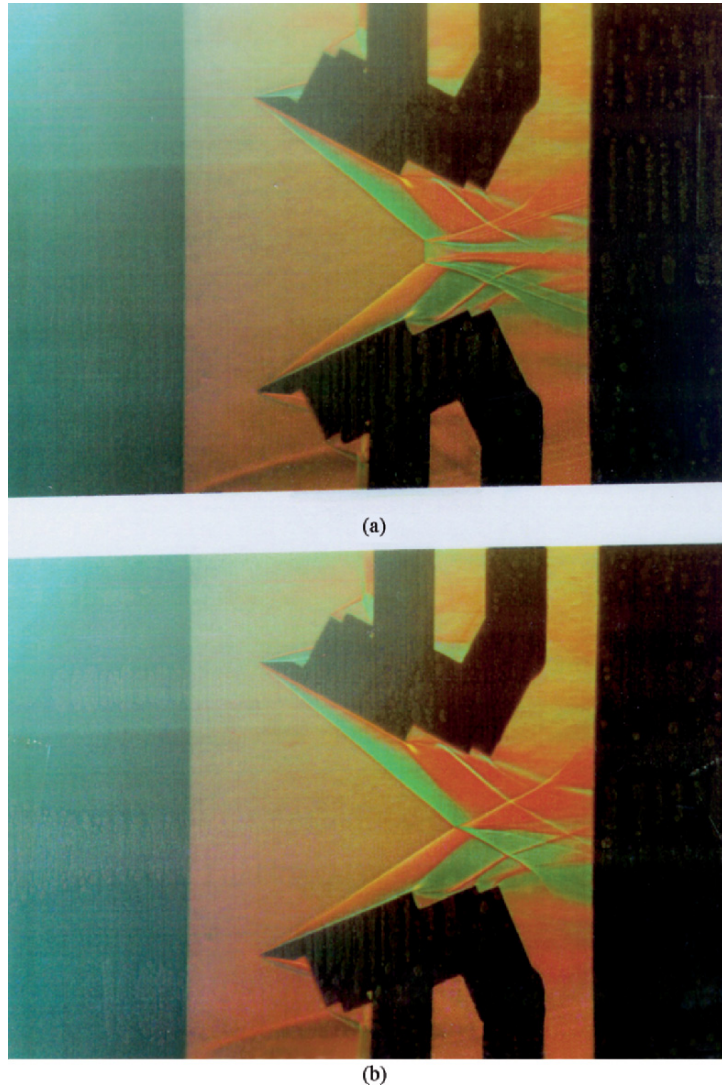


Fig. 2.39. Typical color schlieren photographs, taken from the experimental study of Li et al. (1999), showing (a) an overall MR wave configuration, and (b) an overall RR wave configuration for identical values of $M_0 = 4.96$, $\theta_{w1} = 28^\circ$ and $\theta_{w2} = 24^\circ$

configuration is an oMR[DiMR + InMR] in which the upper MR wave configuration is a DiMR wave configuration and the lower MR wave configuration is an InMR wave configuration. When θ_{w2} is decreased from $\theta_{w2} = 36^\circ$ back to its initial value, i.e., $\theta_{w2} = 22^\circ$, the oMR[DiMR + InMR] wave configuration

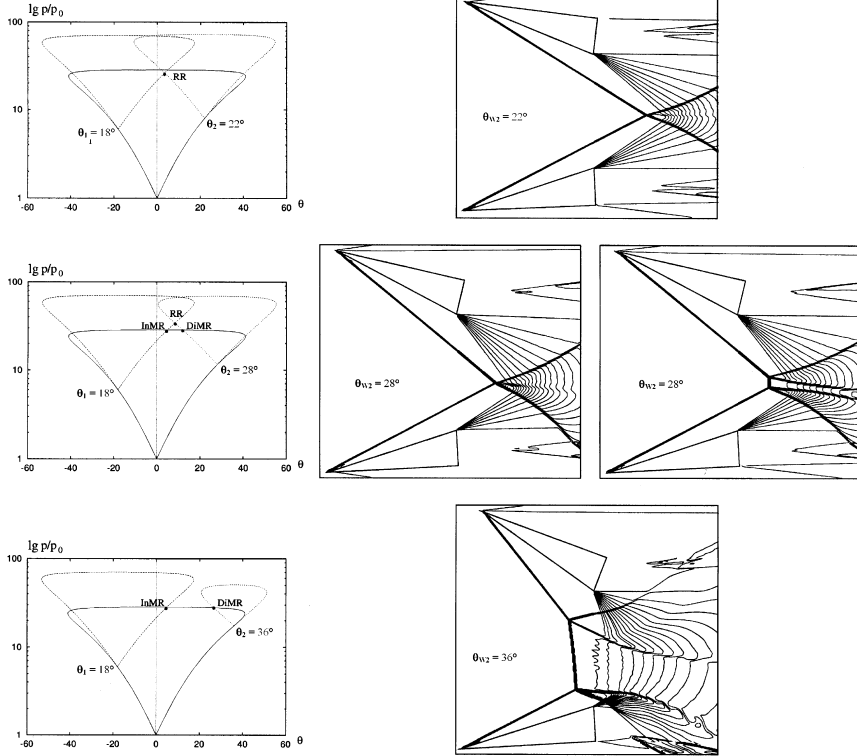


Fig. 2.40a.

is maintained in the dual-solution domain. Thus, for example, at $\theta_{w2} = 28^\circ$ two different shock wave configurations, one oRR and one oMR, are actually observed, in perfect agreement with the analysis. This sequence can be marked oRR $\xrightarrow{\text{at } \theta_{w2}^E}$ oMR[DiMR + InMR] $\xrightarrow{\text{at } \theta_{w2}^T}$ oRR.

The sequence in Fig. 2.40b starts with an oRR wave configuration at $\theta_{w2} = 12^\circ$. When θ_{w2} is increased the oRR wave configuration still exists at $\theta_{w2} = 24^\circ$. At $\theta_{w2} = 30^\circ > \theta_{w2}^E$ the overall reflection wave configuration is an oMR[DiMR + DiMR] in which both the upper and the lower MR wave configurations are DiMR wave configurations. When θ_{w2} is decreased from $\theta_{w2} = 30^\circ$ back to its initial value, i.e., $\theta_{w2} = 12^\circ$, the orientation of the slipstream of the lower MR wave configuration changes continuously. As a result at $\theta_{w2} = 21^\circ$, which is very close to the analytical value $\theta_{w2}^N = 20.87^\circ$, the upper wave configuration is close to being an StMR (i.e., its slipstream is almost parallel to the oncoming flow at the triple point). Upon a further decrease in θ_{w2} the lower wave configuration changes to an InMR, and

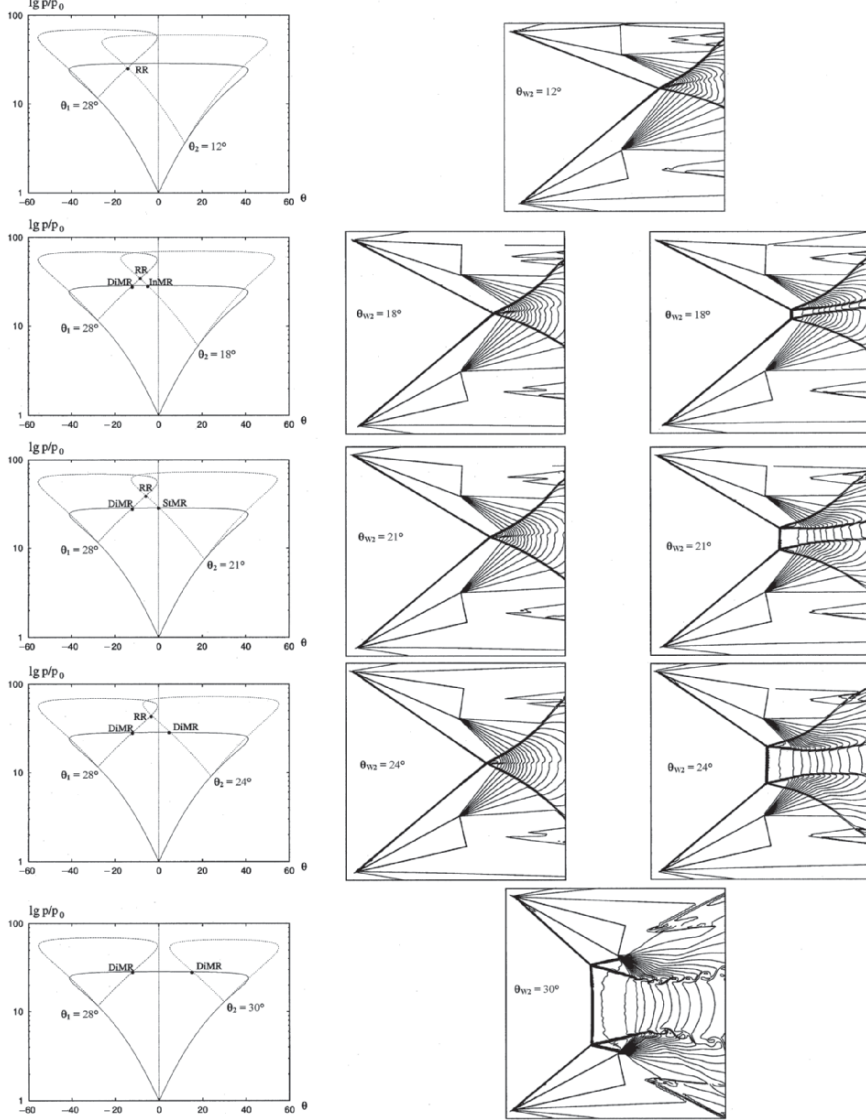


Fig. 2.40b. Numerical frames, taken from Ivanov et al.'s (2002) numerical investigation, illustrating the hysteresis loop or $M_0 = 4.96$ and $\theta_{w1} = 18^\circ$ and for $M_0 = 4.96$ and $\theta_{w1} = 28^\circ$. Constant density contours are displayed

the oMR wave configuration consists now of a DiMR and an InMR, i.e., it is an oMR[DiMR + InMR] wave configuration, as shown for $\theta_{w2} = 18^\circ$. This sequence can be marked oRR $\xrightarrow{\text{at } \theta_{w2}^E}$ oMR[DiMR + DiMR] $\xrightarrow{\text{on } \theta_{w2}^N}$ oMR[DiMR + StMR] $\xrightarrow{\text{at } \theta_{w2}^N}$ oMR[DiMR + InMR] $\xrightarrow{\text{at } \theta_{w2}^T}$ oRR.

Flow-Mach-Number-Variation-Induced Hysteresis

In similar to the flow-Mach-number-variation-induced hysteresis process, in the reflection of symmetric shock waves (see Sect. 2.4.2), which was numerically illustrated and verified both by Onofri & Nasuti (1999) and Ivanov et al. (2001), it is hypothesized that a similar flow-Mach-number-variation-induced hysteresis process also exists in the reflection of asymmetric shock waves.

2.4.4 Hysteresis Process in the Reflection of Axisymmetric (Conical) Shock Waves

In spite of the above-presented good to excellent agreement that was evident when the experimentally recorded hysteresis processes in the RR \rightleftharpoons MR transition were compared with predictions based on two-dimensional analytical models for both symmetric and asymmetric shock waves (see e.g., Chpoun et al. 1995 and Li et al. 1999), some investigators (see e.g., Skews et al. 1996, Skews 1997 and 1998, Fomin et al. 1996, Ivanov et al. 1998c, and Kudryavtsev et al. 1999) claimed and showed that these hysteresis processes were influenced and/or triggered and thereby promoted by three-dimensional edge effects, and therefore are not purely two-dimensional. This in turn, led to the questions whether an actual RR wave configuration is indeed stable inside the dual-solution domain, and whether the hysteresis process indeed exists in a purely two-dimensional flow. For this reason, Chpoun et al. (1999) and Ben-Dor et al. (2001) designed an axisymmetric geometrical set-up, which by definition was free of three-dimensional effect.

A schematic illustration of their experimental set-up is shown in Fig. 2.41. A 70-mm in diameter and 28-mm wide conical ring was placed in the center of a 127-mm supersonic jet, which emanated from the wind tunnel. The

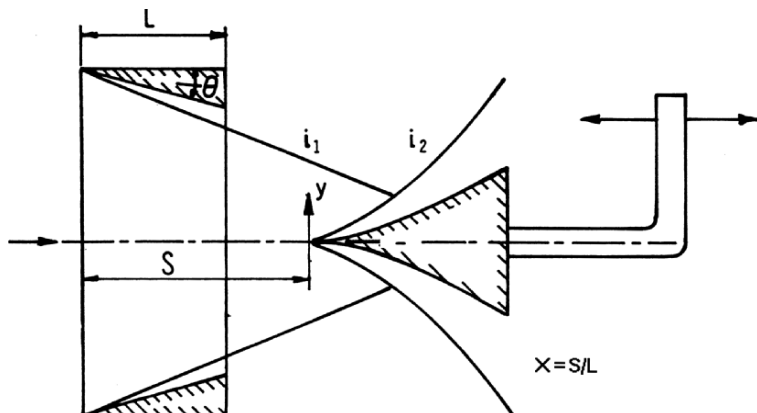


Fig. 2.41. Schematic illustration of the geometrical set-up for investigating the reflection of conical shock waves

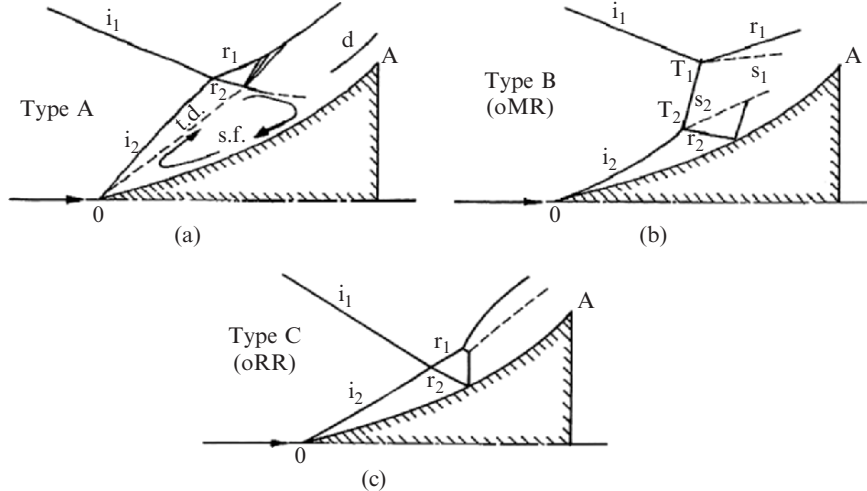


Fig. 2.42. Schematic illustrations of the three different types of wave configurations that were obtained by Chpoun et al. (1999) in their course of experimental investigation of the reflection of conical shock waves, in the geometrical set-up shown in Fig. 2.41: (a) Type A; (b) Type B (oMR); and (c) Type C (oRR)

head angle of the conical ring was 8.5° . A curvilinear cone was placed downstream of the conical ring. Their axes of symmetry coincided. The shape of the curvilinear cone was $y(x) = 0.000115x^3 + 0.002717x^2 + 0.08749x$ (x and y are in mm). The base diameter and the length of the curvilinear cone were 30.4 mm and 40 mm, respectively. The conical ring generated an incident converging straight conical shock wave, i_1 , and the curvilinear cone generated an incident diverging curvilinear conical shock wave, i_2 . Depending on the angle of interaction between these two incident shock waves, three different types of overall wave configurations, which are shown schematically in Fig. 2.42, were recorded in the course of the experimental investigation of Chpoun et al. (1999).

The Type A wave pattern, shown in Fig. 2.42a, consists of a straight diverging conical shock wave attached to the nose of the curvilinear cone that interacts with the converging straight conical shock wave, which is generated by the conical ring. As a result, the boundary layer separates, and a large slow re-circulation zone is induced near the surface of the cone. The re-circulation zone is the mechanism supporting the straight incident diverging conical shock wave that is attached to the nose of the curvilinear cone. In Fig. 2.42a, i_1 and i_2 are the converging and diverging incident conical shock waves, respectively, r_1 and r_2 are the reflected fronts of i_1 and i_2 after their interaction, d is the shock wave formed by the flow over the rear edge of the curvilinear cone (point A), s.f. denotes the separated flow zone with the slow re-circulation, and t.d. is a tangential discontinuity. The tangential discontinuity interacts with the reflected shock wave, r_2 , to result in a rarefaction wave, which

interacts with the reflected shock wave, r_1 . The existence of the separated flow zone indicates that viscous effects play an important role in the formation of the Type A wave configuration. It should be noted here that the above description of the detailed structure of the Type A wave configuration is based on the Navier–Stokes simulations of Burstchell et al. (2001). In the experiments of Chpoun et al. (1999) only the overall wave configurations was observed.

The Type B wave configuration, shown in Fig. 2.42b, is similar to the overall Mach reflection wave configuration in the interaction of asymmetric plane shock waves (see Fig. 2.35b). It consists of two MR wave configurations that have a common Mach stem that bridges their two triple points from which two slipstreams emanate. For this reason, the Type B wave configuration is also referred to as an overall Mach reflection wave configuration, oMR.

In the Type C wave configuration, Fig. 2.42c, the converging straight conical shock wave, i_1 , interacts with the weak diverging curvilinear conical shock wave, i_2 , and results in two refracted shock waves, r_1 and r_2 . The Type C wave configuration is similar to the overall regular reflection wave configuration in the interaction of asymmetric plane shock waves (see Fig. 2.35a). For this reason, the Type C wave configuration is also referred to as an overall regular reflection wave configuration, oRR.

An inspection of the geometrical set-up shown in Fig. 2.41 indicates that the angle of interaction between the converging and diverging incident conical shock waves, i_1 and i_2 , depends on either the axial distance between the conical ring and the curvilinear cone or the oncoming flow-Mach number. This gives rise to two possible hysteresis processes in the oRR \rightleftharpoons oMR transition:

- A *geometrical-variation-induced hysteresis*, in which the axial distance between the conical ring and the curvilinear cone is changed for a given oncoming flow-Mach number
- A *flow-Mach-number-variation-induced hysteresis*, in which the oncoming flow-Mach number is changed for a fixed axial distance between the conical ring and the curvilinear cone.

It is noted again that the change in the angle of interaction between the two incident shock waves is, in fact, the mechanism inducing the hysteresis in both processes.

Geometrical-Variation-Induced Hysteresis

Ben-Dor et al. (2001) investigated this hysteresis process both experimentally and numerically. In their numerical investigation, they used an inviscid flow. Figure 2.43 shows a sequence of 10 frames taken from one of their experimentally recorded videotapes. The sequence shows the evolution of the wave pattern during the shift of the curvilinear cone in the course of $X : 1.56 \rightarrow 0.70 \rightarrow 1.68$ where $X = S/L$ (S is the distance between the

entrance cross-section of the conical ring and the nose of the curvilinear cone, and $L = 28\text{ mm}$ is the width of the conical ring, see Fig. 2.41). The above-mentioned three different wave patterns, Types A, B and C, are clearly seen in Fig. 2.43.

From the initial position [frame (a)] with coordinate $X = 1.56$ the curvilinear cone was slowly moved with the velocity 0.22 mm/s along the axis of symmetry towards the conical ring. Whenever a drastic change, in the wave pattern, took place, the curvilinear cone was stopped and the flow was allowed to stabilize. Type A wave patterns are seen in frames (a)–(d). When the curvilinear cone was moved from $X = 0.86$ [frame (d)] to $X = 0.70$ [frame (e)] the wave configuration changed suddenly from Type A to Type B. This transition involved a reattachment of the boundary layer and, a disappearance of the separated zone. As a result the incident shock wave that was attached to the nose of the curvilinear cone, changed suddenly from a strong straight diverging conical shock wave to a weak curvilinear diverging conical shock wave. This transition, the Type A \rightarrow Type B transition, occurred at $X \approx 0.78$. The subsequent frames (f)–(j) correspond to the shift of the curvilinear cone in the reverse direction. Two transitions in the wave pattern were encountered, in the course of shifting the curvilinear cone from $X = 0.70$ [frame (e)] to $X = 1.68$ [frame (j)]. While shifting the curvilinear cone from $X = 0.70$ [frame (e)] to $X = 1.29$ [frame (h)] the height of the Mach stem continuously decreased until it disappeared between $X = 1.29$ [frame (h)] and $X = 1.56$ [frame (i)], and the wave pattern changed from Type B to Type C. This transition, the Type B \rightarrow Type C transition, occurred at $X \approx 1.38$. While shifting the curvilinear cone from $X = 1.56$ [frame (i)] to $X = 1.68$ [frame (j)] the boundary layer was separated from the surface of the curvilinear cone. As a result, the incident shock wave that was attached to the nose of the curvilinear cone suddenly changed from a weak diverging curvilinear conical shock wave to a strong diverging nearly straight conical shock wave, and the Type A wave pattern was formed again. This transition, the Type C \rightarrow Type A transition, occurred at $X \approx 1.61$. The pairs of frames (a) and (i), (b) and (h), (c) and (g) and (d) and (f), which correspond to the same X -position of the curvilinear cone, clearly demonstrate the existence of two different wave patterns for the same flow conditions. The entire set of frames in Fig. 2.43 provides a clear experimental evidence for the existence of a hysteresis process, which consists of the following three transitions:

- Type A \rightarrow Type B at $X \approx 0.78$ on the course of decreasing X
- Type B \rightarrow Type C at $X \approx 1.38$ on the course of increasing X
- Type C \rightarrow Type A at $X \approx 1.61$ on the course of increasing X

The hysteresis loop is Type A $\xrightarrow{X \approx 0.78}$ Type B $\xrightarrow{X \approx 1.38}$ Type C $\xrightarrow{X \approx 1.61}$ Type A.

Ben-Dor et al. (2001) also found that the just mentioned Type B \rightarrow Type C transition at $X \approx 1.38$ was the origin of an additional internal hysteresis loop. In some of the experiments, immediately after encountering the

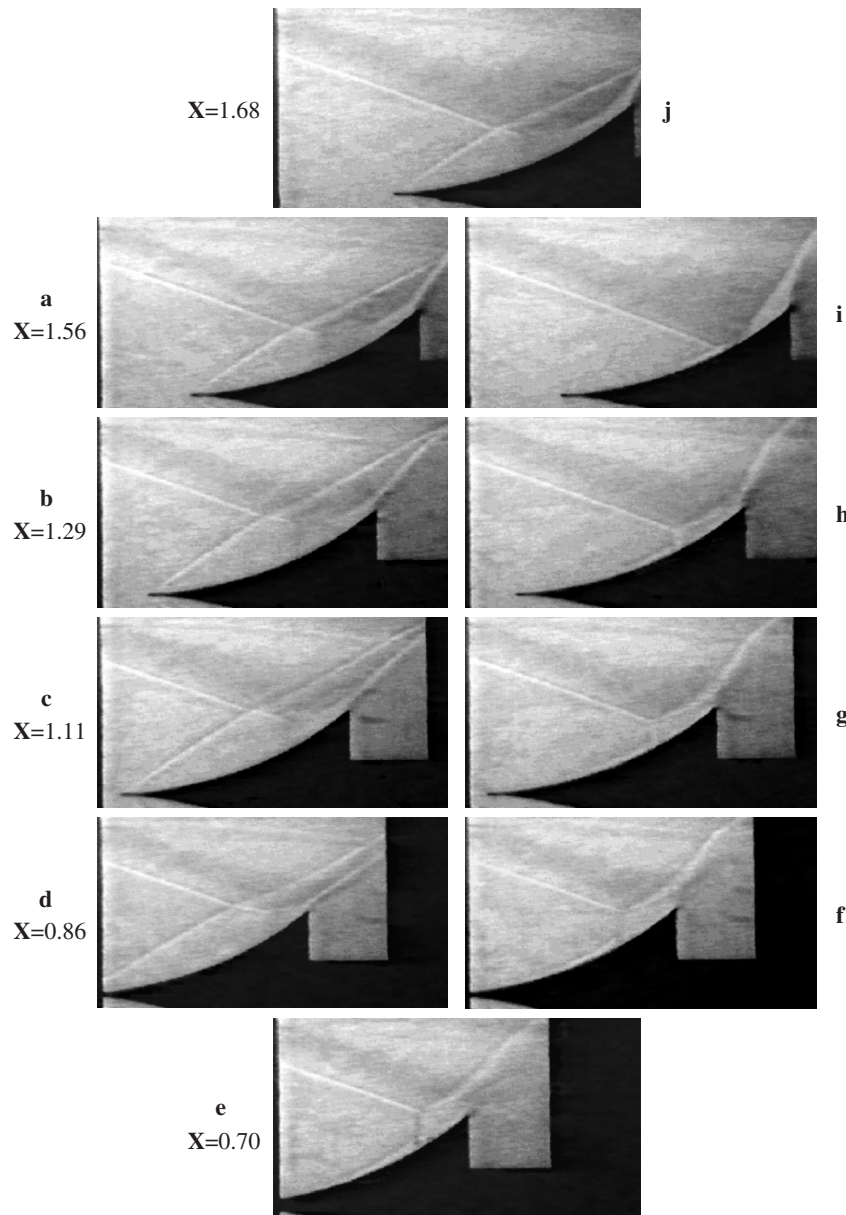


Fig. 2.43. A sequence of 10 frames taken from one of the experimentally recorded videotapes of Ben-Dor et al. (2001). The sequence shows the evolution of the wave pattern during the shift of the curvilinear cone in the course of $X : 1.56 \rightarrow 0.70 \rightarrow 1.68$. The three different wave patterns, Types A, B and C, which are shown in Fig. 2.42, are clearly seen

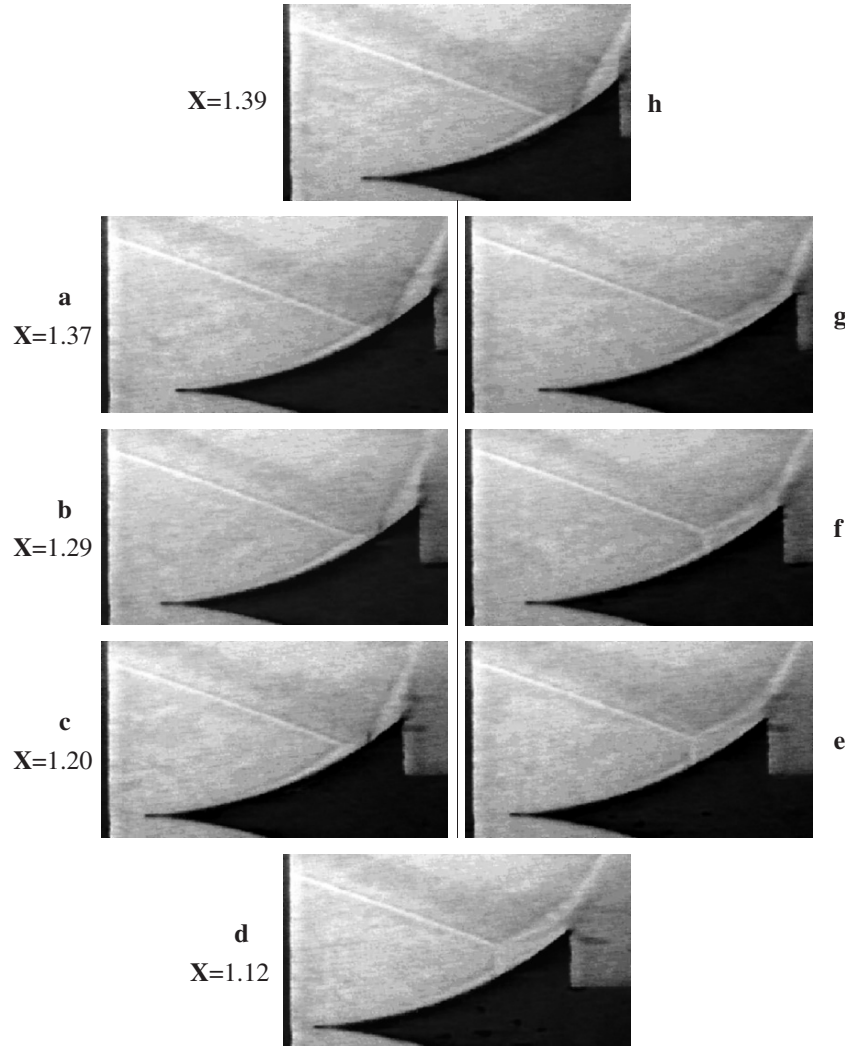


Fig. 2.44. A sequence of eight frames taken from one the experimentally recorded videotapes of Ben-Dor et al. (2001). The sequence shows the evolution of the wave pattern during the shift of the curvilinear cone in the course of $X : 1.39 \rightarrow 1.12 \rightarrow 1.39$. Two transitions of the wave pattern are evident

Type B \rightarrow Type C transition, at $X \approx 1.38$, the curvilinear cone was stopped and its shifting direction was reversed.

Figure 2.44 shows a sequence of 8 experimental frames corresponding to this case. The coordinate of the curvilinear cone was changed in the course of $X : 1.39 \rightarrow 1.12 \rightarrow 1.39$. Two transitions of the wave pattern were evident:

- Type C \rightarrow Type B transition took place at $X \approx 1.16$, when X was changed from 1.20 [frame (c)] to 1.12 [frame (d)], and an opposite
- Type B \rightarrow Type C transition occurred at $X \approx 1.38$, when X was changed from 1.37 [frame (g)] to 1.39 [frame (h)].

It should be noted here that, based on the experiments, the Type B \rightarrow Type C transition occurred when the Mach stem had a finite height. This was not the case in the inviscid numerical simulations, where the Mach stem decreased continuously until it vanished at the Type B \rightarrow Type C transition. Probably viscous effects behind the Mach stem were the cause for this peculiar behavior. It is noted again, that the Type C \rightarrow Type B hysteresis loop, shown in Fig. 2.44, is an internal hysteresis loop of the major hysteresis loop shown in Fig. 2.43. The sequence of this internal hysteresis loop is Type C $\xrightarrow{X \approx 1.16}$ Type B $\xrightarrow{X \approx 1.38}$ Type C.

Finally, it should be noted that frames (b) and (h) in Fig. 2.43 and frames (b) and (f) in Fig. 2.44, which all correspond to the same X -position of the curvilinear cone, $X = 1.29$, clearly demonstrate that three different shock wave patterns, Type A, Type B and Type C, were obtained experimentally, for the same flow conditions.

The above-described experimental double-loop hysteresis is shown in Fig. 2.45. The frames shown in Fig. 2.43 describe a viscous-dependent major hysteresis loop, which is accompanied by three transitions:

- Type A \rightarrow Type B at $X \approx 0.78$
- Type B \rightarrow Type C at $X \approx 1.38$
- Type C \rightarrow Type A at $X \approx 1.61$

In similar, the frames shown in Fig. 2.44 describe an internal (nonviscous-dependent) hysteresis loop with two transitions:

- Type B \rightarrow Type C (or oMR \rightarrow oRR) at $X \approx 1.38$
- Type C \rightarrow Type B (or oRR \rightarrow oMR) at $X \approx 1.16$.

The frames shown in Figs. 2.43 and 2.44 were added to Fig. 2.45. Each one of them is labeled as (Nn) where “N” is the number of the Fig. 2.43 or 2.44 and “n” is the letter designation of the frame in the appropriate figure.

It should be noted that the above given values of X are directly related to the geometrical dimensions and shapes of the conical ring and the curvilinear cone. It is believed that different dimensions and/or shapes would result in a similar hysteresis phenomenon with transitions at different values of X .

The experimental results in Fig. 2.45 provide a clear proof of the existence of a hysteresis phenomenon in the oRR \rightleftharpoons oMR transition in an axisymmetric flow, which by definition is free of three-dimensional effects.

As will be shown subsequently, the Euler code, which was applied by Ben-Dor et al. (2001), failed, as expected, to reproduce the viscous dependent Type A wave configuration and the hysteresis loop that is associated with it. As a result, only the nonviscous-dependent internal hysteresis

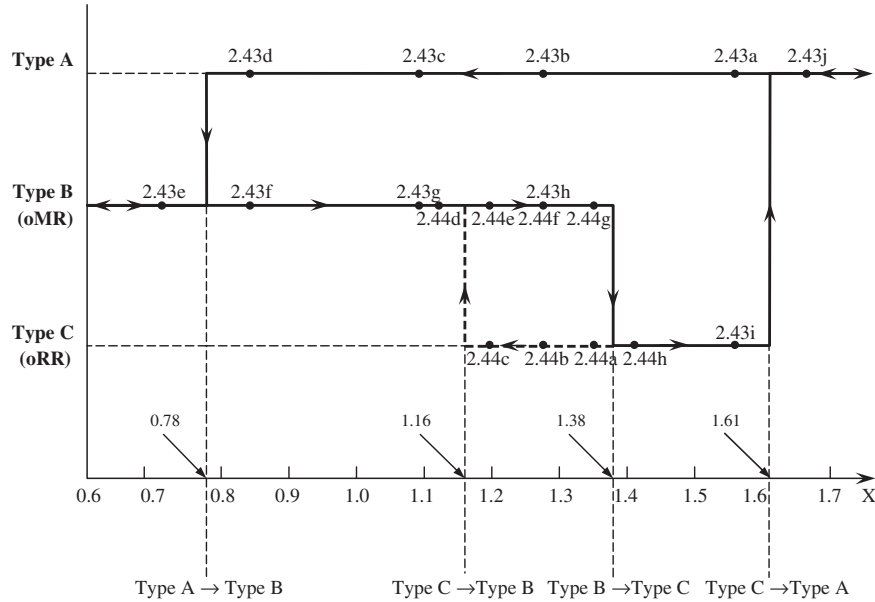


Fig. 2.45. The experimental double-loop hysteresis

loop, i.e., the Type B \leftrightarrow Type C hysteresis loop, was simulated. However, in addition, a few secondary hysteresis loops, associated with the interaction between the overall shock wave configuration and the rear edge of the curvilinear cone were obtained. Burstchell et al. (2001), who simulated the process using a Navier–Stokes code, did succeed in obtaining the Type A wave configuration.

The overall multi-loop hysteresis as obtained with an Euler code is shown in Fig. 2.46 in the (X, \bar{H}_m) -plane. Here $\bar{H}_m = H_m/L$ is the nondimensional length of the Mach stem, where H_m , is the length of the common Mach stem (i.e., the distance between the two triple points when the resulted overall wave configuration is an oMR). Evidently, $\bar{H}_m = 0$ for an oRR wave configuration for which $H_m = 0$. The stable flow states that were encountered when the curvilinear cone was shifted along the $X : 0 \rightarrow 2.2$ path and along the reversed $X : 2.2 \rightarrow 0$ path were A–B–C–D–E–F–G–H–I–J–K–L–M–N–O–P–Q and Q–P–R–S–M–T–K–J–U–H–G–V–E–D–W–B–A, respectively. These two different paths of stable flow states consisted of two different types of hysteresis loops. The first one, the major one, described by the S–N–O–P–R–S loop, which is similar to the one obtained experimentally (see Fig. 2.45), consists of both oMR and oRR wave configurations for the same flow conditions. The second one, the minor one, has not been recorded experimentally, probably because of the poor experimental resolution along the surface of the curvilinear cone. It consists of only oMR wave configurations, which have different Mach-stem lengths and respective flow patterns for the same flow conditions.

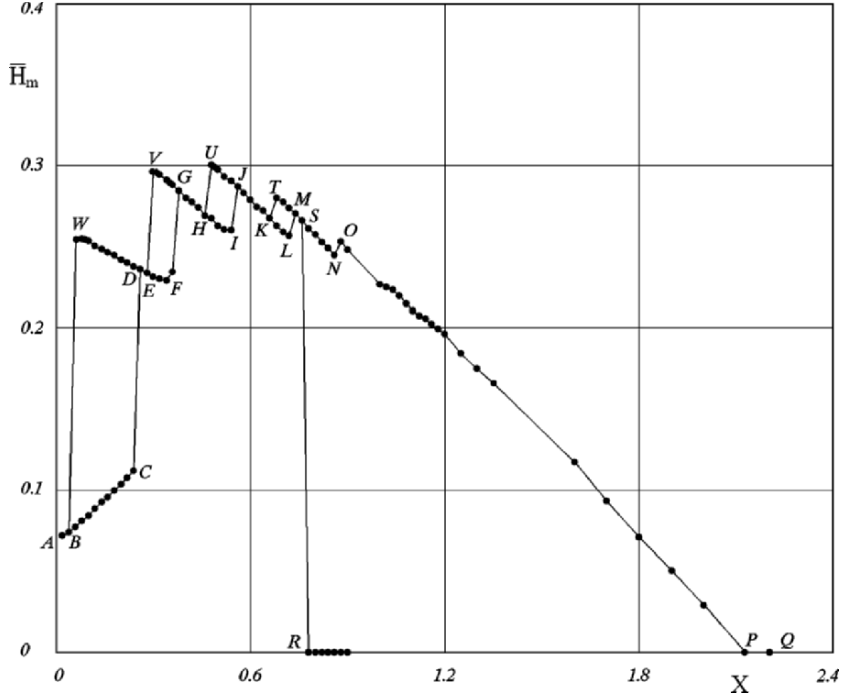


Fig. 2.46. The numerical overall multiloop hysteresis (Euler calculation)

Figure 2.46 reveals four such minor hysteresis loops: B–C–D–W–B, E–F–G–V–E, H–I–J–U–H and K–L–M–T–K.

Frames corresponding to the major S–N–O–P–R–S hysteresis loop are shown in Fig. 2.47. This hysteresis, which is nonviscous dependent, probably originates from the existence of a dual-solution domain. The wave configuration for $X = 1.3$, shown in frame (a), is an oRR. The incident converging straight conical and the incident diverging curvilinear conical shock waves interact with each other in a regular manner. The refracted converging conical shock wave reflects from the surface of the curvilinear cone as an RR. The reflected shock wave of this RR interacts with the refracted diverging curvilinear conical shock wave. When X is decreased to 0.80 [frame (c)] the reflection of the transmitted converging conical shock wave from the surface of the curvilinear cone changes from an RR to an MR. When X is decreased to 0.70 [frame (d)] the overall wave configuration changes suddenly from an oRR to an oMR. If now the direction of shifting the curvilinear cone is reversed and X is increased back to its initial value, the flow patterns shown in frames (e)–(g) are encountered. The length of the Mach stem, of the oMR wave configurations, gradually decreases. It is also seen in frames (d)–(g) that once an oMR wave configuration is formed the interaction of the wave reflected from the surface of the curvilinear cone and the contact surface results in a special

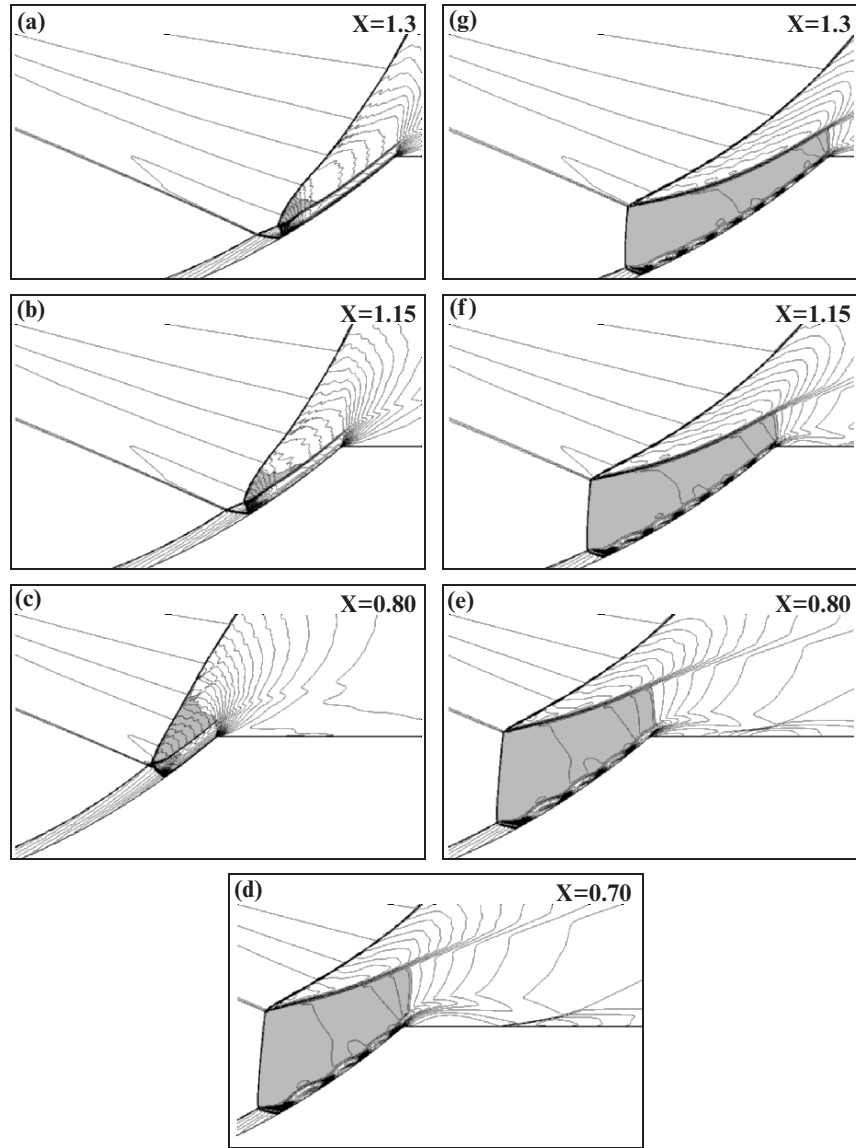


Fig. 2.47. Numerical frames showing the wave patterns associated with the major S–N–O–P–R–S hysteresis loop, (see Fig. 2.46 for details)

structure of “humps” of the contact surface. The number of the humps is seen to increase as X is increased. There are three full humps for $X = 0.7$ and 0.80 [frames (d) and (e), respectively], five full humps for $X = 1.15$ [frame (f)] and seven full humps for $X = 1.3$ [frame (g)]. Ben-Dor et al. (2004) showed that the edges of these humps are associated with extremely high pressure peaks.

The three pairs of frames, (c) and (e) for $X = 0.8$, (b) and (f), for $X = 1.15$, and (a) and (g) for $X = 1.3$, which show different overall shock wave configurations for identical flow conditions provide a clear evidence of the hysteresis phenomenon. Based on Fig. 2.46 the oRR \rightarrow oMR transition takes place at $X \approx 0.75$.

Ben-Dor et al. (2001) found that the location of the curvilinear cone when a given hump was detached from the rear edge of the curvilinear cone was different from its location when the same hump was reattached. The attachment/detachment mechanism led to the identification of the above-mentioned additional minor hysteresis loops in which the wave configurations were always oMRs, but the flow patterns along the surface of the curvilinear cone were different. Four such hysteresis loops are shown in Fig. 2.46. They are B–C–D–W–B, E–F–G–V–E, H–I–J–U–H and K–L–M–T–K.

The B–C–D–W–B hysteresis loop is shown in Fig. 2.48. At $X = 0.02$ [frame (a)] an oMR wave configuration was obtained. It should be noted that unlike the previously discussed oMR wave configurations where the reflected shock wave of the lower MR interacted with the surface of the curvilinear cone upstream of its rear edge, here it interacted with the surface of the curvilinear cone downstream of its rear edge. When X was increased [frames (b) and (c)] the Mach stem bridging the two triple points moved upstream and its length increased. Note that a situation in which the reflected shock wave of the lower MR touched the rear edge of the curvilinear cone was reached at $X \approx 0.20$ [frame (c)]. An increase of X beyond this value resulted in a sudden jump of the Mach stem upstream that was associated with a sudden increase in its length, as can be seen in frame (d) for $X = 0.26$. When X was decreased back to $X = 0.02$ the stable solutions shown in frames (e)–(g) were obtained. The two pairs (c) and (e) for $X = 0.20$, and (b) and (f) for $X = 0.12$, which show different overall wave configurations for identical flow conditions are clear evidences of the hysteresis. The hysteresis is typified by a sudden increase in the length of the common Mach stem at $X = 0.23 \pm 0.03$ and a reversed sudden decrease in its length at $X = 0.07 \pm 0.05$. The calculations revealed that the mechanism, which triggered the sudden transition from an oMR with a short Mach stem [frame (c)] to an oMR with a much larger Mach stem [frame (d)], was the interaction of the reflected shock wave of the lower MR wave configuration with the rear edge of the curvilinear cone [frame (c)]. Once the transition took place [(frame (d))] the reflected shock wave of the lower MR wave configuration reflected from the surface of the curvilinear cone as an RR wave configuration. The reflected shock wave of this RR wave configuration interacted with the contact surface of the lower MR wave configuration. The result of this interaction was an expansion wave, which hit the solid surface of the curvilinear cone and reflected back towards the contact surface as an expansion wave. The reflected expansion wave interacted with the contact surface and turned it back towards the curvilinear cone. Had X been further increased, as will be shown subsequently, this turn of the contact surface would have been developed to become the first full hump of the contact surface

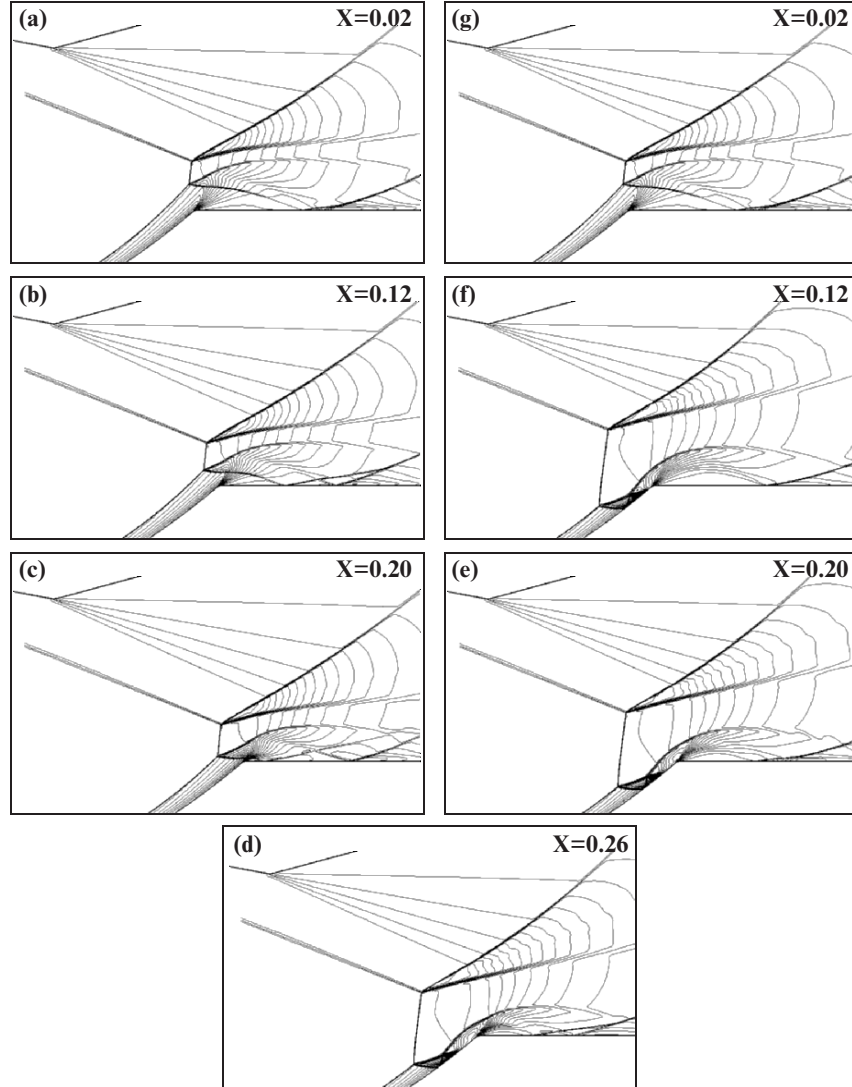


Fig. 2.48. Numerical frames showing the wave patterns associated with the B–C–D–W–B hysteresis loop (see Fig. 2.46 for details)

over the surface of the curvilinear cone. Frames (f) and (g) indicated that the reverse transition was driven by the interaction of the above-mentioned expansion wave with the rear edge of the curvilinear cone.

The minor E–F–G–V–E hysteresis loop is shown in Fig. 2.49. At $X = 0.26$ an oMR wave configuration was obtained. When X was increased, the common Mach stem moved upstream and its length increased. The flow patterns in

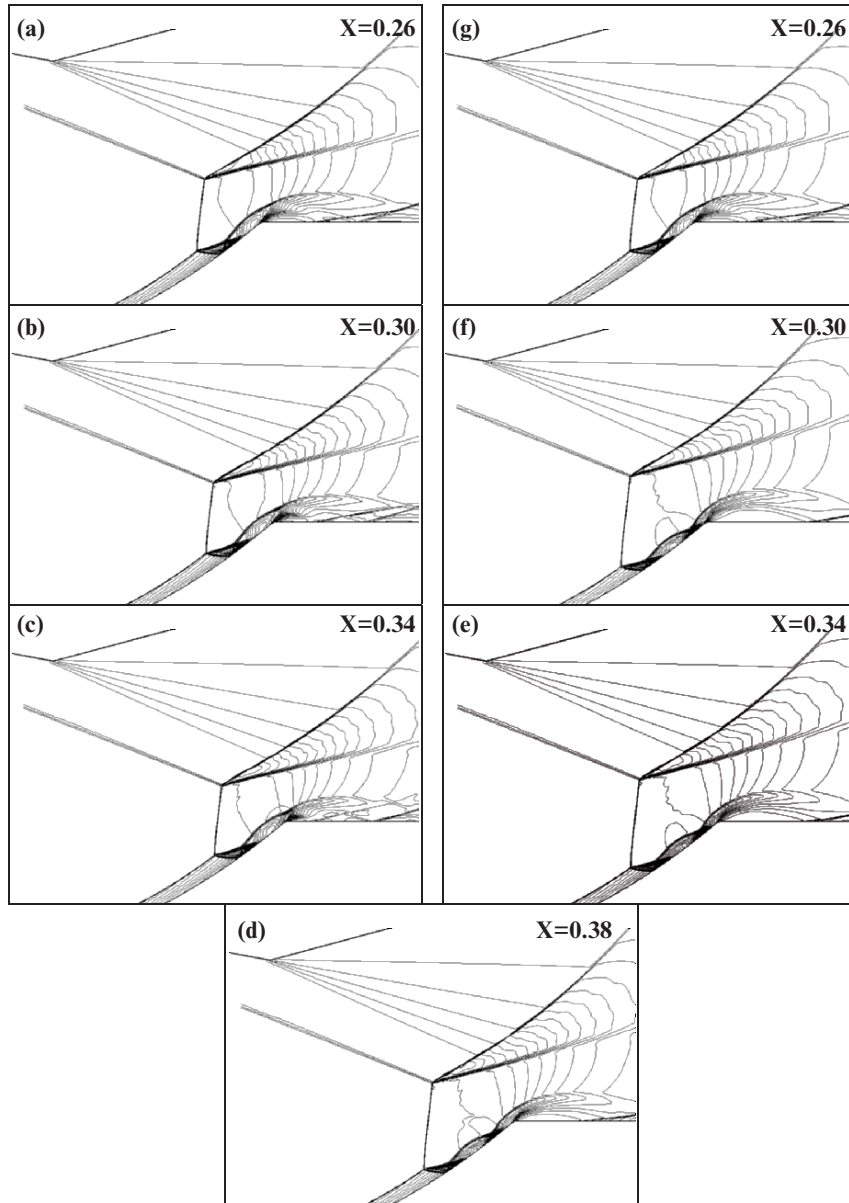


Fig. 2.49. Numerical frames showing the wave patterns associated with the E–F–G–V–E hysteresis loop, (see Fig. 2.46 for details)

frames (a)–(c) for $X = 0.26$, 0.30 , and 0.34 , respectively, were similar to those shown in Fig. 2.48f. A further increase to $X = 0.38$, resulted in the flow pattern shown in frame (d), in which the expansion wave that was mentioned earlier succeeded to develop a full hump of the contact surface of the lower MR wave configuration. When X was decreased back to $X = 0.26$ the stable flow patterns shown in frames (e)–(g) were obtained. The pairs (c) and (e) and (b) and (f) that show different flow patterns for identical flow conditions are clear evidences of the hysteresis. It is evident from Fig. 2.49 that the hysteresis is driven by a mechanism associated with the attachment/detachment of the first hump of the contact surface to the surface of the curvilinear cone. For this reason, the E–F–G–V–E hysteresis is termed as the $0\text{ hump} \rightleftharpoons 1\text{ hump}$ hysteresis. The transitions of this hysteresis loop are:

$$\begin{aligned} 0\text{ hump} &\xrightarrow{X=0.36} 1\text{ hump}, \\ 1\text{ hump} &\xrightarrow{X=0.28} 0\text{ hump}. \end{aligned}$$

Ben-Dor et al. (2001) showed that the minor H–I–J–U–H–E hysteresis loop was driven by a mechanism associated with the attachment/detachment of the second hump to the surface of the cone. For this reason, this hysteresis it is termed as the $1\text{ hump} \rightleftharpoons 2\text{ humps}$ hysteresis. The transitions of this hysteresis loop are

$$\begin{aligned} 1\text{ hump} &\xrightarrow{X \approx 0.55} 2\text{ humps}, \\ 2\text{ humps} &\xrightarrow{X \approx 0.47} 1\text{ hump}. \end{aligned}$$

In similar, the minor K–L–M–T–K hysteresis loop was driven by a mechanism associated with the attachment/detachment of the third hump to the surface of the cone. For this reason, this hysteresis is termed as the $2\text{ humps} \rightleftharpoons 3\text{ humps}$ hysteresis. The transitions of this hysteresis loop are

$$\begin{aligned} 2\text{ humps} &\xrightarrow{X \approx 0.69} 3\text{ humps}, \\ 3\text{ humps} &\xrightarrow{X \approx 0.67} 2\text{ humps} \end{aligned}$$

As mention earlier, Ben-Dor et al. (2001), who used an Euler code, failed, as expected, to numerically reproduce the Type A wave configuration, shown in Fig. 2.42a, which involves a boundary layer separation, and as a result is viscous dependent. Burstchell et al. (2001) also investigated the reflection process associated with the geometry shown in Fig. 2.41 using both Euler and Navier–Stokes numerical codes. While the results of their Euler calculations were similar to those of Ben-Dor et al. (2001), they did succeed to reproduce the Type A wave configuration in their Navier–Stokes calculations. Furthermore, their Navier–Stokes calculations revealed a strong dependence of the number of the humps and their intensities on the viscosity. Hence, the role of viscous effects in forming the humps and determining their intensities, and as a result the existence of the above-described minor hysteresis

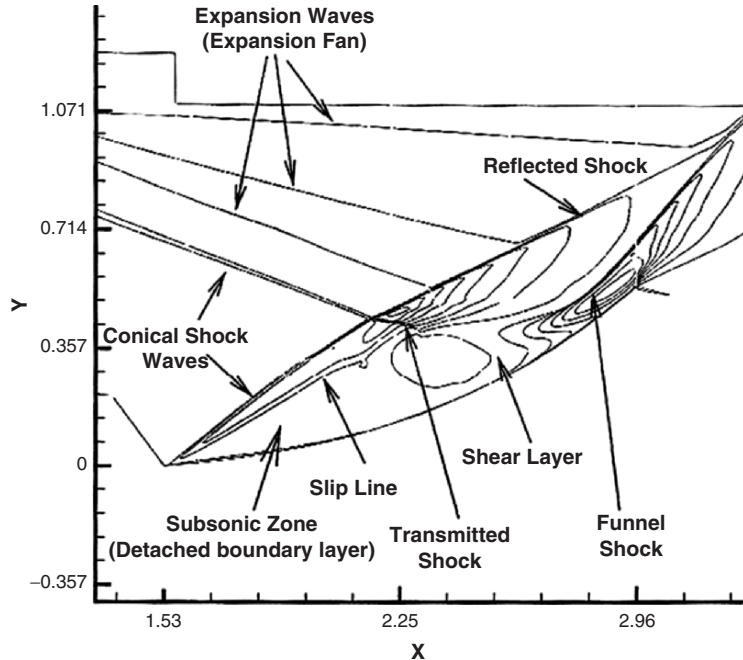


Fig. 2.50. A Navier–Stokes numerical simulation of the experiment shown in Fig. 2.43. The Type A viscous-dependent wave configuration is seen

loops is yet to be investigated and understood. Finally it is noted again that Ben-Dor et al. (2004) showed that the edges of the humps are associated with extremely high pressures.

A Navier–Stokes numerical simulation of the experiment shown in Fig. 2.43a is shown in Fig. 2.50. The numerically generated Type A viscous-dependent wave configuration supports the hypothetical description of the fine details of the flow field as was forwarded by Ben-Dor et al. (2001).

Flow-Mach-Number-Variation-Induced Hysteresis

Ben-Dor et al. (2003) numerically investigated the flow-Mach-number-variation-induced hysteresis process in the interactions of conical shock wave over the axisymmetric geometry shown in Fig. 2.41. Three cases, which differed in the location of the curvilinear cone with respect to the conical ring, X , were investigated: $X = -0.3$, $X = -0.2$ and $X = -0.1$ (the minus sign indicates that the nose of the curvilinear cone was located upstream of the entrance cross section of the conical ring).

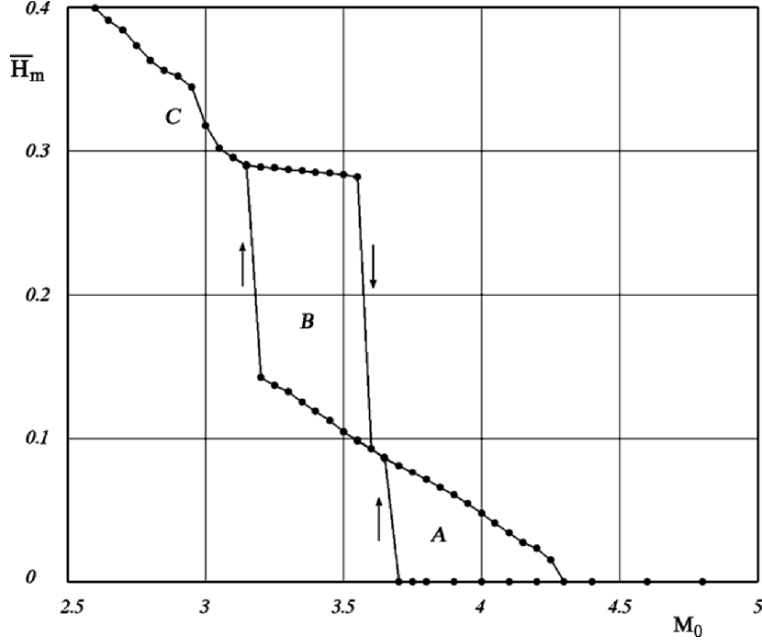


Fig. 2.51. The flow-Mach-number-induced hysteresis loop for $X = -0.3$ when the flow-Mach was changed in the course $4.8 \rightarrow 2.6 \rightarrow 4.8$

Case 1: $X = -0.3$

The dependence of the nondimensional common Mach stem length, \bar{H}_m , on the free-stream-flow-Mach number, M_0 , when the latter was changed in the course $4.8 \rightarrow 2.6 \rightarrow 4.8$ is shown in Fig. 2.51. ($\bar{H}_m = 0$ for an oRR). It is seen that the wave configuration was an oRR during the variation of the flow-Mach number from 4.8 to 3.8. A sudden transition from an oRR wave configuration to an oMR wave configuration occurred at $M_0 \cong 3.65$. Further reductions of M_0 were associated with a gradual increase in the length of the common Mach stem. This trend continued until $M_0 \cong 3.15$ where a sharp increase of the common Mach stem length was observed. As it turned out, this transition was caused by the intersection of the reflected shock wave of the lower MR wave configuration with the rear edge of the curvilinear cone. When the direction of changing M_0 was reversed and it was increased the reversed transitions, occurred at different values of M_0 . Consequently, two hysteresis loops, A and B, were observed. While loop A involved both oRR and oMR wave configurations loop B involved only oMR wave configurations that were associated with different flow patterns. More details regarding the wave configurations associated with hysteresis loops A and B can be found in Ben-Dor et al. (2003).

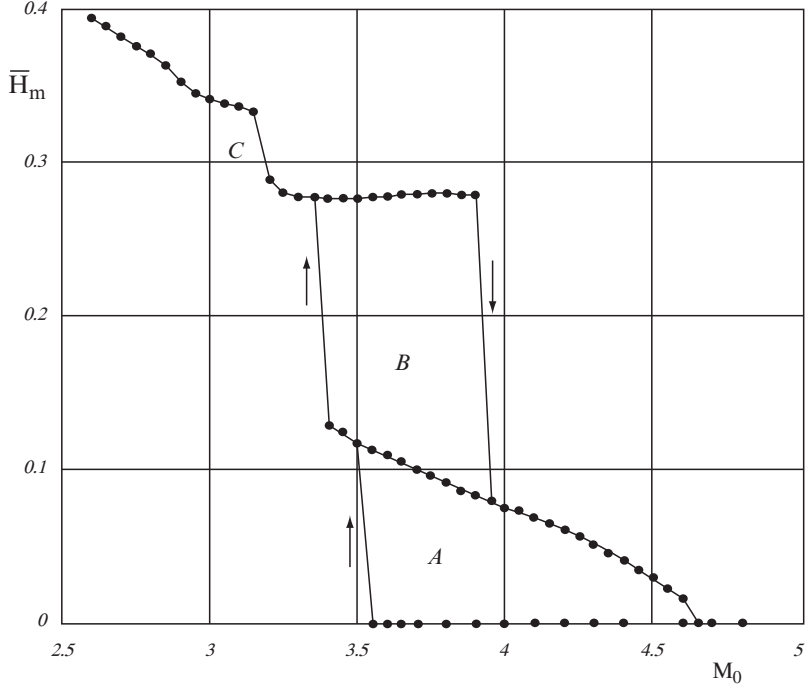


Fig. 2.52. The flow-Mach-variation-number-induced hysteresis loop for $X = -0.2$ when the flow-Mach was changed in the course $4.8 \rightarrow 2.6 \rightarrow 4.8$

Case 2: $X = -0.2$

The dependence of the nondimensional common Mach stem length, \bar{H}_m , on the free-stream-flow-Mach number, M_0 , when the latter was changed in the course $4.8 \rightarrow 2.6 \rightarrow 4.8$ is shown in Fig. 2.52. It is seen that the change in the location of the curvilinear cone resulted in a significant increase of the range of the hysteresis loop A. As a result hysteresis loops A and B overlap. This in turn results in a situation in which there is a flow-Mach-number range for which three stationary wave configurations, one oRR and two different oMRs, are possible. More details regarding the wave configurations associated with hysteresis loops A and B can be found in Ben-Dor et al. (2003).

Case 3: $X = -0.1$

The dependence of the nondimensional common Mach stem length on the free-stream-flow-Mach number when the latter was changed in the course $5.0 \rightarrow 2.6 \rightarrow 5.0$ is shown in Fig. 2.53. It is evident from Fig. 2.53 that the change in the location of the curvilinear cone resulted in a further significant increase of the range of the hysteresis loop A. Furthermore, unlike the previous two cases, now there are three hysteresis loops: the previously

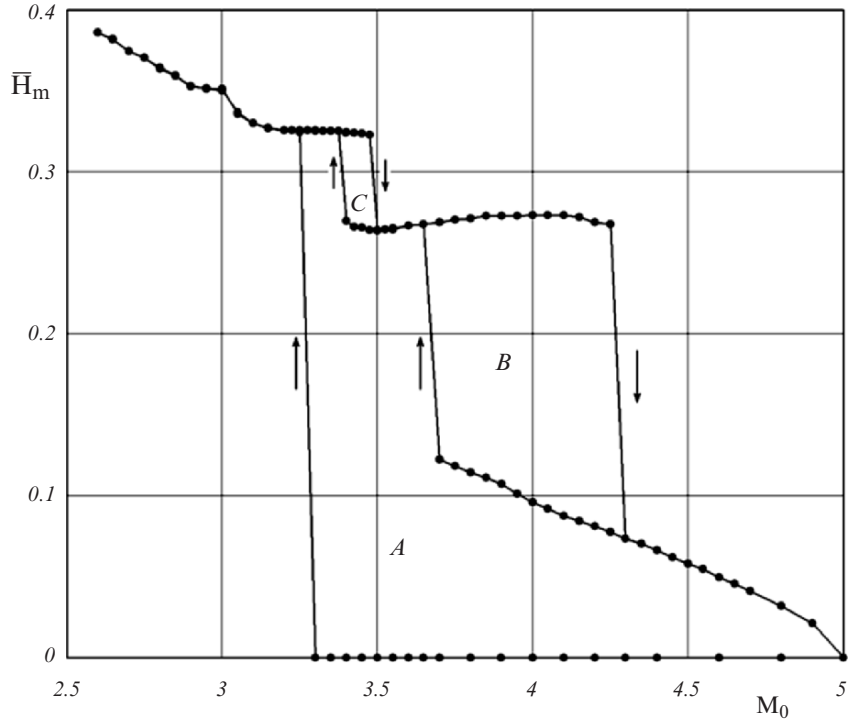


Fig. 2.53. The flow-Mach-number-induced hysteresis loop for $X = -0.1$ when the flow-Mach was changed in the course $5.0 \rightarrow 2.6 \rightarrow 5.0$

observed loops A and B and a small additional hysteresis loop, loop C. In similar to the previous case here again the hysteresis loops overlap. There is an overlap of loops A and C, and an overlap of loops A and B. Consequently, once again three different wave configurations for identical flow conditions are possible. The wave configurations associated with the hysteresis loops A, B, and C are shown in Figs. 2.54–2.56, respectively. The important role of the rear edge of the curvilinear cone in forming the hysteresis loops A, B, and C is clearly seen. More details can be found in Ben-Dor et al. (2003).

Ben-Dor et al. (2003) showed that the different wave configurations for identical flow-Mach numbers were associated with significantly different pressure distributions along the cone surface. Figure 2.57 shows the pressure distributions for $M_0 = 3.45$ (for which loops A and C overlap). Three different wave configurations; an oRR, an oMR having a short Mach stem and an oMR having a longer Mach stem are possible for this flow Mach numbers (see Fig. 2.53). The pressure distribution associated with the oMR having the longer Mach stem (solid line) has two pressure peaks. While the first peak reaches a value of about 37 times the ambient pressure the second peak

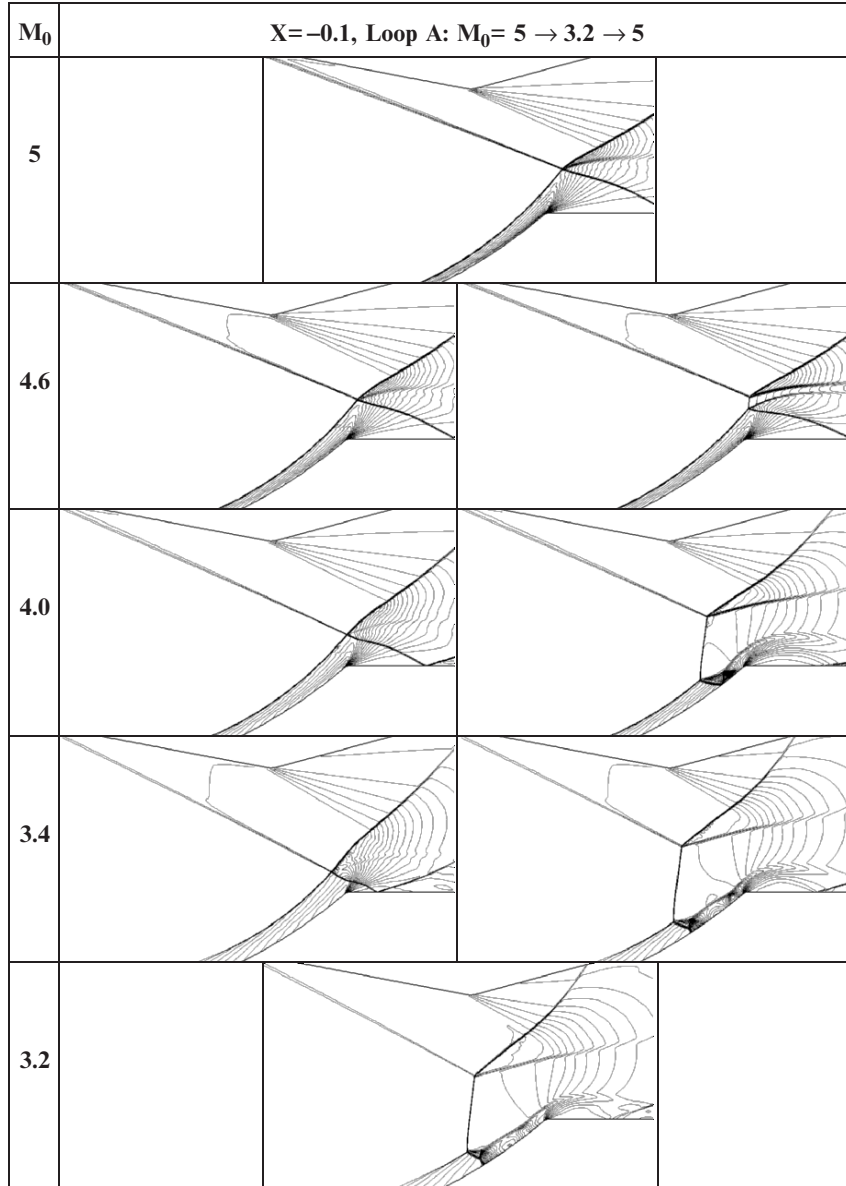


Fig. 2.54. The wave configurations associated with hysteresis loops A of Fig. 2.53

reaches a value of about 24 times the ambient pressure. The reason for the double peak is clearly understood when the actual wave configuration that is shown in Fig. 2.56 ($M_0 = 3.45$, left frame) is consulted. The first peak is due to the reflection of the lower Mach reflection from the surface of the curvilinear

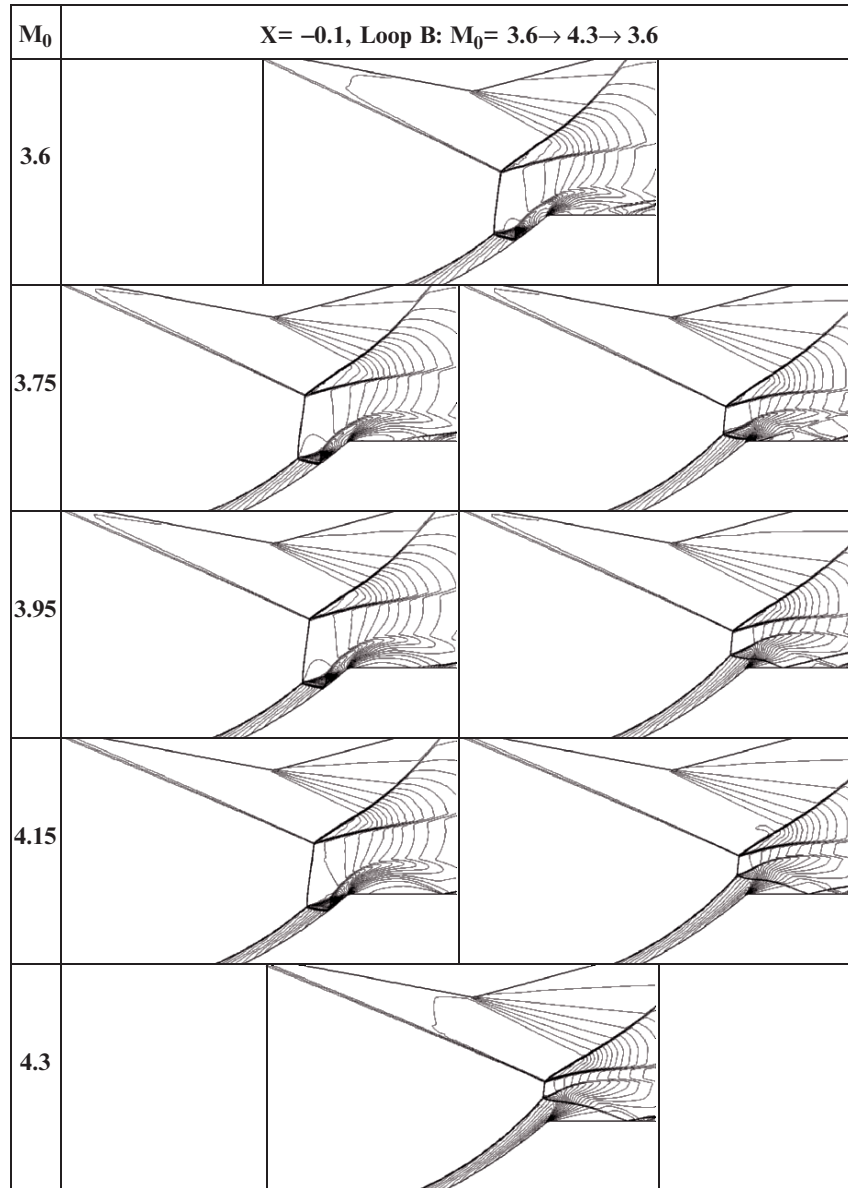


Fig. 2.55. The wave configurations associated with hysteresis loops B of Fig. 2.53

cone. The second peak arises from the strong compression near the shoulder of the curvilinear cone, where a hump in the contact discontinuity is seen to develop over the curvilinear cone surface. Ben-Dor et al. (2001) addressed the pressure enhancement at the edges of such a hump. The pressure distribution

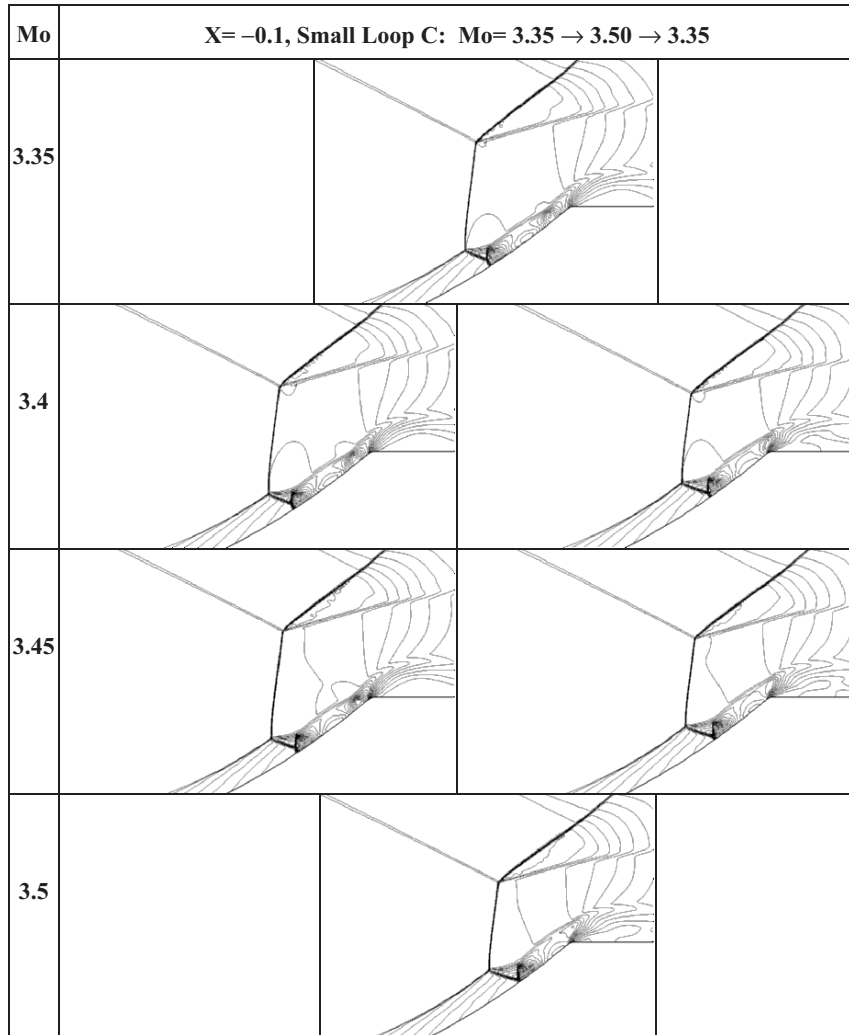


Fig. 2.56. The wave configurations associated with hysteresis loops C of Fig. 2.53

of the oMR having the shorter Mach stem (dash-dotted line) has only one pressure peak that reaches a pressure almost 40 times the ambient pressure. The reason is self-explanatory in view of the foregoing explanations and the inspection of the actual wave configurations in Fig. 2.56 (compare the two frames for $M_0 = 3.45$). The pressure distribution associated with the oRR (dashed line) is seen to gradually increase to a value that is only about 10 times larger than the ambient pressure.

Ben-Dor et al.'s (2003) numerical study revealed that in all the cases in which the common Mach stem of the oMR wave configuration was long enough, pressure peaks that were 40–50 times larger than the ambient pres-

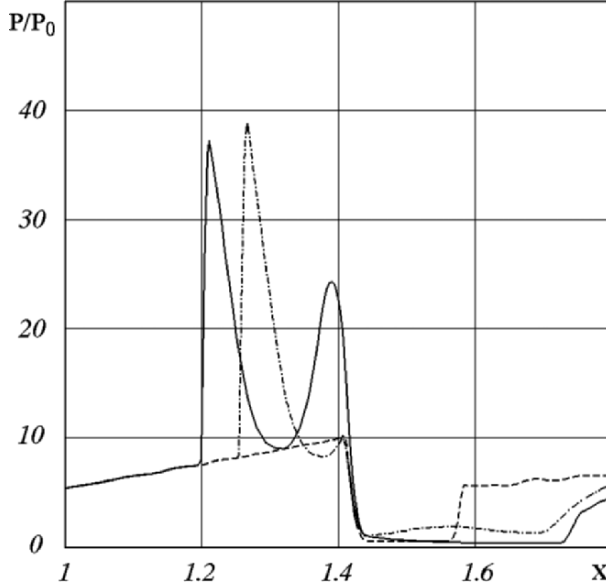


Fig. 2.57. The pressure distribution along the surface of the curvilinear cone for $M_0 = 3.45$ (loops A and C of Fig. 2.53). The distance is measured from the tip of the curvilinear cone. *Solid line*, oMR wave configuration having a long Mach stem; *Dash-Dotted line*, oMR wave configuration having a short Mach stem; *Dashed line*, ORR wave configuration

sure were reached. More details regarding the pressure distributions along the curvilinear cone surface for the wave configurations that are associated with the above-mentioned hysteresis loops in the above-described three cases can be found in Ben-Dor et al. (2003).

Downstream-Pressure-Variation-Induced Hysteresis

In all the above-treated flow fields, the shock wave reflection processes were free of downstream influences. Henderson & Lozzi (1979) hypothesized that the RR \rightleftharpoons MR transition could be promoted or suppressed by suitable choice of the downstream boundary conditions. Ben-Dor et al. (1999) investigated, numerically and analytically, the effect of the downstream pressure (i.e., the wake pressure behind the tail of the reflecting wedge.) on the shock wave reflection. They discovered a downstream-pressure-variation-induced hysteresis. Thus, their study confirmed the hypothesis of Henderson & Lozzi (1979) and showed both numerically and analytically how the RR and the MR wave configurations depend on the downstream pressure.

The numerically obtained downstream-pressure-variation-induced hysteresis is shown in Fig. 2.58. The initial conditions for these simulations were $M_0 = 4.96$ and $\beta_1 = 29.5^\circ$. The results were obtained in the following way.

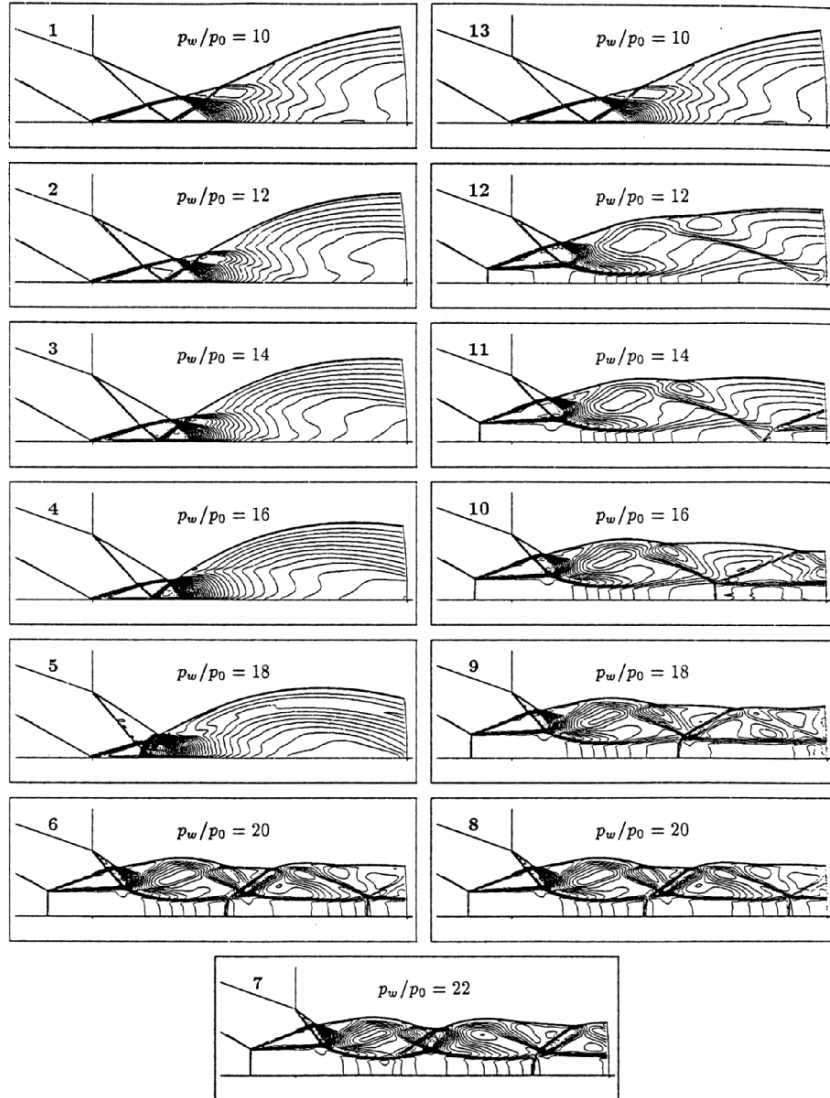


Fig. 2.58. The numerical downstream-pressure-variation-induced hysteresis

First the case with $p_w/p_0 = 10$ was solved (p_w is the downstream pressure, i.e., the wake pressure behind the tail of the reflecting wedge). Then, the final results for $p_w/p_0 = 10$ were used as the initial conditions for $p_w/p_0 = 12$. This procedure was repeated until $p_w/p_0 = 22$ was reached. Then p_w/p_0 was decreased, again by using the results of the previous case as the initial conditions for the next case until $p_w/p_0 = 10$ was reached again.

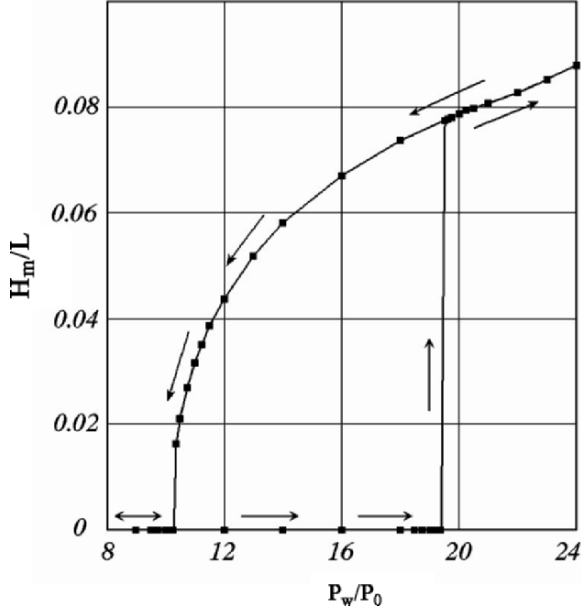


Fig. 2.59. The numerical downstream-pressure-variation-induced hysteresis loop in the $(H_m/L, p_w/p_0)$ -plane

Figure 2.58 indicated that a hysteresis exists in the reflection process. While the RR \rightarrow MR transition took place between frames (5) and (6), the reversed MR \rightarrow RR transition occurred between frames (12) and (13).

The downstream-pressure-variation-induced hysteresis loop is shown in Fig. 2.59 in the $(H_m/L, p_w/p_0)$ -plane (H_m is the height of the Mach stem and L is the length of the reflecting wedge surface). As can be seen the RR \rightarrow MR transition occurs at $p_w/p_0 = 19.63$ and the reversed MR \rightarrow RR transition takes place at $p_w/p_0 = 10$. Both transitions were associated with a sudden disappearance and appearance of a finite size Mach stem. These observations contradict Henderson & Lozzi's (1975) postulation that a mechanical equilibrium should exist at these transitions.

Effect of Free-Stream Perturbations on the RR \rightleftharpoons MR Transition

As both RR and MR wave configurations are observed inside the dual-solution domain both in numerical simulations and experiments, these wave configurations are stable to infinitesimal perturbations. However, large-amplitude perturbations may trigger a transition between these two wave configurations. Experimental facilities have certain levels of perturbations that differ from each other in their nature and magnitude. Hence, a question arises whether the discrepancies between the data on the transition angles that were obtained by means of different experimental facilities and the numerical results could be

attributed to the presence of disturbances in the experimental facilities and by their absence in the numerical computations.

Vuillon et al. (1995) investigated numerically the stability of an RR wave configuration by introducing perturbations behind the reflection point (the velocity was set to zero in several rows of the grid cells). Ivanov et al. (1996b) investigated, using a similar method, i.e., velocity perturbations, the influence of the disturbances near the reflection point using a DSMC method. It was revealed, in these studies, that velocity perturbations could indeed promote the transition from RR to MR.

Ivanov et al. (1996b and 1998d) with a DSMC method and Ivanov et al. (1998e) with an Eulerian code also investigated the influence of more physical short-time strong perturbations of the free stream. The perturbation, in their investigation, consisted of a short duration change in the free-stream velocity at the upstream boundary. The computations showed that such perturbations indeed affected the RR \rightarrow MR transitions.

The RR \rightarrow MR transition process is shown in Fig. 2.60. The perturbation consisted of a short duration 40% increase in the free-stream velocity at the upstream boundary. The early stages of the interaction of the perturbation with the RR wave configuration are seen in Fig. 2.60a. Following the interaction of the perturbations with the RR wave configuration the RR was changed to an MR wave configuration (Fig. 2.60d). Obviously, the reason for the formation of an MR wave configuration was a temporary existence of the shock wave with a large angle of incidence during this unsteady interaction.

The reversed MR \rightarrow RR transition by means of impulsive free stream perturbations (a short duration decrease in the free stream velocity) was observed also in the DSMC computations of Ivanov et al. (1996b and 1998d). The computations revealed that it was easier to promote the RR \rightarrow MR transition in the greater part of the dual-solution domain than the reversed MR \rightarrow RR transition, where stronger perturbations had to be applied. It is important to note that the Mach stem height was found to solely depend on the flow geometry and to be independent of the way the MR wave configuration was obtained.

Khotyanovsky et al. (1999) investigated numerically the effect of free-stream density perturbations. Moderate amplitude density perturbations were introduced in a thin layer near the reflection point. Unlike the just-discussed perturbation in the free stream velocity, this form of perturbing the flow had an advantage that it did not affect the entire flow field and was convected simply downstream, while being separated from the undisturbed flow with a contact surface. By perturbing the flow in this way both the RR \rightarrow MR and the MR \rightarrow RR transitions could be promoted inside the dual-solution domain. Such a “forced” transition between RR and MR wave configurations is illustrated in Fig. 2.61 for the following conditions inside the dual-solution domain: $M_0 = 4$ and $\beta_i = 36^\circ$. The steady RR wave configuration shown in Fig. 2.61a, was exposed to a short duration density perturbation, i.e., the density was decreased at the inflow in the 10 lower cells by 25%, i.e., $\Delta\rho/\rho_0 = -0.25$.

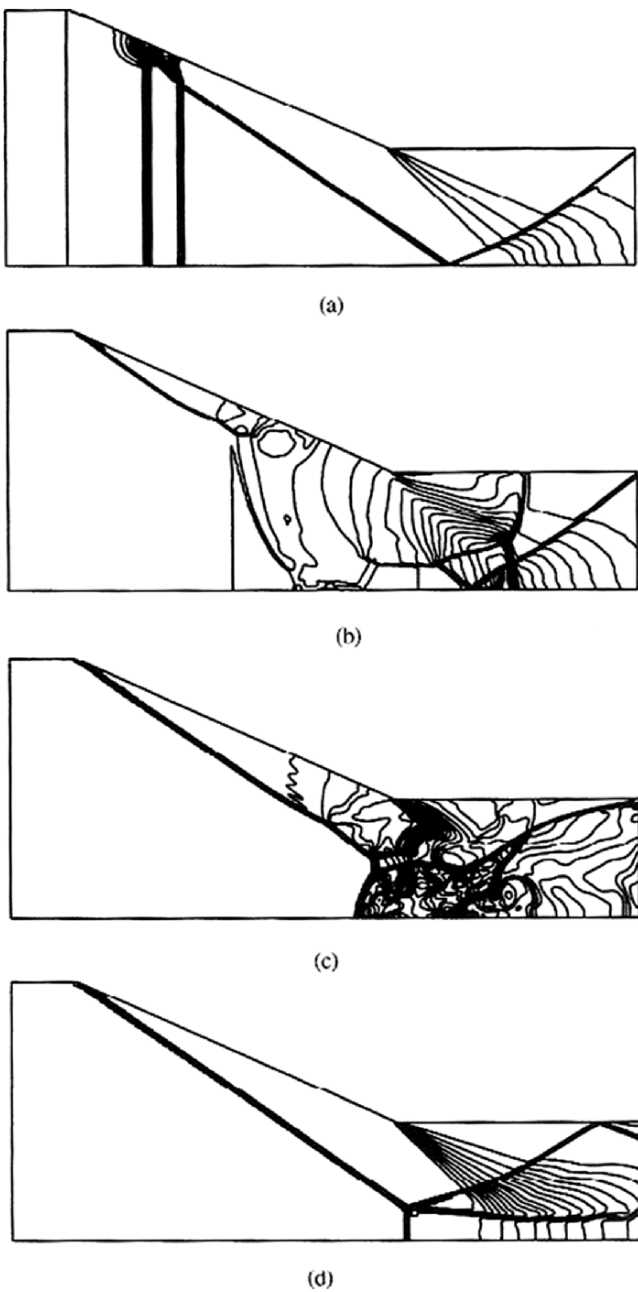


Fig. 2.60. The perturbation induced RR \rightarrow MR transition process

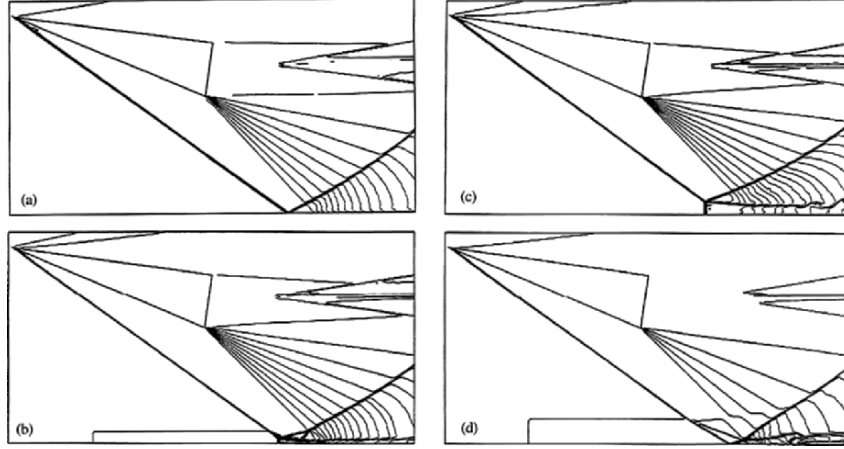


Fig. 2.61. The promotion of the RR \rightarrow MR and the MR \rightarrow RR transitions by density perturbations for $M_0 = 4$ and $\beta_i = 36^\circ$. (a) The RR wave configuration prior to the perturbation; (b) the beginning of the RR \rightarrow MR transition as a result of a density perturbation of $\Delta\rho/\rho_0 = -0.25$; (c) the steady-state MR wave configuration that was finally obtained after the perturbation was “switched off”; (d) the beginning of the MR \rightarrow RR transition as a result of a density perturbation of $\Delta\rho/\rho_0 = 0.5$. After the perturbation was “switched off” the RR wave configuration shown in (a) was established

As a result, the RR \rightarrow MR transition was promoted and an MR wave configuration started to be formed (see Fig. 2.61b). The flow field in Fig. 2.61b corresponds to a nondimensional time $\tau = 2.4\ell_w/u_0$ after the flow perturbation began (here ℓ_w is the length of the slope of the reflecting wedge along the windward plate and u_0 is the free-stream velocity). The perturbation was “switched off” after that moment, and the Mach stem persisted and continued growing. Finally, a steady-state MR wave configuration, shown in Fig. 2.61c was obtained.

The forced reversed MR \rightarrow RR transition is also shown in Fig. 2.61. The density was increased in the 20 lower cells by 50%, i.e., $\Delta\rho/\rho_0 = 0.5$, so that the triple point of the MR wave configuration was inside the perturbed layer. Because of the interaction of the perturbation with the triple shock configuration, the Mach stem height started to decrease until it finally disappeared. This is shown in Fig. 2.61d, which corresponds to a nondimensional time $\tau = 10w/u_0$ from the beginning of flow perturbation. At this time, the perturbation was already “switched off” and its “tail” was upstream from the

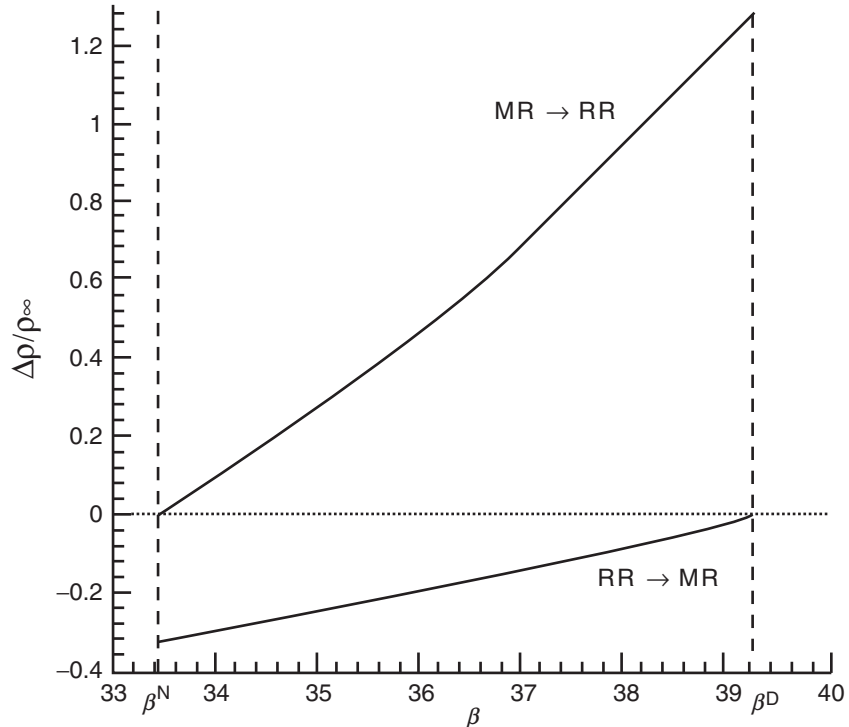


Fig. 2.62. The theoretically evaluated threshold levels of the perturbations, which are required to promote the $RR \rightarrow MR$ and the $MR \rightarrow RR$ transitions

reflection point. Once the perturbation disappeared an RR wave configuration was formed. It should be noted that the time required for the $MR \rightarrow RR$ transition to be completed was much greater than that required for the completion of the $RR \rightarrow MR$ transition.

The reason for the “switch” between the two shock wave configurations was the refraction of the incident shock wave in the perturbed region (see Fig. 2.61d). As a result, the shock wave angle near the reflection point was changed. If the level of the perturbation was high enough then the refracted shock angle in the perturbed layer could become larger than the detachment criterion or smaller than the von Neumann criterion. As a result, the $RR \rightarrow MR$ or $MR \rightarrow RR$ transitions became inevitable. The resulted shock wave configuration continued to exist after the perturbation was “switched off.”

The threshold levels of the perturbations that were required to cause the transitions were evaluated theoretically, and are shown in Fig. 2.62. It was found also that the $RR \rightarrow MR$ transition could be promoted with smaller perturbation intensities than the reversed $MR \rightarrow RR$ transition. It is apparent from Fig. 2.62 that the slope of the line corresponding to the $MR \rightarrow RR$ transition is much larger than that of the $RR \rightarrow MR$ transition. Consequently,

the levels of the perturbation capable of changing the MR wave configuration into an RR wave configuration are very high and comparable in magnitude, for some angles of incidence, to the free-stream density. Moreover, there is another reason making the promotion of the RR \rightarrow MR transition much easier to achieve than that of the reversed MR \rightarrow RR transition. For promoting the RR \rightarrow MR transition it is enough to have a perturbation localized in a very thin region near the reflection point. The thickness of this layer depends on the grid resolution, and is usually a few grid cells, so that the formation of the triple shock configuration inside the perturbed region could be resolved. The perturbation that is required for promoting the MR \rightarrow RR must have much larger scales both in space and in time. As mentioned above, its spatial extent must exceed the height of the Mach stem and its temporal duration must be long enough so that the relatively slow process of the decrease of the Mach stem height could be completed and the Mach stem can vanish before the perturbation is over.

Possible Application to Flight Dynamics

It has been shown that the theoretical prediction that multiple shock wave configuration could exist for identical flow conditions in a variety of shock wave related problems in steady flows, could lead to the existence of hysteresis processes. The analytically predicted hysteresis processes were verified both numerically and experimentally for a variety of steady reflection processes.

Since the investigated geometries resemble the geometry of supersonic intakes, the findings regarding the hysteresis loops could be relevant to flight performances at high supersonic and hypersonic speeds. The possible dependence of the flow pattern, in general, and the pressure distribution, in particular, on the preceding variations in the speed of flight of a supersonic/hypersonic aircraft should be taken into account in designing intakes and flight conditions for supersonic and hypersonic vehicles.

Consider Fig. 2.63 in which the upper part is a reproduction of Fig. 2.52. The overlap of the hysteresis loops A and B suggest that there is a flow-Mach number range for which three different wave configurations are possible. For example for the flow-Mach number $M_f = 3.8$ one can obtain an oMR wave configuration with a long Mach stem, or an oMR wave configuration with a short Mach stem or an oRR wave configuration. These three wave configurations are marked in Fig. 2.63 as (1), (2), and (3), respectively. The flow-Mach number at which the transition from an oMR wave configuration with a long Mach stem to an oMR wave configuration with a short Mach stem is labeled M_{tr_1} and the flow-Mach number at which the transition from an oMR wave configuration to an oRR wave configuration is labeled M_{tr_2} . The lower part of Fig. 2.63 shows possible flight-Mach number histories of a supersonic vehicle whose intake is geometrically identical to that shown in Fig. 2.41 and the leading edge of the curvilinear cone is

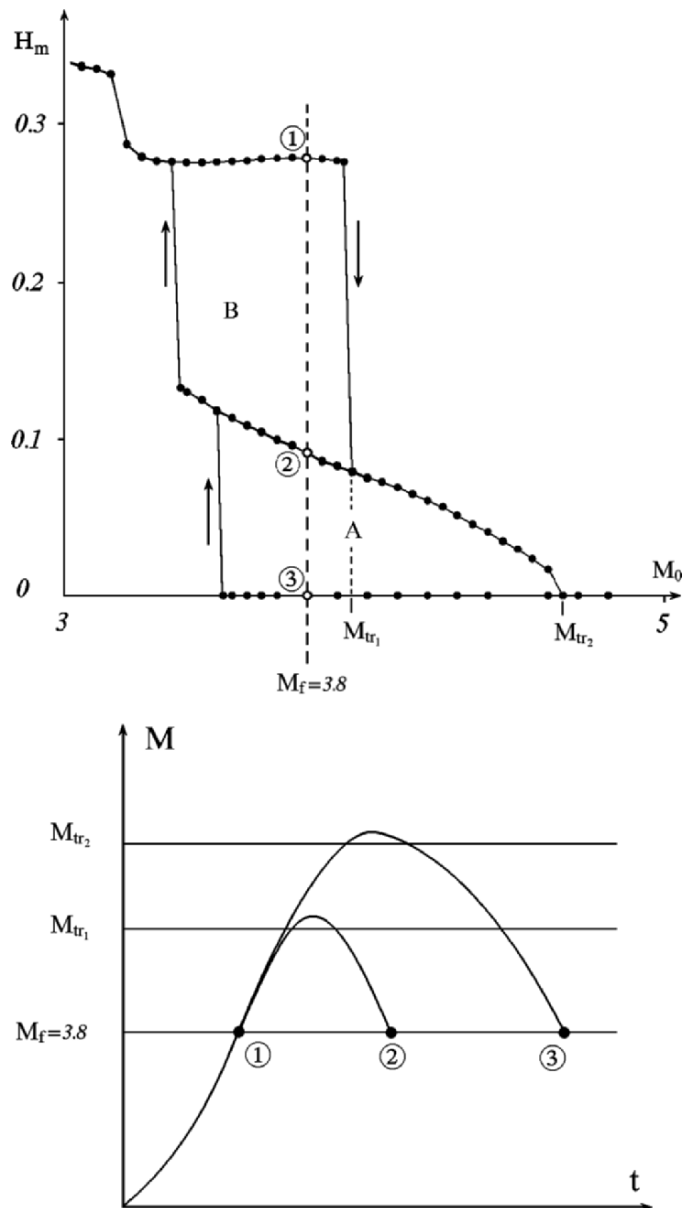


Fig. 2.63. Schematic illustration of the possibility of having a supersonic vehicle flying at the same speed and having different wave configurations in its supersonic intake

at $X = -0.2$. At $t = 0$ the vehicle starts accelerating to reach $M_f = 3.8$ [(state (1) in the figure]. Having reached this speed the wave configuration in its supersonic intake will be an oMR wave configuration with a long Mach stem. If at this stage the vehicle accelerates to a speed in the range $M_{tr_1} < M_f < M_{tr_2}$ and then returns to $M_f = 3.8$ then the wave configuration in the supersonic intake will change to an oMR with a short Mach stem [state (2) in the figure]. If, however, the vehicle accelerates to a speed in the range $M_f > M_{tr_2}$ and then returns to $M_f = 3.8$ then the wave configuration in the supersonic intake will change to an oRR [state (3) in the figure]. Hence, at identical supersonic flight speeds, i.e., $M_f = 3.8$, three different wave configurations might exist in the supersonic intake. As shown earlier (see Fig. 2.57), these different wave configurations are associated with different pressure distributions and hence different dynamic and thermodynamic properties.

References

- Azevedo, D.J. & 2 Liu, C.S., "Engineering approach to the prediction of shock patterns in bounded high-speed flows", AIAA J., 31(1), 83–90, 1993.
- Ben-Dor, G., *Shock Wave Reflection Phenomena*, Springer-Verlag, New York, NY, USA, 1991.
- Ben-Dor, G., Elperin, T. & Golshtain, E., "Monte Carlo analysis of the hysteresis phenomenon in steady shock wave reflections", AIAA J., 35(11), 1777–1779, 1997.
- Ben-Dor, G., Elperin, T., Li, H. & Vasiliev, E.I., "The influence of downstream-pressure on the shock wave reflection phenomenon in steady flows", J. Fluid Mech., 386, 213–232, 1999.
- Ben-Dor, G., Elperin, T. & Vasilev, E.I., "Flow-Mach-number-induced hysteresis phenomena in the interaction of conical shock waves - A numerical investigation", J. Fluid Mech., 496, 335–354, 2003.
- Ben-Dor, G., Elperin, T. & Vasilev, E.I., "Shock wave induced extremely high oscillating pressure peaks", Materials Sci. Forum, 465–466, 123–130, 2004.
- Ben-Dor, G. & Takayama, K., "The phenomena of shock wave reflection - A review of unsolved problems and future research needs", Shock Waves, 2(4), 211–223, 1992.
- Ben-Dor, G., Vasiliev, E.I., Elperin, T. & Chpoun, A., "Hysteresis phenomena in the interaction process of conical shock waves: Experimental and numerical investigations", J. Fluid Mech., 448, 147–174, 2001.
- Burstchell, Y., Zeitoun, D.E., Chpoun, A. & Ben-Dor, G., "Conical shock interactions in steady flows: Numerical study", 23rd Int. Symp. Shock Waves, Fort Worth, Texas, U.S.A, 2001.
- Chpoun, A. & Ben-Dor, G., Numerical confirmation of the hysteresis phenomenon in the regular to the Mach reflection transition in steady flows", Shock Waves, 5(4), 199–204, 1995.

- Chpoun, A., Chauveux, F., Zombas, L. & Ben-Dor, G., "Interaction d'onde de choc coniques de familles opposees en ecoulement hypersonique stationnaire", Mecanique des Fluides/Fluid Mechanics, C.R. Acad Sci Paris, 327(1), 85–90, 1999.
- Chpoun, A. & Lengrand, J.C., "Confermation experimentale d'un phenomene d'hysteresis lors de l'interaction de deux chocs obliques de familles differentes", C.R. Acad. Sci. Paris, 304, 1, 1997.
- Chpoun, A., Passerel, D., Lengrand, J.C., Li, H. & Ben-Dor, G., "Mise en evidence experimentale et numerique d'un phenomene d'hysteresis lors de la transition reflexion de Mach-reflexion reguliere", C. R. Acad. Sci. Paris, 319(II), 1447–1453, 1994.
- Chpoun, A., Passerel, D., Li, H. & Ben-Dor, G., "Reconsideration of oblique shock wave reflection in steady flows. Part 1. Experimental investigation", J. Fluid Mech., 301, 19–35, 1995.
- Courant, R. & Friedrichs, K.O., *Hypersonic Flow and Shock Waves*, Wiley Interscience, New York, NY, USA, 1959.
- Emanuel, G., *Gasdynamics: Theory and Applications*, AIAA Education Series, AIAA Inc., New York, U.S.A., 1986.
- Fomin, V.M., Hornung, H.G., Ivanov, M.S., Kharitonov, A.M., Klemenkov, G.P., Kudryavtsev, A.N. & Pavlov, A.A., "The study of transition between regular and Mach reflection of shock waves in different wind tunnels", in Proc. 12th Int. Mach Reflection Symp, Ed. B. Skews, Pilanesberg, South Africa, 137–151, 1996.
- Henderson, L.F., "The reflection of a shock wave at a rigid wall in the presence of a boundary layer", J. Fluid Mech., 30, 699–722, 1967.
- Henderson, L.F., "On the refraction of shock waves", J. Fluid Mech., 198, 365–386, 1989.
- Henderson, L.F. & Lozzi, A., "Experiments of transition to Mach reflection", J. Fluid Mech., 68, 139–155, 1975.
- Henderson, L.F. & Lozzi, A., "Further experiments of transition to Mach reflection", J. Fluid Mech., 94, 541–560, 1979.
- Hornung, H.G., Oertel, H. Jr. & Sandeman, R.J., "Transition to Mach reflection of shock waves in steady and pseudo-steady flow with and without relaxation", J. Fluid Mech., 90, 541–560, 1979.
- Hornung, H.G. & Robinson, M.L., "Transition from regular to Mach reflection of shock waves. Part 2. The Steady-Flow Criterion", J. Fluid Mech., 123, 155–164, 1982.
- Ivanov, M.S., Ben-Dor, G., Elperin, T., Kudryavtsev, A.N., Khotyanovsky & D.V., "Mach-number-variation-induced hysteresis in steady flow shock wave reflections", AIAA J., 39(5), 972–974, 2001.
- Ivanov, M.S., Ben-Dor, G., Elperin, T., Kudryavtsev, A.N. & Khotyanovsky, D.V., "The reflection of asymmetric shock waves in steady flows: A numerical investigation", J. Fluid Mech., 469, 71–87, 2002.
- Ivanov, M.S., Gimelshein, S.F. & Beylich, A.E., "Hysteresis effect in stationary reflection of shock waves", Phys. Fluids, 7, No. 4, 685–687, 1995.

- Ivanov, M.S., Gimelshein, S.F., Kudryavtsev, A.N. & Markelov, G.N., "Transition from regular to Mach reflection in two- and three-dimensional flows", in Proc. 21st Int Symp Shock Waves, Eds. A.F.P. Houwing, A. Paull, R.R. Boyce, R.R. Xanehy, M. Hannemann, J.J. Kurtz, T.J. McIntyre, S.J. McMahon, D.J. Mee, R.J. Sandeman & H. Tanno, Panther Publ., Fyshwick, Australia, II, 813–818, 1998e.
- Ivanov, M.S., Gimelshein, S.F. & Markelov, G.N., "Statistical simulation of the transition between regular and Mach reflection in steady flows", Computers & Math. with Appl., 35(1/2), 113–125, 1998d.
- Ivanov, M.S., Gimelshein, S.F., Markelov, G.N. & Beylich, A.E., "Numerical investigation of shock-wave reflection problems in steady flows", in Proc. 20th Int. Symp. Shock Waves, Eds. B. Sturtevant, J.E. Shepherd & H.G. Hornung, World Scientific Publ., 1, 471–476, 1996b.
- Ivanov, M.S., Kharitonov, A.M., Klemenkov, G.P., Kudryavtsev, A.N., Nikiforov, S.B. & Fomin, V.M., "Influence of test model aspect ratio in experiments on the RR ⇌ MR transition", in Proc. 13th Int. Mach Reflection Symp Ed. G. Ben-Dor, Beer-Sheva, Israel, 3, 1998a.
- Ivanov, M.S., Klemenkov, G.P., Kudryavtsev, A.N., Nikiforov, S.B., Pavlov, A.A., Fomin, V.M., Kharitonov, A.M., Khotyanovsky, D.V. & Hornung, H.G., "Experimental and numerical study of the transition between regular and Mach reflections of shock waves in steady flows", in Proc. 21st Int. Symp. Shock Waves, Eds. A.F.P. Houwing, A. Paull, R.R. Boyce, R.R. Xanehy, M. Hannemann, J.J. Kurtz, T.J. McIntyre, S.J. McMahon, D.J. Mee, R.J. Sandeman, & H. Tanno, Panther Publ., Fyshwick, Australia, II, 819–824, 1998b.
- Ivanov, M.S., Markelov, G.N., Kudryavtsev, A.N. & Gimelshein, S.F., "Numerical analysis of shock wave reflection transition in steady flows", AIAA J., 36(11), 2079–2086, 1998c.
- Ivanov, M., Zeitoun, D., Vuillon, J., Gimelshein, S. & Markelov, G.N., "Investigation of the hysteresis phenomena in steady shock reflection using kinetic and continuum methods", Shock Waves, 5(6), 341–346, 1996a.
- Khotyanovsky, D.V., Kudryavtsev, A.N. & Ivanov, M.S., "Numerical study of transition between steady regular and Mach reflection caused by free-stream perturbations", in Proc. 22nd Int. Symp. Shock Waves, Eds. G.J. Ball, R. Hillier & G.T. Roberts, University of Southampton, 2, 1261–1266, 1999.
- Kudryavtsev, A.N., Khotyanovsky, D.V., Markelov, G.N. & Ivanov, M.S., "Numerical simulation of reflection of shock waves generated by finite-width wedge", in Proc. 22nd Int. Symp. Shock Waves, Eds. G.J. Ball, R. Hillier & G.T. Roberts, University of Southampton, 2, 1185–1190, 1999.
- Landau, L.D. & Lifshitz, E.M., *Fluid Mechanics*, Pergamon, 1987.
- Li, H. & Ben-Dor, G., "Application of the principle of minimum entropy production to shock wave reflections. I. Steady flows", J. Appl. Phys., 80(4), 2027–2037, 1996.

- Li, H. & Ben-Dor, G., "Oblique-shock/expansion-fan interaction: Analytical solution", AIAA J., 34, No. 2, 418–421, 1996.
- Li, H. & Ben-Dor, G., "A parametric study of Mach reflection in steady flows", J. Fluid Mech., 341, 101–125, 1997.
- Li, H., Chpoun, A. & Ben-Dor, G., "Analytical and experimental investigations of the reflection of asymmetric shock waves in steady flows", J. Fluid Mech., 390, 25–43, 1999.
- Liepmann, H.W. & Roshko, A., 1957, *Elements of Gasdynamics*, John Wiley & Sons, Inc.
- Molder, S., "Reflection of curved shock waves in steady supersonic flow", CASI Trans., 4, 73–80, 1971.
- Molder, S., "Particular conditions for the termination of regular reflection of shock waves", CASI Trans., 25, 44–49, 1979.
- Onofri, M. & Nasuti, F., "Theoretical considerations on shock reflections and their implications on the evaluations of air intake performance", in Proc. 22nd Int. Symp. Shock Waves, Eds. G.J. Ball, R. Hillier & G.T. Roberts, Univ. Southampton, 2, 1285–1290, 1999.
- Pant, J.C., "Reflection of a curved shock from a straight rigid boundary", Phys. Fluids, 14, 534–538, 1971.
- Shapiro, A.H., *The Dynamics and Thermodynamics of Compressible Fluid Flow*, II, The Ronald Press Co., New York, N.Y., U.S.A., 1953.
- Shirozu, T. & Nishida, M., "Numerical studies of oblique shock reflection in steady two dimensional flows", Memoirs Faculty Eng. Kyushu Univ., 55, 193–204, 1995.
- Skews, B.W., "Aspect ratio effects in wind tunnel studies of shock wave reflection transition", Shock Wave, 7, 373–383, 1997.
- Skews, B.W., "Oblique shadowgraph study of shock wave reflection between two wedges in supersonic flow", in Proc. 13th Int. Mach Reflection Symp., Ed. G. Ben-Dor, Beer-Sheva, Israel, p. 3, 1998.
- Skews, B.W., "Three dimensional effects in wind tunnel studies of shock wave reflection", J. Fluid Mech., 407, 85–104, 2000.
- Skews, B.W., Vukovic, S. & Draxl, M., "Three-dimensional effects in steady flow wave reflection transition", in Proc. 12th Int. Mach Reflection Symp., Ed. B. Skews, Pilanesberg, South Africa, 152–162, 1996.
- Sternberg, J., 1959 "Triple shock-wave intersections", Phys. Fluids, 2(2), 178–206.
- Takayama, K. & Ben-Dor, G., "The inverse Mach reflection", AIAA J., 23(12), 1853–1859, 1985.
- Teshukov, V.M., "On stability of regular reflection of shock waves", Pril. Mekhanika i Techn. Fizika, 2, 26–33, 1989, (in Russian). (Translated to English in Appl. Mech. & Tech. Phys.).
- Vuillon, J., Zeitoun, D. & Ben-Dor, G., "Reconsideration of oblique shock wave reflection in steady flows. Part 2. Numerical investigation", J. Fluid Mech., 301, 37–50, 1995.

3

Shock Wave Reflections in Pseudosteady Flows

List of symbols

Latin Letters

a_i	Local speed of sound in state (i)
A_{ij}	$= a_i/a_j$
C	Constant
C_p	Specific heat capacity at constant pressure
C_v	Specific heat capacity at constant volume
H_m	Distance from the first triple point to the reflecting surface (= Length of the Mach stem when it is assumed to be straight)
h_i	Enthalpy in state (i)
k	Thermal conductivity
l_d	Dissociational relaxation length
l_v	Vibrational relaxation length
L	Horizontal distance traveled by the triple point
L_G	Distance of the foot of the Mach Stem from the leading edge of the reflecting wedge
L_K	Horizontal distance by which the kink, K, lags behind the triple point, T
L_T	Horizontal distance of the first triple point from the leading edge of the reflecting wedge
$L_{T'}$	Horizontal distance of the second triple point from the leading edge of the reflecting wedge
L_1	Thickness of the shock front
L_2	Thickness of the relaxation zone behind a shock wave
M_S	Incident shock wave Mach number
M_i	Flow Mach number in state (i)
M_i^J	Flow Mach number in state (i) with respect to point (J)
p_i	Static pressure in state (i)
p_b	Pressure behind the bow shock wave near its interaction with the reflected shock wave

Pr	Prandtl number
P_{ij}	$= p_i/p_j$
Re	Reynolds number
t	Time
T_i	Flow temperature in state (i)
T_{1f}	Frozen temperature behind the shock front
T_w	Temperature of the reflecting surface
u_i	Flow velocity in state (i) with respect to R in RR or T in MR
u_i^j	Flow velocity in state (i) with respect to the flow velocity in state (j)
u_i^J	Flow velocity in state (i) with respect to point J
u_S	Incident shock wave velocity
V_A^B	Velocity of point A with respect to point B
V_i	Flow velocity in state (i) in a laboratory frame of reference
V_{ij}	$= V_i/a_j$
V_S	Incident shock wave velocity
x	Coordinate
x_{char}	Characteristic length
y	Coordinate

Greek Letters

α	Orientation of the flow behind the incident shock wave, in a frame of reference attached to the triple point, with respect to a horizontal line (Fig. 3.22)
χ	First triple point trajectory angle in MR (SMR, TMR, PTMR or DMR)
χ'	Second triple point trajectory angle in DMR
χ_K	Kink trajectory angle
δ	Kinematic boundary layer thickness
δ_T	Thermal boundary layer thickness
δ^*	Boundary layer displacement thickness
Δt	Time interval
ϵ	Roughness
ϕ_i	Angle of incidence between the flow and the stationary oblique shock wave across which the flow enters state (i)
γ	Specific heat capacities ratio ($= C_p/C_v$)
η	$= \theta_w^{\text{tr}}(\epsilon)/\theta_w^{\text{tr}}(0)$
λ	Mean free path
μ	Dynamic viscosity
θ_i	Deflection angle of the flow while passing across a stationary oblique shock wave into state (i)
θ_w	Reflecting wedge angle
θ_w^C	Complementary wedge angle
$\theta_w^{\text{tr}}(0)$	RR \rightleftharpoons IR transition wedge angle over smooth surface ($\epsilon = 0$)
$\theta_w^{\text{tr}}(\epsilon)$	RR \rightleftharpoons IR transition wedge angle over a surface having a roughness – ϵ
ρ_i	Flow density in state (i)
ω_{ij}	Angle between the discontinuities i and j

ξ	Inverse pressure ratio across the incident shock wave ($= P_{01} = p_0/p_1$)
ξ'	Angle between the reflecting surface of a slotted wedge and the contact discontinuity below it
Ψ	Discharge coefficient
ζ	Boundary layer displaced angle; also the divergence angle of the angular contact zone, as shown in Fig. 3.59b
ζ'	Matching coefficient

Subscripts

0	Flow state ahead of the incident shock wave, i
1	Flow state behind the incident shock wave, i
2	Flow state behind the reflected shock wave, r
3	Flow state behind the Mach stem, m
4	Flow state behind the secondary Mach stem, m'
5	Flow state behind the secondary reflected shock wave, r'

Superscripts

'	With respect to the second triple point
---	---

Abbreviations

Waves and Points

B	Bow shock wave
D	Point where r' of a DMR reaches the reflecting surface (Fig. 3.23)
i	Incident shock wave
m	Mach stem
m'	Secondary Mach stem
r	Reflected shock wave
r'	Secondary reflected shock wave
s	Slipstream
s'	Secondary slipstream
K	Kink
K'	Second kink
L	Laboratory
R	Reflection point
T	First triple point
T'	Second triple point
T''	Third triple point

Wave Configuration

DMR	Double-Mach reflection
DMR^+	Positive-double-Mach reflection
DMR^-	Negative-double-Mach reflection
DiMR	Direct-Mach reflection
GR	Guderley reflection
InMR	Inverse-Mach reflection
IR	Irregular reflection

MR	Mach reflection
NR	No reflection
PTMR	Pseudotransitional Mach reflection
RR	Regular reflection
SMR	Single-Mach reflection
StMR	Stationary-Mach reflection
TDMR	Transitional-double Mach reflection
TerDMR	Terminal-double Mach reflection
TMR	Transitional-Mach reflection
TrMR	Triple-Mach reflection
TRR	Transitioned regular reflection
vNR	von Neumann reflection
VR	Vasilev reflection

A shock wave that is propagating with a constant velocity with respect to the laboratory frame of reference could be investigated using steady flow concepts and theories by attaching a frame of reference to it. In such a frame of reference, the shock wave is stationary, and the entire flow field is known as either pseudostationary or pseudosteady. The just-mentioned transformation, known as the Galilean transformation, is shown schematically in Fig. 3.1. In Fig. 3.1a a constant velocity shock wave having a velocity of V_s is seen to propagate from left to right, towards a flow having a velocity V_i and to induce behind it a flow velocity V_j . The velocities with respect to a frame of reference attached to the shock wave are shown in Fig. 3.1b. In this frame of reference the flow in state (i) propagates towards the stationary shock wave with the velocity $u_i = V_s - V_i$. Upon passing through the shock wave its velocity is reduced to $u_j = V_s - V_j$. The velocity field shown in Fig. 3.1b is obtained actually by superimposing a velocity equal to the shock-wave velocity but opposite in its direction on the velocity field shown in Fig. 3.1a. The flow field of Fig. 3.1b is pseudosteady, and hence can be treated using the steady flow theories.

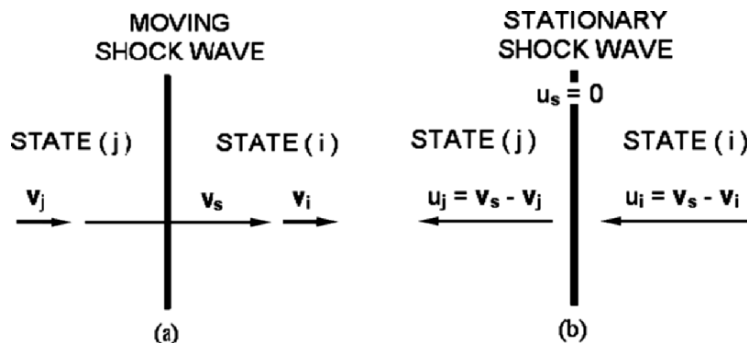


Fig. 3.1. Schematic illustration of the Galilean transformation

Experimental observations of the wave configurations of RR, SMR, TMR, and DMR in shock-tube experiments indicated that by and large any point on these wave configurations, having a radius vector, \mathbf{r} , with the leading edge of the reflecting wedge as the origin was transformed at a later time to a new point located at $C\mathbf{r}$, where C is a scalar constant. This observation means that x and y may be measured relative to any point moving with constant velocity with respect to the reflecting wedge and that instead of three independent variables, x , y and t , the reflection phenomenon is describable in terms of x/t and y/t . In other words, the flow is self-similar and as such, it could be treated as pseudosteady. Further considerations regarding this issue can be found in Jones et al. (1951). Some doubts regarding the accuracy of these observations, which have been raised in the past, will be discussed in subsequent sections.

The analytical investigation of the reflection phenomenon of shock waves in pseudosteady flows is more difficult than that in steady flows for the following reasons:

- Unlike the reflection process in steady flows where the process is independent of any other process, in pseudosteady flows the reflection process is coupled with the flow deflection process around the reflecting wedge (see Sect. 3.2.2).
- Unlike in steady flows where the three-shock theory [(1.14)–(1.27)] is sufficient to calculate the transition boundaries between the various shock reflection configurations in the (M_0, ϕ_1) -domain (see Fig. 2.5a, b), in pseudosteady flows there is a need to analytically predict the first triple point trajectory angle, χ , in order to transform the results from the (M_S, θ_w^C) -plane (see Fig. 1.25), which is analogous to the (M_0, ϕ_1) -plane since $M_S = M_0 \sin \phi_1$ and $\theta_w^C = 90^\circ - \phi_1$, to the more physically meaningful and more applicable (M_S, θ_w) -plane. In order to present the results in this plane the equations of the three-shock theory [(1.14)–(1.27)] should be solved together with an additional expression for χ [see e.g., (3.23)].
- Unlike steady flows where the irregular reflection, IR, can be only one type of Mach reflection, MR, in pseudosteady flows the IR consists of many more different shock wave reflection configurations.

3.1 “Old” State-of-the-Knowledge

The first edition of this monograph, which was published in 1991 summarized the state-of-the-knowledge that existed until then. A study by Li & Ben-Dor (1995), which re-introduced an alternative analytical approach of considering the shock wave reflection phenomenon in pseudosteady flows, was in fact one of the reasons for writing this second edition. However, for the reader’s convenience the results regarding the types of shock reflection configurations and the transition criteria between them, which were published in the first edition,

will be summarized in this section. They will be referred to as the “*old*”-*State-of-the-Knowledge* as opposed to the “*new*”-*State-of-the-Knowledge* that arose following the study of Li & Ben-Dor (1995).

When a planar incident shock wave moving with a constant velocity encounters a sharp compressive straight wedge in a shock tube, it reflects over the wedge surface. Depending upon the incident shock wave Mach number, M_S , and the reflecting wedge angle, θ_w , different reflection wave configurations can be obtained. Since the shock wave moves with a constant velocity over a straight wedge, the reflection process is pseudosteady.

3.1.1 Reflection Configurations

In general, the shock-wave reflection configurations could be:

- A regular reflection, RR, or
- An irregular reflection, IR.

The irregular reflection could be either:

- A von-Neumann reflection, vNR, or
- A Mach reflection, MR.

In general, the Mach reflection could be one of the following three types:

- A direct-Mach reflection, DiMR, whose triple point moves away from the reflecting wedge surface
- A stationary-Mach reflection, StMR, whose triple point moves parallel to the reflecting wedge surface
- An inverse-Mach reflection,¹ InMR, whose triple point moves towards the reflecting wedge surface

Upon the collision of the triple point of the inverse-Mach reflection with the reflecting surface, the inverse-Mach reflection terminates and gives rise to a transitioned-regular reflection, TRR. In pseudosteady flows, the Mach reflection is always a direct-Mach reflection.

The DiMR could be divided further into three different types:

- A single-Mach reflection, SMR
- A transitional-Mach reflection, TMR
- A double-Mach reflection, DMR

Depending on whether the triple point trajectory angle of the first triple point is larger or smaller than that of the second triple point, the double-Mach reflection could be further divided into two types:

- A positive double-Mach reflection, DMR⁺
- A negative double-Mach reflection, DMR⁻

¹ Courant & Friedrichs (1948) called it originally inverted-Mach reflection.

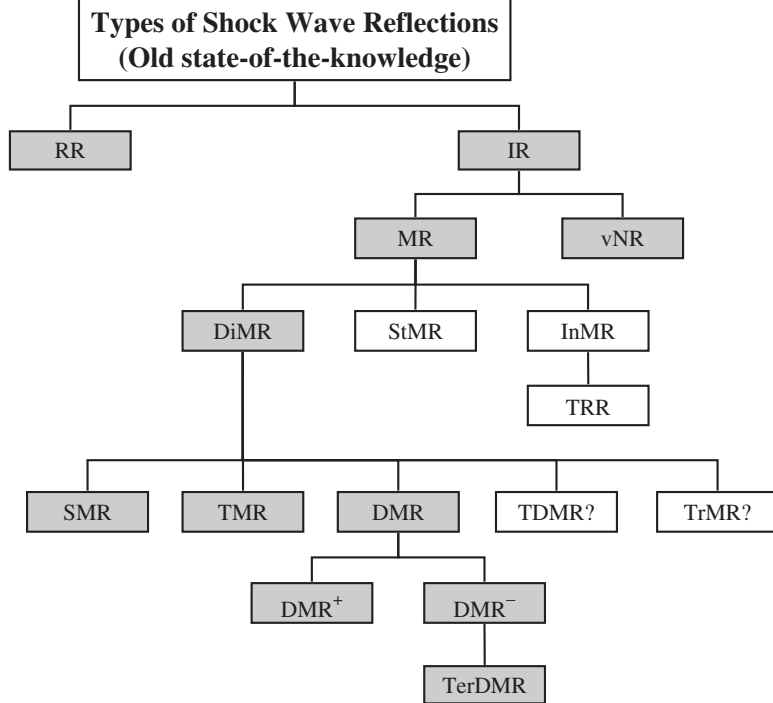


Fig. 3.2. Evolution-tree type presentation of the various types of shock wave reflection configurations according to the “old” state-of-the-knowledge that existed until the mid-1990s and was summarized in Ben-Dor (1991). The shadowed shock wave reflections have been observed actually in pseudosteady experiments

An additional wave configuration, the terminal double-Mach reflection, TerDMR, in which the second triple point of the double-Mach reflection lies on the reflecting wedge surface, was also mentioned as a possible wave configuration.

Illustrations of the evolution-tree of the just-mentioned various types of shock-wave reflection configurations and a schematic illustration of them are shown in Figs. 3.2 and 3.3, respectively. The shock wave reflection wave configurations that have been observed actually in pseudosteady experiments are marked with gray background in Fig. 3.2.

In addition, Ben-Dor & Takayama (1986/7) hypothesized that under some circumstances two additional shock wave reflection wave configurations could materialize in pseudosteady flows. They are a DMR with a kink or a reversal of curvature in its second Mach stem, i.e., a transitional-double-Mach reflection, TDMR, and a triple-Mach reflection, TrMR.

As mentioned in Chap. 1 the RR and the SMR were first observed and mentioned by Mach (1878); the TMR was first reported by Smith (1945); the DMR was discovered and first reported by White (1951); the DiMR, StMR,

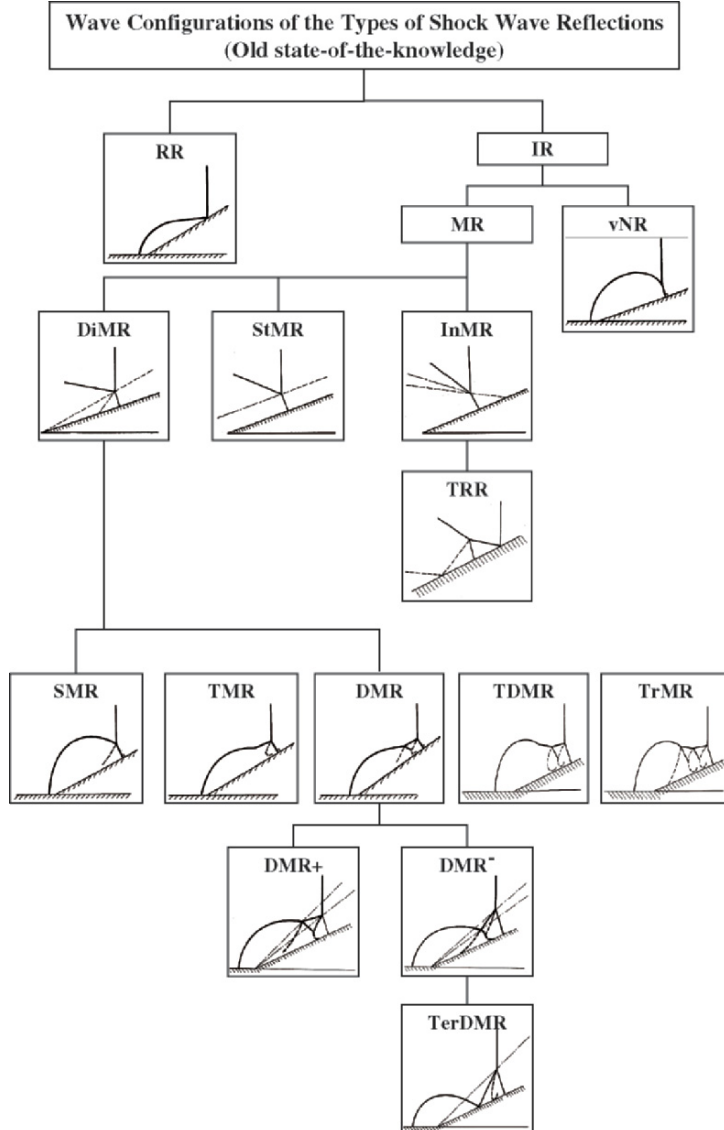


Fig. 3.3. Evolution-tree type presentation of the wave configurations of the various types of shock wave reflections that appear in Fig. 3.2

and InMR were first mentioned by Courant & Friedrichs (1948). Although Ben-Dor (1981) was the first to mention the possibility of the existence of DMR^+ and DMR^- their names were assigned by Lee & Glass (1984); the TerDMR was first mentioned by Lee & Glass (1984). The vNR was first introduced by Colella & Henderson (1990).

3.1.2 The Transition Criteria

The accepted transition criteria between the above-mentioned various reflection configurations that could result from the reflection of a constant-velocity planar shock wave over a straight surface are summarized in Chap. 2.3 of Ben-Dor (1991), and Ben-Dor & Takayama (1992).

Out of the various suggested criteria for the termination of RR (Figs. 3.4a, b), the one which best agrees with pseudosteady experimental data, arises

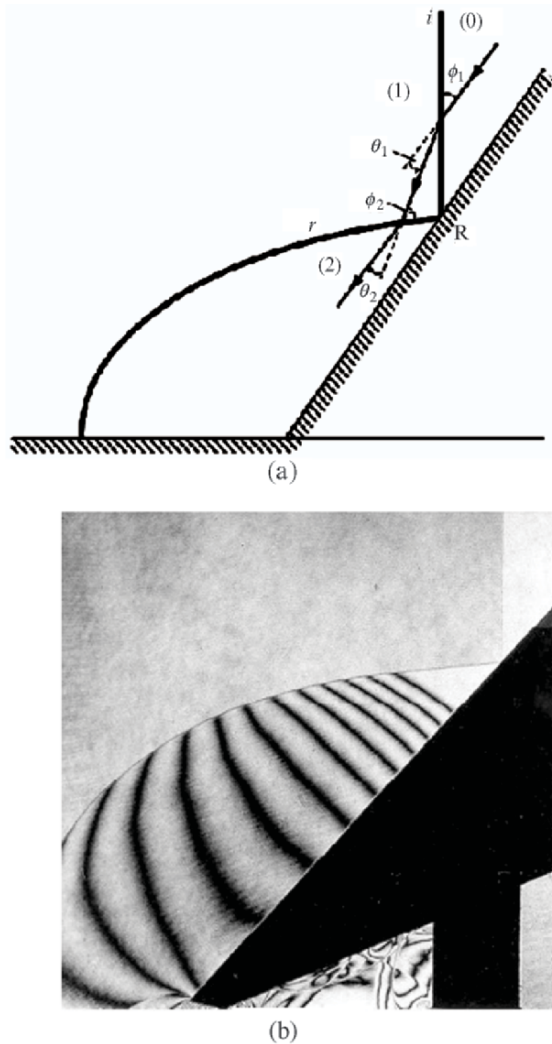


Fig. 3.4. Pseudosteady regular reflection, RR: (a) schematic illustration of the wave configuration and definition of some parameters; (b) photograph (Courtesy of Professor K. Takayama)

from the length scale concept of Hornung et al. (1979), which suggests that the RR terminates, in pseudosteady flows, when the flow behind the reflection point, R , of the RR (see Fig. 3.4a) becomes sonic in a frame of reference attached to R . This criterion implies that the $\text{RR} \Leftarrow \text{IR}$ (IR stands for irregular reflection, i.e., MR or vNR) transition occurs when

$$M_2^R = 1, \quad (3.1)$$

where M_2^R is the flow Mach number in state (2), behind the reflected shock wave of the RR, with respect to the reflection point R . As long as the flow behind the reflection point is supersonic, $M_2^R > 1$, the corner-generated signals cannot catch-up with the reflection point, R , and communicate to it a physical length scale. As a result, an IR-wave configuration, which is typified by a finite length shock wave, the Mach stem, is impossible, since the existence of a finite length shock wave requires the presence of a physical length scale at the reflection point. Clear evidence to this situation is the fact that the reflected shock wave has a straight part near the reflection point (see Fig. 3.4). In fact, the point along the reflected shock wave that has been reached by the corner-generated signals is also seen in Fig. 3.4b. The uniform bright zone downstream of it is the supersonic zone that isolates the reflection point from the corner-generated signals.

Once the corner-generated signals have caught up with the reflection point, R , they communicate to it a physical length scale, and an IR-wave configuration, typified by a finite length shock wave (i.e., the Mach stem), becomes possible and in fact is formed. The IR can be either an MR (Fig. 3.5) in which three shock waves and one contact discontinuity (usually referred to as slip-stream) meet at one point, the triple point, T , or a vNR (Fig. 3.6) depending on the angle of incidence, ϕ_2 , between the flow in state (1) behind the incident

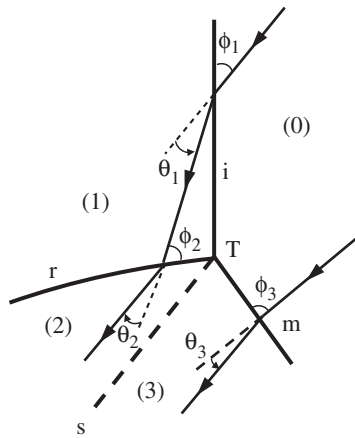
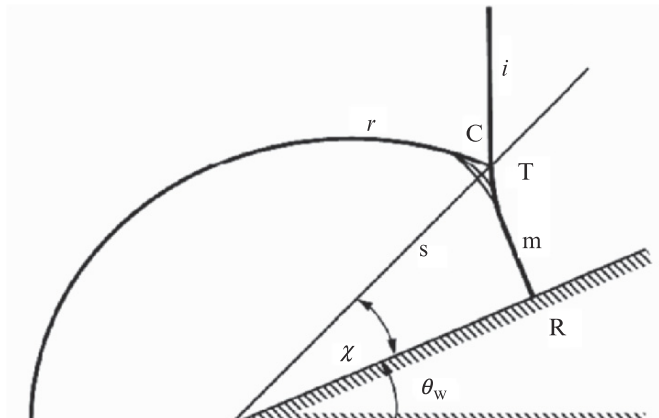
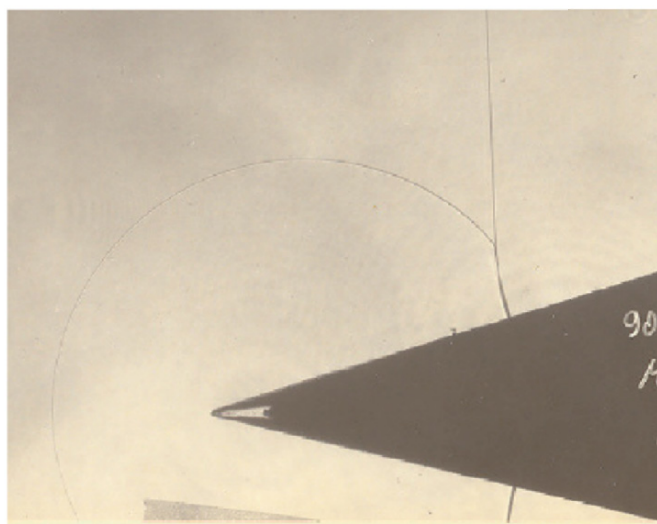


Fig. 3.5. Schematic illustration of the three-shock confluence of a Mach reflection and definition of some parameters



(a)



(b)

Fig. 3.6. Pseudosteady von Neumann reflection, vNR: (a) schematic illustration of the wave configuration and definition of some parameters; (b) photograph (Courtesy of Professor K. Takayama)

shock wave, i , and the reflected shock wave, r , in a frame of reference attached to the triple point, T (see Fig. 3.5). The reflection is an MR as long as $\phi_2 < 90^\circ$. Consequently, the $MR \rightleftharpoons vNR$ transition takes place when:

$$\phi_2 = 90^\circ. \quad (3.2a)$$

When $\phi_2 = 90^\circ$, i.e., when the flow in state (1) is perpendicular to the reflected shock wave, r , it is not deflected while passing through the reflected shock wave. Since the flow behind the reflected shock wave, r , must be parallel to the slipstream, s , it is obvious that the condition given by (3.2a) can be also expressed as:

$$\omega_{rs} = 90^\circ, \quad (3.2b)$$

where ω_{rs} is the angle between the reflected shock wave, r , and the slipstream, s .

Unlike a clear and sharp change in the orientation of the Mach stem with respect to the incident shock wave at the triple point of a Mach reflection (see e.g., Figs. 3.5, 3.7–3.9) in a von Neumann reflection (Fig. 3.6) the Mach stem is seen to smoothly merge into the incident shock wave. In addition, while the reflected wave is a clear shock wave in a Mach reflection it is only a band of compression waves in a von Neumann reflection.

Once the condition for the existence of a Mach reflection is met, i.e., $\phi_2 < 90^\circ$, the value of the flow Mach number, in state (2) behind the reflected shock wave, r , of the Mach reflection with respect to the triple point, T , i.e., M_2^T , becomes the significant parameter in determining the particular type of the obtained Mach reflection.

As long as $M_2^T < 1$, the reflection is an SMR (Figs. 3.7a, b) typified by a reflected shock wave, which is curved along its entire length. This implies that a physical length scale, which is required in order for a radius of curvature to exist, is communicated through state (2) all the way to the triple point, T , from which the curved reflected shock wave emanates. Gas dynamic considerations imply that this communication path is possible only if $M_2^T < 1$.

When the flow in state (2) becomes supersonic with respect to the triple point, T , i.e., $M_2^T > 1$ (see Fig. 3.7), the just-mentioned communication path is blocked by a supersonic flow zone and the reflected shock wave develops a straight portion that terminates at a point known as the kink,² K, which indicates the point along the reflected shock wave, r , that has been reached by the corner-generated signals. Thus the SMR terminates and gives rise to a TMR (Fig. 3.8a, b), when

$$M_2^T = 1. \quad (3.3)$$

Shirouzu & Glass (1986) proposed an additional necessary (but not sufficient) condition for the SMR \rightleftharpoons TMR transition that was based on experimental evidences (see Fig. 3.33). Their additional condition slightly shifted the transition line based on (3.3). They showed experimentally that in an SMR wave configuration $\omega_{ir} \leq 90^\circ$ where ω_{ir} is the angle between the incident, i , and the reflected, r , shock waves. A theoretical explanation for this experimental fact is still unavailable.

² Note that the kink is not a sharp discontinuity as could be anticipated from Fig. 3.8a but a point along the reflected shock wave where it starts to experience a reversal of curvature.

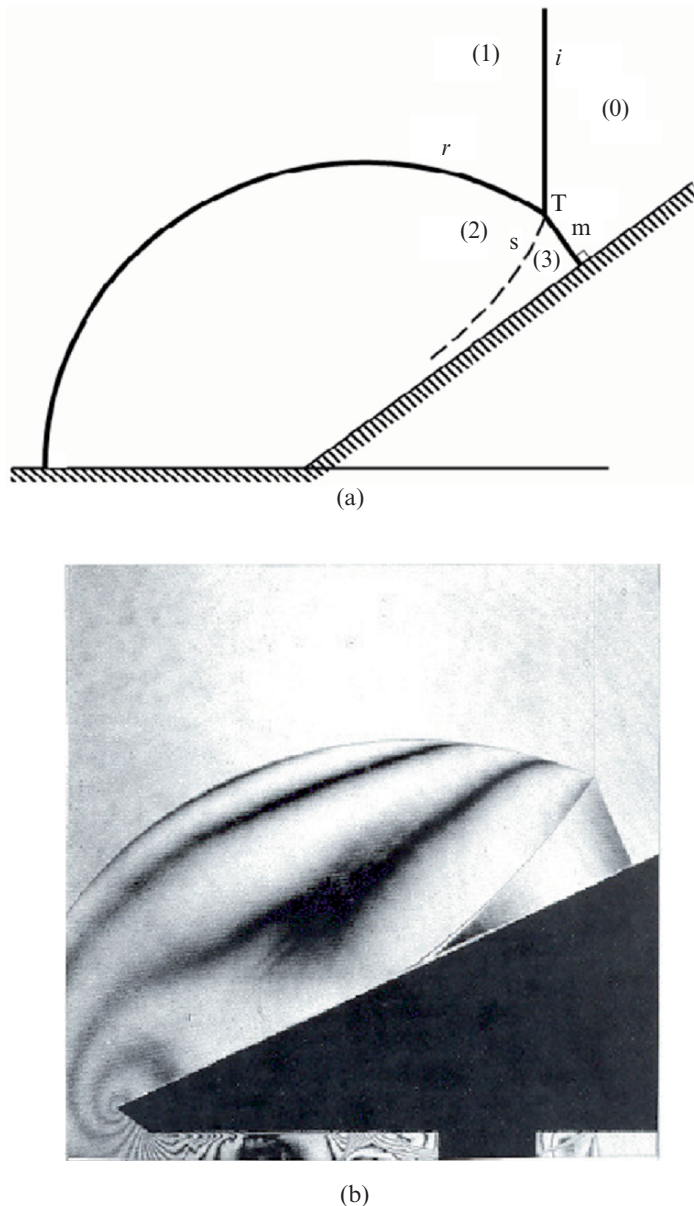


Fig. 3.7. Pseudosteady single-Mach reflection, SMR: (a) Schematic illustration of the wave configuration and definition of some parameters; (b) photograph (Courtesy of Professor K. Takayama) Note that since $\xi' > \xi$ the OMR is positive, i.e., DMR⁺

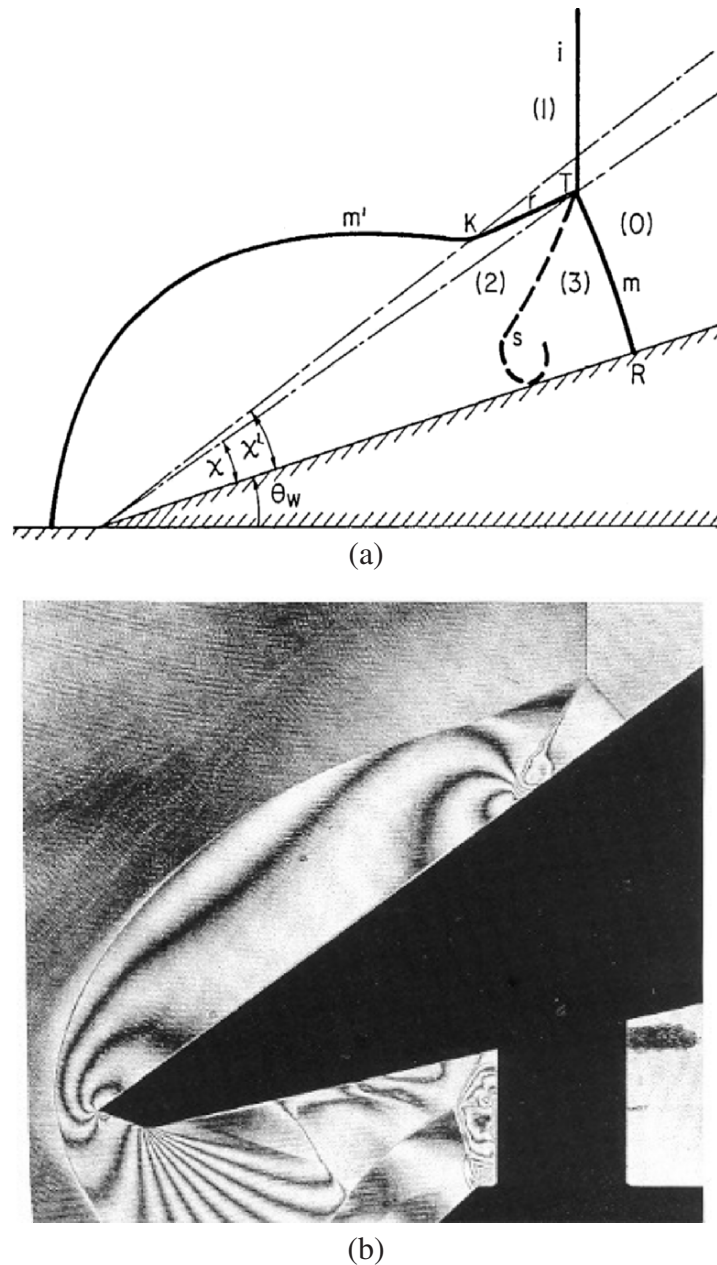


Fig. 3.8. Pseudosteady transitional-Mach reflection, TMR: (a) Schematic illustration of the wave configurations and definition of some parameters; (b) photograph (Courtesy of Professor K. Takayama)

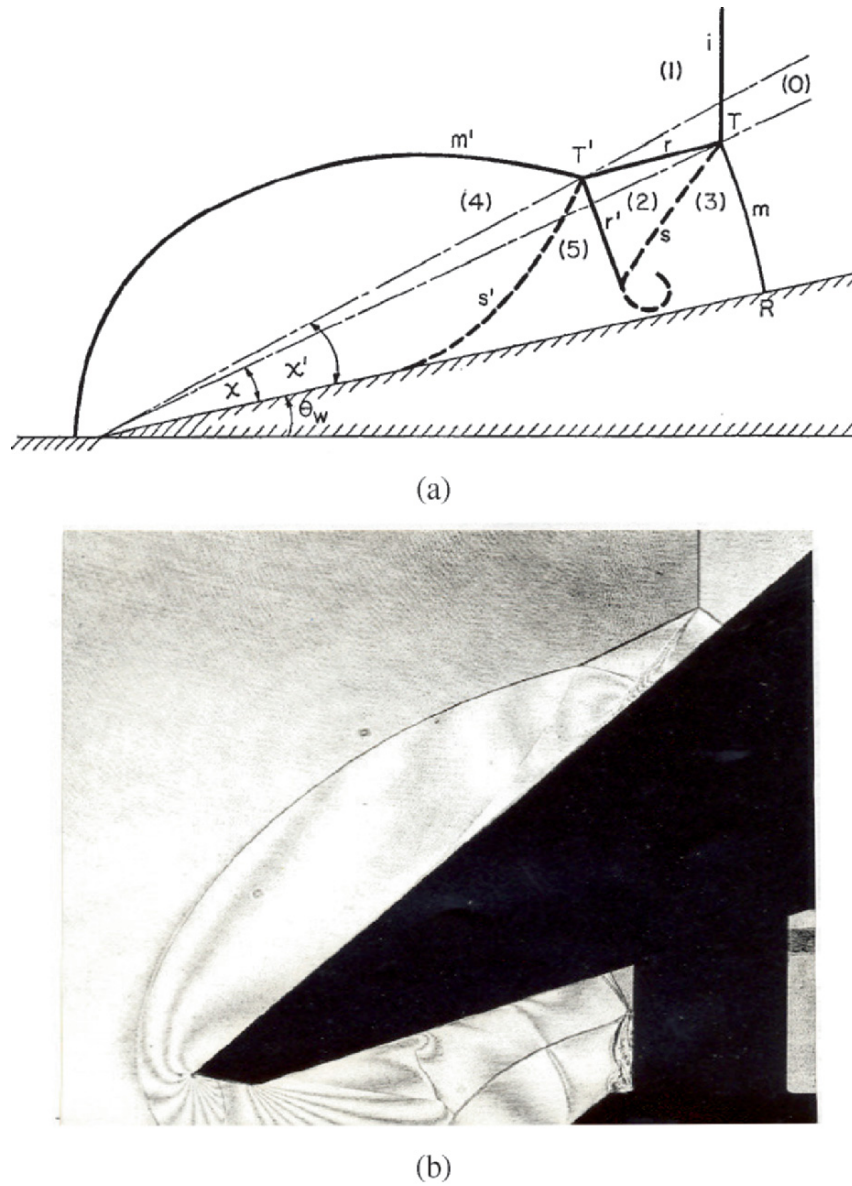


Fig. 3.9. Pseudosteady double-Mach reflection, DMR: (a) schematic illustration of the wave configuration and definition of some parameters; (b) photograph (Courtesy of Professor K. Takayama) Note that since $x' > x$ the DMR is positive, i.e., DMR⁺

Once a kink in the reflected shock wave has been formed, the value of the flow Mach number in state (2) behind the reflected shock wave, r , of the MR with respect to the kink, K , i.e., M_2^K (see Fig. 3.8), becomes the significant parameter in determining whether the reflection remains a TMR or changes to a DMR. As long as $M_2^K < 1$, the reflection is a TMR, typified by a band of compression waves that emanate from kink and its vicinity. When the flow in state (2) behind the reflected shock wave becomes supersonic with respect to the kink, K , i.e., $M_2^K > 1$, the compression waves converge to form a shock wave, the kink sharpens and becomes a second triple point, T' , and a DMR is formed (Fig. 3.9). Thus, the TMR \rightleftharpoons DMR transition occurs when

$$M_2^K = M_2^{T'} = 1. \quad (3.4)$$

Note that based on the foregoing presentation the kink, K , of the TMR and the second triple point, T' , of the DMR are practically the same point. As will be shown subsequently, in the “new”-state-of-the-knowledge these two points are different!

Following the just-described logic of the reasons for the sequence of transitions from SMR to TMR and then from TMR to DMR, it was hypothesized by Ben-Dor (1978) that if the flow in state (4) behind the Mach stem, m' , of the second triple point (see Fig. 3.9) becomes supersonic with respect to the second triple point (i.e., if $M_4^{T'} > 1$) a second kink (reversal of curvature), say K' , could develop in the reflected shock wave and as a result the DMR would terminate and give way to a TDMR, which is a DMR with a kink in its Mach stem, m' . Applying the just-mentioned logic even further implies that if the flow behind the second Mach stem, m' , becomes supersonic with respect to the new kink (i.e., if $M_4^{K'} > 1$) then the just-mentioned new kink could change and become a third triple point, T'' , and a triple-Mach reflection, TrMR, could be obtained. The just-mentioned two hypothetical wave configurations are shown in Fig. 3.10. The above logic could be further extended and based on it, more wave configurations could be hypothesized.

Once a DMR wave configuration is formed it could be either a DMR^+ or a DMR^- depending on whether the first triple point trajectory angle, χ , is larger or smaller than the second triple point trajectory angle, χ' (see Fig. 3.11). Hence the $DMR^+ \rightleftharpoons DMR^-$ transition criterion is:

$$\chi = \chi' \quad (3.5)$$

As mentioned earlier Lee & Glass (1984) presented a photograph showing a situation in which the second triple point of the DMR was seen to be grazing the reflecting wedge surface. They termed this wave configuration as terminal-double-Mach reflection, TerDMR (Fig. 3.12). The requirement for the existence of this wave configuration is simply:

$$\chi' = 0 \quad (3.6)$$

For the reader’s convenience, all the above-mentioned transition criteria are summarized in an evolution tree type presentation in Fig. 3.13.

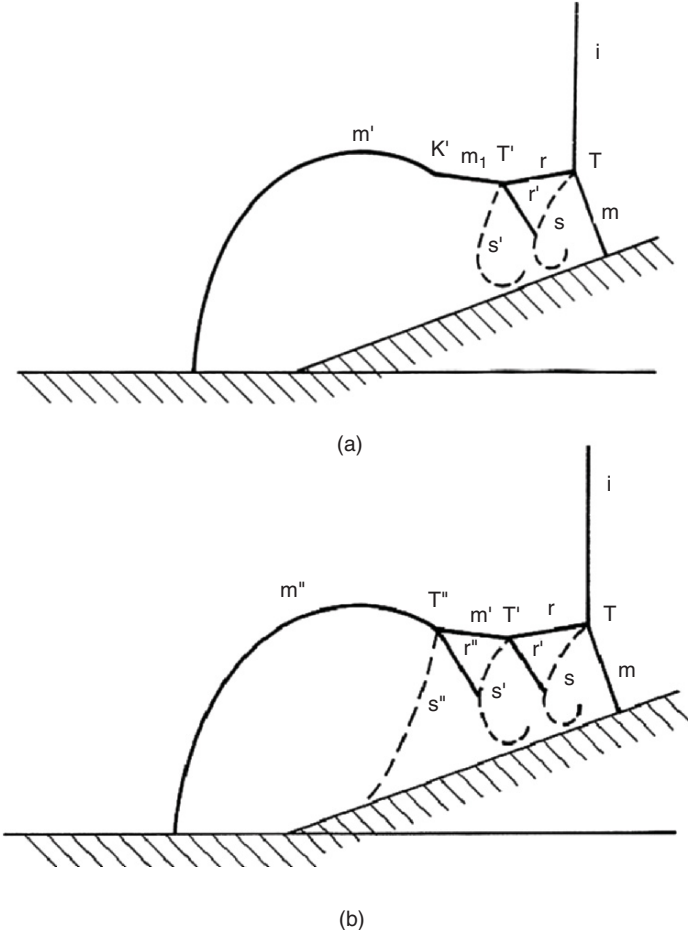


Fig. 3.10. Schematic illustration of the wave configurations of two hypothetical shock wave reflections and definition of some parameters: (a) transitional-double-Mach reflection, TDMR; (b) triple-Mach reflection, TrMR. (Note that Li & Ben-Dor (1995) proved that these wave configurations are not physical)

3.1.3 Second Triple Point Trajectory and Some Critical Remarks Regarding the Old State-of-the-Knowledge

The two- and three-shock theories (see Sects. 1.3.1 and 1.3.2) were solved together with the above-presented transition criteria in order to obtain the transition boundaries and the domains of the above-mentioned major different types of reflection configurations (i.e., RR, SMR, TMR, and DMR) in the (M_S, θ_w) -plane. The calculation of the TMR \rightleftharpoons DMR transition line (3.4) required a transformation of the frame of reference from the first, T, to the second, T', triple point. This transformation was done with the aid of the

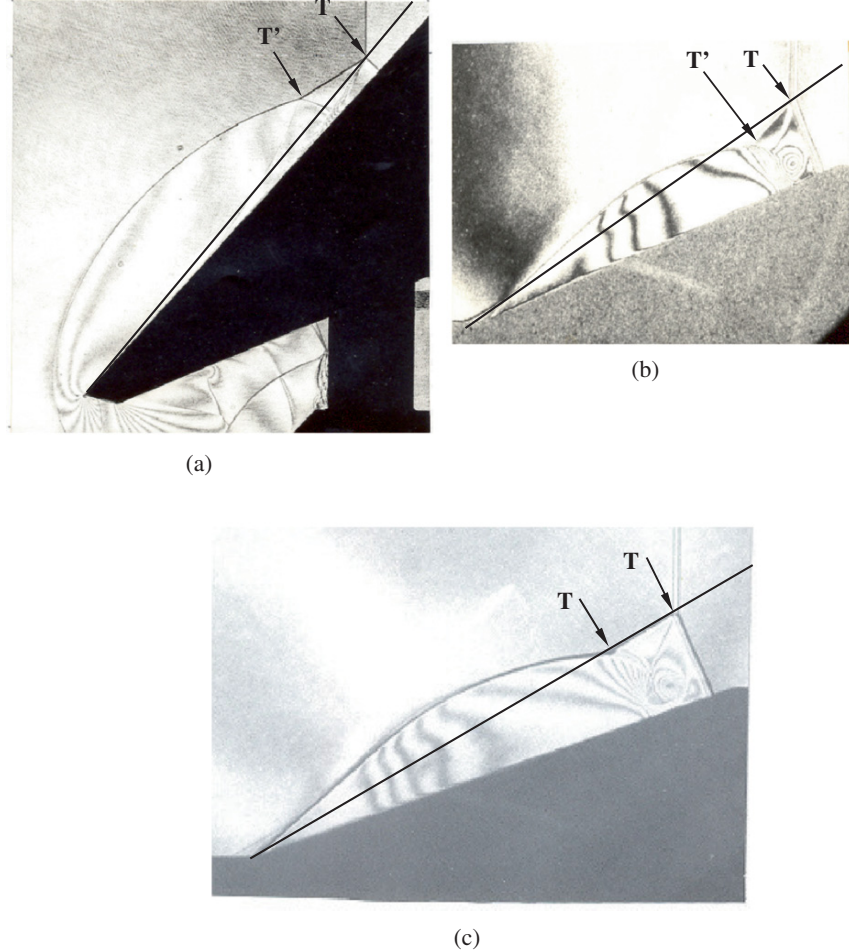
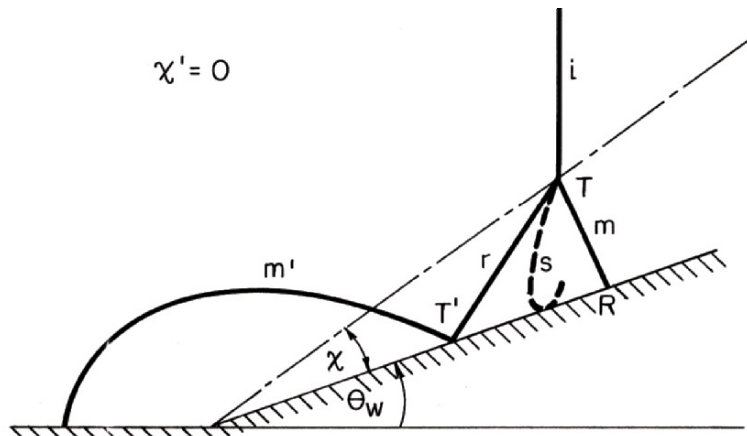


Fig. 3.11. Photographs of (a) a positive-double-Mach reflection, DMR⁺; (b) a negative-double-Mach reflection, DMR⁻; (c) an intermediate wave configuration (DMR⁰) between a DMR⁺ and a DMR⁻

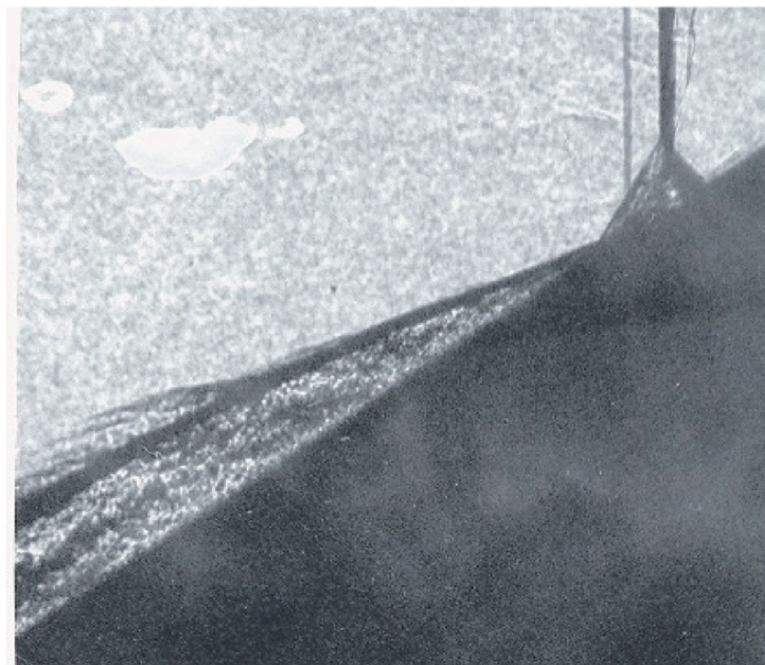
Law-Glass assumption [for details see Law & Glass (1971) and Ben-Dor (1991)] by which the relative velocity between the two triple points, $V_{T'}^T$, could be calculated. The Law-Glass assumption reads

$$V_K^T = \frac{\rho_0}{\rho_1} V_S \cos \text{ec}(\phi_1 + \phi_2 - \theta_1), \quad (3.7)$$

where ρ is the density, V_S is the incident shock wave velocity, ϕ and θ are the angle of incidence and the deflection angle, respectively. It should be noted that the above transformation by which the location of the kink, K, is calculated is based only on the reflection process and completely neglects



(a)



(b)

Fig. 3.12. Pseudosteady terminal-double-Mach reflection, TerDMR: (a) schematic illustration of the wave configuration and definition of some parameters; (b) photograph (Courtesy of Professor I.I. Glass). Note that based on simple gasdynamic considerations a TerDMR wave configuration is impossible

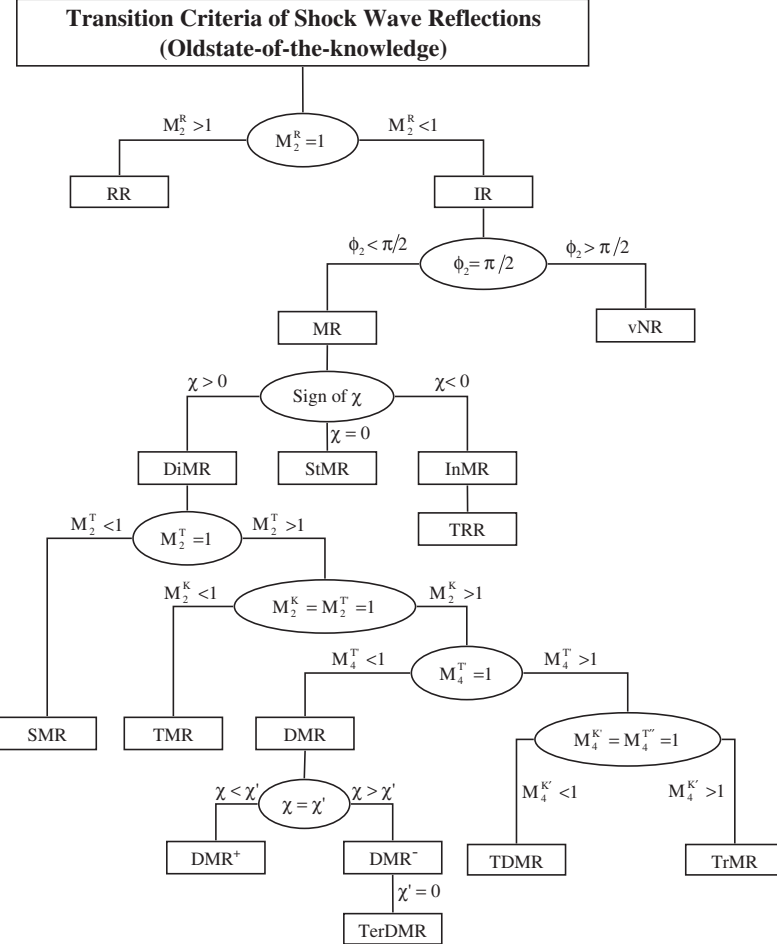


Fig. 3.13. Evolution-tree type presentation of the transition criteria of the wave configurations of the various types of shock wave reflections that appear in Figs. 3.2 and 3.3

the corner-generated signals that arise from the flow-deflection process around the leading edge of the reflecting wedge. The importance of this comment will become clearer when the new state-of-the-knowledge will be presented.

In the following, an expression for the trajectory angle, χ_K , of the kink, K, or χ' of the second triple point, which is based on the just-mentioned Law-Glass assumption is developed. In terms of the parameters shown subsequently in Fig. 3.18 the horizontal distance between the kink, K, and the triple point, T, is

$$L_K = L_{T'} = L - M_1^L a_1 \Delta t, \quad (3.8)$$

where M_1^L is the incident shock induced flow Mach number in the laboratory frame of reference. In similar, the horizontal distance, L, traveled by the triple point can be obtained from

$$L = u_S^L \Delta t = M_S a_0 \Delta t, \quad (3.9)$$

where u_S^L is the incident shock wave velocity in a laboratory frame of reference and Δt is the time measured from the moment the incident shock wave passed through the leading edge of the reflecting wedge. Dividing (3.8) by (3.9) results in

$$\frac{L_K}{L} = \frac{L_{T'}}{L} = 1 - \frac{M_1^L a_1}{M_S a_0}, \quad (3.10)$$

where

$$\frac{a_1}{a_0} = \frac{\left[2\gamma M_S^2 - (\gamma - 1)\right]^{1/2} \left[(\gamma - 1) M_S^2 + 2\right]^{1/2}}{(\gamma + 1) M_S}. \quad (3.11)$$

Based on (3.8) the expression for the kink trajectory angle that is

$$\chi_K = \chi' = \operatorname{tg}^{-1} \left\{ \frac{M_S a_0 [\operatorname{tg}(\theta_w + \chi) + \operatorname{ctg} \omega_{ir}] - m_1 a_1 \operatorname{ctg} \omega_{ir}}{m_1 a_1} \right\} - \theta_w. \quad (3.12)$$

It is important to note here that based on the foregoing developments of the first, χ , and the second, χ' , triple point trajectory angles, an entire section (Sect. 2.2) was dedicated to these angles in the first edition of this monograph (Ben-Dor 1991). Although as will be shown subsequently according to the new-state-of-the-knowledge, in contrast to expression (3.12), $\chi_K \neq \chi'$, and each of these angles is calculated by means of a different model. However, in spite of this fact, the information and data that are provided in Sect. 2.2 of Ben-Dor (1991) are still important from an engineering point of view. For this reason, the main figures of Sect. 2.2 of the first edition of this monograph are added to the Appendix of this chapter.

It should be noted here that Dewey & van Netten (1991 and 1995) raised some serious doubt on the boundaries of the domains various reflection regions as presented in Ben-Dor (1991). They claimed that the experiments that were used to verify the boundaries were based on experiments that were done at low density and with short wedges, about 5- or 6-cm long that gave misleading results. They claimed that their experiments, which were done with up to 20-cm long wedges, revealed that at the low initial pressures, the final reflection configuration was not achieved until 20 or 30-cm up the wedge. They also showed that in reaching the final state, the reflection appears to go from RR to SMR, to TMR and eventually to DMR. As a result, it is easy to mistake the final type of reflection if the wedge is not long enough.

As shown by Ben-Dor (1991) and Ben-Dor & Takayama (1992) a comparison of the analytically predicted domains of the different types of reflection wave configurations and the transition boundaries between them with experimental results in a large variety of gases (O_2 , N_2 , Ar, air, CO_2 , SF_6

and Freon 12) indicated that the transition lines do not separate accurately enough between the various reflection configurations, although, from an engineering point of view, they could be regarded as quite good in most of the reflection domain. The lack of a satisfactory agreement between the analytical predictions and the experimental results was attributed by Ben-Dor & Takayama (1992) to the over-simplifying assumptions on which the two- and three-shock theories were based and the use of the Law–Glass assumption which, as will be shown subsequently, is not accurate enough. Various attempts to relax some of the assumptions by accounting for viscous and real-gas effects practically failed (see Sect. 3.4 for details).

3.2 “New” (Present) State-of-the-Knowledge

The subsequent presentation is based on Li & Ben-Dor’s (1995) study just over a decade ago. In that study, analytical models for describing the transitional-Mach, TMR, and the double-Mach, DMR, reflections were presented.

3.2.1 Introductory Remarks

As mentioned earlier, the kink, K, of the TMR or the second triple point, T', of the DMR were considered, in the old state-of-the-knowledge to be the same point. As a result the location of these two points (K and T') was calculated by one analytical model, which was based on the Law–Glass assumption (3.7). This analytical model ignored the flow deflection process around the leading edge of the reflecting wedge and the resulted interaction of the corner-generated signals with the shock-wave reflection process. This practice was used in spite of the earlier mentioned fact that the intersection of the leading disturbance of the corner-generated signals and the reflected shock wave marks the location of the kink along the reflected shock wave. Li & Ben-Dor’s (1995) developed analytical models that replaced the Law–Glass assumption and enabled one to determine the locations of the kink, K, of the TMR and the second triple point, T', of the DMR. It is noted here that unlike the “old” state-of-the-knowledge where the kink and the second triple point were the same point, in the “new” state-of-the-knowledge, these points are different and their locations along the reflected shock wave are calculated using two different theoretical models.

The basis of the new approach can be traced back to the studies of Law & Glass (1971) and Ben-Dor (1978). In those studies, the entire reflection process was considered to be a combination of two sub-processes, namely:

- *The shock-reflection process*, i.e., the reflection of the planar shock wave over the reflecting surface
- *The flow-deflection process*, i.e., the deflection of the incident-shock-induced flow around the reflecting wedge

The interaction of these two subprocesses, namely the overall process, was referred to by Law & Glass (1971) and Ben-Dor (1978) as *the shock-diffraction process*. This approach, which was initiated more than 30 years ago, was, in fact, ignored for almost two decades and almost all the researchers who investigated the transition criteria between the various Mach reflection wave configurations limited their studies to deriving the transition criteria from the shock-reflection process only. All the above-mentioned transition criteria as well as the Law–Glass assumption were derived by applying various gas dynamic considerations to the shock-reflection process only, and completely ignoring the flow-deflection process. As a result, the possible contribution of the flow-deflection process to the various transition criteria was neglected completely.

As will be shown subsequently, by accounting for the flow-deflection process and its interaction with the shock-reflection process, many of the unsolved questions that were raised by Ben-Dor & Takayama (1992) were resolved and a better agreement between analytical predictions and the experimental results regarding the transition boundaries were obtained.

3.2.2 Shock-Diffraction Process

The shock-wave diffraction process is a result of an interaction of two subprocesses: the shock-wave reflection process and the shock-induced flow-deflection process (see Fig. 3.14).

Consider Fig. 3.15 in which two conceptual models of the interaction of the shock-wave reflection and the flow-deflection processes are schematically illustrated. The shock-wave reflection is an MR with a triple point, T, and a reflected shock wave, r , which extends to point Q and behind which the flow state is denoted by (2). For the reader’s convenience and the sake of clarity the other parts, e.g., the slipstream, of the MR are not shown in Fig. 3.15. The incident-shock-wave Mach number and the incident-shock-induced flow Mach number, in the laboratory frame of reference,

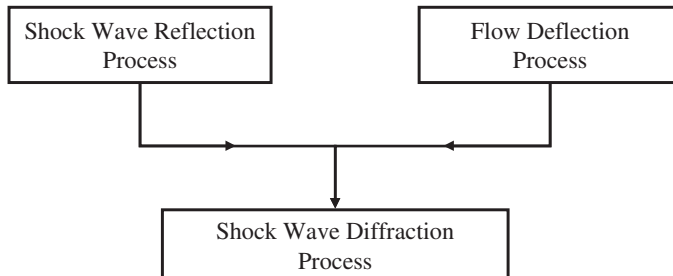


Fig. 3.14. Block diagram type presentation of the basic approach for analyzing the shock wave reflection phenomenon in pseudosteady flows

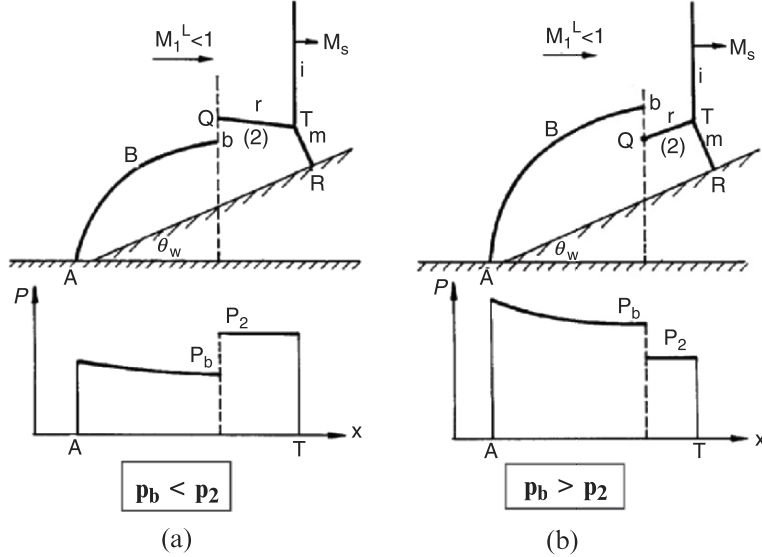


Fig. 3.15. Schematic illustration of the two possible interaction models between the shock-wave reflection and the flow-deflection processes: (a) the shock-induced flow is subsonic in a laboratory frame of reference, $M_1^L < 1$; and (b) The shock-induced flow is supersonic in a laboratory frame of reference, $M_1^L > 1$

are M_S and M_1^L , respectively. The bow shock wave, B, which arises from the flow-deflection process, extends up to point b. The flow domain that extends between points b and Q is the domain in which the interaction between the two processes takes place. Let us define the pressure behind the reflected shock wave as p_2 and that behind the bow shock wave, near Q, as p_b . The relative magnitudes of these two pressures define the mechanism of the interaction between the shock-wave reflection and flow-deflection processes:

- If $p_b < p_2$ (see Fig. 3.15a) then a band of expansive disturbances propagates towards region (2) to bridge the pressure gap.
- If $p_b > p_2$ (see Fig. 3.15b) then a band of compressive disturbances propagates towards region (2) to bridge the pressure gap.

Based on Semenov & Syshchikova (1975) the boundary between these two situations, i.e., $p_b = p_2$, is associated with the situation in which the shock-induced flow, in the laboratory frame of reference, is sonic, i.e., $M_1^L = 1$. Consequently, it is apparent that:

- $p_b < p_2$ when $M_1^L < 1$
- $p_b > p_2$ when $M_1^L > 1$

as is indicated in Fig. 3.15a, b, respectively.

3.2.3 Transition Criteria

In the foregoing presentation of the “old” state-of-the-knowledge, (see Sect. 3.1), the role of the corner-generated signals, which resulted from the flow-deflection process around the leading edge of the reflecting wedge, in affecting the transition criteria was mentioned and accounted for, twice:

- The RR exists as long as the corner-generated signals do not catch-up with its reflection point, R
- The SMR exists as long as the corner-generated signals do catch up with its triple point, T

Hence, since the corner-generated signals are a mechanism that results from the flow-deflection process around the leading edge of the reflecting wedge it is obvious that this process was accounted for when the formation and the termination criteria of the RR and SMR wave configurations were treated. As a result, these two criteria remain the same in the “new” state-of-the-knowledge. However, for the reader’s convenience they are repeated here.

RR \rightleftharpoons IR Transition

The RR terminates when the corner-generated signals catch-up with its reflection point, R. This occurs when the flow Mach number behind the reflected shock wave with respect to the reflection point is subsonic. Therefore, the RR \rightleftharpoons IR transition criterion is:

$$M_2^R = 1. \quad (3.13)$$

As was mentioned earlier, based on the “old” state-of-the-knowledge, the IR wave configuration could be a von Neumann reflection, vNR, or a Mach reflection, MR. Colella & Henderson (1990) originally forwarded the vNR concept during their trial to resolve the von Neumann paradox. However, their proposed and generally accepted criterion for the SMR \rightleftharpoons vNR transition that is given by (3.2a or 3.2b) implies that it is derived from a solution of the three-shock theory. Hence, the vNR concept does not resolve the von Neumann paradox, which refers to the existence of reflection configurations that look similar to the SMR configuration in a domain where the three-shock theory does not have a solution. In fact, as mentioned in Sect. 1.3.2 the three-shock theories could be divided into two parts:

- The *standard three-shock theory* for which $\theta_1 - \theta_2 = \theta_3$
- The *nonstandard three-shock theory* for which $\theta_1 + \theta_2 = \theta_3$

The SMR \rightleftharpoons vNR transition occurs when $\theta_2 = 0$, i.e., when the reflected shock wave is normal to the oncoming flow:

$$\phi_2 = 90^\circ \quad (3.14a)$$

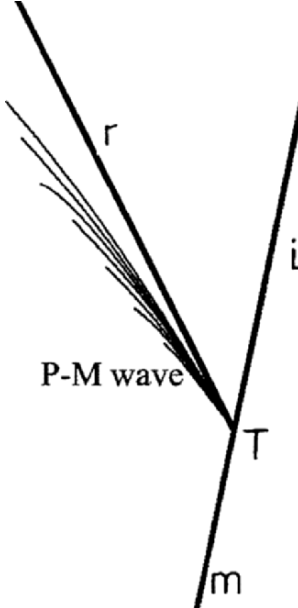


Fig. 3.16. A schematic drawing of a Guderley reflection, GR

As mentioned earlier, since the flow behind the reflected shock wave, r , must be parallel to the slipstream, s , it is obvious that the condition given by (3.14a) can be rewritten to read:

$$\omega_{rs} = 90^\circ \quad (3.14b)$$

As will be shown subsequently, there is a domain inside which the three-shock theory does not have any solution but experimental evidence show wave configurations that are similar to SMR or vNR wave configurations. Vasiliev & Kraiko (1999) indicated through a high-resolution numerical study, using the Euler equations, that this configuration is a four-wave pattern (Fig. 3.16) that was originally suggested by Guderley (1947) about 60 years ago. Based on their numerical study an expansion wave exists immediately behind the reflected shock wave. Skews & Ashworth (2005) who investigated recently the weak shock wave reflection domain claimed that a solution of the inviscid transonic equations indicated the possible existence of a very small, multi-wave structure immediately behind the three-shock confluence. In their experimental study, they obtained schlieren photographs that showed a structure consisting of an expansion wave followed by a small shock situated behind the confluence point, with some indication of smaller scale structures in some experiments.

Skews & Ashworth (2005) suggested naming this four-wave reflection pattern, which was hypothesized first by Guderley (1947) as Guderley reflection, GR. In the conclusion of their paper Skews & Ashworth (2005) mentioned that since their experiments only covered a very small part of the parameter space

identified in the literature as falling within the weak shock reflection domain (see e.g., Olim & Dewey 1992) further research is needed to better understand the reflection phenomenon in this domain. An up-to-date description of the evolution of the reflections process in this domain is given in Sect. 3.2.12.

Owing to the foregoing presentation in the following discussion, only the domain in which the three-shock theory has a standard solution for which $\theta_1 - \theta_2 = \theta_3$ will be considered. The other two domains, i.e., the domain in which the three-shock theory has a nonstandard solution for which $\theta_1 + \theta_2 = \theta_3$ and the domain inside which the three-shock theory has no solution will be discussed in Sect. 3.2.12.

3.2.4 Single-Mach Reflection (SMR)

The earlier-mentioned condition for the existence of a single-Mach reflection, SMR, given by (3.3), is still valid. This condition, i.e., $M_2^T < 1$, implies that the corner-generated signals reach the triple point, T, and as a result the reflected shock wave of an SMR is curved along its entire length since a physical length scale is communicated to the triple point. Consequently, the SMR terminates and gives rise to another reflection when the flow Mach number behind the reflected shock wave with respect to the triple point, becomes supersonic, i.e., $M_2^T > 1$. As will be shown subsequently, the termination of the SMR can give rise to the formation of either a TMR or a DMR. Thus the $\text{SMR} \rightleftharpoons \text{TMR/DMR}$ transition criterion is

$$M_2^T = 1. \quad (3.15)$$

3.2.5 Formation of Transitional-Mach Reflection (TMR) or Double-Mach Reflection (DMR)

If the flow Mach number behind the reflected shock wave, in a frame of reference attached to the triple point, becomes supersonic, i.e., $M_2^T > 1$, the reflected shock wave near the triple point, T, straightens up since part of it is isolated from the corner-generated signals by the supersonic flow region, and the SMR terminates.

The resulted wave configuration, after the termination of the SMR, depends on both the mechanism and the strength of the interaction between the earlier-mentioned shock-wave reflection and flow-deflection processes. The mechanism and strength of the interaction are determined by the relative magnitudes of the pressures p_b and p_2 (see Fig. 3.15):

- When $p_b < p_2$ the reflection is a pseudotransitional-Mach reflection, PTMR. The leading disturbance propagating towards region (2) in order to bridge the pressure gap is a band of expansive waves in this reflection. As a result, the reflected shock wave, r, does not develop a reversal of curvature as in a regular TMR.

- When $p_b > p_2$ the reflection is either a TMR or a DMR. The specific type of reflection (TMR or DMR) depends on whether the interaction between the shock-wave reflection and the flow-deflection processes is strong or weak. This, in turn, depends, for a given gas, on the incident shock wave Mach number, M_S , and the reflecting wedge angle, θ_w .

3.2.6 Transitional-Mach Reflection (TMR)

If the interaction between the shock-wave reflection and the shock-induced flow-deflection processes is weak, the resulted wave configuration is a TMR. An analytical model and a detailed derivation of the governing equations of a TMR appear in the followings.

In the case of a TMR a distributed band of compressive waves propagates towards region (2) and bridges the pressure gap. The leading disturbance is a compressive wave that interacts with the reflected shock wave, r , at point K. At this point the reflected shock wave, r , develops a reversal of curvature. Thus, based on this explanation and in contrast to (3.4), the flow in state (2) behind the reflected shock wave is always sonic with respect to the kink, i.e., $M_2^K = 1$ in a TMR. In fact a situation in which $M_2^K < 1$ that was allowed by the transition criteria of the “old” state-of-the-knowledge is not physical. The distributed band of the compressive waves, which interacts with the reflected shock wave, r , forces the reflected shock wave to curve and reverse its curvature.

Analytical Model of Transitional-Mach Reflection

The analytical model for a TMR is based on the following assumptions:

- (1) The wave configuration of a TMR is self-similar.
- (2) The wave configuration of a TMR is stable.
- (3) The gas is an ideal fluid (i.e., $\mu = 0$ and $k = 0$ where μ is the dynamic viscosity and k is the thermal conductivity).
- (4) The gas obeys the equation of state of a perfect gas.

The flow field near the triple point T of a TMR is given by the well-known three-shock theory, which is constructed from the oblique shock waves relations across the three shock waves, which consist of the triple point together with the matching conditions across the slipstream.

Based on Fig. 3.17 one can write

$$\theta_j = \operatorname{tg}^{-1} \left[2\operatorname{ctg}\phi_j \frac{(M_k \sin \phi_j)^2 - 1}{M_k^2 (\gamma + \cos 2\phi_j) + 2} \right], \quad (3.16)$$

$$p_j = p_k \frac{2\gamma (M_k \sin \phi_j)^2 - (\gamma - 1)}{\gamma + 1}, \quad (3.17)$$

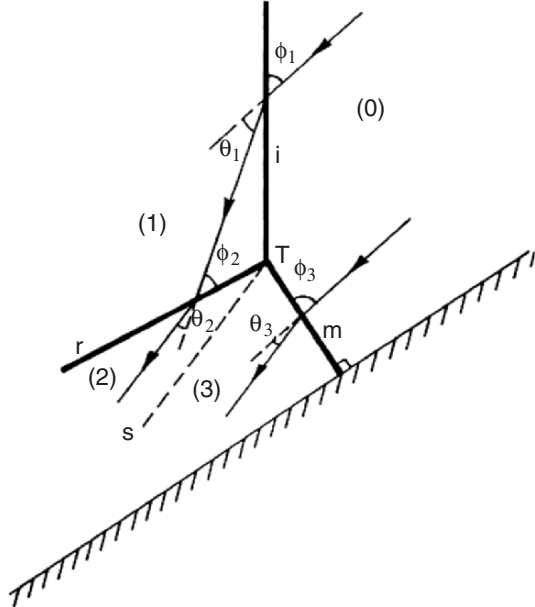


Fig. 3.17. Schematic illustration of a three-shock confluence and definition of parameters

where subscripts k and j indicate flow states ahead and behind the oblique shock wave, M is the flow Mach number, ϕ_j is its angle of incidence with the oblique shock wave across which the flow passes to state (j) , θ_j is the flow deflection angle and p is the pressure. The relations across the incident shock wave, i , are obtained by setting $j = 1$ and $k = 0$, the relations across the reflected shock wave, r , are obtained by setting $j = 2$ and $k = 1$, and the relations across the Mach stem, m , are obtained by setting $j = 3$ and $k = 0$. In addition to the above equations, we have

$$M_0 = \frac{M_S}{\cos(\theta_w + \chi)} \quad (3.18)$$

$$M_1 = \frac{\left\{1 + (\gamma - 1) M_0^2 \sin^2 \phi_1 + \left[\left(\frac{\gamma+1}{2}\right)^2 - \gamma \sin^2 \phi_1\right] M_0^2 \sin^2 \phi_1\right\}^{1/2}}{\left[\gamma M_0^2 \sin^2 \phi_1 - \frac{\gamma-1}{2}\right]^{1/2} \left[\frac{\gamma-1}{2} M_0^2 \sin^2 \phi_1 + 1\right]^{1/2}}, \quad (3.19)$$

$$\phi_1 = \frac{\pi}{2} - (\theta_w + \chi). \quad (3.20)$$

The matching conditions across the slipstream are

$$p_2 = p_3 \quad (3.21)$$

and

$$\theta_1 - \theta_2 = \theta_3. \quad (3.22)$$

The above set of 11 governing equations [note that the general equations (3.16) and (3.17) are in fact six equations] consists of 12 unknowns, namely M_0 , M_1 , p_1 , p_2 , p_3 , ϕ_1 , ϕ_2 , ϕ_3 , θ_1 , θ_2 , θ_3 , and χ provided M_S , θ_w and the thermodynamic properties in state (0) are known. Consequently, in order to have a solvable set of equations, an additional relation is required. If the Mach stem, m , is assumed to be straight and perpendicular to the reflecting wedge surface, then

$$\phi_3 = \frac{\pi}{2} - \chi. \quad (3.23)$$

As mentioned earlier the so-called kink, K , in the case of a TMR is at the point along reflected shock wave, r , which has been reached by the leading corner generated signal, which propagates towards region (2).

Consider Fig. 3.18 in which the wave configuration of a TMR together with the leading disturbance (dashed line) is schematically illustrated. The

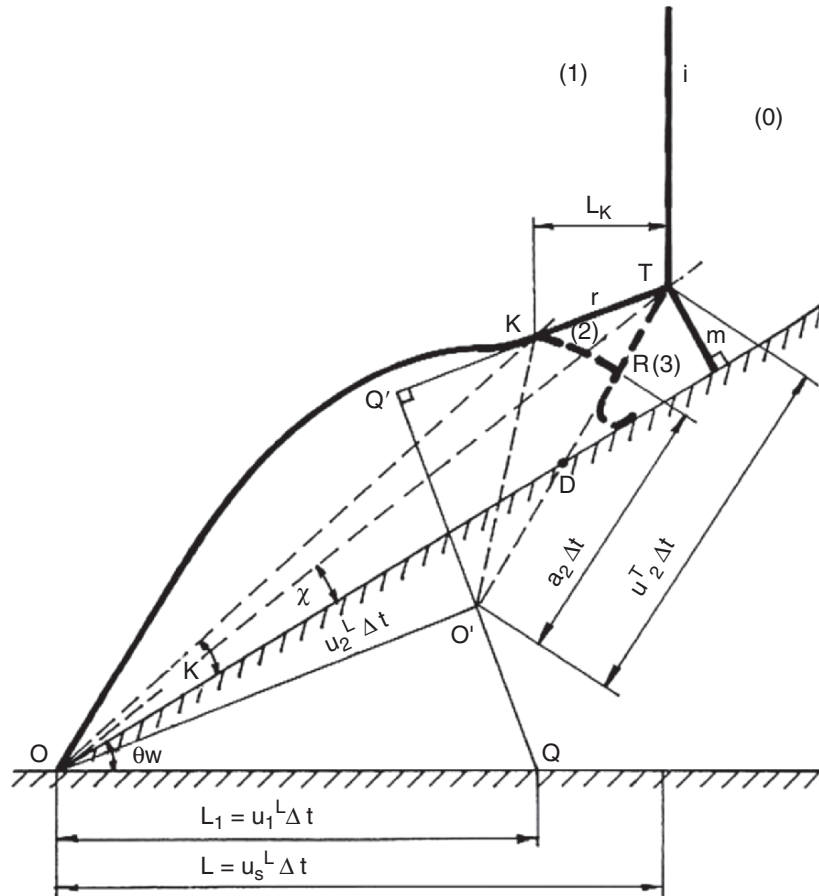


Fig. 3.18. Schematic illustration of a transitional-Mach reflection and definition of various parameters

origin, O' , of the leading disturbance is located at the point where the line QQ' is intersected by the extension of the slipstream s. Point Q from which the line QQ' originates is located at $L_1 = u_1^L \Delta t$ where u_1^L is the incident shock induced flow velocity in the laboratory frame of reference. The line QQ' is perpendicular to the extension of the reflected shock wave, r. It coincides with the direction of the relative velocity between states (2) and (1), i.e., u_2^1 . Since the flow in state (2) is at rest in a frame of reference attached to O' , the leading disturbance is located along a circular arc originating from O' and having a radius equal to $a_2 \Delta t$. As shown in Fig. 3.18, the leading disturbance intersects the slipstream at point R and the reflected shock wave at point, K, i.e., the kink. An inspection of Fig. 3.18 indicates that

$$\overline{O'T} = u_2^T \Delta t = M_2 a_2 \Delta t \quad (3.24)$$

and

$$\overline{O'R} = \overline{O'K} = a_2 \Delta t. \quad (3.25)$$

In addition

$$\omega_{ir} = \frac{\pi}{2} + (\theta_w + \chi + \theta_1 - \phi_2) \quad (3.26)$$

and

$$\omega_{rs} = \phi_2 - \theta_2, \quad (3.27)$$

where ω_{ir} is the angle between the incident, i, and the reflected, r, shock waves and ω_{rs} is the angle between the reflected shock wave, r, and the slipstream, s.

Applying the cosine law to the triangle $O'TK$ results in:

$$(\overline{O'K})^2 = (\overline{KT})^2 - 2\overline{KT} \overline{O'T} \cos \omega_{rs} + (\overline{O'T})^2. \quad (3.28)$$

Inserting (3.9), (3.24) and (3.25) into (3.28) yields

$$\frac{\overline{KT}}{L} = \frac{a_2 \left[M_2 \cos \omega_{rs} - (1 - M_2^2 \sin^2 \omega_{rs})^{1/2} \right]}{a_0 M_s}, \quad (3.29)$$

where

$$\frac{a_2}{a_0} = \frac{\left\{ [2\gamma M_s^2 - (\gamma - 1)] [\gamma M_s^2 + 2] [2\gamma (M_1 \sin \phi_2)^2 - (\gamma - 1)] [(\gamma - 1) (M_1 \sin \phi_2)^2 + 2] \right\}^{1/2}}{(\gamma + 1)^2 M_s M_1 \sin \phi_2}. \quad (3.30)$$

The horizontal distance, L_K in Fig. 3.18, by which the kink, K, lags behind the triple point, T, can be calculated from

$$\frac{L_K}{L} = \frac{\overline{KT}}{L} \cos \left(\omega_{ir} - \frac{\pi}{2} \right) = \frac{\overline{KT}}{L} \sin \omega_{ir}, \quad (3.31)$$

where $\frac{\bar{K}\bar{T}}{L}$ is given by (3.29). Using simple geometrical relations, the following expression for the kink trajectory angle, χ_K , can be developed:

$$\chi_K = \operatorname{tg}^{-1} \left\{ \frac{M_S a_0 \operatorname{tg}(\theta_w + \chi) + \bar{K}\bar{T} \sin \omega_{ir}}{M_S a_0 - \bar{K}\bar{T} \cos \omega_{ir}} \right\} \quad (3.32)$$

Recall that in the “old”-state-of-the-knowledge the kink trajectory angle, χ_K , was developed with the aid on the Law–Glass assumption (see Sect. 3.1.3 and 3.7), i.e., that the horizontal velocity of the kink, K , of a TMR or the second triple point, T' , of a DMR, in a laboratory frame of reference is equal to the incident shock induced flow velocity. The expressions for the kink trajectory angle that is appropriate to the “old”-state-of-the-knowledge was given by (3.12). For the reader’s convenience, it is repeated here:

$$\chi_K = \operatorname{tg}^{-1} \left\{ \frac{M_S a_0 [\operatorname{tg}(\theta_w + \chi) + \operatorname{ctg} \omega_{ir}] - m_1 a_1 \operatorname{ctg} \omega_{ir}}{m_1 a_1}, \right\} - \theta_w \quad (3.33)$$

Location of the Point – K

The location, L_K , of the point, K, of a TMR could be determined by two different methods:

- The method presented originally by Law & Glass (1971), which is based on the Law–Glass assumption (3.10).
- The method presented originally by Li & Ben-Dor (1995) (3.31).

A comparison of the predictions based on these two ways together with some experimental results are shown in Figs. 3.19a, b for fixed values of θ_w and M_S , respectively. The location, L_K , as predicted by the “new” model excellently

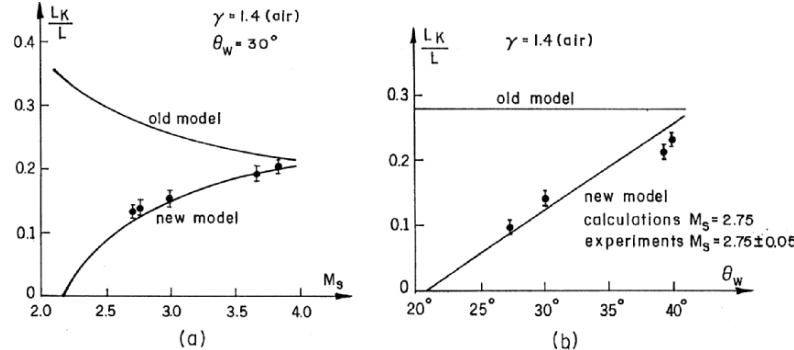


Fig. 3.19. Comparison of the location, L_K , of the kink of a TMR with experimental results: (a) for a fixed reflecting wedge angle, θ_w ; and (b) for a fixed incident shock wave Mach number, M_S . The “old” model is based on the Law–Glass assumption. Experiments were received by private communications from Profs. K. Takayama and J. M. Dewey

agrees with the experimental results. The predictions, which are based on the “old” model (Law–Glass assumption), are very poor. In contrast to Bazhenova et al. (1976) who, based on their experimental results, concluded that the Law–Glass assumption becomes better as θ_w decreases below 40° , Fig. 3.19b clearly indicates that as θ_w decreases in the range $\theta_w < 40^\circ$ the predictions based on the Law–Glass assumption become poorer. Note that the predictions of the new model indicate that $L_K \rightarrow 0$ as M_S or θ_w decreases towards the appropriate TMR \rightarrow SMR transition point. The “old” model does not predict this logical behavior. For example, it is seen in Fig. 3.19b that for $M_S = 2.75$, $L_K/L = 0.277$ independently of how far the conditions are from the transition point. It should also be noted finally that results similar to those shown in Figs. 3.19a, b were obtained for gases having other values of γ , e.g., 1.14, 1.29, 1.33 and 1.67.

3.2.7 Double-Mach Reflection – DMR

If the interaction between the shock-wave reflection and the shock-induced flow-deflection processes is strong, the compression waves converge to form a shock wave, r' . This shock wave forces the reflected shock wave, r , to develop a strong discontinuity (a sharp kink), which becomes the second triple point, T' . Owing to gas dynamic considerations, a secondary slipstream complements this three shock wave confluence. The only way by which the exact location of the second triple point T' can be determined is to solve the entire flow field associated with the DMR, i.e., to solve the full Navier–Stokes equations. This task can be done only numerically.

Fortunately, by using some simplifying assumptions, Li & Ben-Dor (1995) succeeded in developing two simplified analytical models that result in very good predictions. The two models arise from the fact that there are two different possible double-Mach reflection wave configurations.

The two wave configurations, which are schematically illustrated in Fig. 3.20a, b, differ in the way the shock wave, r' , interacts with the primary slipstream, s :

- In the wave configuration, shown in Fig. 3.20a, the r' -shock wave terminates somewhere along the slipstream, s . Gasdynamic considerations imply that the r' -shock wave is perpendicular to slipstream, s .
- In the wave configuration, shown in Fig. 3.20b, the r' -shock wave terminates at (or near) the point where slipstream, s , reaches the reflecting wedge surface. In this case the r' -shock wave does not have to be perpendicular to the slipstream, s .

Photographs of these two different DMR wave configurations are shown in Fig. 3.21a, b, respectively.

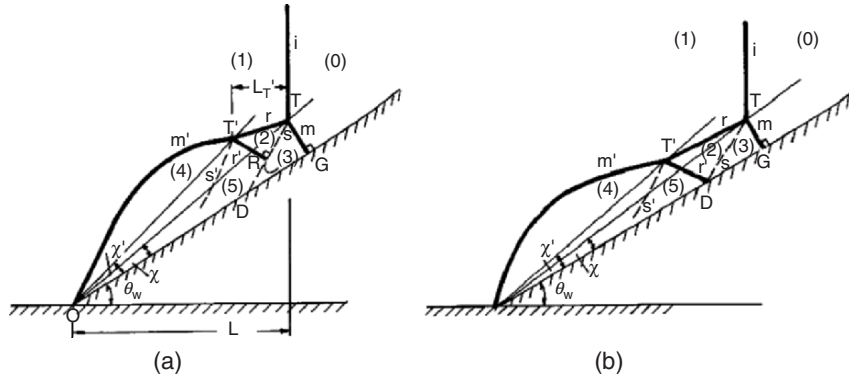


Fig. 3.20. Schematic illustration of two different possible wave configurations of a double-Mach reflection: (a) the r' -shock wave terminates perpendicularly on the primary slipstream, s ; and (b) the r' -shock wave terminates on the reflecting wedge surface at the point where the primary slipstream, s , reaches the reflecting surface

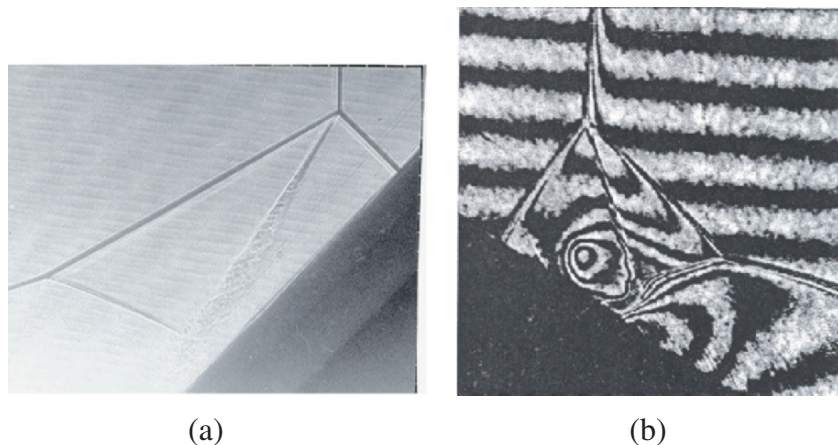


Fig. 3.21. Photographs of the two DMR wave configurations that are shown schematically in Figs. 3.20a, b

Analytical Model of Double-Mach Reflection

The analytical models describing the two DMR wave configurations that are shown in Fig. 3.20 are developed, in the followings under the following assumptions:

- (1) The wave configuration of a DMR is self-similar.
- (2) The second reflected shock wave, r' , is straight (although this assumption is not strictly valid, it can be regarded as reasonable, in view of the fact that r' is short relative to its radius of curvature).

Case I: r' Intersects s and is Perpendicular to It

In addition to the above-mentioned two general assumptions, it is assumed that the shock wave r' does not bifurcate when it encounters the slipstreams.

The wave configuration of a DMR appropriate to this case was shown schematically in Fig. 3.20a. An enlargement of the flow field of interest together with the definition of some parameters is shown in Fig. 3.22.

If a frame of reference is attached to the second triple point, T' , and the three-shock theory is applied, one can write (similar to 3.16)

$$\theta'_j = \operatorname{tg}^{-1} \left[2 \operatorname{ctg} \phi'_j \frac{(M'_k \sin \phi'_j)^2 - 1}{M'_k (\gamma + \cos 2\phi_j) + 2} \right], \quad (3.34)$$

where subscripts k and j indicate flow states ahead and behind the oblique shock wave, M is the flow Mach number, ϕ_j is its angle of incidence with the oblique shock wave across which the flow passes to state (j) , θ_j is the flow deflection angle and p is the pressure. The superscript prime, $'$, means that

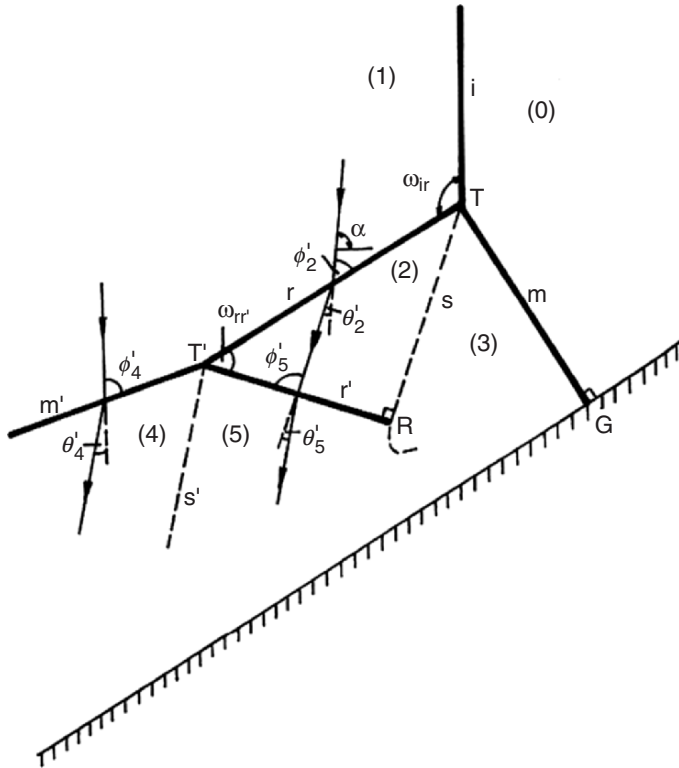


Fig. 3.22. Enlarged schematic illustration of the DMR wave configuration shown in Fig. 3.20a and definition of various parameters

the properties are with respect to the second triple point T' . The relation across the shock wave r is obtained by setting $j = 2$ and $k = 1$, the relation across the shock wave m' is obtained by setting $j = 4$ and $k = 1$, and the relations across the shock wave r' is obtained by setting $j = 5$ and $k = 2$.

The pressures in regions (4) and (5) can be obtained from

$$p_j = p_k \frac{2\gamma (M'_k \sin \phi'_j)^2 - (\gamma - 1)}{\gamma + 1}, \quad (3.35)$$

which is similar to (3.17). In order to get the pressure in state (4) one should set $j = 4$ and $k = 1$ and in order to get the pressure in state (5) one should set $j = 5$ and $k = 2$.

The matching conditions across the slipstream are:

$$p_4 = p_5 \quad (3.36)$$

and

$$\theta'_2 - \theta'_5 = \theta'_4. \quad (3.37)$$

Note that unlike the kinematic properties, which depend on the frame of reference and hence are marked with a prime superscript, the thermodynamic properties, which do not depend on the frame of reference, do not carry a prime.

M'_1 that appears in (3.34) and (3.35), can be obtained from

$$M'_1 = \left[(M_1^L)^2 + \left(\frac{V_{T'}}{a_1} \right)^2 - \frac{2M_1^L V_{T'} \cos(\theta_w + \chi')}{a_1} \right]^{1/2}, \quad (3.38)$$

$$V_{T'} = \frac{M_S a_0 - V_T^{T'} \sin \omega_{ir}}{\cos(\theta_w + \chi')}, \quad (3.39)$$

$$V_T^{T'} = \frac{V_T \sin(\chi' - \chi)}{\sin(\phi_2 + \chi' - \chi - \theta_1)}, \quad (3.40)$$

$$V_T = \frac{M_S a_0}{\cos(\theta_w + \chi)}. \quad (3.41)$$

In the above relations V_T and $V_{T'}$ are the velocities of the first, T , and the second, T' , triple points in the laboratory frame of reference, respectively, $V_T^{T'}$ is the velocity of T relative to T' . The other parameters, i.e., ω_{ir} , a_1 , χ , ϕ_2 and θ_1 can all be obtained by solving the flow field around the first triple point, T , as was shown in Sect. 3.2.6. In addition, one can write

$$\alpha = \operatorname{tg}^{-1} \left[\frac{V_{T'} \sin(\theta_w + \chi')}{V_{T'} \cos(\theta_w + \chi') - M_1^L a_1} \right], \quad (3.42)$$

where α , as defined in Fig. 3.22, is the orientation of the flow in state (1) with respect to a horizontal line, in a frame of reference attached to T' . The angle α is related to the angle of incidence ϕ'_2 through

$$\phi'_2 = \alpha - \left(\omega_{ir} - \frac{\pi}{2} \right). \quad (3.43)$$

In addition

$$\omega_{rr'} = \frac{\pi}{2} - (\phi_2 - \theta_2) \quad (3.44)$$

and

$$\phi'_5 = \pi - (\omega_{rr'} + \phi'_2 - \theta'_2) \quad (3.45)$$

and

$$M'_2 = \frac{\left\{ 1 + (\gamma - 1) (M'_1 \sin^2 \phi'_2)^2 + \left[\left(\frac{\gamma+1}{2} \right)^2 - \gamma \sin^2 \phi'_2 \right] (M'_1 \sin^2 \phi'_2)^2 \right\}^{1/2}}{\left[\gamma (M'_1 \sin^2 \phi'_2)^2 - \frac{\gamma-1}{2} \right]^{1/2} \left[\frac{\gamma-1}{2} (M'_1 \sin^2 \phi'_2)^2 + 1 \right]^{1/2}}. \quad (3.46)$$

The above set of equations consists of 16 equations and 16 unknowns, namely: $\phi'_2, \phi'_4, \phi'_5, \theta'_2, \theta'_4, \theta'_5, p_4, p_5, M'_1, M'_2, V_{T'}, V_T, V_{T'}^{T'}, \alpha, \omega_{rr'}$ and χ' provided $M_S, M_1^L, a_0, a_1, \theta_w, \chi, \phi_2, \theta_1, \theta_2$, and ω_{ir} are known, as indeed is the case since they are obtained from the solution of the flow field around the first triple point, T, as was shown in Sect. 3.2.6.

Case II: r' Intersects the Reflecting Wedge at the Point Where s Reaches It

The wave configuration of the DMR appropriate to this case was shown schematically in Fig. 3.20b. An enlargement of the flow field of interest together with the definition of some parameters is shown in Fig. 3.23.

As can be seen in Fig. 3.23, the second reflected shock wave r' does not cause the flow in region (5) to be parallel to the reflecting wedge surface. This is because the interaction between the slipstream, s, and the wall-boundary layer results in a separation zone. In fact, the second reflected shock wave, r' , never reaches the reflecting wedge surface. Instead, it is pushed over the separation zone [see Landau & Lifshitz (1987, p. 425)]. Therefore, requiring that the flow immediately behind r' near point D where the slipstream s reaches the reflecting surface should be parallel to the reflecting wedge surface is wrong. However, in view of the fact that the size (length) of the separation zone is small relative to the entire wave configuration, it could be assumed that the intersection point of the second reflected shock wave, r' , and the slipstream, s, is located on the reflecting wedge surface. Based on this assumption, the following set of relations is self-explanatory.

$$\overline{DT} = \frac{\overline{GT}}{\cos \omega_{sm}} \quad (3.47)$$

$$\omega_{sm} = \phi_3 - \theta_3, \quad (3.48)$$

$$\overline{GT} = V_T \Delta t \sin \chi \quad (3.49)$$

and

$$V_T^D = \frac{\overline{DT}}{\Delta t}. \quad (3.50)$$

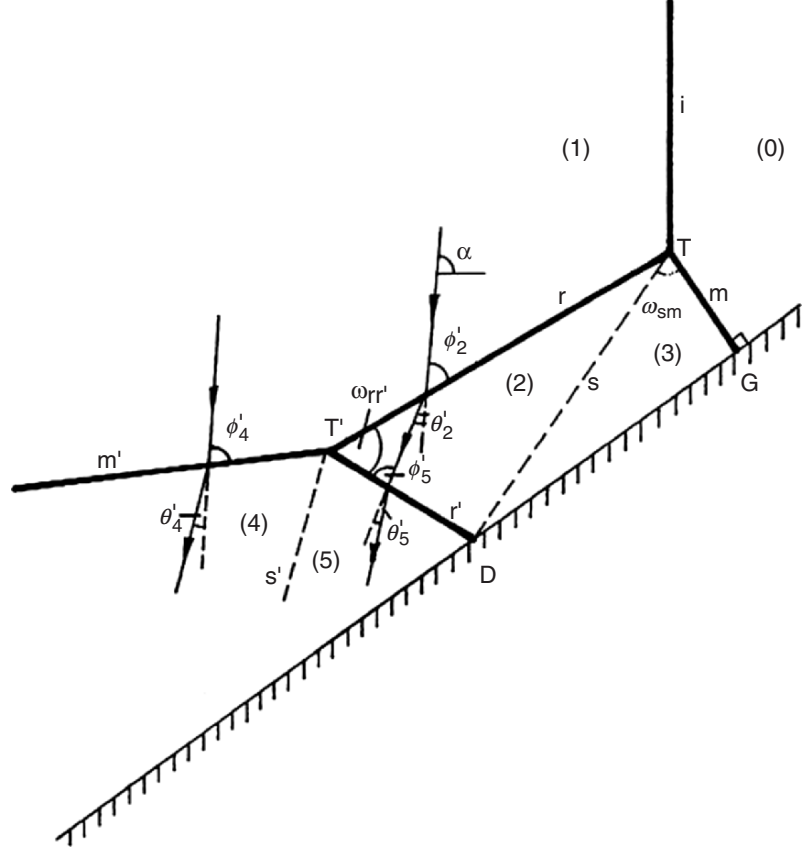


Fig. 3.23. Enlarged schematic illustration of the DMR wave configuration shown in Fig. 3.20b and definition of various parameters

Inserting (3.47)–(3.49) into (3.50) results in

$$V_T^D = \frac{V_T \sin \chi}{\cos(\phi_3 - \theta_3)}. \quad (3.51)$$

In the above equations V_T^D is the velocity of T relative to D. Applying the sine-law to the triangle TT'D yields:

$$\frac{\overline{TT'}}{\sin(\omega_{rr'} + \phi_2 - \theta_1)} = \frac{\overline{DT}}{\sin \omega_{rr'}}. \quad (3.52)$$

In addition

$$\overline{TT'} = V_T^{T'} \Delta t. \quad (3.53)$$

Combining (3.52) and (3.53) yields:

$$\omega_{rr'} = \operatorname{tg}^{-1} \left[\frac{V_T^D \sin(\phi_2 - \theta_2)}{V_T^{T'} - V_T^D \cos(\phi_2 - \theta_2)} \right]. \quad (3.54)$$

Equations (3.34)–(3.46), excluding (3.44), together with (3.51) and (3.54) form a set of 17 equations and 17 unknowns. The 17 unknowns are: $\phi'_2, \phi'_4, \phi'_5, \theta'_2, \theta'_4, \theta'_5, p_4, p_5, M'_1, M'_2, V_{T'}, V_T, V_T^{T'}, \alpha, \omega_{rr'}, \chi$ and V_T^D . Note that the first 16 unknowns are identical to the 16 unknowns in Case I (see Sect. 3.2.7). Consequently, the set of the governing equations of Case II is solvable in principle.

Separating Criterion between Case I and Case II

The transition criterion between the two different DMR wave configurations can be expressed as:

$$V_T^{T'} \cos(\phi_2 - \theta_2) = V_T^D \quad (3.55)$$

which, in turn, could be rewritten as

$$\frac{\sin(\chi' - \chi)}{\sin(\phi_2 + \chi' - \chi - \theta_1)} = \frac{\sin \chi}{\cos(\phi_3 - \theta_3)} \quad (3.56)$$

Location of the Second Triple Point (T')

The location of the second triple point, T', of a DMR, was determined with the aid of the above-mentioned two analytical models. Since the location is calculated using two models that are different from the model that was used to calculate point K in the case of a TMR, the location of T' is different from that of K. This is in contrast to the “old” state-of-the-knowledge where K and T' were considered as the same point, and their location was calculated using one model that was based on the Law–Glass assumption, which completely neglected the flow-deflection process.

A comparison between predictions based on the “new” models (solid lines), the “old” model (dashed lines) and experimental results, is shown in Fig. 3.24a–c. The second triple point trajectory angle, χ' , as a function of the incident shock wave Mach number, M_S , is shown in Fig. 3.24a for $\theta_w = 30^\circ$ and $\theta_w = 40^\circ$ and $\gamma = 1.4$. The superiority of the “new” models over the “old” model is evident. While the predictions of the latter model become progressively worse as M_S decreases below $M_S = 6$, the predictions of the “new” models are seen to excellently agree with the experimental results in that range. Note that at $M_S > 6$, the predictions of the three models approach each other until the difference between them becomes smaller than the experimental uncertainty.

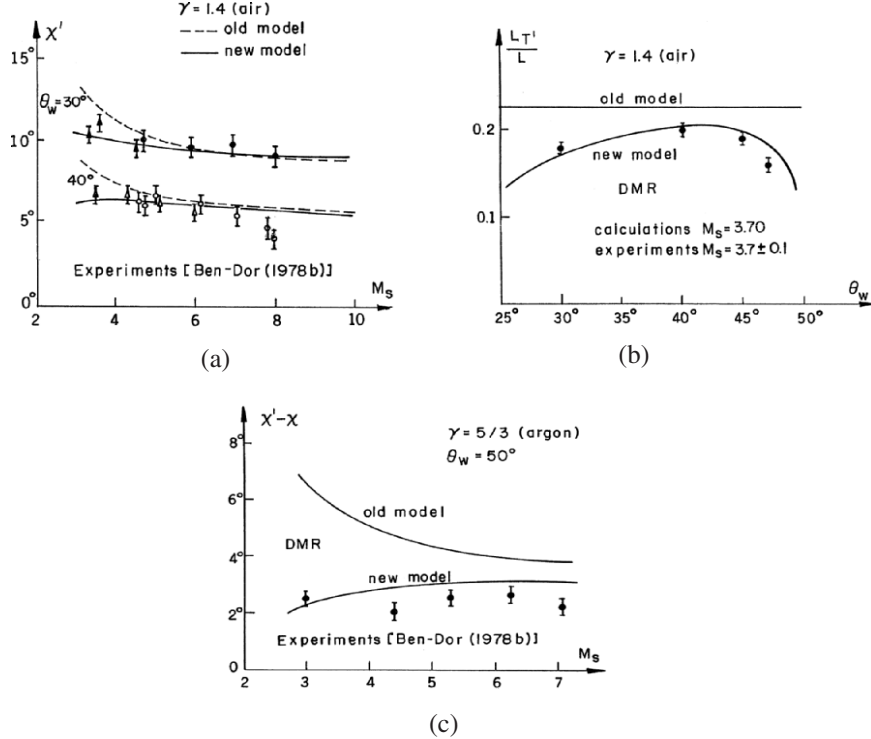


Fig. 3.24. Comparison between analytical predictions of the “new” and the “old” models and experimental results of the (a) second triple point trajectory angle χ' for fixed values of the reflection wedge angles, θ_w ; (b) location of the second triple point of a DMR, $L_{T'}$, for a fixed incident shock wave Mach number, M_s ; (c) difference between the first and the second triple point trajectory angles, $\Delta\chi = \chi - \chi'$, for a fixed reflecting wedge angle, θ_w . The experimental results were obtained by private communication from Profs. K. Takayama and J.M. Dewey

Comparison between the predictions of the just-mentioned three models regarding the location of the second triple point, $L_{T'}$, as a function of the reflecting wedge angle, θ_w , for $M_s = 3.7$ and air is shown in Fig. 3.24b. While the “old” model that is based on the Law–Glass assumption, which predicts a location independent of the reflecting wedge angle, θ_w , completely misses the experimental results, the predictions of Li & Ben-Dor’s (1995) models are very good as they reproduce the strong dependence of $L_{T'}$ on θ_w . The decrease in $L_{T'}$ as θ_w increases towards the value at which the DMR \rightleftharpoons RR transition takes place is missed completely by the results of the “old” model since it predicts a constant value of $L_{T'}$ regardless of how close the DMR is to its termination and transition to RR.

Comparison of the analytical predictions of the three models with experimental results for argon is shown in Fig. 3.24c. The superiority of the “new” models over the “old” model in predicting the difference between the first and the second triple point trajectory angles is clear. In addition, the predictions of the “old” model are also seen to resemble a trend different from that of the experimental results, as the predicted values increase while M_S decreases.

3.2.8 $\text{SMR} \rightleftharpoons \text{PTMR/TMR/DMR}$ and the $\text{TMR} \rightleftharpoons \text{DMR}$ Transition Criteria and Domains of Different Types of Reflection

The conditions and requirements for the transitions between SMR, TMR and DMR are summarized in this section. The necessary and sufficient condition for the termination of SMR and formation of PTMR or TMR or DMR, i.e., the $\text{SMR} \rightleftharpoons \text{PTMR/TMR/DMR}$ transition, is

$$M_2^T = 1, \quad (3.57)$$

where M_2^T is the flow Mach number in region (2) in a frame of reference attached to the first triple point, T,

The wave configuration that is obtained when SMR terminates depends on the incident-shock-induced flow Mach number. If this flow is subsonic then the resulted wave configuration is a PTMR, which has no reversal of curvature in its reflected shock wave. If, however, this flow is supersonic, then the resulted wave configuration is either a TMR or a DMR. Hence the $\text{PTMR} \rightleftharpoons \text{TMR/DMR}$ transition criterion is:

$$M_1^L = 1, \quad (3.58)$$

where M_1^L is the incident-shock-induced flow Mach number, i.e., the flow Mach number in region (1) in the laboratory frame of reference.

Determination of the conditions that sharply distinguish between the TMR and the DMR wave configurations is much more difficult. This is because the TMR, as its name indicates is, in fact, a primary stage of a DMR. Consequently, these two reflection wave configurations are compatible and distinguishing between them is sometimes impossible. In general, it can be said that the condition for the existence of TMR is:

$$M_2^K = 1, \quad (3.59)$$

where M_2^K is the flow Mach number in region (2) in a frame of reference attached to the kink, K.

Similarly, the condition for the existence of DMR is

$$M_2^{T'} > 1, \quad (3.60)$$

where $M_2^{T'}$ is the flow Mach number in region (2) in a frame of reference attached to the second triple point, T' . Hence the $\text{TMR} \rightleftharpoons \text{DMR}$ transition criterion is:

$$M_2^{T'} = 1 \quad (3.61)$$

Note that based on the “old” approach the locations of the kink K and the second triple point T' were determined using the same analytical model and hence these two points were the same point. In the “new” approach there is one model for determining the location of the point, K, of a TMR, and two models for determining the location of the second triple point, T' , of the two different DMR wave configurations that are shown in Fig. 3.20a, b. Furthermore, for all the TMR wave configurations $M_2^K = 1$.

Once a DMR wave configuration is formed it could be either a DMR^+ or a DMR^- depending on whether the first triple point trajectory angle, χ , is larger or smaller than the second triple point trajectory angle, χ' . Hence the $\text{DMR}^+ \rightleftharpoons \text{DMR}^-$ transition criterion is:

$$\chi = \chi' \quad (3.62)$$

As mentioned earlier Lee & Glass (1984) presented a photograph (see Fig. 3.12b) showing a situation in which the second triple point of the DMR is seen to be grazing the reflecting surface. They termed this wave configuration as terminal-double-Mach reflection, TerDMR. The requirement for the existence of this wave configuration is simply

$$\chi' = 0. \quad (3.63)$$

It should be noted here that based on gasdynamic considerations a wave configuration similar to that shown in Fig. 3.12 in which the second triple point actually lies on the reflecting surface is impossible.

3.2.9 Triple-Mach Reflection

As mentioned earlier, based on the gasdynamic logic that was applied in the “old” state-of-the-knowledge in order to determine the conditions for the termination of the TMR and formation of the DMR that led to the establishment of the $\text{TMR} \rightleftharpoons \text{DMR}$ transition criterion, Ben-Dor (1978) and Ben-Dor & Takayama (1992) hypothesized that if the flow Mach number behind the second triple point, T' , becomes supersonic with respect to the second triple point, i.e., if $M_4^{T'} > 1$, a second kink, K' , could develop in the shock wave m' (see Fig. 3.10a). This second kink could eventually develop to become a third triple point, T'' and form a triple-Mach reflection, TrMR, if the flow at that region becomes supersonic with respect to the second kink, i.e., if $M_4^{K'} > 1$ (see Fig. 3.10b).

By applying simple thermodynamic and gasdynamic concepts, Li & Ben-Dor (1995) proved that the just-mentioned conditions could not be met and hence a triple-Mach reflection is not physical and hence impossible.

3.2.10 Summary of the New State-of-the-Knowledge

Figure 3.25 shows an evolution-tree type presentation of the various types of shock wave reflection configurations according to the present state-of-the-knowledge. This figure replaces Fig. 3.2 that summarizes the state-of-the-knowledge that existed until the mid-1990s. It should be noted that Fig. 3.25 presents only a partial picture since it is limited to the domain for which the three-shock theory has a standard solution, i.e., for the case for which $\theta_1 - \theta_2 = \theta_3$. The reflection process in the two additional domains, i.e., the

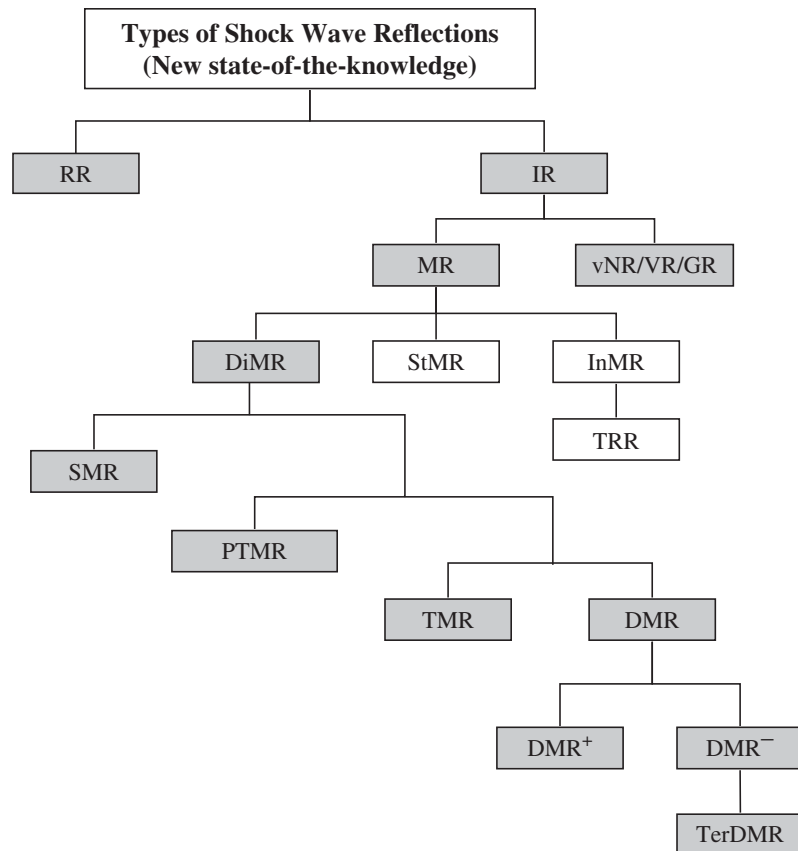


Fig. 3.25. Evolution-tree type presentation of the various types of shock wave reflection according to the new state-of-the-knowledge for the case in which the three-shock theory has a standard solution. The shadowed shock wave reflections have been observed actually in pseudosteady experiments. For the difference between the old and the new states-of-the-knowledge, compare with Fig. 3.2. Note that the cases in which the three-shock theory either has a nonstandard solution or no solution at all emanate from the vNR/VR/GR branch (see the complementary evolution tree in Fig. 3.31)

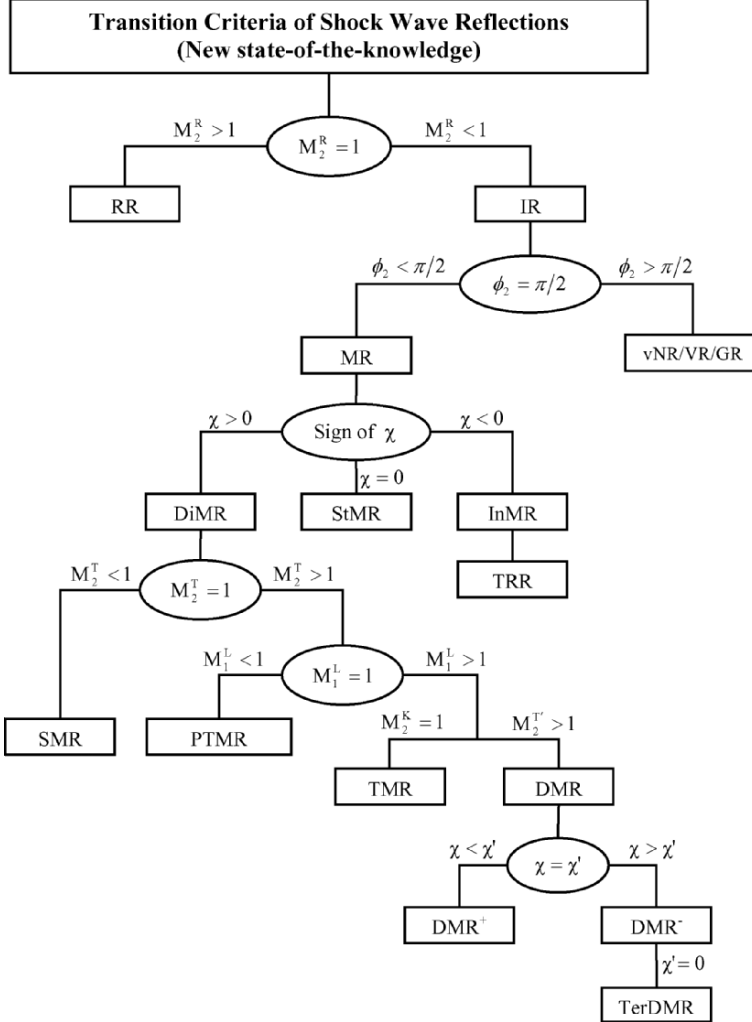


Fig. 3.26. Evolution-tree type presentation of the transition criteria of the wave configurations of the various types of shock wave reflections following the new state-of-the-knowledge. For the difference between the old and the new states-of-the-knowledge, compare with Fig. 3.13

domain in which the three-shock theory has a nonstandard solution and a domain in which the three-shock theory does not have any solution is described in Sect. 3.2.12

In similar Fig. 3.13 that shows an evolution-tree type presentation of the wave transition criteria between the various shock wave reflection configurations should be replaced by Fig. 3.26.

3.2.11 Domains and Transition Boundaries

Figure 3.27 presents the domains of SMR (domain A), PTMR (domain B), TMR (domain C), and DMR (domain D) in the (M_S, θ_w) -plane for air. Note that inside the TMR-domain, i.e., inside domain C, $M_2^K = 1$ everywhere! The line separating the A-domain from the B- and C-domains is given by (3.57), i.e., $M_2^T = 1$. The line separating the C- and D-domains is given by (3.61), i.e., $M_2^{T'} = 1$. The transition line was calculated from $M_2^{T'} = 1 + \varepsilon$ where $\varepsilon \rightarrow 0$. The reason for not calculating a line for which $M_2^{T'} = 1$ lies in the fact that such a requirement implies that the r' -shock wave, is, in fact, not a shock wave. Consequently, in order to ensure that the r' -shock wave remains a shock wave, the condition $M_2^{T'} = 1 + \varepsilon$ was used. The exact location of the line separating the TMR- and the DMR-domains depends on the value chosen for ε . For the line shown in Fig. 3.27 $\varepsilon = 0.01$. Larger values of ε would shift the transition line further into the DMR-domain.

Note that since the existence of TMR and DMR implies that the shock-induced flow should be supersonic [see (3.58)] the transition lines $M_2^T = 1$ and $M_2^{T'} = 1$ are terminated at $M_S = 2.07$ for which $M_1^L = 1$.

An inspection of Fig. 3.27 indicates that five TMR experiments lie in the DMR-domain. This might be misleading since in the past wave configurations were defined as DMR only if the r' -shock wave, was visible. As a result, wave configurations in which a clear sharp kink was evident but the r' -shock wave was not visible were defined as TMR. However, gas dynamic considerations

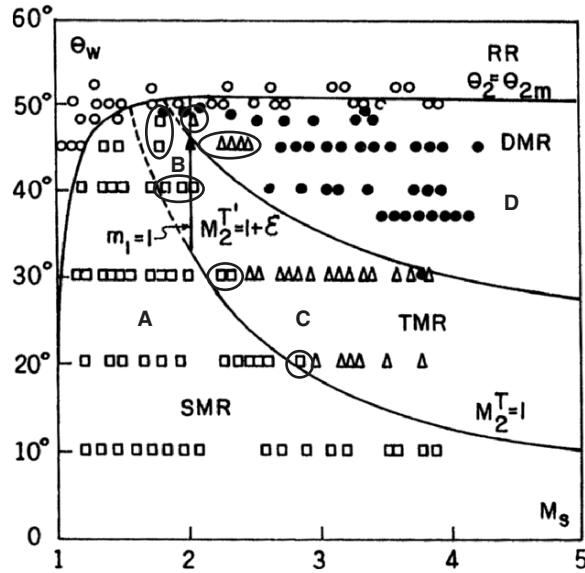


Fig. 3.27. Verification of the transition lines as calculated using the models of the new state-of-the-knowledge and with experimental results

(Courant & Friedrichs, 1948) imply that an additional shock wave and a slipstream should complement a sharp kink in a shock wave. Hence, all wave configurations having a sharp kink are DMR wave configurations regardless of whether the r' -shock wave is visible or not. There are also a few SMR wave configurations inside the PTMR domain. This should not be surprising since SMR and PTMR wave configurations have, in fact, the same appearance, and the PTMR was not known when these experiments were classified.

3.2.12 Weak Shock Wave Reflection Domain

As mentioned in Chap. 1 the IR-domain is divided, in general, into four sub-domains:

- A subdomain inside which the three-shock theory (see Sect. 1.3.2) has a “standard” solution ($\theta_1 - \theta_2 = \theta_3$) that corresponds to an MR,
- A subdomain inside which the three-shock theory has a “nonstandard” solution ($\theta_1 + \theta_2 = \theta_3$) that corresponds to a vNR,
- A subdomain inside which the three-shock theory does not have any solution, but experimental evidences reveal in it wave configurations that resemble MR wave configuration.³ The wave configuration in this case is a GR
- A subdomain, which extends between the just-mentioned vNR- and the GR-domains inside which a yet not fully understood reflection takes place. The wave configuration in this case is a VR.

The subdomains of vNR, VR and GR, which are typified by weak shock waves and small reflecting wedge angles, have been referred to by many investigators as the weak-shock wave reflection domain.

As will be shown subsequently a mathematical solution of the standard three-shock theory yields an MR while a solution of the nonstandard three-shock theory yields two cases: a case in which the solution is physical, and a case in which the solution is not physical. While in the former case, the resulted reflection is a vNR, in the latter case it could be one of two different types: a Guderley reflection, GR, or a Vasilev reflection, VR. In the VR the flow between the Mach stem and contact surface is subsonic, and a logarithmic singularity with infinite gradients at the triple point exists in this patch. A similar situation occurs also in the patch between the reflected shock wave and the expansion fan.

The just-mentioned three different wave configurations are shown in Fig. 3.28. In the vNR all the flow regions behind the reflected shock wave and the Mach stem are subsonic. Hence, the triple point is embedded in a subsonic flow with a logarithmic singularity (except for the incoming flow behind the reflected shock wave). In the VR there is one supersonic patch (white area) that extends from the slipstream towards the reflected shock

³ This phenomenon is known as the von Neumann paradox.

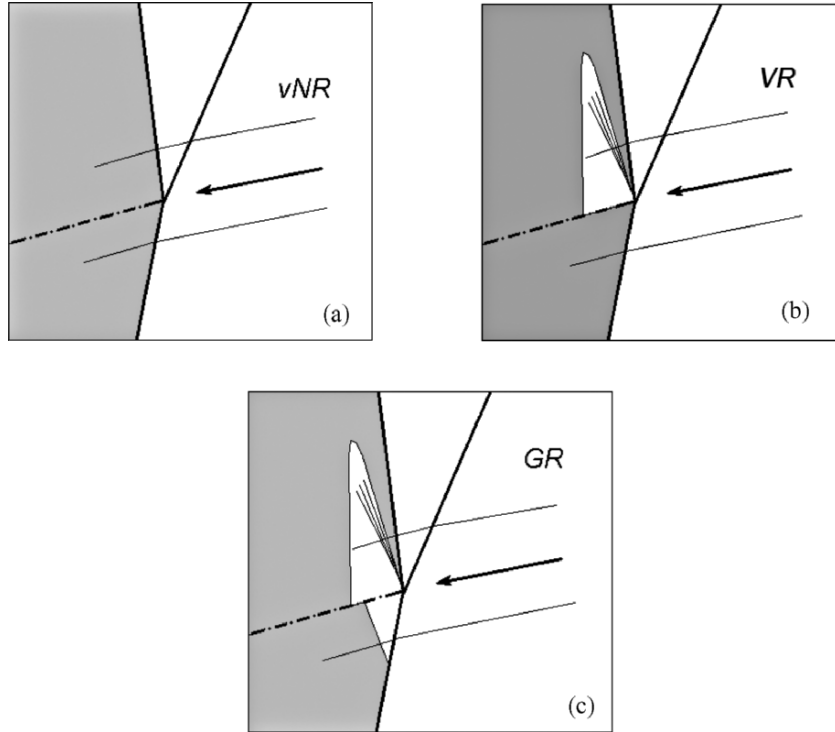


Fig. 3.28. Schematic illustration of the wave configurations of a von Neumann reflection, vNR, a Vasilev reflection, VR, and a Guderley reflection, GR. The gray denotes subsonic flow

wave with a Prandtl–Meyer expansion fan inside it. In the GR there are two supersonic patches. One, similar to the just-mentioned one in the VR, that extends from the slipstream toward the reflected shock wave with a Prandtl–Meyer expansion fan inside it, and one that extends between the slipstream and the Mach stem. Hence while in the VR there are two subsonic patches near the triple point, one behind the reflected shock wave and one behind the Mach stem, in the GR there is only one subsonic patch near the triple point, behind the reflected shock wave. Thus, different number of subsonic patches, with logarithmic singularity at the triple point, characterizes the vNR, VR and GR. It should be noted that the size of the patches is significant. The larger is the patch the smaller is the characteristic size of the singularity. Therefore, in vNR the size of the singularity is smaller than in the VR, which is smaller than in GR.

The evolution of the reflection wave configurations will be described in the following with the aid of (p, θ) -shock polars (for details see Sect. 1.4). Three interesting $(p_i/p_0, \theta_i^T)$ -polar solutions that are also known as (I–R)-polars combinations, corresponding to detachment, are shown in Fig. 1.19a–c.

Figure 1.19a presents an (I–R)-polars combination for which the net deflection of the flows in state (2), with respect to the triple point, is smaller than that in state (1). Hence the flow originating from state (0) at a point above the triple point trajectory is first deflected by the incident shock wave towards the reflecting wedge surface, and then it is deflected by the reflected shock wave away from the reflecting wedge surface to result in a situation in which $\theta_2^T = \theta_3^T < \theta_1^T$. This situation implies that $\theta_1 - \theta_2 = \theta_3$ (1.28a) and hence it represents a “standard” solution of the three-shock theory. The (I – R)-polars combination shown in Fig. 1.19b illustrates a different solution. It is seen that the flow that is deflected towards the reflecting wedge surface while passing through the incident shock wave is not deflected away from the reflecting wedge surface when it passes through the reflected shock wave but it is further deflected towards the reflecting wedge surface to result in a situation in which $\theta_2^T = \theta_3^T > \theta_1^T$. This situation implies that $\theta_1 + \theta_2 = \theta_3$ (1.28b) and hence it represents a “nonstandard” solution of the three-shock theory. Note that in the wave configuration corresponding to this case the reflected shock wave is directed against the flow. The limiting (I–R)-polars combination between the “standard” and “nonstandard” solutions is shown in Fig. 1.19c that indicates that the flow passing through the reflected shock wave is not deflected at all, i.e., $\theta_2 = 0$ and hence $\theta_2^T = \theta_3^T = \theta_1^T$. The boundary condition of the three-shock theory for this case is simply $\theta_1 = \theta_3$. The fact that the flow passing through the reflected shock wave is not deflected implies that the reflected shock wave is normal to the oncoming flow in state (1), i.e., $\phi_2 = 0$. Based on Colella & Henderson (1990) this condition is, in fact, the transition criterion from the Mach to the von Neumann reflection, i.e., the MR \rightleftharpoons vNR transition [see (3.14a and 3.14b and relevant text)]. The three wave configurations that correspond to the three (I–R)-polars combinations that are shown in Fig. 1.19a–1.19c are shown in Fig. 1.20a–c. The earlier remark regarding the orientation of the reflected shock wave is clearly evident in Fig. 1.20b.

Colella & Henderson (1990) concluded their study as follows:

- When the solution of the governing equations of the three-shock theory results in a standard solution for which $\theta_1 - \theta_2 = \theta_3$ the reflection is a Mach reflection, MR, and
- When the solution of the governing equations of the three-shock theory results in a nonstandard solution for which $\theta_1 + \theta_2 = \theta_3$ the reflection is a von Neumann reflection, vNR.

However, as will be shown subsequently while their first conclusion is correct the second one is only partially correct since there are cases in which the three-shock theory does have a nonstandard solution but the solution is not physical. Hence, their second conclusion should be modified to read:

- When the solution of the governing equations of the three-shock theory results in a nonstandard solution for which $\theta_1 + \theta_2 = \theta_3$ the reflection is a von Neumann reflection, vNR, *if the solution is physical*.

It should be noted here that this conclusion contradicts the concept forwarded by Colella & Henderson (1990) that the vNR resolves the “von Neumann paradox” in which wave configurations that resemble Mach reflection wave configurations occur in situations for which the three-shock theory does not have a solution. As just indicated the vNR takes place not when the three-shock theory does not have a solution (i.e., when the I- and R-polars do not intersect at all) but when the three-shock theory provides a “nonstandard” solution, i.e., a solution for which $\theta_1 + \theta_2 = \theta_3$ rather than $\theta_1 - \theta_2 = \theta_3$ as is the case of a “standard” solution, which results in an MR.

Now that the picture is clear when the three-shock theory provides standard and nonstandard solutions that are physical there are still two situations:

- The three-shock theory does provide a “nonstandard” solution, which is not physical.
- The three-shock theory does not have any solution (i.e., the I- and R-polars do not intersect). Experimental results show in this domain wave configurations that resemble vNR or MR. In fact, this is the “von Neumann paradox”.

As it turns out, this paradox was resolved almost over 60 years ago by Guderley (1947), who claimed that in addition to the above-mentioned well-known three shock waves that meet at a single point (i.e., the triple point) there are cases in which a tiny Prandtl–Meyer expansion fan complements the wave configuration. Hence, rather than a three-shock wave confluence there is a four-wave confluence (three shocks and one expansion). For this reason, it should not be surprising that the three-shock theory failed to describe this reflection since it never intended to model a four-wave confluence. Following Skews & Ashworth’ (2005) suggestion this reflection, which is shown schematically in Fig. 3.16, is named after Guderley and is called *Guderley reflection*, GR.

However, as it turned out, the forgoing presentation still does not provide a full picture of the entire phenomenon, since as will be shown subsequently, there are situations between the vNR- and the GR-domain for which none of these two reflection configurations is possible and there is a yet another wave configuration there.

This is shown in the followings by means of the evolution of the (I–R)-polars combinations as the complementary wedge angle, $\theta_w^C = 90^\circ - \phi_1$, is decreased from an initial value of 41° , for which the reflection is an MR, to $38.2^\circ, 34.5^\circ, 33.9^\circ, 32.5^\circ, 31.8^\circ$, and finally to 30° , for $M_S = 1.47$ and $\gamma = 5/3$. The (I–R)-polars combinations for these seven cases are shown in Fig. 3.29. (Note that for reasons that will become clear later the sonic point is marked as a open circle on all shock polars.)

Figures 3.30a–g are enlargements of the 7 (I–R)-polars combinations that appear in Fig. 3.29. Figure 3.30a shows the (I–R)-polars combination for $\theta_w^C = 41^\circ$ ($\phi_1 = 49^\circ$). The intersection of the I and R polars results in a standard solution of the three-shock theory (i.e., $\theta_1 - \theta_2 = \theta_3$) and hence the resulting reflection is an MR. Figure 3.30a also reveals that the I and R polars intersect

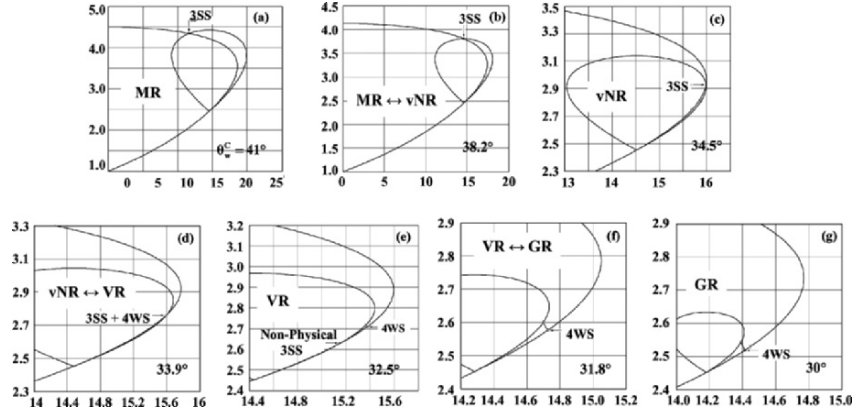


Fig. 3.29. The (I-R)-polars combinations for $M_S = 1.47$ and $\gamma = 5/3$ and $\theta_w^C = 41^\circ$ (MR), 38.2° ($MR \rightleftarrows vNR$), 34.5° (vNR), 33.9° ($vNR \rightleftarrows VR$), 32.5° (VR), 31.8° ($VR \rightleftarrows GR$) and 30° (GR). Recall that $\theta_w^C = 90^\circ - \phi_1$. The sonic point is marked on all the shock polars

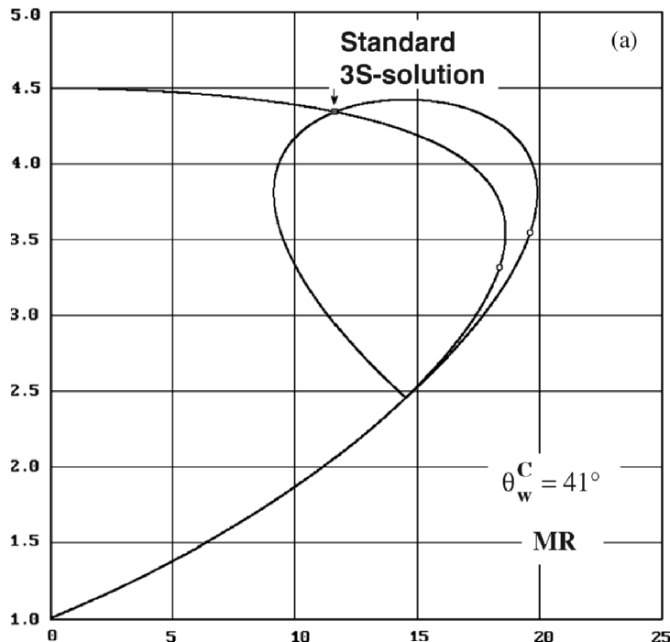


Fig. 3.30. (Continued)

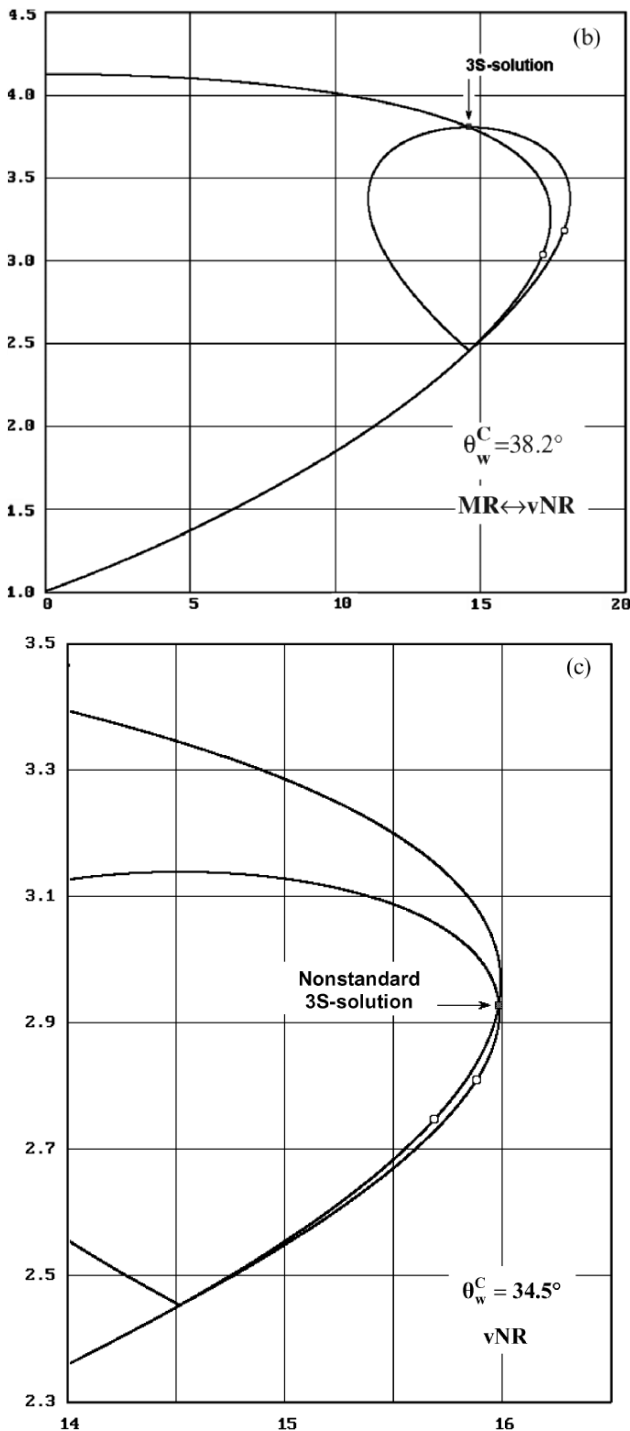


Fig. 3.30. (Continued)

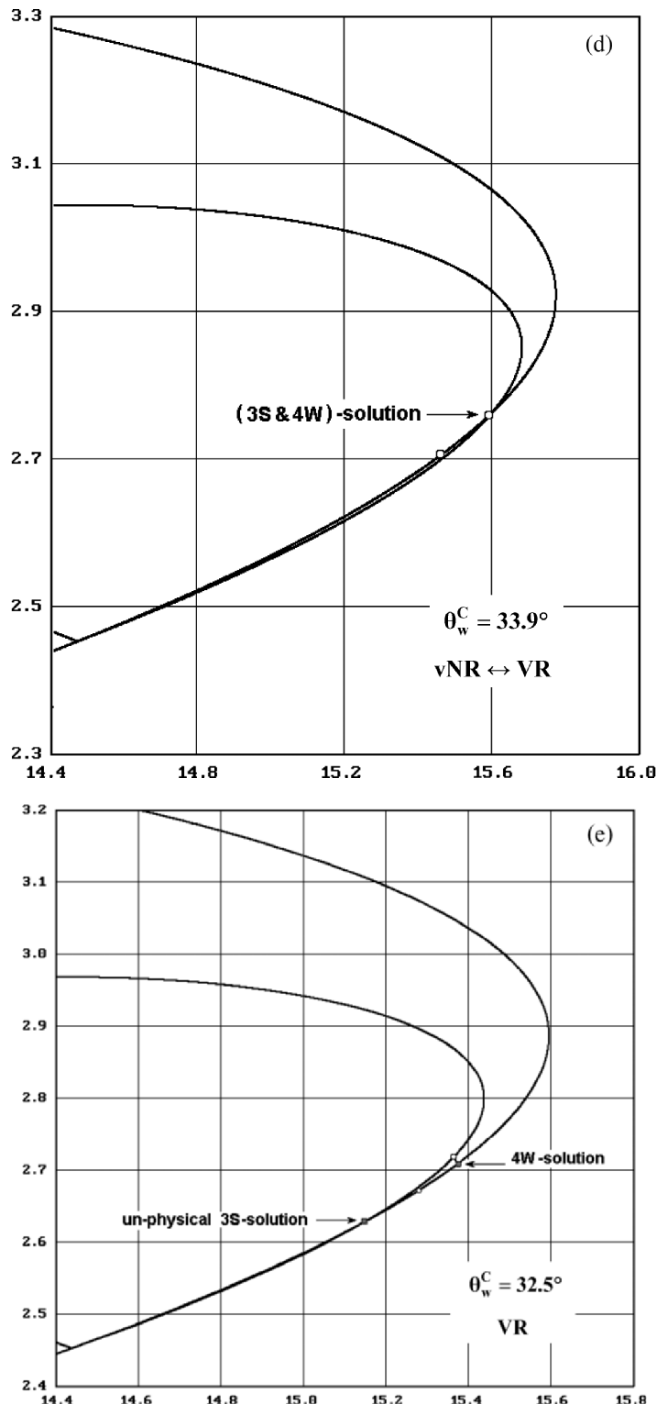


Fig. 3.30. (Continued)

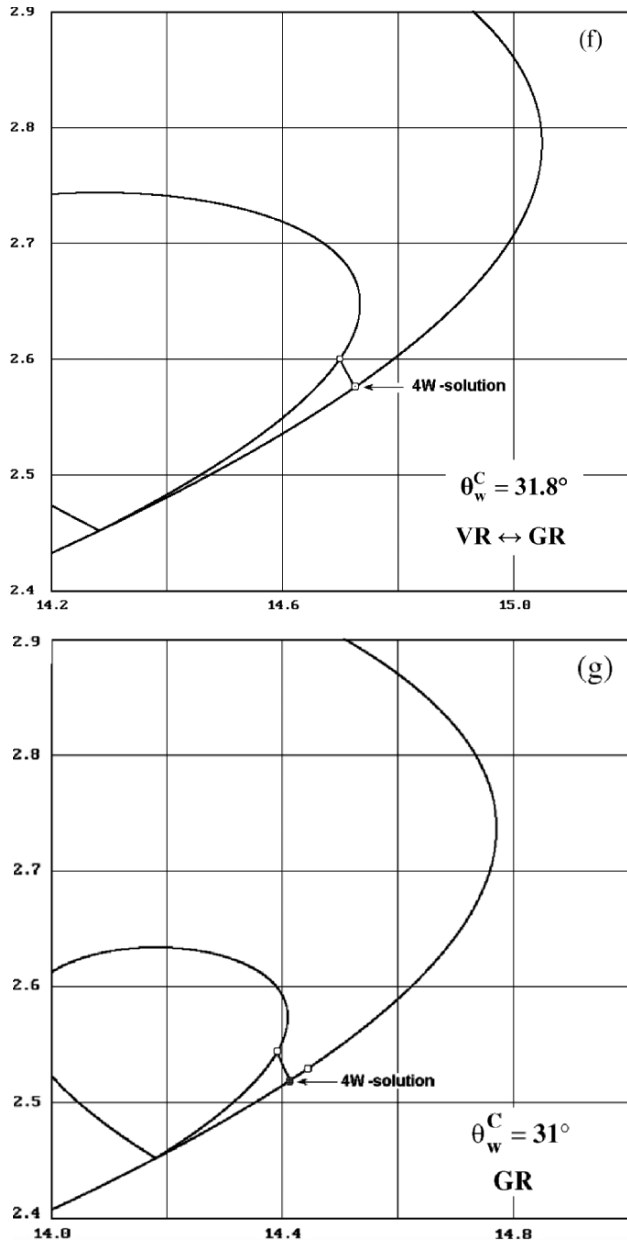


Fig. 3.30. Enlargement of the (I-R)-polars combination that is shown in:
 (a) Fig. 3.29a, (b) Fig. 3.29b (c) Fig. 3.29c (d) Fig. 3.29d, (e) Fig. 3.29e (f) Fig. 3.29f;
 (g) Fig. 3.29g

at their strong segments, i.e., along their subsonic branches. Hence the flows on both sides of the slipstream of the resulted MR wave configuration, in the vicinity of the triple point, are subsonic, i.e., $M_2 < 1$ and $M_3 < 1$. This implies that in the case of a pseudosteady flow the MR is a single-Mach reflection, SMR.

When θ_w^C is reduced to $\theta_w^C = 38.2^\circ$ ($\phi_1 = 51.8^\circ$) the situation for which $\theta_2 = 0$, i.e., $\theta_1 \pm \theta_2 = \theta_3$ or $\theta_1 = \theta_3$, is reached (see Fig. 3.30b). This is, in fact, the point at which the MR terminates and the vNR forms, i.e., this is the $\text{MR} \rightleftharpoons \text{vNR}$ transition point (Colella & Henderson, 1990). Figure 3.30b also reveals that $M_2 < 1$ and $M_3 < 1$. The wave configuration corresponding to this situation is presented in Fig. 1.20c.

Figure 3.30c shows the (I-R)-polars combination for $\theta_w^C = 34.5^\circ$ ($\phi_1 = 55.5^\circ$). The intersection of the I and R polars results in a nonstandard solution of the three-shock theory (i.e., $\theta_1 + \theta_2 = \theta_3$) and hence the resulting reflection is a vNR. Figure 3.30c also reveals that the flows on both sides of the slipstream of the resulted vNR are subsonic, i.e., $M_2 < 1$ and $M_3 < 1$, since the I and R-polars intersect along their subsonic branches. The wave configuration of a vNR is shown in Fig. 3.28a.

When θ_w^C is reduced to $\theta_w^C = 33.9^\circ$ ($\phi_1 = 56.1^\circ$) the situation that is shown in Fig. 3.30d is reached. Now the subsonic branch of the I-polar intersects the R-polar exactly at the sonic point of the R-polar. Hence, for this situation $M_2 = 1$ and $M_3 < 1$. As will be shown subsequently, this situation marks the point beyond which the three-shock theory has a solution, which is not physical! Hence, this is the point at which the vNR terminates and gives rise to a VR. The VR wave configuration is shown in Fig. 3.28b. Thus the situation that is presented in Fig. 3.30d represents the point at which the vNR terminates and the VR forms, i.e., the $\text{vNR} \rightleftharpoons \text{VR}$ transition point and also the point at which solutions of the three-shock theory (3ST) are not physical anymore and hence it should be replaced by another theory, a four-wave theory (4WT), i.e., this situation marks the $\text{3ST} \rightleftharpoons \text{4WT}$.

When θ_w^C is further reduced to $\theta_w^C = 32.5^\circ$ ($\phi_1 = 57.5^\circ$) the situation that is shown in Fig. 3.30e is reached. As can be seen the I- and R-polars still intersect, i.e., the 3ST still provides a solution. However, the polars intersect along their weak-solution branches, which means that the flows on both sides of the slipstream are supersonic, i.e., $M_2 > 1$ and $M_3 > 1$. This solution, which implies that the flow in state (3) is supersonic and is directed towards the reflecting wedge surface, is not physical! The (I-R)-polars combinations of the alternative 4WT, which results in a VR, is shown by the line bridging a subsonic state on the I-polar [state (3)] with the sonic point of the R-polar [state (2)]. As just-mentioned, the wave configuration of a VR is shown in Fig. 3.28b. The fact that a Prandtl–Meyer expansion fan is seen to exist between two flow zones which are not supersonic can be explained in the following way. A Prandtl–Meyer expansion fan cannot exist in a homogeneous subsonic flow. However, in the particular case there is a strongly inhomogeneous converging flow ahead of the fan, and therefore the Prandtl–Meyer

expansion fan can exist. If we consider two adjacent stream lines the flow between them is similar to the flow inside the Laval nozzle with the minimum cross-section at the boundary of the expansion fan.

When θ_w^C is reduced to $\theta_w^C = 31.8^\circ$ ($\phi_1 = 58.2^\circ$) the situation that is shown in Fig. 3.30f is reached. Now the I- and R-polars do not intersect at all and the 3ST does not provide any solution. Based on the 4WT of Vasiliev (1999) the sonic points of the I- and the R-polars are bridged, hence $M_2 = 1$ and $M_3 = 1$. In fact this is the point at which the VR terminates and the GR forms, i.e., $VR \rightleftharpoons GR$.

A further reduction of θ_w^C to $\theta_w^C = 31^\circ$ ($\phi_1 = 59^\circ$) results in the situation shown in Fig. 3.30g. The I- and R-polars do not intersect and the 3ST does not provide any solution. Based on the 4WT of Vasiliev (1999) the I- and the R-polars are bridged at $M_2 = 1$ and $M_3 > 1$. The resulted reflection is a GR that is shown in Fig. 3.28c. A Prandtl-Meyer expansion fan is responsible for bridging the flows in states (2) and (3).

The above-presented evolution of the types of reflection that are encountered when θ_w^C is reduced for $M_S = 1.47$ and $\gamma = 5/3$ and the transition criteria between them is summarized in Table 3.1.

The above presented transition criteria are shown in Fig. 3.31 in an evolution tree type presentation.

Based on the foregoing discussion Fig. 3.32a, b presents the domains of and the transition boundaries between the various shock wave reflection configurations in the (M_S, θ_w^C) -plane for (a) a diatomic ($\gamma = 7/5$) and (b) a monatomic ($\gamma = 5/3$) gas, respectively. Line 1 is the $MR \rightleftharpoons vNR$ transition line, i.e., $\phi_2 = 90^\circ$ on this line. Above this line $\phi_2 < 90^\circ$ and the reflection is an MR. Line 2 is the $vNR \rightleftharpoons VR$ transition line, i.e., $M_2 = 1$ on this line. This line also separates between the domains in which the 3ST does or does not have a physical solution, i.e., the $3ST \rightleftharpoons 4WT$. Line 3 is the $VR \rightleftharpoons GR$ transition line, i.e., $M_3 = 1$ on this line. Line 4 is the line on which $M_1 = 1$.

Table 3.1. Summary of the reflection processes that take place when θ_w^C is decreased for $M_S = 1.47$ and $\gamma = 5/3$

$\theta_w^C \& \phi_1$	Mach Number in state (2)	Mach Number in state (3)	
$\theta_w^C = 41.0^\circ$ ($\phi_1 = 49.0^\circ$)	$M_2 < 1$	$M_3 < 1$	MR
$\theta_w^C = 38.2^\circ$ ($\phi_1 = 51.8^\circ$)		$\phi_2 = 90^\circ$	$MR \rightleftharpoons vNR$
$\theta_w^C = 34.5^\circ$ ($\phi_1 = 55.5^\circ$)	$M_2 < 1$	$M_3 < 1$	vNR
$\theta_w^C = 33.9^\circ$ ($\phi_1 = 56.1^\circ$)		$M_2 = 1$	$vNR \rightleftharpoons VR$ also $3ST \rightleftharpoons 4WT$
$\theta_w^C = 33.4^\circ$ ($\phi_1 = 56.6^\circ$)	$M_2 = 1$	$M_3 < 1$	VR
$\theta_w^C = 31.8^\circ$ ($\phi_1 = 58.2^\circ$)		$M_3 = 1$	$VR \rightleftharpoons GR$
$\theta_w^C = 31.0^\circ$ ($\phi_1 = 59.0^\circ$)	$M_2 = 1$	$M_3 > 1$	GR

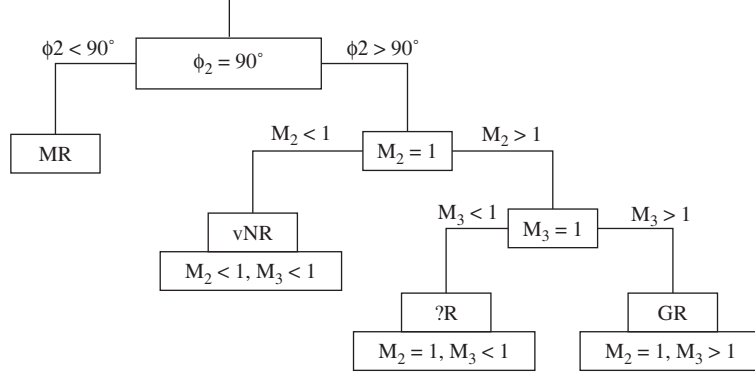


Fig. 3.31. Evolution tree type presentation of the transition criteria between the various reflections

Below this line the flow behind the incident shock wave is subsonic and no reflection can take place! The domain below this line is sometimes referred to as the no-reflection domain (NR-domain). The NR-domain exists only in the (M_S, θ_w^C) -plane. It vanishes in the more physical (M_S, θ_w^C) -plane (recall that $\theta_w^C = \theta_w + \chi$ where χ is the triple point trajectory angle). Line 5 divides the (M_S, θ_w^C) -plane into two domains: above it, the 3ST has at least one solution (not necessarily a physical one) and below it, the 3ST does not have any solution. Consequently, between lines 2 and 5 the 3ST has a solution, which is not physical. The von Neumann paradox existed inside the domain bounded by lines 2 and 4. Guderley (1947) resolved the paradox in the domain bounded by lines 3 and 4 by forwarding the four-wave concept (three shock waves and one expansion wave). The reflection in this domain is a GR (see Fig. 3.28c). The reflection that takes place inside the domain bounded by lines 2 and 3 is VR, which is shown in Fig. 3.28b.

In summary, the MR-domain is above line 1; the vNR-domain is between lines 1 and 2; the VR-domain is between lines 2 and 3; the GR-domain is between lines 3 and 4; and the NR-domain is below line 4. The 3ST has at least one (not necessary physical) solution in the domain above line 5 and no solutions in the domain below line 5.

3.3 Summary, Critique, and Discussion

Comparisons between the analytical predictions of the various transition lines (those that are based on the “old” and “new”-states-of-the-knowledge, see e.g., Sect. 2.4.3 in the first edition of this monograph, Ben-Dor 1991) and experimental have revealed that, in general, the (M_S, θ_w) -plots for the various gases provide the experimenter with good engineering results.

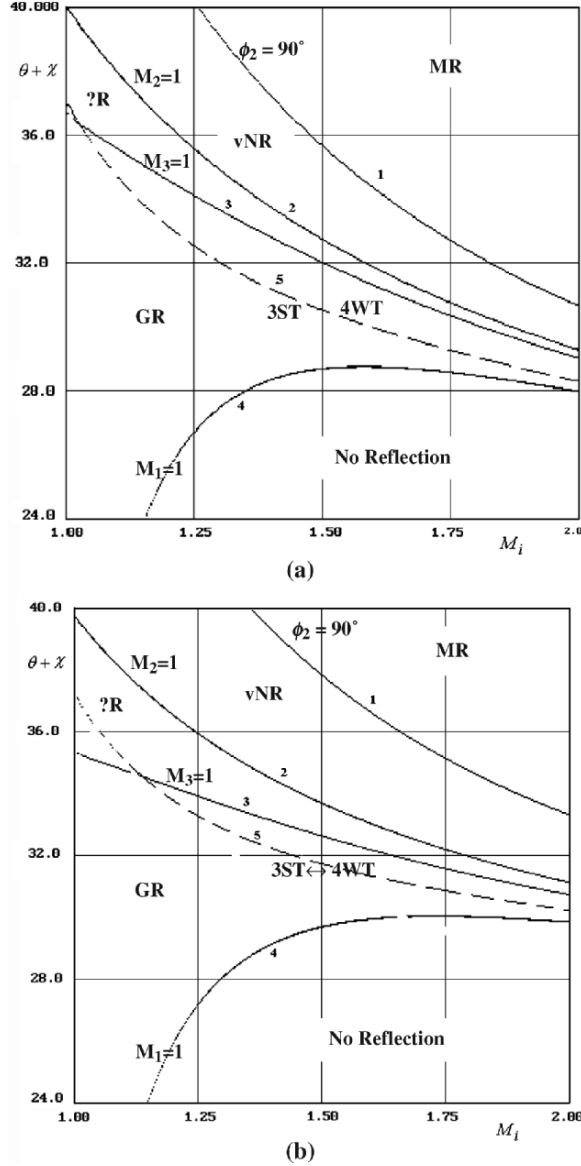


Fig. 3.32. Domains of and the transition boundaries between the various shock wave reflection configurations in the (M_s, θ_w^C) -plane for a: (a) diatomic gas $\gamma = 7/5$ and (b) monatomic gas $\gamma = 5/3$: Line 1: The $MR \rightleftharpoons vNR$ transition line, i.e., $\phi_2 = 90^\circ$; Line 2: The $vNR \rightleftharpoons VR$ transition line, i.e., $M_2 = 1$. This line also separates between the domains in which the 3ST does or does not have a physical solution; Line 3: The $VR \rightleftharpoons GR$ transition line, i.e., $M_3 = 1$; Line 4: The line on which $M_1 = 1$. Below this line the flow behind the incident shock wave is subsonic and a reflection cannot take place! Line 5: Above this line the 3ST has at least one mathematical solution (not necessarily physical) and below it the 3ST does not have any mathematical solution

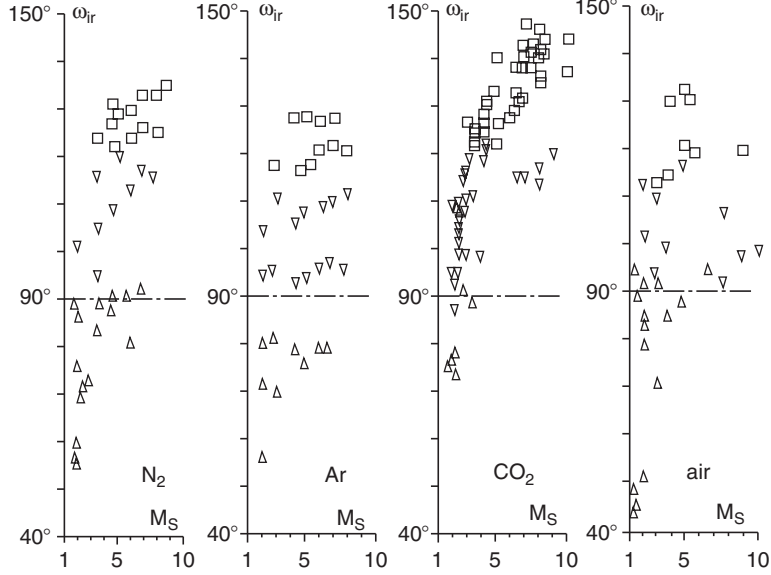


Fig. 3.33. The value of ω_{ir} as measured in actual SMR and TMR experiments for N_2 , Ar, CO_2 and air. The experimental data is from UTIAS (Courtesy of Professor I.I. Glass)

Figure 3.33 illustrates the distribution of SMR- and TMR-experiments for N_2 , Ar, CO_2 , and air in the (ω_{ir}, M_S) -plane. All the TMR-experiments except one for CO_2 satisfy the condition $\omega_{ir} > 90^\circ$. These results provide very good evidence that $\omega_{ir} \geq 90^\circ$ is a necessary condition for the $SMR \rightleftharpoons TMR/DMR$ transition. Several SMR-experiments which lie above the $\omega_{ir} = 90^\circ$, in the case of N_2 and air, if they are not PTMR suggest that $\omega_{ir} \geq 90^\circ$ might not a sufficient condition. In spite of this clear evidence, which is completely based on experimental observations and hence, includes neither calculations nor assumptions, when the calculated $\omega_{ir} = 90^\circ$ transition line is added to the (M_S, θ_w) -plots (see e.g., Figs. 2.41–2.45 in Ben-Dor 1991 and respective discussion) it does not help in clearly and better separating the SMR- and the TMR-domains. As is evident from Figs. 2.42a, 2.42c, 2.43c, 2.43e, and 2.44b of Ben-Dor (1991) the calculated $\omega_{ir} = 90^\circ$ line has the potential for sometimes placing SMR-experiments, which violated the $M_2^T = 1$ transition line, in their appropriate domain. Not even one SMR-experiment, which was in its appropriate domain as defined by the $M_2^T = 1$ transition line, was moved into the TMR-domain due to the additional calculated $\omega_{ir} \geq 90^\circ$ requirement. This was not the case for many TMR-experiments which originally were in their appropriate TMR-domain as defined by the $M_2^T = 1$ transition line and were pushed into the SMR-domain as defined by the calculated $\omega_{ir} = 90^\circ$

boundary (see Figs. 2.43a, 2.43f, 2.44a, 2.44b, 2.45a and 2.45c in Ben-Dor 1991). This contradictory result clearly suggests that an error is introduced into the analytical calculation of ω_{ir} . As will be shown in Sect. 3.4.4 the inviscid three-shock theory does indeed fail to predict accurately the angles between the various discontinuities near the triple point, T. Thus, it is expected that the $\omega_{ir} = 90^\circ$ transition line would better agree with the experimental results if its calculation accounts for viscous effects.

Figures 2.41–2.45 (in Ben-Dor 1991) also indicate that the $M_2^{T'}$ transition line is not accurate enough in distinguishing clearly and sharply between the TMR- and DMR-domains. This is probably due to the oversimplifying assumptions used in calculating the triple point trajectory angles χ and χ' as well as the motion of the second triple point with respect to the first triple point. The modification presented by the new-state-of-knowledge resulted in, as expected, much better agreements.

Unlike the fairly good agreement between the analysis and the experiments for monatomic and diatomic gases, which as mentioned earlier could be assumed to behave as perfect gases under the experimental conditions, the experimental results for the more complex gases, e.g., CO₂, Freon-12 and SF₆, did not indicate good agreement with the perfect gas analysis. The main reason is probably that these gases, which are already excited at room temperature, result in nonequilibrium flows behind the shock waves. Thus, neither a perfect gas solution nor a real equilibrium solution could be expected to reproduce the experimental results. At most, these solutions could be regarded as upper and lower limits of the actual solution. The obvious persistence of DMR-experiments far into the RR-domain suggests that the RR \rightleftharpoons IR transition line should be calculated with more realistic assumptions. Since this transition line is calculated by solving the flow field near the reflection point, R, of an RR, which lies on the reflecting wedge surface, perhaps heat transfer and viscosity are important in calculating this transition line. However, as it turns out real gas effects (see Figs. 2.41–2.45 in Ben-Dor 1991) and viscosity (see Fig. 2.53 in Ben-Dor 1991) cause the RR \rightleftharpoons IR transition line to shift downwards in a direction opposite to that required by the dashed lines in Figs. 2.44a and 2.44b of Ben-Dor (1991). Thus, it might be that heat transfer is the additional mechanism that should be accounted for in order to obtain a more accurate RR \rightleftharpoons IR transition line.

The fact that all the TDMR-experiments (see Figs. 2.44–2.45 in Ben-Dor 1991) lie outside their predicted domain clearly suggests that the $\chi' = 0$ transition line is not calculated accurately enough. This again is probably due to the inadequate way in which real gas effects were accounted for, i.e., equilibrium rather than nonequilibrium, and the oversimplifying assumptions that were used to calculate χ' . In addition, the fact that $\chi' = 0$ forces the second triple point to be on the reflecting wedge surface, probably means that viscosity and heat transfer effects should not be neglected if one wishes to get a more realistic $\chi' = 0$ transition line.

In summary, the fact that the above-presented two- and three-shock theories failed to predict accurately the two- and three-shock wave reflection configurations in pseudosteady flows could be attributed to two major causes:

1. Some of the assumptions upon which the two- and three-shock theories were based are not justified, and
2. There are some additional factors in the experimental set-up that are used to generate shock wave reflections in shock tubes, which influence the actual two- and three-shock wave configurations.

In the following, both of these major causes are examined. Wherever possible, modifications are introduced into the two- and three-shock theories.

3.4 Modifications of the Perfect Inviscid Two- and Three-Shock Theories

Comparisons between the analytical predictions based on the two- and three-shock theories and the experimental results clearly indicated that these theories must be modified in order to improve their predictions and obtain better agreement with the experimental results.

The major assumptions upon which the two- and three-shock theories were based are:

1. The flow field is steady
2. The discontinuities at the reflection point of an RR and at the triple points of an MR are straight, i.e., the flow regions bounded by each pair of neighboring discontinuities is uniform
3. The fluid obeys the equations of state of a perfect gas ($p = \rho RT$)
4. The fluid is inviscid ($\mu = 0$)
5. The fluid is thermally nonconductive ($k = 0$)
6. The contact discontinuity of the triple point is a slipstream, i.e., it is infinitely thin

In the following, the validity of each of these assumptions is discussed. Whenever possible, a modified model in which the assumption under consideration is relaxed is presented.

3.4.1 Nonsteady Effects

The two- and three-shock theories assume that the flow fields in the vicinities of the reflection point of an RR and the triple points of an MR are steady. Hence, strictly speaking, if these theories are used to investigate shock wave reflection configurations in steady flows (e.g., reflections which are obtained in wind tunnels) then the requirement of steady flow is fulfilled.

However, in shock tube experiments, the flow is not steady. The use of the two- and three-shock theories for investigating shock-wave reflection configurations in this case was justified by experimental observations in the early 1940s, which reported that the reflection configurations were self-similar, and hence, the flow field could be considered as pseudosteady.

However, experimental investigations regarding the point of formation of the first triple point raised some doubts about the validity of the self-similar behavior of the MR wave configuration. Reichenbach (1985) and Schmidt (1989) provided experimental evidences that the triple point does not form at the leading edge of the reflecting wedge, but at some distance up the reflecting wedge surface. Furthermore, they showed that the triple point trajectory is not straight near the point along the reflecting wedge surface where it is formed. Consequently, an MR in its early stages, cannot have a self-similar structure. However, it is possible that the MR approaches a self-similar structure after its triple point assumes a straight trajectory. It should be noted here that Dewey & van Netten (1991 and 1995) who showed experimentally that the evolution of the reflection is indeed not self-similar, also claimed that all their experimental results showed that if someone waits long enough a final reflection configuration develops in which the triple point trajectory extends back to the leading edge of the reflecting wedge.

Further comments regarding the self-similarity of the reflection configurations in pseudosteady flows are given in Sect. 3.4.7.

3.4.2 Nonstraight Discontinuities

The two- and three-shock theories assume that the discontinuities at the reflection point of an RR and the triple point of an MR are straight. This assumption implies that the flow region bounded by any two neighboring discontinuities is uniform.

In the case of an RR (see Fig. 3.4), which exists as long as the flow behind the reflection point, R, is supersonic with respect to the reflection point, i.e., $M_2^R > 1$, this assumption is justified since both the incident shock wave, i, and the reflected shock wave, r, are separating supersonic flow regions. Thus, the assumption of straight discontinuities near the reflection point of an RR should not introduce any error into predictions based on the two-shock theory when it is used to calculate the flow properties near the reflection point.

Unfortunately, however, this is not the case with the three-shock theory. While the incident shock wave, i, of the triple point, T, of an MR is always straight, both the Mach stem, m, and the slipstream, s, are curved always near the triple point (see Figs. 3.7–3.9). Thus, the assumption of straight discontinuities near the triple point introduces an inherent error into predictions based on the three-shock theory.

Furthermore, the reflected shock wave, r, of the first triple point, is straight in the vicinity of the triple point, T, only for TMR (see Fig. 3.8) PTMR, and DMR (see Fig. 3.9) which exist only for $M_2^T > 1$. In the case of an SMR

(see Fig. 3.7), the reflected shock wave is curved in the vicinity of T since an SMR exists only for $M_2^T < 1$. This fact introduces further inherent errors into predictions based on the three-shock theory when it is used to calculate the flow properties near the triple point of an SMR.

Similarly, the discontinuities near the second triple point, T' , of a DMR (see Figs. 3.9 and 3.21) are not all straight. Both the second Mach stem, m' , and the second slipstream, s' , are curved. Thus, the use of the assumption of straight discontinuities introduces an inherent error into predictions based on the three-shock theory when it is used to calculate the flow properties near the second triple point of a DMR.

3.4.3 Real Gas Effects

When a shock wave propagates through a gas, the translational and rotational degrees of freedom of the gas molecules are excited to a new state of equilibrium. The distance along which this occurs is known as the relaxation length. Its length is equal to a few mean-free-paths, which is of the order of the thickness of the shock wave front. The other internal degrees of freedom require a longer time (or distance) to reach equilibrium. Thus, in the analysis of gasdynamic shock wave phenomena the role of the relaxation length is very important. If the relaxation length of an internal degree of freedom is much longer than a characteristic length of the phenomenon, then the internal degree of freedom can be treated as frozen at its preshock state. If, however, the relaxation length of an internal degree of freedom is considerably shorter than a characteristic length of the phenomenon, it can be assumed to be in equilibrium immediately behind the shock wave front. Note that this is only a simplifying assumption, since equilibrium is approached only at a distance of the order of the relaxation length. The gas is in nonequilibrium when the relaxation length is of the order of the characteristic length of the phenomenon. In such a case, the frozen and the equilibrium solutions might be considered as two extreme cases bounding the real nonequilibrium solution.

Although there are no straightforward rules for choosing a characteristic length of a given phenomenon, there are cases where the choice is quite simple and obvious. In the case of the TMR \rightleftharpoons DMR transition, which is based on the flow Mach number behind the reflected shock wave with respect to the second triple point, $M_2^{T'}$, the distance between the first, T, and the second, T' , triple points can be considered as a characteristic length. This is because the flow state near the second triple point depends on the length of the relaxation zone behind the incident shock wave.

Figure 3.34 illustrates a DMR reflection at three different locations along a given reflecting wedge. The vibrational and the dissociational relaxation lengths, l_v and l_d , respectively, are drawn behind the incident shock wave. These relaxation lengths, which depend solely on the incident shock wave Mach number and the flow properties ahead of it as is shown in Fig. 3.35 for N_2 , O_2 and CO_2 . The wave configuration, however, grows linearly with time.

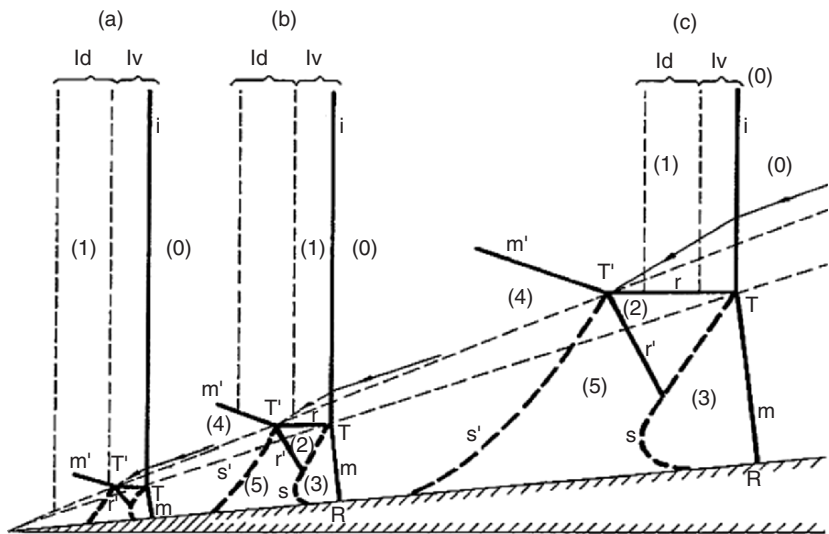


Fig. 3.34. Schematic illustration of the way by which real gas effects might affect a DMR

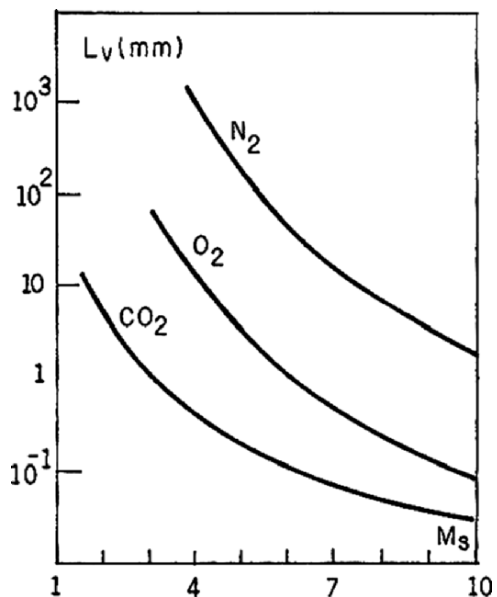


Fig. 3.35. Dependence of the vibrational relaxation lengths of N_2 , O_2 and CO_2 on the incident shock wave for $p_0 = 15$ Torr and $T_0 = 300$ K

When the incident shock wave is at position "a" the second triple point, T' , is still inside the zone where the vibrational degree of freedom has not yet reached its equilibrium and the dissociational degree of freedom is still frozen at that position, as its excitation can be assumed to start only after vibrational equilibrium is reached. Thus, if the flow field near the second triple point is to be solved, the flow approaching the second triple point from state (1) should be treated as a nonequilibrium flow. Later, the incident shock wave reaches position "b". At this position the second triple point, T' , lies beyond the vibrational relaxation zone, and hence the flow is already in vibrational equilibrium. However, the dissociational degree of freedom, which is already excited at this position, is not in equilibrium yet. Thus, the treatment of the flow field near the second triple point, T' , in this situation is different from that in the previous situation. When the incident shock wave reaches position "c", the second triple point, T' , is already located beyond the dissociational relaxation zone. Thus, the flow approaching the second triple point, T' , from state (1) is in dissociational-equilibrium.

The foregoing illustration and discussion clearly indicate the important role of the various relaxation lengths in accurately solving the flow field near the second triple point. It is clear that the flow field in the vicinity of the second triple point depends on the continuously changing distance between the second triple point, T' , and the incident shock wave, i, or alternatively on the location of the incident shock wave along the reflecting wedge surface.

Note, that unlike the second triple point, which moves backwards with respect to the incident shock wave, the first triple point is a part of the incident shock wave and hence all the internal degrees of freedom are frozen in its vicinity and retain their preshock states. Therefore, while real gas effects must be accounted for when the flow field near the second triple point is solved, a frozen gas solution could be carried out for the flow near the first triple point. This implies that the SMR \rightleftharpoons TMR/DMR transition criterion, i.e., $M_2^{T'} = 1$, should be based on a frozen flow in states (1), (2), and (3) while the TMR \rightleftharpoons DMR transition criterion, i.e., $M_2^T = 1$, depends on the thermodynamic state of the flow in state (1), which depends on the location of the incident shock wave along the reflecting wedge.

It is evident from the foregoing discussion that the choice of a characteristic length in the case of a DMR is obvious if the flow near the second triple point is to be solved. In other cases, such as RR or SMR, the choice of a characteristic length is more difficult. However, as long as the flow fields near the reflection point, R, of an RR, or the first triple point, T, in an MR, are to be solved, it is justified to assume that the internal degrees of freedom of the flow remain frozen and hence retain their preshock level of excitation. Thus, gases such as Ar, N₂, O₂, and air, which at room temperature can be assumed to behave as perfect gases, should be treated as perfect gases near the reflection point of an RR or the first triple point of an MR. Similarly, gases which are already excited at room temperature, such as Freon-12, SF₆ and even CO₂ should be treated as frozen at their excited level in the vicinities of R and T.

The foregoing discussion also suggests that even in the case of a single reflection configuration, it is not possible to determine one single characteristic length. In the case of DMR, for example, two different characteristic lengths should be considered for treating each of the two triple points. The two characteristic lengths might differ by orders of magnitude. In addition, the internal degrees of freedom do not relax in the simplified manner shown in Fig. 3.34. The dissociational relaxation does not start only after vibrational equilibrium is reached, but earlier. Therefore, there are situations where both the vibrational and dissociational degrees of freedom are not fully excited. Furthermore, when the temperatures are high enough, electronic excitation and ionization further complicate the phenomenon. The situation is even further complicated if one recalls that the relaxation processes themselves do not have a precise length, for it takes a considerably longer distance than the relaxation length [usually defined as the distance where the flow properties reach $(1-1/e)$ of their equilibrium value which is reached theoretically at infinity] to achieve the final equilibrium state.

The foregoing discussion suggests that obtaining a real nonequilibrium solution could be too complicated. Therefore, it is a common practice to model real gas behavior by assuming equilibrium of the most likely activated degree of freedom, i.e., vibrational-, dissociational-, electronic excitational-, or ionizational-equilibrium. Such a model should therefore be regarded as bounding limit on the phenomenon, where the perfect gas model results in the other bounding limit. Further discussions concerning the assumptions regarding the excitation of the internal degrees of freedom can be found in Shirouzu & Glass (1986) and Glaz et al. (1988).

Figure 3.36a illustrates the domains of different types of reflections (based on the “old” state-of-the-knowledge in the (M_S, θ_w^C) -plane for perfect nitrogen (solid lines) and nitrogen in dissociational-equilibrium (dashed lines). The real gas model assumes a dissociational-equilibrium everywhere. At relatively low incident shock wave Mach numbers, the transition lines for the imperfect nitrogen diverge from their appropriate perfect gas transition lines due to the excitation of the vibrational degree of freedom. Each of the real gas boundary lines splits up, at a higher incident shock wave Mach number (i.e., higher temperature), into four lines (numbered 1–4). This split is due to the excitation of the dissociational degree of freedom. Each of these four lines corresponds to a different initial pressure, p_0 . The lower is the initial pressure the greater is the shift from the appropriate perfect gas line. Unlike the dissociational relaxation, which is pressure and temperature dependent, the vibrational relaxation does not depend on the pressure but on the temperature only. Therefore, the transition lines for different initial pressures, but identical initial temperatures, converge to a single line. Figure 3.36a clearly indicates that, for a given M_S and θ_w , the resulting reflection depends on the thermodynamic state of the gas. If the gas can be assumed to be in dissociational-equilibrium, then at high incident shock wave Mach numbers the phenomenon depends also on the initial pressure. For example, at $M_S = 10$ and $\theta_w^C = 44^\circ$ an RR should be

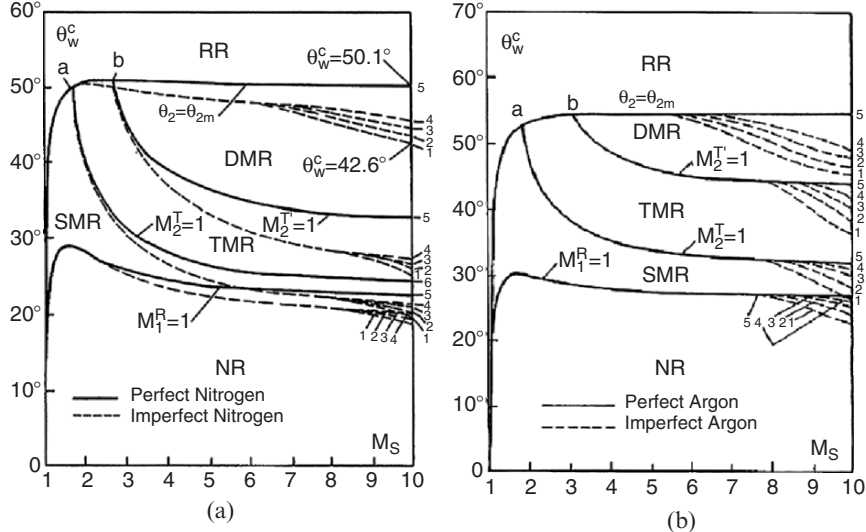


Fig. 3.36. Domains and transition boundaries of different types of shock wave reflections in the (M_S, θ_w^C) -plane: (a) nitrogen and (b) argon. Solid lines are for perfect gas behavior ($\gamma = 7/5$ for nitrogen and $\gamma = 5/3$ for argon). Dashed lines are for imperfect behavior with $T_0 = 300$ K and $p_0 = 1, 10, 100, 1,000$ Torr for lines 1–4, respectively (dissociational-equilibrium in nitrogen and ionizational-equilibrium in argon)

expected if $p_0 < 1$ Torr, while a DMR should be expected if $p_0 > 1,000$ Torr. Since, however, the real flow is most likely not in dissociational-equilibrium, one can conclude from Fig. 3.36a that for $M_S = 10$ and $p_0 = 1$ Torr an RR could not be obtained for $\theta_w^C < 42.6^\circ$ and an MR is impossible for $\theta_w^C > 50.1^\circ$. In the intermediate range $42.6^\circ < \theta_w^C < 50.1^\circ$ either an RR or a DMR could be obtained, depending upon the actual thermodynamic state of the gas (nitrogen in this example).

A similar plot for argon is shown in Fig. 3.36b. In addition to the translational degree of freedom, a monatomic gas has two other degrees of freedom, namely, electronic excitation and ionization. Therefore, the transition lines for the imperfect argon diverge from their appropriate perfect gas transition lines due to the excitation of the ionizational degree of freedom. Each of the transition lines splits up into four lines (numbered 1–4). Each of these four lines corresponds to a different initial pressure, p_0 . The lower is the initial pressure the greater is the shift from the appropriate perfect gas transition line. Unlike the ionizational relaxation, which is pressure and temperature dependent, the electronic excitational relaxation is only temperature dependent. Therefore, the transition lines for different initial pressures, but identical initial temperatures, converge to a single line.

Note that both Fig. 3.36a, b indicates that real gas effects cause the transition lines to shift away from the perfect gas transition lines to lower values

of reflecting wedge angles. In addition, the smaller the initial pressure, the smaller is the incident shock wave Mach number at which this shift starts.

3.4.4 Viscous Effects

One of the assumptions in the analytical models of the two- and three-shock theories was that the fluid is inviscid. This, however, is not true, since in reality all fluids have a finite viscosity. This viscosity will cause a momentum exchange between the fluid and the reflecting surface over which it flows in the case of RR and MR, and between the fluids on both sides of the slipstream in the case of MR. In the following, the viscous effects on RR and MR are treated separately.

Viscous Effects on RR

Consider Fig. 3.37a where an RR over a straight surface is schematically drawn. The figure is, in general, similar to Fig. 3.4. However, unlike Fig. 3.4 the boundary layer $\delta(x)$, which develops in state (2) along the reflecting surface in a frame of reference attached to the reflection point, R, is added to Fig. 3.37a. This boundary layer, which starts to grow at the reflection point ($x = 0$), indicates the flow region in which viscous effects are dominant, and hence should not be neglected.

Figure 3.37a reveals that if the boundary condition of an RR, i.e., $\theta_1 - \theta_2 = 0$ (see 1.13) is to be retained then the gas in state (2) cannot be treated as inviscid. Instead the full Navier–Stokes equations should be solved in state (2). This is not the case in states (0) and (1). In state (0) there is no friction

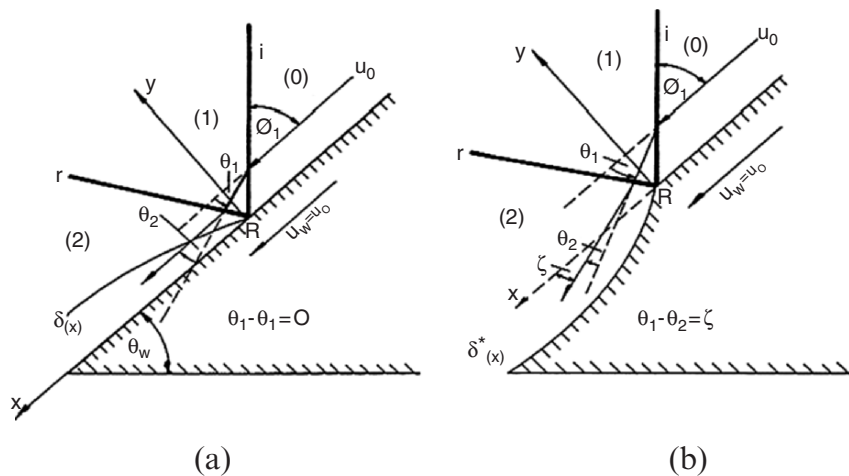


Fig. 3.37. Schematic illustration of: (a) viscous RR over the real reflecting surface; (b) inviscid RR over the displaced reflecting surface

between the gas and the reflecting surface as both of them move (in a frame of reference attached to R) with the same velocity, and state (1) is isolated from the reflecting surface. Therefore, the fluid in states (0) and (1) can be still assumed to be inviscid, and a full solution of the Navier–Stokes equations is not required in these flow regions.

There is, however, a simple way, known as the *boundary layer displacement technique*, to overcome the above difficulty. By applying the boundary layer displacement technique, it is possible to change the geometry of the reflecting wedge surface in such a way that the flow over it can be treated as inviscid. The idea to use this technique for shock wave reflections was proposed first by Hornung & Taylor (1982) who tried to resolve the so-called von Neumann paradox concerning the persistence of RR beyond its theoretical limit. Consider Fig. 3.37b where the reflecting wedge surface behind the reflection point, R , has been displaced by $\delta^*(x)$, which can be simply calculated from $\delta(x)$ in the way described by classical text books on fluid mechanics (see e.g., Shames 1982). Fig. 3.37b indicates that due to the displacement of the reflecting surface $\theta_1 - \theta_2 \neq 0$ i.e., the flow behind the reflected shock wave is not parallel to the real reflecting wedge surface. Instead, it moves towards it with an angle $-\zeta$, which, in principle, could be obtained from $\delta^*(x)$. Unfortunately, however, a straightforward procedure by which ζ could be deduced from does not exist. Consider Fig. 3.38 where $\delta^*(x)$ is plotted (x is measured from the reflection

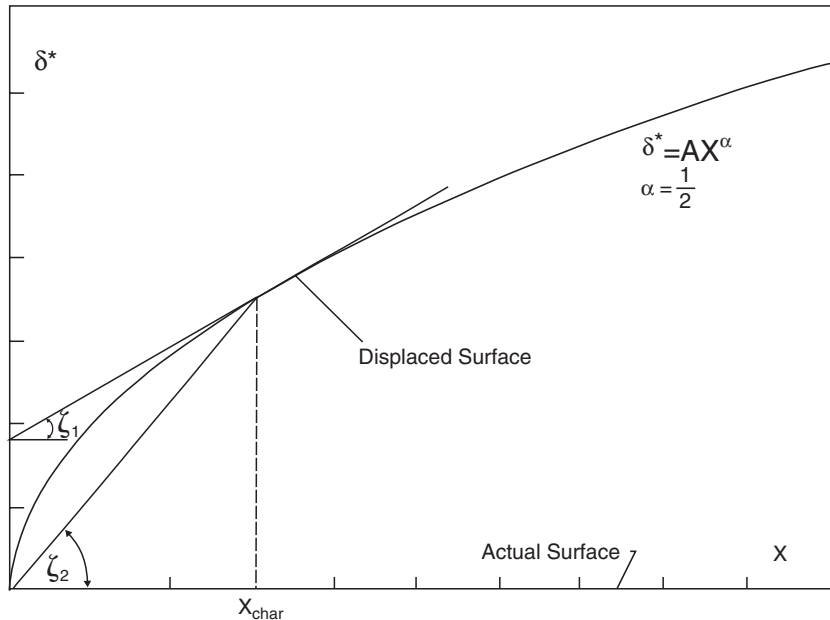


Fig. 3.38. Schematic illustration of the displacement thickness profile over a straight surface and definition of various displacement angles, for a laminar boundary layer

point, R). Since, in general, $\delta^*(x) = Ax^\alpha$ where $\alpha < 1$ (see, e.g., Shames 1982), $d\delta^*/dx \rightarrow \infty$ at ($x = 0$). Hence, ζ cannot be equal to $d\delta^*/dx$ at $x = 0$ since no flow can smoothly negotiate a sudden 90° turn. Instead, Shirouzu & Glass (1982) proposed to use either of the two following ways to calculate the value of ζ from $\delta^*(x)$:

The slope of the displaced boundary at a characteristic distance, x_{char}

$$\zeta_1 = \tan^{-1} \frac{d\delta^*}{dx} \Big|_{x_{\text{char}}}. \quad (3.63a)$$

The average slope of the displaced boundary at a characteristic distance, x_{char}

$$\zeta_2 = \tan^{-1} \frac{\delta^*}{x} \Big|_{x_{\text{char}}}. \quad (3.63b)$$

Both of these suggested ways require a choice of a characteristic length in order to define ζ . Shirouzu & Glass (1982) suggested using the average slope method and using $x_{\text{char}} = 1 \text{ mm}$, which according to them is most realistic since it is the smallest practical resolved length on experimental photograph. Unfortunately, neither they nor others followed their proposed procedure, i.e., evaluated the boundary layer $\delta(x)$ to finally obtain ζ , for this case of RR. Instead, (1.5)–(1.12) together with the following boundary condition which replaces (1.13) were solved by assigning different values to ζ and thereby forcing the $\text{RR} \rightleftharpoons \text{IR}$ transition line to lower values of θ_w .

$$\theta_1 - \theta_2 = \zeta. \quad (3.64)$$

Figure 3.39 illustrates the results of the just-mentioned procedure for air. It can be clearly seen that the $\text{RR} \rightleftharpoons \text{IR}$ transition line is shifted to lower

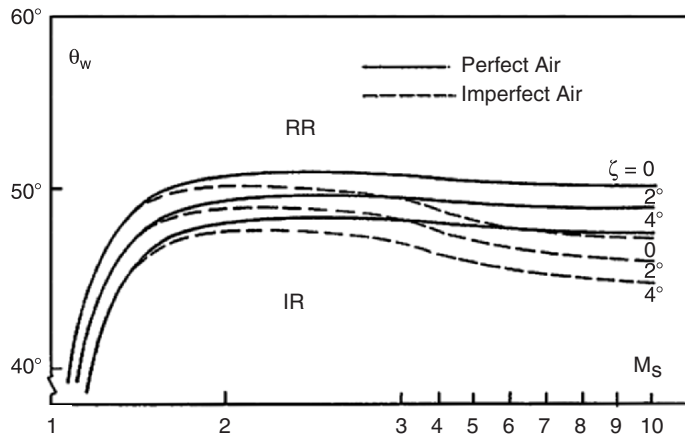


Fig. 3.39. The dependence of the $\text{RR} \rightleftharpoons \text{IR}$ transition line on the boundary layer displacement thickness angle. *Solid lines* are for frozen air with $\gamma = 1.4$; *dashed lines* are for air in dissociational-equilibrium

values of transition wedge angles by assigning nonzero values to ζ . The larger is ζ the greater is the shift of the RR \rightleftharpoons IR transition line. The shift is seen to be independent of whether or not real gas effects are accounted for. Thus, it is clear that, by using the boundary layer displacement concept, it is possible to explain the persistence of RR wave configurations below the RR \rightleftharpoons IR transition line as predicted by the inviscid two-shock theory.

The boundary layer displacement concept implies that if a solution accounting for viscosity is to be solved then, the real reflecting surface is negotiated by the flow. However, if one wishes to use an inviscid approach, then the flow must be assumed to negotiate an imaginary reflecting surface. This imaginary surface has a change in its slope at the reflection point, R, as is shown in Fig. 3.40. In order to further prove the validity of the boundary layer displacement concept, Shirouzu & Glass (1982) illustrated that viscous effects are also responsible for the disagreement between the values predicted by the two-shock theory for the angle between the incident and the reflected shock waves, ω_{ir} , and those measured in actual experiments. Consider Fig. 3.40 and note that if the flow negotiates an imaginary wedge surface, the reflected shock wave, r, (solid line) should assume a new orientation, r^d , (dashed line) because it is required to deflect the flow only by an angle θ_2^d , which is smaller than θ_2 since $\theta_2 - \theta_2^d = \zeta$.

This effect is clearly illustrated for Ar in Fig. 3.41, where the experimentally measured values of the angle between the reflected shock wave and the reflecting wedge surface, ω_r (note $\omega_r = 180^\circ - \phi_1 - \omega_{ir}$) are compared with

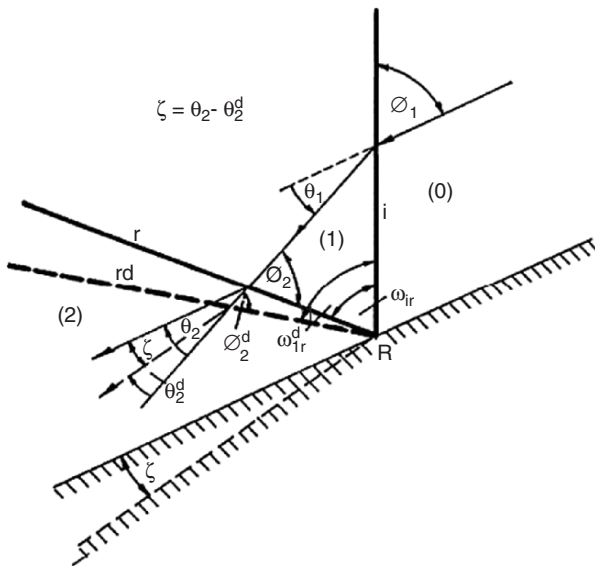


Fig. 3.40. Schematic illustration of the displaced reflected shock wave, r, of an RR to IR transition due to the neglect of viscous effects

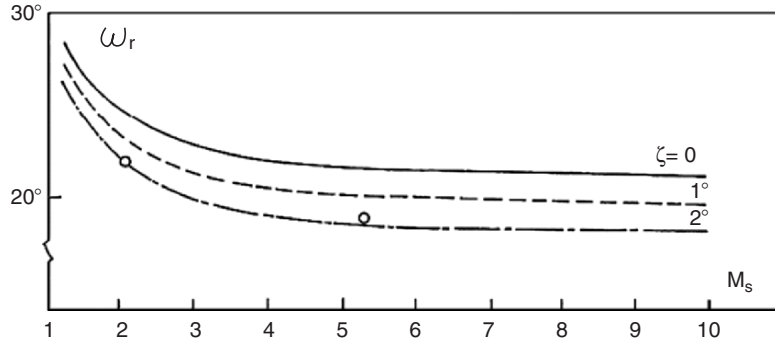


Fig. 3.41. The dependence of the reflected-shock wave angle on the boundary layer displacement angle for $\theta_w = 60^\circ$

the predictions of the two-shock theory for $\zeta = 0, 1^\circ$ and 2° . If $\zeta = 0$, i.e., the value appropriate to the inviscid two-shock theory is used, then the predicted values of ω_r are higher than those measured experimentally, by about 2.6° . A value of $\zeta = 2^\circ$, which could be attributed to viscous effects, results in excellent agreement with the experimentally measured values.

Although neither Shirouzu & Glass (1982) nor others tried to systematically obtain the correct value of ζ (2° for the case shown in Fig. 3.41) from the boundary layer, $\delta(x)$, which develops over the reflecting surface, the foregoing discussion leaves little doubt about the fact that viscous effects should be accounted for if an RR is to be accurately solved using the two-shock theory.

Wheeler (1986) has further illustrated that the persistence of RR below the RR \rightleftharpoons IR transition line, as predicted by the inviscid two-shock theory, is probably due to viscous effects. He showed experimentally that the deviation of the actual RR \rightleftharpoons IR transition line from the one predicted using the inviscid two-shock theory increases with a drop in the initial pressure, p_0 , in a manner consistent with the boundary layer theory.

Viscous Effects on MR

Figure 3.42 indicates that in the case of an MR wave configuration, viscous effects are dominant not only along the reflecting wedge surface but also on both sides of the slipstream. The viscous effects along the reflecting wedge surface have little to do with the solution of the flow field near the triple point, T. They do have, however, some influence because they affect the flow field near reflection point, R, where the foot of the Mach stem touches the reflecting surface. Since the flow behind the Mach stem is subsonic, in a frame of reference attached to the triple point, T, the influence of the boundary layer, which develops along the reflecting surface, could be communicated to the triple point, and influence it too. Dewey & McMillin (1985) who experimentally observed that the foot of the Mach stem is not exactly perpendicular

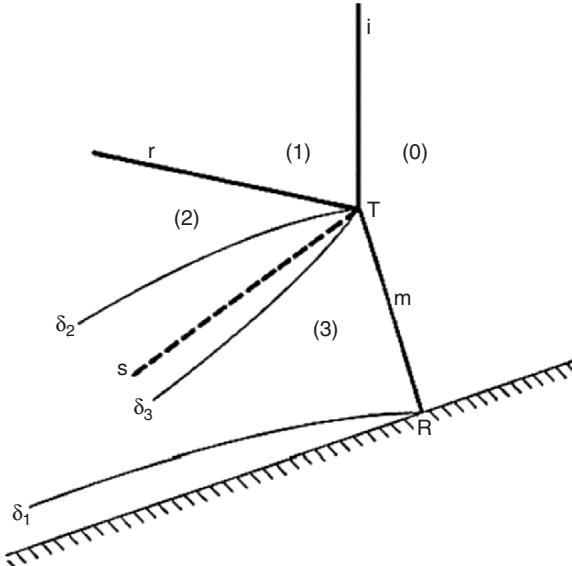


Fig. 3.42. Schematic illustration of the various boundary layers associated with a Mach reflection

to the reflecting wedge surface first reported the fact that the boundary layer affects the foot of the Mach stem. Their observation could again be explained by the earlier-mentioned argument that, if the flow is assumed to be inviscid, it should not be required to negotiate the real reflecting surface and hence the condition of zero flow deflection through the foot of the Mach stem is incorrect. Instead, if the flow is assumed to be inviscid, it should be required to negotiate an imaginary displaced reflecting surface over which the foot of the Mach stem should be oblique. Unfortunately, no analytical work has been done so far to study the nonperpendicular nature of the foot of the Mach stem and its influence on the flow field near the triple point.

Viscous effects on both sides of the slipstream probably have significant influence on the flow field in the vicinity of the triple point, upon which the predictions of the $\text{SMR} \rightleftharpoons \text{TMR/DMR}$ and $\text{TMR} \rightleftharpoons \text{DMR}$ transition criteria and the angles between the four discontinuities, i , r , m and s , using the three-shock theory, are based.

Figure 3.43a illustrates the situations appropriate to the inviscid three-shock theory. The flows above and below the slipstream are uniform with velocities U_2 and U_3 , respectively. At the slipstream there is a discontinuity in the velocity field. However, since all fluids have a finite viscosity, the situation shown in Fig. 3.43a is not physical. Instead, the fluids on both sides of the slipstream exchange momentum to result in a smooth transition from U_2 to U_3 as is shown in Fig. 3.43b. It is evident that the inviscid three-shock theory cannot be used to treat this case. Instead, the full Navier-Stokes equations must be solved in states (2) and (3).

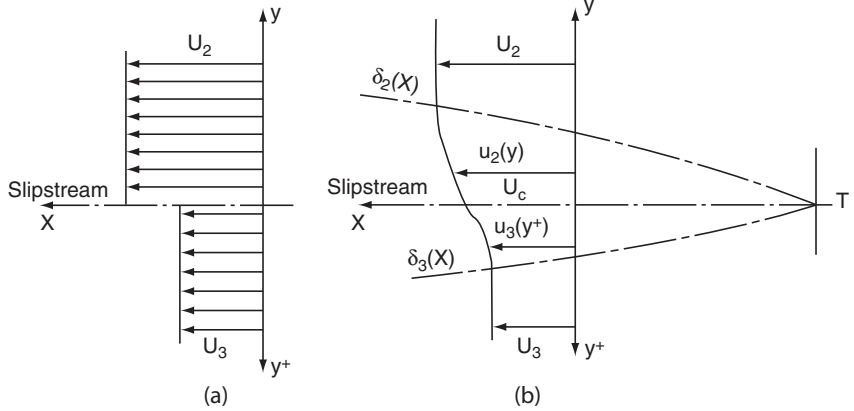


Fig. 3.43. Illustration of the flow field on both sides of the slipstream of a Mach reflection: (a) inviscid flow; (b) viscous flow

If, however, one still wishes to use the model given by the inviscid three-shock theory then the displacement thickness technique, which was introduced in Sect. 3.4.4.1, could again be applied. This was done, quite successfully, by Ben-Dor (1987). Consider Fig. 3.44 where the actual velocity profiles, shown previously in Fig. 3.43b, are redrawn on the left side. Each of these two velocity profiles is plotted separately. If uniform flow profiles are to be used in states (2) and (3), then the slipstream should be displaced. Owing to the shape of the velocity profiles, the displacement thickness of the flow field in state (2), above the slipstream, is positive while that of state (3), below the slipstream, is negative. However, since both flows have a common surface along which they flow, i.e., the slipstream, the displacement thicknesses above and below the slipstreams must satisfy the condition $\delta_2^* = \delta_3^*$.

In a detailed study, Ben-Dor (1987) compared the angles between the various discontinuities at the triple point, namely, ω_{ir} , ω_{im} and ω_{rs} , as predicted by the inviscid three-shock theory with actual experiments and found a discrepancy too large to be explained by experimental uncertainties. Then the boundary layers that develop on both sides of the slipstream, δ_2 and δ_3 , were calculated. These boundary layers were used to obtain the respective displacement thicknesses δ_2^* and δ_3^* . By imposing the condition $\delta_2^* = \delta_3^*$ the orientation of the imaginary slipstream was obtained. The orientation of the imaginary slipstream was then used to define the imaginary flow streamlines in states (2) and (3) which were assumed to be parallel to it. Then the reflected and Mach stem shock waves were displaced in such a way, that they resulted in the required imaginary flow deflections. The obtained results agreed perfectly with those measured experimentally. Note that in order to obtain the angular displacement of the slipstream, a displacement thickness angle had to be obtained from the analysis. This angle is analogous to the angle ζ that was mentioned in the previous section for the case of RR. In order to obtain this

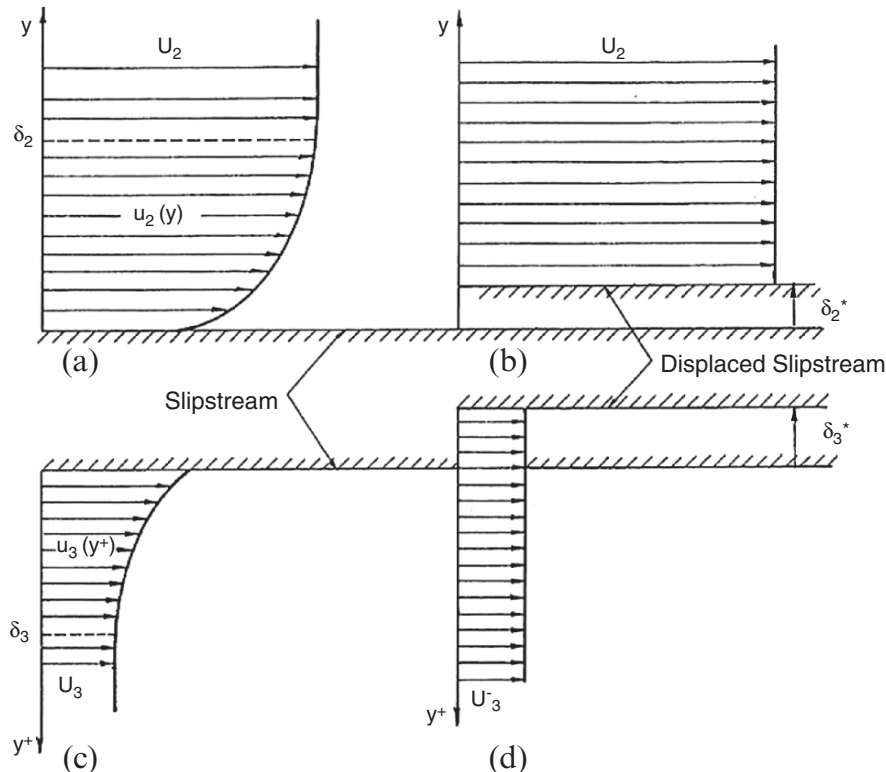


Fig. 3.44. Definition of the displacement thicknesses on both sides of the slipstream

angle a characteristic length was needed. It was found by Ben-Dor (1987) that the most appropriate characteristic length was of the order of the thickness of the incident shock wave.

Table 3.2 summarizes the results of Ben-Dor (1987) for the case of an MR with $M_S = 2.71$, $\phi_1 = 39.9^\circ$, $T_0 = 296\text{ K}$ and $p_0 = 760\text{ Torr}$ in nitrogen. The results indicate that the predictions of the inviscid perfect three-shock theory for ω_{ir} and ω_{rs} are about 5° greater and smaller than the respective measured values from the experimental record that is shown in Fig. 3.45. When the foregoing boundary layer displacement technique (viscous) model is used, the agreement between the theory and the experimental results is excellent. Table 3.2 also indicates that when the three-shock theory is used without viscous effects but assumes that the air is in rotational-vibrational equilibrium in the vicinity of the triple point, it provided better values for ω_{ir} , ω_{im} and ω_{rs} than those predicted by the inviscid perfect gas theory. Unfortunately, however, as indicated in Fig. 3.35 the vibrational relaxation length of N_2 at $M_S = 2.71$ is more than 1m. This implies that the flow in the vicinity of the triple point must be considered as frozen with $\gamma = 1.4$. Thus, the better agreement due to the inclusion of real gas effects must be considered as accidental.

Table 3.2. Comparison between the experimental results and the predictions of the wave angles by the various modified models of the three-shock theory

Type of model	ω_{ir}	ω_{im}	ω_{rs}
Experimental results	$118^\circ \pm 1^\circ$	$132^\circ \pm 1^\circ$	$32^\circ \pm 1^\circ$
Three-shock theory for an inviscid perfect gas	123.19° $(+5.19^\circ)$	132.74° $(+0.74^\circ)$	27.16° (-4.84°)
Three-shock theory for a perfect gas with viscous effects along the slipstream	118.02° $(+0.02^\circ)$	131.70° (-0.30°)	32.32° $(+0.32^\circ)$
Three-shock theory for an inviscid real gas in rotational-vibrational equilibrium	117.32° (-0.68°)	131.95° (-0.05°)	29.81° (-2.19°)
Three-shock theory for a real gas in rotational-vibrational equilibrium with viscous effects along the slipstream	120.04° $(+2.04^\circ)$	130.70° (-1.30°)	27.09° (-4.91°)

$M_S = 2.71, \phi_1 = 39.9^\circ, T_0 = 296 \text{ K}, p_0 = 760 \text{ Torr}$

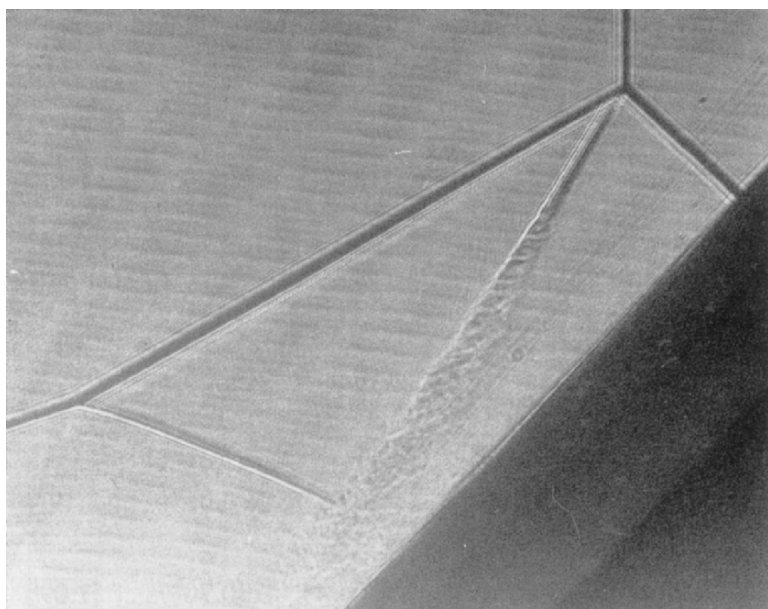


Fig. 3.45. Enlarged photograph of a double-Mach reflection illustrating the structure of the slipstream with $M_S = 2.71$ and $\theta_w = 47^\circ$ in air at $T_0 = 296 \text{ K}$ and $p_0 = 760 \text{ Torr}$ (Courtesy of Professor K. Takayama, Shock Wave Research Center, Institute of Fluid Science, Tohoku University, Sendai, Japan)

It is also evident from Table 3.2, that when both viscous and real gas effects are integrated into the three-shock theory the predicted values of ω_{ir} , ω_{im} and ω_{rs} are poorer than the results that are obtained when these effects are separately integrated into the inviscid three-shock theory model.

The foregoing comparisons imply that viscous effects should be accounted for if the flow field near the triple point is to be calculated. Unfortunately, to the best of the author's knowledge, the SMR \rightleftharpoons PTMR/TMR/DMR and the TMR \rightleftharpoons DMR transition lines and the additional requirement for the SMR \rightleftharpoons PTMR/TMR/DMR transition have not been evaluated using the modified viscous three-shock theory model described in this section.

It should also be mentioned that the above method of accounting for viscous effects in the solution of the flow field near the triple point must also be adopted when the second triple point is treated, since it also has a slipstream across which momentum exchange takes place.

Wheeler (1986) found experimentally that the initial pressure influences the height of the Mach stem of an MR. Lower initial pressures, which result in greater viscous effects because both δ and δ^* depend on $p_0^{-0.5}$, reduced the height of the Mach stem to values which were smaller than those predicted by the inviscid three-shock theory.

Finally, it should be noted that the incident shock wave thickness, which was found by Ben-Dor (1987) to be the most appropriate characteristic length for evaluating the value of the displacement angle of the slipstream, ζ , is also p_0 dependent, since the mean free path λ is proportional to p_0^{-1} . Thus the experimental results of Wheeler (1986) might serve as verification for the choice made by Ben-Dor (1987) for x_{char} .

Special Reflecting Surface Conditions

The understanding of the manner by which the kinematic boundary layer influences the RR \rightleftharpoons IR transition line, and thereby successfully explaining the persistence of RR-experiments below the theoretical RR \rightleftharpoons IR transition line as predicted by the inviscid two-shock theory, has been the impetus for various investigations of the reflection of shock waves over wedges, where the surface conditions were such that they could either enhance or reduce the rate of growth of the boundary layers. Some of these investigations are discussed in the followings.

Rough Reflecting Surface

By imposing a roughness on the reflecting wedge surface, the rate of the boundary layer growth could be enhanced. Figures 3.46a and 3.46b are shadowgraphs of an RR and a TMR over rough reflecting straight surfaces. Ben-Dor et al. (1987) carried out a detailed experimental and analytical study on the influence of surface roughness on the RR \rightleftharpoons IR transition. The results of their study are summarized in Fig. 3.47 for nitrogen. The experimental

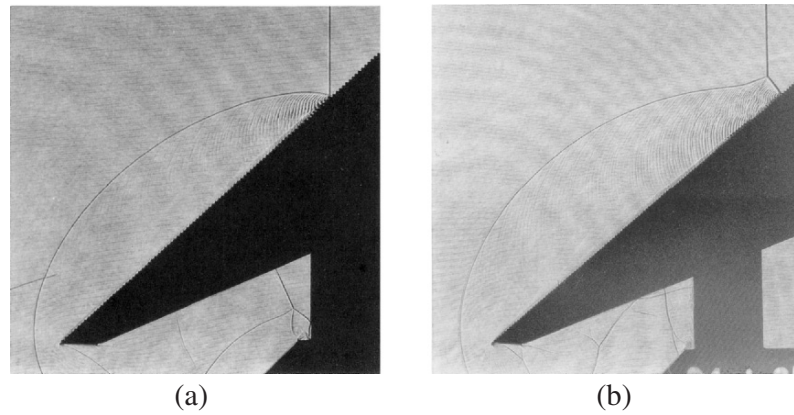


Fig. 3.46. Shadowgraph of reflections over a rough reflecting surface: (a) RR with $M_S = 2.74$ and $\theta_w = 43^\circ$ in air at $T_0 = 283.5\text{ K}$ and $p_0 \approx 760\text{ Torr}$, and (b) TMR with $M_S = 2.30$ and $\theta_w = 39^\circ$ in air at $T_0 = 283.4\text{ K}$ and $p_0 \approx 760\text{ Torr}$ (Courtesy of Professor K. Takayama, Shock Wave Research Center, Institute of Fluid Science, Tohoku University, Sendai, Japan)

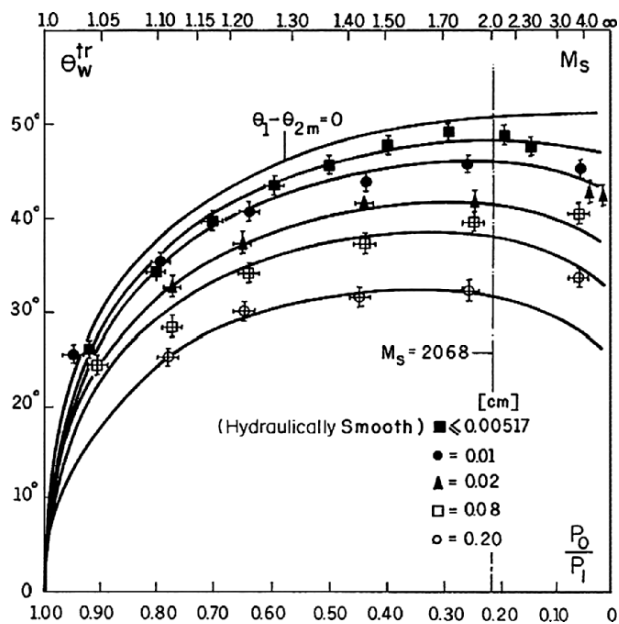


Fig. 3.47. The dependence of the RR ⇌ IR transition line on the reflecting surface roughness and comparison with experiments

results indicate that for a given incident shock wave Mach number the surface roughness results in a reduction in the wedge angle, at which the RR \rightleftharpoons IR transition occurs. The greater is the roughness size the larger is the reduction in the transition wedge angle. This behavior is consistent with the earlier discussion on the effect of viscosity on the RR wave configuration, since the roughness results in an increase in the rate of growth of the boundary layer which, in turn, results in an increase in the rate of growth of the displaced boundary, i.e., larger values of ζ (see Sect. 3.4.4) at the required characteristic length.

Ben-Dor et al. (1987) developed an analytical model by which the boundary layer growth for a supersonic compressible flow over a flat rough surface could be predicted. Then the surface was displaced in a way similar to that mentioned in Sect. 3.4.4. By again using a characteristic length of the order of the thickness of the incident shock wave, a value the angle of ζ was obtained. This value was then used in the two-shock theory with the modified boundary condition [(3.54) instead of (1.13)]. The analytical results using this procedure are shown in Fig. 3.47. Excellent agreement between the experiments and the analytical predictions is evident in the range $1 < M_S \leq 2$. In the range $M_S > 2$ the predicted results failed to reproduce the experiments. Ben-Dor et al. (1987) hypothesized that this might be due to the fact that the shock induced flow behind the incident shock wave, in air, is subsonic for $M_S < 2.068$, while it is supersonic for $M_S > 2.068$. Thus, it is possible that this fact has an effect, unfortunately not yet understood, on the reflection process. The persistence of RR-experiments below the theoretical limit as predicted by the inviscid two-shock theory, is clearly seen in Fig. 3.47 where the experimentally recorded transition wedge angles, for a smooth wedge, are seen to lie below the corresponding RR \rightleftharpoons IR transition line as calculated using the inviscid perfect gas two-shock theory. Based on these findings, and on the fact that no surface is perfectly smooth, it must be concluded that the surface roughness, regardless of how small it is, does have some effect on the rate of growth of the boundary layer developing over the reflecting surface. This boundary layer affects the actual wave configuration in the manner described earlier.

Two more points regarding the surface roughness effect on the shock reflection phenomenon in pseudosteady flows should be mentioned:

- The first is that the most appropriate characteristic length to be used in (3.63b) was found to be of the order of the thickness of the incident shock wave. This is surprisingly identical to the findings mentioned earlier in Sect. 3.4.4.2, where the most appropriate characteristic length was also found to be of the same order of magnitude when the viscous effects were integrated into the inviscid three-shock theory. This is in spite of the fact that while integrating viscous effects into the three-shock theory the boundary layer was assumed laminar, and in the case of a boundary layer over a rough reflecting surface, it was assumed to be turbulent. These findings might suggest that, in shock wave reflection phenomena,

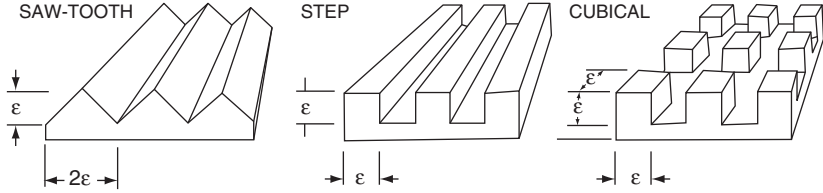


Fig. 3.48. Definition and illustration of various types of surface roughness

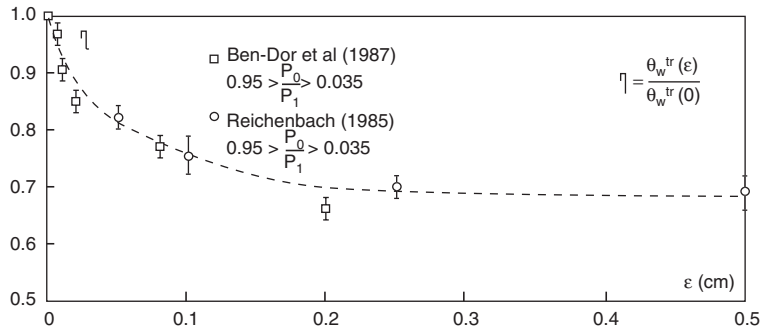


Fig. 3.49. The dependence of the RR ⇌ IR transition angle ratio on the roughness height

the thickness of the incident shock wave is the characteristic length that should be used whenever viscous effects are accounted for by means of the boundary layer displacement technique.

- The second striking point is that while Ben-Dor et al. (1987) used in their experiments a saw-tooth shaped roughness, Reichenbach (1985) who used in his experiments different shapes of roughness reported the same shifts in the transition wedge angle for identical heights of the roughness. The saw-tooth shape of the roughness used by Ben-Dor et al. (1987) and the step and cubical shapes of the roughness used by Reichenbach (1985) are shown in Fig. 3.48, with the definition of the roughness height ϵ . Reichenbach (1985) defined the ratio between the transition wedge angle over a rough reflecting surface and the transition wedge angle over a smooth reflecting surface as η , and presented his own and Ben-Dor et al.'s (1987) experimental results in the (η, ϵ) -plane as shown in Fig. 3.49. Figure 3.49 clearly indicates that the roughness height, ϵ , rather than its shape, is the dominant factor in determining the transition wedge angle. In his experimental study, Reichenbach (1985) also measured the height of the Mach stem, H_m , as a function of the distance of its foot from the leading edge of the reflecting wedge, L_G . The results for a step shape roughness are shown in Fig. 3.50. The results clearly indicated that the triple point was not formed at the leading edge of the reflecting wedge, i.e., at $L_G = 0$, but at some distance up the reflecting wedge surface. Reichenbach (1985)

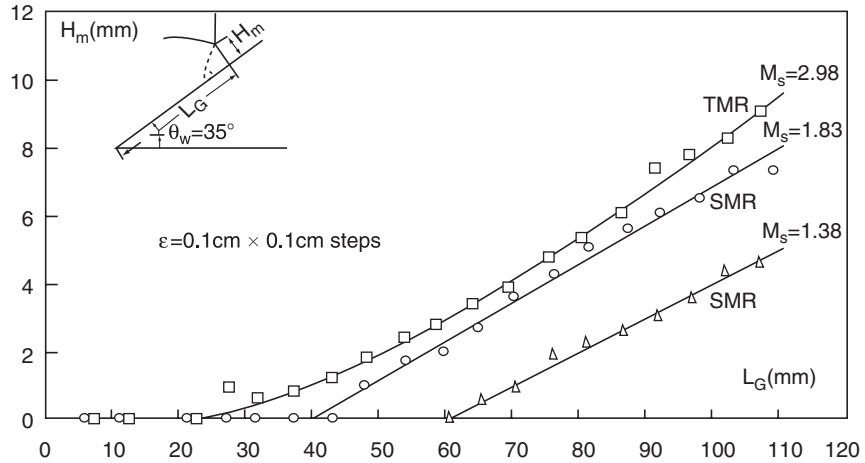


Fig. 3.50. Experimentally measured Mach stem height of an MR as function of distance from the leading edge of the reflecting wedge for a rough surface

further found that the distance from the leading edge of the reflecting wedge to the point along the reflecting surface, where the triple point was formed, increased with decreasing incident shock wave Mach numbers. It is important to note here that Dewey & van Netten (1991 and 1995) that in spite of this non self-similar effect if one waited long enough a final reflection configuration developed in which the triple point trajectory extended back to the leading edge of the reflecting wedge.

Perforated Reflecting Surface

Onodera (1986) reinitiated an experimental investigation of the reflection of a planar shock wave over a perforated plate, which was originally done by Friend (1958). The effect of a perforated plate should be similar to that of a rough surface, because in the case of a rough surface, the boundary layer displacement technique results in a situation in which the flow behind the reflection point assumes a direction parallel to an imaginary reflecting wedge surface, which extends below the real reflecting wedge surface. Thus, fluid is being drawn away from the flow field since it is allowed to flow into the real reflecting wedge surface. A similar effect occurs when the plate is perforated since in this case too the fluid is drawn away from the flow field as it penetrates the perforated plate and flows across it. A typical experimental record from Onodera's (1986) study is shown in Fig. 3.51 for $M_S = 2.93$, $\theta_w = 33^\circ$ and a perforation ratio of 0.355 (i.e., the ratio between the perforated area and the overall surface area). The very complex structure of the wavelets, which are generated along the reflecting surface, is clearly seen. The structure of these wavelets shows a similarity to those in Fig. 3.46a, b, where an RR and a TMR over rough surfaces are shown.

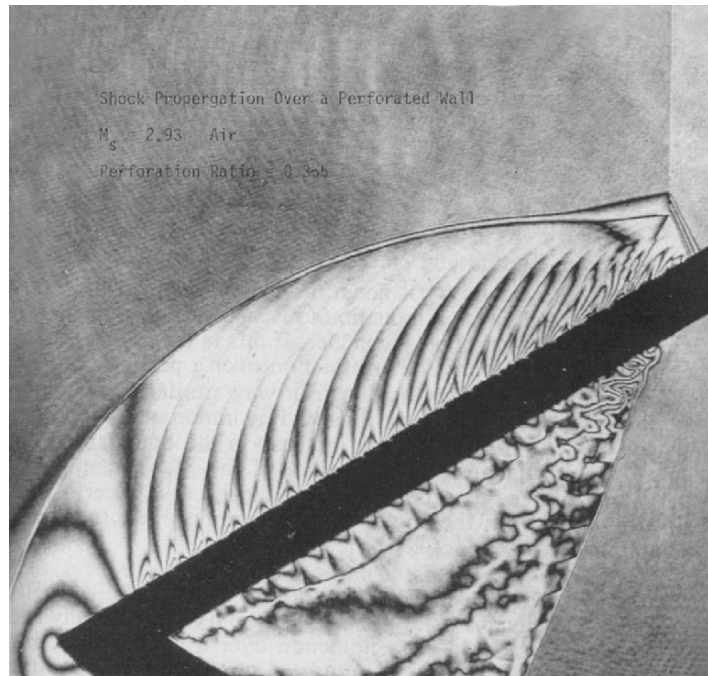


Fig. 3.51. An interferogram of an MR in air over a perforated flat plate with a perforation ratio of 0.355 for $M_S = 2.93$ and $\theta_w = 33^\circ$ (Courtesy of Professor K. Takayama, Shock Wave Research Center, Institute of Fluid Science, Tohoku University, Sendai, Japan)

Since there are not enough experimental data regarding the reflection phenomenon of planar shock waves over perforated plates, not much can be said, at this stage, about it. Perhaps the only encouraging conclusion, which could be drawn from Fig. 3.51, is that the MR does seem to respond in the expected way to the fact that the reflecting surface is perforated. Based Fig. 2.26 of Ben-Dor (1991) the experimentally measured first triple point trajectory angle for $M_S = 2.93$ and $\theta_w = 33^\circ$ is $\chi = 8^\circ$. In the case of a reflection over a perforated plate (Fig. 3.51) with identical initial conditions $\chi = 6^\circ$. This means that the triple point is lower and hence a transition to RR should be expected to occur at lower reflecting wedge angles. If this is the case, then the flow sucking effect in the case of a reflection over a perforated plate influences the $RR \rightleftharpoons IR$ transition in a manner similar to that of a reflection over a rough surface.

Finally, it is important to note that Wheeler (1986) reported that an increase in the boundary layer height causes a decrease in the height of the Mach stem. This observation further supports the fact that the effect of a perforated reflecting surface on the shock wave reflection phenomenon is similar to that of viscous effects.

Slitted Reflecting Surface

Onodera & Takayama (1990) investigated both experimentally and analytically the reflection phenomenon over a slitted reflecting surface. Their experimental study was conducted using three different models. In their models A and B the slits were open (as in a perforated plate), whereas in their model C the slits were closed. Models A, B and C had 58, 36, and 36 slits, respectively. The perforation ratios, i.e., the ratio between the perforated area and the overall surface area, were 0.34, 0.40, and 0.40 for models A, B and C, respectively.

A schematic drawing of the wave configuration and the various flow velocity vectors, for the case of a reflection over a slitted surface, is shown in Fig. 3.52. In a laboratory frame of reference, the flow velocity along the slitted reflecting surface has two components, namely, V_2^L parallel to and V_4^L perpendicular to the reflecting surface.

Similar to the above-mentioned change in the boundary condition of an RR, from (1.13) to equation (3.64), when viscous effects are accounted for by means of the boundary layer displacement technique, Onodera & Takayama (1990) suggested that, for the case of a slitted surface, the boundary condition of an RR should be

$$\theta_1 - \theta_2 = \zeta. \quad (3.65)$$

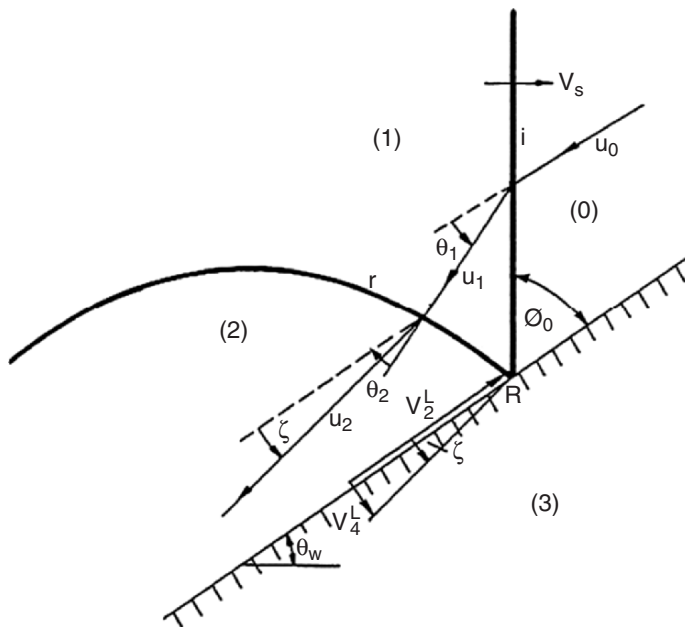


Fig. 3.52. Schematic illustration of an RR over a slitted surface and definition of various velocity vectors

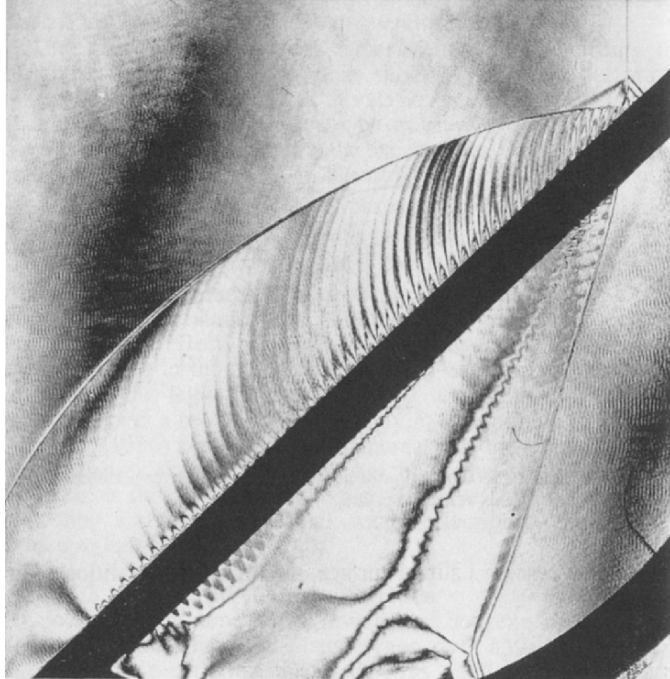


Fig. 3.53. A holographic interferogram of an RR over an inclined slitted surface with $M_S = 2.96$ and $\theta_w = 44^\circ$

Furthermore, they argued that ζ could be related to V_2^L and V_4^L in the following way

$$\tan \zeta = \psi \frac{V_2^L}{V_4^L}, \quad (3.66)$$

where ψ is the discharge coefficient through the perforated area.

Unfortunately, they did not pursue this idea to calculate the RR \rightleftharpoons IR transition for a slitted surface. Instead, they proposed the following empirical approach based on their experimental observation. Consider Fig. 3.53 where a holographic interferogram of a shock wave having a Mach number $M_S = 2.96$ is seen to reflect as an RR over an inclined slitted surface (model A) having $\theta_w = 44^\circ$. Note that an oblique shock wave is driven by a contact discontinuity in region (3) below the slitted surface. If the angle between the reflecting surface and the contact discontinuity is defined as ζ' then according to Onodera & Takayama (1990)

$$\zeta = \xi' \zeta', \quad (3.67)$$

where ξ' is an experimental matching coefficient. This matching coefficient was determined empirically by Onodera & Takayama (1990) to be equal to 0.61 and 0.55 for models A and B, respectively.

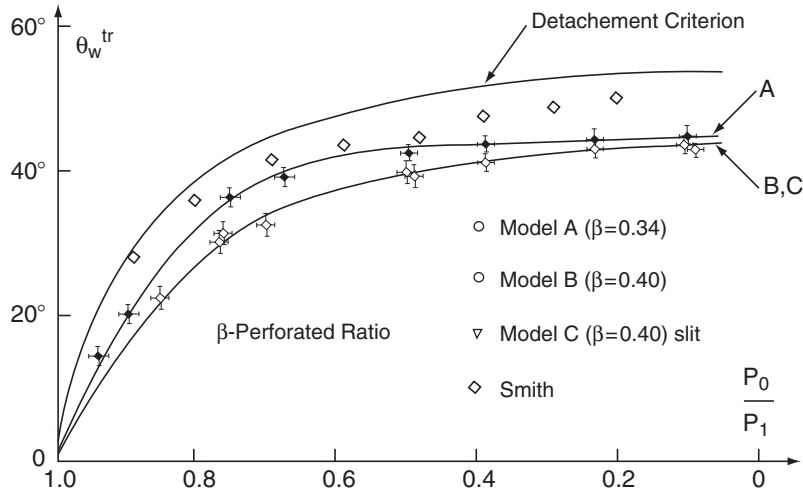


Fig. 3.54. The empirical $\text{RR} \rightleftharpoons \text{IR}$ transition lines over an inclined slitted surface with experimental results (Courtesy of Professor K. Takayama)

Their experimental and empirical results for the $\text{RR} \rightleftharpoons \text{IR}$ transition over a slitted surface are shown in Fig. 3.54. The predicted transition lines for models A, B, and C are seen to agree excellently with the corresponding experimental results. Furthermore, the transition wedge angles, for models A and B, approach each other at strong incident shock waves, and differ by about 5° at moderate incident shock waves. In addition, the results indicate that the transition wedge angles for models B and C are almost the same. Hence, it was concluded that the transition wedge angle does not depend on whether the slits are open or closed.

Figure 3.54 also implies that the transition wedge angle depends on the perforation ratio. The larger is the perforation ratio the greater is the reduction in the transition wedge angle. However, for incident shock wave Mach numbers with $M_S > 1.5$ ($p_0/p_1 < 0.4$) the dependence of the transition wedge angle on the perforation ratio seems to be negligible, as the results indicate that the transition wedge angle attains a value of about 43.5° for models A, B, and C.

Porous Reflecting Surface

The interaction of shock waves with porous wedges has been a recurring subject of research since the early 1980s. The investigations on the interactions of shock waves with porous media were conducted with two types of porous materials: compressible and rigid. The physical approach was summarized in Li et al. (1995) and Malamud et al. (2003) for the interaction with rigid porous wedges and in Malamud et al. (2005) for the interaction with wedges made of compressible foams.

When an oblique shock wave interacts with a porous layer both a regular (RR) and an irregular reflection (IR) wave configurations are possible. Both types have well-known solutions when the oblique shock wave interacts with a solid wall. However, when it interacts with a porous layer, the gaseous phase can penetrate into the porous layer and modify the wave configurations. Furthermore, additional waves and discontinuities can develop inside the porous layer (e.g., a transmitted oblique shock or compression wave and a slipstream).

Kobayashi et al. (1995) proposed two different analytical models for describing the RR. Then they solved the less realistic analytical model, where the coupling between the pure gas and the porous layer was neglected. Their more realistic model for the RR wave configuration was analyzed and solved by Li et al. (1995). The more realistic model for an RR wave configuration over a rigid porous media is shown in Fig. 3.55. In this model, an incident shock wave that moves relative to the porous layer collides with the porous interface and generates two shock waves: the first is the reflected shock wave, which is the product of the solid phase interaction with the gas, and the second is a transmitted shock wave into the gaseous phase inside the porous layer. In addition due to the transfer of mass into the porous layer a contact discontinuity is formed.

An analytical model for solving the flow field associated with regular reflections of oblique shock waves over rigid porous layers was developed by Li et al. (1995). The governing equations of the gaseous phase inside the porous layer were similar to those of the gaseous phase outside the porous layer.

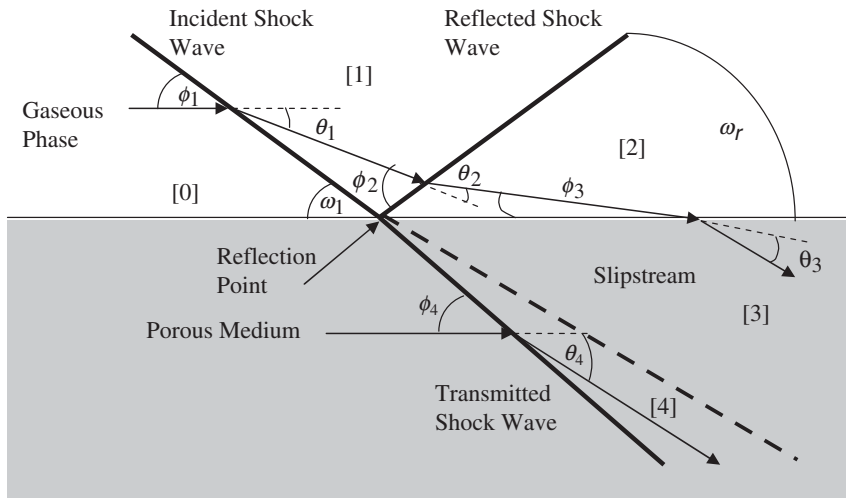


Fig. 3.55. Physical model for an RR over a porous surface. State (0) is ahead of the incident and transmitted shock waves; state (1) is behind the incident shock wave; state (2) is behind the reflected shock wave, and state (4) is behind the transmitted shock wave. State (3) is obtained from state (2) when the flow penetrates the porous material. States (3) and (4) are separated by the contact discontinuity

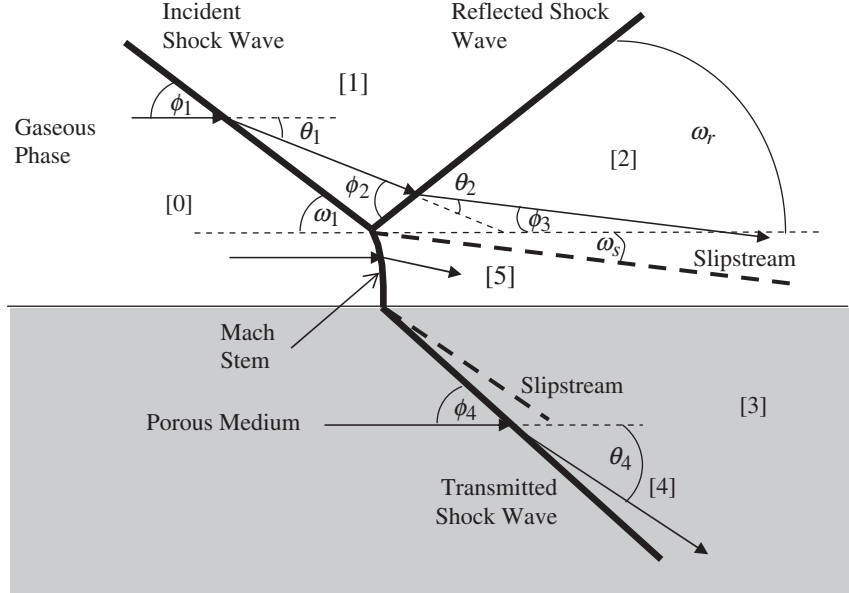


Fig. 3.56. Schematic illustration of the wave configuration of an MR over a rigid porous layer. State (0) is ahead of the incident and transmitted shock waves; state (1) is behind the incident shock wave; state (2) is behind the reflected shock wave, state (4) is behind the transmitted shock wave and state (5) is behind the Mach stem. State (3) is obtained from state (5) when the flow penetrates the porous material. States (3) and (4) are separated by the contact discontinuity inside the porous material and states (2) and (5) are separated by the contact discontinuity, which starts at the triple point

The predictions of the analytical model were validated by comparing them to the experimental data of Kobayashi et al. (1995) and Skews (1994). The analytical model solved a set of 17 governing equations, and could predict the properties of the fluid phase, the angles of the reflection and the diversion of the fluid velocity vectors from the shock waves and the porous surface. The sonic criterion together was implemented in the analytical model to predict the RR \rightleftharpoons MR transition.

Malamud et al. (2003) proposed model for an MR is shown in Fig. 3.56. A Mach stem and a slipstream are formed outside the porous medium. In this case, at least one uniform flow zone has been formed. Because of that, the physical description of the MR is much more complicated than that of the RR. The MR contains 5 or more uniform flow zones instead of the 4 shown in the RR wave configuration. Since the physical phenomenon of the MR over a porous layer was not fully understood, it could not be simplified. Hence, it was very difficult to develop an analytical model for a Mach reflection over a porous layer. Instead, Malamud et al. (2003) developed a two dimensional model for numerically predicting the flow field of various reflection phenomena.

The predictions of the numerical simulations were compared with the predictions of the two-dimensional analytical model of Li et al. (1995) for the case of an RR from a rigid porous surface in pseudosteady flow and good agreement was evident. Comparisons between the predictions of the numerical simulations and the two-dimensional experimental data of Kobayashi et al. (1995), confirmed the validity of the physical model and the numerical code. In addition, the comparison between the predictions of the two-dimensional numerical simulations and the experimental data of Skews (1994) confirmed the validity of the code for both RR and IR waves configurations. Although the predictions of the numerical model for the RR and the IR were validated by the flow field outside the porous material, it was the first time that the flow field characteristics inside the porous material, which resulted from the interaction of oblique shock waves with porous wedges were predicted. In addition, it was the first time that the IR configuration over a porous surface was solved.

Nonsolid Reflecting Surface

Using a nonsolid reflecting surface, i.e., a liquid reflecting surface, is another situation in which the boundary layer could be changed from that developing over a solid wedge. This is due to the following two reasons:

- (1) Unlike a solid reflecting surface, a liquid reflecting surface, such as water, is extremely smooth
- (2) The viscous interaction of the gas with the liquid surface is different from that with a solid surface

An experimental investigation of the reflection of a planar shock wave over a water surface was conducted by Takayama et al. (1989), Takayama & Ben-Dor (1989) and Henderson et al. (1990). The shock wave was reflected over a water surface by means of a special shock tube that could be tilted in the vertical plane. By using this technique, it was possible to adjust the shock tube inclination to obtain any desired water wedge angle. The experimentally measured transition wedge angles for water and a solid surface are shown in Fig. 3.57 together with the $\text{RR} \rightleftharpoons \text{IR}$ transition line arising from the detachment criterion. It is evident that for $1.47 \leq M_S \leq 2.25$ ($0.174 \leq \xi \leq 0.425$) the actual transition wedge angles over the water wedge agree excellently with those predicted by the detachment criterion, and there is no evidence of the well-known persistence of RR-configurations below the $\text{RR} \rightleftharpoons \text{IR}$ transition line. However, for $1 < M_S \leq 1.47$ ($0.425 \leq \xi \leq 1$) an opposite behavior is evident. While the experimental results, both over the solid and the water reflecting surfaces, exhibit the well-known persistence of RR-configurations below their theoretical limit, the actual transition wedge angles over the water reflecting surface show worse agreement with the theoretical inviscid $1.47 \leq M_S \leq 2.25$ ($0.174 \leq \xi \leq 0.425$) transition line than the transition wedge angles over the solid reflecting surface.

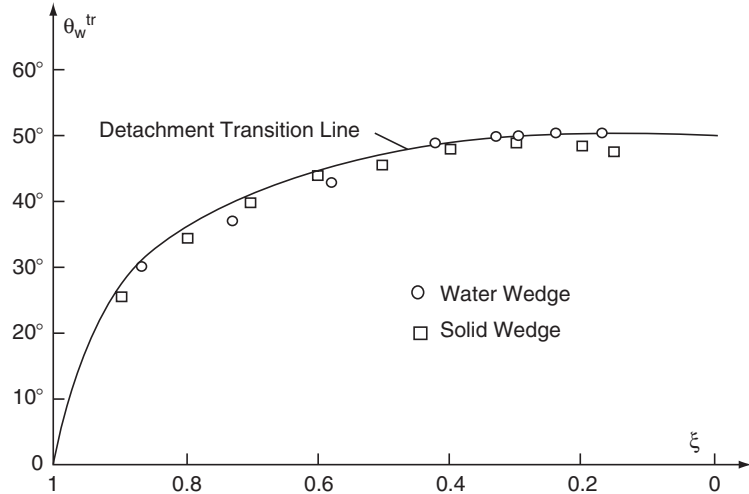


Fig. 3.57. The RR \rightleftharpoons IR transition over a water and a solid surface and comparison with experimental results

The reason for this peculiar behavior could lie in the fact that for air the SMR \rightleftharpoons TMR transition line intersects the RR \rightleftharpoons IR transition line at $M_S \approx 1.5$ ($\xi \approx 0.4$). Thus for $[M_S < 1.5]$ ($\xi > 0.4$) the termination of an RR results in an SMR while for $M_S > 1.5$ ($\xi < 0.4$) the termination of an RR results in a TMR. In a TMR the flow behind the reflected shock wave in the vicinity of the triple point is supersonic with respect to the triple point, $M_2^T > 1$, and hence the triple point is isolated from pressure signals generated along the reflecting surface. However, in the case of an SMR the flow behind the reflected shock wave is subsonic with respect to the triple point, $M_2^T < 1$, and therefore pressure signals generated along the reflecting surface can reach the triple point and influence it.

3.4.5 Thermal Conduction Effects

The possibility that thermal conduction might also have a non-negligible effect on the solutions of the flow fields in the vicinities of the reflection point of an RR and the triple point of an MR have already been mentioned as a possible explanation for the persistence of TDMR-experiments beyond the RR \rightleftharpoons DMR transition line (see Sects. 2.4.3 and 2.4.4 in Ben-Dor 1991).

When the gas is assumed to be an ideal fluid, i.e., $\mu = 0$ and $k = 0$, the two- and three-shock theories inherently assume a discontinuity in the temperature field along the reflecting wedge surface, which is usually at room temperature, and along the slipstream. Consider Fig. 3.58a, c where the temperature profiles, as assumed by the three-shock theory, on both sides of the slipstream of an MR and behind the Mach stem over the reflecting wedge surface are drawn.

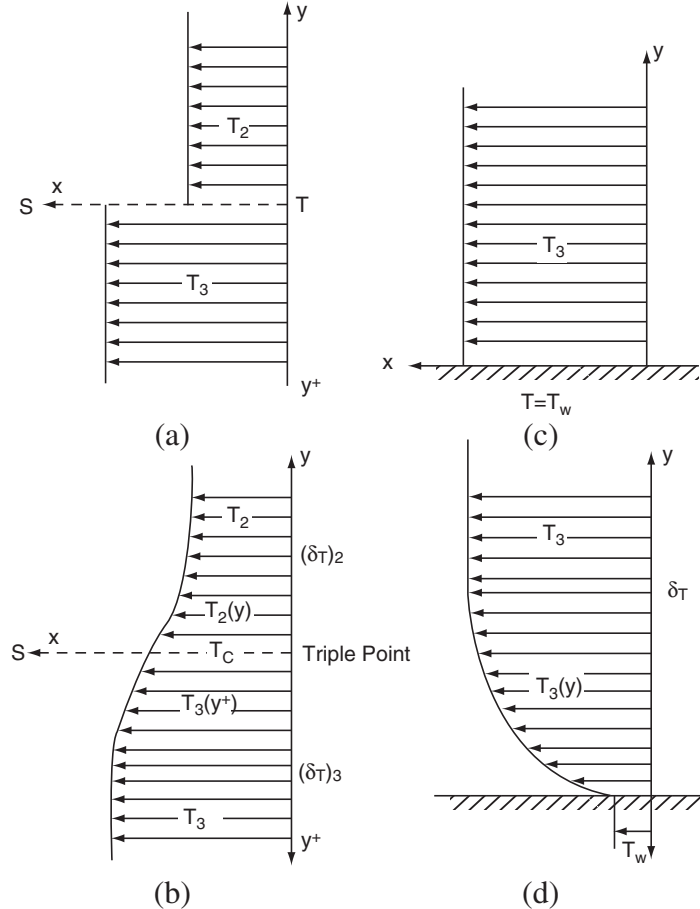


Fig. 3.58. Illustration of the temperature fields on both sides of the slipstream and behind the foot of the Mach stem: (a) and (c) nonconductive flow; (b) and (d) conductive flow

In reality, however, due to thermal conductivity the temperature profiles must change smoothly as is shown in Fig. 3.58b, d. The change takes place inside the thermal boundary layer, δ_T . Outside the thermal boundary layer, the temperatures are uniform and thermal conduction could be neglected. However, inside the thermal boundary layers, heat transfer due to thermal conduction must be accounted for, if one wishes to accurately solve the flow fields. Note that depending upon the Prandtl number, Pr , the thermal boundary layer δ_T could be either smaller or greater than the kinematic boundary layer, δ .

The solution of the flow field near the triple point with thermal conduction could affect the $SMR \rightleftharpoons PTMR/TMR/DMR$ and $TMR \rightleftharpoons DMR$ transition lines. The solution of the flow field at the foot of the Mach stem with thermal

conduction could contribute to the experimental observation by Dewey & McMillin (1985) that the Mach stem is not perpendicular to the reflecting wedge surface. In the case of an RR (see Fig. 3.37) heat conduction might be important in state (2) behind the reflection point, R, where a high temperature gas flows over the cold reflecting wedge, which is initially at room temperature.

The following two examples illustrate the magnitude of the heat fluxes due to the assumed temperature discontinuities in an RR and an MR. In the case of an RR with $M_S = 4.68$, $\phi_1 = 30^\circ$, $p_0 = 15.31$ Torr and $T_0 = 300$ K in nitrogen, the inviscid two-shock theory predicts a flow with temperature $T_2 = 2907$ K over the reflecting wedge surface which has a temperature $T_w = 300$ K. In a case of an MR with $M_S = 2.71$, $\phi_1 = 39.9^\circ$, $p_0 = 760$ Torr and $T_0 = 296$ K in nitrogen the inviscid three-shock theory predicts $T_2 = 920.6$ K and $T_3 = 1305$ K. The heat conductivity of N₂ is about $0.064 \text{ W m}^{-1} \text{ K}^{-1}$ at 920 K and $0.084 \text{ W m}^{-1} \text{ K}^{-1}$ at 1305 K. Thus assuming an average value of $0.074 \text{ W m}^{-1} \text{ K}^{-1}$ implies that the heat flux across the slipstream, which could be assumed to have a thickness similar to that of the incident shock wave (about ten mean free paths), i.e., about 6.6×10^{-7} m, is of the order of $4.3 \times 10^7 \text{ W m}^{-2}$. In the case of the high temperature flows over the reflecting wedges the heat flux might be even greater because the temperature differences are larger, e.g., $\Delta T = 1,005$ K for the MR and 2,607 K for the RR in the above examples. In addition to the larger temperature differences, the heat conductivity, which increases with increasing temperatures, further increases the heat flux.

Unfortunately, an analysis of either the two- nor the three-shock theories in which thermal conduction is accounted for has ever been undertaken. Therefore, it is impossible at this stage to quantitatively assess its influence. However, owing to the fact that both viscous and real gas effects cause a shift in the RR \rightleftharpoons IR transition line to lower values of reflecting wedge angles, and owing to the fact that TDMR-experiments were recorded above the RR \rightleftharpoons IR transition line as calculated by the inviscid, nonconductive perfect two-shock theory, it is possible that the inclusion of heat transfer would shift the RR \rightleftharpoons IR transition line to higher values of reflecting wedge angles.

3.4.6 Noninfinitely Thin Contact Discontinuity

Skews (1971 and 1971/2) and Zaslavskii & Safarov (1973) suggested that the failure of the inviscid three-shock theory to predict correctly the angles between the four discontinuities of a triple point could arise from inadequate choice of the boundary conditions across the contact discontinuity. As discussed in Sect. 1.3.2 the contact discontinuity of the triple point was assumed, in the three-shock theory, to be infinitely thin, i.e., a slipstream. Hence, the flows on both sides of the slipstream were assumed to be parallel, i.e.,

$$\theta_1 - \theta_2 = \theta_3, \quad (3.68)$$

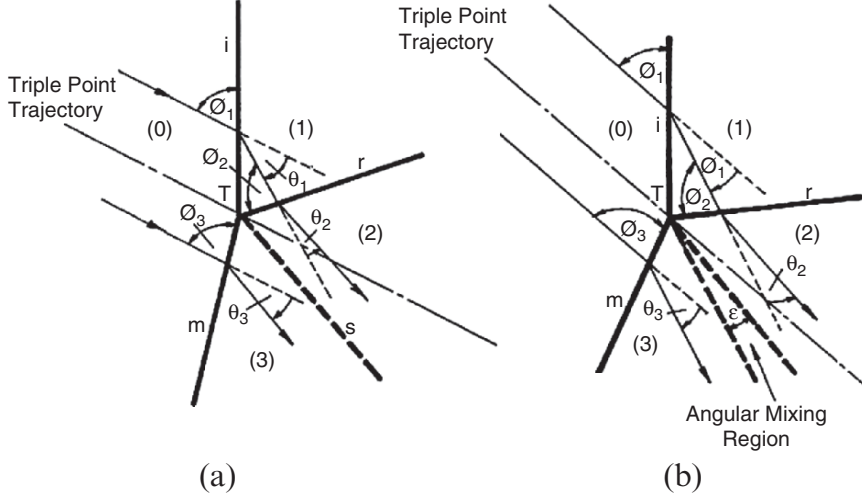


Fig. 3.59. The wave configuration of an MR with an: (a) infinitely thin slipstream; (b) angular contact zone

Alternatively, Skews (1971/2) hypothesized that perhaps the contact discontinuity is an angular contact zone rather than an infinitely thin slipstream. Courant & Friedrichs (1948) originally suggested the possibility of such a wave configuration.

An inspection of the enlarged photograph of the triple point of the DMR, shown in Fig. 3.45, indicates that the contact discontinuity indeed seems to be diverging.⁴ If this is the case, then, according to Skews (1971/2), (3.68) should be replaced by

$$\theta_1 - \theta_2 = \theta_3 - \zeta, \quad (3.69)$$

where ζ is the divergence angle of the angular contact zone, as shown in Fig. 3.59b.

Ben-Dor (1990) followed Skews' (1971/2) hypothesis and analyzed the photograph shown in Fig. 3.45 from which the measured value of ζ is $\zeta = 4^\circ$. The results of Ben-Dor's (1990) study are summarized in Table 3.3 for $M_S = 2.71$, $\phi_1 = 39.9^\circ$, $T_0 = 296$ K and $p_0 = 760$ Torr in nitrogen. The results indicate that the predictions of the inviscid perfect three-shock theory with an infinitely thin contact discontinuity, i.e., a slipstream, for ω_{ir} and ω_{rs} are about 5° greater or smaller than the respective measured.

It is evident from Table 3.3 that the analytical predictions using an angular diverging contact discontinuity are not much better than those obtained using

⁴ Many more photographs of MR wave configurations with clear diverging contact discontinuities can be found in Deschambault's (1984) comprehensive report and Rikanati et al.'s (2006) recent study, which showed that small-scale growth of the Kelvin-Helmholtz shear flow instability is the cause for the slipstream thickening.

Table 3.3. Comparison between the experimental results, shown in Fig. 3.45, and the predictions of the wave angles by the various modified models of the three-shock theory

Type of model	ω_{ir}	ω_{im}	ω_{rs}
Experimental results	$118^\circ \pm 1^\circ$	$132^\circ \pm 1^\circ$	$32^\circ \pm 1^\circ$
Three-shock theory with a slipstream (inviscid perfect gas)	123.19° $(+5.19^\circ)$	132.74° $(+0.74^\circ)$	27.16° (-4.84°)
Three-shock theory with $\zeta = 4^\circ$ (inviscid perfect gas)	123.25° $(+5.25^\circ)$	133.95° $(+1.95^\circ)$	30.311° (-1.89°)
Three-shock theory with $\zeta = 4^\circ$ (inviscid gas in vibrational-relaxation)	117.38° (-0.62°)	133.19° $(+1.19^\circ)$	31.65° (-0.35°)

$M_S = 2.71, \phi_1 = 39.9^\circ, T_0 = 296\text{ K}$ and $p_0 = 760\text{ Torr}$

a slipstream. The three-shock theory with a 4° divergence angular contact zone results in slightly worse values for ω_{ir} and ω_{im} and a much better value for ω_{rs} than the three-shock theory with a slipstream.

If the assumption that the gas behaves as a perfect gas is replaced, and the gas is allowed to be in vibrational equilibrium, the analytical predictions become fairly good. The discrepancies between the analytical predictions and the measured values for this model are within the experimental uncertainty. However, as mentioned in Sect. 3.4.4 accounting for real gas effects for calculating the flow field near the triple point is not justified.

The above results also imply that the shock polar solution of an MR, such as the one shown in Fig. 1.16, is incorrect. The shock polar solution of an MR with $\zeta \neq 0$ is shown in Fig. 3.60. Here states (2) and (3) lie along a constant pressure line, but they are separated by the angle of divergence of the angular contact zone, ζ .

Finally, it should be mentioned that Rikanati et al. (2006) showed recently that small-scale growth of the Kelvin–Helmholtz shear flow instability is the cause for the slipstream thickening. Previously reported growth rates of the large scale Kelvin–Helmholtz instability (Rikanati et al. 2003) combined with the perfect gas three-shock theory were analytically implemented in predicting the growth rates of the slipstream instability. The predictions of the suggested model were validated through a complementary experimental investigation. In the experiments, the instability growth rates were measured for a wide range of incident shock-wave Mach numbers and reflecting wedge angles. The results showed very good agreements with the model predictions for Reynolds numbers greater than $Re > 2 \times 10^4$. Rikanati et al.’s (2006) study demonstrated, for the first time, the use of well-known large-scale models of the Kelvin–Helmholtz instability, in modeling secondary turbulent mixing in hydrodynamic flows.

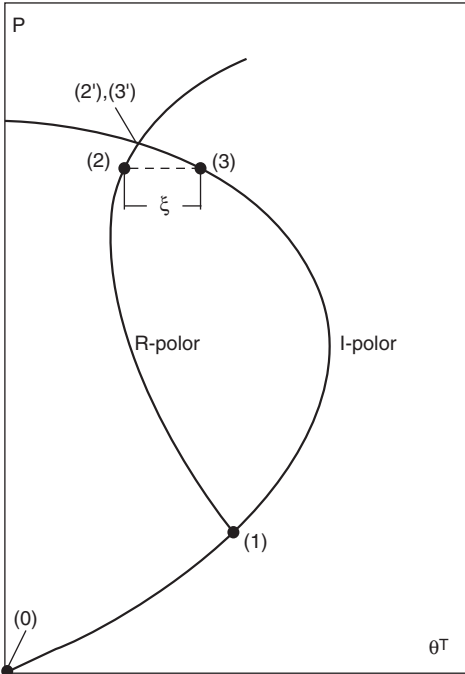


Fig. 3.60. (p, θ) -solution of a Mach reflection with an angular contact zone

3.4.7 Non-Self-Similar Effects

Some comments suggesting that the flow field associated with shock wave reflections in pseudosteady flows cannot be self-similar were given earlier in Sect. 3.4.1, where nonsteady effects were considered.

The assumption of self-similarity was checked and verified experimentally by many investigators. However, in light of the foregoing discussions on viscous, heat transfer, and real gas effects one is left to wonder whether poor experimental resolution techniques mistakenly led to an incorrect conclusion of a self-similar behavior. The three flow zones arising from the above-mentioned three effects, namely, the kinematic boundary layer, the thermal boundary layer and the relaxation zone, are all non-self-similar. The kinematic boundary layer thickness depends solely on the Reynolds number, Re , the thermal boundary layer thickness depends on both the Reynolds, Re , and the Prandtl, Pr , numbers, and the relaxation lengths depend solely on the shock wave Mach number, M_S . Thus, while the wave configurations grows with time, these three lengths remain constant in a frame of reference attached to either the reflection point of an RR or the triple point of an MR. For these reasons it is unavoidable to conclude that actual shock wave reflections in pseudosteady flows cannot be self-similar.

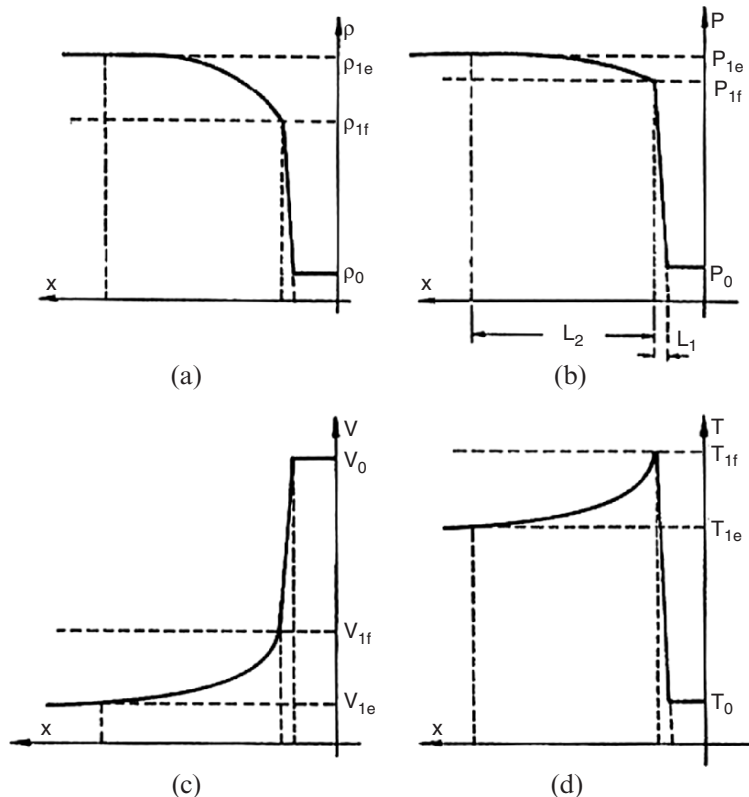


Fig. 3.61. Illustration of the change in the flow properties behind normal stationary shock wave due to the relaxation of the internal degrees of freedom: (a) density; (b) pressure; (c) flow velocity; (d) temperature

To justify further this conclusion consider Fig. 3.61 where four parameters (density, pressure, flow velocity, and temperature) of the flow field inside the relaxation zone behind a shock wave are schematically illustrated. All the flow conditions immediately behind the shock front (which has a thickness of L_1) could be obtained from the R-H equations. They are known as the frozen jump conditions. Once they are reached, the internal degrees of freedom of the gas are excited (provided the temperature T_{1f} is high enough) to result in a further increase in both the density (a) and the pressure (b) and a decrease in both the flow velocity (c) and the temperature (d). The changes asymptotically approach the equilibrium values which are reached at the end of the relaxation zone, L_2 . Thus, it is clear that the properties of the flow field depend on the distance from the shock wave front. Consider now Fig. 3.34 where a DMR at three different positions along a straight reflecting wedge is drawn. The second triple point of this DMR, which was initially adjacent to the first triple point, moves away from the triple point, as the DMR propagates up the reflecting

wedge surface. Consequently, the properties of the gas in state (1), which flows through the second triple point, are changing continuously from their frozen values, immediately behind the shock wave, to their equilibrium values. Similarly, the second reflected shock wave, r' , faces continuously changing flow properties in region (2). Thus, it is clear that the second triple point encounters different flow properties as long as it is inside the relaxation zones behind the incident and reflected shock waves. This suggests that the flow in its vicinity cannot be self-similar, and the orientation of the four discontinuities must be continuously changing with time, to negotiate the continuous change in the flow properties.

Note that the above argument could not be applied to the first triple point as it always faces frozen flow conditions. However, it is possible that while the wave configuration of the first triple point resembles self-similar behavior, the flow fields around it are changing with time in such a way that they are not self-similar. This behavior could be understood better if one refers to the study of Ben-Dor & Glass (1978) where the early attempts to numerically simulate RR and SMR were compared with actual reflections. In the different numerical approaches, the predicted wave configurations were almost identical to those recorded experimentally. However, the shapes of the isopycnics (constant density contours) were different. Thus, one must conclude that the fact that the wave configurations seem to be self-similar does not necessarily imply that the flow fields associated with them are also self-similar. If this is true, then the location along the reflecting wedge where an actual experiment is recorded might play some role in determining the details of the wave structure of the reflection configuration.

Furthermore, the experimental results about the formation of the triple point, i.e., the fact that it does not form at the leading edge of the reflecting wedge, suggests that even the wave configuration of an MR is not self-similar in the very beginning of the reflection but only after it reaches asymptotically a self-similar stage downstream of the leading edge of the reflecting wedge.

Relaxing the assumption of self-similarity can be accomplished only by numerically solving the complete Navier–Stokes equations for an imperfect gas. Since this has not been investigated yet, it is difficult to assess if and how the various transition lines would shift in the (M_S, θ_w^C) - or (M_S, θ_w) -planes. However, in view of the earlier remarks on the need for a mechanism to shift the $\text{RR} \rightleftharpoons \text{IR}$ transition to higher wedge angles in order to account for the TDMR-experiments, which lie above the $\text{RR} \rightleftharpoons \text{IR}$ transition line, it is possible that the inclusion of non-self-similar effects would indeed cause a shift in the required direction. Note also, that the TDMR-experiments are obtained in the case of heavy gases at high Mach numbers where real gas effects undoubtedly play a significant role. Thus, the fact that the second triple point encounters different flow properties as it moves along the relaxation zone might suggest that this is indeed the mechanism causing the $\text{TMR} \rightleftharpoons \text{DMR}$ and the $\text{DMR} \rightleftharpoons \text{TDMR}$ transition lines not to show satisfactory agreement with the experiments.

3.5 Additional Considerations

As mentioned earlier (see Sects. 3.2.1 and 3.2.2), two sub-processes take place when a planar incident shock wave interacts with a straight wedge:

- The shock wave reflection process
- The shock-induced flow deflection process

The entire phenomenon, the shock-wave diffraction process, is a result of an interaction of these two subprocesses (see Fig. 3.15).

The shock wave reflection process has been dealt with, in detail, in the foregoing sections. In the following, brief descriptions of the flow deflection process and the shock diffraction process, are given.

3.5.1 Flow Deflection Domains

When a planar shock wave propagates along the shock tube towards a reflecting wedge it induces a flow behind it. Depending on the incident shock wave Mach number, this flow can be either subsonic or supersonic. The incident shock wave Mach number for which the induced flow is exactly sonic can be obtained from

$$M_1^L = \frac{V_{10}}{A_{10}} = 1, \quad (3.70)$$

where V_{10} and A_{10} , which depend solely on the incident shock wave Mach number, M_S , are given by

$$V_{10} = \frac{2(M_S^2 - 1)}{(\gamma + 1) M_S} \quad (3.71)$$

and

$$A_{10} = \frac{\gamma + 1}{\gamma - 1} \frac{1}{M_S} \left[\left(\frac{2\gamma}{\gamma - 1} M_S^2 - 1 \right) \left(M_S^2 + \frac{2}{\gamma - 1} \right) \right]^{1/2}. \quad (3.72)$$

In the case of N_2 and Ar , for example, the limiting incident shock wave Mach numbers are 2.068 and 2.758, respectively.

As discussed earlier (see Sect. 1.2 and Fig. 1.6), the shock induced flow can negotiate the wedge through a subsonic turning if it is subsonic or with the aid of a shock wave if it is supersonic. In the latter, the shock wave can be either attached or detached (see Fig. 1.6b, c, respectively) depending upon the shock-induced flow Mach number and the reflecting wedge angle.

Figure 3.62a, b illustrates the various domains of flow deflection in the (M_S, θ_w) -plane for N_2 and Ar , respectively. The solid lines are for a perfect gas and the dashed lines are for dissociational-equilibrium in the case of N_2 and ionizational-equilibrium in the case of Ar .

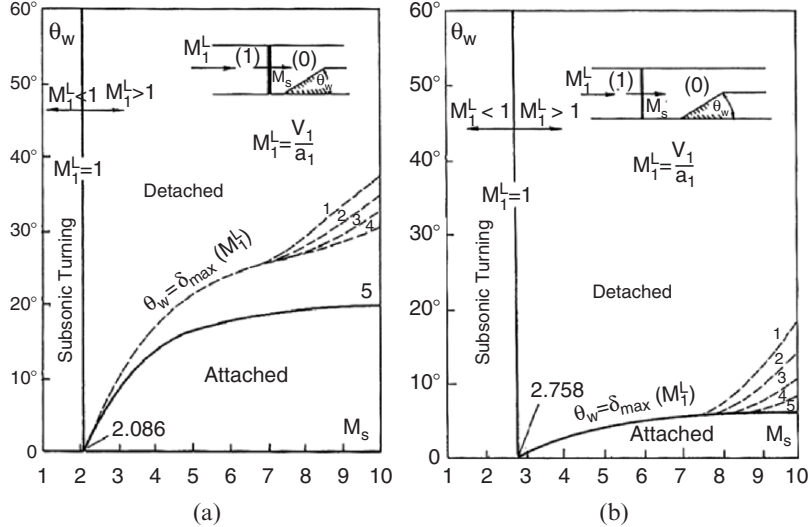


Fig. 3.62. Domains and transition boundaries of different types of flow deflection processes in the $(M_s \theta_w)$ -plane. Solid lines are for perfect gas. Dashed lines are for imperfect gas for $T_0 = 300\text{ K}$ and $p_0 = 1, 10, 100, 1, 000\text{ Torr}$ for lines 1–4, respectively. (a) Nitrogen with $\gamma = 7/5$ for perfect an in dissociational-equilibrium for imperfect; (b) argon with $\gamma = 5/3$ for perfect an in ionizational equilibrium for imperfect

Consider first the region for which the shock induced flow is supersonic in a laboratory frame of reference, i.e., $M_1^L > 1$. This region is divided by the line $\theta_w = \delta_{\max}(M_1^L)$ where $\delta_{\max}(M_1^L)$ is the maximum deflection that a flow having a Mach number $M_1^L > 1$ could experience by passing through an oblique shock wave. Based on the discussion in Sect. 1.2, one can conclude that

- If $\theta_w < \delta_{\max}(M_1^L)$ then the deflecting shock wave is attached to the leading edge of the reflecting wedge.
- If $\theta_w > \delta_{\max}(M_1^L)$ then the deflecting shock wave is detached. In this case, it continuously moves towards the oncoming flow since the entire wave configuration grows with time.

The region for which $M_1^L < 1$, where a subsonic turning (see Fig. 1.6a) should be expected, does not materialize in reality. Instead, because of the sudden change in the boundary condition that is experienced by the subsonic shock-induced flow, when the shock wave reaches the leading edge of the reflecting wedge, and the flow is suddenly exposed to the reflecting wedge (see Sect. 1.2.2 and the discussion regarding Fig. 1.8b) a detached shock wave is obtained in this region too. Hence, this domain degenerates to become a part of the region marked in Fig. 3.62a, b as “detached.”

3.5.2 Shock Wave Diffraction Domains

A superposition of figures of the type shown in Fig. 3.27, but for N₂ and Ar with Fig. 3.60a, b, respectively, results in Fig. 3.63a, b where the domains and transition boundaries of the shock wave diffraction processes are shown in the (M_s, θ_w)-plane. Figure 3.63a, b clearly indicates that the four general types of strong shock wave reflections, i.e., RR, SMR, TMR and DMR, can all have either an attached or a detached shock wave at the leading edge of the reflecting wedge, although sometimes a reflection configuration with an attached shock wave requires a very high incident shock wave Mach number. The PTMR, on the other hand, has always a detached reflected shock wave since it requires $M_1^L < 1$. In general, the domain of an attached shock wave at the leading edge of the reflecting wedge is larger for N₂ than for Ar. Therefore, reflections having attached shock waves are easier to obtain with gases having smaller values of γ , where γ is the specific heat capacities ratio.

Furthermore, real gas effects shift the transition lines between the domains of various types of reflections to smaller wedge angles while they shift the attached/detached transition line to larger wedge angles. Hence, it is easier to obtain reflections having attached shock waves when the internal degrees of freedom of the gas are excited. Recall that the practical effect of the excitation of the internal degrees of freedom is a reduction in γ .

An interferogram of an RR and a shadowgraph of an SMR having attached reflected shock waves are shown in Figs. 3.64 and 3.65, respectively. For comparison with an RR and an SMR having detached reflected shock waves, the reader is referred to Figs. 3.4 and 3.7, respectively.

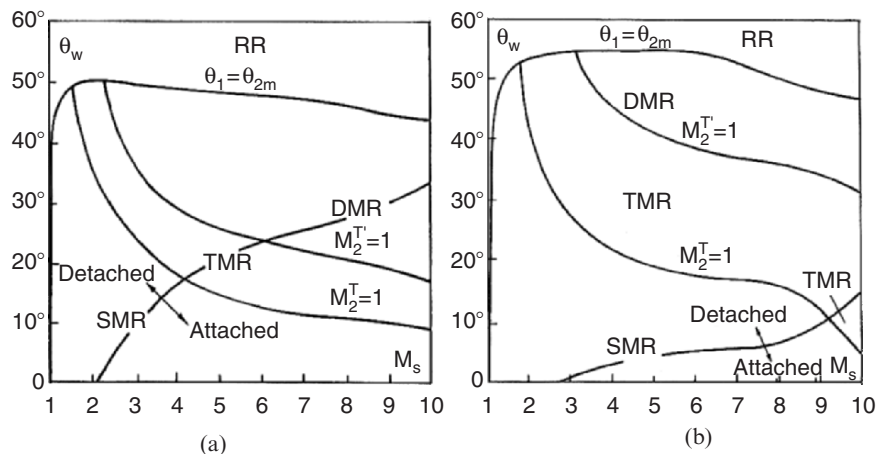


Fig. 3.63. Domains and transition boundaries of different types of shock wave diffraction processes in the $(M_s \theta_w)$ -plane for $T_0 = 300\text{ K}$ and $p_0 = 15\text{ Torr}$. (a) nitrogen in dissociational-equilibrium; (b) argon in ionizational-equilibrium

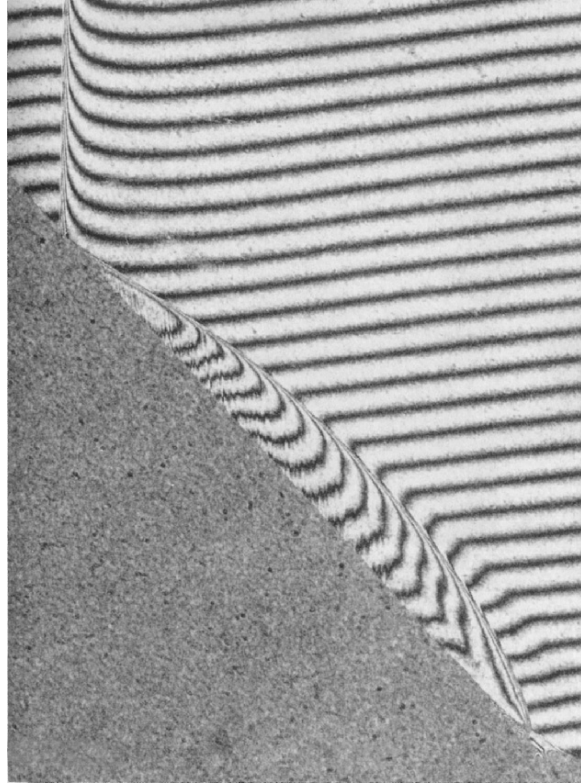


Fig. 3.64. An interferogram showing an RR with a reflected shock wave attached to the leading edge of the reflecting wedge with $M_S = 9.9$ and $\theta_w = 47^\circ$ in air at $T = 296.4\text{ K}$ and $p_0 = 15\text{ Torr}$ (Courtesy of Professor I.I. Glass, Institute for Aerospace Studies, University of Toronto, Toronto, Ontario, Canada)

3.5.3 Comparison Between Steady and Pseudosteady Reflection Domains

It was mentioned earlier (see Sect. 1.5.5) that the $\text{RR} \rightleftharpoons \text{IR}$ transition line in pseudosteady flows differs from that in steady flows. The difference between these two transition lines for N_2 in dissociational-equilibrium is shown in Fig. 3.66 in the (M_0, ϕ_1) -plane. In the case of pseudosteady flows M_0 and ϕ_1 are obtained using the following relations:

$$M_0 = M_S / \cos \theta_w^C$$

and

$$\phi_1 = 90^\circ - \theta_w^C$$

Thus the transition lines in Fig. 3.66 for the pseudosteady case are those shown in the (M_S, θ_w^C) -plane (e.g., see Fig. 3.36a) transformed by the above relations.

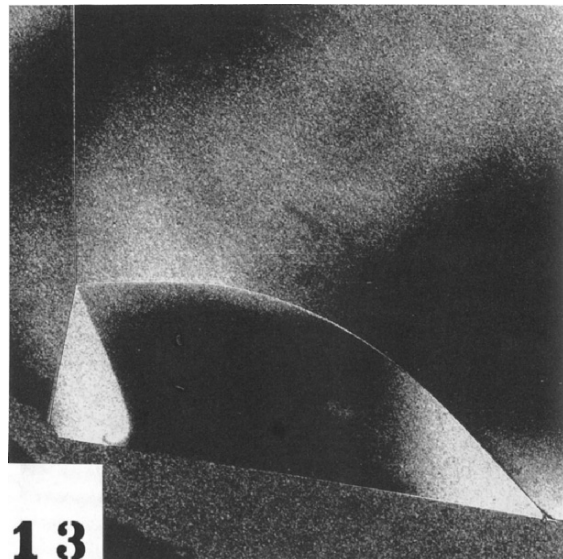


Fig. 3.65. An interferogram showing an SMR with a reflected shock wave attached to the leading edge of the reflecting wedge with $M_S = 4.73$ and $\theta_w = 10^\circ$ in air at $T = 296.6\text{ K}$ and $p_0 = 15\text{ Torr}$ (Courtesy of Professor I.I. Glass, Institute for Aerospace Studies, University of Toronto, Toronto, Ontario, Canada)

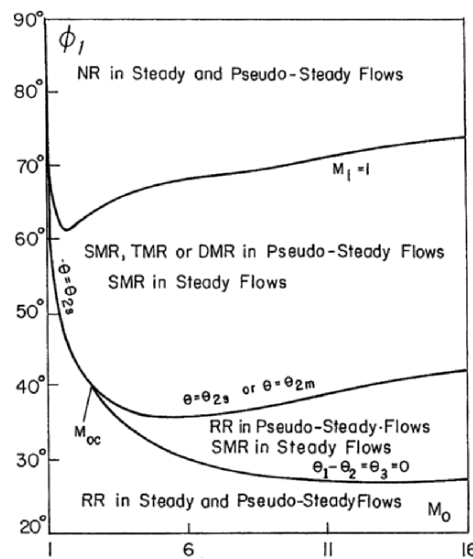


Fig. 3.66. Comparison between the domains of RR and MR in steady and pseudosteady flows in the (M_0, ϕ_1) -plane. Nitrogen in dissociational-equilibrium at $T_0 = 300\text{ K}$ and $p_0 = 15\text{ Torr}$

Figure 3.66 indicates that there is a large area in which the type of the reflection, i.e., RR or MR, depends on the type of the flow under consideration, i.e., steady or pseudosteady. In pseudosteady flows, the RR-domain is larger than the corresponding domain in steady flows. In addition, while in steady flows the MR is always an SMR, in pseudosteady flows the MR-domain is divided further into SMR-, PTMR-, TMR- and DMR-domains.

References

- Bazhenova, T.V., Fokeev, V.P. & Gvozdeva, L.G., "Regions of various forms of Mach reflection and its transition to regular reflection", *Acta Astro.*, 3, 131–140, 1976.
- Ben-Dor, G., "Regions and transitions on nonstationary oblique shock-wave diffractions in perfect and imperfect gases", *UTIAS Rep. 232, Inst. Aero. Studies, Univ. Toronto, Toronto, Ont., Canada*, 1978.
- Ben-Dor, G., "Relation between first and second triple point trajectory angles in double Mach reflection", *AIAA J.*, 19, 531–533, 1981.
- Ben-Dor, G., "A reconsideration of the three-shock theory for a pseudo-steady Mach reflection", *J. Fluid Mech.*, 181, 467–484, 1987.
- Ben-Dor, G., "Structure of the Contact Discontinuity of Nonstationary Mach Reflections", *AIAA J.*, Vol. 28, pp. 1314–1316, 1990.
- Ben-Dor, G., *Shock Wave Reflection Phenomena*, Springer-Verlag, New York, NY, USA, 1991.
- Ben-Dor, G. & Glass, I.I., "Nonstationary oblique shock wave reflections: Actual isopycnics and numerical experiments", *AIAA J.*, 16, 1146–1153, 1978.
- Ben-Dor, G., Mazor, G., Takayama, K. & Igra, O., "The influence of surface roughness on the transition from regular to Mach reflection in a pseudo-steady flow", *J. Fluid Mech.*, 176, 336–356, 1987.
- Ben-Dor, G. & Takayama, K., "The dynamics of the transition from Mach to regular reflection over concave cylinders", *Israel J. Tech.*, 23, 71–74, 1986/7.
- Ben-Dor, G. & Takayama, K., "The phenomena of shock wave reflection – A review of unsolved problems and future research needs", *Shock Waves*, 2(4), 211–223, 1992.
- Colella, P. & Henderson, L.F., "The von Neumann paradox for the diffraction of weak shock waves", *J. Fluid Mech.*, 213, 71–94, 1990.
- Courant, R. & Friedrichs, K.O., *Hypersonic Flow and Shock Waves*, Wiley Interscience, New York, 1948.
- Deschambault, R.L., "Nonstationary oblique-shock-wave reflections in air", *UTIAS Rep. 270, Inst. Aero. Studies, Univ. Toronto, Toronto, Ont., Canada*, 1984.
- Dewey, J.M. & McMillin, D.J., "Observation and analysis of the Mach reflection of weak uniform plane shock waves. Part 1. Observation", *J. Fluid Mech.*, 152, 49–66, 1985.

- Dewey, J.M. & van Netten, A.A., "Observations of the initial stages of the Mach reflection process", Proc. 18th Int. Symp. Shock Waves, Ed. K. Takayama, Springer-Verlag, 227–232, 1991.
- Dewey, J.M. & van Netten, A.A., "Non-self-similarity of the initial stages of Mach reflection", Proc. 20th Int. Symp. Shock Waves, Ed. B. Sturtevant, J.E. Shepherd & H.G. Hornung, 1, 399–404, 1995.
- Friend, W.H., "The interaction of plane shock wave with an inclined perforated plate", UTIAS Tech. Note 25, Inst. Aero. Studies, Univ. Toronto, Toronto, Ont., Canada, 1958.
- Glaz, H.M., Colella, P., Collins, J.P. & Ferguson, E., "Nonequilibrium effects in oblique shock-wave reflection", AIAA J., 26, 698–705, 1988.
- Guderley, K.G., "Considerations on the structure of mixed subsonic-supersonic flow patterns", Tech. Rep. F-TR-2168-ND, Wright Field, USA, 1947.
- Henderson, L.F., Ma, J.H., Sakurai, A. & Takayama, K., "Refraction of a shock wave at an air-water interface", Fluid Dyn. Res., 5, 337–350, 1990.
- Hornung, H.G., Oertel, H. Jr. & Sandeman, R.J., "Transition to Mach reflection of shock waves in steady and pseudo-steady flows with and without relaxation", J. Fluid Mech., 90, 541–560, 1979.
- Hornung, H.G. & Taylor, J.R., "Transition from regular to Mach reflection of shock waves. Part 1. The effect of viscosity on the pseudo-steady case", J. Fluid Mech., 123, 143–153, 1982.
- Jones, D.M., Martin, P.M. & Thornhill, C.K., "A note on the pseudo-stationary flow behind a strong shock diffracted or reflected at a corner", Proc. Roy. Soc. Lond., Ser. A209, 238–248, 1951.
- Kobayashi S., Adachi T. & Suzuki T., "Regular reflection of a shock wave over a porous layer: Theory and experiment", *Shock Waves @ Marseille IV*, Eds. R. Brun, R. & L.Z. Dumitrescu, Springer, 175–180, 1995.
- Landau, L.D. & Lifshitz, E.M., *Fluid Mechanics*, 2nd Ed., p. 425, Pergamon Press, Oxford, England, 1987.
- Law, C.K. & Glass, I.I., "Diffraction of strong shock waves by a sharp compressive corner", CASI Trans., 4, 2–12, 1971.
- Lee, J.-H. & Glass, I.I., "Pseudo-stationary oblique-shock-wave reflections in frozen and equilibrium air", Prog. Aerospace Sci., 21, 33–80, 1984.
- Li, H. & Ben-Dor, G., "Reconsideration of pseudo-steady shock wave reflections and the transition criteria between them", Shock Waves, 5(1/2), 59–73, 1995.
- Li, H., Levy, A. & Ben-Dor, G., "Analytical prediction of regular reflection over rigid porous surfaces in pseudo-steady flow", J. Fluid Mech., 282, 219–232, 1995.
- Mach, E., "Über den verlauf von funkenwellen in der ebene und im raume", Sitzungsbr. Akad. Wiss. Wien, 78, 819–838, 1878.
- Malamud, G., Levi-Hevroni D. & Levy A., "Head-on collision of a planar shock wave with deformable porous foams", AIAA J., 43(8), 1776–1783, 2005.

- Malamud, G., Levi-Hevroni D. & Levy A., "Two-dimensional model for simulating the shock wave interaction with rigid porous materials", *AIAA J.*, 41(4), 663–673, 2003.
- Olim, M. & Dewey, J.M., "A revised three-shock solution for the Mach reflection of weak shock waves", *Shock Waves*, 2, 167–176, 1992.
- Onodera, H., "Shock propagation over perforated wedges", M.Sc. Thesis, Inst. High Speed Mech., Tohoku Univ., Sendai, Japan, 1986.
- Onodera, H. & Takayama, K., "Shock wave propagation over slotted wedges", *Inst. Fluid Sci. Rep.*, 1, 45–66, Tohoku Univ., Sendai, Japan, 1990.
- Reichenbach, H., "Roughness and heated layer effects on shock-wave propagation and reflection – Experimental results", Ernst Mach Inst., Rep. E24/85, Freiburg, West Germany, 1985.
- Rikanati, A., Alon, U. & Shvarts, D., "Vortex-merger statistical-mechanics model for the late time self-similar evolution of the Kelvin–Helmholtz instability", *Phys. Fluids*, 15(12), 3776–3785, 2003.
- Rikanati, A., Sadot, O., Ben-Dor, G., Shvarts, D., Kurabayashi, T. & Takayama, K., "Shock-wave Mach-reflection slip-stream instability: A secondary small-scale turbulent mixing phenomenon", *Physical Review Letters*, 96, 174503:1–174503:4, 2006.
- Schmidt, B., "Structure of Incipient Triple Point at the Transition from Regular Reflection to Mach Reflection", in *Rarefied Gas Dynamics: Theoretical and Computational Techniques*, Eds. E.P. Muntz, D.P. Weaver & D.H. Campbell, *Progress in Astronautics and Aeronautics*, 118, 597–607, 1989.
- Semenov, A.N., Syshchikova, M.P., "Properties of Mach reflection in the interaction of shock waves with a stationary wedge", *Comb. Expl. & Shock Waves*, 11, 506–515, 1975.
- Shames, I.H., *Mechanics of Fluids*, McGraw Hill, 2nd Ed., 1982.
- Shirouzu, M. & Glass, I.I., "An assessment of recent results on pseudo-steady oblique shock-wave reflection", UTIAS Rep. 264, Inst. Aero. Studies, Univ. Toronto, Toronto, Ont., Canada, 1982.
- Shirouzu, M. & Glass, I.I., "Evaluation of assumptions and criteria in pseudo-stationary oblique shock-wave reflections", *Proc. Roy. Soc. Lond.*, Ser. A406, 75–92, 1986.
- Skews, B.W., "The flow in the vicinity of a three-shock intersection", *CASI Trans.*, 4, 99–107, 1971.
- Skews, B.W., "The effect of an angular slipstream on Mach reflection", Dept. Note, McMaster Univ., Hamilton, Ont., Canada, 1971/2.
- Skews B.W., "Oblique reflection of shock waves from rigid porous materials", *Shock Waves*, 4, 145–154, 1994.
- Skews, B. & Ashworth J.T., "The physical nature of weak shock wave reflection", *J. Fluid Mech.*, 542, 105–114, 2005.
- Smith, L.G., "Photographic investigation of the reflection of plane shocks in air", OSRD Rep. 6271, Off. Sci. Res. Dev., Washington, DC., U.S.A., or NORC Rep. A-350, 1945.

- Takayama, K. & Ben-Dor, G., "Pseudo-steady oblique shock-wave reflections over water wedges", *Exp. in Fluids*, 8, 129–136, 1989.
- Takayama, K., Miyoshi, H. & Abe, A., "Shock wave reflection over gas/liquid interface", *Inst. High Speed Mech. Rep.*, 57, 1–25, Tohoku Univ., Sendai, Japan, 1989.
- Vasilev, E. & Kraiko, A., "Numerical simulation of weak shock diffraction over a wedge under the von Neumann paradox conditions", *Comp. Math. & Math. Phys.*, 39, 1335–1345, 1999.
- Wheeler, J., "An interferometric investigation of the regular to Mach reflection transition boundary in pseudo-stationary flow in air", *UTIAS Tech. Note 256*, Inst. Aero. Studies, Univ. Toronto, Toronto, Ont., Canada, 1986.
- White, D.R., "An experimental survey of the Mach reflection of shock waves", Princeton Univ., Dept. Phys., Tech. Rep. II–10, Princeton, N.J., U.S.A., 1951.
- Zaslavskii, B.I. & Safarov, R.A., "Mach reflection of weak shock waves from a rigid wall", *Zh. Prik. Mek. Tek. Fiz.*, 5, 26–33, 1973.

Appendix: First and Second Triple Point Trajectory Angles

As was shown in Sects. 3.2.6 and 3.2.7 the analytical models of the “new” state-of-the-knowledge result in better predictions of the location of the kink, K , of a TMR (see Fig. 3.19), and the first, T , and second, T' , triple points (see Fig. 3.24) than those of the model of the “old” state-of-the-knowledge”.

In spite of this fact, it should be noted here that the predictions of the first, χ , and second, χ' , triple point trajectory angles of the “old” model were quite good from an engineering point of view. For this reason, the main figures of Sect. 2.2 of the first edition of this monograph (Ben-Dor 1991) are included in this Appendix (Figs. A1–A11).

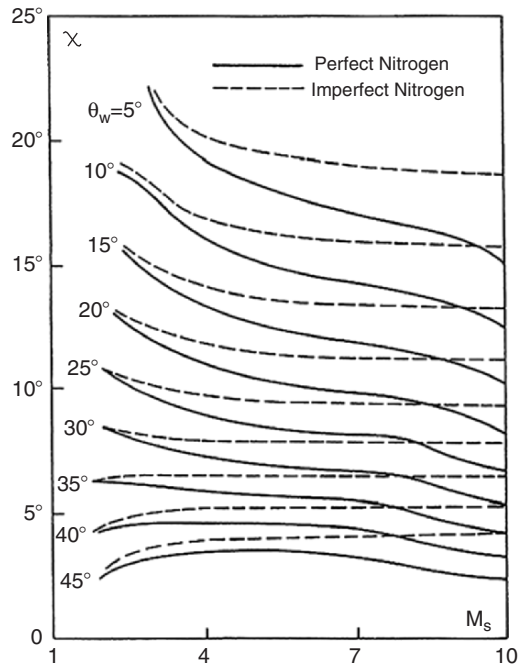


Fig. A1. Variation of χ with M_s for given θ_w . *Solid lines* – perfect nitrogen with $\gamma = 1.4$. *Dashed lines* – nitrogen in dissociational-equilibrium with $p_0 = 15$ Torr and $T_0 = 300$ K

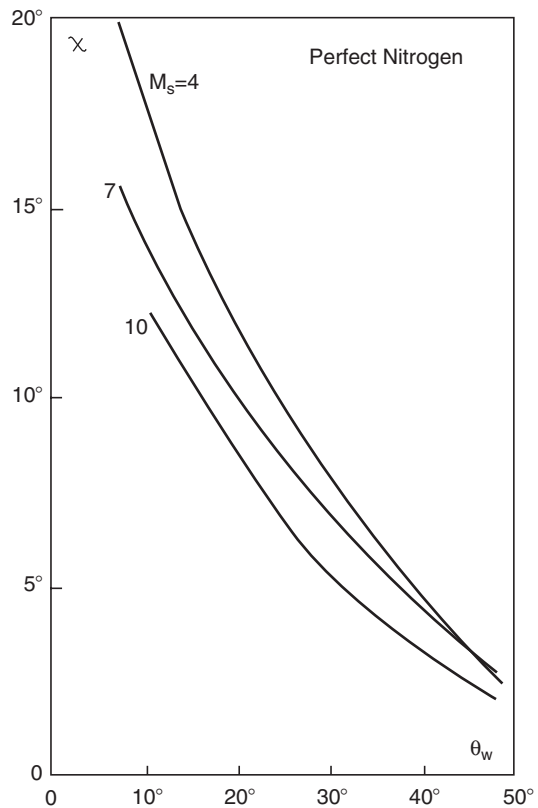


Fig. A2. Variation of χ with θ_w for given M_s for perfect nitrogen with $\gamma = 1.4$

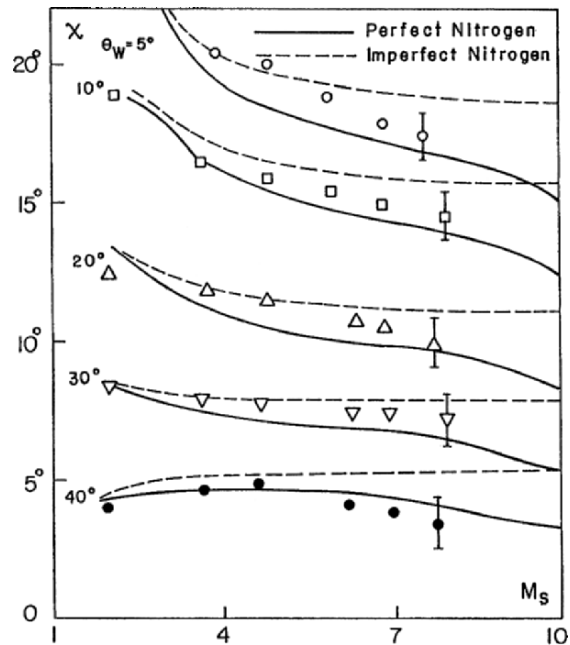


Fig. A3. Variation of χ with M_S for given θ_w and comparison with Ben-Dor's (1978) experiments. *Solid lines* – perfect nitrogen with $\gamma = 1.4$. *Dashed lines* – nitrogen in dissociational-equilibrium with $p_0 = 15$ Torr and $T_0 = 300$ K

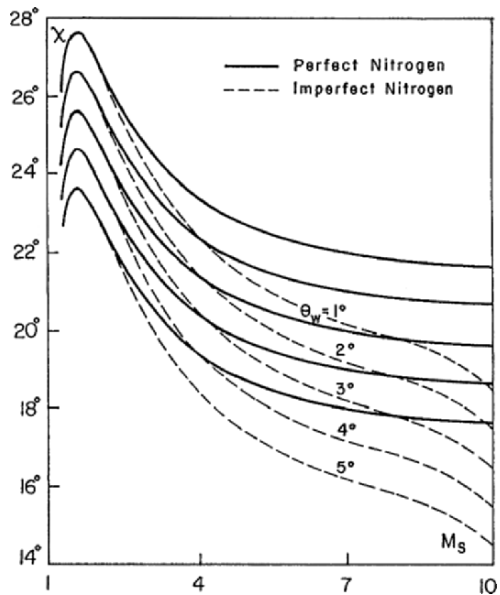


Fig. A4. Variation of χ with M_S for small given θ_w . *Solid lines* – perfect nitrogen with $\gamma = 1.4$. *Dashed lines* – nitrogen in dissociational-equilibrium with $p_0 = 15$ Torr and $T_0 = 300$ K

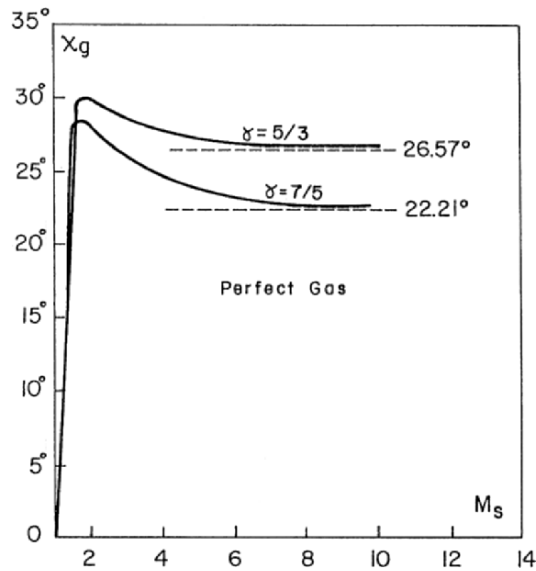


Fig. A5. Variation of the triple point trajectory angle at glancing incidence

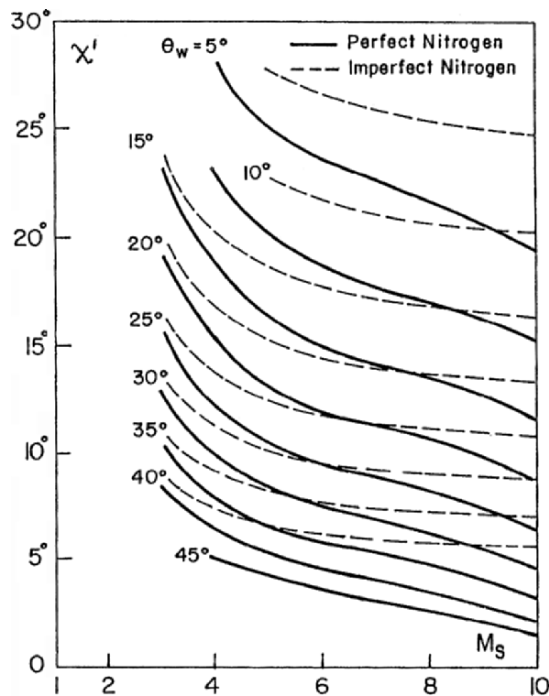


Fig. A6. Variation of χ' with M_s for given θ_w . Solid lines – perfect nitrogen with $\gamma = 1.4$. Dashed lines – nitrogen in dissociational-equilibrium with $p_0 = 15$ Torr and $T_0 = 300$ K

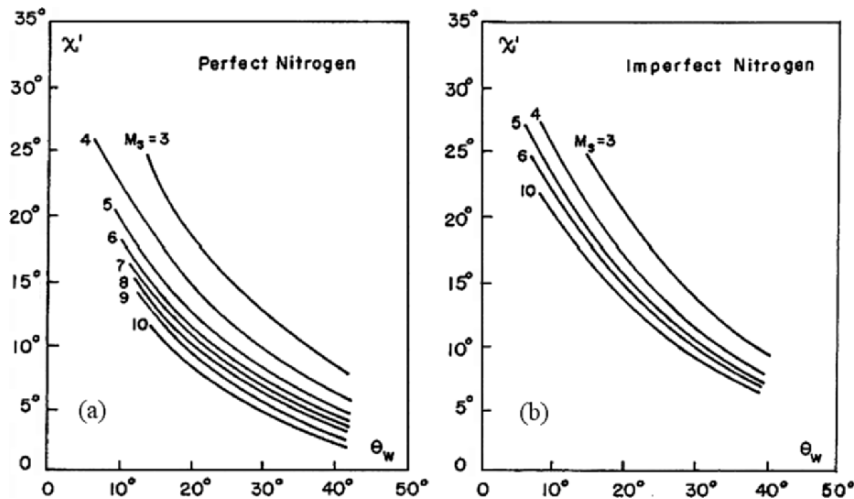


Fig. A7. of χ' with θ_w for given M_s for: (a) perfect nitrogen with $\gamma = 1.4$, and (b) nitrogen in dissociational-equilibrium with $p_0 = 15$ Torr and $T_0 = 300$ K

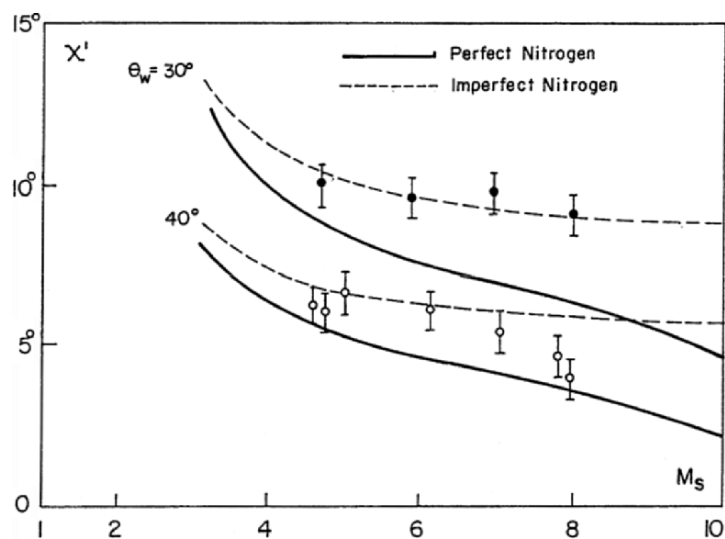


Fig. A8. Variation of χ' with M_s for given θ_w and comparison with Ben-Dor's (1978) experiments. Solid lines – perfect nitrogen with $\gamma = 1.4$. Dashed lines – nitrogen in dissociational-equilibrium with $p_0 = 15$ Torr and $T_0 = 300$ K

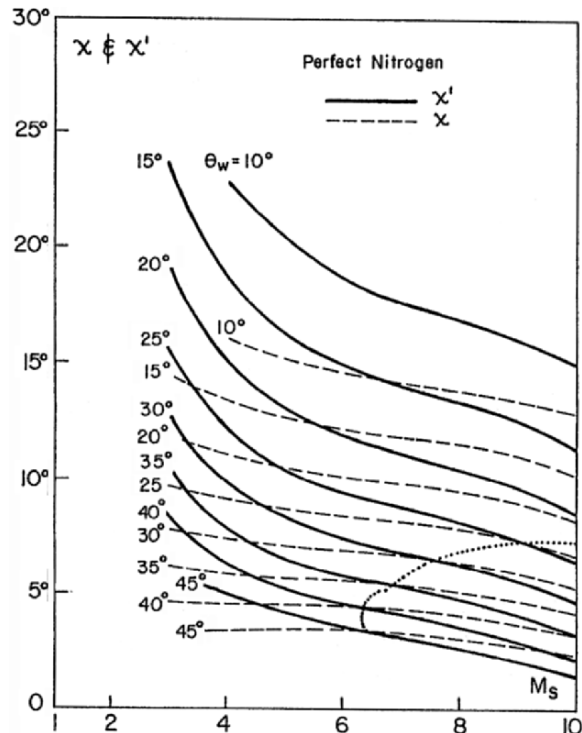


Fig. A9. Comparison of χ and χ' for a perfect nitrogen with $\gamma = 1.4$. The *dashed line* separates between the DMR^+ and DMR^- wave configurations

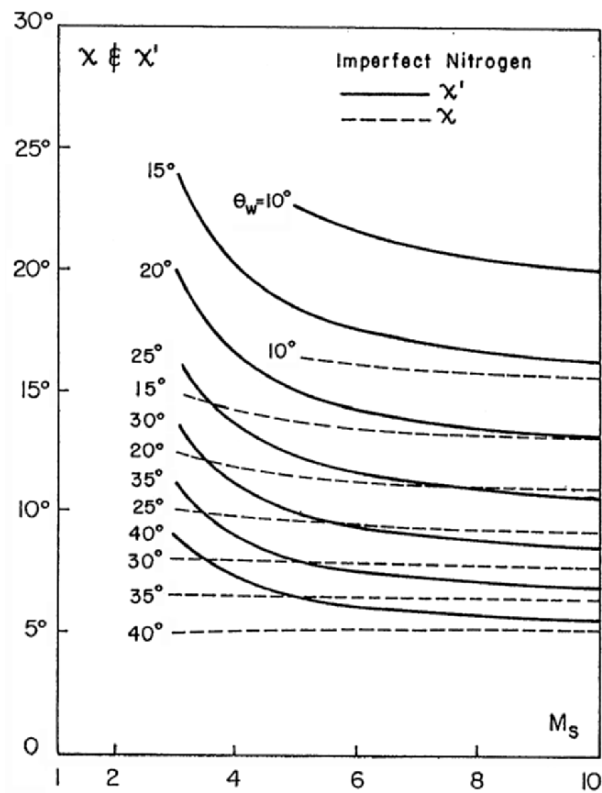


Fig. A10. Comparison of χ and χ' for a nitrogen in dissociational-equilibrium with $p_0 = 15$ Torr and $T_0 = 300$ K

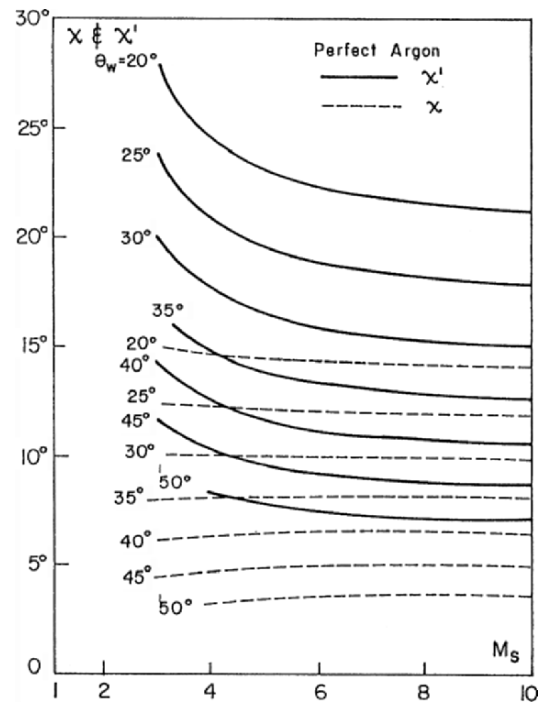


Fig. A11. Comparison of χ and χ' for a perfect argon with $\gamma = 5/3$

Shock Wave Reflections in Unsteady Flows

List of symbols

Latin Letters

a	Local speed of sound
a_i	Local speed of sound in state (i)
A_{ij}	$= a_i/a_j$
H_m	Height of the Mach stem in MR
L_r	Length of the reflected shock wave in TRR
l	Particle path
m_3	The mass of the flow in region (3) of a TRR
M_i	Flow Mach number in state (i) ($= V_i/a_i$)
M_m	Mach stem Mach number
M_S	Incident shock wave Mach number
p_a	Atmospheric pressure
p_i	Pressure in state (i)
r	Disturbance path
R	Radius of curvature of cylindrical wedges
s	Coordinate along the cylindrical wedge surface
S	Distance propagated by the corner-generated signals
t	Time
T_i	Temperature in state (i)
u_i	Flow velocity in state (i) with respect to R in RR and TRR and T in MR
u_n	Velocity of the foot of the normal shock wave of a TRR (point Q) with respect to the reflection point R
V	Flow velocity
V_i	Flow velocity in state (i) in a laboratory frame of reference
V_{ij}	$= V_i/a_j$
V_n	Velocity of the normal shock wave of a TRR with respect to the reflection point R
V_S	Incident shock wave velocity
W	Weight (equivalent to TNT) of the explosive charge

x	Coordinate
x^{tr}	x coordinate of the MR \rightarrow TRR transition point
x_T	x coordinate of the triple point of an MR
y	Coordinate
y_T	y coordinate of the triple point of an MR

Greek Letters

α	Angle between the incident shock wave and the reflecting wedge surface in a TRR (Fig. 4.9)
β	Angle between the slipstream and the reflecting wedge surface in a TRR (Fig. 4.9)
χ	Triple point trajectory angle
χ_g	Triple point trajectory angle at glancing incidence
χ_{tr}	Triple point trajectory angle at transition
Δt	Time interval
$\Delta\theta_w$	Change of the slope of the reflecting surface of a double wedge
ϵ	Roughness
ϕ_i	Angle of incidence between the flow and the oblique shock wave across which the flow enters state (i) with respect to R in RR and TRR and T in MR
γ	Specific heat capacities ratio
θ	Angular position of a flow particle along a curved wedge
θ_i	Deflection angle of the flow while passing across an oblique shock wave into state (i) with respect to R in RR and TRR and with respect to T in MR
θ_T	Angular position of the triple point
θ_w	Reflecting wedge angle
$\theta_w[A \rightleftharpoons B]$	Transition wedge angle from reflection A to reflection B
θ_w^C	Complementary reflecting wedge angle ($90^\circ - \phi_1$)
$\theta_w^{\text{initial}}$	Initial wedge angle of a cylindrical concave or convex wedge
θ_w^{tr}	Transition wedge angle
$\theta_w^{\text{tr}} _M$	Transition wedge angle for shock wave Mach number M
θ_w^1	Wedge angle of the first surface of a double wedge
θ_w^2	Wedge angle of the second surface of a double wedge
ρ_i	Flow density in state (i)

Subscripts

0	Flow state ahead of the incident shock wave, i
1	Flow state behind the incident shock wave, i
2	Flow state behind the reflected shock wave, r
3	Flow state behind the Mach stem, m, of an MR or the normal shock wave, n, of a TRR
r	Reference

Abbreviations

Waves and Points

i	Incident shock wave
m	Mach stem
n	Additional (normal) shock wave in a TRR
r	Reflected shock wave
s	Slipstream
s_1	Slipstream of a TRR
HOB	Height of burst
O	Leading edge of the reflecting wedge
P	Point where the slipstream of a TRR reflects from the reflecting surface
Q	Point where the foot of n touches the reflecting surface
R	Reflection point
T	First triple point
T'	Second triple point
T^*	Triple point of a TRR

Wave Configuration

DMR	Double-Mach reflection
DiMR	Direct-Mach reflection
InMR	Inverse-Mach reflection
MR	Mach reflection
PTMR	Pseudotransitional Mach reflection
RR	Regular reflection
SMR	Single-Mach reflection
StMR	Stationary-Mach reflection
TMR	Transitional-Mach reflection
TRR	Transitioned regular reflection

Unlike the shock reflection phenomena in steady flows (Chap. 2) and in pseudosteady flows (Chap. 3), where the flow fields basically depend on two independent variables, namely x and y in the former and x/t and y/t in the latter, here the flow field depends on three parameters x , y , and t . For this reason, the analytical consideration of the reflection phenomenon in unsteady flows is more difficult.

In addition, to this difficulty, all the difficulties, which were mentioned for the case of shock wave reflections in pseudosteady flows, exist also in the case of shock wave reflections in unsteady flows.

Unsteady shock wave reflections can basically be obtained in one of the following ways:

1. Reflecting a shock wave propagating with a constant velocity over a non-straight surface

2. Reflecting a shock wave propagating with a nonconstant velocity over a straight surface
3. Reflecting a shock wave propagating with a nonconstant velocity over a nonstraight surface

4.1 Constant Velocity Shock Wave Reflections Over Nonstraight Surfaces

If the reflecting wedge surface is not straight but curved, either concavely or convexly, then point R at which the foot of the incident shock wave touches the reflecting wedge surface (see e.g., Fig. 1.8a) would have a constant velocity (the incident shock wave velocity) in the horizontal direction only. The velocity of the reflection point, point R, in the vertical direction would not be constant as in the case of a straight reflecting surface.

Thus, if a frame of reference is attached to point R, then the angle of incidence of the oncoming flow, ϕ_1 , would change continuously as the shock wave propagates. Furthermore, since $M_0 = M_S / \sin \phi_1$, it is clear that the flow Mach number of the oncoming flow, M_0 , would also change continuously.

4.1.1 Shock Wave Reflections Over Cylindrical Concave Surfaces

When an incident planar shock wave encounters a cylindrical concave surface it reflects over it either as an RR or as an MR depending upon the initial wedge angle and the incident shock wave Mach number. The initial type of reflection can be determined using the pseudosteady shock reflection theory presented in Chap. 3.

Consider, for example, Fig. 3.27 and note that if one draws a constant M_S -line (i.e., a vertical line for a given M_S) then the number of transition boundaries intersected by this line depends on the chosen value of M_S . In the case of nitrogen for example if $M_S < 2.07$ then the RR \rightleftharpoons SMR and the SMR \rightleftharpoons PTMR transition lines are intersected. In the range $M_S > 2.07$ the SMR \rightleftharpoons TMR, TMR \rightleftharpoons DMR, and DMR \rightleftharpoons RR transition lines are intersected.

Let us consider the most general case of an incident shock wave having a Mach number, $M_S > 2.07$, for which all the four types of reflection, i.e., SMR, TMR, DMR, and RR are possible. Let us also define the corresponding three transition wedge angles as θ_w [SMR \rightleftharpoons TMR], θ_w [TMR \rightleftharpoons DMR], and θ_w [DMR \rightleftharpoons RR]. Let us also consider Fig. 4.1 where four different cylindrical concave wedges are drawn. While they all have the same radius of curvature, R , their initial wedge angles (i.e., the slopes of the cylindrical wedges at their leading edges) are different. The initial slopes are:

1. $\theta_w = 0$ the wedge aa'e
2. θ_w [SMR \rightleftharpoons TMR] for the wedge bb'e

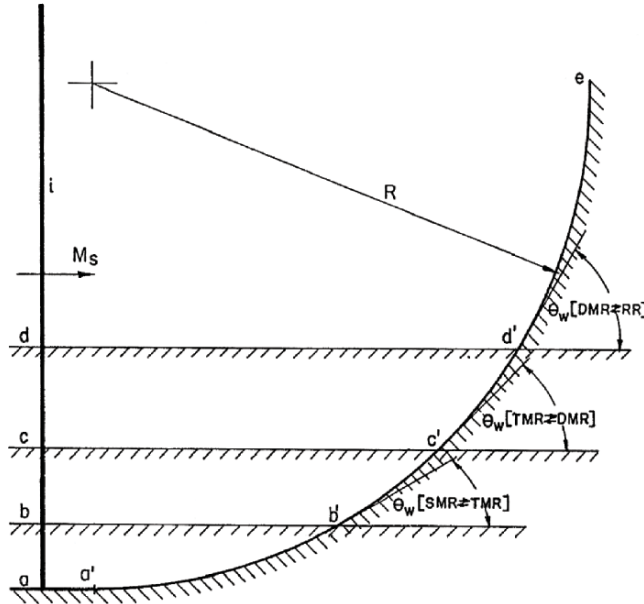


Fig. 4.1. Schematic illustration of four different cylindrical concave surfaces over which different reflection processes are obtained

3. $\theta_w[\text{TMR} \rightleftharpoons \text{DMR}]$ for the wedge cc'e
4. $\theta_w[\text{DMR} \rightleftharpoons \text{RR}]$ for the wedge dd'e

Thus, for all the cylindrical wedges with an initial angle in the range:

1. $0 < \theta_w^{\text{initial}} < \theta_w[\text{SMR} \rightleftharpoons \text{TMR}]$ the initial reflection will be an SMR
2. $\theta_w[\text{SMR} \rightleftharpoons \text{TMR}] < \theta_w^{\text{initial}} < \theta_w[\text{TMR} \rightleftharpoons \text{DMR}]$ the initial reflection will be a TMR
3. $\theta_w[\text{TMR} \rightleftharpoons \text{DMR}] < \theta_w^{\text{initial}} < \theta_w[\text{DMR} \rightleftharpoons \text{RR}]$ the initial reflection will be a DMR
4. $\theta_w[\text{DMR} \rightleftharpoons \text{RR}] < \theta_w^{\text{initial}} < 90^\circ$ the initial reflection will be an RR

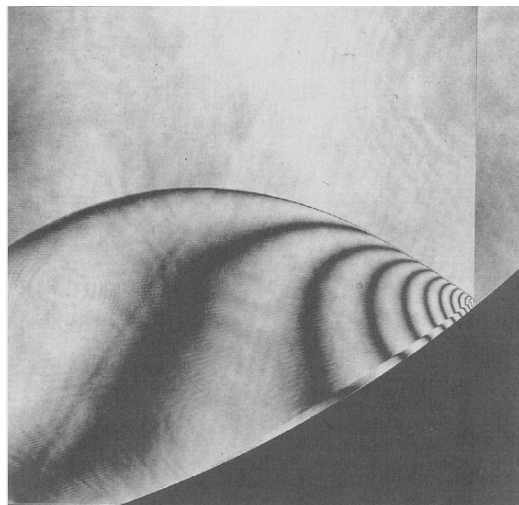
If the initial reflection is an MR (i.e., $\theta_w^{\text{initial}} < \theta_w[\text{DMR} \rightleftharpoons \text{RR}]$) then the incident shock wave propagates along the cylindrical concave wedge, and encounters an ever increasing wedge angle, which will eventually force the MR to change into an RR. If, however, the initial reflection is an RR (i.e., $\theta_w^{\text{initial}} > \theta_w[\text{DMR} \rightleftharpoons \text{RR}]$) then the RR will persist.

The foregoing discussion implies that the initial reflection over a cylindrical concave wedge can be an SMR, a TMR, a DMR, or an RR depending upon the initial wedge angle (provided the incident shock wave Mach number is high enough):

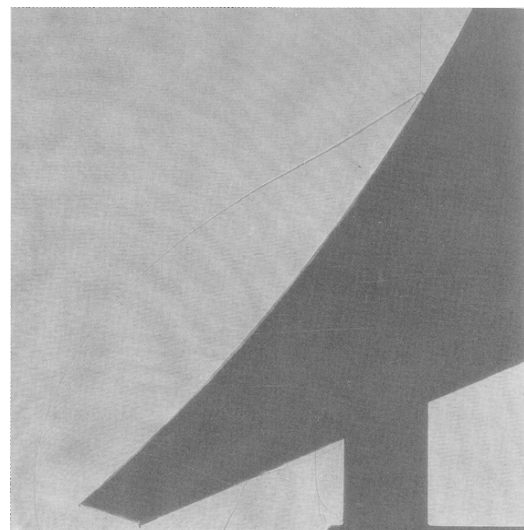
1. If it the initial reflection an SMR, it will change first to a TMR, then to a DMR and finally to an RR

2. If the initial reflection is a TMR, it will first change to a DMR and then to an RR
3. If the initial reflection is a DMR it will change to an RR
4. If the initial reflection is an RR it will remain an RR

Photographs of an SMR, a TMR, a DMR, and an RR over a cylindrical concave surface are shown in Fig. 4.2a-d, respectively.

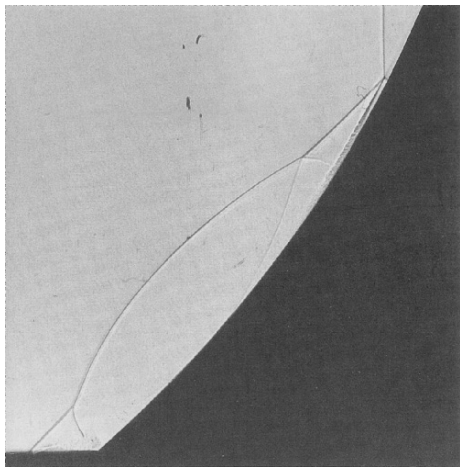


(a)

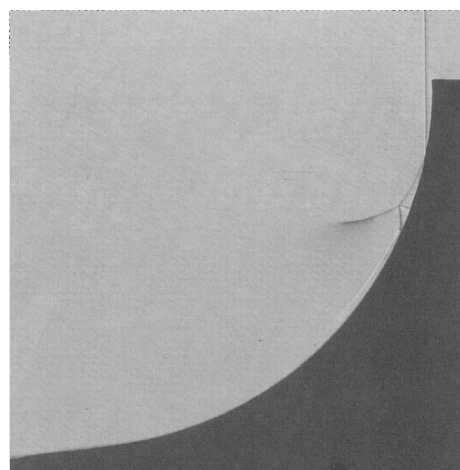


(b)

Fig. 4.2. (Continued)



(c)



(d)

Fig. 4.2. (a) A holographic interferogram illustrating an actual SMR over a cylindrical concave surface with $M_S = 1.7$ in air at $T_0 = 290\text{ K}$ and $p_0 = 760\text{ Torr}$. (Courtesy of Professor K. Takayama, Shock Wave Research Center, Institute of Fluid Science, Tohoku University, Sendai, Japan.) (b) A shadowgraph illustrating an actual TMR over a cylindrical concave surface with $M_S = 2.19$ in air at $T_0 = 291.3\text{ K}$ and $p_0 = 760\text{ Torr}$. (Courtesy of Professor K. Takayama, Shock Wave Research Center, Institute of Fluid Science, Tohoku University, Sendai, Japan.) (c) A shadowgraph illustrating an actual DMR over a cylindrical concave surface with $M_S = 3.02$ in air at $T_0 = 292.4\text{ K}$ and $p_0 = 760\text{ Torr}$. (Courtesy of Professor K. Takayama, Shock Wave Research Center, Institute of Fluid Science, Tohoku University, Sendai, Japan.) (d) A shadowgraph illustrating an actual RR over a cylindrical concave surface with $M_S = 2.1$ in air at $T_0 = 290\text{ K}$ and $p_0 = 760\text{ Torr}$. (Courtesy of Professor K. Takayama, Shock Wave Research Center, Institute of Fluid Science, Tohoku University, Sendai, Japan.)

MR → RR Transition

As mentioned in Sect. 4.1.1, if an incident shock wave reflects initially over a cylindrical concave wedge as an MR it will eventually change to an RR.

In an extensive experimental study Takayama and Sasaki (1983) showed that the MR → RR transition wedge angle, θ_w^{tr} , depends in addition to the incident shock wave Mach number, M_S , on both the radius of curvature of the cylindrical wedge, R , and the initial wedge angle $\theta_w^{initial}$. The results of their experimental study are shown in Fig. 4.3 together with the $MR \rightleftharpoons RR$ transition lines of steady (line AB) and pseudosteady flows (line AC).

It is evident that all the experimentally recorded transition wedge angles lie above the $RR \rightleftharpoons MR$ transition line of steady flows. Furthermore, as the radius of curvature increases, the transition wedge angles decrease and approach the steady flow $RR \rightleftharpoons MR$ transition line. Similarly, the experimental results indicate that the transition wedge angle decreases with increasing initial wedge angles. The dependence of θ_w^{tr} on $\theta_w^{initial}$ is shown in a different way in Fig. 4.4 for two incident shock wave Mach numbers. The results for $M_S = 1.6$ reveal a continuous nonlinear decrease of θ_w^{tr} as $\theta_w^{initial}$ increases. The solid line is hand-drawn to illustrate the dependence of θ_w^{tr} on $\theta_w^{initial}$. Since θ_w^{tr} cannot be smaller than $\theta_w^{initial}$ this line must terminate at the point $\theta_w^{initial} = \theta_w^{tr}$. The initial wedge angle at this point results in an RR for $M_S = 1.6$. Similar behavior is evident for $M_S = 3.1$; however, due to the lack of enough experimental data points the hand-drawn line should not be trusted. It should also be

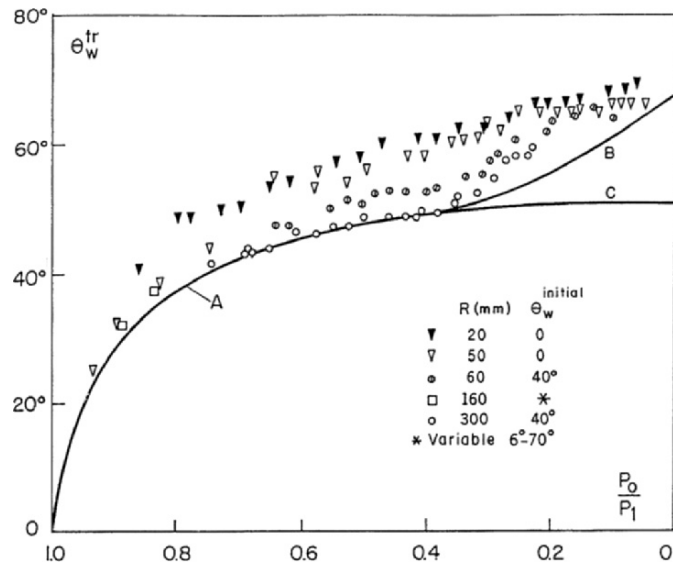


Fig. 4.3. Experimental data with air illustrating the dependence of the transition wedge angle over a cylindrical concave surface on the radius of curvature and the initial wedge angle

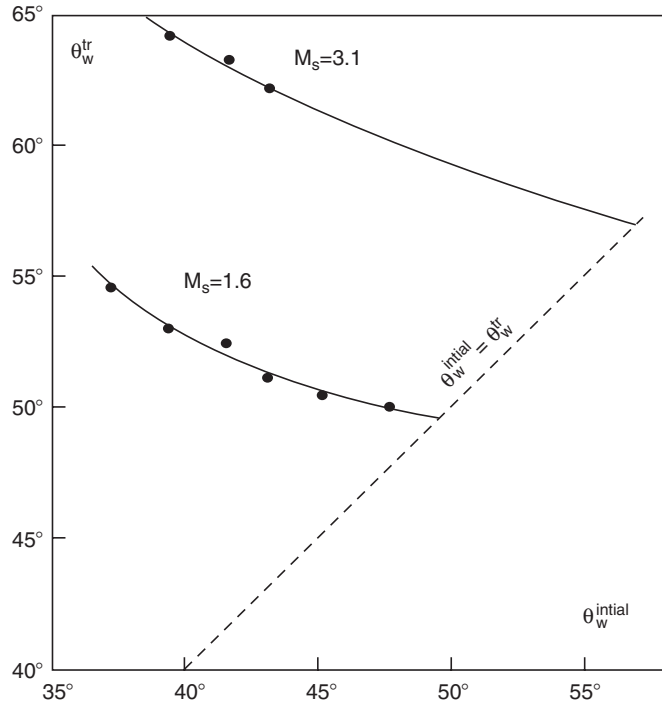


Fig. 4.4. Experimental data with air illustrating the dependence of the transition wedge angle over a cylindrical concave surface on the initial wedge angle for $M_S = 1.6$ and 3.1

noted that the experimental results suggest that as the radius of curvature approaches infinity, i.e., $R \rightarrow \infty$, the actual transition wedge angles approach the transition line appropriate to a steady flow.

Effect of Surface Roughness

Takayama et al. (1981) investigated experimentally the effect of surface roughness on the MR \rightleftharpoons RR transition. The roughness was imposed on the surface by pasting sand paper with different mesh sizes on the reflecting wedge surface. Their results for a cylindrical concave wedge with $R = 50$ mm, $\theta_w^{\text{initial}} = 0$ and three different sizes of roughness are shown in Fig. 4.5. Again, the MR \rightleftharpoons RR transition lines of steady (line AB) and pseudosteady (line AC) flows are added.

Figure 4.5 reveals that the transition wedge angle, θ_w^{tr} , decreases as the roughness of the reflecting surface increases. In the case of an extremely rough surface (mesh No. 40 sand paper) θ_w^{tr} is almost independent of the incident shock wave Mach number as it assumes a value of about 54.5° . Furthermore, while for the case of a smooth wedge, θ_w^{tr} was always greater than the

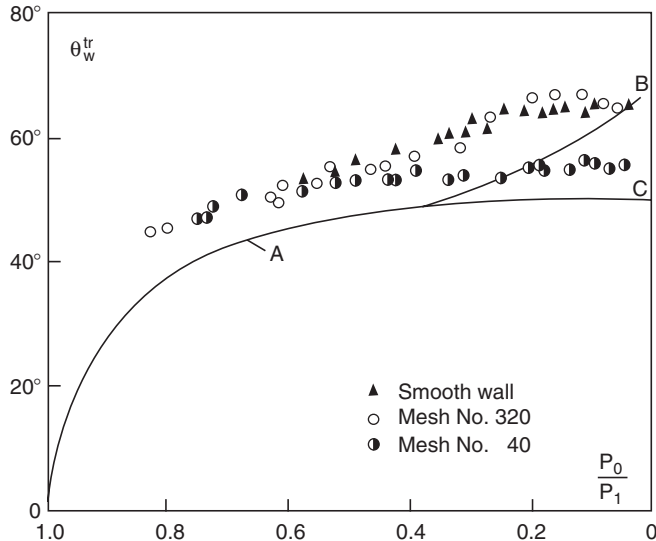


Fig. 4.5. Experimental data with air illustrating the dependence of the transition wedge angle over a cylindrical concave surface on its roughness

appropriate value in steady flows (see Fig. 4.3), here there are cases where θ_w^{tr} is smaller than the appropriate value in steady flows. However, even with the extremely high roughness the recorded transition wedge angles were always larger than those appropriate to pseudosteady flows.

Dynamics of the MR \rightarrow RR Transition

Figure 4.6 illustrates the measured triple point trajectory of an MR with $M_S = 1.4$ over a cylindrical concave surface. The experimental results indicate that the height of the Mach stem, H_m , increases from $H_m = 0$ at the leading edge of the reflecting wedge, to a maximum after which it decreases until it vanishes at the point where the MR terminates and a TRR is formed. It should be noted that the first measured point is quite far away from the leading edge of the reflecting wedge; however, since H_m must start from zero a reasonable trajectory is drawn (dashed lines) in the region where experimental data are unavailable.

The triple point trajectory, as shown in Fig. 4.6, can be divided into two parts:

1. A part along which $dH_m/ds > 0$
2. A part along which $dH_m/ds < 0$

where s is a distance measured along the wedge surface.

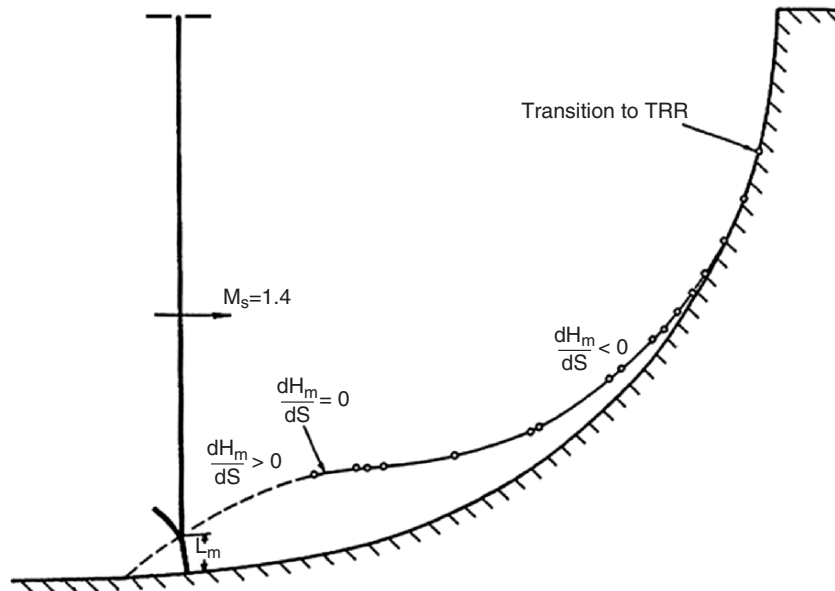


Fig. 4.6. Measured triple point trajectory of an MR with $M_s = 1.4$ over a cylindrical concave surface

Courant and Friedrichs (1948) indicated that, theoretically, three different types of MR-configuration are possible, depending on the direction of propagation of the triple point of the MR with respect to the reflecting surface:

1. If the triple point moves away from the reflecting surface, then the MR is a direct-Mach reflection – DiMR
2. If the triple point moves parallel to the reflecting surface, then it is a stationary-Mach reflection – StMR
3. If the triple point moves towards the reflecting surface then it is an inverse-Mach reflection – InMR

(More details on DiMR, StMR, and InMR are given in Sect. 1.1 and Fig. 1.3)

Following these definitions one can conclude that the experimental data shown in Fig. 4.6 suggest that the reflection of a planar shock wave over a cylindrical concave surface goes through the following sequence of events:

1. A direct-Mach reflection, DiMR, along the part where $dH_m/ds > 0$
2. A momentarily stationary-Mach reflection, StMR, at the point where $dH_m/ds = 0$, an inverse-Mach reflection, InMR, along the part where $dH_m/ds < 0$
3. Termination of the InMR and a formation of an RR at the point where $H_m = 0$. Since the RR-configuration that is formed after the termination of an InMR has a special structure attached to it (see Sect. 4.1.1.2), it is called transitioned regular reflection-TRR.

In summary, experimental investigations of the MR \rightarrow RR transition over cylindrical concave surfaces suggest that the reflection process follows the following sequence of events:

$$\text{DiMR} \rightarrow \text{StMR} \rightarrow \text{InMR} \rightarrow \text{TRR}$$

More details can be found in Ben-Dor and Takayama (1986/7).

Figure 4.7 illustrates this sequence of events in the (p, θ) -plane:

1. The intersection of the $I_1 - R_1$ shock polars at point "a", which is on the right branch of the I_1 -polar, results in a DiMR
2. The intersection of the $I_2 - R_2$ shock polars at point "b", which lies also on the p -axis, results in an StMR

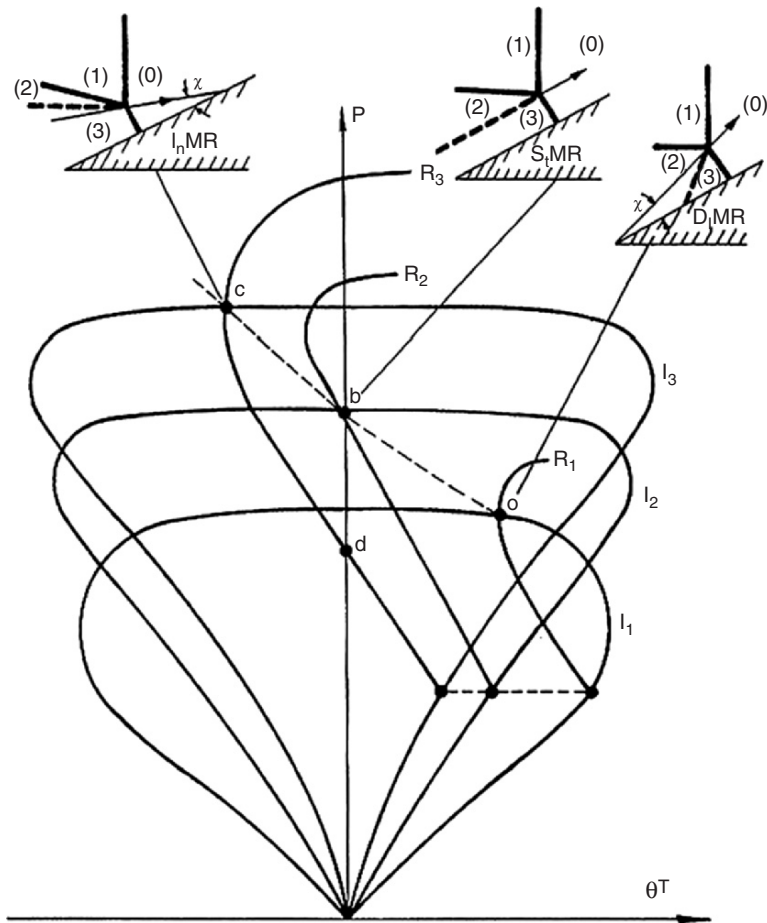


Fig. 4.7. Schematic illustration of the transition from DiMR to TRR in the (p, θ) -plane

3. The intersection of the $I_3 - R_3$ shock polars at point “c”, which is on the left branch of the I_3 -polar, results in an InMR
4. The intersection of the R_3 -polar with the p -axis at point “d” results in a TRR

Note that since the pressure in state (1) is determined solely by the incident shock wave Mach number, all the R -polars emanate from their corresponding I -polars at the same pressure. The dashed line connecting points “a”, “b”, and “c” in the locus of the Mach reflection configurations which are obtained from the moment a DiMR was formed at point “a” until the moment the InMR was terminated at point “c” to form a TRR at point “d”.

1. DiMR wave configurations exist along the portion “a” and “b”
2. A momentary StMR wave configuration exists at point “b”
3. InMR wave configurations exist along the portion “b and c”

Figures 4.6 and 4.7 indicate that the part along which $dH_m/ds > 0$ corresponds to the section “a and b”, the point where $dH_m/ds = 0$ corresponds to point “b”, and the part along which $dH_m/ds < 0$ corresponds to the section “b and c.”

Unlike the DiMR, which is obtainable in pseudosteady flows also, the StMR and the InMR can be obtained only in unsteady flows.

Stationary-Mach Reflection (StMR)

The wave configuration of an StMR and the I-R shock polar combination of an StMR are shown in Fig. 4.7. The wave configuration of an StMR is basically the same as that of a DiMR. The only difference is that its slipstream is parallel to the reflecting surface. This is because the triple point of an StMR moves parallel to the reflecting surface.

Inverse-Mach Reflection (InMR)

The wave configuration of an InMR and the I-R shock polar combination of an InMR are also shown in Fig. 4.7. The wave configuration of an InMR is very similar to that of a DiMR. The only difference is in the orientation of the slipstream. While in a DiMR the slipstream extends from the triple point towards the reflecting surface (see e.g., Fig. 3.7), in the case of an InMR the slipstream emanating from the triple point extends away from the reflecting surface, because the triple point moves toward the reflecting surface. For this reason, the InMR is a temporary reflection. It terminates as soon as its triple point collides with the reflecting surface. Upon the termination of an InMR, a new wave structure, transitioned regular reflection, TRR, is formed.

Transitioned Regular Reflection (TRR)

Figure 4.8 is a schematic illustration showing the dynamics of the termination of an InMR and the formation of a TRR. Figure 4.8a shows an InMR moving

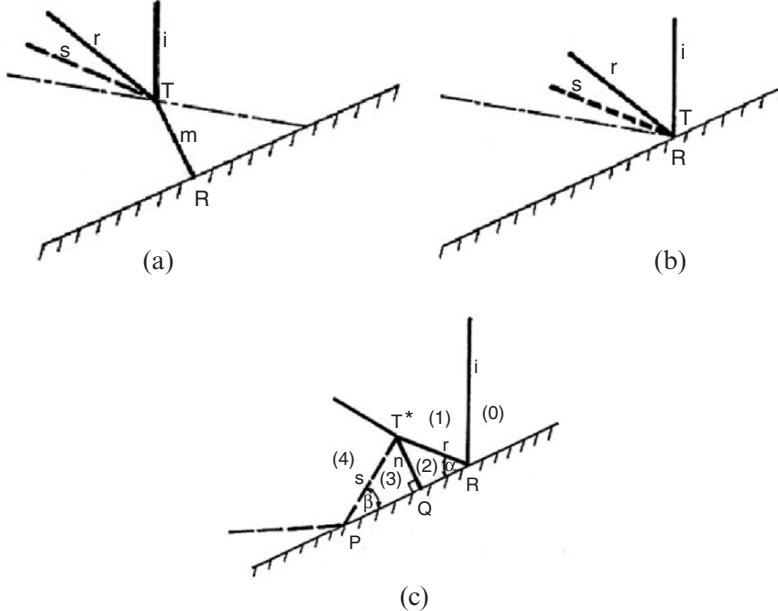


Fig. 4.8. Schematic illustration showing the dynamics of the termination of an InMR and the formation of a TRR

toward the reflecting surface. Figure 4.8b illustrates the wave configuration at the moment the triple point, T , collides with the reflecting surface. The Mach stem, m , vanishes and the incident shock wave, i , and the reflected shock wave, r , meet on the reflecting surface. The wave configuration, which is obtained after the termination of an InMR, is shown in Fig. 4.8c. The major part of the wave structure is an RR (i and r meet on the reflecting surface). In addition a new triple point, T^* , is formed on the reflected shock wave. The nature of this triple point is yet to be investigated. Figure 4.8c also indicates that an additional shock wave connects this triple point with the reflecting surface. This additional shock wave, which is not necessarily straight, is perpendicular to the reflecting surface at its foot.

The physical reason for the formation of this additional shock wave is the need to support a sudden pressure drop, which is associated with the InMR \rightarrow TRR transition. Henderson and Lozzi (1975) were the first to hypothesize the need for this additional shock wave. Consider Fig. 4.7 and note that the termination of an InMR at point “c” and the formation of a TRR at point “d” is associated with a sudden pressure drop from p_c to p_d . The additional shock wave supports this sudden pressure drop. Hence, the pressure ratio across the additional shock wave should be p_c/p_d . (Note that based on Fig. 4.8 $p_c = p_2$ and $p_d = p_3$).

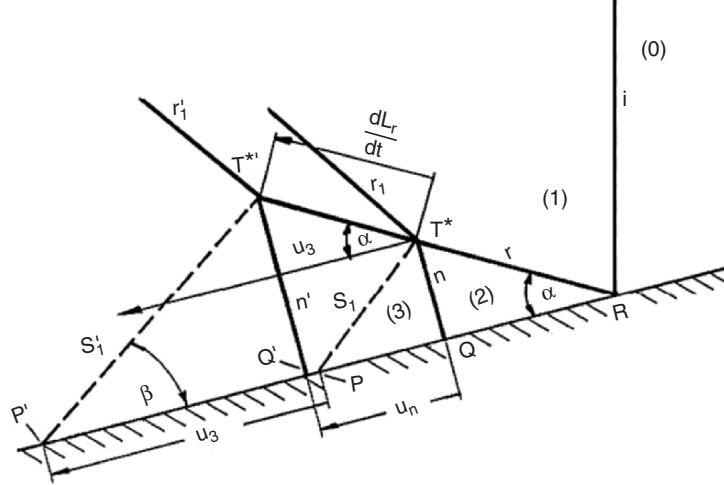


Fig. 4.9. The wave configuration of a transitioned regular reflection at two different times

Analytical Solution of a TRR

The various flow regions of a TRR are shown in Fig. 4.8c. The reflection point of the RR is R, the foot of the additional shock wave, n, is at point Q, and the slipstream reflects from the reflecting surface at point P.

If one assumes that the wave configuration of a TRR is self-similar, then the entire structure shown in Fig. 4.8c grows linearly with time. Consider Fig. 4.9 where the wave configuration of a TRR is drawn at two different times, say t and $t + \Delta t$. Within the time interval Δt the points Q, P, and T^* moved to the locations marked Q' , P' , and $T^{*\prime}$. Let us define the velocity of point Q with respect to the reflection point R as u_n , and the velocity of the triple point T^* with respect to the reflection point R as dL_r/dt where L_r is the length of the reflected shock wave, r , as shown in Fig. 4.9. In addition, it is important to note that since point P is on the slipstream, s_1 , its velocity must be equal to u_3 where u_3 is the flow velocity in state (3) with respect to point R. For the reader's convenience, the velocity vectors u_n , u_3 , and dL_r/dt are added to Fig. 4.9.

As mentioned earlier, the additional shock wave, n, is not necessarily straight. However, experimental evidence indicates that its curvature is very small. Thus, if one assumes that the additional shock wave, n , is straight, then it is normal to the flow passing through it from state (2) to state (3). Thus, the conservation equations across the normal shock wave for a perfect gas are as follows:

- Conservation of mass:

$$\rho_2 (u_2 - u_n) = \rho_3 (u_3 - u_n) \quad (4.1)$$

– Conservation of linear momentum:

$$p_2 + \rho_2 (u_2 - u_n)^2 = p_3 + \rho_3 (u_3 - u_n)^3 \quad (4.2)$$

– Conservation of energy

$$\frac{\gamma}{\gamma-1} \frac{p_2}{\rho_2} + \frac{1}{2} (u_2 - u_n)^2 = \frac{\gamma}{\gamma-1} \frac{p_3}{\rho_3} + \frac{1}{2} (u_3 - u_n)^2 \quad (4.3)$$

Note that since the additional normal shock wave is moving with a velocity u_n in the frame of reference under consideration, the relative velocities $(u_2 - u_n)$ and $(u_3 - u_n)$ are used in the above conservation equations. It is also important to note that all the flow properties in state (2) could be easily calculated by solving the RR of the incident shock wave over the reflecting surface.

The above set of conservation equations consists of three equations, (4.1)–(4.3), and four unknowns, namely, u_3 , p_3 , ρ_3 , and u_n . Thus, an additional equation is required to have a closed set which can, in principle, be solved.

Consider Fig. 4.8c and note that the gas that flows from region (2) into region (3) through the normal shock wave cannot leave region (3) because region (3) is bounded by a slipstream, s_1 , and the reflecting surface. It could easily be shown that the mass of the fluid in region (3) is:

$$m_3 = \frac{1}{2} \rho_3 (L_r)^2 \frac{\sin^2 \alpha}{\tan \beta}, \quad (4.4)$$

where, L_r is the length of the reflected shock wave, r , and α and β are defined in Fig. 4.9. Differentiating (4.4) with respect to t results in the rate by which the fluid mass increases in region (3) i.e.,

$$\frac{dm_3}{dt} = \rho_3 L_r \frac{dL_r}{dt} \frac{\sin^2 \alpha}{\tan \beta}. \quad (4.5)$$

The rate by which the fluid mass increases in region (3) is equal to the rate of flow from region (2) to region (3) through the normal shock wave, n , i.e.,

$$\frac{dm_3}{dt} = \rho_2 (u_2 - u_n) L_r \sin \alpha. \quad (4.6)$$

Setting (4.5) equal to (4.6), results in:

$$\frac{dL_r}{dt} = \frac{\rho_2}{\rho_3} (u_2 - u_n) \frac{\tan \beta}{\sin \alpha}. \quad (4.7a)$$

It could easily be shown that $\alpha = \phi_2 - \theta_1$; thus, (4.7a) could be rewritten to read:

$$\frac{dL_r}{dt} = \frac{\rho_2}{\rho_3} (u_2 - u_n) \frac{\tan \beta}{\sin (\phi_2 - \theta_1)}. \quad (4.7b)$$

From simple geometrical considerations it is obvious that:

$$u_n = \frac{dL_r}{dt} \cos \alpha = \frac{dL_r}{dt} \cos (\phi_2 - \theta_1). \quad (4.8)$$

Inserting dL_r/dt from (4.8) into (4.7b) results in:

$$u_n = \frac{\rho_2}{\rho_3} (u_2 - u_n) \frac{\tan \beta}{\tan (\phi_2 - \theta_1)}. \quad (4.9)$$

Equation (4.8) can be simplified by combining it with (4.1) to result in:

$$u_n = \frac{u_3}{1 + \frac{\tan (\phi_2 - \theta_1)}{\tan \beta}}. \quad (4.10)$$

The information upon which (4.10) is based has not been used in (4.1)–(4.3), and hence it is an additional independent equation. However, it carries with it an additional unknown, β , and hence one now has a set of four equations [(4.1), (4.2), (4.3), and (4.10)] and five unknowns (u_3 , p_3 , ρ_3 , u_n , and β). Thus, there is still a need for an additional equation to have a solvable set of governing equations.

Since the wave configuration under consideration does not provide any information that can lead toward an additional independent equation, let us assume that due to the similarity between the general wave configurations of a TRR and a DMR, (see comparison in Fig. 4.10) the triple point T^* of a TRR has features similar to those of the second triple point T' of a double-Mach reflection, DMR.

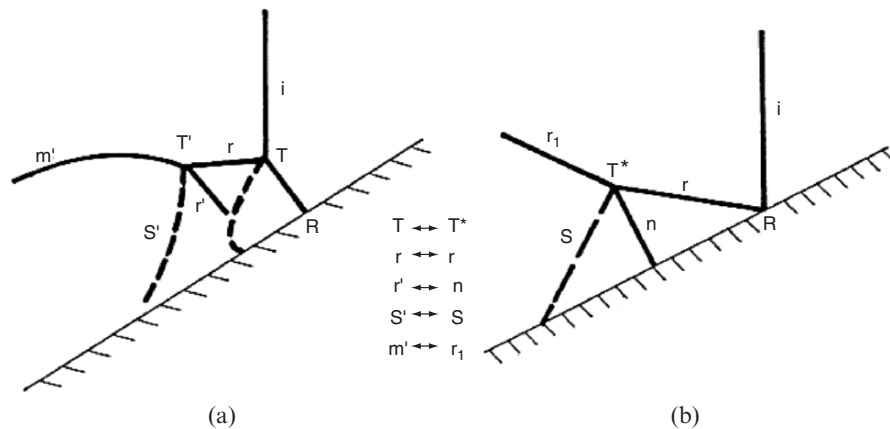


Fig. 4.10. A comparison between the wave configurations around the triple point T' of a DMR and T^* of a TRR

Once this assumption is made, we recall that while investigating the DMR, Law and Glass (1971) assumed that the second triple point of a DMR, i.e., T' , moves with a velocity identical to that induced by the incident shock wave (see Sect. 3.1.3). This assumption, known as the Law-Glass assumption, which was adopted by Ben-Dor (1980) who presented an analytical solution of a DMR, was found to be quite good for a wide range of incident shock wave Mach numbers and reflecting wedge angles. Although a physical explanation for the validity of this assumption does not exist as yet, it is hypothesized here that it should be related to the communication of a geometrical length scale to the triple points T^* or T' since both the DMR and the TRR wave configurations involve shock waves having finite lengths. Recall that Bazhenova et al. (1976) showed that the “Law-Glass” assumption was fairly good for DMRs in the range $\theta_w < 40^\circ$. Consequently, it is possible that the Law-Glass assumption is not good enough in the entire range of wedge angles where a TRR is possible. More details about the inaccuracy introduced by using the Law-Glass assumption were provided in Sects. 3.2.5 and 3.2.6.

Defining the shock induced flow velocity in state (1) in a laboratory frame of reference as V_1 and using the conservation of mass across the incident shock wave one obtains:

$$V_1 = V_S \left(1 - \frac{\rho_0}{\rho_1} \right). \quad (4.11)$$

Thus while the reflection point R moves with the velocity V_S in the x -direction, the triple point T^* moves, in the x -direction, with the velocity V_1 . Using this fact it can be shown easily that the rate at which the length of the reflected shock wave increases is:

$$\frac{dL_r}{dt} = \frac{V_S - V_1}{\cos(\alpha - \theta_w)}.$$

Inserting (4.11) into the above relation yields:

$$\frac{dL_r}{dt} = V_S \frac{\rho_0}{\rho_1} \frac{1}{\cos(\alpha - \theta_w)}$$

which together with (4.8) finally results in

$$u_n = V_S \frac{\rho_0}{\rho_1} \frac{\cos(\phi_2 - \theta_1)}{\cos(\phi_2 - \theta_1 - \theta_w)} \quad (4.12)$$

Equation (4.12) is the additional independent equation needed to have a closed set of governing equations for solving a TRR. The set of the five governing equations, (4.1), (4.2), (4.3), (4.10), and (4.12), contains five unknowns, u_3 , p_3 , ρ_3 , u_n , and β . Thus, in principle, the set of equations is solvable.

There are only a few reported experiments illustrating the wave configuration of a TRR, which is formed after an inverse-Mach reflection terminates at the reflecting wedge. Figure 31b in Ben-Dor et al. (1987) illustrates such a wave configuration that was obtained by reflecting a planar incident shock

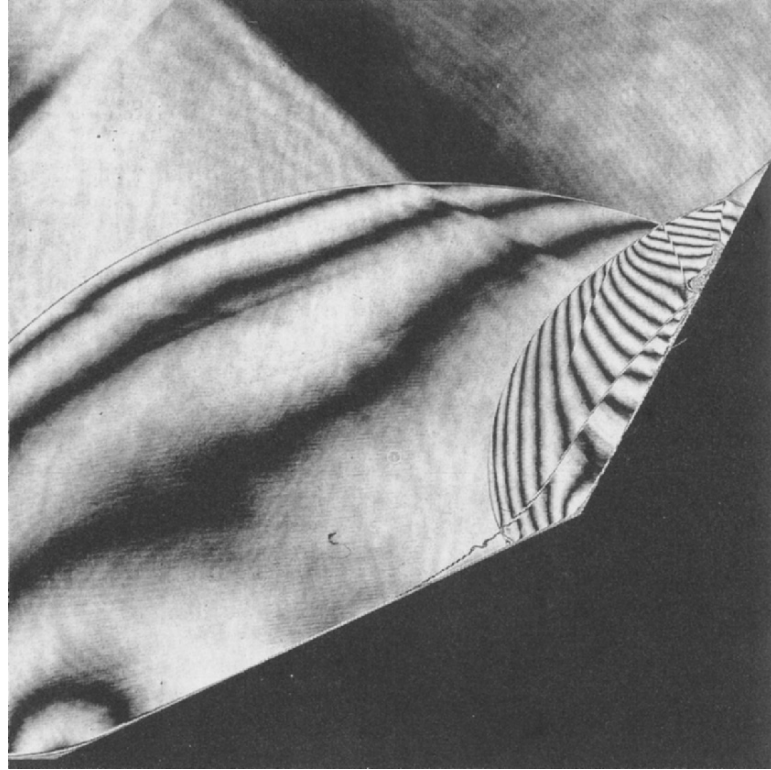


Fig. 4.11. A holographic interferogram illustrating the wave configuration of a TRR as obtained from the reflection of a planar shock wave with $M_S = 1.52$ over a double wedge with $\theta_w^1 = 25^\circ$ and $\theta_w^2 = 60^\circ$ in air at $T_0 = 290\text{ K}$ and $p_0 = 760\text{ Torr}$. (Courtesy of Professor K. Takayama, Institute of Fluid Science, Tohoku University, Sendai, Japan)

wave having a Mach number $M_S = 1.3$ over a double wedge with $\theta_w^1 = 25^\circ$ and $\theta_w^2 = 60^\circ$. The value of the angle β as measured from the photograph is 21.5° . The predicted value of β using the above described analytical model is 21.7° .

The photograph shown in Fig. 4.11 again illustrates the wave configuration of a TRR for another reflection of a planar incident shock wave over a double wedge. The initial conditions for this case were: $M_S = 1.52$, $\theta_w^1 = 25^\circ$, and $\theta_w^2 = 60^\circ$. The value of β as measured from this photograph is about 19° . The value of β as predicted by the above described model is 18.6° .

The foregoing comparison clearly indicates that the above developed model is capable of accurately predicting the wave structure of a TRR, which results following the termination of an inverse-Mach reflection. It should be noted that the fact that the just-presented analytical model provided excellent predictions of β should and could not be used as a verification of the Law-Glass assumption, which as mentioned earlier is problematic. The excellent agreement only suggests that β is probably a not too sensitive variable.

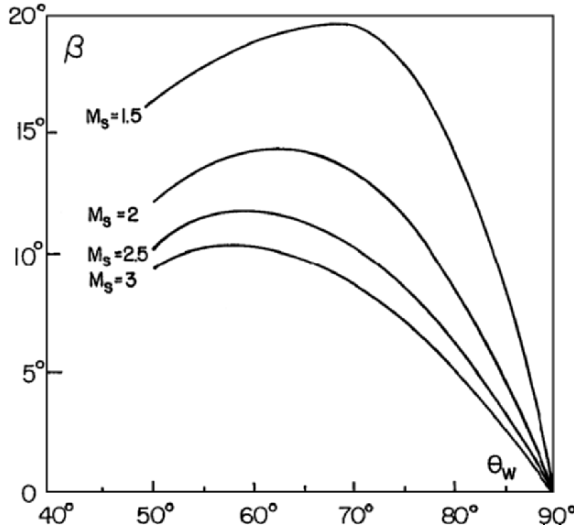


Fig. 4.12. The dependence of β on the reflecting wedge angle θ_w for various incident shock wave Mach numbers, M_s

Figure 4.12 illustrates the dependence of the angle β on the reflecting wedge angle, θ_w , for various incident shock wave Mach numbers, $M_s = 1.5, 2, 2.5$, and 3 . It is evident that the value of β increases as the incident shock wave Mach number decreases for a given reflecting wedge angle, θ_w . In addition, it can be seen that for a given incident shock wave Mach number, M_s , the value of β increases as the reflecting wedge angle θ_w is increased, until it reaches a maximum value after which β decreases and approaches 0 as θ_w approaches 90° regardless of the incident shock wave Mach number. It is seen also that the smaller is the incident shock wave Mach number, the larger is the value of the reflecting wedge angle at which β reaches its maximum. While for $M_s = 1.5$, β reaches its maximum at about $\theta_w = 68^\circ$, it reaches its maximum at about $\theta_w = 59^\circ$ for $M_s = 3$.

The dependence of the angle β on the incident shock wave Mach number, M_s , for various reflecting wedge angles, θ_w , is shown in Fig. 4.13. In general, it is seen that as the incident shock wave Mach number increases, the value of β decreases. It is also seen that as $M_s \rightarrow \infty$ the value of β asymptotically approaches a constant value. The smaller is the reflecting wedge angle, the larger is the asymptotic value approached by β .

Analytical Considerations

Although the analytical consideration of the reflection phenomenon over cylindrical concave wedges is very difficult for the reasons outlined in the introduction to this chapter, there exist some simplified analytical models predicting

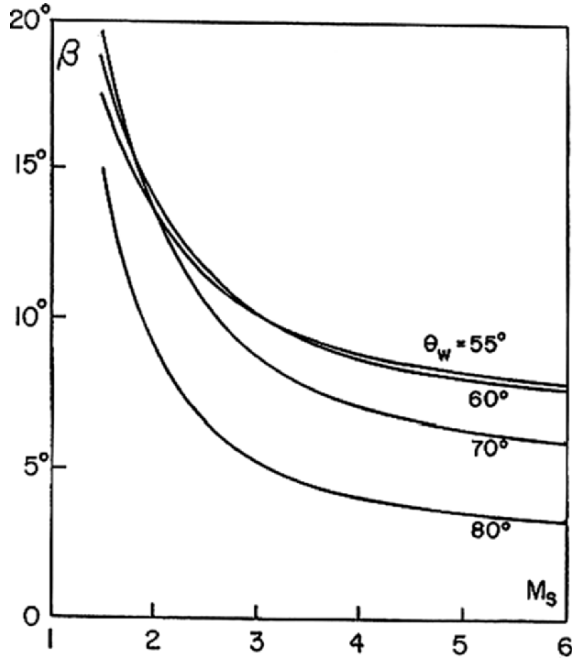


Fig. 4.13. The dependence of β on the incident shock wave Mach number, M_s , for various reflecting wedge angles, θ_w

the MR \rightarrow TRR transition, and some other aspects related to the reflection phenomenon. Unfortunately, however, these simplified analytical models are limited to relatively weak incident shock waves.

Analytical Prediction of the MR \rightarrow TRR Transition

The first approach to predict analytically the MR \rightarrow TRR transition over cylindrical concave wedges was presented by Ben-Dor and Takayama (1985). Their analysis was based on the length-scale concept of Hornung et al. (1979) that was presented in Sect. 1.5.4. Predictions based on this concept were found to the correct transition criteria in steady and in pseudosteady flows. The length scale criterion implies that an MR cannot exist unless a physical length scale is communicated to its triple point.

Figure 4.14 illustrates an MR over a cylindrical concave wedge prior to its transition that occurs when its triple point T reaches point R. Since the transition occurs at a point beyond which an MR cannot exist, one must conclude that based on the length scale concept an MR with a triple point in the vicinity of point R (just before transition) represents the last time the corner-generated signals can catch-up with the triple point. Upon a further propagation of the incident shock wave, i , an MR will become impossible. The actual reflection, which is formed after the termination of the MR (shown in Fig. 4.2c), is a

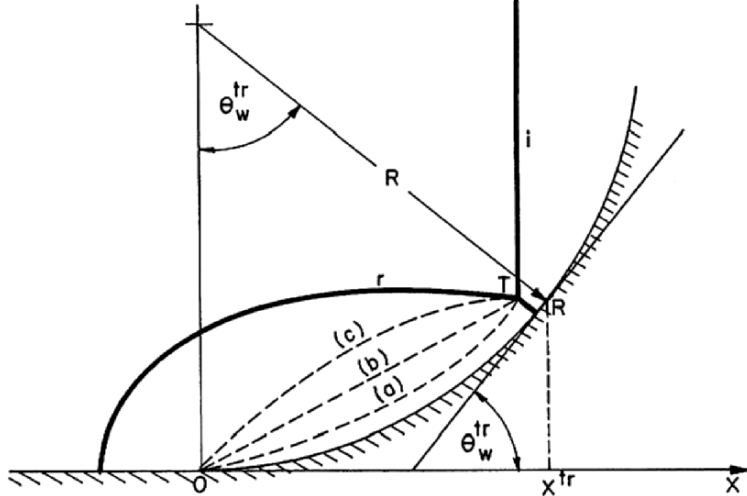


Fig. 4.14. Illustration of an MR over a cylindrical concave wedge just before transition

TRR (shown in Fig. 4.2d). In a TRR the incident shock wave reflects from the reflecting surface as an RR, and a triple point is formed along the reflected shock wave of the RR. A short shock wave, which emanates from this triple point, terminates perpendicularly on the reflecting surface. The triple point probably indicates the position reached by the corner-generated signals. The corner-generated signals cannot precede the additional shock wave. Thus, the reflected point, R, of the RR is isolated from the corner-generated signals by a supersonic flow region. Let us assume that the signals, which are generated at the leading edge of the reflecting wedge (point 0), move with a velocity $V + a$ where V is the flow velocity and a is the local speed of sound. In general, $V + a$ changes inside the flow field. If Δt is the time required for the incident shock wave to travel from $x = 0$ to $x = x^{\text{tr}}$, where x^{tr} is the point along the x -axis where the corner-generated signals have caught-up with the triple point for the last time, then the corner generated signals have propagated during this time interval a distance of

$$S = \int_0^{\Delta t} (V + a) dt. \quad (4.13)$$

Since the variation of $V + a$ inside the flow field is unknown, the integration on the right hand side of equation (4.13) cannot be carried out. However, inspecting a typical MR over a concave wedge (see e.g., Fig. 4.2a) indicates that, as the reflected shock wave approaches the surface, it becomes very weak. This, in turn, implies that the flow properties do not change significantly while passing through the reflected shock wave. Consequently, they can be assumed to retain their prereflected shock values (i.e., the values behind the incident

shock wave). Therefore, it can be assumed that

$$V + a = V_1 + a_1, \quad (4.14)$$

where V_1 and a_1 are the flow velocity and the local speed of sound behind the incident shock wave, respectively. Using this assumption, the integration on the right hand side of equation (4.13) can be easily carried out to result in

$$S = (V_1 + a_1) \Delta t. \quad (4.15)$$

Unfortunately, the exact path of the corner-generated signals is also unknown. Consequently, the value of S in (4.15) is unknown.

In the following, two possible propagation paths will be examined. The first path is along the reflecting surface and the second path is along a straight line connecting the leading edge of the reflecting wedge (point O in Fig. 4.14) and the triple point, T, when it coincides with the reflection point R (i.e., exactly at transition). These two propagation paths are shown in Fig. 4.14 as lines (a) and (b), respectively. It should be noted again that the actual propagation path need not be either of these two suggested propagation paths. It could be any path connecting the leading edge of the reflecting wedge and the triple point, e.g., line (c) in Fig. 4.14. In the following, two such paths will be examined.

Case A: *The propagation path is assumed to be along the reflecting surface*
This assumption implies that:

$$S = R\theta_w^{\text{tr}}, \quad (4.16)$$

where θ_w^{tr} is the reflecting wedge angle at the point where the MR \rightarrow TRR transition takes place, and R is the radius of curvature of the cylindrical concave wedge. Combining (4.15) and (4.16) results in:

$$R\theta_w^{\text{tr}} = (V_1 + a_1) \Delta t. \quad (4.17)$$

However, $\Delta t = x^{\text{tr}}/V_S$ where V_S is the velocity of the incident shock wave. Thus, (4.17) could be rewritten as:

$$R\theta_w^{\text{tr}} = (V_1 + a_1) \frac{x^{\text{tr}}}{V_S}. \quad (4.18)$$

From Fig. 4.14 it is clear that:

$$x^{\text{tr}} = R \sin \theta_w^{\text{tr}} \quad (4.19)$$

Combining (4.18) and (4.19) yields:

$$\frac{\sin \theta_w^{\text{tr}}}{\theta_w^{\text{tr}}} = \frac{V_S}{V_1 + a_1}. \quad (4.20)$$

Dividing both the numerator and the denominator on the right-hand side of (4.20) by the local speed of sound ahead of the incident shock wave, a_0 , finally results in:

$$\frac{\sin \theta_w^{\text{tr}}}{\theta_w^{\text{tr}}} = \frac{M_S}{V_{10} + A_{10}}, \quad (4.21)$$

where M_S is the incident shock wave Mach number, $V_{10} = V_1/a_0$ and $A_{10} = a_1/a_0$. For a perfect gas both V_{10} and A_{10} depend solely on M_S through (3.71) and (3.72).

Case B: *The propagation path is assumed to be the shortest path (straight line) connecting the leading edge of the reflecting wedge and the triple point.* The above assumption together with the assumption that the height of the Mach stem, H_m , is much shorter than the radius of curvature of the reflecting wedge, i.e., $H_m \ll R$, imply that (see Fig. 4.14):

$$\frac{S}{2} = R \sin \frac{\theta_w^{\text{tr}}}{2}. \quad (4.22)$$

Inserting S from (4.22) and x^{tr} from (4.19) into (4.15) results in:

$$\cos \frac{\theta_w^{\text{tr}}}{2} = \frac{V_S}{V_1 + a_1}. \quad (4.23)$$

Nondimensionalizing the velocities on the right-hand side of equation (4.23) by the local speed of sound ahead of the incident shock wave, a_0 , yields:

$$\cos \frac{\theta_w^{\text{tr}}}{2} = \frac{M_S}{V_{10} + A_{10}}, \quad (4.24)$$

where M_S is the incident shock wave Mach number, $V_{10} = V_1/a_0$ and $A_{10} = a_1/a_0$. For a perfect gas both V_{10} and A_{10} depend solely on M_S through (3.71) and (3.72).

Experimental results of the transition wedge angle for $R = 50$ mm and $\theta_w^{\text{initial}} = 0$ are presented in Fig. 4.15 with the transition lines as obtained from the transition formulae given by (4.21) and (4.24).

Lines AB and AC are the RR \rightleftharpoons MR transition lines in steady and pseudosteady flows, respectively. Lines D and E are the transition lines as predicted by (4.21) and (4.24), respectively. Line F will be referred to subsequently. As can be seen, the agreement between the experiments and the transition line predicted by (4.21), line D, is quite good in the range $1.125 < M_S < 4$. (The upper limit arises from the lack of experimental results for larger incident shock wave Mach numbers.) At the smaller Mach number range, $1 < M_S < 1.125$, the agreement between line D and the experiments is very poor (see the three experiments marked with an arrow which lie 4.5° – 7.5° above line D). The transition line predicted by (4.24), line E, shows excellent agreement with these three experimental points only, i.e., it is good in the range $1 < M_S < 1.125$. Outside this narrow range, the analytical predictions based on (4.24) are 10° – 15° larger than those obtained experimentally.

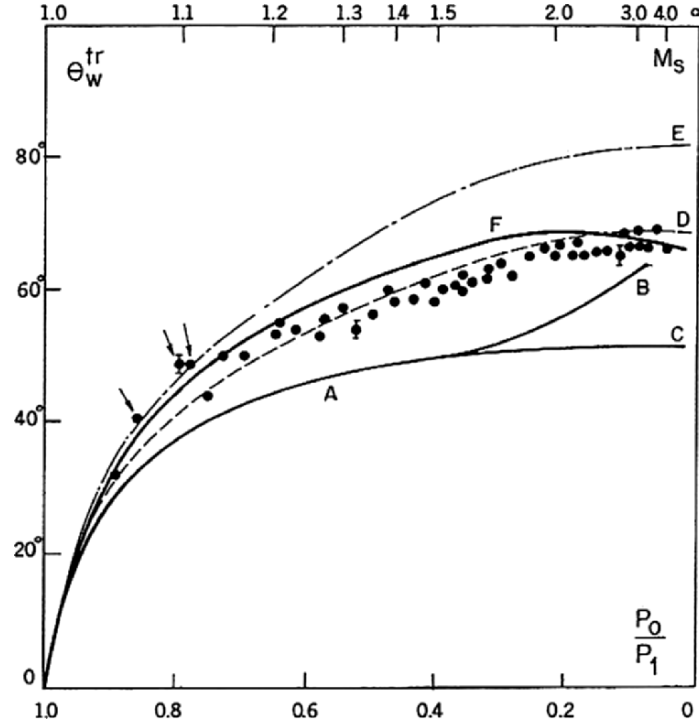


Fig. 4.15. Experimental results of the transition wedge angle over a cylindrical concave surface with $R = 50$ mm and $\theta_w^{\text{initial}} = 0$ with different analytical transition lines

In order to improve the analytical prediction of the MR \rightleftharpoons TRR transition over cylindrical concave wedges the foregoing two analytical approaches of Takayama and Ben-Dor (1985) were reconsidered, and an additional analytical approach was put forward by Takayama and Ben-Dor (1989).

Consider Fig. 4.16 where an MR is illustrated exactly at its transition. Let us assume that a gas particle that propagated along the cylindrical wedge and reached an angular position, θ , generated a disturbance, which propagated with the local speed of sound, a , and reached a circle having radius, r . Thus, the distance to which the corner-generated signals propagated can be obtained by a vector summation of the particle path, l , and the disturbance path, r , as shown by the dashed line in Fig. 4.16. Unlike the previous assumption that $V + a = V_1 + a_1$ let us assume that $V = V_1$ and $a = a_1$. Using these simplifying assumptions one can write

$$l = R\theta = V_1 \Delta t \quad (4.25)$$

$$r = a_1 \Delta t \quad (4.26)$$

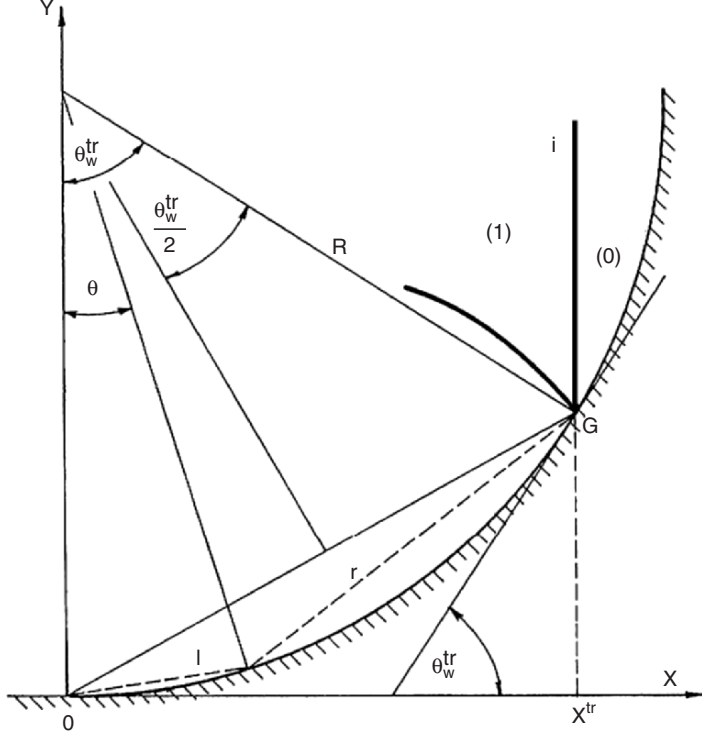


Fig. 4.16. A Mach reflection over a cylindrical concave surface exactly at transition

From Fig. 4.16 it is clear that:

$$(R \sin \theta_w^{\text{tr}} - R \sin \theta)^2 + (R \cos \theta - R \cos \theta_w^{\text{tr}})^2 = r^2. \quad (4.27)$$

Inserting (4.26) into (4.27) results in:

$$(\sin \theta_w^{\text{tr}} - \sin \theta)^2 + (\cos \theta - \cos \theta_w^{\text{tr}})^2 = \left(\frac{a_1 \Delta t}{R} \right)^2. \quad (4.28)$$

From (4.25) we have

$$\theta = \frac{V_1 \Delta t}{R}. \quad (4.29)$$

Using the incident shock wave velocity, V_S , one can write:

$$\cos \theta_w^{\text{tr}} = \frac{V_S \Delta t}{R}. \quad (4.30)$$

Inserting (4.29) into (4.28) and (4.30), while eliminating $\frac{\Delta t}{R}$ yields:

$$\theta = \frac{V_1}{V_S} \sin \theta_w^{\text{tr}} \quad (4.31)$$

and

$$\frac{2 - 2 \cos(\theta_w^{\text{tr}} - \theta)}{\sin^2 \theta_w^{\text{tr}}} = \left(\frac{a_1}{V_S} \right)^2 \quad (4.32)$$

Nondimensionalizing the velocities on the right-hand side of (4.31) and (4.32) by the local speed of sound ahead of the incident shock wave, a_0 , and simplifying (4.32) by using well-known trigonometric relations, finally results in

$$\theta = \frac{V_{10}}{M_S} \sin \theta_w^{\text{tr}} \quad (4.33)$$

and

$$\frac{2 \sin \frac{\theta_w^{\text{tr}} - \theta}{2}}{\sin \theta_w^{\text{tr}}} = \frac{A_{10}}{M_S}, \quad (4.34)$$

which for a given incident shock wave Mach number, M_S , can be solved iteratively to obtain θ_w^{tr} and θ . The transition line as predicted by (4.33) and (4.34) is shown in Fig. 4.15 as curve F. Unlike the previous transition lines, D and E, which were good only at $M_S > 1.125$ and $M_S < 1.125$, respectively, and very poor beyond these ranges, line F shows, in general, fairly good agreement with the experiments in the entire range of M_S . In the range $1 < M_S < 1.125$ it lies slightly below line E and shows good agreement with the experiments marked with arrows. In the range $1.125 < M_S < 2$ line F is about 5° too high while for $2 < M_S < 4$ the agreement becomes good again. Note that in the range $1.125 < M_S < 2$ the predictions of line D are better than those of line F, but as mentioned earlier, in the lower Mach number regime the predictions of line D are very poor.

Unfortunately, the foregoing three models for predicting the analytical MR \Leftrightarrow TRR transition, which are all based on the length-scale concept, are independent of the radius of curvature of the reflecting wedge, R , and the initial angle of the cylindrical reflecting wedge, $\theta_w^{\text{initial}}$, which as shown in Fig. 4.3, do affect the actual MR \rightarrow TRR transition.

An approach partially overcoming these problems was suggested by Ben-Dor and Takayama (1985) who included the initial wedge angle in the transition criterion given by (4.21) to obtain

$$\frac{\sin \theta_w^{\text{tr}} - \sin \theta_w^{\text{initial}}}{\theta_w^{\text{tr}} - \theta_w^{\text{initial}}} = \frac{M_S}{V_{10} + A_{10}}. \quad (4.35)$$

The transition lines as predicted by (4.35) are compared with the experimental results of Itoh and Itaya (1980) in Fig. 4.17. The transition lines as predicted by (4.35) exhibit the same trend as the experiments. However, the agreement between the transition lines for a given value of $\theta_w^{\text{initial}}$ becomes poorer as $\theta_w^{\text{initial}}$ increases. This is probably because the larger is $\theta_w^{\text{initial}}$, the poorer is the assumption that $V + a = V_1 + a_1$. This indeed should be the case since when $\theta_w^{\text{initial}} > 0$ the reflected shock wave can no longer be assumed to be weak in the vicinity of the leading edge of the reflecting wedge.

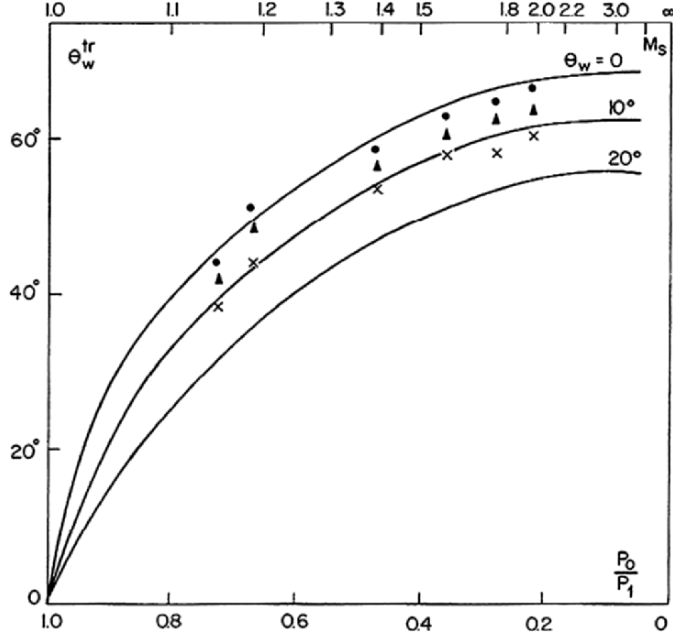


Fig. 4.17. Comparison between the measured transition wedge angles over a cylindrical concave surface with different wedge angles and a simplified analytical transition criterion. (Data are for nitrogen)

When the initial wedge angle is included in (4.24) it becomes:

$$\frac{\sin \theta_w^{tr} - \sin \theta_w^{\text{initial}}}{\sin \frac{1}{2} (\theta_w^{tr} - \theta_w^{\text{initial}})} = 2 \frac{M_s}{V_{10} + A_{10}}. \quad (4.36)$$

Another analytical approach for calculating the transition wedge angle, \$\theta_w^{tr}\$, which accounts for the radius of curvature of the reflecting cylindrical wedge, was suggested by Ben-Dor and Takayama (1986/7). Unfortunately, the suggested model is not complete, for it requires further information regarding the reflection.

Consider Fig. 4.18 where two wave configurations of an MR over a concave cylindrical wedge are drawn. For the sake of simplicity, only the incident and the Mach stem shock waves are shown. When the triple point is at point A, the length of the Mach stem is \$H_m\$. During the time interval, \$\Delta t\$, the triple point moved to point B, and the length of the Mach stem decreases to \$H_m - \Delta H_m\$.

From simple geometry one can write:

$$\overline{AB} = \frac{V_s \Delta t}{\sin \phi_1}, \quad (4.37)$$

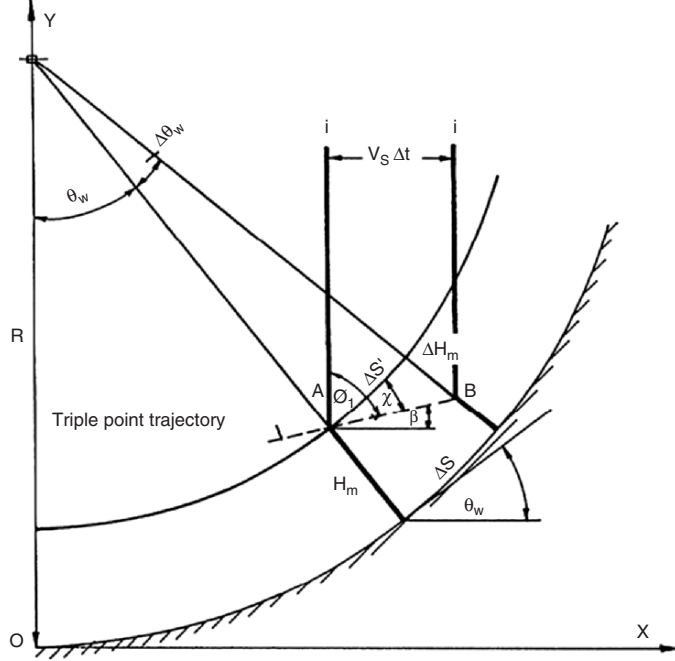


Fig. 4.18. Schematic illustration of the wave configuration of an MR over a cylindrical concave surface at two different times

where ϕ_1 is the angle of incidence between the incident shock wave, i, and the oncoming flow, as measured from a frame of reference attached to the triple point when it is at point A. In addition,

$$\frac{\Delta S'}{\overline{AB}} \approx \cos \chi, \quad (4.38)$$

where χ is the effective triple point trajectory angle. Combining (4.37) and (4.38) results in

$$\frac{\Delta S' \sin \phi_1}{V_s \Delta t} \approx \cos \chi. \quad (4.39)$$

However, it is evident from Fig. 4.18 that:

$$\theta_w - \chi = 90^\circ - \phi_1. \quad (4.40)$$

Consequently, (4.39) becomes

$$\frac{V_s \Delta t}{\Delta S'} \cos \chi \approx \cos (\theta_w - \chi). \quad (4.41)$$

From simple geometry $\Delta S' = (R - H_m) \Delta \theta_w$ and $\Delta S = R \Delta \theta_w$ thus,

$$\frac{\Delta S'}{\Delta S} = \left(1 - \frac{H_m}{R} \right). \quad (4.42)$$

Combining (4.41) and (4.42) results in

$$\frac{V_S \Delta t}{\Delta S} \cos \chi \approx \left(1 - \frac{H_m}{R}\right) \cos(\theta_w - \chi)$$

or alternatively:

$$\frac{V_S \Delta t}{R \Delta \theta_w} \cos \chi \approx \left(1 - \frac{H_m}{R}\right) \cos(\theta_w - \chi)$$

Under the requirement $\Delta t \rightarrow 0$ one obtains:

$$\frac{d\theta_w}{dt} \approx \frac{V_S}{R} \frac{\cos \chi}{\left(1 - \frac{H_m}{R}\right) \cos(\theta_w - \chi)}. \quad (4.43)$$

Equation (4.43) gives the rate of change of the wedge angle as the shock wave reflection sweeps it. Defining the transition wedge angle as, θ_w^{tr} , and recalling that at transition $H_m = 0$ yields:

$$\frac{d\theta_w^{tr}}{dt} \approx \frac{V_S}{R} \frac{\cos \chi}{\cos(\theta_w^{tr} - \chi)}. \quad (4.44)$$

If (4.44) could be integrated, i.e., if $\chi(t)$ was known, a relation of the form $\theta_w^{tr}(V_S, R, t)$ could be obtained. This relation could then be used to calculate the transition wedge angle, θ_w^{tr} , for a given incident shock wave Mach number, M_S , and a radius of curvature of the cylindrical reflecting surface, R . Unfortunately, however, $\chi(t)$ is as yet unknown, and hence (4.44) cannot be further used to analytically calculate θ_w^{tr} .

However, as is shown subsequently, (4.44) provides important information regarding the behavior of the triple point trajectory as the MR \rightarrow TRR transition is approached. In order to deduce this information, let us first obtain another expression for $d\theta_w^{tr}/dt$, from the geometrical relation describing the cylindrical reflecting surface, i.e.,

$$x^2 + (y - R)^2 = R^2. \quad (4.45)$$

Differentiating this relation results in

$$\frac{dy}{dx} = \frac{x}{R - y}. \quad (4.46)$$

Inserting y from (4.45) into (4.46) results in

$$\frac{dy}{dx} = \left[\left(\frac{R}{x} \right)^2 - 1 \right]^{-1/2}. \quad (4.47)$$

But $\theta_w = \tan^{-1} \frac{dy}{dx}$, and hence,

$$\theta_w = \tan^{-1} \left[\left(\frac{R}{x} \right)^2 - 1 \right]^{-1/2}. \quad (4.48)$$

Differentiating (4.48) by t , yields:

$$\frac{d\theta_w}{dt} = \tan^{-1} \left[\left(\frac{R}{x} \right)^2 - 1 \right]^{-1/2} \frac{1}{x} \frac{dx}{dt}. \quad (4.49)$$

However, at the transition point $V_S = dx/dt$ and $x/R = \sin \theta_w^{\text{tr}}$. Therefore, (4.49) assumes at transition the form:

$$\frac{d\theta_w^{\text{tr}}}{dt} = \tan^{-1} \left[\left(\frac{1}{\sin \theta_w^{\text{tr}}} \right)^2 - 1 \right]^{-1/2} \frac{1}{\sin \theta_w^{\text{tr}}} \frac{V_S}{R}. \quad (4.50)$$

Comparing (4.44) and (4.50) results in:

$$\frac{\cos \chi}{\cos(\theta_w^{\text{tr}} - \chi)} = \left[\left(\frac{1}{\sin \theta_w^{\text{tr}}} \right)^2 - 1 \right] \frac{1}{\sin \theta_w^{\text{tr}}}$$

This relation can be further simplified to obtain:

$$\sin \theta_w^{\text{tr}} \sin \chi = 0. \quad (4.51)$$

Since $\theta_w^{\text{tr}} \neq 0$, (4.51) implies that $\sin \chi = 0$ at the moment of transition. This condition suggests that at the MR \rightarrow TRR transition:

$$\chi = 0. \quad (4.52)$$

This result, which was obtained purely from analytical considerations, is fully supported by experimental results. Consider Fig. 4.6 where the experimentally measured triple point trajectory of an MR over a cylindrical concave surface is shown. It is evident that as the triple point approaches the MR \rightarrow TRR transition point the triple point trajectory angle $\chi \rightarrow 0$.

Triple Point Trajectory for Weak Incident Shock Waves

Using the assumptions of the model by which (4.33) and (4.34) were developed, Ben-Dor et al. (1987) developed an analytical model for predicting the triple point trajectory for relatively weak incident shock waves.

If the location of the triple point is denoted by x_T and y_T , measured from the leading edge of the reflecting cylindrical wedge, then

$$x_T = \frac{M_S}{V_{10}} R \theta \quad (4.53)$$

and

$$y_T = R\theta \left[\frac{1}{M_1^2} - \left(\frac{M_S}{V_{10}} - \frac{\sin \theta}{\theta} \right)^2 \right]^{1/2} + R(1 - \cos \theta), \quad (4.54a)$$

which for small values of θ adopts the form

$$y_T = R\theta \left[\frac{1}{M_1^2} - \left(\frac{M_S}{V_{10}} - 1 \right)^2 \right]^{1/2}, \quad (4.54b)$$

where $M_S = V_S/a_0$, $M_1 = V_1/a_1$, $V_{10} = V_1/a_0$, R is the radius of curvature, V_S is the incident shock wave velocity, V_1 the shock induced flow velocity, a_0 and a_1 are the local speeds of sound ahead of and behind the incident shock wave, and θ is the angular position of the flow particles, which were initially at $x = 0$, as shown in Fig. 4.16. The triple point trajectory angle, χ , can thus be calculated from

$$\chi = \tan^{-1} \frac{dy_T}{dx_T}. \quad (4.55)$$

Inserting (4.53) and (4.54) into (4.55) yields:

$$\chi = \tan^{-1} \left\{ \frac{1}{M_S} \left[A_{10}^2 - (M_S - V_{10})^2 \right]^{1/2} + \frac{V_{10}}{M_S} \theta \right\}. \quad (4.56)$$

The triple point trajectory angle at glancing incidence, χ_g , can be obtained from (4.56) by calculating $\chi_g = \lim_{\theta \rightarrow 0} \chi$. This yields:

$$\chi_g = \tan^{-1} \left\{ \frac{1}{M_S} \left[A_{10}^2 - (M_S - V_{10})^2 \right]^{1/2} \right\}. \quad (4.57)$$

The values of χ_g vs. M_S is shown in Fig. 4.19. The angular position of the triple point, θ_T , can simply be obtained from:

$$\theta_T = \tan^{-1} \left(\frac{x_T}{R - y_T} \right). \quad (4.58)$$

The triple point trajectories for $M_S = 1.01, 1.05, 1.10, 1.15$, and 1.2 over a cylindrical concave wedge with $R = 15$ cm are shown in Fig. 4.20. As can be seen, the predicted triple point trajectories are close to being straight lines. This should indeed be the case, since for small values of M_S , the value of θ is less than 10° (see Table 4.2) and its influence in (4.56) is negligible.

The values of χ_g , χ_{tr} , and θ_w^{tr} for different values of M_S in the range $1 < M_S \leq 1.15$ are given in Table 4.1. The values of θ_T and χ vs. θ for $M_S = 1.15$ (last line in Table 4.1) are given in Table 4.2. Plotting these results shows that there is an almost perfect linear relationship between χ

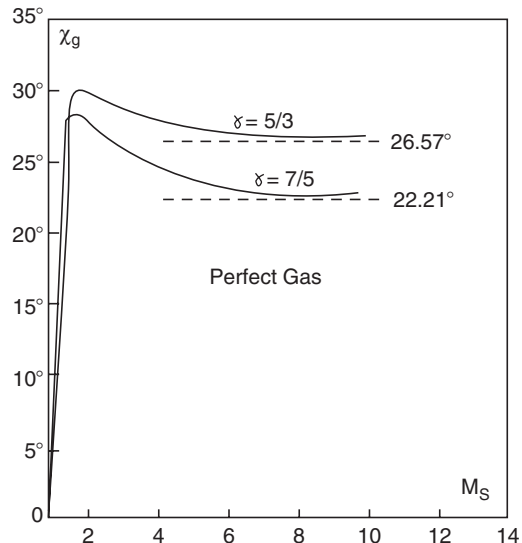


Fig. 4.19. Variation of the triple point trajectory angle at glancing incidence with the incident shock wave Mach number

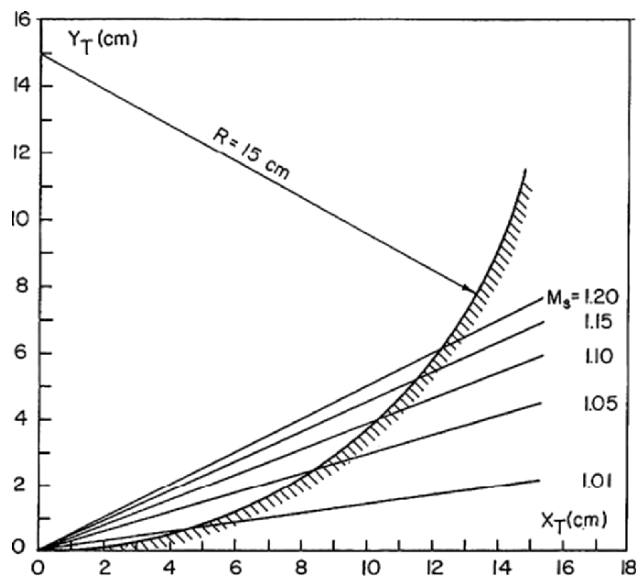


Fig. 4.20. Analytical prediction of the triple point trajectories of MR with different incident shock wave Mach numbers over a cylindrical concave surface

Table 4.1. The triple point trajectory angles at glancing incidence, χ_g , and at transition, χ_{tr} , and values of θ_w^{tr} for incident shock wave Mach numbers in the range $1 < M_S \leq 1.15$

M_S	χ_g	χ_{tr}	$\Delta\chi$	θ_w^{tr}
1.00	—	—	—	—
1.01	7.92	7.93	0.01	15.89
1.02	10.97	10.99	0.02	21.95
1.03	13.16	13.21	0.05	26.37
1.04	14.89	15.00	0.11	29.88
1.05	16.32	16.49	0.17	32.81
1.06	17.54	17.79	0.25	35.32
1.07	18.60	18.94	0.34	37.52
1.08	19.52	19.98	0.46	39.47
1.09	20.34	20.92	0.58	41.22
1.10	21.07	21.78	0.71	42.80
1.11	21.73	22.57	0.84	44.24
1.12	22.32	23.31	0.99	45.55
1.13	22.86	24.00	1.14	46.76
1.14	23.34	24.65	1.31	47.88
1.15	23.79	25.26	1.47	48.92

Details of θ vs. θ_T for $M_S = 1.15$ (last line) are given in Table 4.2

Table 4.2. Comparison between the triple point trajectory angle as calculated from the simplified theory and the empirical relation for $M_S = 1.15$

θ	θ_T	χ (theoretical) (4.56)	χ (empirical) (4.59)
0	0	23.788	23.790
1	5.101	23.957	23.943
2	10.535	24.127	24.107
3	16.231	24.296	24.279
4	22.096	24.465	24.454
5	28.016	24.633	24.631
6	33.871	24.800	24.808
7	39.548	24.968	24.978
8	44.953	25.134	25.141
8.777	48.920	25.264	25.260

and θ_T . Hence, following empirical relation is self-explanatory:

$$\chi = \frac{\chi_{tr} - \chi_g}{\theta_w^{tr}} \theta_T + \chi_g. \quad (4.59)$$

The values of χ as calculated from the empirical relation (4.59) are also added to Table 4.2 for comparison with the value of χ as calculated from the analytical equation (4.56). It is clear that the differences are insignificant.

A comparison of the analytical predictions of the triple point location [(4.53) and (4.54)] and the experimental results for two incident shock wave Mach numbers are shown in Fig. 4.21. The squares represent the triple point

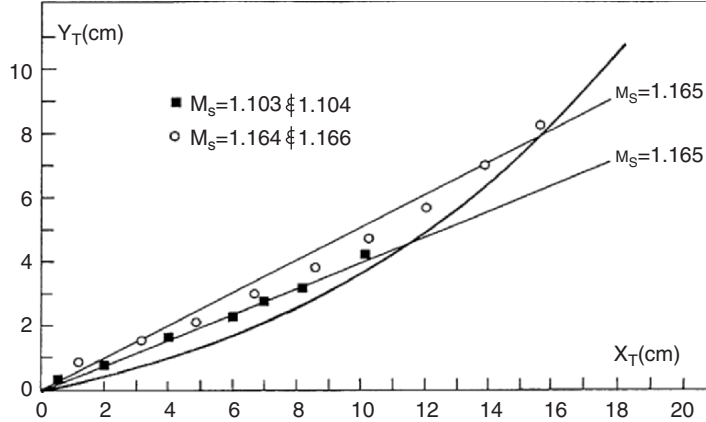


Fig. 4.21. Comparison between the measured triple point locations and the analytical predictions for $M_S = 1.1035$ and 1.165 (Data are for air)

locations for $M_S = 1.103$ and 1.104 and the circles are for $M_S = 1.164$ and 1.166 . The solid lines are the results of the analytical calculations for $M_S = 1.1035$ and 1.165 . In the case of $M_S = 1.1035$ the recorded locations of the triple point lie almost on a straight line which excellently agrees with the analytical calculations. However, for the higher incident shock wave Mach number $M_S = 1.165$, the experimentally measured triple point trajectory is no longer a straight line and it is seen to approach the wedge at a glancing angle. Thus it can be concluded that the analytical model presented in this section is probably good only for $M_S < 1.10$. In the range $M_S > 1.16$ the predictions of the model are not good enough. In order to determine accurately the upper limit of the incident shock wave Mach number for which the model presented in this section is valid, more experiments are needed in the range $1.10 < M_S < 1.161$.

Application of Steady Shock Polars to Unsteady Flows

In order to better understand the phenomenon of shock wave reflection in unsteady flows Ben-Dor and Takayama (1986) suggested dividing the unsteady flow into a sequence of momentarily pseudosteady states and thereby using the (p, θ) -shock polars. It is of interest to note that Marconi (1983) used shock polars in his study of the MR \rightleftharpoons RR transition in three-dimensional steady flows. The third dimension in his study might be considered similar to the additional time dimension in the two-dimensional unsteady flows.

A multishock polar diagram is shown in Fig. 4.7. When the incident shock wave propagates along the reflecting wedge, its Mach number remains constant. However, the complementary wedge angle of ϕ_1 , θ_w^C (i.e., $\theta_w^C = 90^\circ - \phi_1$) increases and hence the oncoming flow Mach number, M_0 , with respect to the triple point increases. Thus, for a given location of the incident shock wave

along the cylindrical concave surface, the momentary value of M_0 could be calculated, and the corresponding momentary pseudosteady shock polar could be drawn.

Three combinations of the I-R shock polars are shown in Fig. 4.7. Since the incident shock wave moves with a constant velocity, the pressure jump across it remains constant. Therefore, all the R-polars emanate from their corresponding I-polars at the same pressure. Figure 4.7 shows a DiMR at a point “a” (the I_1 - and R_1 -polars intersect on the right branch of the I_1 -polar), an StMR at point “b” (the I_2 - and R_2 -polars intersect on the p -axis), and an InMR reflection at point “c” (the I_3 - and R_3 -polars intersect on the left branch of the I_3 -polar) and finally an RR at point “d” (where the R_3 -polar intersects the p -axis). Consequently, the multishock polar suggests that the reflection goes through the following sequence of events; a DiMR from point “a” along the dashed line up to point “b” where a momentary StMR is obtained. The momentary StMR changes immediately into an InMR. The InMR is maintained along the dashed line between points “b” and “c”. When the InMR reaches point “c” the InMR suddenly transitions to an RR at point “d”.

Note that the multishock polar diagram suggests that when the InMR terminates at point “c” and an RR forms at point “d” the pressure drops from p_c to p_d . According to Henderson and Lozzi (1975) “if a pressure discontinuity occurs during transition then an unsteady wave of finite amplitude or a finite amplitude band of waves will be generated in the flow.” Therefore, based on the shock polars shown in Fig. 4.7, one might expect that since the InMR → RR transition is associated with a sudden pressure drop, the RR, behind which the pressure is lower, should be followed by either a compression wave or a shock wave, which should support the sudden drop in the pressure.

As shown in Sect. 4.1.1.2 the RR, which is formed after an InMR terminates, is followed by an additional shock wave structure. The overall wave configuration (the RR including the additional shock wave structure) was termed transitioned-regular reflection – TRR.

The fact that this additional shock wave does actually appear when an InMR terminates to form a TRR might serve as a justification for using steady shock polars for better understanding the reflection phenomena in unsteady flows as well as for explanatory purposes.

4.1.2 Shock Wave Reflections Over Cylindrical Convex Surfaces

When a planar incident shock wave encounters a cylindrical convex surface it reflects over it either as an RR or as an MR depending upon the initial wedge angle and the incident shock wave Mach number. The initial type of reflection can be determined in a way similar to that presented in Sect. 4.1.1.

Consider Fig. 4.22 where four different cylindrical convex wedges are drawn. While they all have the same radius of curvature, R , their initial wedge angles are different. The initial wedge angles are:

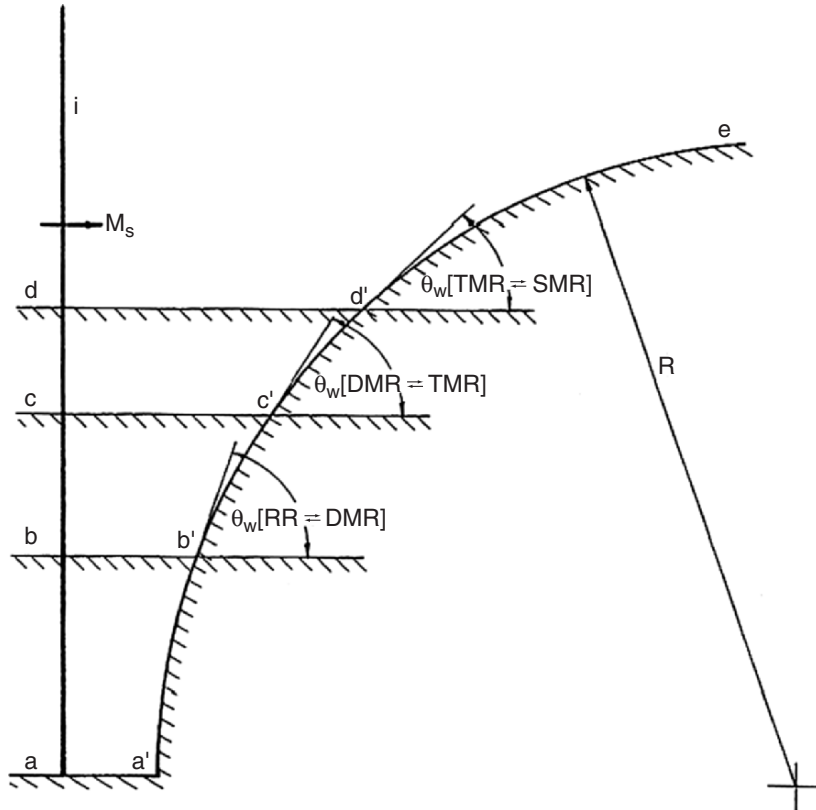


Fig. 4.22. Schematic illustration of four different cylindrical convex surfaces over which different reflection processes are obtained

1. $\theta_w = 90^\circ$ for the wedge aa'e
2. $\theta_w [RR \rightleftharpoons DMR]$ for the wedge bb'e
3. $\theta_w [DMR \rightleftharpoons TMR]$ for the wedge cc'e
4. $\theta_w [TMR \rightleftharpoons SMR]$ for the wedge dd'e

Thus for all the cylindrical wedges with an initial wedge angle, $\theta_w^{\text{initial}}$, in the range:

1. $\theta_w [RR \rightleftharpoons DMR] < \theta_w^{\text{initial}} < 90^\circ$ the initial reflection will be an RR
2. $\theta_w [DMR \rightleftharpoons TMR] < \theta_w^{\text{initial}} < \theta_w [RR \rightleftharpoons DMR]$ the initial reflection will be a DMR
3. $\theta_w [TMR \rightleftharpoons SMR] < \theta_w^{\text{initial}} < \theta_w [DMR \rightleftharpoons TMR]$ the initial reflection will be a TMR
4. $\theta_w^{\text{initial}} < \theta_w [TMR \rightleftharpoons SMR]$ the initial reflection will be an SMR

If the initial reflection is an RR (i.e., $\theta_w [RR \rightleftharpoons DMR] < \theta_w^{\text{initial}} < 90^\circ$) then as the incident shock wave propagates along the cylindrical concave wedge

it encounters an ever decreasing wedge angle, which will eventually force the RR to change into an MR. If, however, the initial reflection is an MR (i.e., $0 < \theta_w^{\text{initial}} < \theta_w$ [RR \rightleftharpoons DMR]) then the MR will persist.

The foregoing discussion implies that the initial reflection over a cylindrical convex wedge can be an RR, a DMR, a TMR, or an SMR depending upon the initial wedge angle (provided the incident shock wave Mach number is high enough).

1. If it is an RR, then it will change first to a DMR, then to a TMR and finally to an SMR
2. If the initial reflection is a DMR then it will first change to a TMR and then to an SMR
3. If the initial reflection is a TMR it will change to an SMR
4. If the initial reflection is an SMR it will remain an SMR

Shadowgraphs of an RR, a DMR, a TMR, and an SMR over cylindrical concave surfaces are shown in Fig. 4.23a–d, respectively.

RR \rightarrow MR Transition

If an incident shock wave reflects initially over a cylindrical convex wedge as an RR then it will eventually change to an MR.

Takayama and Sasaki (1983) showed experimentally that the RR \rightarrow MR transition wedge angle θ_w^{tr} , depends in addition to the incident shock wave Mach number, M_S , on both the radius of curvature of the cylindrical wedge, R , and the initial wedge angle, $\theta_w^{\text{initial}}$. The results of their experimental study are shown in Fig. 4.24 together with the RR \rightleftharpoons MR transition lines in steady (line AB) and pseudosteady (line AC) flows.

Figure 4.24 reveals that all the experimentally recorded transition wedge angles lie below the RR \rightleftharpoons MR transition line of pseudosteady flows. Furthermore, as the radius of curvature increases the transition wedge angle increases and approaches the pseudosteady RR \rightleftharpoons MR transition line. Similarly, the results indicate that the transition wedge angle decreases with decreasing initial wedge angles. The dependence of θ_w^{tr} on $\theta_w^{\text{initial}}$ is shown in a different way in Fig. 4.25 for $M_S = 1.6$. The results reveal a continuous nonlinear decrease of θ_w^{tr} as $\theta_w^{\text{initial}}$ decreases. The solid hand-drawn line illustrates the dependence of θ_w^{tr} on $\theta_w^{\text{initial}}$. Since θ_w^{tr} cannot be greater than $\theta_w^{\text{initial}}$ this line must terminate at the point $\theta_w^{\text{initial}} = \theta_w^{\text{tr}}$. The initial wedge angle at this point will result in for $M_S = 1.6$ an MR.

It should also be mentioned that the experimental results suggest that as the radius of curvature approaches infinity, i.e., $R \rightarrow \infty$, the actual transition wedge angles approach the transition line appropriate to pseudosteady flows. Recall that in the case of a reflection of a planar shock wave over a cylindrical concave surface $R \rightarrow \infty$ resulted in an approach to the transition line appropriate to steady flows (see Fig. 4.3). Thus, one can conclude that the actual transition line in pseudosteady flows, which is the case when $R \rightarrow \infty$

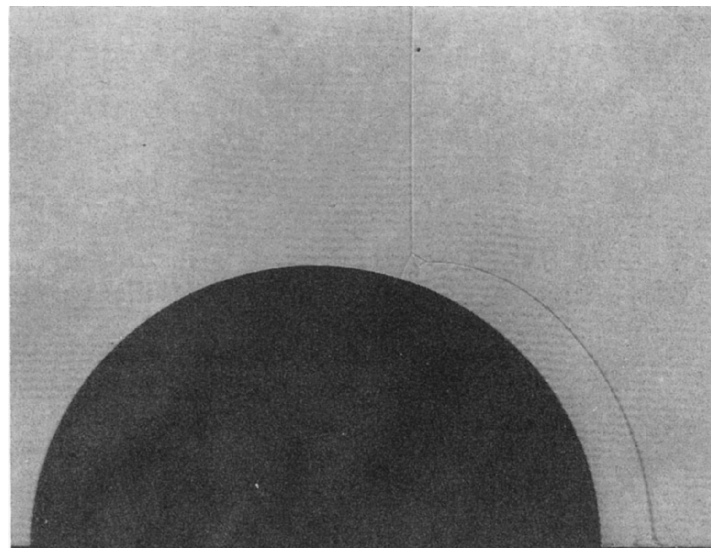
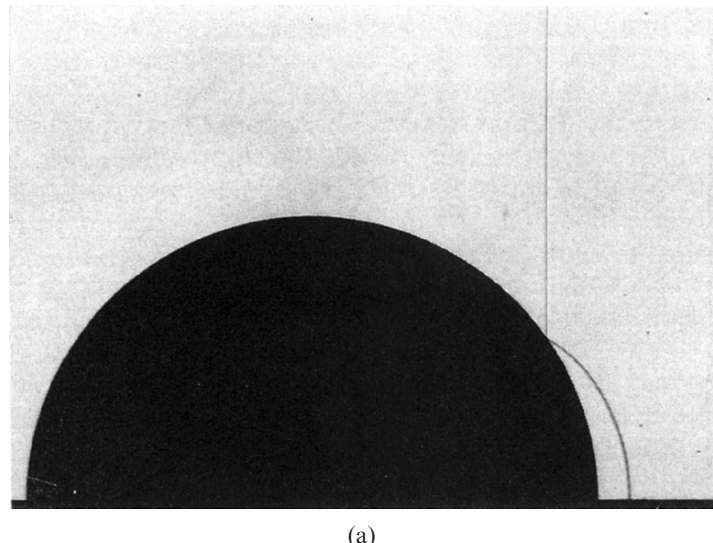
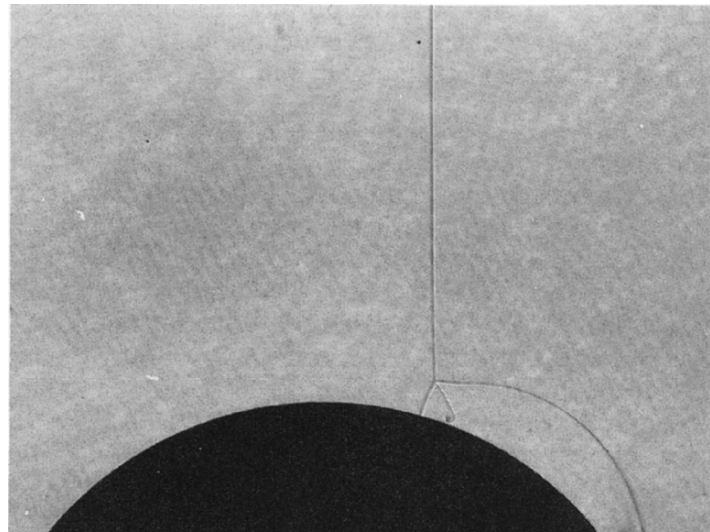
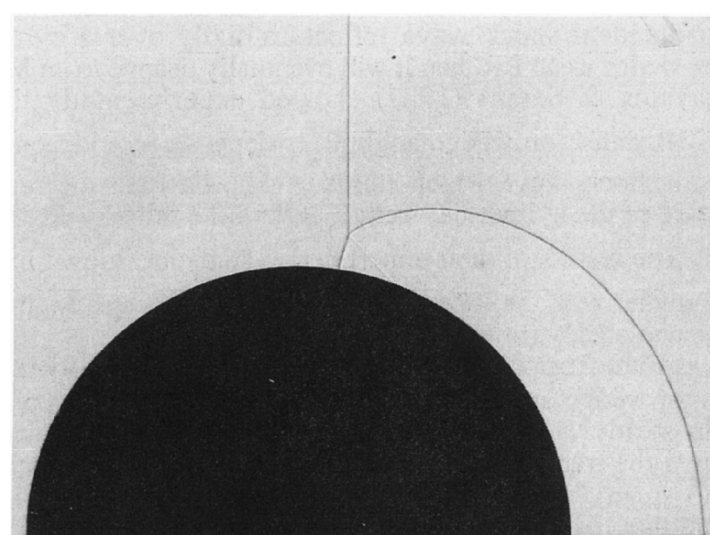


Fig. 4.23. (*Continued*)



(c)



(d)

Fig. 4.23. Shadowgraphs illustrating actual shock wave reflections over a cylindrical convex surface: (a) regular reflection; (b) double-Mach reflection (Courtesy of Professor K. Takayama, Shock Wave Research Center, Institute of Fluid Science, Tohoku University, Sendai, Japan); (c) transitional-Mach reflection; (d) single-Mach reflection (Courtesy of Professor K. Takayama, Shock Wave Research Center, Institute of Fluid Science, Tohoku University, Sendai, Japan)

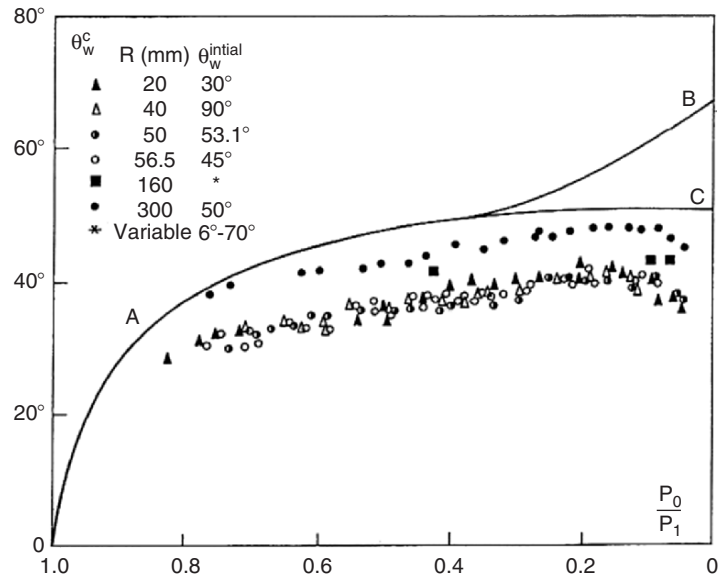


Fig. 4.24. Experimental data with nitrogen illustrating the dependence of the transition wedge angle over a cylindrical convex surface on the radius of curvature and the initial wedge angle

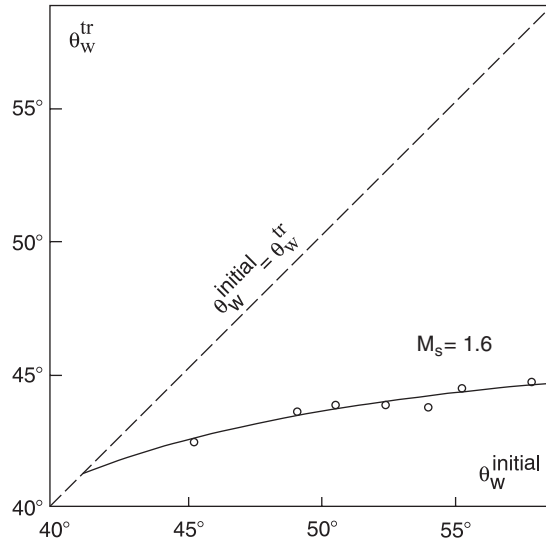


Fig. 4.25. Experimental data with nitrogen illustrating the dependence of the transition wedge angle over a cylindrical convex surface on the initial wedge angle for $M_s = 1.6$

is approached, is not a unique one, but depends on the way the reflection was initiated and generated.

Effect of Surface Roughness

Takayama et al. (1981) investigated experimentally the effect of surface roughness on the RR \rightarrow MR transition. The roughness was imposed on the surface by pasting sand paper with different mesh sizes on the reflecting wedge surface. Their results for a cylindrical convex wedge with $R = 50$ mm, $\theta_w^{\text{initial}} = 90^\circ$, and three different sizes of roughness are shown in Fig. 4.26. Again, the RR \rightleftharpoons MR transition lines for steady (line AB) and pseudosteady (line AC) flows are added.

Figure 4.26 reveals that the transition wedge angle, θ_w^{tr} , decreases as the size of the roughness of the reflecting surface increases. In the case of the extremely rough surface (mesh No. 40 sand paper) θ_w^{tr} is almost independent of the incident shock wave Mach number since it assumes a value of about 28.7° throughout the entire range of the inverse pressure ratio across the incident shock wave $- p_0/p_1$. This behavior of reduction in the actual transition wedge angle with increasing roughness was also evident in the case of shock wave reflection over a cylindrical concave surface (see Sect. 4.1.1.1).

Reichenbach (1985) experimentally investigated the RR \rightarrow MR transition over rough cylindrical surfaces, using cylindrical wedges whose surfaces were machined to obtain step and cubical shapes of roughness (see Fig. 3.48). Reichenbach (1985) defined the ratio between the transition wedge angle of

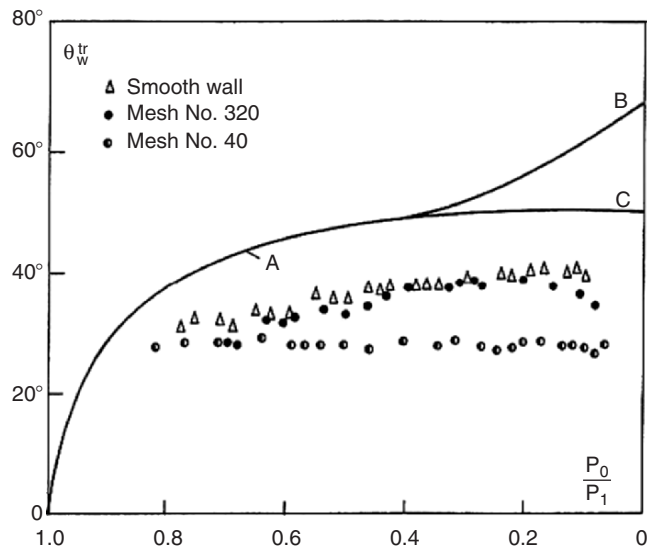


Fig. 4.26. Experimental data with nitrogen illustrating the dependence of the transition wedge angle over a cylindrical convex surface on its roughness

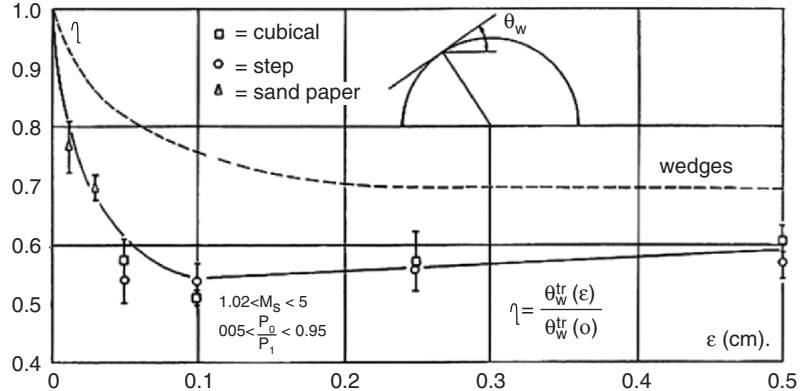


Fig. 4.27. The dependence of the RR → MR transition angle ratio over cylindrical convex surfaces on the roughness height

rough reflecting surfaces and the transition wedge angle over smooth reflecting surfaces as $-\eta$, and presented the experimental results in the (η, ϵ) -plane shown in Fig. 4.27. Figure 4.27 clearly indicates that the roughness height, ϵ , rather than its shape, is the dominant factor in determining the transition wedge angle. For comparison purposes, the line from Fig. 3.49, which is appropriate to straight surfaces (pseudosteady flow), is added as a dashed line to Fig. 4.27.

Analytical Considerations

In view of the fact that the length scale concept of Hornung et al. (1979) was successful in predicting the transition lines in steady and pseudosteady shock wave reflections as well as in the case of unsteady shock wave reflections over cylindrical concave surfaces, it is the author's belief that the race between the corner-generated signals and the incident shock wave is the dominant factor in determining the RR → MR transition phenomenon over cylindrical convex surfaces as well. Thus, the RR → MR transition lines should be obtained, in principle, using models similar to those described for concave cylinders. Unfortunately, however, similar analytical considerations for convex surfaces are much more difficult than for concave surfaces because the reflected shock wave, at the leading edge of the reflecting wedge, is much stronger when the incident shock wave reflects over a convex surface. Therefore, the simplifying assumptions used to analyze shock wave reflections over concave surfaces, that the reflected shock wave is weak and therefore the flow field behind it is close to being uniform (i.e., $V + a = V_1 + a_1$ or $V = V_1$ and $a = a_1$) cannot be applied in the case of shock wave reflection over convex surfaces. Thus if one wishes to calculate analytically the catch-up condition then V and a must be known in the flow field in order to carry out the integration $\int (V + a) dt$, which appears on the right hand side of equation (4.13).

Numerical Predictions of the RR → MR Transition

Although there are no available analytical models predicting the RR → MR transition over cylindrical convex surfaces, there are fortunately, relatively simple numerical codes capable of predicting this transition.

Consider Fig. 4.28 where the recorded transition wedge angles, θ_w^{tr} , over a convex cylindrical wedge with $R = 50$ mm and $\theta_w^{\text{initial}} = 90^\circ$ are plotted with some analytical and numerical transition lines. Lines AB and AC are the RR \rightleftharpoons MR transition lines in steady and pseudosteady flows, respectively. Line D was numerically calculated by Heilig (1969) who applied Whitham's (1957) classical ray-shock theory. Line E is a similar calculation of Itoh et al. (1981) who used Milton's (1975) modification of Whitham's (1957) theory. A comparison between curves D and E and the experimental results indicates that Milton's modification of Whitham's theory improves the agreement between the numerical predictions and the experimental results. The numerical predictions of Heilig (1969) and Itoh et al. (1981) become poorer as M_s increase beyond $M_s \approx 2$, when the transition lines gradually increase with increasing M_s while the experimental results level out and even exhibit a slight decrease in the actual transition wedge angle. This could be because for $M_s > 2$ the shock-induced flow becomes supersonic.

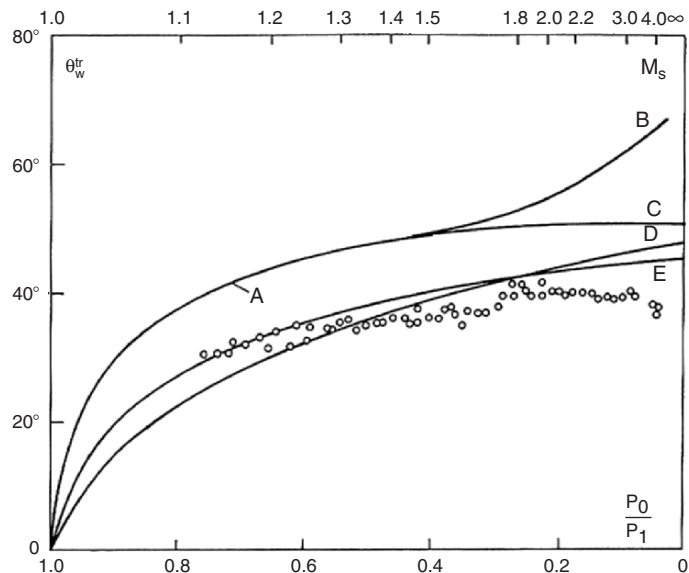


Fig. 4.28. Comparison between the measured transition wedge angles over a cylindrical convex surface and various numerical criteria (Data are for nitrogen)

Additional Remark

Heilig (1969) has also experimentally investigated the shock wave reflection over elliptical convex surfaces. The experimental results were, in general, similar to those obtained over cylindrical convex surfaces with an appropriate radius of curvature.

4.1.3 Shock Wave Reflections Over Double Wedges

Ginzburg and Markov (1975) initiated an experimental investigation of the reflection of a planar shock wave over a two-facet concave wedge. Srivastava and Deschambault (1984) experimentally investigated a two-facet convex wedge. Ben-Dor et al. (1987) who termed it shock wave reflection over double concave or convex wedges reinitiated a detailed experimental and analytical study of this reflection phenomenon. Schematic drawings of a concave and a convex double wedge are shown in Fig. 4.29a, b, respectively. For both wedges, θ_w^1 and θ_w^2 are the angles of the first and second surfaces and $\Delta\theta_w$ is the inclination of the second surface with respect to the first surface, i.e., $\Delta\theta_w = \theta_w^2 - \theta_w^1$. For a concave double wedge $\Delta\theta_w > 0$ while for a convex double wedge $\Delta\theta_w < 0$. $\Delta\theta_w = 0$ corresponds to a single face straight wedge.

Domains of Different Types of Reflection Processes

The analytical results of Ben-Dor et al. (1987) are shown in Fig. 4.30 in the (θ_w^1, θ_w^2) -plane. The third parameter, M_S , is kept constant. Thus for any given value of incident shock wave Mach number, M_S , there is a specific plot such as the one shown in Fig. 4.30.

There are four transition lines in Fig. 4.30 that divide the (θ_w^1, θ_w^2) -plane into seven domains of different types of reflection processes over any double wedge.

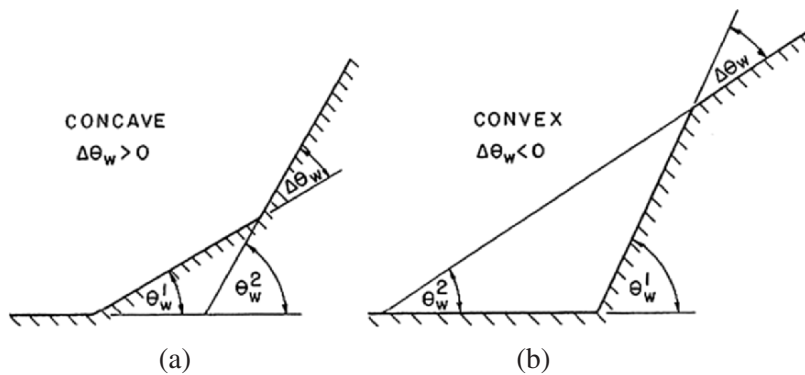


Fig. 4.29. Schematic illustrations of a double wedge: (a) concave and (b) convex

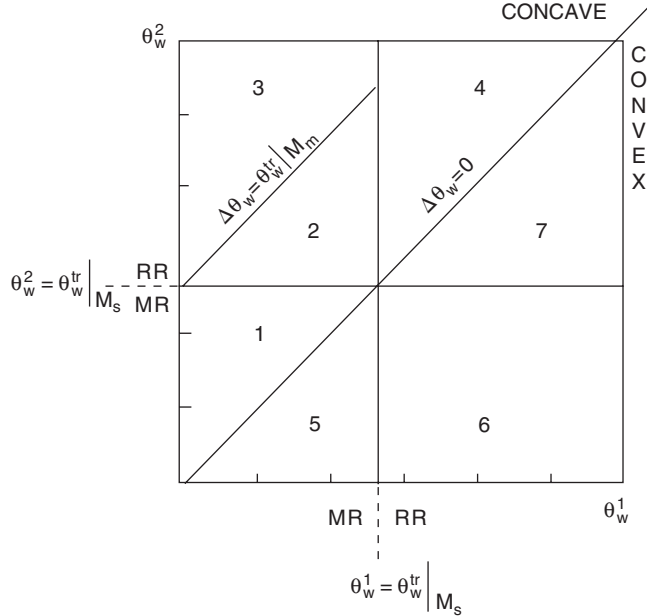


Fig. 4.30. Domains and analytical transition boundaries of different types of reflection processes over a double wedge in the $\theta_w^2 = \theta_w^{\text{tr}}|_{M_s}$ -plane for a given M_s

1. The line $\Delta\theta_w = 0$ divides the (θ_w^1, θ_w^2) -plane into two domains of different geometries:
 - Concave double wedge
 - Convex double wedge
2. The line $\theta_w^1 = \theta_w^{\text{tr}}|_{M_s}$ determines the type of the reflection of the incident shock wave over the first reflecting surface
 - If $\theta_w^1 < \theta_w^{\text{tr}}|_{M_s}$ then the incident shock wave reflects over the first reflecting surface is an MR, however,
 - If $\theta_w^1 > \theta_w^{\text{tr}}|_{M_s}$ then the incident shock wave reflects over the first reflecting surface as an RR
3. The line $\theta_w^2 = \theta_w^{\text{tr}}|_{M_s}$ determines the final type of reflection of the incident shock wave over the second reflecting surface
 - If $\theta_w^2 < \theta_w^{\text{tr}}|_{M_s}$ then the final reflection of the incident shock wave over the second reflecting surface is an MR
 - If $\theta_w^2 > \theta_w^{\text{tr}}|_{M_s}$ then the final incident shock wave reflection over the second reflecting surface is an RR

When $\theta_w^1 < \theta_w^{\text{tr}}|_{M_s}$ then, as mentioned earlier, the incident shock wave reflects over the first reflecting surface as an MR. If in addition, the wedge is concave, i.e., $\Delta\theta_w > 0$, then the Mach stem of this MR encounters a compressive corner from which it can reflect either as an MR or as an RR depending on whether $\Delta\theta_w$ is smaller or greater than $\theta_w^{\text{tr}}|_{M_m}$.

Table 4.3. The reflection processes in each of the seven domains shown in Fig. 4.30

Region	Type of double wedge	Initial reflection over the 1st surface	Initial reflection over the 2nd surface	Final reflection over the 2nd surface
1	Concave	MR	MR	MR
2	Concave	MR	MR	TRR
3	Concave	MR	RR	RR
4	Concave	RR	RR	RR
5	Convex	MR	MR	MR
6	Convex	RR	MR	MR
7	Convex	RR	RR	RR

4. If $\Delta\theta_w < \theta_w^{\text{tr}}|_{M_m}$ then the Mach stem reflects over the second reflecting surface as an MR
5. If $\Delta\theta_w > \theta_w^{\text{tr}}|_{M_m}$ then the Mach stem reflects over the second reflecting surface as an RR

If the Mach stem is assumed straight and perpendicular to the reflecting surface then:

$$M_m = M_S \frac{\cos \chi}{\cos(\theta_w^1 + \chi)}, \quad (4.60)$$

where χ is the triple point trajectory angle and M_S and M_m are the Mach numbers of the incident and Mach stem shock waves, respectively.

It is clear from this relation that $M_m > M_S$. However, from Fig. 3.27 it is evident that for $M_S > 2$ the RR \rightleftharpoons MR transition wedge angle does not depend too strongly on the shock wave Mach number. Hence, it can be assumed that:

$$\theta_w^{\text{tr}}|_{M_m} \approx \theta_w^{\text{tr}}|_{M_S}. \quad (4.61)$$

For example, for $M_S = 2.5$ and $\theta_w^1 = 20^\circ$ the MR solution results in $\chi = 12.88^\circ$. This, in turn, results in $M_m = 2.902$. The corresponding transition wedge angles for these values of M_S and M_m are 50.77° and 50.72° , respectively. This example indicates that although the difference in the shock wave Mach numbers is about 15%, the difference in the corresponding RR \rightleftharpoons MR transition wedge angles is only 0.05° .

The seven domains of different types of reflection processes, numbered in Fig. 4.30 from 1 to 7, are described in Table 4.3.

RR \rightleftharpoons MR Transition Over Double Wedges

The experimental study of Ben-Dor et al. (1987) indicated that the RR \rightleftharpoons MR transition wedge angle, θ_w^{tr} , over a double wedge depends on $\Delta\theta_w$.

Typical results for a concave double wedge with $M_S = 2.45$ are shown in Fig. 4.31. When $\Delta\theta_w = 0$, i.e., a straight single surface wedge, the value of θ_w^{tr}

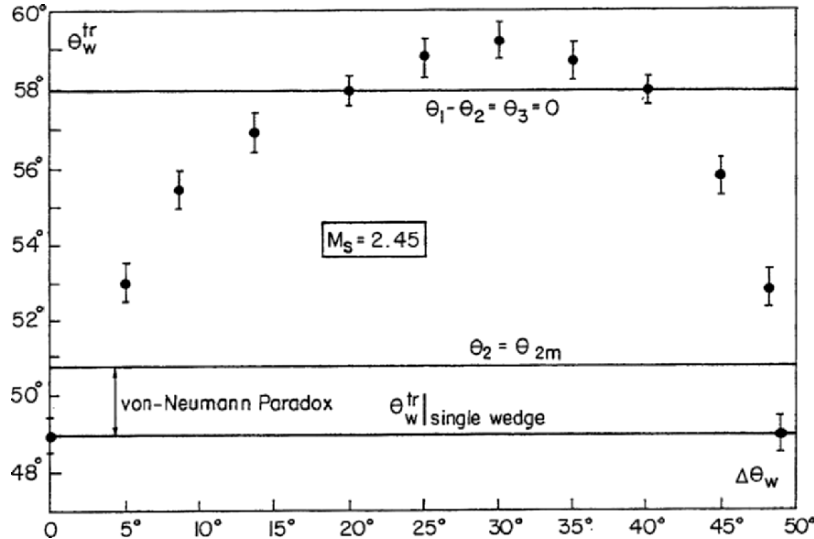


Fig. 4.31. The RR \rightleftharpoons MR transition wedge angle over a concave double wedge in nitrogen with $M_s = 2.45$

is about 49° . This value is about 1.75° below the RR \rightleftharpoons MR transition wedge angle as predicted by the sonic criterion. As $\Delta\theta_w$ increases, θ_w^{tr} increases until a maximum of $\theta_w^{\text{tr}} \approx 59.5^\circ$ at $\Delta\theta_w = 30^\circ$. From there on θ_w^{tr} decreases with increasing $\Delta\theta_w$ until it again reaches the value of 49° at about $\Delta\theta_w = 48.8^\circ$. Note that in this plot the value of θ_w^{tr} is actually the value of θ_w^2 at which the MR \rightarrow RR transition was recorded. Thus for each experimental point $\theta_w^2 = \theta_w^{\text{tr}}$ and $\theta_w^1 = \theta_w^{\text{tr}} - \Delta\theta_w$.

The measured transition wedge angles for a convex double wedge with $M_s = 1.3$ are shown in Fig. 4.32. At $\Delta\theta_w = 0$ the value of θ_w^{tr} is about 44.5° . This value is about 1.65° below the RR \rightleftharpoons MR transition wedge angle as predicted by the sonic criterion. As $\Delta\theta_w$ decreases (note $\Delta\theta_w$ is negative), θ_w^{tr} decreases until a minimum of $\theta_w^{\text{tr}} \approx 43^\circ$ at $\Delta\theta_w = -25.5^\circ$. From there on θ_w^{tr} increases with decreasing $\Delta\theta_w$ until it reaches again the value of 44.5° at about $\Delta\theta_w = -45.5^\circ$. Similar to the previous case of a concave double wedge, here again: $\theta_w^2 = \theta_w^{\text{tr}}$ and $\theta_w^1 = \theta_w^{\text{tr}} - \Delta\theta_w$, where $\Delta\theta_w$ is negative and hence $\theta_w^1 > \theta_w^2$.

It is evident from Figs. 4.30 and 4.31 that for a concave double wedge θ_w^{tr} is greater than the one predicted by the sonic criterion, while for a convex double wedge θ_w^{tr} is smaller than that predicted by the sonic criterion. This behavior is similar to that shown earlier for cylindrical concave and convex wedges (see Figs. 4.3 and 4.24). However, while for the case of shock wave reflections over cylindrical concave wedges the transition wedge angles were above those predicted by the steady flow RR \rightleftharpoons MR transition line (see line B in Fig. 4.3), for the case of shock wave reflections over concave double wedges

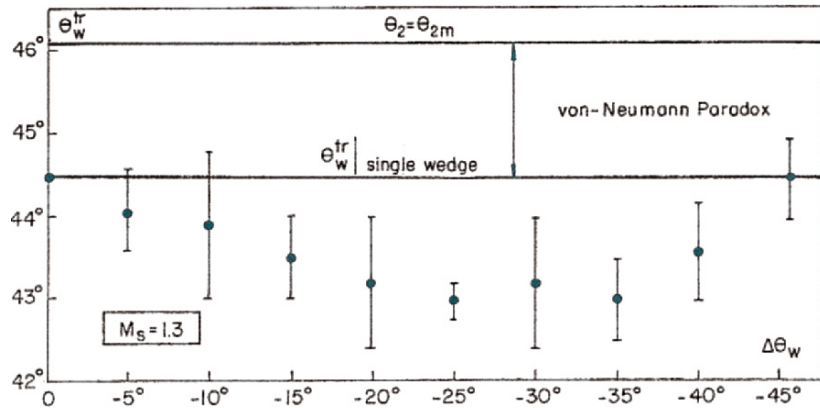


Fig. 4.32. The RR \rightleftarrows MR transition wedge angle over a convex double wedge in nitrogen with $M_s = 1.3$

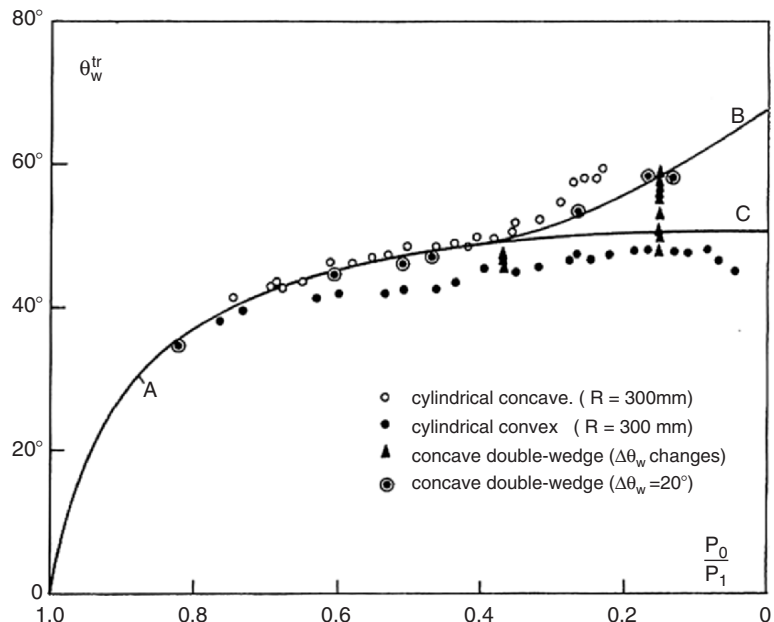


Fig. 4.33. Actual transition wedge angles over various cylindrical concave, cylindrical convex, and double wedges

it is possible to obtain transition wedge angles below this transition line as shown in Fig. 4.31.

Figure 4.33 illustrates the transition wedge angle, θ_w^{tr} , for four cases: reflection over a cylindrical concave wedge with $R = 300 \text{ mm}$, over a cylindrical convex wedge with $R = 300 \text{ mm}$, over a concave double wedge with various

values of $\Delta\theta_w$, and a concave double wedge with $\Delta\theta_w = 20^\circ$. Note that for $R = 300$ mm the transition wedge angles over a cylindrical concave wedge approach those appropriate to pseudo steady flows, while the transition wedge angles over a cylindrical convex wedge approach those appropriate to steady flows. The transition wedge angles are expected to reach the appropriate transition line at $R \rightarrow \infty$. In view of the earlier discussion the other results shown in Fig. 4.33 are self-explanatory.

Additional Remarks

The shock wave reflection phenomenon over double wedges still requires further analytical and experimental studies. The experimental studies concerning the RR \rightleftharpoons MR transition over double wedges as well as the experimentally recorded transition wedge angles over single wedges are sufficient for redrawing two of the transition lines shown in Fig. 4.30, namely the lines $\theta_w^1 = \theta_w^{\text{tr}}|_{M_s}$ and $\theta_w^2 = \theta_w^{\text{tr}}|_{M_s}$. The $\Delta\theta_w = 0$ line is a geometrical condition, and hence is correct. Thus, more data are needed to obtain the actual boundary separating domains 2 and 3. Figure 4.34 is a reproduction of Fig. 4.30 with the actual transition lines replacing the corresponding analytical transition lines for $M_s = 1.3$.

It is of interest to note that although the reflection of a shock wave over a double wedge has not yet been completely explained from a theoretical point of view, the fact that the reflection over concave or convex double wedges

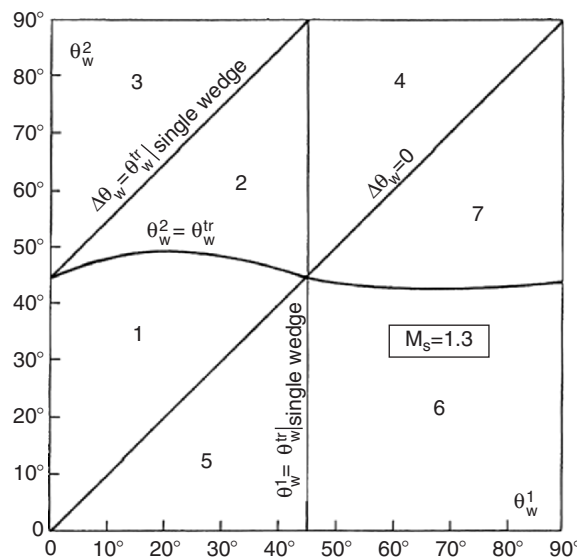


Fig. 4.34. Domains and experimental transition boundaries of the different types of reflection processes over a double wedge in the (θ_w^1, θ_w^2) -plane for a given M_s

shows similar behavior to the reflection over concave or convex cylindrical surfaces should be encouraging, since the analytical study of the former might be easier. Once the reflection over a double wedge is understood, a natural step would be to go over to a triple wedge or a multiple faceted wedge.

As a final remark it should be mentioned that Ben-Dor et al. (1988) showed experimentally that if the second surface of a double wedge is long enough then the final reflection which develops over it (i.e., an RR on an MR) asymptotically approaches the wave configuration which would have been obtained, had the incident shock wave reflected over a straight wedge having an angle equal to θ_w^2 .

4.2 Nonconstant Velocity Shock Wave Reflections Over Straight Surfaces

The interaction of a nonconstant velocity shock wave over straight surfaces is another example of a truly unsteady reflection process. Although the analytical treatment of a reflection of this type might be important to better understand the more complex reflection of a spherical shock wave (nonconstant velocity shock wave) reflection over the ground surface (straight surface), which is dealt with in the next section, unfortunately no analytical work has been done on this reflection process. This is in spite of the fact that experimental investigations of this type of shock wave reflection processes can be performed relatively easily in a shock tube. The only requirement is to generate an accelerating or decelerating (decaying) planar shock wave and reflect it over a wedge with a straight surface. Techniques for generating decaying planar shock waves in shock tubes can be found in the literature related to shock tubes.

4.3 Spherical Shock Wave Reflections Over Straight and Nonstraight Surfaces

The reflection of a spherical shock wave, e.g., a blast wave that is generated when a large amount of energy is released in short times (explosion), over straight and nonstraight surfaces has been experimentally investigated quite extensively in the past few decades, e.g., Dewey et al. (1977), Dewey and McMillin (1981), Hu and Glass (1986), etc.

When a spherical shock wave is generated from an explosion detonated above the ground it reflects over the surface initially as an RR, which then, depending upon the strength of the spherical shock wave, changes into a DMR, a TMR, and finally to an SMR as it propagates outwards. Figure 4.35a, b illustrates an RR and an SMR of a spherical shock wave over a straight surface.

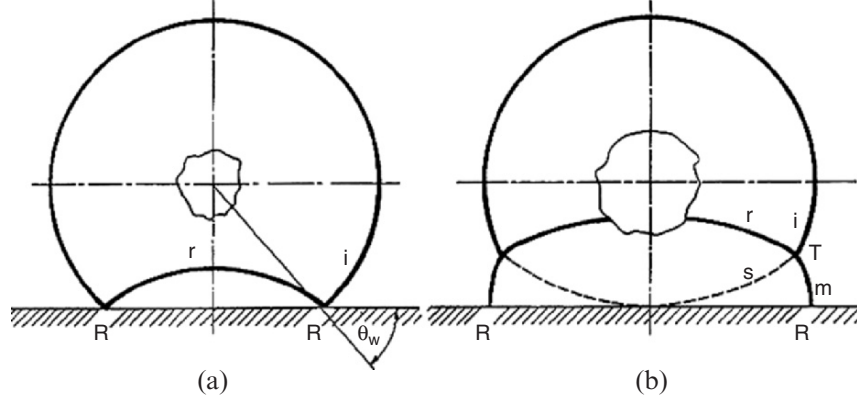


Fig. 4.35. Schematic illustrations of spherical shock wave reflections over a straight surface: (a) regular reflection and (b) single-Mach reflection

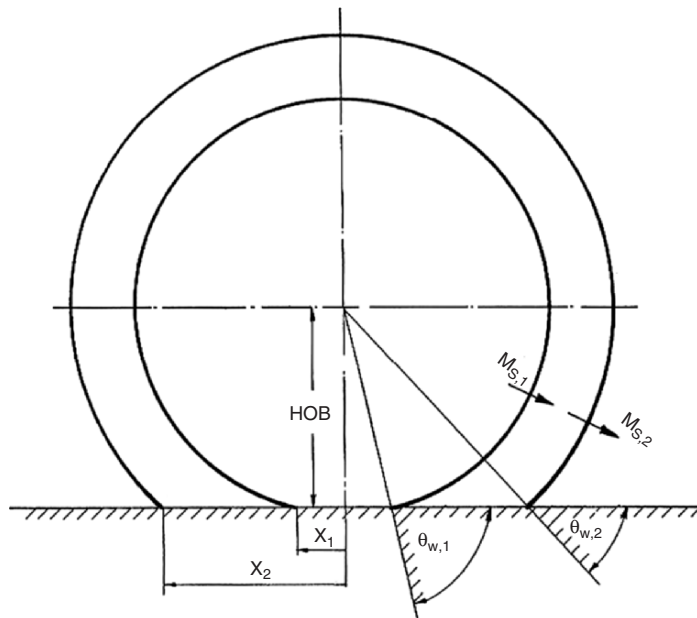


Fig. 4.36. Schematic illustration of the instantaneous incident shock wave Mach number and the instantaneous reflecting wedge angle of a spherical shock wave propagating over a straight surface

Consider Fig. 4.36 where the spherical shock wave at two different times is drawn, and note that as the spherical shock wave propagates outward the point where it touches the reflecting surface encounters an ever decreasing effective reflecting wedge angle, i.e., $\theta_{w,2} < \theta_{w,1}$. Thus beside the fact that the

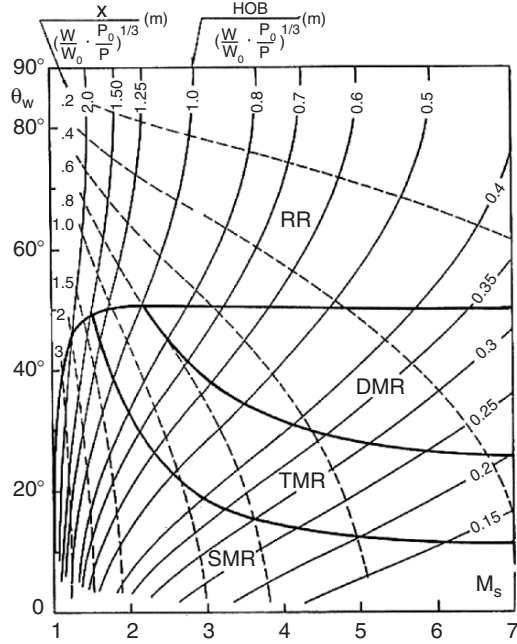


Fig. 4.37. Domains of different types of reflections in pseudosteady flows and spherical shock wave trajectories (Courtesy of Professor I. I. Glass)

instantaneous blast wave Mach number, M_S , decreases with time ($M_{S,2} < M_{S,1}$), the effective reflecting wedge angle also decreases with time. Correlations on the attenuation of blast waves propagating into pure and inert dusty gases can be found in Aizik et al. (2001).

Figure 4.37 [originally plotted by Hu and Glass (1986)] shows the domain of different types of reflections (in pseudosteady flows) in the (M_S, θ_w) -plane for air. Spherical shock wave trajectories, i.e., $M_S(\theta_w)$, are added to Fig. 4.37. The trajectories differ from each other by the nondimensionalized height of burst, HOB (see Fig. 4.36). The nondimensionalizing factor is $(W p_a / W_r p_a)^{1/3}$ where W and p are the weight (equivalent to TNT) of the explosive charge, used to generate the blast (spherical shock) wave, and the atmospheric pressure, respectively, and $W_r = 1 \text{ Kg TNT}$ and $p_r = 1 \text{ atm}$. The nondimensionalized distance X denotes the radial location (measured from the center of explosion on the ground, see Fig. 4.36). The $X = 0$ line coincides with the $\theta_w = 90^\circ$ line. It is seen that for an explosive charge of 1 Kg TNT at a height of burst of 0.8 m and an ambient pressure of 1 atm the blast wave has a strength equivalent to $M_S \approx 3.7$ upon colliding with the reflecting surface. The initial reflection for this case is an RR that changes later to a DMR, then to a TMR, and finally to an SMR until it degenerates to a sound wave, $M_S \rightarrow \infty$.

On the other hand, if the HOB for the same charge is 2 m, the instantaneous Mach number when the blast wave collides with the ground surface is $M_S \approx 1.5$ and the RR changes directly to an SMR before it degenerates to a sound wave. The trajectories shown in Fig. 4.37 are fits based on the best experimental data. However, the foregoing discussion should be regarded only as explanatory from a phenomenological point of view, since the pseudosteady transition lines shown in Fig. 4.37 are not applicable for unsteady flows.

An experimental test of the applicability of the transition lines between the various types of reflections in pseudosteady flows, for the case of blast wave reflections is shown in Fig. 4.38, where the actual RR \rightleftharpoons MR transition angles for seven experiments with different heights of burst are connected by a dashed line. The experimental RR \rightleftharpoons MR transition wedge angles are up to 10° smaller or larger than the pseudosteady RR \rightleftharpoons MR transition line. Furthermore, while the pseudosteady RR \rightleftharpoons MR transition line slightly decreases as M_S increases, the unsteady experimental RR \rightleftharpoons MR transition line shows a gradual increase with increasing values of M_S . Thus, beside the

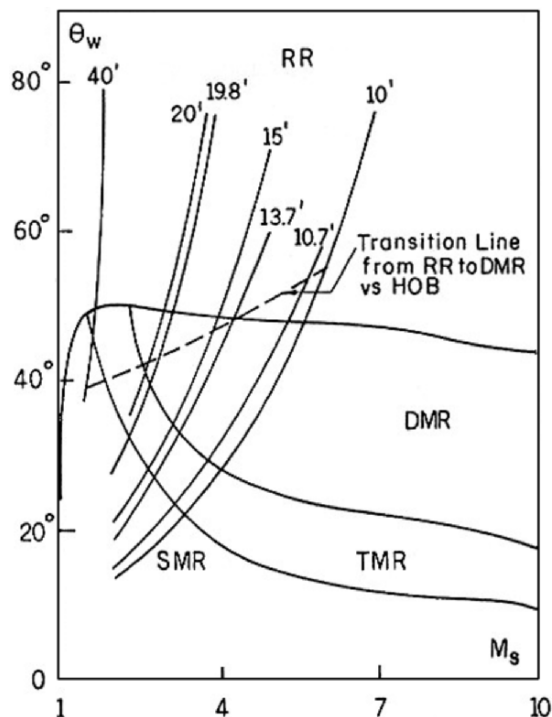
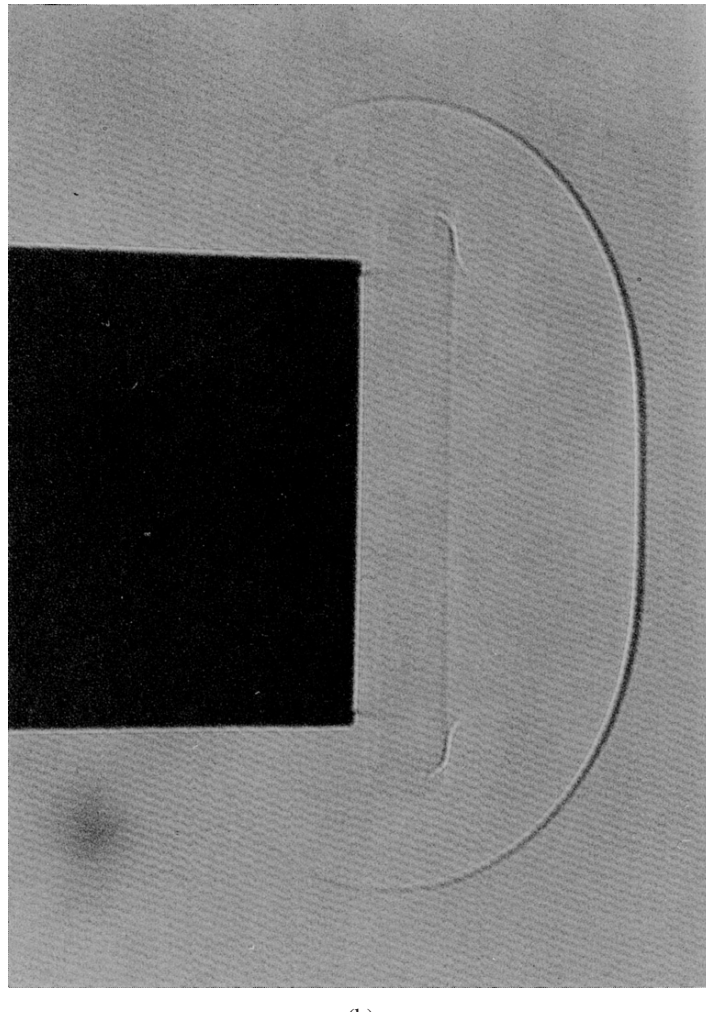


Fig. 4.38. Comparison of average transition lines of actual blast wave experiments as compared to the transition boundaries appropriate to pseudosteady reflections in imperfect nitrogen (Courtesy of J. Wisotski, Denver Research Institute, Denver, Colorado)

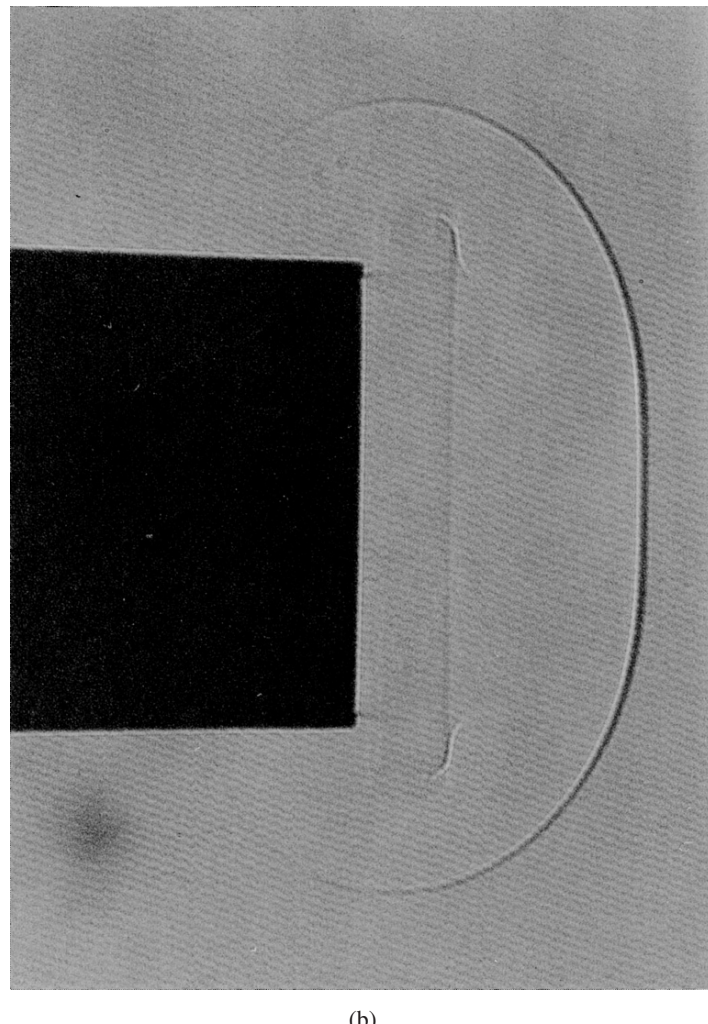
fact that the (M_S, θ_w) -plot is helpful in determining the sequence of events during the RR \rightleftharpoons MR transition, it is obvious that it cannot predict the actual transition angles.

Spherical shock waves can be generated in shock tubes by producing a planar shock wave inside a circular shock tube and allowing it to emerge from it. The formation of such a blast wave as it emerges from the tube is shown in Fig. 4.39a, b. While at early stages the shape of the shock wave emerging from the end of the tube is not spherical, at later times (Fig. 4.39b) it attains a



(b)

Fig. 4.39. (*Continued*)



(b)

Fig. 4.39. The generation of a spherical shock wave by means of a shock tube: (a) The shape of the incident shock wave a short time after it emerges out of the open ended circular shock tube. (Courtesy of Professor K. Takayama, Shock Wave Research Center, Institute of Fluid Science, Tohoku University, Sendai, Japan). (b) After a relatively long time a perfect spherical shape is approached. (Courtesy of Professor K. Takayama, Shock Wave Research Center, Institute of Fluid Science, Tohoku University, Sendai, Japan)

perfectly spherical shape. Takayama and Sekiguchi (1981a & 1981b) used this technique of producing spherical shock waves in a shock tube to investigate the reflection of spherical shock waves from various surfaces, in general, and cones in particular. The reflection of the spherical shock wave shown in Fig. 4.39b from a cylindrical reflecting surface is shown in Fig. 4.40.

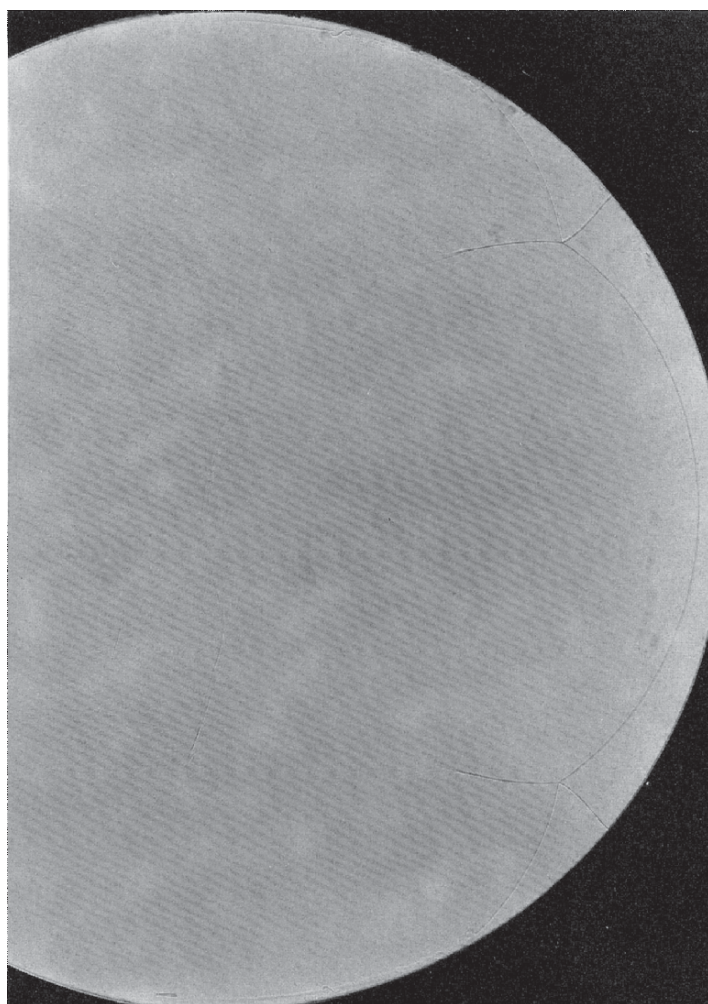


Fig. 4.40. The reflection of a spherical shock wave as generated by the experimental set-up shown in Fig. 4.39, from a cylindrical reflecting surface. (Courtesy of Professor K. Takayama, Shock Wave Research Center, Institute of Fluid Science, Tohoku University, Sendai, Japan)

References

- Aizik, F., Ben-Dor, G., Elperin, T. & Igra, O., "General attenuation laws for spherical shock waves propagating in pure and particle laden gases", AIAA J., 39(5), 969–972, 2001.
- Bazhenova, T.V., Fokeev, V.P. & Gvozdeva, L.G., "Regions of various forms of Mach reflection and Its transition to regular reflection", Acta Astro., 3, 131–140, 1976.
- Ben-Dor, G., "Analytical solution of a double-Mach reflection", AIAA J., 18, 1036–1043, 1980.
- Ben-Dor, G., Dewey, J.M., McMillin, D.J. & Takayama, K., "Experimental investigation of the asymptotically approached Mach reflection over the second surface in the reflection over a double wedge", Exp. Fluids, 6, 429–434, 1988.
- Ben-Dor, G., Dewey, J.M. & Takayama, K., "The reflection of a planar shock wave over a double wedge", J. Fluid Mech., 176, 483–520, 1987.
- Ben-Dor, G. & Takayama, K., "Analytical prediction of the transition from Mach to regular reflection over cylindrical concave wedges", J. Fluid Mech., 158, 365–380, 1985.
- Ben-Dor, G. & Takayama, K., "Application of steady shock polars to unsteady shock wave reflections", AIAA J., 24, 682–684, 1986.
- Ben-Dor, G. & Takayama, K., "The dynamics of the transition from Mach to regular reflection over concave cylinders", Israel J. Tech., 23, 71–74, 1986/7.
- Ben-Dor, G., Takayama, K. & Dewey, J.M., "Further analytical considerations of the reflection of weak shock waves over a concave wedge", Fluid Dyn. Res., 2, 77–85, 1987.
- Courant, R. & Friedrichs, K.O., *Hypersonic Flow and Shock Waves*, Wiley Interscience, New York, U.S.A., 1948.
- Dewey, J.M. & McMillin, D.J., "An analysis of the particle trajectories in spherical blast waves reflected from real and ideal surfaces", Canadian J. Phys., 59, 1380–1390, 1981.
- Dewey, J.M., McMillin, D.J. & Classen, D.F., "Photogrammetry of spherical shocks reflected from real and ideal surfaces", J. Fluid Mech., 81, 701–717, 1977.
- Ginzburg, I.P. & Markov, Y.S., "Experimental investigation of the reflection of a shock wave from a two-facet wedge", Fluid Mech.-Soviet Res., 4, 167–172, 1975.
- Heilig, W.H., "Diffraction of shock wave by a cylinder", Phys. Fluids Suppl. I., 12, 154–157, 1969.
- Henderson, L.F. & Lozzi, A., "Experiments on transition of Mach reflection", J. Fluid Mech., 68, 139–155, 1975.
- Hornung, H.G., Oertel, H. Jr. & Sandeman, R.J., "Transition to Mach reflection of shock waves in steady and pseudo-steady flow with and without relaxation", J. Fluid Mech., 90, 541–560, 1979.

- Hu, T.C.J. & Glass, I.I., "Blast wave reflection trajectories from a height of burst", AIAA J., 24, 607–610, 1986.
- Itoh, S. & Itaya, M., "On the transition between regular and Mach reflection", in "Shock Tubes and Waves", Eds. A. Lifshitz and J. Rom, Magnes Press, Jerusalem, 314–323, 1980.
- Itoh, S., Okazaki, N. & Itaya, M., "On the transition between regular and Mach reflection in truly non-stationary flows", J. Fluid Mech., 108, 383–400, 1981.
- Law, C.K. & Glass, I.I., "Diffraction of strong shock waves by a sharp compressive corner", CASI Trans., 4, 2–12, 1971.
- Marconi, F., "Shock reflection transition in three-dimensional flow about interfering bodies", AIAA J., 21, 707–713, 1983.
- Milton, B.E., "Mach reflection using ray-shock theory", AIAA J., 13, 1531–1533, 1975.
- Reichenbach, H., "Roughness and heated layer effects on shock wave propagation and reflection – Experimental results", Ernst Mach Institute Rep. E 24/85, Freiburg, West Germany, 1985.
- Srivastava, R.S. & Deschambault R.L., "Pressure distribution behind a non-stationary reflected-diffracted oblique shock wave", AIAA J., 22, 305–306, 1984.
- Takayama, K. & Ben-Dor, G., "A reconsideration of the transition criterion from Mach to regular reflection over cylindrical concave surfaces", KSME J., 3, 6–9, 1989.
- Takayama, K., Ben-Dor, G. & Gotoh, J., "Regular to Mach reflection transition in truly nonstationary flows – Influence of surface roughness", AIAA J., 19, 1238–1240, 1981.
- Takayama, K. & Sasaki, M., "Effects of radius of curvature and initial angle on the shock transition over concave and convex walls", Rep. Inst. High Speed Mech., Tohoku Univ., Sendai, Japan, 46, 1–30, 1983.
- Takayama, K. & Sekiguchi, H., "Triple-point trajectory of strong spherical shock wave", AIAA J., 19, 815–817, 1981a.
- Takayama, K. & Sekiguchi, H., "Formation and diffraction of spherical shock waves in shock tube", Rep. Inst. High Speed Mech., Tohoku Univ., Sendai, Japan, 43, 89–119, 1981b.
- Whitham, G.B., "A new approach to problems of shock dynamics. Part 1. Two dimensional problems", J. Fluid Mech., 2, 145–171, 1957.

5

Source List

Ben-Dor (1991) included a comprehensive list of papers and reports dealing with the various aspects of shock wave reflection phenomenon. An updated list is provided in this chapter.

The list is divided into two parts:

- The first contains papers which were published in refereed scientific journals and which are, in principle, available to the scientific community.
- The second contains departmental reports from institutions and universities which have been involved in the study of shock wave reflection.

An effort was made to try and include most of the papers and the reports which have been published so far in the area of shock wave reflection. In addition, an effort was made to provide full reference to each of the listed references.

Finally, since only papers published in refereed scientific journals and departmental reports are listed in the following, the interested reader is advised to look for more papers on the subject of shock-wave reflections in the proceedings of the following conferences:

- (1) The International Symposium on Shock Waves (ISSW).¹
- (2) The International Symposium on Military Applications of Blast and Shock (MABS).²
- (3) The International Colloquium on Dynamics of Explosions and Reactive Systems (ICDERS).
- (4) The International Mach Reflection Symposium (IMRS).
- (5) The International Symposium on the Interaction of Shocks (ISIS).

¹ Formerly known as The International Symposium on Tubes and Shock Waves (ISTS).

² Formerly known as The International Symposium on Military Applications of Blast Simulation (MABS).

5.1 Scientific Journals

References

- Adachi, T., Kobayashi, S. & Suzuki, T., "An analysis of the reflected shock wave structure over a wedge with surface roughness", *Dyn. Image Anal.*, 1, 30–37, 1988.
- Adachi, T., Kobayashi, S. & Suzuki, T., "An experimental analysis of oblique shock reflection over a two-dimensional multi-guttered wedge", *Fluid Dyn. Res.*, 9, 119–132, 1992.
- Adachi, T., Kobayashi, S. & Suzuki, T., "Reflection of plane shock waves over a dust layer – The effects of permeability", *Theor. & Appl. Mech.*, 37, 23–30, 1989.
- Adachi, T., Kobayashi, S. & Suzuki, T., "An experimental study of reflected shock wave structure over a wedge with surface roughness", *Trans. Japan Soc. Mech. Eng.*, B56, 1244–1249, 1990.
- Adachi, T., Kobayashi, S. & Suzuki, T., "Unsteady behavior of Mach reflection of a plane shock wave over a wedge with surface roughness", *Theor. & Appl. Mech.*, 39, 285–291, 1990.
- Adachi, T., Sakurai, A., & Kobayashi, S., "Effect of boundary layer on Mach reflection over a wedge surface" *Shock Waves*, 11(4), 271–278, 2002.
- Adachi, T., Suzuki, T. & Kobayashi, S., "Unsteady oblique reflection of a plane shock wave over a wedge with surface roughness", *Dyn. Image Anal.*, 2, 31–36, 1990.
- Adachi, T., Suzuki, T. & Kobayashi, S., "Mach reflection of a weak shock waves", *Trans. Japan Soc. Mech. Eng.*, 60(575), 2281–2286, 1994.
- Arutyunyan, G.M., "On interaction of shock waves with a wedge", *Dokl. Akad. Nauk Arm. SSSR*, 46, 160–167, 1968.
- Arutyunyan, G.M., "On diffraction of shock waves", *Prikl. Math. & Mekh.*, 34, 693–699, 1970.
- Arutyunyan, G.M., "Theory of anomalous regimes in the regular reflection of shock waves", *Izv. Akad. Nauk SSSR, Mekh. Zh. i Gaza*, 5, 117–125, 1973.
- Arutyunyan, G.M., Belokon, V.A. & Karchevsky, L.V., "Effect of adiabatic index on reflection of shocks", *Zh. Prikl. Mekh. i Teor. Fiz.*, 4, 62–66, 1970.
- Arutyunyan, G.M. & Karchevsky, L.F., *Reflected Shock Waves*, Mashinostroyeniye Press, Moscow, SSSR, 1975.
- Auld, D.J. & Bird, G.A., "Monte Carlo simulation of regular and Mach reflection", *AIAA J.*, 15, 638–641, 1977.
- Azevedo, D.J. & Liu, C.S., "Engineering approach to the prediction of shock patterns in bounded high-speed flows", *AIAA J.*, 31(1), 83–90, 1993.
- Barbosa, F.J. & Skews, B.W., "Experimental confirmation of the von Neumann theory of shock wave reflection transition", *J. Fluid Mech.*, 472, 263–282, 2002.

- Barkuhudarov, E.M., Mdivnishvili, M.O., Sokolov, I.V., Taktakishvili, M.I. & Terekhin, "Reflection of ring shock wave from a rigid wall", *Shock Waves*, 3(4), 273–278, 1994.
- Bartenev, A.M., Khomik, S.V., Gelfand, B.E., Grönig, H. & Olivier, H., "Effect of reflection type on detonation initiation at shock-wave focusing", *Shock Waves* 10(3), 205–215, 2000.
- Bazhanov, K.A., "The regular case of shock wave diffraction on a wedge partially submerged in fluid", *Appl. Math. & Mech.*, 46, 628–634, 1982.
- Bazhenova, T.V., Fokeev, V.P. & Gvozdeva, L.G., "Regions of various forms of Mach reflection and its transition to regular reflection", *Acta Astro.*, 3, 131–140, 1976.
- Bazhenova, T.V., Fokeev, V.P. & Gvozdeva, L.G., "Reply to the comments of C.K. Law & I.I. Glass", *Acta Astro.*, 4, 943–944, 1977.
- Bazhenova, T.V. & Gvozdeva, L.G., *Unsteady Interactions of Shock Waves*, Nauka, Moscow, SSSR, 1977.
- Bazhenova, T.V. & Gvozdeva, L.G., "The reflection and diffraction of shock waves", *Fluid Dyn. Trans.*, 11, 7–16, 1983.
- Bazhenova, T.V., Gvozdeva, L.G., Komarov, V.S. & Sukhov, B.G., "Pressure and temperature change on the wall surface in strong shock wave diffraction", *Astro. Acta*, 17, 559–566, 1972.
- Bazhenova, T.V., Gvozdeva, L.G., Komarov, V.S. & Sukhov, B.G., "Diffraction of strong shock waves by convex corners", *Izv. Akad. Nuak SSSR, Mekh. Zh. Gaza*, 4, 122–134, 1973.
- Bazhenova, T.V., Gvozdeva, L.G. & Nettleton, M.A., "Unsteady interactions of shock waves", *Prog. Aero. Sci.*, 21, 249–331, 1984.
- Bazhenova, T.V., Gvozdeva, L.G. & Zhilin, Yu.V., "Change in the shape of a diffracting shock wave at a convex corner", *Acta Astro.*, 6, 401–412, 1979.
- Ben-Dor, G., "A reconsideration of the shock polar solution of a pseudo-steady single-Mach reflection", *CASI Trans.*, 26, 98–104, 1980.
- Ben-Dor, G., "Analytical solution of double-Mach reflection", *AIAA J.*, 18, 1036–1043, 1980.
- Ben-Dor, G., "Steady oblique shock wave reflections in perfect and imperfect monatomic and diatomic gases", *AIAA J.*, 18, 1143–1145, 1980.
- Ben-Dor, G., "Relation between first and second triple point trajectory angles in double-Mach reflection", *AIAA J.*, 19, 531–533, 1981.
- Ben-Dor, G., "A reconsideration of the three-shock theory of a pseudo-steady Mach reflection", *J. Fluid Mech.*, 181, 467–484, 1987.
- Ben-Dor, G., "Steady, pseudo-steady and unsteady shock wave reflections", *Prog. Aero. Sci.*, 25, 329–412, 1988.
- Ben-Dor, G., "Structure of the contact discontinuity of nonstationary Mach reflections", *AIAA J.*, 28, 1314–1316, 1990.
- Ben-Dor, G., "Interaction of a planar shock wave with a double wedge-like structure", *AIAA J.*, 30(1), 274–278, 1992.

- Ben-Dor, G., "Reconsideration of the-state-of-the-art of shock-wave-reflection-phenomenon in steady-flows", Japan Soc. Mech. Eng. Int. J., Ser. B, 38(3), 325–334, 1995.
- Ben-Dor, G., "Hysteresis phenomena in shock wave reflection in steady flows", Math. Proc. Tech., 85, 15–19, 1999.
- Ben-Dor, G., "Comments on 'On stability of strong and weak reflected shocks' by S. Mölder, E.V. Timofeev, C.G. Dunham, S. McKinley & P.A. Voinovich", Shock Waves, 11(4), 327–328, 2002.
- Ben-Dor, G., "Pseudo-steady shock wave reflections wave configurations and transition criteria: State-of-the knowledge", Comp. Fluid Dyn. J., 12(2), 132–138, 2003.
- Ben-Dor, G., "A state-of-the-knowledge review on pseudo-steady shock-wave reflections and their transition criteria", Shock Waves, 15(3/4), 277–294, 2006.
- Ben-Dor, G. & Dewey, J.M., "The Mach reflection phenomenon – A suggestion for an international nomenclature", AIAA J., 23, 1650–1652, 1985.
- Ben-Dor, G., Dewey, J.M., McMillin, D.J. & Takayama, K., "Experimental investigation of the asymptotically approached Mach reflection over the second surface in a reflection over a double wedge", Exp. Fluids, 6, 429–434, 1988.
- Ben-Dor, G., Dewey, J.M. & Takayama, K., "The reflection of a planar shock wave over a double wedge", J. Fluid Mech., 176, 483–520, 1987.
- Ben-Dor, G. & Elperin, T., "Analysis of the wave configuration resulting from the termination of an inverse Mach reflection", Shock Waves, 1(3), 237–241, 1991.
- Ben-Dor, G., Elperin, T. & Golshtain, E., "Monte Carlo analysis of the hysteresis phenomenon in steady shock wave reflections", AIAA J., 35(11), 1777–1779, 1997.
- Ben-Dor, G., Elperin, T., Li, H. & Vasilev, E., "Downstream pressure induced hysteresis in the regular → Mach reflection transition in steady flows", Phys. Fluids, 9(10), 3096–3098, 1997.
- Ben-Dor, G., Elperin, T., Li, H. & Vasilev, E., "The influence of downstream-pressure on the shock wave reflection phenomenon in steady flows", J. Fluid Mech., 386, 213–232, 1999.
- Ben-Dor, G., Elperin, T. & Vasiliev, E.I., "Flow-Mach-number-induced hysteresis phenomena in the interaction of conical shock waves – A numerical investigation", J. Fluid Mech., 496, 335–354, 2003.
- Ben-Dor, G., Elperin, T. & Vasilev, E.I., "Shock wave induced extremely high oscillating pressure peaks", Materials Science Forum, 465/466, 123–130, 2004.
- Ben-Dor, G., Elperin, T., Li, H., Vasilev, E., Chpoun, A. & Zeitoun, D., "Dependence of steady Mach reflections on the reflecting-wedge-trailing-edge-angle", AIAA J., 35(1), 1780–1282, 1997.

- Ben-Dor, G. & Glass, I.I., "Nonstationary oblique shock wave reflections: Actual isopycnics and numerical experiments", *AIAA J.*, 16, 1146–1153, 1978.
- Ben-Dor, G. & Glass, I.I., "Domains and boundaries of nonstationary oblique shock wave reflections:1. Diatomic gas", *J. Fluid Mech.*, 92, 459–496, 1979.
- Ben-Dor, G. & Glass, I.I., "Domains and boundaries of nonstationary oblique shock wave reflections:2. Monatomic gas", *J. Fluid Mech.* 96, 735–756, 1980.
- Ben-Dor, G., Ivanov, M., Vasilev, E.I. & Elperin, T., "Hysteresis processes in the regular reflection \rightleftharpoons Mach reflection transition in steady flows", *Prog. Aerospace Sci.*, 38(4/5), 347–387, 2002.
- Ben-Dor, G., Mazor, G., Takayama, K. & Igra, O., "The influence of surface roughness on the transition from regular to Mach reflection in a pseudo steady flow", *J. Fluid Mech.*, 176, 333–356, 1987.
- Ben-Dor, G. & Rayevsky, D., "Shock wave interaction with a high density step like layer", *Fluid Dyn. Res.*, 13(5), 261–279, 1994.
- Ben-Dor, G. & Takayama, K., "Analytical prediction of the transition from Mach to regular reflection over cylindrical concave wedges", *J. Fluid Mech.*, 158, 365–380, 1985.
- Ben-Dor, G. & Takayama, K., "Application of steady shock polars to unsteady shock wave reflections", *AIAA J.*, 24, 682–684, 1986.
- Ben-Dor, G. & Takayama, K., "The dynamics of the transition from Mach to regular reflection over concave cylinders", *Israel J. Tech.*, 23, 71–74, 1986/7.
- Ben-Dor, G. & Takayama, K., "The reflection of a planar shock wave over a water wedge", *Israel J. Tech.*, 23, 169–173, 1986/7.
- Ben-Dor, G. & Takayama, K., "Streak camera photography with curved slits for the precise determination of shock wave transition phenomena", *CASI J.*, 27, 128–134, 1981.
- Ben-Dor, G., Takayama, K. & Dewey, J.M., "Further analytical considerations of the reflection of a weak shock wave over a concave wedge", *Fluid Dyn. Res.*, 2, 77–85, 1987.
- Ben-Dor, G., Takayama, K. & Kawauchi, T., "The transition from regular to Mach reflection and from Mach to regular reflection in truly nonstationary flows", *J. Fluid Mech.* 100, 147–160, 1980.
- Ben-Dor, G., Takayama, K. & Needham, C.E., "The thermal nature of the triple point of a Mach reflection", *Phys. Fluids*, 30, 1287–1293, 1987.
- Ben-Dor, G. & Takayama, K., "The phenomena of shock wave reflection – A review of unsolved problems and future research needs", *Shock Waves*, 2(4), 211–223, 1992.
- Ben-Dor, G., Vasilev, E.I., Elperin, T. & Chpoun, A., "Hysteresis phenomena in the interaction process of conical shock waves: Experimental and numerical investigations", *J. Fluid Mech.*, 448, 147–174, 2001.
- Ben-Dor, G., Vasilev, E.I., Elperin, T. & Zenovich, A.V., "Self-induced oscillations in the shock wave flow pattern formed in a stationary supersonic flow over a double wedge", *Phys. Fluids*, 15(2), L85–L88, 2003.

- Berezkina, M.K., Syshchikova, M.P. & Semenov, A.N., "Interaction of two consecutive shock waves with a wedge", Sov. Phys. Tech. Phys., 27, 835–841, 1982.
- Beryozkina, M.K., Syshchikova, M.P., Semenov, A.N. & Krassovskaya, I.V., "Some properties of the nonstationary interaction of two shock waves with a wedge", Arch. Mech., 32, 621–631, 1980.
- Beryozkina, M.K., Syshchikova, M.P. & Semenov, A.N., "Interaction of two successive shock waves with a wedge", Zh. Tekh. Fiz., 52, 1375–1385, 1982.
- Bleakney, W., Fletcher, C.H. & Weimer, D.K., "The density field in Mach reflection of shock waves", Phys. Rev. 76, 323–324, 1949.
- Bleakney, W. & Taub, A.H. "Interaction of shock waves", Rev. Mod. Phys., 21, 584–605, 1949.
- Bleakney, W., White, D.R. & Griffith, W.C., "Measurement of diffraction of shock waves and resulting loading of structure", J. Appl. Mech., 17, 439–445, 1950.
- Bogatko, V.I. & Kolton, G.A., "On regular reflection of strong shock waves by a thin wedge", Izv. Akad. Nauk SSSR, Mekh. Zh. i Gaza, 5, 55–61, 1974.
- Bogatko, V.I. & Kolton, G.A., "Regular reflection of a strong shock wave by the surface of a wedge", Izv. Akad. Nauk SSSR, Mekh. Zh. i Gaza, 2, 92–96, 1983.
- Bryson, A.E. & Gross, R.F.W., "Diffraction of strong shocks by cones, cylinders and spheres", J. Fluid Mech., 10, 1–16, 1961.
- Buggisch, H., "The steady two-dimensional reflection of an oblique partly dispersed shock wave from a plane wall", J. Fluid Mech., 61, 159–172, 1973.
- Burtschell, Y., Zeitoun, D.E. & Ben-Dor, G., "Steady shock wave reflections in thermochemical nonequilibrium flows", Shock Waves, 11(1), 15–21, 2001.
- Burtschell, Y. & Zeitoun, D.E., "Shock/shock and shock/boundary layer interactions in axisymmetric laminar flows", Shock Waves, 12(6), 487–495, 2003.
- Burtschell, Y. & Zeitoun, D.E., "Real gas effects and boundary layer suction in reflected shock tunnel", Comp. Fluid Dyn., 4(6), 277–284, 2004.
- Chang, K.S. & Kim, S.W., "Reflection of shock wave from a compression corner in the particulate laden gas region", Shock Waves, 1(1), 65–74, 1991.
- Chang, T.S. & Laporte, O., "Reflection of strong blast waves", Phys. Fluids, 7, 1225–1232, 1964.
- Chester, W., "The diffraction and reflection of shock waves", Quart. J. Mech. & Appl. Math., 7, 57–82, 1954.
- Chopra, M.G., "Diffraction and reflection of shock from corners", AIAA J., 11, 1452–1453, 1973.
- Chpoun, A. & Ben-Dor, G., "Numerical confirmation of the hysteresis phenomenon in the regular to the Mach reflection transition in steady flows", Shock Waves, 5(4), 199–204, 1995.
- Chpoun, A., Chauveux, F., Zombas, L. & Ben-Dor, G., "Interaction d'onde de choc coniques de familles opposées en écoulement hypersonique stationnaire", Mécanique des Fluides/Fluid Mech., C.R. Acad. Sci. Paris, 327(1), IIb, 85–90, 1999.

- Chpoun, A. & Lengrand, J.C., "Conformation experimentale d'un phénomène d'hysteresis lors de l'interaction de deux chocs obliques de familles différentes", C.R. Acad. Sci. Paris, 304, 1, 1997.
- Chpoun, A., Passerel, D. & Ben-Dor, G., "Stability of regular and Mach reflection wave configurations in steady flows", AIAA J. 34(10), 2196–2198, 1996.
- Chpoun, A., Passerel, D., Lengrand, J.C., Li, H. & Ben-Dor, G., "Mise en évidence expérimentale et numérique d'un phénomène d'hysteresis lors de la transition réflexion de Mach-réflexion réguliare", Mécanique des Fluides/Fluid Mech., C.R. Acad. Sci. Paris, 319(II), 1447–1453, 1994.
- Chpoun, A., Passerel, D., Lengrand, J.C., Li, H. & Ben-Dor, G., "Etudes expérimentale et numérique de la réflexion d'une onde de choc oblique en écoulement stationnaire hypersonique", La Recherche Aérospatiale, 2, 95–105, 1996.
- Chpoun, A., Passerel, D., Li, H. & Ben-Dor, G., "Reconsideration of oblique shock wave reflection in steady flows. Part I: Experimental investigation", J. Fluid Mech., 301, 19–35, 1995.
- Clarke, J.F., "Regular reflection of a weak shock wave from a rigid porous wall", Quar. J. Mech. & Appl. Math., 37, 87–111, 1984.
- Clarke, J.F., "Reflection of a weak shock wave from a perforated plug", J. Eng. Math., 18, 335–350, 1984.
- Clarke, J.F., "The reflection of weak shock waves from absorbent surfaces", Proc. Roy. Soc. London, A396, 365–382, 1984.
- Colella, P. & Henderson, L.F., "The von Neumann paradox for the diffraction of weak shock waves", J. Fluid Mech., 213, 71–94, 1990.
- Courant, R. & Friedrichs, K.O., *Supersonic Flow and Shock Waves*, Wiley Interscience, New York, U.S.A., 1948.
- Deschambault, R.L. & Glass I.I., "An update on non-stationary oblique shock wave reflections. Actual isopycnics and numerical experiments", J. Fluid Mech., 131, 27–57, 1983.
- Davis, J.L., "On the nonexistence of four confluent shock waves", J. Aero. Sci., 20, 501–502, 1953.
- Dewey, J.M., "The Mach reflection of spherical blast waves", Nucl. Eng. & Des., 55(3), 363–373, 1979.
- Dewey, J.M. & Lock, G.D., "An experimental investigation of the sonic criterion for transition from regular to Mach reflection of weak shock waves", Expts. Fluids, 7, 289–292, 1989.
- Dewey, J.M., McMillin, D.J. & Classen, D.F., "Photogrammetry of spherical shocks reflected from real and ideal surfaces", J. Fluid Mech., 81(4), 701–717, 1977.
- Dewey, J.M. & McMillin, D.J., "An analysis of the particle trajectories in spherical blast waves reflected from real and ideal surfaces", Canadian J. Phys., 59(10), 1380–1390, 1981.
- Dewey, J.M. & McMillin, D.J., "Observation and analysis of the Mach reflection of weak uniform plane shock waves, Part 1. Observations", J. Fluid Mech., 152, 49–66, 1985.

- Dewey, J.M., & McMillin, D.J., "Observation and analysis of the Mach reflection of weak uniform plane shock waves. Part 2. Analysis", *J. Fluid Mech.*, 152, 67–81, 1985.
- Dewey, J.M., McMillin, D.J. & Classen, D.F., "Photogrammetry of spherical shocks reflected from real and ideal surfaces", *J. Fluid Mech.*, 81, 701–717, 1977.
- Dewey, J.M. & Walker, D.K., "A multiply pulsed double-pass laser schlieren system for recording the movement of shocks and particle tracers within a shock tube", *J. Appl. Phys.*, 46, 3454–3458, 1975.
- Druguet, M-C & Zeitoun, D.E., "Influence of numerical and viscous dissipation on shock wave reflection in supersonic steady flows", *Int. J. Computers & Fluids*, 32(4), 515–533, 2002.
- Dulov, V.G., "About the motion of a triple shock wave configuration with wake formation behind the branching point", *J. Appl. Mech. & Tech. Phys.*, 6, 67–75, 1973. (In Russian)
- Dunayev, Yu.A., Syschikova, M.P., Berezkina, M.K. & Semenov, A.N., "The interaction of a shock wave with a body in the presence of ionization relaxations", *Acta Astro.*, 14, 491–495, 1969.
- Dunne, B.B., "Mach reflection of 700-kbar shock waves in gases", *Phys. Fluids*, 4, 1565–1566, 1961.
- Dunne, B.B., "Mach reflection of detonation waves in condensed high explosives", *Phys. Fluids*, 4, 918–924, 1961.
- Dunne, B.B., "Mach reflection of detonation waves in condensed high explosives. II", *Phys. Fluids*, 7, 1707–1712, 1964.
- Duong, D.Q. & Milton, B.E., "The Mach reflection of shock waves in converging cylindrical channels", *Exp. Fluids*, 3, 161–168, 1985.
- Durand, A., Chanetz, B., Benay, R. & Chpoun, A., "Investigation of shock waves interference and associated hysteresis effect at variable Mach upstream flow", *Shock Waves*, 12(6), 469–477, 2003.
- Falcovitz, J., Alfandary, G. & Ben-Dor, G., "Numerical simulation of the head-on reflection of a regular reflection", *Int. J. Num. Methods Fluids*, 17(2), 1055–1078, 1993.
- Felthun, L.T. & Skews, B.W., "Dynamic shock wave reflection", *AIAA J.*, 42(8), 1633–1639, 2004.
- Fletcher, C.H., Taub, A.H. & Bleakney, W., "The Mach reflection of shock waves at nearly glancing incidence", *Rev. Mod. Phys.*, 23, 271–286, 1951.
- Fletcher, C.H., Weimer, D.K. & Bleakney, W., "Pressure behind a shock wave diffracted through a small angle", *Phys. Rev.*, 78, 634–635, 1950.
- Gelfand, B.E., Bartenev, A.M., Medvedev, S.P., Polenov, A.N., Khomik, S.V., Lenartz, M. & Grönig, H., Specific features of incident and reflected blast waves, *Shock Waves*, 4(3), 137–143, 1994.
- Ginzberg, I.P. & Markov, Yu.S., "Experimental investigation of the reflection of a shock wave from a two-facet wedge", *Fluid Mech.-Sov. Res.*, 4, 167–172, 1975.

- Glass, I.I., "Present status of oblique-shock-wave reflections", *Physicochem. Hydrody.*, 6, 863–864, 1985.
- Glass, I.I., "Some aspects of shock-wave research", *AIAA J.*, 25, 214–229, 1987.
- Glass, I.I., "Over forty years of continuous research at UTIAS on nonstationary flows and shock waves", *Shock Waves*, 1(1), 75–86, 1991.
- Glass, I.I. & Heuckroth, L.G., "Head-on collision of spherical shock waves", *Phys. Fluids*, 2, 542–546, 1959.
- Glaz, H.M., Colella, P., Collins, J.P. & Ferguson, R.E., "Nonequilibrium effects in oblique shock wave reflection", *AIAA J.*, 26, 698–705, 1988.
- Glaz, H.M., Colella, P., Glass, I.I. & Deschambault, R.L., "A numerical study of oblique shock-wave reflections with experimental comparisons", *Proc. Roy. Soc. London*, A398, 117–140, 1985.
- Grasso, F., Purpura, C., Chanetz, B. & Délery, J., "Type III and Type IV shock/shock interferences : Theoretical and experimental aspects", *Aero. Sci. & Tech.*, 7, 93–106, 2003.
- Griffith, W.C., "Shock Waves", *J. Fluid Mech.*, Vol. 106, pp. 81–101, 1981.
- Griffith, W.C. & Bleakney, W., "Shock waves in gases", *Amer. J. Phys.*, 22, 597–612, 1954.
- Griffith, W.C. & Brickle, D.E., "The diffraction of strong shock waves", *Phys. Rev.*, 89, 451–453, 1953.
- Grove, J.W., & Menikoff, R., "Anomalous reflection of a shock wave at a fluid interface", *J. Fluid Mech.*, 219, 313–336, 1990.
- Grudnitskii, V.G. & Prokhorchuk, Yu.A., "Analysis of the diffraction of a shock wave at a curvilinear surface", *J. Num. Anal. & Math. Phys.*, 15, 1525–1534, 1975.
- Gun'ko, Yu.P., Kudryavtsev, A.N. & Rakhimov, R.D., "Supersonic inviscid corner flows with regular and irregular shock interaction", *Fluid Dynamics*, 39(2), 304–318, 2004.
- Gvozdeva, L.G., Bazhenova, T.V., Lagutov, Yu.P. & Fokeev, V.P., "Shock wave interaction with cylindrical surfaces", *Arch. Mech.*, 32, 693–702, 1980.
- Gvozdeva, L.G., Bazhenova, T.V., Predvoditeleva, O.A. & Fokeev, V.P., "Mach reflection of shock waves in real gases", *Astro. Acta*, 14, 503–508, 1969.
- Gvozdeva, L.G. Bazhenova, T.V., Predvoditeleva, O.A. & Fokeev, V.P., "Pressure and temperature at the wedge surface for Mach reflection of strong shock waves", *Astro. Acta*, 15, 503–510, 1970.
- Gvozdeva, L.G. & Fokeev, V.P., "Experimental study of irregular shock wave reflection from the surface of a wedge", *Fiz. Gorenia i Vzryva*, 12, 260–269, 1976.
- Gvozdeva, L.G. & Fokeev, V.P., "Transition from Mach to regular reflection and domains of various Mach reflection configurations", *Comb. Exp. & Shock Waves*, 13, 86–93, 1977.

- Gvozdeva, L.G., Lagutov, Yu.P. & Fokeev, V.P., "Transition from regular reflection to Mach reflection in the interaction of shock waves with a cylindrical surface", Sov. Tech. Phys. Lett., 5, 334–336, 1979.
- Gvozdeva, L.G., Lagutov, Yu.P. & Fokeev, V.P., "Transition from Mach reflection to regular reflection when strong shock waves interact with cylindrical surfaces", Izv. Akad. Nauk SSSR, Mekh. Zh. i Gaza, 2, 132–138, 1982.
- Gvozdeva, L.G. & Predvoditeleva, O.A., "Experimental investigation of Mach reflection of shock waves with velocities of 1000–3000 m/sec in carbon dioxide gas, nitrogen and Air", Sov. Phys. Dokl., 10, 694–697, 1965.
- Gvozdeva, L.G., Predvoditeleva, O.A. & Fokeev, V.P., "Double Mach reflection of strong shock waves", Izv. Akad. Nauk SSSR, Mekh. Zh. i Gaza, 14, 112–119, 1968.
- G., Predvoditeleva, O.A., "A study of triple configuration of detonation waves in gases", Comb. Exp. & Shock Waves, 4, 451–461, 1969.
- Hadjadj, A., Kudryavtsev, A.N. & Ivanov, M.S., "Numerical investigation of shock-reflection phenomena in overexpanded supersonic jets", AIAA J., 42(3), 570–577, 2004.
- Han, Z.Y., Milton, B.E. & Takayama, K., "The Mach reflection triple-point locus for internal and external conical diffraction of a moving shock wave", Shock Waves, 2(1), 5–12, 1992.
- Handke, E. & Obermeier, F., "Theoretical results from the Mach reflection of weak shock waves", Z. Angew. Math. & Mech., 65, 202–204, 1985.
- Heilig, W.H., "Diffraction of shock wave by a cylinder", Phys. Fluids Suppl. I, 12, 154–157, 1969.
- Henderson, L.F., "On the confluence of three shock waves in a perfect gas", Aero. Quart., 15, 181–197, 1964.
- Henderson, L.F., "The three shock confluence on a simple wedge intake", Aero. Quart., 16, 42–54, 1965.
- Henderson, L.F., "The reflection of a shock wave at a rigid wall in the presence of a boundary layer", J. Fluid Mech., 30, 699–723, 1967.
- Henderson, L.F., "On the Whitham theory of shock wave diffraction at concave corners", J. Fluid Mech., 99, 801–811, 1980.
- Henderson, L.F., "Exact expressions for shock reflection transition criteria in a perfect gas", Z. Ang. Math. & Mech., 62, 258–261, 1982.
- Henderson, L.F., "Regions and boundaries for diffracting shock wave systems", Z. Ang. Math. & Mech., 67, 1–14, 1987.
- Henderson, L. F., "On the refraction of shock waves", J. Fluid Mech., 198, 365–386, 1989.
- Henderson, L.F., Crutchfield, W.Y. & Virgona, R.J., "The effects of thermal conductivity and viscosity of argon on shock waves diffracting over rigid ramps", J. Fluid Mech., 331, 1–36, 1997.
- Henderson, L.F. & Gray, P.M., "Experiments on the diffraction of strong blast waves", Proc. Roy. Soc. London, Ser. A377, pp. 363–378, 1981.
- Henderson, L.F. & Lozzi, A., "Experiments on transition of Mach reflection", J. Fluid Mech., 68, 139–155, 1975.

- Henderson, L.F. & Lozzi, A., "Further experiments on transition to Mach reflection", *J. Fluid Mech.*, 94, 541–559, 1979.
- Henderson, L.F., Ma, J-H, Sakurai, A. & Takayama, K., "Refraction of a shock wave at an air-water interface", *Fluid Dyn. Res.*, 5, 337–350, 1990.
- Henderson, L.F. & Menikoff, R., "Triple-shock entropy theorem and its consequences", *J. Fluid Mech.*, 366, 179–210, 1998.
- Henderson, L.F. & Siegenthaler, A., "Experiments on the diffraction of weak blast waves: The von Neumann paradox", *Proc. Roy. Soc. London*, A369, 537–555, 1980.
- Henderson, L.F., Takayama, K., Crutchfield, W.Y. & Itabashi, S., "The persistence of regular reflection during strong shock diffraction over rigid ramps", *J. Fluid Mech.*, 431, 273–296, 2001.
- Henderson, L.F., Vasilev, E.I., Ben-Dor, G. & Elperin, T., "The wall-jetting effect in Mach reflection: Theoretical consideration and numerical investigation", *J. Fluid Mech.*, 479, 259–286, 2003.
- Higashino, F., Henderson, L.F. & Shimizu, F., "Experiments on the interaction of a pair of cylindrical weak blast waves in air", *Shock Waves*, 1(4), 275–284, 1991.
- Honma, H., Glass, I.I., Wong, C.H., Holst-Jensen, O., "Experimental and numerical studies of weak blast wave in air", *Shock waves*, 1(2), 111–119, 1991.
- Honma, H. & Henderson, L.F., "Irregular reflections of weak shock waves in polyatomic gases", *Phy. Fluids A*, 1, 597–599, 1989.
- Honma, H., Maekawa, H. & Usui, T., "Numerical analysis of non stationary oblique reflection of weak shock waves", *Computer & Fluids*, 21(2), 201–210, 1992.
- Hornung, H.G., "The effect of viscosity on the Mach stem length in unsteady shock reflection", *Lecture Notes Phys.*, 235, 82–91, 1985.
- Hornung, H.G., "Regular and Mach reflection of shock waves", *Ann. Rev. Fluid Mech.*, 18, 33–58, 1986.
- Hornung, H.G., "Mach reflection of shock-waves", *Zeitschrift fur Flugwissenschaften und Weltraumforschung*, 12(4), 213–223, 1988.
- Hornung, H.G., "On the stability of steady-flow regular and Mach reflection", *Shock Waves*, 7(2), 123–125, 1997.
- Hornung, H.G., "Oblique shock reflection from an axis of symmetry", *J. Fluid Mech.*, 409, 1–12, 5 2000.
- Hornung, H.G., Oertel, H.Jr. & Sandeman, R.J., "Transition to Mach reflection of shock waves in steady and pseudosteady flow with and without relaxation", *J. Fluid Mech.*, 90, 541–560, 1979.
- Hornung, H.G. & Robinson, M.L., "Transition from regular to Mach reflection of shock waves. Part 2. The steady flow criterion", *J. Fluid Mech.*, 123, 155–164, 1982.
- Hornung, H.G. & Schwendeman, D.W., "Oblique shock reflection from an axis of symmetry: shock dynamics and relation to the Guderley singularity", *J. Fluid Mech.*, 438, 231–245, 2001.

- Hornung, H.G. & Taylor, J.R., "Transition from regular to Mach reflection of shock waves. Part 1. The effect of viscosity in the pseudosteady case", *J. Fluid Mech.*, 123, 143–153, 1982.
- Hosseini, S.H.R. & Takayama, K., "Implosion of a spherical shock wave reflected from a spherical wall", *J. Fluid Mech.*, 530, 223–239, 2005.
- Hu, T.C.J. & Glass, I.I., "Blast wave trajectories from height of burst", *AIAA J.*, 24, 607–610, 1986.
- Hu, T.C.J. & Glass, I.I., "Pseudostationary oblique shock wave reflections in sulphur hexafluoride (SF_6): Interferometric and numerical results", *Proc. Roy. Soc. London A* 408, 321–344, 1986.
- Hunt, B.L., "Calculation of two-dimensional and three-dimensional regular shock interactions", *Aero. J.*, 828, 285–289, 1980.
- Hunt, B.L. & Lamont, P.J., "The confluence of three shock waves in a three-dimensional flow", *Aero. Quart.*, 29, 18–27, 1978.
- Hunter, J.K. & Brio, M., "Weak shock reflection", *J. Fluid Mech.* 410, 235–261, 2000.
- Ikui, T., Matsuo, K., Aoki, T. & Kondoh, N., "Investigations of Mach reflection of a shock wave. Part 1. Configurations and domains of shock reflection", *Bull. Japan Soc. Mech. Eng.*, 25, 1513–1520, 1982.
- Irving Brown, Y.A. & Skews, B.W., "Three-dimensional effects on regular reflection in steady supersonic flows", *Shock Waves*, 13(5), 339–349, 2004.
- Itoh, S., Okazaki, N. & Itaya, M., "On the transition between regular and Mach reflection in truly non-stationary flows", *J. Fluid Mech.*, 108, 383–400, 1981.
- Itoh, K., Takayama, K. & Ben-Dor, G., "Numerical simulation of the reflection of a planar shock wave over a double wedge", *Int. J. Num. Methods Fluids*, 13, 1153–1170, 1991.
- Ivanov, M.S., Ben-Dor, G., Elperin, T., Kudryavtsev, A.N. & Khotyanovsky, D.V. "Mach-number-variation-induced hysteresis in steady flow shock wave reflections", *AIAA J.*, 39(5), 972–974, 2001.
- Ivanov, M.S., Ben-Dor, G., Elperin, T., Kudryavtsev, A.N. & Khotyanovsky, D.V., "The reflection of asymmetric shock waves in steady flows: A numerical investigation", *J. Fluid Mech.*, Vol. 462, pp. 285–306, 2002.
- Ivanov, M.S., Gimelshein, S.F. & Beylich, A.E. "Hysteresis effect in stationary reflection of shock waves", *Phys Fluids*, 7(4), 685–687, 1995.
- Ivanov, M.S., Gimelshein, S.F. & Markelov, G.N., "Statistical simulation of the transition between regular and Mach reflection in steady flows", *Computers in Math. with Appl.*, 35(1/2), 113–125, 1998.
- Ivanov, M.S., Klemenkov, G.P., Kudryavtsev, A.N., Fomin, V.M. & Kharitonov, A.M., "Experimental investigation of transition to Mach reflection of steady shock waves", *Doklady Phys.*, 42(12), 691–695, 1997.
- Ivanov, M.S., Kudryavtsev, A.N. & Khotyanovski, D.V., "Numerical simulation of the transition between the regular and Mach reflection of shock waves under the action of local perturbations", *Doklady Phys.*, 45(7), 353–357, 2000.

- Ivanov, M.S., Kudryavtsev, A.N. Nikiforov, S.B. & Khotyanovsky, D.V., "Transition between regular and Mach reflection of shock waves: new numerical and experimental results", Aeromech. & Gas Dyn., 2002, No.3, pp. 3–12 (in Russian).
- Ivanov, M.S., Kudryavtsev, A.N., Nikiforov, S.B., Khotyanovsky, D.V. & Pavlov, A.A., "Experiments on shock wave reflection transition and hysteresis in low-noise wind tunnel", Phys. Fluids, 15(6), 1807–1810, 2003.
- Ivanov, M.S., Markelov, G.N., Kudryavtsev, A.N. & Gimelshein, S.F., "Numerical analysis of shock wave reflection transition in steady flows", AIAA J., 36(11), 2079–2086, 1998.
- Ivanov, M.S., Vandromme, D., Fomin, V.M., Kudryavtsev, A.N., Hadjadj, A. & Khotyanovsky, D.V., "Transition between regular and Mach reflection of shock waves: new numerical and experimental results", Shock Waves, 11(3), 199–207, 2001.
- Ivanov, M., Zeitoun, D., Vuillon, J., Gimelshein, S. & Markelov, G.N., "Investigation of the hysteresis phenomena in steady shock reflection using kinetic and continuum methods", Shock Waves 5(6), 341–346, 1996.
- Jahn, R.G., "Transition process in shock wave interactions", J. Fluid Mech., 2, 33–48, 1956.
- Jones, D.M., Martin, P.M.E. & Thornhill, C.K., "A note on the pseudo-stationary flow behind a strong shock diffracted or reflected at a corner", Proc. Roy. Soc. London, A209, 238–248, 1951.
- Kaliski, S. & Włodarczyk, E., "The influence of the parameters of state on the characteristics of regular reflection of oblique shock waves", Proc. Vib. Problems, 14, 4–5, 1973.
- Kaliski, S. & Włodarczyk, E., "Regular reflection of intense oblique shock waves from a rigid wall in a solid body", Proc. Vib. Problems, 15, 271–282, 1974.
- Kawamura, R. & Saito, H., "Reflection of shock waves-1. Pseudo-stationary case", J. Phys. Soc. Japan, 11, 584–592, 1956.
- Khotyanovsky, D.V., Kudryavtsev, A.N. & Ivanov, M.S., "Effects of a single-pulse energy deposition on steady shock wave reflection", Shock Waves, 15(5), 353–362, 2006.
- Kim, S-W. & Chang, K-S., "Reflection of shock wave from a compression corner in a particle-laden gas region", Shock Waves, 1(1), 65–73, 1991.
- Kireev, V.T., "On the reflection of a strong shock wave by a sphere or a cylinder", Izv. Akad. Nauk SSSR, Mekh. Zh. i Gaza, 3, 31–40, 1969.
- Klein, E.J., "Interaction of a shock wave and a wedge: An application of the hydraulic analogy", AIAA J., 3, 801–808, 1965.
- Kobayashi, S., Adachi, T. & Suzuki, T., "An investigation on the transition criterion for reflection of a shock over a dusty surface", Dyn. Image Anal., 1, 67–73, 1988.
- Kobayashi S., Adachi T. & Suzuki T., "Examination of the von Neumann paradox for a weak shock wave", Fluid Dyn. Res., 17(1), 13–25, 1995.

- Kobayashi S., Adachi T. & Suzuki T., "Non-self-similar characteristics of weak Mach reflection: the von Neumann paradox", *Fluid Dyn. Res.*, 35(4), 275–286, 2004.
- Kobayashi, S., & Suzuki, T., "Non-self-similar behavior of the von Neumann reflection", *Phys. Fluids*, 12(7), 1869–1877, 2000.
- Kolgan, V.P. & Fonarev, A.C., "Development of the flow in shock incidence on a cylinder or sphere", *Izv. Akad. Nauk SSSR, Mekh. Zh. i Gaza*, 5, 97–103, 1972.
- Krehl, P. & van der Geest, M., "The discovery of the Mach reflection effect and its demonstration in an auditorium", *Shock Wave*, 1, 3–15, 1991.
- Krishnan, S., Brochet, C. & Cheret, R., "Mach reflection in condensed explosives", *Propellants & Explosives*, 6, 170–172, 1981
- Kudryavtsev, A.N., Khotyanovsky, D.V., Ivanov, M.S., Hadjadj, A. & Vandromme, D., "Numerical investigations of transition between regular and Mach reflections caused by free-stream disturbances", *Shock Waves*, 12(2), 157–165, 2002.
- Kutler, P. & Sakell, L., "Three-dimensional shock on shock interaction problem", *AIAA J.*, 13, 1360–1367, 1975.
- Kutler, P., Sakell, L. & Aiello, G., "Two-dimensional shock on shock interaction problem", *AIAA J.*, 13, 361–367, 1975.
- Kutler, P. & Shankar, V., "Diffraction of a shock wave by a compression corner: I. Regular reflection", *AIAA J.*, 15, 197–203, 1977.
- Law, C., Felthun, L.T. & Skews, B.W., "Two-dimensional numerical study of planar shock-wave/moving-body interactions. Part I: Plane shock-on-shock interactions", *Shock Waves*, 13(5), 381–394, 2004.
- Law, C.K. & Glass, I.I., "Diffraction of strong shock waves by a sharp compressive corner", *CASI Trans.*, 4, 2–12, 1971.
- Law, C.K. & Glass, I.I., "Comments on regions of various forms of Mach reflection and its transition to regular reflection", *Acta Astro.*, 4, 939–941, 1977.
- Law, C. & Skews, B.W., "Two-dimensional numerical study of planar shock-waves/moving-body interactions. Part II: Non-classical shock-wave/moving-body interactions", *Shock Waves*, 13(5), 395–408, 2004.
- Le Kuok Khyu, "Geometrical investigation of the regular reflection of shock waves from a wall", *Izv. Akad. Nauk SSSR, Mekh. Zh. i Gaza*, 5, 182–185, 1980.
- Lee, J.-H. & Glass, I.I., "Pseudo-stationary oblique shock wave reflections in frozen and equilibrium air", *Prog. Aero. Sci.*, 21, 33–80, 1984.
- Li, H. & Ben-Dor, G., "Interaction of regular reflection with a compressive wedge: Analytical solution", *AIAA J.*, 33(5), 955–958, 1995.
- Li, H. & Ben-Dor, G., "Reconsideration of pseudo-steady shock wave reflections and the transition criteria between them", *Shock Waves*, 5(1/2), 59–73, 1995.
- Li, H. & Ben-Dor, G., "Head-on Interaction of weak planar shock waves with flexible porous materials – Analytical model", *Int. J. Multiphase Flow*, 21(5), 941–947, 1995.

- Li, H. & Ben-Dor, G., "Reconsideration of the shock-shock relations for the case of a nonquiescent gas ahead of the shock and verification with experiments", Proc. Roy. Soc. London, A451, 383–397, 1995.
- Li, H. & Ben-Dor, G., "A shock dynamics theory based analytical solution of double Mach reflections", Shock Waves, 5(4), 259–264, 1995.
- Li, H. & Ben-Dor, G., "Oblique-shock/expansion-wave interaction analytical solution", AIAA J., 34(2), 418–421, 1996.
- Li, H. & Ben-Dor, G., "Application of the principle of minimum entropy production to shock wave reflections. I. Steady flows", J. Appl. Phys., 80(4), 2027–2037, 1996.
- Li, H. & Ben-Dor, G., "Application of the principle of minimum entropy production to shock wave reflections. II. Pseudo-steady flows", J. Appl. Phys., 80(4), 2038–2048, 1996.
- Li, H. & Ben-Dor, G., "Analytical investigation of two-dimensional unsteady shock-on-shock interactions", J. Fluid Mech., 340, 101–128, 1997.
- Li, H. & Ben-Dor, G., "A parametric study of Mach reflection in steady flows", J. Fluid Mech., 341, 101–125, 1997.
- Li, H. & Ben-Dor, G., "A modified CCW theory of detonation waves", Comb. & Flame, 113, 1–12, 1998.
- Li, H. & Ben-Dor, G., "Mach reflection wave configuration in two-dimensional supersonic jets of overexpanded nozzles", AIAA J., 36(3), 488–491, 1998.
- Li, H. & Ben-Dor, G., "Interaction of two Mach reflections over concave double wedges-Analytical model", Shock Waves, 9(4), 259–268, 1999.
- Li, H. & Ben-Dor, G., "Analysis of double-Mach-reflection wave configurations with convexly curved Mach stems", Shock Waves, 9(5), 319–326, 1999.
- Li, H., Ben-Dor, G. & Grönig, H., "Analytical study of the oblique reflection of detonation waves", AIAA J., 35 (11), 1712–1720, 1997.
- Li, H., Ben-Dor, G. & Han, Z.Y., "Modification on the Whitham theory for analyzing the reflection of weak shock waves over small wedge angles", Shock Waves, 4(1), 41–45, 1994.
- Li, H., Ben-Dor, G. & Han, Z.Y., "Analytical prediction of the reflected-diffracted shock wave shape in the interaction of a regular reflection with an expansive corner", Fluid Dyn. Res., 14(5), 229–239, 1994.
- Li, H., Chpoun, A. & Ben-Dor, G., "Analytical and experimental investigations of the reflection of asymmetric shock waves in steady flows", J. Fluid Mech., 390, 25–43, 1999.
- Li, H., Levy, A. & Ben-Dor, G., "Analytical prediction of regular reflection over porous surfaces in pseudo-steady flows", J. Fluid Mech., 282, 219–232, 1995.
- Li, H., Levy, A. & Ben-Dor, G., "Head-on interaction of planar shock waves with ideal rigid open-cell porous materials – Analytical model", Fluid Dyn. Res., 16(4), 203–215, 1995.
- Li, Y., Zhang, D. & Cao, Y., "The computational numerical experimental research of Mach reflection", Acta Mech. Sin., 17, 162–167, 1985.

- Liang, S.M., Hsu, J.L. & Wang, J.S., "Numerical Study of Cylindrical Blast-Wave Propagation and Reflection", AIAA J., 39(6), 1152–1158, 2001.
- Liang, S.M. & Liao, C.Y. "Numerical simulation of blast-wave reflection over a wedge using a high-order scheme", Trans. Aero. & Astro. Soc. Rep. China, 34, 69–74, 2002.
- Liang, S.M., Wang, J.S. & Chen, H., "Numerical study of spherical blast-wave propagation and reflection", Shock Waves, 12(1), 59–68, 2002.
- Lighthill, M.J., "The diffraction of blast. I", Proc. Roy. Soc. London, A198, 454–470, 1949.
- Lighthill, M.J., "The diffraction of blast. II", Proc. Roy. Soc. London, A, V200, 554–565, 1950.
- Lipnitskii, Yu.M. & Lyakhov, V.N., "Numerical solution of the problem of shock wave diffraction at a wedge", Izv. Akad. Nauk SSSR, Mekh. Zh. i Gaza, 6, 88–93, 1974.
- Lipnitskii, Yu. M. & Panasenko, A.V., "Investigation into the interaction of a shock wave with an acute case", Izv. Akad. Nauk SSSR, Mech. Zh. i Gaza, 3, 98–104, 1980.
- Lock, G.D. & Dewey, J.M., "An experimental investigation of the sonic criterion for transition from regular to Mach reflection of weak shock waves", Exp. Fluids, 7, 289–292, 1989.
- Logvenov, A.Yu., Misonochnikov, A.L. & Rumyanstev, B.V., "Mach reflection of shock waves in condensed media", Sov. Tech. Phys. Lett., 13, 131–132, 1987.
- Ludloff, H.F. & Friedman, M.B., "Mach reflection of shocks at an arbitrary incidence", J. Appl. Phys., 24, 1247–1248, 1953.
- Ludloff, H.F. & Friedman, M.B., "Aerodynamics of blasts-diffraction of blast around finite corners", J. Aero. Sci., 22, 27–34, 1955.
- Ludloff, H.F. & Friedman, M.B., "Difference solution of shock diffraction problem", J. Aero. Sci., 22, 139–140, 1955.
- Lyakhov, V.N., "Unsteady loads in shock wave diffraction", Izv. Akad. Nauk SSSR, Mekh. Zh. i Gaza, 4, 123–129, 1975.
- Lyakhov, V.N., "Mathematical simulation of Mach reflection of shock waves in media with different adiabatic indices", Izv. Akad. Nauk SSSR, Mekh. Zh. i Gaza, 3, 90–94, 1976.
- Lyakhov, V.N., "Concerning the evaluation of pressure in unsteady reflection of shock waves", Izv. Akad. Nauk SSSR, Mekh. Zh. i Gaza, 2, 100–106, 1977.
- Lyakhov, V.N., "Interaction of shock waves of moderate intensity with cylinders", Izv. Akad. Nauk SSSR, Mekh. Zh. i Gaza, 2, 113–119, 1979.
- Lyakhov, V.N. & Ryzhov, A.S., "On the law of similarity in nonlinear reflection of shock waves by a rigid wall", Izv. Akad. Nauk SSSR, Mekh. Zh. i Gaza, 3, 116–123, 1977.
- Mach, E., "Über den verlauf von funkenwellen in der ebene und im raume", Sitzungsber. Akad. Wiss. Wien, 78, 819–838, 1878.

- Makarevich, G.A., Lisenkova, G.S., Tikhomirov, N.A. & Khodstev, A.V., "Experimental study of Mach reflection of weak shock waves", Sov. Phys.-Tech. Phys., 29, 370–372, 1984.
- Makarevich, G.A., Predvoditeleva, O.A. & Lisenkova, G.S., "Reflection of shock waves from a wedge", Tepl. Vys. Temp., 12, 1318–1321, 1974.
- Makomaski, A.H., "Some effects of surface roughness on two dimensional Mach reflection of moving plane shock waves in Air", CASJ., 12, 109–111, 1966.
- Malamud, G., Levi-Hevroni D. & Levy A., "Head-on collision of a planar shock wave with deformable porous foams", AIAA J., 43(8), 1776–1783, 2005.
- Malamud, G., Levi-Hevroni D. & Levy A., "Two-dimensional model for simulating the shock wave interaction with rigid porous materials", AIAA J., 41(4), 663–673, 2003.
- Marconi, F., "Shock reflection transition in three-dimensional steady flow about interfering bodies", AIAA J., 21, 707–713, 1983.
- Matsuo, K., Aoki, T. & Hirahara, H., "Visual studies of characteristics of slip-stream in Mach reflection of a shock wave", Flow Visualization, 4, 543–548, 1987.
- Matsuo, K., Aoki, T., Hirahara, H., Kondoh, N. & Kuriwaki, K., "Investigations of Mach reflection of a shock wave. Part 3: Strength of a reflected shock wave", Bull. Japan Soc. Mech. Eng., 29, 428–433, 1986.
- Matsuo, K., Aoki, T., Hirahara, H., Kondoh, N. & Kishigami, T., "Investigations of Mach reflection of a shock wave. Part 4: The transition between regular and Mach reflection", Bull. Japan Soc. Mech. Eng., 29, 434–438, 1986.
- Matsuo, K., Aoki, T., Hirahara, H. & Kondoh, N., "Nonlinear problem on interaction between a shock wave and rigid wall", Theor. & Appl. Mech., 33, 51–57, 1985.
- Matsuo, K., Aoki, T., Kondoh, N. & Hirahara, H., "Investigations of Mach reflection of a shock wave. Part 2: Shape of a reflected shock wave", Bull. Japan Soc. Mech. Eng., 29, 422–427, 1986.
- Matsuo, K., Ikui, T. Aoki, T., & Kondoh, N., "Interaction of a propagating shock wave with an inclined wall", Theor. & Appl. Mech., 31, 429–437, 1983.
- Meguro, T. Takayama, K. & Onodera, O., "Three-dimensional shock wave reflection over a corner of two intersecting wedges", Shock Waves, 7(2), 107–121, 1997.
- Merritt, D.L., "Mach reflection on a cone", AIAA J., 6, 1208–1209, 1968.
- Milton, B.E., "Mach reflection using ray-shock theory", AIAA J., 13, 1531–1533, 1975.
- Milton, B.E. & Archer, R.D., "Conical Mach reflection of moving shock waves. Part 1: Analytical considerations", Shock Waves, 6(1), 29–39, 1996.
- Milton, B.E. & Archer, R.D., "Generation of implosions by area change in a shock tube", AIAA J., 7, 779–780, 1969.

- Milton, B.E. & Takayama, K, "Conical Mach reflection of moving shock waves. Part 2: Physical and CFD experimentation", *Shock Waves*, 8(2), 93–104, 1998.
- Mirels, H., "Mach reflection flowfields associated with strong shocks", *AIAA J.*, 23, 522–529, 1985.
- Mogilevich, L.I. & Shindyapin, G.P., "On nonlinear diffraction of weak shock waves", *Prikl. Math. & Mekh.*, 35, 492–498, 1971.
- Mölder, S., "Reflection of curved shock waves in steady supersonic flow", *CASI Trans.*, 4, 73–80, 1971.
- Mölder, S., "Polar streamline directions at the triple point of a Mach interaction of shock waves", *CASI Trans.*, 5, 88–89, 1972.
- Mölder, S., "Particular conditions for the termination of regular reflection of shock waves", *CASI Trans.*, 25, 44–49, 1979.
- Mölder, S. & Timofeev, E.V., "Reply to 'On stability of strong and weak reflected shocks' by G. Ben-Dor", *Shock Waves*, 11(4), 329, 2002.
- Mölder, S., Timofeev, E.V., Dunham, C.G., McKinley, S. & Voinovich, P.A., "On stability of strong and weak reflected shocks", *Shock Waves*, 10(5), 389–393, 2001.
- Morgan, K., "The diffraction of a shock wave by a slender body", *J. Appl. Math. & Phys.*, 26, 13–29, 1975.
- Morgan, K., "The diffraction of a shock wave by an inclined body of revolution", *J. Appl. Math. & Phys.*, 26, 299–306, 1975.
- Moran, T.P. & Moorhem, W.K., "Diffraction of a plane shock by an analytic blunt body", *J. Fluid Mech.*, 38, 127–136, 1969.
- Morro, A., "Oblique interaction of waves with shocks", *Acta Mech.*, 38, 241–248, 1981.
- Murdoch, J.W., "Shock wave interaction with two dimensional bodies", *AIAA J.*, 13, 15–17, 1975.
- Neumann, J. von, *Collected Works*, 6, 238–308, Pergamon Press, 1963.
- Obermeier, F. & Handke, E., "Theoretische ergebnisse zur Mach reflexion schwacher stobwellen", *Z. Ang. Math. & Mech.*, 65, 202–204, 1985.
- Oertel, H. Jr., "Oxygen vibrational and dissociation relaxation behind regular reflected shocks", *J. Fluid Mech.* 74, 477–495, 1976.
- Oertel, H. Jr., "Oxygen dissociation relaxation behind oblique reflected and stationary oblique shocks", *Arch. Mech.*, 30, 123–133, 1978.
- Ofengeim, D.K. & Drikakis, D., "Simulation of blast wave propagation over a cylinder", *Shock Waves*, 7(5), 305–317, 1997.
- Olim, M & Dewey, J.M., "Least energy as a criterion for transition between regular and Mach reflection", *Shock Waves*, 1(4), 243–249, 1991.
- Olim, M & Dewey, J.M., "A revised three-shock solution for the Mach reflection of weak shocks ($1.1 < M_i < 1.5$)", *Shock Waves*, 2(3), 167–176, 1992.
- Olivier, H. & Grönig, H., "The random-choice method applied to two-dimensional shock focusing and diffraction", *J. Comp. Phys.*, 63, 85–106, 1986.

- Omang, M., Børve, S. & Trulsen, J., "Numerical simulations of shock wave reflection phenomena in non-stationary flows using regularized smoothed particle hydrodynamics", *Shock Waves*, 16(2), 167–177, 2006.
- Omang, M., Børve, S. & Trulsen, J., "SPH in spherical and cylindrical coordinates", *J. Comp. Phys.*, 213(1), 391–412, 2006.
- Onodera, H. & Takayama, K., "Interaction of a plane shock wave with slotted wedge", *Exp. Fluids*, 10, 109–115, 1990.
- Onofri, M. & Nasuti, F., "Theoretical considerations on shock reflections and their implications on the evaluations of air intake performance", *Shock Waves*, 11(2), 151–156, 2001.
- Pack, D.C., "The reflection and diffraction of shock waves", *J. Fluid Mech.*, 18, 549–576, 1964.
- Pant, J.C., "Reflection of a curved shock from a straight rigid boundary", *Phys. Fluids*, 14, 534–538, 1971.
- Pant, J.C., "Regular reflection of a shock wave in the presence of a transverse magnetic field", *Z. Ang. Math. & Mech.*, 47, 73–85, 1968.
- Pant, J.C., "Reflection of a curved shock from a straight rigid boundary", *Phys. Fluids*, 14, 534–538, 1971.
- Pekurovskii, L.E., "Shock wave diffraction on a thin wedge moving with a slip relative to the wave front with irregular shock interaction", *Prikl. Math. & Mekh.*, 44, 183–190, 1981.
- Piechór, K., "Reflection of a weak shock wave from an isothermal wall", *Arch. Mech.*, 32, 233–249, 1980.
- Piechór, K., "Regular interaction of two weak shock waves", *Arch. Mech.*, 33, 829–843, 1981.
- Piechór, K., "Regular reflection of a weak shock wave from an inclined plane isothermal wall", *Arch. Mech.*, 33, 337–346, 1981.
- Podlubnyi, V.V. & Fonarev, A.S., "Reflection of a spherical blast wave from plane surface", *Izv. Akad. Nauk SSSR, Mekh. Zh. i Gaza*, 6, 166–172, 1974.
- Poluboyarinov, A.K., "On the motion of the shock front reflected from a blunt body", *Fluid Dynamics*, 6(2), 239–245, 2005.
- Poluboyarinov, A.K. & Tsirkunov, V.E., "Concerning the reflection of a shock wave by a cylinder or a sphere", *Fluid Mech.-Sov. Res.*, 10, 85–91, 1981.
- Ram, R. & Sharma, V.D., "Regular reflection of a shock wave from a rigid wall in a steady plane flow of an ideal dissociating gas", *Tensor*, 26, 185–190, 1972.
- Rawling, G. & Polacheck, H., "On the three shock configuration", *Phys. Fluids*, 1, 572–577, 1950.
- Rayevsky, D. & Ben-Dor, G., "Shock wave interaction with a thermal layer", *AIAA J.*, 30(4), 1135–1139, 1992.
- Reichenbach, H., "Contribution of Ernst Mach to fluid mechanics", *Ann. Rev. Fluid Mech.*, 15, 1–28, 1983.
- Rikanati, A., Sadot, O., Ben-Dor, G., Shvarts, D., Kurabayashi, T. & Takayama, K., "Shock-wave Mach-reflection slip-stream instability: A secondary

- small-scale turbulent mixing phenomenon”, Phys. Rev. Lett., 96, 174503: 1-174503:4, 2006.
- Rusanov, V.V., “Calculation of the interaction of non-stationary shock waves and obstructions”, J. Num. Anal. & Math. Phys., 1, 267–279, 1961.
- Ryzhov, O.S. & Khristianovich, S.A., “Nonlinear reflection of weak shock waves”, Prikl. Math. & Mekh., 22, 586–599 1958.
- Sakurai, A., “On the problem of weak Mach reflection”, J. Phys. Soc. Japan, 19, 1440–1450, 1964.
- Sakurai, A., Henderson, L.F., Takayama, K., Walenta, Z. & Colella, P., “On the von Neumann paradox of weak Mach reflection”, Fluid Dyn. Res., 4, 333–345, 1989.
- Sakurai, A., Srivastava, R.S., Takahashi, S. & Takayama, F., “A note on Sandeman’s simple physical theory of weak Mach reflection”, Shock Waves, 11(5), 409–411, 2002.
- Sakurai, A. & Takayama, F., “Analytical solution of a flow field for weak Mach reflection over a plane surface”, Shock Waves, 14(4), 225–230, 2005.
- Sandeman, R.J., “A simple physical theory of weak Mach reflection over plane surfaces”, Shock Waves, 10(2), 103–112, 2000.
- Sanderson, S.R., Hornung, H.G. & Sturtevant, B., “Aspects of planar, oblique and interacting shock waves in an ideal dissociating gas”, Phys. Fluids, 15(6), 1638–1649, 2003.
- Sasoh, A. & Takayama, K., “Characterization of disturbance propagation in weak shock-wave reflections”, J. Fluid Mech., 277, 331–345, 1994.
- Sasoh, A., Takayama, K. & Saito, T., “A weak shock wave reflection over wedges”, Shock Waves, 2(4), 277–281, 1992.
- Schmidt, B., “Shock-wave transition from regular to Mach reflection on a wedge-shaped edge”, Z. Ang. Math. & Mech., 65, 234–236, 1985.
- Schneyer, G.P., “Numerical simulation of regular and Mach reflections”, Phys. Fluids, 18, 1119–1124, 1975.
- Schotz, M., Levy, A., Ben-Dor, G. & Igra, O., “Analytical prediction of the wave configuration size in steady flow Mach reflections”, Shock Waves, 7(6), 363–372, 1997.
- Semenov, A.N. & Syshchikova, M.P., “Properties of Mach reflection in the interaction of shock waves with a stationary wedge”, Comb. Expl. & Shock Waves, 11, 506–515, 1975.
- Semenov, A.N., Syshchikova, M.P. & Berezkina, M.K., “Experimental investigation of Mach reflection in a shock tube”, Sov. Phys.-Tech. Phys., 15, 795–803, 1970.
- Shankar, V., Kutler, P. & Anderson D.A., “Diffraction of a shock wave by a compression corner: Part II: Single Mach reflection”, AIAA J., 16, 4–5, 1978.
- Sharma, V.D. & Shyman, R., “Regular reflection of a shock wave from a rigid wall in a steady plane flow of a vibrationally relaxing gas”, Indian J. Pure & Appl. Math., 15, 15–22, 1984.

- Shindyapin, G.P., "Irregular reflection of weak shock waves from a rigid wall", *Zh. Prikl. Mekh. i Tekh. Fiz.*, 2, 22–28, 1964.
- Shindyapin, G.P., "Regular reflection of weak shock waves from a wall", *Zh. Prikl. Math. Mekh.*, 29, 114–121, 1965.
- Shindyapin, G.P., "Irregular interaction of weak shock waves of different intensity", *Prikl. Math. Mech.*, 38, 105–114, 1974.
- Shindyapin, G.P., "Numerical solution of the problem of non-regular reflection of a weak shock wave by a rigid wall in a perfect gas", *Zh. Vyehisl. Math. Math. Fiz.*, 20, 249–254, 1980.
- Shindyapin, G.P. "Mach reflection and interaction of weak shock waves under the conditions of von Neumann paradox", *Mekh. Zid. i Gaza*, 2, 183–190, 1996. (In Russian).
- Shirouzu, M. & Glass, I.I., "Evaluation of assumptions and criteria in pseudo-stationary oblique Shock Wave Reflections", *Proc. Roy. Soc. London*, A406, 75–92, 1986.
- Shirozu, T. & Nishida, M., "Numerical studies of oblique shock reflection in steady two dimensional flows", *Memoirs Faculty Eng. Kyushu Univ.*, 55, 193–204, 1995.
- Skews, B.W., "The shape of a diffracting shock wave", *J. Fluid Mech.*, 29, 297–304, 1967.
- Skews, B.W., "Shock-shock reflection", *CASI Trans.*, 4(1), 16–19, 1971.
- Skews, B.W., "The flow in the vicinity of a three-shock intersection", *CASI Trans.*, 4(2), 99–107, 1971.
- Skews B.W., "The shape of a shock in regular reflection from a wedge", *CASI Trans.*, 5(1), 28–32, 1972.
- Skews B.W., "Shock wave shaping", *AIAA J.*, 10(6), 839–841, 1972.
- Skews, B.W., "Oblique reflection of shock waves from rigid porous materials", *Shock Waves*, 4(3), 145–154, 1994.
- Skews B.W., "Synchronised shock tubes for wave reflection studies", *Rev. Sci. Instr.* 66, 3327–3330, 1995.
- Skews, B.W., "Aspect ratio effects in wind tunnel studies of shock wave reflection transition", *Shock Waves*, 7(6), 373–383, 1997.
- Skews, B.W., "Three-dimensional effects in wind tunnel studies of shock wave reflection", *J. Fluid Mech.*, 407, 85–104, 2000.
- Skews, B.W. & Ashworth, J.T., "The physical nature of weak shock wave reflection", *J. Fluid Mech.*, 542, 105–114, 2005.
- Skews, B.W., Menon, N., Bredin, M. & Timofeev, E.V., "An experiment on imploding conical shock waves", *Shock Waves*, 11(4), 323–326, 2002.
- Smith, W.R., "Mutual Reflection of Two Shock Waves of Arbitrary Strengths", *Phys. Fluids*, 2, 533–541, 1959.
- Sokolov, V.B., "Reflection of a strong shock wave by an ellipsoid of revolution and elliptical cylinder", *Izv. Akad. Nauk SSSR Mekh. Zh. i Gaza*, 4, 173–174, 1974.
- Srivastava, R. & Chopra, M.G., "Diffraction of blast waves for the oblique case", *J. Fluid Mech.*, 40, 821–831, 1970.

- Srivastava, R.S. & Deschambault, R.L., "Pressure distribution behind a non-stationary reflected-diffracted oblique shock wave", *AIAA J.*, 22, 305–306, 1984.
- Sternberg, J., "Triple-shock-wave intersections", *Phys. Fluids*, 2, 179–206, 1959.
- Sudani, N., & Hornung H.G., "Stability and analogy of shock wave reflection in steady flow", *Shock Waves*, 8(6), 367–374, 1998.
- Sudani, N., Sato, M., Karasawa, T., Kanda, H. & Toda, N., "Irregular phenomena of shock reflection transition in a conventional supersonic wind tunnel", *AIAA J.*, 41(6), 1201–1204, 2003.
- Sudani, N., Sato, M., Karasawa, T., Noda, J., Tate, A. & Watanabe, M., "Irregular effects on the transition from regular to Mach reflection of shock waves in wind tunnel flows", *J. Fluid Mech.*, 459, 167–185, 2002.
- Suhindyapin, G.P., "On irregular reflection of weak shock waves by a rigid wall", *Zh. Prikl. Math. Tekh. Fiz.*, 2, 22–28, 1964.
- Suhindyapin, G.P., "On the regular reflection of weak shock waves by a rigid wall", *Prikl. Math. & Mekh.*, 29, 114–121, 1965.
- Suhindyapin, G.P., "Irregular interaction of weak shock waves of different intensity", *Prikl. Math. & Mekh.*, 38, 105–114, 1974.
- Suhindyapin, G.P., "Numerical solution of the problem of non regular reflection of a weak shock wave by a rigid wall in a perfect gas", *J. Num. Anal. & Math. Phys.*, 20, 249–254, 1980.
- Sun, M. & Takayama, K., "The formation of a secondary shock wave behind a shock wave diffracting at a convex corner", *Shock Waves*, 7(5), 287–295, 1997.
- Sun, M. & Takayama, K., "A note on numerical simulation of vortical structures in shock diffraction", *Shock Waves*, 13(1), 25–32, 2003.
- Sun, M. & Takayama, K., "Vorticity production in shock diffraction", *J. Fluid Mech.*, 478, 237–256, 2003.
- Sun, M. Yada, K. Jagadeesh, G. Onodera, O. Ogawa, T. & Takayama, K., "A study of shock wave interaction with a rotating cylinder", *Shock Waves*, 12(6), 479–485, 2003.
- Suzuki, T. & Adachi, T., "The reflection of a shock wave over a wedge with dusty surface", *Trans. Japan Soc. Aero. & Astro.*, 28, 132–139, 1985.
- Suzuki, T. & Adachi, T., "Comparison of shock reflection from a dust layer with those from a smooth surface", *Theo. & Appl. Mech.*, 35, 345–352, 1987.
- Suzuki, T. & Adachi, T., "An experimental study of oblique shock wave reflection over a dusty surface", *Trans. Japan Soc. Aero. & Astro.*, 31, 104–110, 1988.
- Suzuki, T., Adachi, T. & Kobayashi, S., "Experimental analysis of reflected shock behavior over a wedge with surface roughness (Local behavior)", *JSME Int. J., Ser. B: Fluids & Thermal Eng.*, 36(1), 130–134, 1993.
- Suzuki, T., Adachi, T. & Kobayashi, S., "Image analysis of oblique shock reflection over a model wedge", *J. Visualization Soc. Japan*, 10(2), 7–10, 1990.

- Suzuki, T., Adachi, T. & Kobayashi, S., "Nonstationary shock reflection over nonstraight surfaces: An approach with a method of multiple steps", *Shock Waves*, 7(1), 55–62, 1997.
- Suzuki, T., Adachi, T. & Tanabe, K., "Structure of the Mach-type reflection on a dust layer", *Theor. & Appl. Mech.*, 34, 73–80, 1986.
- Syshchikova, M.P. & Krassovskaya, I.V., "Some properties of regular and irregular interaction of shock waves", *Arch. Mech.*, 31, 135–145, 1979.
- Syshchikova, M.P., Semenov, A.N. & Berezhkina, M.K., "Shock wave reflection by a curved concave surface", *Sov. Phys. Tech. Phys.*, 2, 61–66, 1976.
- Sysoev, N.N., "Unsteady reflection of shock waves by a sphere or cylinder", *Ser. Phys. & Astron.*, 20, 90–91, 1979.
- Sysoev, N.N. & Shugaev, F.V., "Transient reflection of a shock wave from a sphere and a cylinder", *Vestnik Moskovskogo Universiteta. Fiz.*, 34, 90–91, 1979.
- Takayama, K. & Ben-Dor, G., "A Reconsideration of the hysteresis phenomenon in the regular \rightleftharpoons Mach reflection transition in truly nonstationary flows", *Israel J. Tech.*, 21, 197–204, 1983.
- Takayama, K. & Ben-Dor, G., "The inverse-Mach reflection", *AIAA J.*, 23, 1853–1859, 1985.
- Takayama, K. & Ben-Dor, G., "Application of streak photography for the study of shock wave reflections over a double wedge", *Exp. Fluids*, 6, 11–15, 1987.
- Takayama, K. & Ben-Dor, G., "A reconsideration of the transition criterion from Mach to regular reflection over cylindrical concave surfaces", *Korean Soc. Mech. Eng. J.*, 3, 6–9, 1989.
- Takayama, K. & Ben-Dor, G., "Pseudo-steady oblique shock wave reflections over water wedges", *Exp. Fluids*, 8, 129–136, 1989.
- Takayama, K. & Ben-Dor, G., "State-of-the-art in research on Mach reflection of shock waves", *Sadhana*, Vol. 18(3/4), pp. 695–710, 1993.
- Takayama, K., Ben-Dor, G. & Gotoh, J., "Regular to Mach reflection transition in truly nonstationary flows – Influence of surface roughness", *AIAA J.*, 19, 1238–1240, 1981.
- Takayama, T. & Jiang, Z., "Shock wave reflection over wedges: a benchmark test for CFD and experiments", *Shock Waves*, 7(4), 191–203, 1997.
- Takayama, K. & Sekiguchi, H., "Triple-point trajectory of a strong spherical shock wave", *AIAA J.*, 19, 815–817, 1981.
- Tan, H.S., "Strength of reflected shock in Mach reflection", *J. Aero. Sci.*, 18, 768–770, 1951.
- Taub, A.H., "Refraction of plane shock waves", *Phys. Rev.*, 72, 51–60, 1947.
- Ter-Minassians, S.M., "The diffraction accompanying the regular reflection of a plane obliquely impinging shock wave from the walls of an obtuse wedge", *J. Fluid Mech.*, 35, 391–410, 1969.
- Tesdall, A.M. & Hunter, J.K., "Self-similar solutions for weak shock reflection", *Siam. J. Appl. Math.*, 63, 42–61, 2002.

- Teshukov, V.M., "On regular reflection of a shock wave from a rigid wall", Prikl. Math. & Mekh., 46, 225–234, 1982.
- Teshukov, V.M., "On the stability of regular reflection of shock waves", Prilk. Mekh. i Tech. Fizika, (translated to English in Appl. Mech. & Tech. Phys.), 2, 26–33, 1989. (In Russian).
- Thomas, G.O. & Williams, R. LI, "Detonation interaction with wedges and bends", Shock Waves, 11(6), 481–492, 2002.
- Ting, L., & Ludloff, H.F., "Difference solution of shock diffraction problem", J. Aero. Sci., 19, 317–328, 1952.
- Trotsyuk, A.V., Kudryavtsev, A.N. & Ivanov, M.S., "Numerical investigation of unsteady Mach reflection of detonation waves", Comp. Fluid Dyn. J., 12(2), 248–257, 2003.
- Tsu-Sien-Shao, "Numerical solution of plane viscous shock reflections", J. Comp. Phys., 1, 367–381, 1977.
- Vasilev, E.I., "Generalization of the von Neumann theory for the Mach reflection of weak shock waves", Math. Fiz., 3, 74–82, 1998. (In Russian)
- Vasilev, E.I., 1999 Four-wave scheme of weak Mach shock wave interaction under von Neumann paradox conditions. Fluid Dyn., 34(3), 421–427.
- Vasilev, E.I., & Kraiko, A.N. "Numerical simulation of weak shock diffraction over a wedge under the von Neumann paradox conditions", Comp. Math. Math. Phys., 39(8), 1335–1345, 1999.
- Voinovich, P.A., Popov, F.D. & Fursenko, A.A., "Numerical simulation of shock wave reflection from a concave surface", Sov. Tech. Phys. Lett., 4, 127–128, 1978.
- Voloshinov, A.V., Kovalev, A.D. & Shindyapin, G.P., "Transition from regular reflection to Mach reflection when a shock wave interacts with a wall in two-phase gas-liquid medium", Izv. Akad. Nauk SSSR, Mekh. Zh. i Gaza, 5, 190–192, 1983.
- Voloshinov, A.V., Kovalev, A.D. & Shindyapin, G.P., "Transition from regular reflection to Mach reflection when a shock wave interacts with a wall in a two-phase gas-liquid medium", Fluid Dyn., 18, 827–829, 1983.
- Vasilev, E.I., Ben-Dor, G., Elperin, T. & Henderson, L.F., "Wall-jetting effect in Mach reflection: Navier-Stokes simulations", J. Fluid Mech., 511, 363–379, 2004.
- Vuillon, J., Zeitoun, D. & Ben-Dor, G., "Reconsideration of oblique shock wave reflection in steady flows. Part II: Numerical Investigation", J. Fluid Mech., 301, 37–50, 1995.
- Vuillon, J., Zeitoun, D. & Ben-Dor, G., "Numerical investigation of shock wave reflections in steady flows", AIAA J., 34(6), 1167–1173, 1996.
- Walenta, Z.A., "Regular reflection of the plane shock wave from an inclined wall", Arch. Mech., 26, 825–832, 1974.
- Walenta, Z.A., "Microscopic structure of the Mach-type reflection of the shock wave", Arch. Mech., 32, 819–825, 1980.
- Walenta, Z.A., "Formation of the Mach-type reflection of shock waves", Arch. Mech., 35, 187–196, 1983.

- Walker, D.K., Dewey, J.M. & Scotten, L.N., "Observations of density discontinuities behind reflected shocks close to the transition from regular to Mach reflection", *J. Appl. Phys.*, 53(3), 1398–1400, 1982.
- Wensheng, H., Onodera, O. & Takayama, K., "Unsteady interaction of shock wave diffracting around a circular cylinder in air", *Acta Mech. Sinica*, 7(4), 295–299, 1991.
- White, D.R., "Reflection of strong shock at nearly glancing incidence", *J. Aero. Sci.*, 18, 633–634, 1951.
- Whitham, G.B., "A new approach to problems of shock dynamics. Part 1. Two dimensional problems", *J. Fluid Mech.* 2, 145–171, 1957.
- Woodward, P.R. & Colella, P., "Numerical solution of two-dimensional fluid flow with strong shocks", *J. Compt. Phys.*, 54, 115–173, 1984.
- Xie, P. & Takayama, K., "A study of the interaction between two triple points", *Shock Waves*, 14(1/2), 29–36, 2005.
- Xu, D.Q. & Honma, H., "Numerical simulation for nonstationary Mach reflection of a shock wave: A kinetic model approach", *Shock Waves*, 1(1), 43–50, 1991.
- Xu, D.Q., Honma, H. & Abe, T., "DSMC approach to nonstationary Mach reflection of strong incoming shock waves using a smoothing technique", *Shock Waves*, 3(1), 67–72, 1993.
- Yan, H., Adelgren, R., Elliott, G., Knight, D. & Beutner, T., "Effect of energy edition on RR → MR transition", *Shock Waves*, 13(2), 123–138, 2003.
- Yang, J.Y., Liu, Y. & Lomax, H., "Computation of shock wave reflection by circular cylinders", *AIAA J.*, 25, 683–689, 1987.
- Yang, J., Sasoh, A. & Takayama, K., "The reflection of a shock wave over a cone", *Shock Waves*, 6(5), 267–273, 1996.
- Yu, Q. & Grönig, H., "Shock waves from an open-ended shock tube with different shapes", *Shock Waves*, 5(4), 249–258, 1996.
- Yu, Sh. & Grönig, H., "A simple approximation for axially symmetric diffraction of plane shocks by cones", *Z. Naturforsch.* 39a, 320–324, 1984.
- Zakhrian, A.R., Brio, M., Hunter, J.K. & Webb, G.M., "The von Neumann paradox in weak shock reflection", *J. Fluid Mech.* 422, 193–205, 2000.
- Zaslavskii, B.I. & Safarov, R.A., "About Mach reflection of weak shock waves from a rigid wall", *J. Appl. Mech. & Tech. Phys.*, 5, 26–33, 1973. (In Russian).
- Zaslavskii, B.I. & Safarov, R.A., "On the similarity of flows occurring in weak shock wave reflections from a rigid wall or free surface", *Fiz. Gorenija i Vzryva*, 4, 579–585, 1973.
- Zeitoun, D.E. & Burtschell, Y., "Shock/shock and shock/boundary layer interactions in an axisymmetric laminar flows", *Shock Waves*, 12(6), 487–495, 2003.
- Zeng, S. & and Takayama, K., "On the refraction of shock wave over a slow-fast gas interface", *Acta Astro.* 38(11), 829–838, 1996.
- Zhao, H., Yin, X.Z. & Grönig, H., "Pressure measurements on cone surface in 3-D shock reflection processes", *Shock Waves*, 9(6), 419–422, 1999.

- Zhigalko, Y.F., "Concerning the problem of shock wave diffraction and reflection", *Vestnik Moskovskogo Universiteta. Fiz.*, 1, 78–82, 1967.
- Zhigalko, Y.F., "A linear approximation of shock wave diffraction and reflection", *Vestnik Moskovskogo Universiteta. Fiz.*, 3, 94–104, 1969.
- Zhigalko, Y.F., "Approximate locally-nonlinear solutions of the problem on interaction between a shock wave and a rigid wall", *Fluid Mech. Sov. Res.*, 4, 81–91, 1975.
- Zhigalko, Y.F., "Linear approximation of the reflection of shock waves from a concave wall", *Fluid Mech. Sov. Res.*, 10, 60–71, 1981.
- Zhigalko, Y.F., Kolyshkina, L.L. & Shevtsov, V.D., "Vortical singularity of self-similar gas flow in the reflection of a shock wave", *Zh. Prikl. Mekh. i Tekh. Fiz.*, 1, 107–111, 1982.
- Znamenskaya, I.A., Ryazin, A.P. & Shugaev, F.V., "On some features of gas parameter distribution in the early stages of shock reflection by a sphere or cylinder", *Izv. Akad. Nauk SSSR Mekh. Zh. i Gaza*, 3, 103–110, 1979.
- Zumwalt, G.W., "Weak shock reflections at near 90° angle of incidence", *J. Appl. Mech.*, 41, 1142–1143, 1974.

5.2 Reports

References

- Adachi, T., Kobayashi, S. & Suzuki, T., "Unsteady behavior of Mach reflection over a wedge with surface roughness", *Ann. Rep. Japan Soc. Heat Fluid Eng.*, 4, 53–57, 1989.
- Ando, S., "Pseudo-stationary oblique shock wave reflection in carbon dioxide – Domains and boundaries", UTIAS TN 231, Institute for Aerospace Studies, Univ. Toronto, Toronto, Ont., Canada, 1981.
- Bargmann, V., "On nearly glancing reflection of shocks", *Sci. Res. Dev. OSRD Rep. 5171*, Washington, DC, U.S.A. or Nat. Defence Res. Comm., NDRC, 1945.
- Bargmann, V. & Montgomery, D., "Prandtl-Meyer zones in Mach reflection", *Off. Sci. Res. Dev. OSRD Rep. 5011*, Washington, DC, U.S.A., 1945.
- Ben-Dor, G., "Regions and transitions of nonstationary oblique shock wave diffractions in perfect and imperfect gases", UTIAS Rep. 232, Institute for Aerospace Studies, Univ. Toronto, Toronto, Ont., Canada, 1978.
- Ben-Dor, G., "Nonstationary oblique shock wave reflection in nitrogen and argon: Experimental results", UTIAS Rep. 237, Institute for Aerospace Studies, Univ. Toronto, Toronto, Ont., Canada, 1978.
- Bertrand, B.P., "Measurement of pressure in Mach reflection of strong shock waves in a shock tube", *Mem. Rep. 2196*, Ballistic Res. Lab., U.S.A., 1972.
- Bleakney, W., "The effect of Reynolds number on the diffraction of shock waves", Princeton Univ., Dept. Phys. Tech. Rep. II-8, Princeton, N.J., U.S.A., 1951.

- Clarke, J.F., "Regular reflection of a weak shock wave from a rigid porous wall. Some additional results", CoA Memo 8225, Cranfield Inst. Tech., Cranfield, England, 1982.
- Clarke J.F., "Inertia effects on the regular reflection of a weak reflection of a weak shock wave from a rigid porous wall", CoA Rep. NFP84/2, Cranfield Inst. Tech. Cranfield, England, 1984.
- Deschambault, R.L., "Nonstationary oblique-shock-wave reflections in air", UTIAS Rep. 270, Institute for Aerospace Studies, Univ. Toronto, Toronto, Ont., Canada, 1984.
- Fletcher, C.H., "The Mach reflection of weak shock waves", Princeton Univ., Dept. Phys. Tech. Rep. II-4, Princeton, N.J., U.S.A., 1950.
- Friend, W.H., "The interaction of a plane shock wave with an inclined perforated plate", UTIAS TN 25, Institute for Aerospace Studies, Univ. Toronto, Toronto, Ont., Canada, 1958.
- Fry, M., Picone, J.M., Boris, J.P. & Book, D.L., "Transition to double-Mach stem for nuclear explosion at 104-ft height of burst", NRL MR 4630, 1981.
- Fuchs, J. & Schmidt, B., "Entstehungsort des tripelpunktes und seine anschließende spur beim ubergang von regularer reflektion zur Mach reflektion", Stromangsmechanik und Stromeungsmaschinen Rep. 40/89, Universitat Karlsruhe, Karlsruhe, Germany, 1989.
- Glass, I.I., "Beyond three decades of continuous research at UTIAS on shock tubes and waves", UTIAS Rev. 45, Institute for Aerospace Studies, Univ. Toronto, Toronto, Ontario, Canada, 1981.
- Glass, I.I., "Some aspects of shock wave research", UTIAS Rev. 48, Institute for Aerospace Studies, Univ. Toronto, Toronto, Ont., Canada, 1986.
- Glaz, H.M., Colella, P., Glass, I.I. & Deschambault, R.L., "A detailed numerical, graphical and experimental study of oblique shock wave reflections", LBL-20033, Lawrence Berkely Lab., Berkely, CA, U.S.A., 1985.
- Glaz, H.M., Colella, P., Glass, I.I. & Deschambault, R.L., "A numerical and experimental study of pseudostationary oblique-shock-wave reflections in argon and air", UTIAS Rep. 285, Institute for Aerospace Studies, Univ. Toronto, Toronto, Ont., Canada, 1986.
- Guderley, K.G., "Considerations on the structure of mixed Subsonic-supersonic flow patterns", HQ Air Materiel Command, Tech. Rep. F-TR-2168-ND, Wright Field, Dayton, Ohio., U.S.A.
- Guo Chang-Ming, "Numerical calculation of Mach reflection of spherical shock wave on rigid wall", Rep. 9/85, Dept. Modern Mech., Univ. Sci. & Tech. China, Hefei, China, 1985.
- Handke, E. & Obemeier, F., "Some theoretical results on Mach reflection of moderately strong shock waves", Max Planck Inst. Rep. 14, 1983.
- Harrison, F.B. & Bleakney, W., "Remeasurement of reflection angles in regular and Mach reflection of shock waves", Princeton Univ., Dept. Phys. Tech. Rep. II-0, Princeton, N.J., U.S.A., 1947.
- Hisley, D.M., "BLAST2D computations of the reflection of planar shocks from wedge surfaces with comparison to SHARC and SLEATH results",

- Tech. Rep. BRL-TR-3147, Ballistic Res. Lab., Aberdeen Proving Ground, Maryland, U.S.A., 1990.
- Hu, T.C.J., "Pseudo-stationary oblique-shock-wave-reflections in a polyatomic gas-sulfur hexafluoride", UTIAS TN 253, Institute for Aerospace Studies, Univ. Toronto, Toronto, Ont., Canada, 1985.
- Hu, T.C.J. & Shirouzu, M., "Tabular and graphical solutions of regular and Mach reflections in pseudo-stationary frozen and vibrational equilibrium flows", UTIAS Rep. 283, Parts 1 & 2, Institute for Aerospace Studies, Univ. Toronto, Toronto, Ont., Canada, 1985.
- Ikui, T., Matsuo, K. Aoki, T. & Kondoh, N., "Mach reflection of a shock wave from an inclined wall", Memoirs Faculty Eng., Kyushu Univ., 41, 361–380, Fukuoka, Japan, 1981.
- Jahn, R.G., "The refraction of shock waves at a gaseous interface: Regular reflection of weak shocks", Princeton Univ., Dept. Phys. Tech. Rep. II-16, Princeton, N.J., U.S.A., 1954.
- Jahn, R.G., "The refraction of shock waves at a gaseous interface: Regular reflection of strong shocks", Princeton Univ., Dept. Phys. Tech. Rep. II-18, Princeton N.J., U.S.A., 1955.
- Jahn, R.G., "The refraction of shock waves at a gaseous Interface: Irregular refraction", Princeton Univ., Dept. Phys. Tech. Rep. II-19, Princeton, N.J., U.S.A., 1955.
- Kaca, J., "An interferometric investigation of the diffraction of a planar shock wave over a semicircular cylinder", UTIAS TN 269, Institute for Aerospace Studies, Univ. Toronto, Toronto, Ont., Canada, 1988.
- Law, C.K. "Diffraction of strong shock waves by a sharp compressive corner", UTIAS TN 150, Institute for Aerospace Studies, Univ. Toronto, Toronto, Ont., Canada, 1970.
- Lean, G.H., "Report on further experiments on the reflection of inclined shock waves", Nat. Phys. Lab. London, England, 1946.
- Lee, J.H. & Glass, I.I. "Domains and boundaries of pseudo stationary oblique shock wave reflections in air", UTIAS Rep. 262, Institute for Aerospace Studies, Univ. Toronto, Toronto, Ont., Canada, 1982.
- Li, J. -C. & Glass, I.I., "Collision of Mach reflections with a 90-degree ramp in air and CO₂", UTIAS Rep. 290, Institute for Aerospace Studies, Univ. Toronto, Toronto, Ont., Canada, 1985.
- Lottero, R.E. & Wortman, J.D., "Evaluation of the HULL and SHARC hydrocodes in simulating the reflection of a Mach 2.12 non-decaying shock on wedges of various angles", Tech. Rep. BRL-TR-????, Ballistic Res. Lab., Aberdeen Proving Ground, Maryland, U.S.A., 1991.
- Lozzi, A., "Double Mach reflection of shock waves", M.Sc. Thesis, The Univ. Sydney, Sydney, New South Wales, Australia, 1971.
- Meiburg, E., Oertel, H.Jr., Walenta, Z. & Fiszdon, W., "Quasistationary Mach reflection of shock waves, preliminary results of experimental and Monte Carlo investigations", DFVLR-AVA Rep. IB-221-83A, 1983.

- Mirels, H., "Mach reflection flow fields associated with strong shocks", Aerospace Corp., TR-0083(3785)-1, El Segundo, CA, U.S.A.
- Mölder, S., "Head on interaction of oblique shock waves", UTIAS TN 38, Institute for Aerospace Studies, Univ. Toronto, Toronto, Ont., Canada, 1960.
- Neumann, J. von, "Oblique reflection of shocks", *Explosive Research. Rep. 12*, Navy Dept., Bureau of Ordnance, Washington, DC, U.S.A., 1943.
- Neumann, J. von, "Refraction, intersection and reflection of shock waves", NAVORD Rep. 203-245, Navy Dept., Bureau of Ordnance, Washington, DC, U.S.A., 1945.
- Olim, M., "A study of the reflection of weak ($1.1 < M_i < 1.5$) shocks and the development of a revised three shock solution", Ph.D Thesis, Dept. Phys., Univ. Victoria, Victoria, B.C., Canada, 1990.
- Onodera, H. & Takayama, K., "Shock wave propagation over slitted wedges", Rep. Inst. Fluid Sci., Tohoku Univ., Sendai, Japan, Vol. 1, pp. 45-66, 1990.
- Polacheck, H. & Seeger, R.J., "Regular reflection of shocks in water-like substances", Explos. Res. Rep. 14, Navy Dept., Bureau of Ordnance, Washington, DC., U.S.A., 1943.
- Prasse, H.G., "An analytic description of the expansion of the reflected shock wave at the Mach reflection on wedges", Rep. 4/72, Ernst Mach Institute, Freiburg, Germany, 1972.
- Reichenbach, H., "Roughness and Heated Layer Effects on Shock Wave Propagation and Reflection - Experimental Results", Rep. 24/85, Ernst Mach Institute, Freiburg, Germany, 1985.
- Richtmyer, R.D., "Progress report on the Mach reflection calculation", Rep. NYU 9764, Courant Inst., New York Univ., N.Y., U.S.A., 1961.
- Schultz-Grunow, F., "Diffuse reflexion einer stobwelle", Rep. 4/72, Ernst Mach Institute, Freiburg, Germany, 1972.
- Seeger, R.J. & Polacheck, H., "Regular reflection of shocks in ideal gases", Explos. Res. Rep. 13, Navy Dep., Bureau of Ordnance, Washington, DC., U.S.A., 1943.
- Shankar, V., Kutler, P. & Anderson, D., "Diffraction of a shock wave by a compression corner: Regular and single Mach reflection", NASA TM X-73,178, 1976.
- Shirouzu, M. & Glass, I.I. "An assessment of recent results on pseudo stationary oblique-shock-wave reflections", UTIAS Rep. 264, Institute for Aerospace Studies, Univ. Toronto, Toronto, Ont., Canada, 1982.
- Skews, B.W., "Profiles of diffracting shock waves (an analysis based on Whitham's theory)", Univ. Witwatersrand, Dept. Mech. Eng., Rep. 35, Johannesburg, South Africa, 1966.
- Skews, B.W., "Shock wave diffraction a review", Univ. Witwatersrand, Dept. Mech. Eng. Rep. 32, Johannesburg, South Africa, 1966.
- Skews, B.W., "The perturbed region behind a diffracting shock wave", Univ. Witwatersrand, Dept. Mech. Eng. Rep. 44, Johannesburg, South Africa, 1967.

- Skews, B.W., "The deflection boundary condition in the regular reflection of shock waves", Dept. Rep., McMaster Univ., Hamilton, Ontario, Canada, 1972.
- Skews, B.W., "The effect of angular slipstream on Mach reflection", Dept. Rep., McMaster Univ., Hamilton, Ontario, Canada, 1972.
- Smith, L.G., "Photographic investigation of the reflection of plane shocks in Air", Off. Sci. Res. Dev. OSRD Rep. 6271, Washington, DC, U.S.A. or Nat. Defence Res. Comm. NDRC Rep. A-350, 1945.
- Srivastava, R.S., "Diffraction of blast waves for the oblique case", British Aero. Res. Council Rep. 1008, 1968.
- Suzuki, T. & Adachi, K., "Oblique reflection of a plane shock on a rough and porous wedge", Ann. Rep. Japan Soc. Heat Fluid Eng., 2, 23-26, 1987.
- Takayama, K. & Ben-Dor, G., "Reflection and diffraction of shock waves over a circular concave wall", Rep. Inst. High Speed Mech., Tohoku Univ., Sendai, Japan, 51, 44-87, 1986.
- Takayama, K., Miyoshi, H. & Abe, A., "Shock wave reflection over gas/liquid interface", Rep. Inst. High Speed Mech., Tohoku Univ., Sendai, Japan, 57, 1-25, 1989.
- Takayama, K., Onodera, O. & Gotoh, J., "Shock wave reflections over a rough surface wedge and a curved rough surface", Rep. Inst. High Speed Mech., Tohoku Univ., Sendai, Japan, 48, 1-21, 1982.
- Takayama, K. & Sasaki, M., "Effects of radius of curvature and initial angle on the shock transition over concave and convex walls", Rep. Inst. High Speed Mech., Tohoku Univ., Sendai, Japan, 46, 1-30, 1983.
- Takayama, K. & Sekiguchi H., "An experiment on shock diffraction by cones", Rep. Inst. High Speed Mech., Tohoku Univ., Sendai, Japan, 36, 53-74, 1977.
- Takayama, K. & Sekiguchi, H., "Formation and diffraction of spherical shock waves in a shock tube", Rep. Inst. High Speed Mech., Tohoku Univ., Sendai, Japan, 43, 89-119, 1981.
- Tepe, F.R.Jr. & Tabakoff, W., "The interaction of unequal oblique shock waves in a hypersonic flow", Aero. Res. Lab., ARL Rep. 63-146, U.S.A.
- Urbanowicz, J.T., "Pseudo stationary oblique shock wave reflections in low gamma gases - isobutane and sulphur hexafluoride", UTIAS TN 267, Institute for Aerospace Studies, Univ. Toronto, Toronto, Ont., Canada, 1988.
- Weynants, R.R., "An Experimental investigation of shock-wave diffraction over compression and expansion corners", UTIAS TN 126, Institute for Aerospace Studies, Univ. Toronto, Toronto, Ont., Canada, 1968.
- Wheeler, J., "An interferometric investigation of the regular to Mach reflection transition boundary in pseudostationary flow in air", UTIAS TN 256, Institute for Aerospace Studies, Univ. Toronto, Toronto, Ont., Canada, 1986.
- White, D.R., "An experimental survey of the Mach reflection of shock waves", Princeton Univ., Dept. Phys., Tech. Rep. II-10, Princeton, N.J., USA, 1951.
- White, D.R., "An experimental survey of the Mach reflection of shock waves", Ph.D. Thesis, Princeton University, N.J., USA. See also Proc. 2nd Midwest Conf. Fluid Mech., Ohio State Univ., 3, 253-262, 1952.

- Yagla, J.J., "Machine calculation of unsteady Mach reflections and Prandtl-Meyer supersonic flows", NWL Tech. Rep. TN-2897, 1973.
- Zhang, D.L. & Glass, I.I., "An interferometric investigation of the diffraction of planar shock waves over a half diamond cylinder in air", UTIAS Rep. 322, Institute for Aerospace Studies, Univ. Toronto, Toronto, Ont., Canada, 1988.

Index

A

Acoustic impedance 66–67

B

Boundary layer displacement technique
displacement angle 202–203, 207–208,
210, 212–213
displacement thickness in MR
205–210
displacement thickness in RR 201–205
Boundary layer/shock wave interaction
incident shock 50, 102, 103, 105,
Mach stem 205–206

C

Complex-Mach reflection - CMR
definition 8
discovery 8
Compression Wave

D

Direct Mach reflection - DiMR
definition 6, 140–142, 257
in asymmetric reflection 93–94
shock polar of 24, 258
wave configuration of 6, 142
Domains of reflection
comparison between pseudosteady
and steady flows 233–235
in pseudosteady flow
strong shocks 179–180, 190, 192–194
weak shock 189–191
real gas effects on 199–201
in steady flow 47 70–73

in unsteady flow over double wedge
219–293, 296–297

Double-Mach reflection - DMR
analytical model 168–175
definition 8, 140–142, 167
discovery 8, 141
formation and termination 150,
161–162, 167, 175–176, 192, 198
negative and positive 8, 140–142, 150,
152, 176
over concave cylinders 252
over convex cylinders 283, 284, 285
real gas effects on 196–199
spherical shock wave 297
terminal – TerDMR, 8, 141, 142, 150,
153, 176
wave configuration of 142, 149,
167–175

Dual-solution domain
in symmetric reflection 34–35, 78
in asymmetric reflection 95
stability of regular reflection 78, 101
effect of free-stream perturbation
123–128

F

Flow deflection
domains 230–231
in pseudosteady flows 139, 154, 156,
159, 161
in steady flows 9
Four wave theory – 4WT 189, 190
Free stream perturbations
velocity perturbations 124
density perturbations 126

G

- Galilean transformation 138
 Guderley reflection - GR
 definition 3, 160, 180, 183
 discovery 3, 183
 formation and termination 180, 183,
 189
 shock polar of
 wave configuration of 160, 181

H

- Hysteresis phenomena
 application to flight dynamics
 129–130
 asymmetric shock waves
 wedge-angle-variation-induced
 96–99
 flow-Mach-number-variation-
 induced 99
 downstream-pressure-variation-
 induced 121–123
 axisymmetric shock waves
 geometrical-variation induced
 103–114
 flow-Mach-number-variation-
 induced 114–121
 viscous and nonviscous dependence
 107, 108
 symmetric shock waves
 wedge-angle-variation-induced
 79–86
 flow-Mach-number-variation-
 induced 86–90
 three-dimensional edge effects
 100–101

I

- Inverse-Mach reflection – InMR
 definition 6, 140–142, 257
 in asymmetric reflection 93–94
 shock polar of 24, 259
 termination of 259–260
 wave configuration of 6, 142, 259
 Inverted Mach reflection 6, 140–142
 Irregular reflection – IR
 definition 3, 140–142
 discovery 3
 domains 3, 180

L

- Law-Glass assumption 152, 156, 166,
 167, 173, 264

M

- Mach stem
 prediction of height 53–76
 Mach number 293
 Mach reflection – MR
 definition 3, 140–142
 discovery 3
 formation and termination 46,
 144–146, 182, 185, 188
 shock polar of 188
 stability to perturbations 123–128
 viscous effect on 106
 wave configuration of 4, 16, 53–76

N

- von Neumann paradox
 first 159, 183, 190
 second 202, 294, 295
 von Neumann reflection – vNR
 definition 3, 140–142, 145–146
 discovery 3, 142
 formation and termination 145, 159,
 180, 182, 185, 188
 shock polar of 27
 wave configuration of 28, 142,
 145–146, 181

O

- Overall Mach reflection - oMR
 in the reflection of asymmetric shock
 waves 90–91
 in the reflection of conical shock
 waves 91, 102, 110–113,
 115–121
 wave configuration 102
 Overall regular reflection - oRR
 in the reflection of asymmetric shock
 waves 90–91
 in the reflection of conical shock
 waves 91, 103, 115–121
 wave configuration 102

P

- Pseudo transitional-Mach reflection -
 PTMR
 definition 8, 161
 discovery 8, 161
 formation and termination 161, 175
 wave configuration of 161
 Pressure peaks 109, 117–119

R

Real gas effects
 dissociational equilibrium 198, 199–200, 203, 230–231, 233, 239, 241–243, 245
 ionizational equilibrium 199, 200, 230–231
 in Mach reflection 205–210
 in regular reflection 210–205
 on reflection domains 47, 193
 on shock polars 21
 on three-shock theory 52
 on two-shock theory 52
 relaxation length/zone 52, 196–199, 228
 regular reflection 52
 rotational-vibrational equilibrium 208–209
 vibrational equilibrium 196–199, 226

Regular reflection - RR
 definition 3, 140–142
 discovery 3, 141
 formation and termination 46, 143, 159
 over concave cylinders 252
 over convex cylinders 283, 284, 285
 over rigid porous 219–220
 real gas effects on 198
 roughness effect on 210–214
 shock polar of 21
 strong regular reflection-sRR 22, 91
 spherical shock wave 297–298
 stability to perturbations 123–128
 viscous effects on 201–205
 wave configuration of 4, 15, 142, 143
 weak regular reflection-wRR 22, 91

S

Shock polars
 application in unsteady flows 281–282
 at detachment 26, 27
 at mechanical equilibrium 30
 at sonic 31
 definition 18
 real gas effect on 21

Shock waves
 bow 158
 Galilean transformation 138
 conical 101
 oblique 13
 spherical 297–303

Shock wave diffraction

definition 157, 230
 domains 232

Shock wave reflection

definition 157
 historical background 3, 141–142
 in pseudosteady flows
 strong shock domain 135–180
 weak shock domain 180–190
 in steady flows 39–134
 in unsteady flow 247–305
 reasons for 9

Single-Mach reflection - SMR
 definition 8, 140–142
 discovery 3, 141
 formation and termination 146, 159, 161, 175, 192, 198
 over concave cylinders 251, 252
 over convex cylinders 283, 284, 286
 over perforated surfaces 215
 over rigid porous 220
 real gas effects on 198
 roughness effect on 210–211, 213–214
 shock polar of 22
 spherical shock wave 297
 viscous effect on 205–210
 wave configuration of 142, 146, 147

Slipstream

boundary conditions across 17
 boundary layer along 205–210
 diverged 224–227
 humps-like structure 109–114
 Kelvin-Helmholtz instability along 225, 226

Stationary-Mach reflection – StMR
 definition 6, 140–142, 257
 in asymmetric reflection 93–94
 shock polar of 24, 30, 258
 wave configuration of 6, 142, 259

Surface conditions

non-solid 221–222
 perforated 214–215
 porous
 compressible 218
 rigid 218–221
 rough 210–214, 255, 288–289
 slotted 215–218

Surface geometry

concave cylinders 250–282
 convex cylinders 282–291

- Surface geometry (*Continued*)
 curved 43–45
 double wedge 291–297
 elliptical convex 291
- T**
 Terminal double-Mach reflection – TDMR
 definition 8, 141, 150
 discovery 8, 142
 formation and termination 150, 176
 wave configuration of 142, 153
- Thermal conduction effects 222–224
- Three-shock theory – 3ST
 formulation 16
 modifications 48, 194
 non-self-similar effects 155, 195,
 227–229
 non-steady effects 194–195
 nonstraight discontinuity effects 49,
 195–196
 real gas effects 52, 196–200
 standard and nonstandard 17, 27–28,
 159, 182–183, 188
 thermal conduction effects 51,
 222–224
 viscous effects 49, 205–210
- Transition criteria
 detachment 25, 33
 length scale 32, 33, 144, 267, 289
 mechanical equilibrium 29, 33
 sonic 30, 33, 144
- Transitional-double-Mach reflection – TDMR
 definition 141, 150
 wave configuration of 150–151
- Transitional-Mach reflection – TMR
 analytical model 162–167
 definition 8, 140–142
 discovery 8, 141
 formation and termination 146, 150,
 161–162, 175–176, 192, 198
 kink 150, 151–156, 165–167, 173, 176
 over concave cylinders 252
 over convex cylinders 283, 284, 286
 real gas effects 196–199
- spherical shock wave 297
 wave configuration of 142, 146, 148,
 150, 162, 164
- Transitioned regular reflection – TRR
 analytical model 261–266
 definition 7, 140–142, 257
 formulation of 259–260, 282
 over concave cylinders 260, 268
 over double wedge 293
 wave configuration of 7, 142, 260, 268
- Triple-Mach reflection - TrMR
 definition 141, 150, 176
 wave configuration of 150–151, 176
- Triple point
 first 4, 22, 32, 35, 53, 140, 146, 170,
 173–174, 193, 195, 198, 239–241,
 244–246
 formation 155, 195, 213–214, 229
 glancing incidence 242, 278–280
 second 8, 140, 150, 151–156, 170,
 173–175, 176, 196, 198, 242–246
 third 150, 176
 trajectory 155, 195
 trajectory angle 8, 140, 215
- Two-shock theory – 2ST
 formulation 14
 modifications 48, 194
 nonstraight discontinuity effects 49,
 195–196
 nonsteady effects 194–195
 real gas effects 52, 196
 thermal conduction effects 51
 viscous effects 49, 201–205
- V**
 Vasilev reflection - VR
 definition, 180
 discovery 3
 formation and termination 180,
 188–189
 shock polar of 186
 wave configuration of 181, 188–189
- Viscous effects
 on Mach reflection 205–210
 on regular reflection 201–205